



**Proceedings of the
6th Annual Summer Conference**

NASA/USRA

University Advanced Design Program

**Hosted by
NASA Lewis Research Center
June 11-15, 1990**

**NATIONAL AERONAUTICS & SPACE ADMINISTRATION
UNIVERSITIES SPACE RESEARCH ASSOCIATION**

(NASA-CR-187041) PROCEEDINGS OF THE 6TH
ANNUAL SUMMER CONFERENCE: NASA/USRA
UNIVERSITY ADVANCED DESIGN PROGRAM Final
Report (USRA) 319 p CSCL 22A
65/12 0325455
N91-18171
--THRU--
N91-18172
Uncl us







**NASA/USRA
UNIVERSITY ADVANCED DESIGN PROGRAM**

**PROCEEDINGS OF THE
6th ANNUAL SUMMER CONFERENCE**

June 11-15, 1990

**NASA/USRA UNIVERSITY ADVANCED DESIGN PROGRAM
6th ANNUAL SUMMER CONFERENCE**

The NASA/University Advanced Design Program is operated by the Universities Space Research Association (USRA) under a contract with NASA Headquarters (NASW-4435). Inquiries regarding the program may be directed to:

USRA Advanced Design Program Office
17225 El Camino Real, Suite 450
Houston, Texas 77058
(713)480-5939
FAX: (713)480-8862

DEDICATION

We respectfully dedicate this Proceedings Volume to Mr. Melvin J. Hartmann of NASA's Lewis Research Center who retired on July 3 after 46 years of outstanding service to NACA and NASA. Mr. Hartmann's significant technical contributions include advances in both air breathing and rocket propulsion systems, strengthening basic research at Lewis Research Center, and providing a major interface to university based research in the aeronautics and space programs.

FOREWORD

The Program

The NASA/USRA University Advanced Design Program is a unique program that brings together NASA engineers, students, and faculty from United States engineering schools by integrating current and future NASA space/aeronautics engineering design projects into the university curriculum. The Program was conceived in the fall of 1984 as a pilot project to foster engineering design education in the universities and to supplement NASA's in-house efforts in advanced planning for space and aeronautics design. Nine universities and five NASA centers participated in the first year of the pilot project. Close cooperation between the NASA centers and the universities, the careful selection of design topics, and the enthusiasm of the students has resulted in a very successful program that now includes forty-three universities and eight NASA centers.

The study topics cover a broad range of potential space and aeronautics projects that could be undertaken during a 20-30-year period beginning with the deployment of the Space Station Freedom scheduled for the mid-1990s. Both manned and unmanned endeavors are embraced, and the systems approach to the design problem is emphasized. The student teams pursue the chosen problem during their senior year in a one- or two-semester capstone design course and submit a comprehensive written report at the conclusion of the project. Finally, student representatives from each of the universities summarize their work in oral presentations at the annual Summer Conference, held at one of the NASA centers and attended by the university faculty, NASA and USRA personnel, and aerospace industry representatives.

The Proceedings Volume

As the Advanced Design Program has grown in size, it has also matured in terms of the quality of the student projects. The comprehensive final

reports are distributed through the National Technical Information Service. However, the results of the studies reach only a small audience, principally those who attend the Summer Conference. In order to broaden the distribution, a Proceedings volume, which summarizes the project results and roughly parallels the Conference presentations, is published. The present volume represents the student work accomplished during the 1989-90 academic year and reported at the 6th Annual Summer Conference hosted by the Lewis Research Center, June 11-15, 1990.

ACKNOWLEDGMENTS

This publication was made possible through the efforts of a great many people. First of all, we are grateful to the students, the university faculty, and their teaching assistants for the excellent technical work. Second, we are indebted to those individuals from NASA Headquarters and from the NASA centers who conceived the program in the beginning, have provided valuable guidance throughout, and through their keen interest in the student projects, are in large part responsible for the boundless enthusiasm of the students. Finally, we thank the staff of the Publications Services Office of the Lunar and Planetary Institute for the excellent work in the preparation of the final Proceedings volume.

—USRA Advanced Design Program Office

TABLE OF CONTENTS

Opening Remarks—Mel Hartmann	ix
<i>NASA Lewis Research Center</i>	
Keynote Address—Raymond S. Colladay	xi
<i>Martin Marietta Corporation</i>	
SPACE PROJECTS	
THE UNIVERSITY OF ALABAMA, HUNTSVILLE	35
Fluid Phase Separation (FPS) Experiment for Flight on the Shuttle in a Get Away Special (GAS) Canister: Design and Fabrication	
UNIVERSITY OF ARIZONA	1152
Autonomous Space Processor for Orbital Debris	
UNIVERSITY OF CALIFORNIA, LOS ANGELES	2353
Laboratory Simulation of the Rocket Motor Thrust as a "Follower" Force	
UNIVERSITY OF CALIFORNIA, LOS ANGELES	2754
Design of a Scientific Probe for Obtaining Mars Surface Material	
UNIVERSITY OF CENTRAL FLORIDA	3557
Postlanding Optimum Designs for the Assured Crew Return Vehicle	
UNIVERSITY OF COLORADO	4158
Methods for the Development of a Bioregenerative Life Support System	
UNIVERSITY OF FLORIDA	4959
Implementation of Sensor and Control Designs for Bioregenerative Systems	
FLORIDA A&M UNIVERSITY/FLORIDA STATE UNIVERSITY	5360
Conceptual Second-Generation Lunar Equipment	
FLORIDA A&M UNIVERSITY/FLORIDA STATE UNIVERSITY	5561
Lunar Articulated Remote Transportation System	
GEORGIA INSTITUTE OF TECHNOLOGY	6162
Lunar Surface Vehicle Model Competition	
GEORGIA INSTITUTE OF TECHNOLOGY	6363
Bagging System, Soil Stabilization Mat, and Tent Frame for a Lunar Base	
UNIVERSITY OF HOUSTON COLLEGE OF ARCHITECTURE	6964
Spaceport Aurora: An Orbiting Transportation Node	
UNIVERSITY OF HOUSTON COLLEGE OF ARCHITECTURE	7965
In-situ Resource Utilization in the Design of Advanced Lunar Facilities	
UNIVERSITY OF IDAHO	8966
Preliminary Greenhouse Design for a Martian Colony: Structural, Solar Collection, and Light Distribution Systems	
UNIVERSITY OF ILLINOIS, URBANA-CHAMPAIGN	9367
An Unmanned Probe to Pluto	
KANSAS STATE UNIVERSITY	9968
Automation of Closed Environments in Space for Human Comfort and Safety	
UNIVERSITY OF MARYLAND	10569
Project Exodus	

UNIVERSITY OF MARYLAND Manned Mars Mission	111 5/8
UNIVERSITY OF MARYLAND Walking Robot: A Design Project for Undergraduate Students	117 5/8
MASSACHUSETTS INSTITUTE OF TECHNOLOGY Project Artemis	123 5/8
UNIVERSITY OF MICHIGAN Project Egress: The Design of an Assured Crew Return Vehicle for the Space Station	129 5/8
UNIVERSITY OF MINNESOTA Biconic Cargo Return Vehicle with an Advanced Recovery System	137 5/8
UNIVERSITY OF MINNESOTA Winged Cargo Return Vehicle Conceptual Design	145 5/8
NAVAL POSTGRADUATE SCHOOL High-Latitude Communications Satellite (HILACS)	153 5/8
OHIO STATE UNIVERSITY Project WISH: The Emerald City	165 5/8
OLD DOMINION UNIVERSITY Design of an Autonomous Lunar Construction Vehicle	169 5/8
PENNSYLVANIA STATE UNIVERSITY Preliminary Subsystem Designs for the Assured Crew Return Vehicle (ACRV)	175 5/8
PRAIRIE VIEW A&M UNIVERSITY Replenishable Food Supply on Mars	183 5/8
UNIVERSITY OF PUERTO RICO Habitability: CAMELOT IV	187 5/8
RENSSELAER POLYTECHNIC INSTITUTE Investigations into a Potential "Laser-NASP" Transport Technology	195 5/8
THE UNIVERSITY OF TEXAS, AUSTIN 1989-90 Project Summaries	203 5/8
THE UNIVERSITY OF TEXAS, AUSTIN Project Summaries	209 5/8
UNITED STATES NAVAL ACADEMY MIMES and GEOSHACK	213 5/8
UTAH STATE UNIVERSITY Microspacecraft and Earth Observation: Electrical Field (ELF) Measurement Project	217 5/8
VIRGINIA POLYTECHNIC AND STATE UNIVERSITY Three Orbital Transfer Vehicles	221 5/8
UNIVERSITY OF WASHINGTON Megawatt Solar Power Systems for Lunar Surface Operations	229 5/8
UNIVERSITY OF WISCONSIN-MILWAUKEE Genesis Lunar Outpost: An Evolutionary Lunar Habitat	241 5/8
WORCESTER POLYTECHNIC INSTITUTE Integrated Support Structure for GASCAN II	255 5/8

AERONAUTICS PROJECTS

AUBURN UNIVERSITY	267
Summary of 1989-90 Aeronautics Design Projects	
CALIFORNIA STATE UNIVERSITY, NORTHRIDGE	273
Autonomous Martian Flying Rover	
CALIFORNIA STATE POLYTECHNIC UNIVERSITY, POMONA	275
High Altitude Reconnaissance Aircraft	
CALIFORNIA POLYTECHNIC STATE UNIVERSITY, SAN LUIS OBISPO	283
The California Corridor Transportation System: A Design Summary	
CASE WESTERN RESERVE UNIVERSITY	287
O-THREE: A High Altitude, Remotely Piloted Vehicle	
UNIVERSITY OF KANSAS, LAWRENCE	291
Preliminary Design of a Supersonic Short-Takeoff and Vertical-Landing (STOVL) Fighter Aircraft	
UNIVERSITY OF NOTRE DAME	301
Design of a Remotely Piloted Vehicle for a Low Reynolds Number Station Keeping Mission	
THE OHIO STATE UNIVERSITY	309
A Hypersonic Research Vehicle to Develop Scramjet Engines	
ECOLE POLYTECHNIQUE FEMININE	319
Carrier Aircraft	
PURDUE UNIVERSITY	321
Design of a High Speed Business Transport	
WORCESTER POLYTECHNIC INSTITUTE	325
High Altitude, Microwave-Powered Atmospheric Sampling Aircraft	

ALUMNI PROJECTS

TEXAS A&M UNIVERSITY	329
UNIVERSITY OF WISCONSIN-MADISON	333

Opening Remarks

It is a pleasure to take part in the opening session of the University Advanced Design Program Summer Conference.

Over the next several days, we will be reviewing the design concepts developed by the teams and classes involved in the program. Reviews, critiques, and evaluations are a continuing and necessary step in the design and development of advanced aerospace systems. It occurs to me that some of you, having contributed to your team's efforts, may feel that the task is completed. It is only completed to a level where the concepts can be reviewed and further needs and the course of the design and development can be defined.

In the aerospace and similar technical areas, the design process blends neatly into the development and application phase. It is necessary to pass through a series of review steps along the way. Design changes and modifications along with critical reviews may be expected to continue throughout the useful life of aerospace systems. This is the process that is used to continue to update and bring new knowledge and capability to extend the systems' useful life. If this does not occur, it is probable that the design was too conservative to result in a profitable venture.

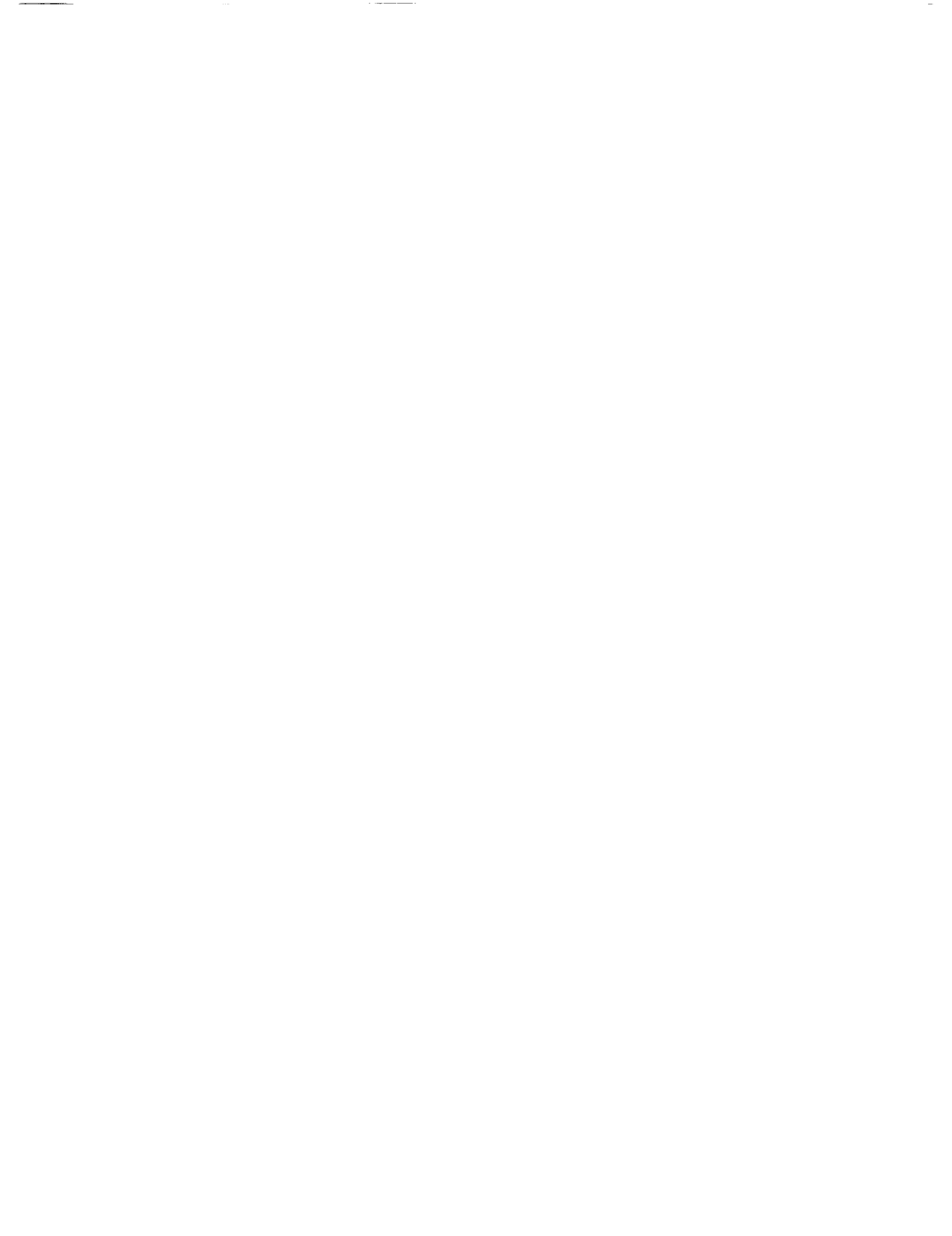
The greatest challenge to engineers engaged in design is the need to be continuously aware of advances that may provide increased capability. This new knowledge must be verified and applied to improved design and analysis methods and reduced to engineering practice as quickly as possible. To provide competitive designs, it is necessary that the latest information be available to the designers as well as the reviewer.

The personnel of the Lewis Research Center are pleased to host this conference and are glad that so many of you have journeyed to the North Coast to attend.

—Mel Hartmann
NASA Lewis Research Center

PAGE viii INTENTIONALLY BLANK

PRECEDING PAGE BLANK NOT FILMED



KEYNOTE ADDRESS

It's good to be here in the backyard of the Lewis Research Center and away from that piece of real estate on the Potomac otherwise known as Washington—the city of southern efficiency and northern charm. As an alumnus of the center, Lewis will always be a special place for me, and I still look back with fond memories of the years I spent here.

These are the best of times and the worst of times. In the next few minutes, I hope to persuade you that they are mostly the best of times. There is no doubt that we are facing the most dramatic change in the aerospace and defense business in 50 years.

The defense budget will continue its already four-year decline coming off the Reagan build-up. A complete reexamination of our national defense strategy of the last 40 years, following the dramatic events in Eastern Europe and the Soviet Union, will result in a major realignment and consolidation of the defense and aerospace industrial base. It's a lot different building up than building down. Trying to grow business in a declining market really sharpens your management skills. But the winners in this shakedown will be profitable. Change brings uncertainty and uncertainty carries with it risk; but with risk comes reward.

What does it mean for aerospace in particular? First of all, there will not be a peace dividend. But the space program will prosper, for NASA and defense, as compliance with new treaties must be verified largely from space national technical means. There is some argument that because defense budgets will decline, we should invest more in space to maintain a strong industrial base, but that downplays the importance of a U.S. space program—makes it sound like a space welfare program. The real reason space exploration will be supported is because the American people want it. They understand what the Congress will eventually realize, that the space program lets the country express its will to achieve great things and to satisfy an innate human desire to explore and learn, while at the same time infusing some of the skills and tools required to rekindle our industrial productivity.

I can be even more bullish on the prospects for design engineering, as companies like mine recognize how important good design engineers are. I hold the view that design is critical to our future for several reasons.

First, because we are often dealing with space systems that cannot be adequately tested, we must rely heavily on design getting it right. The national aerospace plane is a good example; much of the design can't be tested as a system before the flight article. The shuttle is another example; the first test of the full orbiter system was the piloted landing tests and the first test of the complete system occurred on its maiden launch to space. That is trusting design, albeit with lots of subsystem tests.

Second, design, coupled with manufacturing in concurrent engineering, is what lets us build in quality and improve productivity. Since World War II, we have approached product development like a relay race. Research and marketing comes up with an idea, hands it off to design, and they may develop a couple of hand-built prototypes to prove the soundness of the concept, and then it's thrown over to manufacturing to figure out how to build it. The first thing they do is send it back to engineering for changes, and on and on . . . you know the story.

Our problem in this country isn't a lack of technology and innovative ideas; it's getting products to the market on time. It just takes too long to get an idea from laboratory to field. In the U.S., we typically invest 2/3 of the cost of development on product and 1/3 on process. It is just the reverse in Japan.

But we're changing all that, right? We know that the walls between design and manufacturing need to be torn down. That's the social part of the fix and middle management is feeling threatened—you can actually get rid of a layer of management when you get teams of design, software, hardware, purchasing, manufacturing, and field support, all together and empower the people to make decisions. The other thing that has made concurrent engineering possible is the computer and information management systems that let all the functions talk to each other in a common medium.

At Martin Marietta, like our sister companies in the aerospace business, the change in culture is dramatic and the results are incredible.

While design is a small part of the product development effort, it has the major impact on cost.

	Cost Incurred	Total Cost Committed
Concept definition	<5%	>50%
Design engineer	<10%	>70%
Testing	10%	>85%
Process planning	15%	>90%
Production	>60%	95-100%

Through each phase, cost of a design change increases an order of magnitude, so the same design change that would cost, say, \$100 in concept definition, would cost \$1M to change in production.

Bringing design and manufacturing together, along with purchasing and the vendors and subcontractors, also has a major impact on time and quality. Our experience, again, like others, is that:

Development time is reduced by more than 50%; engineering changes are reduced by more than 70%; the time it takes to get a product to market is cut in half; and we gain quality improvement with almost no end in sight.

Quality means continuous improvement, and quality, built-in, costs less. For a long time that was counterintuitive. Augustine's^{*} law of "counterproductivity" is proven over and over again:

"It costs a lot of money to build bad products."

It costs a lot less to do it right the first time, one time.

When you cut through all the rhetoric, the real issues are (1) time to market and (2) quality . . . plus flexibility in responding to changing customers needs and market forces. If you do everything else right, cost takes care of itself.

We've been talking about product development, but let's look at the Washington end of the process for a minute. I use that as a euphemism to refer to the front end of the process of fielding an idea—the planning, budgeting, and acquisition process—when the government is the customer.

I have earned some license to be critical, because I've been there.

It has long been recognized in Washington that the formation of a committee is a powerful technique for avoiding responsibility, deferring difficult decisions, and averting blame while at the same time maintaining a semblance of action.

Kelly Johnson, who built the legacy of the Lockheed Skunk Works had a particular disdain for committees. He described it in the following way: "We're into an era where a committee designs airplanes. You never do anything totally stupid, you never do anything totally bright. You get an average wrong answer."

At Martin, I just formed a committee to deal with an issue so important that we've had meetings every other Friday for two consecutive weeks. Norm [Augustine] really believes in one of his other laws: "The optimum committee has no members . . . or maybe one . . . or at most three as long as one is absent and another is sick."

Congress has carried it to an extreme. They even have a committee on committees. Not only do we need to reduce the time to get things through the factory, we need to give some attention to reducing the time it takes to get programs through the budget and procurement cycle.

^{*}Norman R. Augustine, veteran aerospace executive, now Chairman and CEO of Martin Marietta Corporation.

Recently, I looked at most of the major military systems developed over the last 50 years and plotted the ratio of planning time-to-execution time against year that full-scale development was initiated. A gradual upward trend in the 1950s and 1960s really began to take off beginning in the 1970s to the point where, now, we take nearly as long to plan and sell programs as we do to execute them.

Look at Space Station and how long the planning process has taken to move it through the administration and the congressional budget process. Keeping a program sold is also a challenge and, the longer the program stretches out, the harder it is.

I'm not even going to hazard a guess on what the planning-to-execution time for a mission to Mars will be. Special care will have to be taken in laying that program out to have a series of major accomplishments always before the public to hold their interest.

I am disturbed by the committee approach to overseeing our space program. The National Space Council can be an effective deliberative body for sorting out national priorities, building political consensus, advising the President, and cutting through the Washington bureaucracy. But, if it tries to sort out the best approach to the space exploration program and reserves too many decisions for itself instead of turning the details over to NASA, then I have a problem. We have a civil space agency—the same one that took us to the Moon 20 years ago. It's time to give NASA the total responsibility and the authority to take us back.

Let me turn now to the future. Engineers and scientists, particularly you students in the audience, will be the ones going back to the Moon and to Mars and you will be helping to lead us back to being a productive nation, strong economically, and secure militarily. Only engineering can lead us back—not MBAs, not lawyers, not the service occupations. Engineers are the doers, and design engineering is where it's at, as they say.

We will go back to the Moon to stay and to Mars. Robotics will continue to provide us with a surrogate presence in the universe. New military systems will have smart sensors in things that fly, swim, and drive, that allow us to project military force anywhere in the world. While we will not be in full-rate production on as many new systems because of the DOD budget decline, we will still upgrade existing systems. We can expect increased design activity through R&D and pre-production prototypes. And, when technical breakthroughs occur, we will take those systems to production to keep our defense modern and provide a credible deterrence. There will also be more emphasis on simulation, before, and in lieu of, bending metal. We will become more dependent on advances in communication and intelligent systems that give us information when we need it, where we need it, and in the form we need it.

Of course these will be challenging times. But again, speaking to the students in the audience, don't be discouraged by change. It is exciting and you will affect the course of that change.

When Alan Shepard blasted off on the first U.S. manned space mission, I was in high school and decided right then that I would be part of the space adventure. Ten years later, after collecting a few degrees, I was a green-behind-the-ears research engineer at Lewis. I no sooner reported to work than the notice of layoffs hit—it was in the post-Vietnam build-down in defense and this looked like it might be a bummer of a profession to be in. But just the opposite has been true. It has been, for me, the most rewarding and exciting career one could imagine. We go through these cycles, but the engineering profession rides them out, and the long-term trend is always the same—we need more good engineers.

I went into aerospace engineering and the space program because I wanted to be part of an enterprise that inspires the human spirit. I am glad to see so many of you are motivated by the same interest. Looking over the design projects on display, I'd say the future is in pretty good hands. Thank you and best of luck to all of you.

—Raymond S. Colladay
Vice President, Research and Development
Martin Marietta Corporation

Space Projects



21-27
f. 8³

FLUID PHASE SEPARATION (FPS) EXPERIMENT FOR FLIGHT ON THE SHUTTLE IN A GET AWAY SPECIAL (GAS) CANISTER:

DESIGN AND FABRICATION

N91-18122

THE UNIVERSITY OF ALABAMA, HUNTSVILLE

The separation of fluid phases in microgravity environments is of importance to environmental control and life support systems (ECLSS) and materials processing in space. A successful fluid phase separation experiment will demonstrate a proof of concept for the separation technique and add to the knowledge base of material behavior. The phase separation experiment will contain a premixed fluid that will be exposed to a microgravity environment. After the phase separation of the compound has occurred, small samples of each of the species will be taken for analysis on Earth. By correlating the time of separation and the temperature history of the fluid, it will be possible to characterize the process. The phase separation experiment is totally self-contained, with three levels of containment on all fluids, and provides all necessary electrical power and control. The controller regulates the temperature of the fluid and controls data logging and sampling. An astronaut-activated switch will initiate the experiment and an unmaskable interrupt is provided for shutdown. The experiment has been integrated into space available on a manifested Get Away Special (GAS) experiment, CONCAP 2, part of the Consortium for Materials Complex Autonomous Payload (CAP) Program, scheduled for STS 42 in April 1991. This document presents the design and the production of a fluid phase separation experiment for rapid implementation at low cost.

INTRODUCTION

The separation of fluid phases in microgravity is of interest for materials processing and long-duration life support systems in space. On Earth, phase separation occurs due to buoyancy, but this is not the case in the microgravity environment of space. Therefore, materials processing relying on the phase separation of liquid mixtures will not occur in the same way as on Earth. This difference could be used to advantage to develop new materials not presently available on Earth.

Fluid phase separation has direct application to current research concerning new metal alloys produced in microgravity. To optimize the processing method for the alloys, the relationships between the different phases of the metal must be known (i.e., a phase diagram). Microgravity alters the phase diagram. To construct a new phase diagram, the molten metal needs to be analyzed while in space. It has been proposed that a simpler method could use special fluid mixtures to model the molten metals. This has the advantage that the transition temperature of phase separation for most fluids is significantly lower than that of molten metals, so it will be easier to study the fluids in the laboratory and then correlate the data to the metals. The result will be a new space-based phase diagram that can be used to develop stronger, lighter-weight metals.

Another possible application concerns spacecraft thermal control systems. The heat from components, experiments, and people must be dissipated from the spacecraft environment. Present technology utilizes pumped liquid thermal transport systems for heat exchange. The heat dissipation is controlled by the mass flow rate of the system, which is determined by

the size of the pump. Large heat dissipation requires large pumps that use a prohibitively large amount of electrical power and add significantly to the weight of the spacecraft. A specialized two-phase (liquid-to-liquid) thermal transport system could be more efficient in accomplishing this task. Therefore, understanding the liquid-liquid phase separation process in space could aid in the design of closed environments, such as the Space Station and the Mars mission.

A detailed understanding of the separation process is essential to the application of the fluid phase separation technology. Preliminary research concerning potential fluid mixtures and their behavior in space is underway. However, the fluid phase separation process is a complex interaction between temperature and microgravity that is not possible to duplicate in an earthbound laboratory. An experiment is needed that will characterize the separation process in space and demonstrate a proof of concept for the fluid phase separation technique. Since this is a high priority project, it would be advantageous to fly the experiment as soon as possible. At the University of Alabama in Huntsville, a fluid phase separation experiment has been designed that satisfies all these requirements.

The experiment will record a complete temperature history of the fluids, along with samples of component species to be analyzed on Earth. The phase separation experiment is totally self-contained, with multiple containment levels for all fluids, and provides all necessary electrical power and control. Furthermore, the fluid phase separation experiment has a

unique opportunity to take advantage of space available on a manifested Get Away Special (GAS) Canister, CONCAP 2, which is scheduled for STS 42 in April 1991.

This document presents a summary of the design for the Fluid Phase Separation (FPS) experiment. It includes the description of the process, design of systems, and outline of a construction program.

EXPERIMENTAL PROCESS

A mixture of succinonitrile and cyclohexane is of particular interest. Succinonitrile is a solid at 20°C (room temperature) and has a vaporization temperature of 85°C. This material is highly reactive with most metals except for gold and stainless steel. Plastics and rubber are also reactive, but teflon is not. Cyclohexane is a liquid at room temperature and has a vaporization temperature above 120°C. It is an organic solvent that will dissolve most adhesives. All the materials used to contain and support the fluids must be carefully selected so as not to interact with the liquids to produce erroneous results or jeopardize the safety of the experiment.

The experiment is a mixture of two fluids that are dormant both before and during launch. The mixture will not need to be heated prior to the experiment start-up since the mixture will contract uniformly upon freezing. Just prior to the second sleep period, during a time of low activity, each of the fluid samples will be heated to a predetermined temperature (less than 90°C) and allowed to stabilize at that temperature for four to six hours. The controller will signal the heaters to shut down and the system will begin to cool. When the fluid reaches the transition temperature (a function of composition, density, and initial temperature), the phase separation will then begin, accompanied by a release of heat. This will cause the

fluid temperature to temporarily stabilize. As phase separation continues, the fluid temperature will once again begin to fall and the sampling mechanism will be activated. The temperature of the fluid will be stabilized and maintained constant, permitting small samples of each of the species to be taken for analysis on Earth. By correlating the time of separation and the temperature history of the fluid, it will be possible to characterize the process. After the sampling is complete, the experiment will be deactivated for the duration of the space shuttle mission.

On Earth, differences in density typically drive the separation process. In microgravity, minimal surface energy will be controlling the separation. It is anticipated that this will produce two spherically shaped volumes containing the different component species. One component will be collected at the center of the fluid container, while the other will be wrapped around the first, positioned at the edge of the container. The fluid phase separation experiment will be used to characterize this process.

DESIGN SUMMARY

The fluid phase separation experiment has a total weight of 11.8 lb and a volume of 1105 in³, which is within the initial payload constraints imposed by CONCAP 2. This value includes six fluid containers and the support apparatus, the controller, and power supply. The overall dimensions are 14.5 in (width) × 8.5 in (height) × 9.75 in (depth from the mounting plate). Volume of an individual fluid sample is 0.22 in³ and the complete assembly is 0.8 lb. The GAS canister is shown in Fig. 1 with the relative placement of the components within the GAS Can.

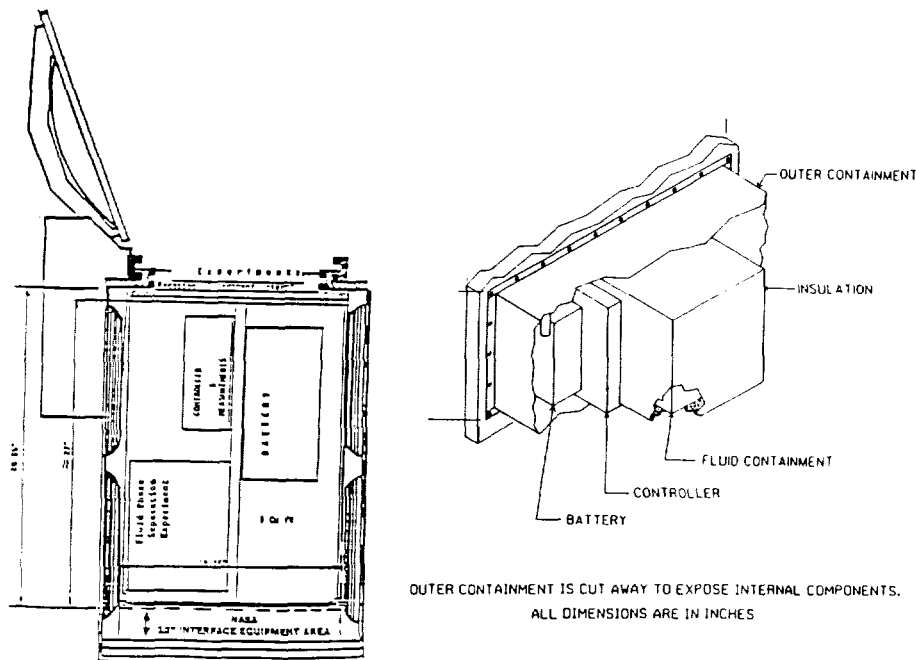


Fig. 1. GAS Canister and Fluid Phase Experiment

ORIGINAL PAGE IS
OF POOR QUALITY

STRUCTURAL SYSTEM

The structure will support the experiment and isolate the fluid phase separation experiment from the rest of the GAS Can. The whole experiment will be contained within this shell and will allow the liquid containers and sampling mechanism to be attached to the GAS Can mounting plate.

Several ideas for the shape of the outer shell were considered. The criteria used to evaluate the proposed shape included size of the enclosed volume, minimization of the weight, ease of fabrication, and structural stability. The dimensions of the GAS canister and the allocated space provided by CONCAP 2 set the maximum dimensions. The experiment was to be located in the bottom, on one side of the canister, and have a height of no more than 10 in. Later, the height was further reduced to 8.5 in due to a change in the primary experiment, CONCAP 2.

It was decided that the volume occupied by the fluid phase experiment should be large enough to fully contain six fluid sample containers, a controller, and a battery. Since the experiment had to be completely isolated from the other experiments in the GAS canister, there needed to be a minimum of seams and joints in the outer shell. To maximize structural stability, the shell needed to be self-supporting.

The semicylinder was chosen as the best shape for the outer shell (Fig. 2). The shell will have a length of 14.5 in, a height of 8.5 in, and a depth (measured out from the mounting plate) of 9.25 in. The shell will be formed from 0.031-in, type-304 stainless steel sheet, which is inert to the chemicals used for the fluids. By using thin steel, we can maintain the high strength and minimize the weight. The 304 stainless steel is easy to form and can be welded to increase the strength of the shell and provide containment.

To reduce the weight, there is no backplane on the shell. The containment is maintained by covering the GAS Can mounting plate with a continuous 3-mm-thick teflon sheet. A 0.125-in-thick teflon O-ring gasket is placed between the outer shell and the mounting plate to absorb the displacements induced by thermal and mechanical loads. This will maintain a tight seal and prevent contamination of the other experiments in the GAS Can.

The shell is held to the mounting plate by 22 #10-24 grade 8 socket head bolts with 0.5-in washers. The bolt material is A-286 corrosion-resistant steel with an allowable stress of 20 Ksi. The bolts are spaced at 2 in centers around the 0.75-in flange on the outer shell. Although 22 bolts are not needed to support the outer shell, they are needed to maintain an adequate distributed pressure between the teflon gasket and the mounting plate to ensure a tight seal under launch loads. This bolt configuration produces a worst-case maximum bolt stress of 3000 psi, for a factor of safety of 6, under a 10-g load applied during the launch. The outer shell experiences a maximum stress of 400 psi at launch, which is well below the yield stress of the stainless steel and should prevent even a fatigue failure of the outer shell.

The shell will be penetrated at three points. A D-type electrical connector is located on the bottom of the shell to connect with control cables from the shuttle (located at the

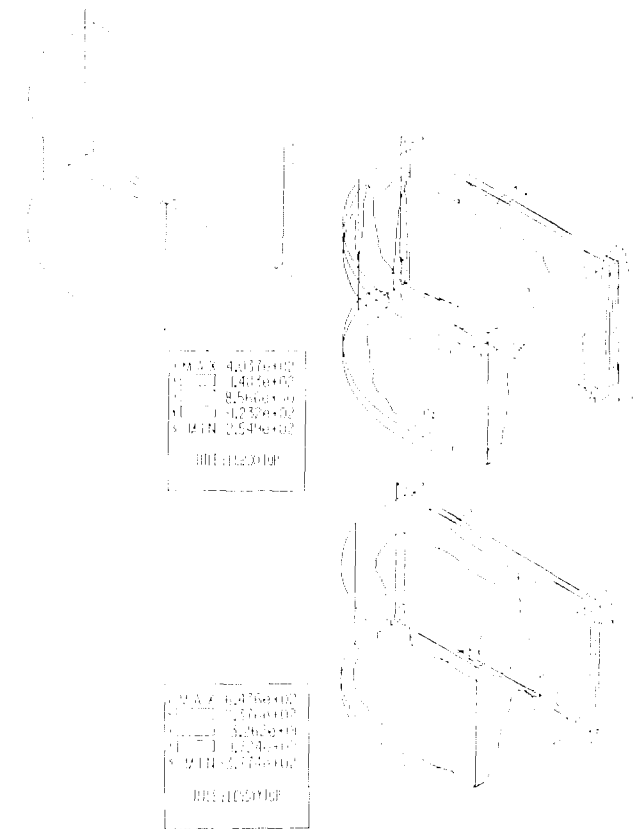


Fig. 2. Outer Shell and Loading Stresses

bottom of the GAS Can). The connector will have gold-plated pins and a teflon gasket on the interior to prevent corrosion and contamination of the GAS Can. The other two openings are covered with 7- μ m teflon filters in a 304 stainless steel housing. The filters are 25 mm in diameter and have a maximum pressure of 100 psi at the inlet, with an allowable pressure difference of 50 psi. This will permit the purging of the fluid phase separation experiment with nitrogen prior to launch. Also, these two ports will permit rapid dissipation of the interior pressure while maintaining containment of the fluid in the event that the GAS Can is depressurized while in space. If this were to occur, the fluid would sublime to a solid and be trapped by the filter while the nitrogen gas could escape, preventing a rupture of the outer shell.

An analysis of displacements showed that deflections of the large diaphragm-like surfaces were acceptable, but a dynamic analysis showed that the fundamental frequency of vibration was too low. To improve the dynamic response of the outer shell, triangular ribs were added to the top, bottom, and side of the shell. These ribs broke up the area that could freely oscillate, and stiffened the surfaces to out-of-plane motion.

FLUID SAMPLING AND SPECIMEN RETRIEVAL SYSTEM

Within the outer shell is the fluid phase separation experiment. The experimental apparatus is composed of three subsystems: the fluid containers, the sampling mechanism, and

**ORIGINAL PAGE IS
OF POOR QUALITY**

the structural frame (inner shell). Size and weight restrictions determined the maximum number of fluid sampling systems to six.

Many materials were considered for the fluid containers. Due to the unusual corrosive nature of the fluids, stainless steel, gold, and teflon were the only materials that were chemically suitable. A material with a low specific gravity was desired to minimize weight. Furthermore, uniform thermal conductivity was necessary to transfer heat from the external heaters into the fluid. Since the external heaters are to be positioned on the outside of the container, it is essential that the material have a high melting point. Finally, a high tensile strength will be needed to withstand the expected loads during the shuttle flight. All these criteria are met by teflon.

The teflon was machined into the desired geometrical shape. A 0.75-in-diameter spherical fluid cavity is inside a truncated cone with a nominal wall thickness of 0.25 in. A flat octahedron plate passes through the sphere/cone dividing it in two halves. Assembly of the fluid containers is accomplished using a ferrule-type joint for alignment with six bolts to ensure an adequate seal. This will also provide the first level of containment for the fluid. The orientation of the fluid containers is shown in Fig. 3.

Although a spherical shape both inside and out would be optimal for heat flow considerations, the exterior sphere is difficult to produce. Therefore, a cone was used since it can be easily machined and still provides a minimum of exposed surface to conduct and radiate heat away from the fluid. The shape will produce an even heat flow through the teflon container and into the fluid sphere.

Provisions had to be made to fill the spherical cavity of each sample container after assembly. This problem was remedied by designing a special fill port that included a stainless steel tube press fit into the fluid container and sealed at the outside with a removable teflon plug. This permits overfilling of the spherical cavity so that no air pockets are present within the sphere.

The teflon container has a maximum tensile strength of 3000 psi, which is strong enough to withstand the increase in internal pressure created by partial vaporization of the fluid

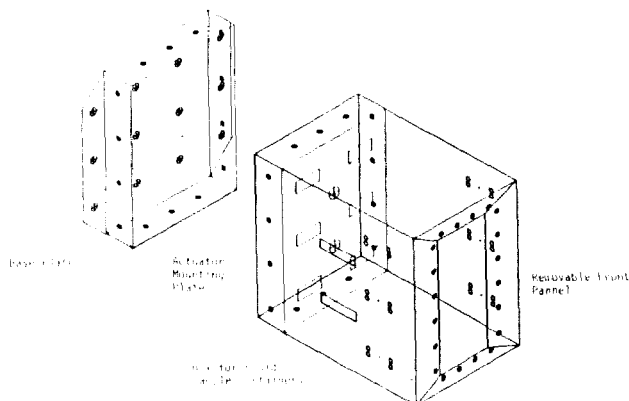


Fig. 3. Inner Shell Showing Two Parts and Mounting Plate

within the cavity (an internal pressure of 100 psi). However, the controller should terminate the heating of the fluid before this pressure is reached.

Surrounding the fluid containers is the inner stainless steel shell, which provides the structural support and acts as the second level of containment. The housing will be fabricated from the same material as the outer shell discussed earlier and will also have welded seams. The fluid containers will be mounted within this housing but separated from the stainless steel shell by an insulating phenolic pad to minimize heat transfer away from the fluid spheres. Each of the fluid containers is attached to the inner shell by four #5-40 socket head screws threaded 0.375 in into the teflon. Under the worst loading case at the time of launch, the maximum load (including the preload) is 84 lb per screw. This gives a safety factor of 9 with respect to tear-out, bearing, and shear stresses.

The inner shell is constructed in two parts. A base plate mounts the shell to the GAS cannister with 12 #10-24 grade 8 socket head screws. The A-286 corrosion-resistant steel used in the screws has a 20-Ksi allowable tensile stress, which is four times greater than the maximum stress of 5000 psi that occurs at launch. The base plate has four flanges that are normal to the surface of the plate for attachment of the box containing the fluid spheres.

The box has four sides (open front and back), and is made slightly larger than the tabs of the base plate. The box is then bolted to the tabs on the base plate. Stainless steel nuts were spot welded to the base plate to accept the twelve #5-40 A-286 steel socket head screws. This was done to permit easier assembly of the experiment by allowing access to the front and back of the fluid spheres. To seal the box onto the base plate, a teflon O-ring gasket fits inside the tabs. To completely seal the box, the front panel is attached using twelve #5-40 A-286 steel socket head screws and a teflon O-ring gasket. As before, stainless steel nuts are welded onto the inside edge of the box to accept the screws. This panel permits access to the spheres to fill them prior to launch.

The whole structure of the inner box has a maximum stress of 900 psi, which is well below the yield stress of the stainless steel, and should prevent failure of the inner shell. To stiffen the inner shell and to provide a rigid plate upon which to mount the rotary actuators, a stainless steel plate is welded across the interior of the box. Once all the components are in place, selected areas inside the box are filled with expanded polystyrene foam, which helps to dampen vibration and provides thermal insulation.

The sampling mechanism is composed of two tubes fitted one inside the other (Fig. 4). The exterior tube is rigidly mounted across the inside of the fluid sphere. It has two holes in the wall of the tube positioned such that one is at the center and the other is near the edge. A rotary actuator will rotate the inner tube to align the inner two holes with the outer two and permit diffusion of the fluid species into the inner tube. After sampling is completed, the inner tube will be rotated in a reverse direction to seal the samples within the innermost tube.

The exterior tube is limited to a diameter of approximately 0.050 in to limit the effects of wetting along the tube, which

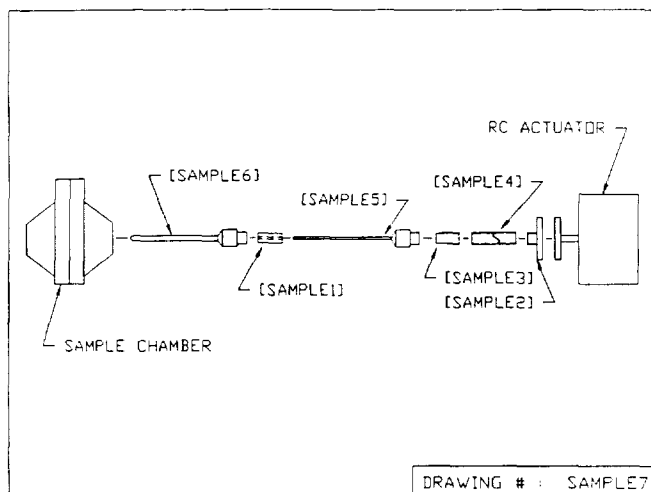


Fig. 4. Fluid Container Assembly

would destroy the concentric sphericity of the two fluids as they separate. To prevent this, the tube has two small disks or fins on it to keep the one fluid from wetting along the whole length of the tube. This will ensure that each component species is sampled.

In order to provide rigidity, precision, and to simplify the design and construction, the sampling tubes are made from stainless steel spinal needles, which are modified as needed. The ends of the needles are closed by a quick touch with a TIG welder. The rotary actuators have a maximum 40° rotation, which limits the size of the holes in the tubes to a diameter of 0.013 in. To make sure that the holes on both tubes are aligned and free of jagged edges that would disrupt the fluid flow into the tube, both holes are simultaneously cut with a file and then the tubes are dipped in nitric acid to remove burrs.

An interference or press fit is used wherever a teflon to stainless steel seal occurs. The outer tube pierces the sampling chamber; the rotary seal between the inner and outer tubes, and the plug in the inner tube are all examples of an interference fit. Adequate pressure is maintained at the seal up to 130°C. This allows for the difference in the thermal expansions of the two materials.

ENVIRONMENTAL CONTROL SYSTEM

The fluid phase separation requires careful control of the fluid temperature during the experiment. Conductive and radiative heat flow will account for the heat transfer within the GAS Can. The design of the environmental control system must compensate for the rapidly changing temperatures of the GAS Can environment while providing enough heat to raise the fluid temperature above the transition temperature so that phase separation can occur.

The problem is not one of steady-state conduction but of time-varying conduction. The orbit (sunlight to darkness every 45 min), periodic turning within orbit, and the attitude of shuttle within orbit (Earth or space viewing) will influence

the ambient GAS Can environment. The environment may vary from -100° to 20°C. Therefore, the design of the heaters and the insulation must consider the rate at which heat will be lost from the fluid so that the cooling time is long enough. Likewise, the cooling period must not be too long or the experiment may not be completed within the allotted time.

Initial calculations modeled a fluid heated to 90°C and cooled to 20°C that is surrounded by a cold environment. The fluid is a sphere, at a uniform temperature, which is suddenly immersed in a colder fluid. Surrounding the fluid is a low-density, high-heat-capacity polystyrene insulative layer. As the thickness of the insulation layer increases, the cooling time increases. However, if the ambient environment is too warm, the cooling time becomes prohibitively long. This means that the insulation layer must be designed for the warmer environment and supplemental heating used to stretch the cooling time in colder environments.

A more detailed model was obtained using SINDA (Systems Improved Numerical Differencing Analyzer). This computer program is well-suited to solving lumped parameter representations of physical problems. The model represents the heat flow paths as a conductor/capacitor network.

The experiment components were first broken into smaller elements and assigned a nodal number. The volume and capacitance of each node was calculated. The nodes are then linked to reflect conductive and radiation heat flow paths between all the possible nodes. The final aspect is to assign boundary nodes to represent the properties of space around the GAS canister. This computer model is then converted into executable Fortran code, and run for a predetermined amount of time or until steady state is reached. The end result is a complete temperature history of each node as it cools and/or warms. The temperatures of the fluid were of interest in the cooling phase, and they were dependent upon the temperature chosen for the heat sink (space node). From these tests, the heaters and the layer of insulation were sized and are shown in Fig. 5.

A polystyrene layer, with nominal thickness of 1 in, will be affixed to the exterior of the fluid container housing. Additional insulation can be added within the cylindrical aluminum container and inside the fluid container housing to shield individual fluid containers from the other containers. This will allow customization of individual fluid samples without affecting the overall performance of the experiment.

Sensors will constantly monitor the temperature of the fluid and activate the heaters to keep the liquid from freezing. In orbit, the expected equilibrium GAS Can temperatures are -100°C during space viewing and -10°C during Earth viewing. Due to occasional rotating of the shuttle, the sun may heat the outside of the GAS Can, which may cause the temperature within the GAS Can to rise to 20°C. Although the effects of the extreme cold can be minimized with heaters and insulation, the warming of the GAS Can will be a problem. There is no adequate means at our disposal to cool the experiment if it should get too warm. Because of this, the thermal heating design was determined for the worst-case temperatures of -100°C and it is assumed that the insulation provided will prevent the experiment from warming too much.

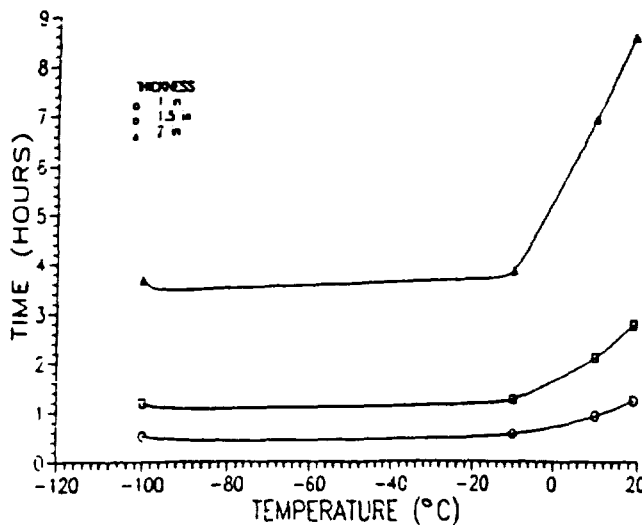


Fig. 5. Thermal Analysis of Cooling Time

Once the experiment begins, the fluid will be heated to a maximum temperature of 90°C over a 1-hr period and then maintained at that temperature for 5 hr. This will require 81 mW/hr or 486 mW total. The fluid will also need to be cooled slowly, so intermittent heating may be required during cooling. Once sampling of the two fluid components begins, the fluid temperature will be stabilized for an additional hour. This heating load is used to determine the size and number of heaters required.

The heat flow for a single fluid container is 81 mW/hr over a 6-hr period. Because there is some thermal lag in transferring the load, and the heaters should not be in continuous operation, the heaters had to have a greater output than the heating load required. It was determined that the heaters should operate only one-third of the time, which requires 243 mW/hr. With six heaters chosen, the output from a single heater must be 40.5 mW/hr. Given that the voltage available from the battery is 6 V, the resistance of an individual heater was calculated to be 0.88 ohms. These requirements can be met by Thermofoil heaters, each having a diameter of 0.5 in, with an effective area of 0.15 sq in.

For control and safety, each heater will have a resistance thermometer laminated within it. The resistance thermometers (RTDs) increase resistance with temperature, and are considered to be accurate and stable sensing devices. The RTD chosen will have either platinum, nickel, copper, or nickel-iron elements.

Temperature sensors will also be needed to monitor the temperature of the sample, as well as the temperature of the battery. They must have an output range from 0-10 V. For the sphere, it will be necessary to have a coated sensor that will resist any type of reaction with the fluid. It must have a temperature range at least from -50° to 150°C. A teflon-coated thermocouple with a length of 0.05 in and a time constant of 1 sec has been selected.

CONTROLLER

The controller executes three primary functions. Function one provides active temperature control of six fluid samples during the experiment cycle. In addition, the temperature of the experiment battery pack will be regulated to maintain optimum battery output throughout the experiment cycle. Function two is the independent timing and control of each of the sample actuators once the phase transition is reached. Function three is the data logging in nonvolatile memory of experiment temperatures for the duration of the experiment's operation. Finally, the controller will monitor safety and control power for the experiment.

The control and data logging requirements for the Fluid Phase Separation Experiment are relatively simple. The requirements fall into four categories. These categories constitute the logical division of work for the controller.

Category one is data storage. The nonvolatile electrically erasable and programmable memory (EEPROM) requirements are driven by the number of temperatures stored multiplied by the sample rate, multiplied by the experiment total operating time. A three-day experiment cycle time will generate 30,240 bytes that need to be stored.

Category two is active temperature control. The active control for temperature requires 13 separate temperature inputs, 2 each from each of the 6 fluid specimens plus 1 from the battery. In addition, there are seven temperature control outputs, one for each of the six experiments plus one output for the battery.

Category three is the control of the experiment actuators. There are six one-bit control outputs for the actuation of the experiment sample mechanisms. The timing for the sample mechanisms will be controlled by the temperature inputs from the experiments themselves. A minimum time delay between sample actuation will be used to prevent overloading of the batteries.

Category four covers the general control requirements. This includes the input from the GCD switch actuated by an astronaut to begin and end the experiment. If there is an indication that the battery charge is low (voltage is less than 4.75 V for an extended period), a nonmaskable interrupt will be sent to the controller to shut itself off. This is done for safety since this is the minimum reliable operating voltage for TTL digital logic. Also, a software timer will be monitored by the processor to indicate that the controller is operating the experiment properly. If the experiment does not seem to be progressing (the fluid is not cooling, etc.), another nonmaskable interrupt will be sent to shut off that portion of the experiment. Furthermore, if any of the heaters should fail in the "on" position, the controller would turn itself off to prevent thermal runaway.

To permit speed in construction and ensure certification for flight, the controller will be a modification of NSC 800 controller from the GAS Explorer Program. To test the logical sections and permit integration of the experiment and controller, simulated mission tests will be performed at the University of Alabama in Huntsville.

POWER SUPPLY

A power supply is needed to provide power to various systems in the experiment: sample actuators, fluid heaters, battery heater, data acquisition and storage, and the experiment controller. Collectively, these systems require 3.2 amphotours for a 60-hr experiment duration. A 6-V, 5-amphour Gates lead-acid monobloc battery, 5.47 in long, 2.11 in wide, and 3.02 in high will provide the necessary electrical power. The battery weighs 2.43 lb, is self-contained in a flame-retardant material and is flight qualified.

SAFETY

Safety has been of primary concern throughout the design process for the experiment. The potential hazards concerning possible collision, corrosion, explosion, and fire were identified. Each was carefully examined and a detailed description of the hazard, hazard causes, and hazard controls are presented. All the safety requirements are referenced from NSTS 1700.7B, "Safety Policy and Requirements for Payloads Using the Space Transportation System." See Fig. 6 for a condensed description of identified hazards and means to deal with them.

Collision is of paramount concern for any experiment on board the space shuttle. Because of structural failure, damage could occur to surrounding experiments or to the shuttle itself. The result could be a loss of control or even the ability

of the shuttle to stay in orbit. The ultimate hazard would be penetration of the crew compartment, placing the safety of the astronauts in jeopardy. To prevent these hazards from occurring, a factor of safety of 1.4 was applied to all structural design. Furthermore, close inspection of all assemblies for quality of materials and workmanship will reduce the potential for material failure. The applicable NASA safety requirements concerning collision (206, 208.1, 208.2, and 208.3) have been met.

Damage of the fluid containment vessels caused by sudden expansion of the sample fluid, collision, or a fire could result in the release of some corrosive material. If the fluid comes in contact with metal, the reaction may weaken the metal and cause the component to fail. To prevent this hazard, the experiment is self-contained with three levels of containment surrounding the experimental fluid. This containment will protect the surrounding experiments by minimizing the spread of shrapnel and corrosive material if a structural failure occurs. These measures fulfill the safety regulations concerning corrosion (206 and 209.1).

Overheating of the battery due to heater runaway, polarity reversal, or short circuit could cause the battery to explode. The battery explosion could spread corrosive material and shrapnel throughout the GAS Can. This is prevented by using a sealed, flight-qualified battery along with a bus board to prevent short circuits. Finally, a pure nitrogen environment around the experiment will deprive a fire of the oxygen necessary to burn. Nonflammable elements will be used near

GAS PAYLOAD SAFETY MATRIX										
PAYLOAD	PAYLOAD ORGANIZATION								DATE	PAGE
G - CONCAP 2-Fluid Phase									4 DEC 89	
HAZARD GROUP	COLLISION	CONTAMINATION	CORROSION	ELECTRICAL	SHOCK	EXPLOSION	FIRE	TEMPERATURE EXTREMES	RADIATION	
BIOLOGICAL										
RADIATION										
STRUCTURES	X									
ELECTRICAL						X	X			
ENVIRONMENTAL CONTROL										
HUMAN FACTORS										
HYDRAULICS										
MATERIALS			X							
MECHANICAL										
OPTICAL										
PRESSURE SYSTEMS										
PIROTECHNICS										

GAS HAZARD LIST		
PAYLOAD	SUBSYSTEM	DATE
CONCAP 2-Fluid Phase Sep. Exp.	MULTIPLE, AS LISTED	4 DEC 89
HAZARD GROUP	HAZARD TITLE	APPLICABLE SAFETY REQUIREMENT
COLLISION G- F1	STRUCTURES, MECHANICAL Failure of support structures.	NSTS 1700.7B 206-208.1 208.2-208.3
CONTAMINATION CORROSION G- F2	MATERIALS Release of contaminating or corrosive materials	206-209.1
EXPLOSION G- F3	ELECTRICAL Rupture of Battery	206-213.2
FIRE, TEMPERATURE EXTREMES G- F4	ELECTRICAL Thermal Runaway	206-213.1 213.2

Fig. 6. NASA Safety Regulations and Identified Hazards

ORIGINAL PAGE IS OF POOR QUALITY

connections and all wiring and heaters will be properly inspected. The design is in line with the NASA safety regulations for explosion and fire (206, 213.1, and 213.2).

PROJECT MANAGEMENT

The design has emphasized the use of prefabricated components whenever possible to quicken the procurement and assembly of the experiment. The delivery of the battery will be set for August so that the battery is not over six months old at the time of launch. The acquisition of the controller is paramount to assembly of the experiment. Adequate time is needed to modify and test the controller.

The project was designed and assembled by engineering students at the University of Alabama in Huntsville. The fall 1989 Senior Student Design class (ME 465) was the nucleus of the design team. The students were responsible for generating all the necessary design documentation. They will also serve as the transition to the construction phase of the experiment. Construction has begun, with anticipated completion by August 1990. The current work is done by students enrolled in a "Special Topics Class: Advanced Space Systems Design."

The planned schedule for the construction of the fluid phase separation experiment is a fast-paced program to permit complete integration of the experiment into CONCAP 2. The development of the phase separation experiment must meet the existing time schedule for CONCAP 2. In the event that the phase separation experiment fails to meet any of the established requirements, it will be divorced from the CONCAP 2 project.

Figure 7 shows the revised time schedule for the phase separation experiment. It is anticipated that CONCAP 2 will fly on the GAS Bridge on STS 42, scheduled for April 1990.

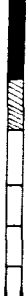
- 
- Optimized design for the FPS Experiment (began preliminary design September, 1989 and finished design May, 1990)
 - Use fast track method for fabrication of flight hardware (anticipate completion by July, 1990)
 - Begin testing and qualifying, summer of 1990
 - Integration of experiment into GAS can by September, 1990
 - Delivery to NASA in November, 1990
 - Fly on STS-42 in April, 1991

Fig. 7. Time Schedule for Project

CONCLUSION

The fluid phase separation experiment will characterize the liquid-liquid phase separation process in a microgravity environment. The experiment allows six samples of fluid to be monitored for three days while in orbit. The system will record temperature data and obtain samples of the component species for analysis on Earth. The data will be analyzed to produce a phase relationship or phase diagram for the fluid mixture. Ultimately, it will add to the knowledge base of material processing and provide information for the design of long-duration life support systems.

The current status of the project is that construction and assembly are underway. It is anticipated that the experiment will be ready for integration into CONCAP 2 by July, and therefore has an excellent chance of flying onboard the shuttle in April 1990.

AUTONOMOUS SPACE PROCESSOR FOR ORBITAL DEBRIS

UNIVERSITY OF ARIZONA

This work continues to develop advanced designs toward the ultimate goal of a GETAWAY special to demonstrate economical removal of orbital debris using local resources in orbit. The fundamental technical feasibility was demonstrated in 1988 through theoretical calculations, quantitative computer animation, a solar focal point cutter, a robotic arm design, and a subscale model. Last year improvements were made to the solar cutter and the robotic arm. Also performed last year was a mission analysis that showed the feasibility of retrieving at least four large (>1500-kg) pieces of debris. Advances made during this reporting period are the incorporation of digital control with the existing placement arm, the development of a new robotic manipulator arm, and the study of debris spin attenuation. These advances are discussed here.

INTRODUCTION

We can hardly improve upon the lucid descriptions of the orbital debris issue by science writers⁽¹⁻⁴⁾ and other popular news media coverage⁽⁵⁻⁹⁾. Without doubt, the problems of orbital debris have grown to be of serious concern to astronomers, space technologists, and to terrestrial dwellers. The specific problems were presented at the 39th IAF Congress. The University of Arizona Space Engineering Design team is developing the design for economical removal of the larger debris pieces through local resource utilization. The fundamental idea is to concentrate solar energy into a point focus, cut the debris into precise shapes that can be added on to the "sweeper" craft, and robotically assemble the pieces into a manageable configuration. This is followed by one of three disposal modes: (1) retrieval by a spacecraft (STS, HERMES, BURAN, etc.), (2) precise ocean splashdown, or (3) planned burnup upon atmospheric reentry. The fundamental space technologies to be demonstrated are solar cutting of candidate space debris materials, robotic assembly, and accurate disposal. In 1988 the University of Arizona began participation in the USRA program and demonstrated solar cutting and a subscale model robotic arm. In 1989, a full-scale robotic arm with manual controls was developed and the solar cutter/robotic arm assembly was shown to be technically feasible. Also in 1989, a mission analysis was performed in which the large debris environment was identified and a four-debris retrieval sample mission analysis showed the propellant requirements to be well within reason. This year, 1990, the existing robotic arm was converted to digital control using an IBM PC, a second robotic arm was developed for precise pick and place operations, and the problem of debris tumbling was addressed and various detumbling methods were investigated. This report is a summary of the work and explains the details of space engineering.

Consistent with the USRA philosophy, new undergraduate students were involved in the design process. This year, 11 new students were involved in the Autonomous Space Processor for Orbital Debris (ASPOD) design. The project continues to draw worldwide attention including correspondence with elementary and high schools.

DEBRIS SPIN ATTENUATION

The purpose of this project was to research and recommend methods of attenuating the rotational spin of orbital debris so that an ASPOD satellite can safely grasp them for retrieval. To avoid possible damage to the ASPOD craft, only passive means of attenuation were investigated. The use of passive means is defined as the use of methods of attenuation that do not involve ASPOD in direct contact with space debris, thereby endangering it. Some of the design criteria and target specifications are (1) attenuate the rotation of an object spinning about one axis; (2) attenuate the rotation of an object having a mass of up to 2000 kg and rotating with rotational speeds of up to 50 rpm; (3) attenuate the rotation of an object up to 7 m in diameter and up to 7 m in height; (4) use a minimal amount of energy; (5) attenuate at least four objects per mission; (6) require no maintenance; (7) must not interfere with the normal operation of other functional satellites; (8) must not create more debris; (9) must weigh less than about 500 lb; and (10) must have a reasonable expense relative to the space industry.

Satellites and most other space debris generally contain a certain amount of rotational energy. The problem of dealing with the rotation of a large, nonsymmetric object containing a lot of mass orbiting the Earth must be solved before the satellites can be safely and effectively collected.

A workable solution dealing with debris capture must allow the rotational energy of the debris to be contained or dissipated without transferring it to the collector satellite. The space debris that is proposed for collection is often very massive, 2000 kg or more, with spin rates of up to 50 rpm. These figures suggest that there can be quite a bit of angular momentum involved.

SOLUTIONS

As a first step, various attenuation methods were researched and evaluated. Of all the methods investigated, four were chosen as possible solutions and merited further analysis. Each of these four solutions uses a different physical principle (for example, conservation of angular momentum or conservation

of energy) to accomplish the attenuation of the satellite. Although each of the four designs merits further investigation, for the present the most promising of the four was singled out for detailed analysis and testing.

Reeled weight mechanism. The physical principle used in this method is to translate the rotational energy into linear kinetic energy, then into potential energy. This design uses a reeled cable capable of attaching itself to the debris by the cable's free end. Also contained in the reel mechanism is a generator allowing the cable to reel out, turning permanent magnets around a stationary armature and storing that energy in a battery. This generator can then act as a motor by turning the stored energy in shaft power, allowing the cable to be reeled in. Once the free end of the cable is attached to the debris in its plane of rotation, the reel is then allowed to freely move away from the debris due to centrifugal acceleration, yet is still tethered by the cable. The reel will move away in a straight path while the debris continues to spin, and the attachment point of the cable on the debris will rotate with the debris, wrapping a portion of the cable around the debris. At this time the reel will create a drag force on the cable by engaging the generator and then storing that energy. Due to the centripetal force of the reel attached to the much more massive piece of debris, the reel will attempt to move into a radial position about the debris' center of mass. Before it comes near this point some of the stored energy will be used to reel the reel mechanism back into the debris, at which point the process will start over. Some of the advantages to this system are the ease of attachment to essentially any shape of debris and the relative simplicity of the mechanism. Some of the problems are the difficulty in analysis and testing of the system and the chance of the cable becoming permanently entangled in protrusions on the debris.

Coiled spring mechanism. Figure 1 presents the proposed configuration for the coiled spring mechanism. This proposed mechanism consists of a component for attaching to the debris, a ratchet, a coiled spring, and a stabilizer. The idea behind this solution is to absorb the rotational energy of the debris and store it in a coiled spring as potential energy. The purpose of the ratchet is to act as a locking mechanism for the spring when it winds up completely. Winding up the spring, though, necessitates the use of a stabilizer to hold the other end of the spring fixed. A stabilizer is thought of as a servo-controlled gyroscopic platform where gyroscopes are to be used only as sensors. The resolver (the "brain" of the control system) will be continually feeding corrections through the feedback controlled loop to keep the attachment to the platform fixed in space. The greatest advantage of this process is that it can attenuate the rotation of the debris quickly, i.e., within minutes. Furthermore, the attenuation of the debris is complete (100%). The disadvantages of this idea are the requirements for powering the gyroscopic sensors and lubricating the ratchet. Another more important problem is that the ASPOD will eventually be involved actively in the process by powering several thrusters as well as its momentum wheels. Since this may create safety problems for the vehicle itself, the idea was abandoned for the time being and our effort was concentrated on developing passive means of attenuation.

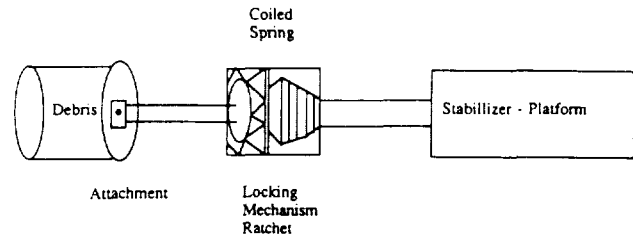


Fig. 1. Coiled Spring Mechanism

Long cable mechanism. For this design there are two ways in which it could work. One would be to let out a cable with a mass attached to the end, thereby increasing the moment of inertia and slowing the satellite down. This would not allow the satellite to come to a complete stop, but it could possibly slow the satellite down enough for a robotic arm to manipulate it. The cable would have to be cut off when maximum attenuation occurs, preferably so that it would reenter the Earth's atmosphere, because once the robotic arm attached to the satellite, the cable would reel in uncontrollably due to the momentum of the cable. The other method would be to leave the cable on for an extended amount of time and allow the gravity gradient to slow the satellite to a complete stop. The satellite could then be grabbed and the cable reeled in since the rotation of the satellite would be fully attenuated. Figure 2 shows a representation of this method.

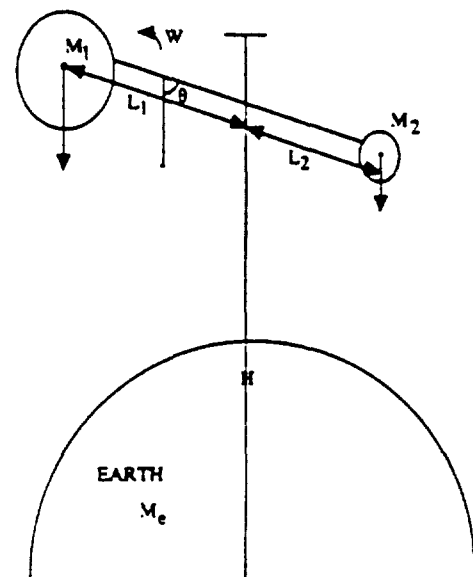


Fig. 2. Long Cable Configuration

Geared-bar mechanism. The geared-bar mechanism is the solution selected by the attenuation research group for further development and is detailed below.

Geared-bar Mechanism

Theory of operation. A representation of the gear bar can be seen in Fig. 3. The centrifugal acceleration acting on the flywheel forces the flywheel radially outward to the end of the geared bar. If the geared bar were smooth, the flywheel would just translate outward without spinning; however, the contact forces between the gear and the bar apply a torque about the center of the gear, forcing the flywheel to spin as well as translate. Mathematical analysis and experimentation show that as the angular rotation of the flywheel increases, the angular rotation of the debris decreases. A ratcheting mechanism is attached to the system so that when the flywheel reaches the end of the bar the flywheel will continue to rotate freely.

The effectiveness of our design depends on the length of the geared bar and the mass moment of inertia of the flywheel. It could happen that the configuration necessary to achieve an adequate amount of attenuation would be unfeasible to take into space due to the size and/or mass of the flywheel and the length of the bar. If this is shown to be true it should be possible to attach a motor to the flywheel and "reel" the flywheel back in, while the ratchet mechanism allows it to maintain its angular velocity and let it move out again. This process could be repeated as many times as necessary.

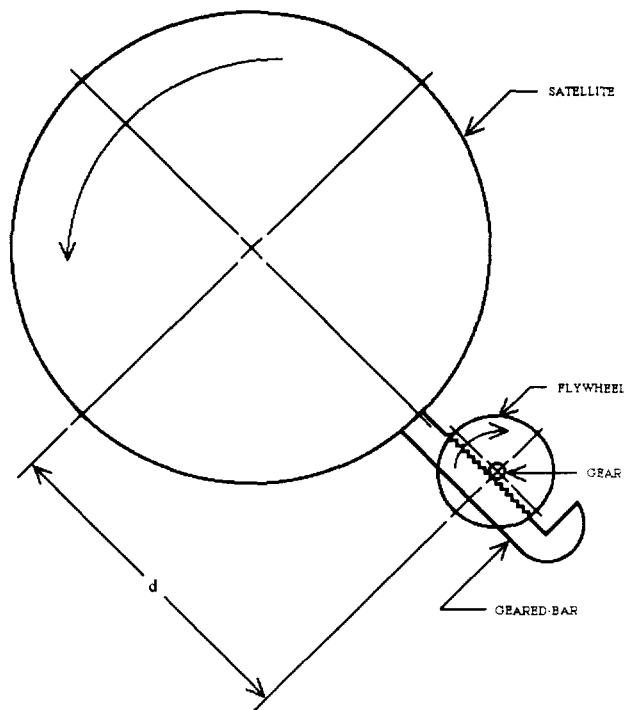


Fig. 3. Geared-bar Mechanism

Design. A rudimentary device was fabricated for experimental purposes. The design that was used included a rubber wheel and friction bar to simulate the rack and pinion system. A small cart supporting the flywheel and friction wheel with a bearing rolled along a track that represented the geared bar. The friction wheel rolled along a friction bar attached to the track forcing the flywheel to rotate. The combination of the flywheel and the cart simulated both the rotation and the translation of the flywheel. To simulate the ratcheting mechanism, the friction bar was cut shorter than the track. This allowed the flywheel to rotate freely once it reached the end of the track. This design was not adaptable to the use of a motor; however, it was felt that showing that the theory mechanism would work for one pass was sufficient to show that this method of attenuation was feasible.

Experiment. Previously, a large model representing space debris was built for attenuation experimentation purposes. This model is an octagonal solid approximately 48 in in diameter and 72 in high with a calculated mass moment of inertia of 655 lbm ft. The "debris" is attached to the ceiling and floor with a large metal rod about which it rotates. Lubricated bearings were used to minimize the frictional effects.

To gather data, a systematic process had to be developed to measure the time per revolution. A computer program was used to record the needed data. A mark was made on the "debris," which was then spun up to an appropriate speed. Each time the mark came into sight, a key was pressed on the computer. The program would then print the number of revolutions and measure the time elapsed. With this data, the program calculated the time between revolutions and revolutions per minute. Finally, this information was exported to a spreadsheet program for further analysis and graphing.

To prove the effectiveness of the geared-bar mechanism, it was necessary to find a way to separate the effects of the changing mass moment of inertia due to the flywheel translating outward vs. the effects of the rotational kinetic energy being transferred to the flywheel. To do this, reference data had to be taken. These reference data consisted of several measurements with the flywheel retracted and several with the flywheel extended. Before measurements could be taken with the geared-bar mechanism fully operational, one additional component needed to be added. Because the debris needed to be brought up to a functioning speed before the flywheel could be released, it was necessary to develop a release mechanism so that the flywheel would not begin to move before the appropriate speed was attained. This was done by including an eyelet on the flywheel, and passing a pin through it that could be easily pulled out when needed without significantly affecting the speed of the debris.

As stated above, these measurements were taken for each case: the flywheel retracted, extended, and operational. Figures 4, 5, and 6 show the relative quality of the measurements for each case and their characteristic curves.

Although the reference data were taken, a standard procedure to spin up the debris at an equal rpm for each run was not developed, nor was there a way to measure the energy added to the system. It was necessary, therefore, to determine

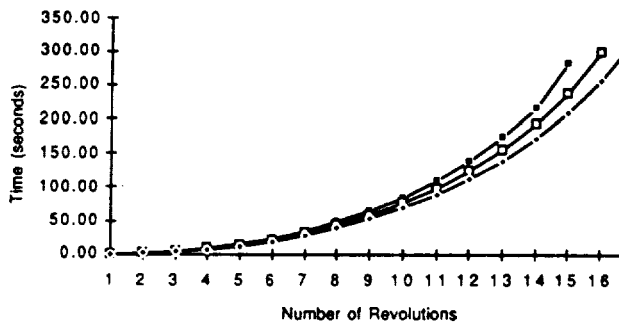


Fig. 4. Flywheel Retracted

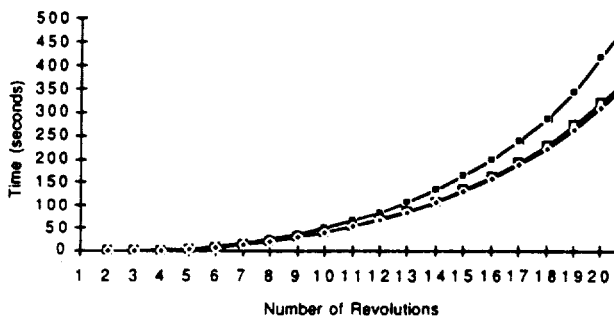


Fig. 5. Flywheel Extended

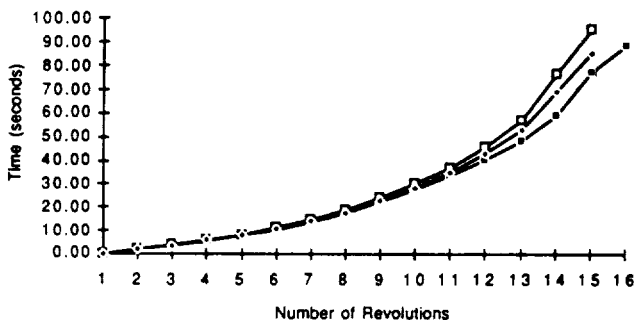


Fig. 6. Flywheel Translating

a method for comparing the data with the three different cases. Because of limitations with the graphing software used, it was felt that taking the points at which the debris came to rest with each case and counting the maximum, common number of data points backward would be a reasonable method for developing a common reference. For example, the working case only included 14 data points, so the last 14 data points for each case were used.

Figure 7 illustrates the effects between the three different cases. The line with the flywheel retracted is steep due to the low relative inertia. The line with the flywheel extended is flatter and the time of rotation longer due to the effects of increased mass moment of inertia. If the working case

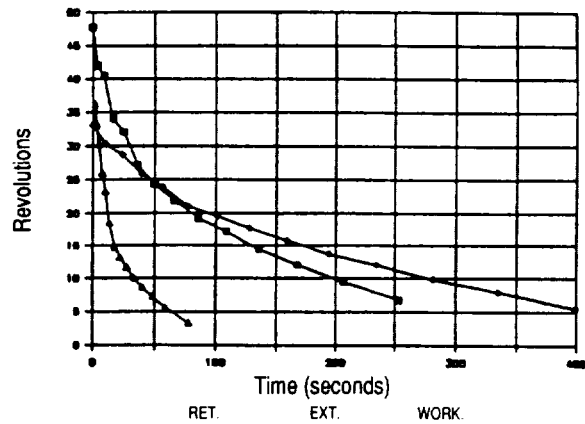


Fig. 7. Experimental Comparison

decreased the rotational speed of the debris solely due to the effects of the changing mass moment of inertia, one would expect the line for the working case to lie somewhere between the retracted and extended cases. In fact, the graph should begin at the approximate point of the retracted case because of the identical value for the mass moment of inertia and end near the same point of the extended case because the same amount of energy should still be in the system. It was not the group's goal to "prove" the effects of changing the mass moment of inertia, but to prove that the flywheel actually absorbs the energy of the debris. To confirm this, the graph of the working case should start near the point of the retracted case and end significantly below the extended case. The working case line does confirm this hypothesis.

This experiment does not exactly model the case of debris spinning in space because satellites in space are not pinned, therefore the center of rotation would change as the flywheel moves out. The mass of the flywheel could be optimized to minimize these effects. Nonetheless, this system of attenuation will still work, because the center of rotation will always lie between the centers of the debris and the flywheel, maintaining the centrifugal component of acceleration moving the flywheel outward.

In conclusion, and most importantly, the geared-bar mechanism of the experimental case does absorb the rotational energy of a spinning body. For the 3 cases mentioned above, the time for the last 14 data points is 253 sec for the retracted case, 400 sec for the extended case, and 59 sec for the working case. The above experiment also proves that the attenuation is not solely due to the change in mass moment of inertia, but actually performs a significant amount of energy transfer.

Computer modeling. In order to investigate the dynamics of the geared-bar mechanism as an attenuator of the rotational energy of a satellite, several approximations to the actual case were considered. The first case, consisting of the two-dimensional analog (Fig. 8) of the actual case (Fig. 9), assuming perfect targeting and neglecting the attachment phase and the endpoint locking of the flywheel, was solved analytically.

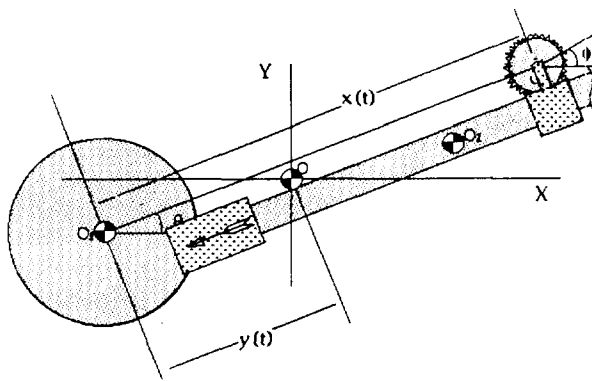


Fig. 8. Attachment Parameters

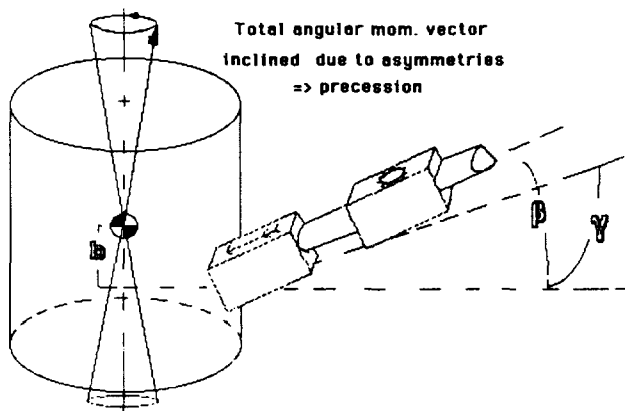


Fig. 9. Attachment Sensitivities

Under the above assumptions, the analysis suggested that an attenuation of about 50% could be attained for a rack length of 4 m, and an operation of 50 sec. These results pertain to a satellite modeled as a 2000-kg cylinder, 4 m in height and 3 m in radius rotating at 50 rpm. The 40-kg flywheel used in the analysis was 1 m in diameter, while the rack was assumed weightless. At this point it should be mentioned that the attenuation effects are highly dependent on the inertial properties of the satellite. Thus, it should be kept in mind that the diversity of satellites to be attenuated adds to the complications and limits the applicability of the design.

In order to investigate the effects of the geared-bar attenuator when it is not attached at right angles to the principal axis of rotation of the debris, as well as when it is attached off-center with respect to the satellite's center of mass (Fig. 9), an analysis was attempted on a software package available at the University of Arizona. This software facilitated a three-dimensional analysis and made it possible to animate the resulting effects, for visual and demonstrational purposes. For a satellite with inertial properties as mentioned above, the software shows attenuation as high as 70% during the first 5 sec for the two-dimensional case, but not more than 25% for the three-dimensional case that involves geometrical

asymmetries and precessions. The fact that the rack and pinion joint is not 100%, as was assumed by the software, will lengthen the time needed for attenuation. Figures 10 and 11 show the angular velocity of the debris for the two- and three-dimensional cases respectively.

The results indicate that the targeting and alignment of our device is essential, and therefore a process of determining the center of mass of the debris before operation is essential. The software can provide results once the device is attached to the satellite; however, impact forces caused by the attachment process were not modeled.

To evaluate the model, a final comment on the effects upon impact needs to be made. Provided that no eccentric forces are present, i.e., perfect targeting, any components directed radially from the Earth will cause oscillations that are estimated to die out. Moreover, any angular components will result in shifting the orbit but not changing the orbit altitude. Thus, the effects on the debris will be mostly translational and will not greatly affect the attenuation process.

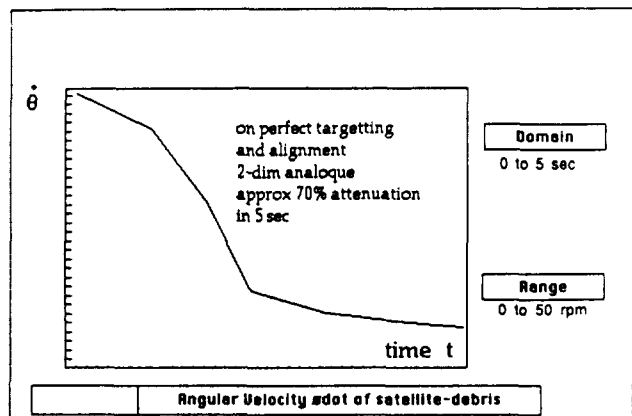


Fig. 10. 2-D Computer Modeling

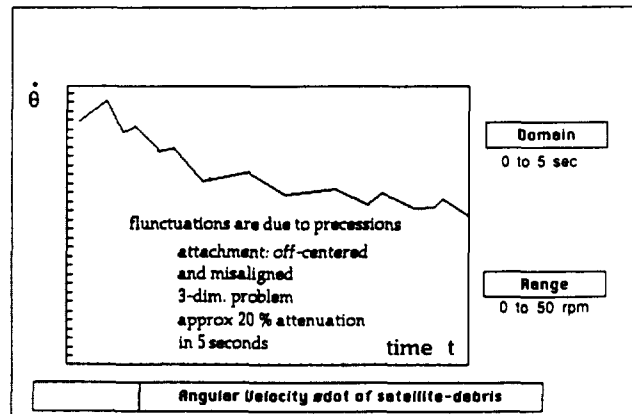


Fig. 11. 3-D Computer Modeling

Attachment. Since the purpose of this project was to test processes for attenuation, the issue of attaching the mechanism to the satellite was not initially addressed. However, it was felt that developing a method of attachment was necessary to complete the subject of attenuating the rotational motion of orbital debris.

Several ideas were considered. Wrapping something around the satellite (similar to lassoing) was discarded because it could not be guaranteed that there would be a perfectly clear path all the way around every satellite due to auxiliary objects such as antennas. Grabbing the satellite was felt to be impractical because the skin of the satellite is very flimsy (since its only purpose is to shield the inside from solar radiation and small particles) and could not sustain very large forces and moments.

The conceptual design of the device that was chosen to build was much like an umbrella. The device would pierce the skin of the satellite and, once inside, open up to prevent the device from slipping back out.

As can be seen in Fig. 12, a motor turns a threaded rod and the collar with the shorter links attached begins to move. Once the collar contacts the back-plate the collar no longer moves along the threaded rod and the shorter links then pull the larger links until both are at right angles to the threaded rod. The mechanism would have worked with only the longer rods; however, the design chosen minimizes the load that each link has to take and increases the mechanical advantage of each link, thereby requiring less energy.

The motor to drive the threaded screw would be a DC motor. The batteries would be charged prior to use using the power source available to ASPOD.

Conclusion. The overall purpose of this part of the project was to research and design a mechanism that would slow or attenuate the rotation of a satellite. The solution found would involve launching a geared-bar mechanism to the piece of debris. The tip would pierce the skin and six links would then open up to keep the device in place. The flywheel would then be disconnected from its locked position and allowed to rotate out. This would transfer the rotational energy from the satellite

to a more manageable form in the flywheel. This method was proven to work through experimentation and mathematical and computer analysis.

DIGITAL CONTROL OF PLACEMENT ARM

The ASPOD design incorporates a solar-powered metal cutter to facilitate dead satellite processing in a cost-effective manner. In order to position debris at the focal point it is necessary that the ASPOD be equipped with robotic arms. The arm function is to hold and move material to be cut in the focal plane of the solar concentrator. After this initial development stage, the gathering arm was controlled with a variable-speed on/off control panel. In order to automate the arm and to better simulate its operation in space, a hardware/software controller was designed. The objective of the digital control was to eliminate the direct human interface initially needed to operate the arm and to replace it with a software interface that would accept commands entered into a PC terminal. The digital control would increase the accuracy of the arms' movements, and with the software interface a program could be developed in order to perform a pick-and-place operation or a more defined cutting operation.

Design Specifications

The robotic arm has five revolute joints as shown in Fig. 13 with axes and degrees of joint rotation. The most important component of the whole robot system is the digital control system whose components are a power supply, voltage regulator, two motion controller boards (from Motion Engineering), five motor drivers, five optical encoders, five DC motors, and an IBM PC. Two of the hardware parts—the power supply and the motor driver—required custom design and fabrication. These components were constructed by members of the team.

The hardware needed to build the power supply included a transformer, a bridge, and two capacitors to produce a dual output of +25 V/-25 V with a smooth signal (resembling DC voltage). The +25 V was also connected to a voltage regulator to produce +5 V for the optical encoder. Figure 14 shows the circuit design for both the power supply and the voltage regulator.

Five individual motor drivers (channels) were built within the motor driver. Each driver consisted of a high-voltage operational amplifier to amplify the input voltage from motion controller boards, transistors, capacitors, and resistors (see Fig. 15). The motor driver receives a voltage from the motion controller board between -10 V/+10 V. The operational amplifier amplifies the voltage at values of +20 to -20 V. The transistor amplifies the current and then sends a voltage to drive the DC motors at each joint of the arm.

The optical encoders (HEDS-5600) are used to provide accurate motion detection. They provide a high-performance, optical incremental encoder that emphasizes high reliability and resolution, low cost, and ease of assembly. The optical encoders were attached at the points of rotation to measure the angle of rotation at each joint, and required a rigid mount and modification to the shaft at each joint.

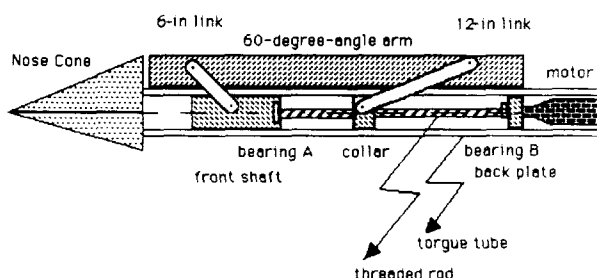


Fig. 12. Attachment Device

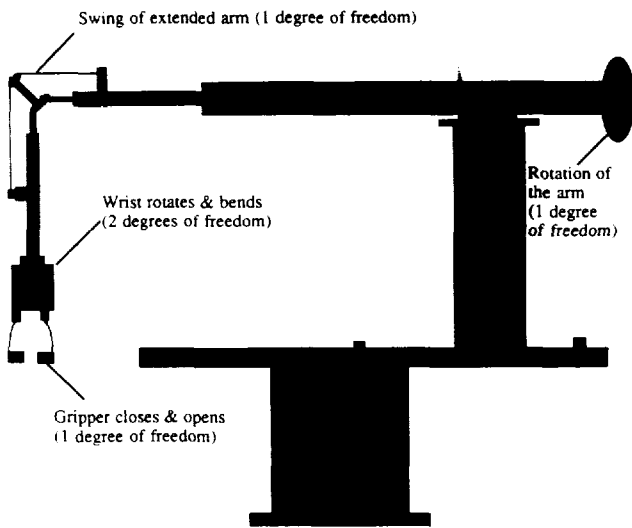


Fig. 13. Robotic Arm Showing Degrees of Freedom at Joints

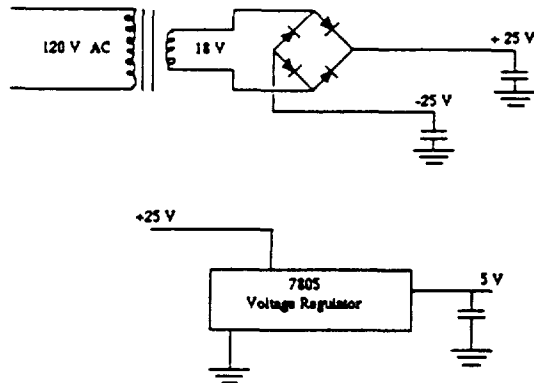


Fig. 14. Power Supply and Voltage Regulator

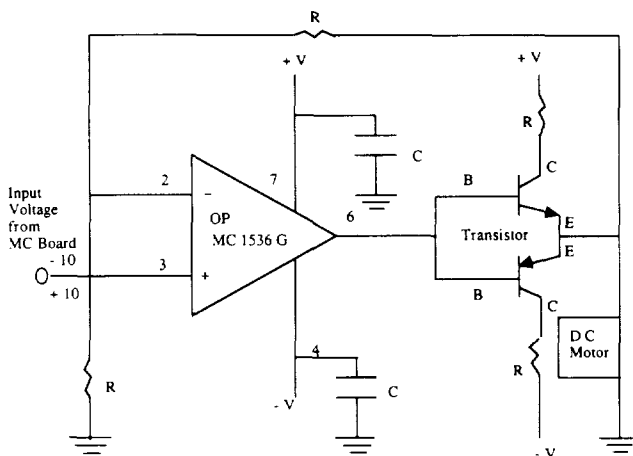


Fig. 15. Circuit Design of Motor Driver

Two motion controller (MC) boards control the five DC motors on the arm. The MC-400 is able to control four motors while MC-200 can control two motors. The two MC boards are connected to the computer and wired to the motor drivers. Included in the package with the controller boards were two types of software: the "Stand Alone Program" aids in the installation and testing of the optical encoders, and the MC boards and the "Utility Subroutine and Program" aid in the development of a customer-written program. The software can be written in either "C" or "BASIC." The MC controller boards were accompanied by a user guide to assist in installation and operation. The block diagram for the control system is shown in Fig. 16.

The decision was made to use these MC boards over other possible choices because the controller cards were designed around the HCTL-1000 general-purpose Motion Control IC. The HCTL-1000 has the capacity to handle all encoder input decoding, phase commutation for steppers and brushless servomotors, digital filtering of the control signal, and generation of analog or pulse-width-modulated motor command signals. It continually performs intensive tasks of digital motion control, thereby freeing the PC for other planning tasks. The HCTL-1000 operation is controlled by a bank of 64 internal registers that, in turn, can be accessed by mapping within the PC memory. There is no need for interrupt-handling during operation.

To develop the control system, the robotic arm is viewed as a continuous time-varying system. The Laplace transform technique is used to simplify the analysis. The block diagram in Fig. 17 depicts the feedback closed-loop system of the robotic arm control. The digital controller is an IBM computer, while the DAC is a digital-to-analog converter, and the ADC is an analog-to-digital converter. The amplifier is the motor driver circuit used to convert the low-level analog torque signal $u(t)$ to a voltage $v(t)$, which directly activates the joint motors. Since the joints are DC motors, the generated torque is proportional to the armature current. Therefore, the amplifier in Fig. 17 is an analog subsystem regulating the

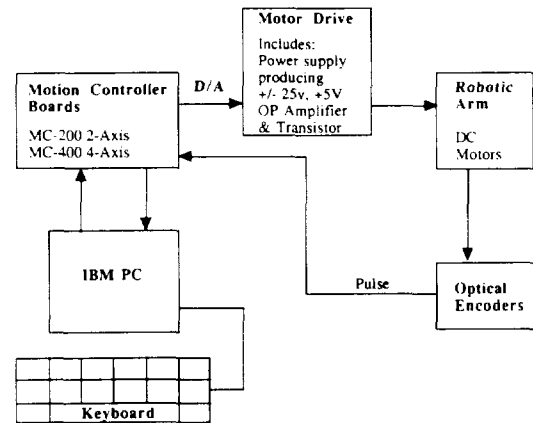


Fig. 16. General Block Diagram for Robotic Arm Control System

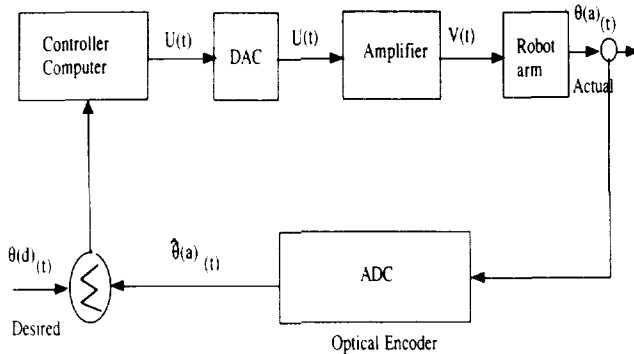


Fig. 17. Feedback Closed Loop System of Digital Control

current through variations in the applied armature voltage. The ADC block detects the position (encoders) and the speed (tachometers) of the joint motors and converts them into a form recognized by the digital controller. Thus, the sensors here represent an encoded disk (optical encoder) of the type ADC.

The status of the project at this point is that we have control of four of the five motors on the arm. A program was written in "C" that can demonstrate a predetermined movement of the arm and its return. Since the initial (zero) position sensors are not installed, the arm can only be controlled using the joint coordinates. Two sample programs were developed for this purpose. One uses the voltage to control the joints. It reads and records the quadrature counts from the optical encoders. The second program uses the trapezoidal profile position control in an interactive mode. It has been modified to execute a sequence of point-to-point positions in the specified envelope. The user at this point may move all joints simultaneously or move one joint at a time to a predefined position. This requires only one keystroke to the keyboard.

Future Plan

The future plan of the software project is to move the arm with all 5 degrees of freedom integrating in a "pick-and-place" fashion. The arm will also be movable to any predetermined position in the physical envelope of the apparatus (i.e., move anywhere defined in polar (r,q) coordinates). Future work involves some hardware and software amplifications. For the hardware, some position sensors need to be installed for the initial (zero) position, and an optical encoder installed at the wrist. For the software aspect, the relationship between the inverse kinematics of the robot arm and the trajectory planning needs to be studied in more depth, and integration of the second arm must also be achieved. Components of this integration include state-of-the-art artificial intelligence and decentralized control algorithms. Additional considerations for the software portion include both error checking and recovery software that must be designed with the focal cutting point in mind as well as an initial (zero) position. All the above points must be intrinsic to the computer software each time

the machine is booted up or loaded. The future work of the project will take place in the succeeding semesters by other design teams.

MANIPULATOR ARM

The ASPOD spacecraft will need two robotic arms to successfully retrieve and process a piece of orbital debris. This year the task was to design and fabricate a new robotic arm. This arm was to be designed with the specific ASPOD mission in mind, and have the flexibility necessary for the handling of large pieces of debris.

Limitations

There will be no subsequent contact with the orbiter once it has been launched; therefore, it must be reliable. The arm must have a hand capable of grabbing most space debris as well as grappling with a larger satellite. Control of the arm must be precise. Vibrations, as well as slop/backlash within the arm's actuator mechanisms, must be minimized. The design must be adaptable to digital control and the electrical system must run off a 24-V power supply.

Design (Target) Specifications

In the process of generating alternative solutions the solar mirror structure was analyzed to determine the necessary DOFs. By approaching the problem in this manner, we would not have to analyze and build models to treat every design that did not have any immediate foreseeable problems. Analysis by this method led to a very unique solution.

First, it was determined that the easiest way to remove the lens from the holding slot was to translate it along an axis contained within the plane of the lens (see Fig. 18). We call this the hand axis from here on to clarify our discussion. Note that we assume the grasping mechanism to be attached to this axis.

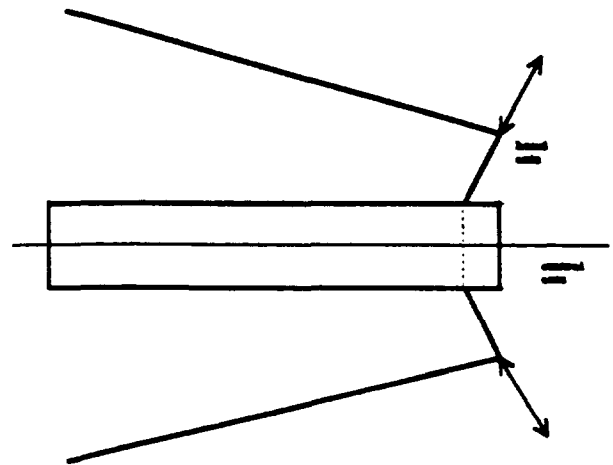


Fig. 18. Hand Axis

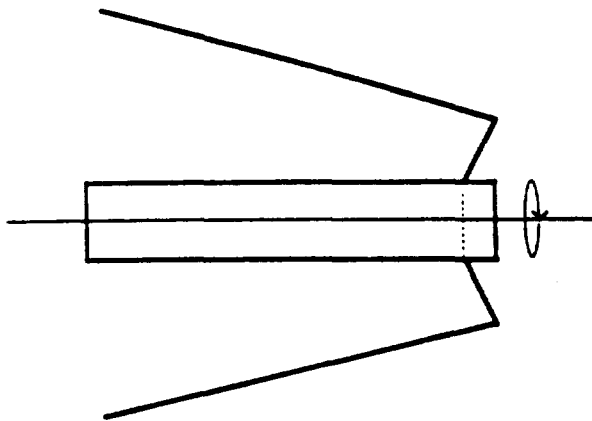


Fig. 19. Central Axis Rotation

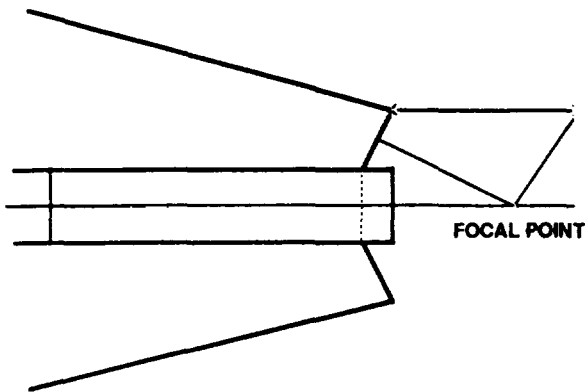


Fig. 20. Focal Point Within Reach

To reach all three lenses with the hand axis in this orientation with respect to each lens individually, it is necessary to rotate about the central axis of the mirror structure (see Fig. 19).

The next requirement is for the arm to be able to reach the focal point. From Fig. 20 it can be seen that we need only to translate along an axis parallel to that of the central axis to meet this requirement. Finally, to reach debris located above the mirror structure the mechanism must be able to rotate about an axis perpendicular to the plane created by both the hand and central axis.

With these three DOFs we have a work area with roughly the shape of a cylinder with half spheres at the ends. Adding more DOFs in the form of joints or extensions would be redundant at this point. The adding of redundancies may decrease the difficulty of specific tasks. For example, in the case where an obstruction prevents the arm from directly reaching an object, it may be necessary to have another joint in the arm to essentially reach around the obstruction.

It is important to note that none of the DOFs required by the hand to perform properly have been considered here. The reason is that the DOFs discussed so far are for location and orientation of the hands—i.e., getting the hand to the desired locations—whereas the DOFs required by the hand are for orientation of the hand to receive the object. Those DOFs will be discussed in the subproblems involving the hand.

Using the three fundamental DOFs, the configuration in Fig. 21 was proposed. Note that the ring was used to accomplish the rotation about the central axis so that no part of the arm would be prone to moving through the focal point (see Figs. 21 and 22).

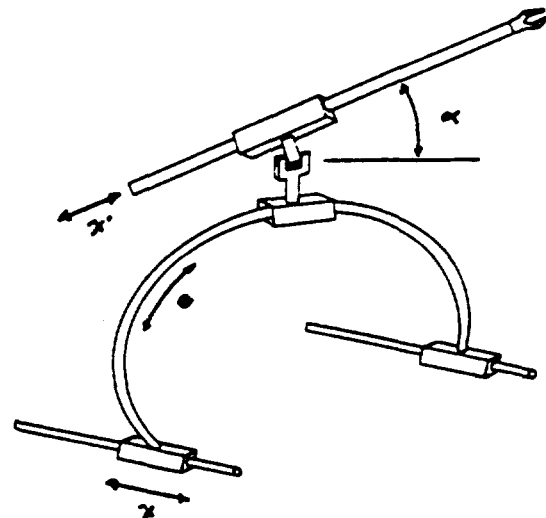


Fig. 21.

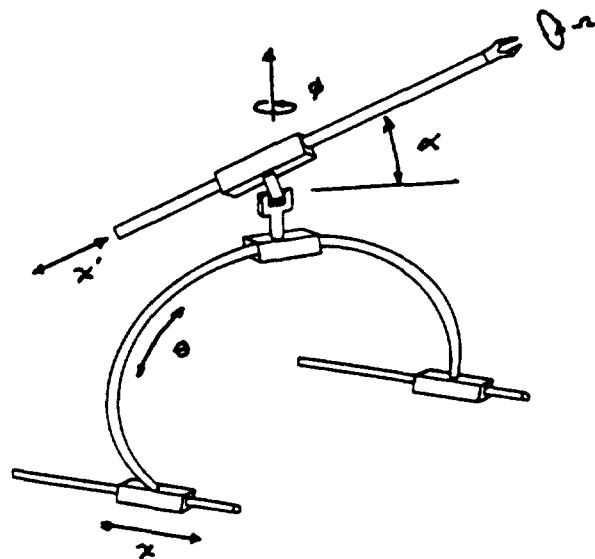


Fig. 22.

Final Design

Polar drive mechanism. The purpose of the axial tracks is to translate the entire robotic arm structure along the body of the collector. This is accomplished through motor driven screws. The motors have an output of 100 oz-in at 30 rpm per motor. This velocity will cause the polar track assembly to move at a rate of 4 in/min. The reason for keeping the velocity low is to prevent unwanted oscillations in the system. The power screws are regular 0.5 in and 13 threads per in.

The main load of the polar tracks is taken up by the bearings inside the pillow blocks. The bearings are 0.75-in linear bearings. Two linear bearings were used to prevent horizontal motion. The bearings ride on 60 case-hardened steel rods. This material was chosen because of its great stiffness capabilities and availability. Alongside the bearings, inside the pillow blocks, there are two couplings. The reason for using two is also to prevent horizontal deflection and to maximize the contact area between the pillow blocks and the driver screws.

The connection between the pillow blocks and the polar track is done through the flat plates that are welded to the polar track and the pillow blocks. The flat plates are bolted together.

The tracks, which were manufactured out of aluminum stock, are supported at the ends.

The circular track allows the arm to rotate about the focal point and align itself in a normal sense to the lens axis. The circular track allows the arm to access the mirror/lens structure without interference. A wide-base channel section (5 × 1.75-in cross-section) provides the necessary contact points to mount the arm and yields a "chamber" of space essential to the drive mechanism. The channel material is 5052 aluminum and initially weighed 24 lb. The weight was reduced to approximately 19 lb by drilling thirty 2.5-in diameter holes along the web, evenly spaced 3.5 in apart center to center. The holes did not weaken the track but did slightly deform it. The track's inside diameter was reduced by approximately 0.5 in, which is not a problem.

The arm is mounted onto the arm-platform, which contacts the channel track at six points: four on the outside and two on the inside. The rollers are Killian bearings that provide normal and lateral stability. The four outside bearings have been modified to prevent derailing. A washer has been pressed against the lip of the bearing. Two pairs of springs are incorporated in the design of the platform: one pair clamps the inside rollers to the platform providing normal stability, and the other pair ensures lateral contact of the bearings to the track. The springs are necessary to account for track irregularities.

The drive is simply a dual chain/sprocket drive. Power is transferred through a 50:1 worm gear reducer. The motor ordered was found to be faulty. It was rated at 10,000 rpm, 9 oz-in torque. Since it was to operate at shaft conditions of 500 rpm, 180 oz-in, this would give more than the needed torque of 500 oz-in. Testing showed motor output was nowhere near these specifications, so it was necessary to use a motor that was found and worked. No characteristics are known about the motor. Testing of the circular track drive

mechanism showed that operation performance was adequate for loads of 15 to 20 lb.

Elbow joint. The elbow joint provides one degree of freedom, which enables objects to be moved in or out of the focal point. It also supports access radially outward from the polar track providing access to objects that lie outside the ASPOD's framework. The elbow consists of two major components.

The first piece holds the motor and worm, and braces the 5/16-in shaft with a 7/8-in OD roller bearing press fit at either side. The selected motor is shown below as motor #1. The worm is steel, single-tooth, and 32 pitch. The shaft is held in place with snap rings.

The second major part of the elbow joint has a 32-pitch, 100-tooth worm wheel pressed into it. The worm wheel mates the worm on the first part when placed on the shaft. The shaft has a flat milled across it and is fixed to the worm wheel with a 5-40 set screw. The set screw is 2 in long so it not only holds the shaft but also fixes the wheel to the second piece.

Both parts of the elbow have a 1-in long hollow male fitting that is placed into a 1.5-in OD 0.0649-in thick pipe. All structural parts are made of aluminum; all fasteners are steel.

Motor rotor assembly. The motor rotor assembly is a gearbox that holds the arm above the polar track and allows the arm to rotate a full 360°. This provides access to objects in front, behind, or to either side of the ASPOD. The gearbox consists of two 9-in × 4-in plates separated 2.5 in by four spacers. The motor drives a 24-pitch, 100-tooth worm wheel that is held on the end of the shaft/endcap with 5-40 set screw. The motor selected for the gearbox is identified as motor #1. The motor is held at the precise height and angle with the motor mount.

The shaft/endcap is machined to have a 3/8-in shaft on one end and a 1/2-in long hollow male fitting on the other. It protrudes through the top of the gearbox so that the 1.5-in pipe that holds the elbow joint can be attached. The part of the endcap that joins the shaft was threaded with 9/32-in 18 threads/in. The shaft fits through a bearing and is held by a 9/32-in nut. The bearing is held in place with a machined cap. The cap was machined to have a snug fit with the bearing circumference and have a 1/1000-in interference fit between the bearing and top plate. The cap is fastened to the plate with four 6/32-in bolts.

Motor selection. The following motors were selected for their torque and speed. The exact weight was unknown but a rough estimate considering their size was also considered. The motors needed to have this great amount of torque as our initial estimates of the arm weight were too low. These motors will allow the arm to retain its original design capabilities of lifting a 2-lb plate at an extension of 33 in.

Motor #	Quantity	Torque (oz-in)	Speed (rpm)
1	2	100	375
2	1	25	1000
3	3	100	75
4	2	75	30

Grasping mechanism. The requirements of the grasping mechanism are that it must be able to grab a thin flat plate ranging in thickness from 0.125 to 0.75 in, grasp a cylinder with a diameter ranging from 0.125 to 4.0 in, and grasp a sphere with a diameter equal to that of the cylinder. Other general requirements for the mechanism are that the weight be minimal, the ratio of the clamping to the actuator force be maximized, and that the force ratio be as nearly constant throughout the range of motion of the mechanism as possible.

For the design that was developed and built to meet the requirements, the ratio of the clamping force to the actuator force is 0.25 and is nearly constant throughout the clamping range. The ratio was determined by constructing a static force vector diagram on each design at intervals in their range of motion. There was a trade-off between the increased ratio and smaller size. The force ratio would increase if the distance between the two sets of four bar linkages were increased. This design was chosen over five others because of its higher clamping force ratio, its smaller size, and its simplicity.

Harmonic vibrations. Vibrations of any space structure create special problems. The payload must be deployed, be able to precisely grab objects, and not suffer damage due to fatigue trying to capture satellites.

The space shuttle has a natural harmonic frequency of 32 Hz that prevents it from carrying a payload with a corresponding harmonic frequency less than or equal to 32 Hz. Such a payload (≤ 32 Hz) would certainly cause resonant vibrations of increasing amplitude. Damage to the shuttle resulting from resonance would be likely since it takes several hours to deploy any payload and the shuttle would be subject to the resonant vibrations until deployment since there is no damping in space.

If the robotic arm is to grasp an object, the exact position of the manipulator must be known. Low frequency vibrations tend to have greater amplitude and the end of the arm could move more than an inch. Use of space-rated composite materials (higher structural stiffness) would help to alleviate this problem.

If the amplitude of harmonic vibrations is too high, the robotic arm will experience high stresses. These stresses will cause fatigue damage if aluminum is the primary construction material of the arm. This is especially dangerous since space structures usually have little or no factor of safety. Composites have better fatiguing properties and should be used in all high-stress areas.

Conclusion. This year's research team designed and constructed the primary grappling arm. The arm has the ability to maneuver large and bulky objects into the focus of the Fresnel lens solar cutting device without obstructing the beam. A secondary function of the arm is to be able to repair or replace any of the Fresnel lenses if they are damaged. Both of these goals are met with the ASPOD robotic arm.

Most of the design specifications have been met. The arm can grasp a variety of objects from round balls to flat plates. It can be adapted to computer control by future design teams. All motors operate at 24 V (some are rated slightly higher but this presents no problem). The arm appears able to replace Fresnel lenses and repair the mirror array. However, the arm is not lightweight; in fact, it is so overweight that the Polar Arc is in distress. The arm is not reliable enough to operate for months or years without service.

Replacement of some aluminum parts with graphite composites would greatly enhance the performance of the robotic arm. Not only will weight be drastically reduced, but problems due to the low harmonics (4 to 10 Hz depending on its position) of the arm will be improved.

ACKNOWLEDGMENTS

The support from USRA and the technical monitoring of Mr. James D. Burke of JPL are gratefully acknowledged. Mr. Milton Schick contributed greatly towards the development of ASPOD.

Design project participants were David Campbell, Micky Marine, Daniel Bertles, Dave Nichols, and Mohamid Saad with Dr. Kumar Ramohalli, faculty.

REFERENCES

1. Discover, December, 1988, p. 22.
2. GEO, March, 1989, p. 154.
3. Danish Science, December, 1988, p. 46.
4. Smithsonian, December, 1988.
5. Arizona Daily Star, February 21, 1987.
6. Tucson Citizen, February 27, 1987.
7. Arizona Republic, August 14, 1988.
8. Tucson Citizen, September 23, 1988.
9. American Way, May 15, 1989.
10. *Artificial Space Debris*, Johnson, Nicholas L., Orbit Book Company, Malabar, Florida, 1987.
11. Ibid
12. Ibid
13. Ibid
14. "Debris Danger Zone," Natural History, November, 1987.
15. "Hypervelocity Impact," NASA Activities, April-May, 1987.



p. 4 23

LABORATORY SIMULATION OF THE ROCKET MOTOR THRUST AS A "FOLLOWER" FORCE

N 9 1 - 1 8 1 2 4

UNIVERSITY OF CALIFORNIA, LOS ANGELES

Ground tests of solid propellant rocket motors have shown that metal-containing propellants produce various amounts of slag (primarily aluminum oxide), which is trapped in the motor case causing a loss of specific impulse. Although not yet definitely established, the presence of a liquid pool of slag also may contribute to nutational instabilities that have been observed with certain spin-stabilized, upper-stage vehicles. Because of the rocket's axial acceleration—absent in the ground tests—estimates of in-flight slag mass have been very uncertain. Yet such estimates are needed to determine the magnitude of the control authority of the systems required for eliminating the instability. A test rig with an eccentrically mounted hemispherical bowl was designed and built that incorporates a "follower" force that properly aligns the thrust vector along the axis of spin. A program that computes the motion of a point mass in the spinning and precessing bowl was written. Using various rpm, friction factors, and initial starting conditions, plots were generated showing the trace of the point mass around the inside of the fuel tank. The apparatus will be used extensively during the 1990-1991 academic year and incorporate future design features such as a variable nutation angle and a film height measuring instrument. Data obtained on the nutational instability characteristics will be used to determine order-of-magnitude estimates of control authority needed to minimize the sloshing effect.

INTRODUCTION

Many rocket motor solid propellants in current use contain a significant amount of aluminum, which, when burned, produces a slag consisting of aluminum oxide and elemental aluminum. Most of this material is expelled through the rocket motor nozzle and adds to the thrust, but some remains trapped in the motor case. The melting point of the α -form of Al_2O_3 is about $2050^\circ C$, below the temperature of the combustion gas. The liquid slag, in the form of small droplets, is subject to a combination of forces that include the drag from the combustion gas, the inertial force resulting from the axial acceleration of the rocket, and (for spin-stabilized vehicles) the centrifugal force resulting from the vehicle spin.

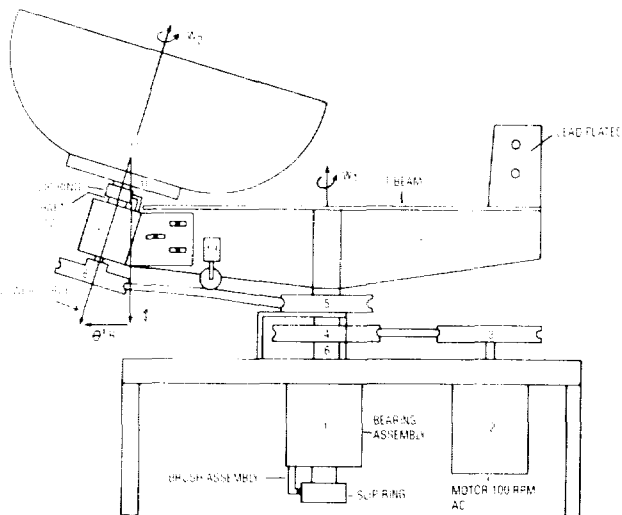
The present analysis postulates that, because of the high level of turbulence in the motor, slag droplets entering the gas stream are ejected, and that trapped slag is formed primarily by liquid slag flowing along the surfaces toward the point of minimum potential energy in the accelerating and spinning motor. Also, the present analysis concludes that slag will accumulate to some degree in all spinning or accelerating rocket motors with aluminum-containing propellants and submerged nozzles.

A number of spin-stabilized vehicles that use aluminized propellant have shown a marked tendency for a "coning" instability, i.e., a precession with steadily increasing nutation angle. These motors have a submerged nozzle geometry, resulting in a downstream annular pocket that is likely to favor slag retention. It has been surmised, therefore, that the sloshing motion of a liquid slag pool may be a contributing cause of the observed flight instability. The effects of liquid slag on the stability of spinning vehicles is similar to the effects produced by fuel slosh in spacecraft. Slag retention also requires examination because of its potentially deleterious effect on specific impulse.

Through installation of witness plates downstream of the nozzle, where some of the (now solid) slag particles are deposited, estimates of the size distribution and total mass of the expelled particles have been made. Ground tests of this type, however, take no account of the precessing of the droplets in the nozzle.

This report consists of a mechanical design that simulates the motion of a spherical fuel tank in a thrusting spacecraft. A true simulation of the thrust was thought to be impossible because of the gravitational forces present in the laboratory. However, through the means of an eccentrically mounted spacecraft model on the top of a turntable, the simulation of thrust aligned with the vehicle axis is possible. The mechanical design was finished during the 1990 winter quarter and the test rig was built in the spring. Comparison of the initial description (see Fig. 1) with the design actually built (see Fig. 2) shows the evolution of the design concept. Qualitative analysis will be provided by photographs of fluid profiles at given time intervals and quantitative analysis by correlation of film thickness from capacitance measurements between two platinum wires located in the bowl. This sensor will be designed, built, and incorporated into the test rig slip-ring assembly during the 1990-1991 academic year. From these data, nutational instability characteristics and order-of-magnitude estimates of control authority needed to eliminate the instability will be determined.

A computer program was written to simulate the shape of a fluid in a spinning and precessing container with a nutation angle equal to zero. The fluid was assumed to be in hydrostatic equilibrium. The fluid depth as a function of position along with the shoreline of the fluid was determined. A more general code was written that computes the motion of a point mass in a spinning and precessing hemispherical container. Using



- | | |
|---------------------------------|---------------------------------|
| 1 general bearing assembly | 8 bowl pulley |
| 2 AC motor (variable rpm) | 9 bowl bearing housing assembly |
| 3 pulley for motor shaft | 10 bowl mounting flange |
| 4 main drive pulley | 11 hemispherical bowl (lucite) |
| 5 secondary pulley (stationary) | 12 bowl support shaft |
| 6 main shaft | 13 idler guide |
| 7 control arm | |

Fig. 1. Apparatus Diagram (Not to scale)

various rpm and friction factors, plots were generated to compare the motion of the point mass and validate the theoretical model (see Fig. 3).

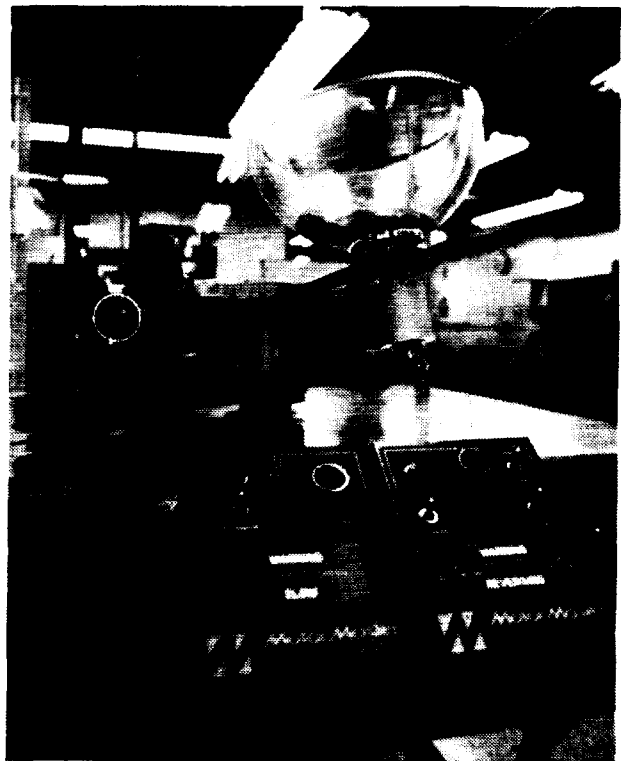
VISCOUS DISSIPATION

The degree of instability of a thrusting, spin-stabilized spacecraft depends strongly on the amount of internal energy dissipation. The dominant energy dissipation mechanism is thought to be the sloshing of liquid slag at the bottom of the solid motor casing, which directly influences the body's motion. Oscillatory, and sometimes violent, motion of the fluid induces corresponding oscillations in the body. Viscous effects in the fluid also influence the body causing the nutation angle to change, thereby affecting stability. It is, therefore, important to estimate the energy losses in the fluid.

Once these energy losses are estimated, one can predict the body motion by reducing its kinetic energy at the same rate. This approach is known as the "energy sink" procedure. Due to the growing nutation angle from energy dissipation, thrust corrections need to be made to stabilize the craft. This requires more fuel to be included for stabilization during launch, which ultimately increases launch mass. Having to fire these correcting thrusters at the right time creates yet another problem in the attitude dynamics and control of the spacecraft. Ideally, nutational instability characteristics and order-of-magnitude estimates of control authority needed to eliminate the instability would allow designers to provide the lightest control system necessary to minimize this phenomenon.



(a)



(b)

Fig. 2. Completed Test Rig: (a) Top View Showing Liquid Sloshing in Bowl; (b) Side View Showing Dual Motor Assembly

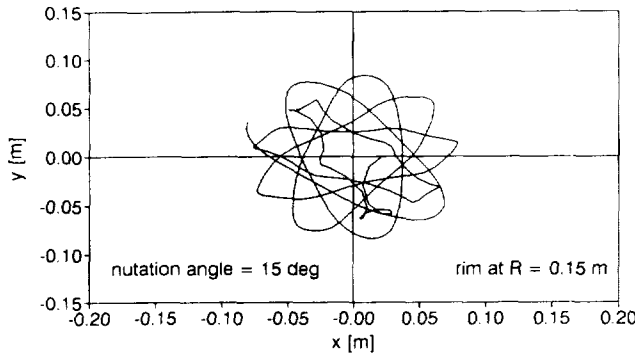


Fig. 3. Follow Force Diagram

SCALE-MODEL PRINCIPLES

Many different models have been developed to test sloshing and its effect on spacecraft. Most of these models, however, are made to simulate the sloshing of a spacecraft in which thrust is absent. One of the recent problems is that an instability evidenced by a growing nutation angle has been observed during the firing of liquid and solid perigee and apogee motors. A new model to simulate this motion was needed that properly aligns the "thrust" vector with the model axis.

A simple design of a spacecraft model mounted eccentrically on a turntable can be used. This rig simulates the thrust as a "follower" force (see Fig. 4). Previous models were subjected to gravity forces acting at the center of mass, but the new model produces a combination of gravity and inertial forces that remains aligned at all times with the vehicle axis. Hence, this thrust "follows" the model as it spins and precesses on the turntable.

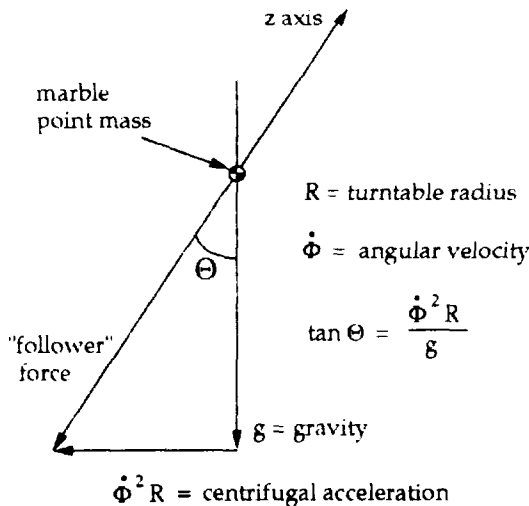


Fig. 4. Computer Code Results: Ten Second Marble Trace

Because of space and cost constraints, it is necessary to have a model that is not full scale. It must then be shown that the model behaves in the same way as the spacecraft. Therefore, it is required for the model to have the same inertia ratio as the spacecraft

$$\left[\frac{I_s}{I_p} \right]_{\text{model}} = \left[\frac{I_s}{I_p} \right]_{\text{spacecraft}}$$

It also follows that the ratio of the precession rate to the spin rate be the same in both the model and the full-scale spacecraft. To simulate the dynamics of the sloshing requires that the Froude numbers of the model and spacecraft be the same

$$\text{Froude number} \equiv \left[\frac{Rt(d\Phi/dt)^2}{g/\cos\theta} \right]_{\text{model}} = \left[\frac{Rt(d\Phi/dt)^2}{T/M} \right]_{\text{spacecraft}}$$

Solving for $(d\Phi/dt)_{\text{model}}$

$$(d\Phi/dt)_{\text{model}} = (d\Phi/dt)_{\text{spacecraft}} \sqrt{\frac{(Rt)_{\text{spacecraft}} g M}{(Rt)_{\text{model}} T \cos\theta}}$$

Using these equations, a good approximation of a thrusting spacecraft can be made in the laboratory.

MECHANICAL DESIGN

A distinct design evolution was experienced in attempting to construct a test rig that would adequately simulate the conditions present during the burn of a solid propellant rocket motor. As a preliminary experiment it was primarily designed to provide a qualitative analysis of fuel and slag sloshing and aid in the development of future experimentation.

The design problem was to simulate rotation about the rocket's own axis and the subsequent precession about an associated axis, both of which are effects of spin stabilization. It was initially agreed that dual rotating shafts were best fitted to produce the kinematics of the situation, and subsequently the design problem was limited to developing a system that would drive the two shafts with correct direction and rates of spin. In order to achieve this effect several proposals were made, the first of which entailed using a set of belts and pulleys driven by a single electric motor. Succeeding designs included such elements as a planetary gear system, a set of rubber wheels, or a set of dual motors. In the end, the initial concept of belts and pulleys was adopted for their availability and ease of use.

The rig is mounted on a half-inch-thick aluminum table, approximately 1 m square and held up by four 9-in-long aluminum legs. The main shaft is positioned vertically through the middle of the table, housed by a bearing assembly mounted to the underface of the table. This shaft is driven by a belt, connected to a variable-rpm electric motor also mounted beneath the table. To the top of the main shaft is mounted a control arm made from an aluminum T beam. On one side of the control arm is the fuel tank assembly and on the other, an equal counterweight made of lead plates.

The hemispherical bowl, turned from a lucite block, is mounted to a second shaft that rotates within the bearing housing mounted to the control arm. Positioned on the main shaft and on the bottom of the second shaft are two pulleys. The pulley on the main shaft is secured and remains stationary with respect to the table. The other pulley is secured to the second shaft and produces the rotation of the bowl about its own axis. A crossing belt connects the two pulleys, and as the main shaft rotates at an average rate of 40 rpm, the second shaft rotates twice as fast in the opposite direction. In order to keep an adequate tension in the belt, the bearing assembly housing the shaft can shift horizontally by ± 0.5 in. In addition, an idler is included on the control arm to guide the belt and maintain its tension.

During the next academic year (1990-1991) a sensor will be designed that determines the film thickness by measuring the capacitance between two platinum wires. This will hopefully provide a means to quantify the force and momentum produced by the rotating liquid in the bowl at various rpm. In order to incorporate this instrument, an electric connection to the bowl is needed through a set of slip rings in the rotating mechanism. Just below the bowl and above the bearing assembly is mounted the first slip ring, and at the bottom of the main shaft below the bearing assembly is mounted the second slip ring. To connect the wires from the control arm to the second ring, a hole is drilled down the center and through the entire length of the shaft. Through this hole the wires are run to the slip ring.

COMPUTER SIMULATION

A theoretical analysis that approximates the fluid in the bowl with a point mass was developed. The result was a system of two ordinary differential equations that can be solved numerically by Heun's method for initial value problems. A code was generated that determines the x, y, and z coordinates of a "marble" rolling around inside the bowl given a friction factor, initial starting coordinates, bowl rpm, and nutation angle. The friction factor was varied to simulate the effects of fluid viscosity and friction of the point mass. The larger the friction value, the more of a damping effect the marble exhibited. For smaller values, the marble took longer to stabilize and rose higher in the bowl (see Fig. 4). When the actual experiments begin this fall, the code can be properly validated with better estimates of the friction factor, rpm, and nutation angles necessary to demonstrate a valid theoretical model and test rig.

ACKNOWLEDGMENTS

Participating students were Oscar Alvarez, Henry Bausley, Sam Cohen, Miguel Falcon-Martin, Gary Furumoto (Group Leader), Asikin Horio, David Levitt, and Amy Walsh. Faculty were James Marcollesco, TA, and R. X. Meyer, Adjunct Professor.

54-71
P. 7²⁷

DESIGN OF A SCIENTIFIC PROBE FOR OBTAINING MARS SURFACE MATERIAL

N 91 - 18125

UNIVERSITY OF CALIFORNIA, LOS ANGELES

INTRODUCTION

Background

With the recent renewed interest in interplanetary and deep space exploratory missions, the Red Planet, Mars, which has captured people's imagination for centuries, has again become a center of attention. In the late 1960s and early 1970s, a series of Mariner missions performed fly-by investigations of the Mars surface and atmosphere. Later, in the mid 1970s, the data gathered by these earlier Mariner missions provided the basis of the much-publicized Viking missions, whose main objective was to determine the possibility of extraterrestrial life on Mars. More recently, with the dramatic changes in international politics, ambitious joint manned missions between the United States and the Soviet Union have been proposed to be launched in the early 21st century.

In light of these exciting developments, the Spacecraft Design course, which was newly established at UCLA under NASA/USRA sponsorship, has developed its curriculum around a design project: the synthesis of an unmanned martian landing probe. The students are required to conceive a preliminary design of a small spacecraft that is capable of landing at a designated site, collecting soil samples, and then returning the samples to orbit. The goal of the project is to demonstrate the feasibility of such a mission.

Mission Requirements

The detailed mission requirements are as follows:

Science objective. To collect 1.0 kg of surface material from the planet Mars for return to Earth for chemical and mineralogical analysis. The surface material is to come from the Hellas depression near Crater 29 at latitude -28.5° , longitude 283.0° .

Engineering objective. To design a Mars Surface Probe (MSP) that will descend from a Mars Orbiting Vehicle (MOV) to the surface of the planet, collect the surface material and return it to the MOV. The material can be in the form of granules obtained from drilling into the surface. The MOV with its attached MSP orbits about Mars in a circular path with the ascending node at 250° longitude, inclination angle $+30^\circ$, altitude above the Mars mean surface of 600 km. As long as the MSP remains attached to the orbiting vehicle, all housekeeping functions such as electric power supply, command and telemetry, maintenance of constant temperature, etc., are provided to the MSP by the orbiting vehicle. The nominal temperature before the MSP is separated from the MOV is 20°C .

Project Organization

The project itself was divided into four areas of specialization: mechanical design, trajectory analysis, propulsion systems, and thermal control.

The main duty of the mechanical design specialist was to develop the general physical configuration of the spacecraft. Details such as the accessibility of the components, integration of subsystems, and mass property calculations had to be taken into account. In addition, the design of the soil collection mechanism, landing gears, and parachutes (if applicable) were also part of the mechanical designer's responsibility.

The trajectory specialist's first concern was to determine the optimum path necessary to allow the MSP to leave Mars orbit and land at the designated site. Detailed calculations were also performed by numerically solving the equations of motion of the vehicle at the vicinity of the planet surface, while taking into account atmospheric resistance. The ascending trajectory was also determined to allow the rendezvous of the landing vehicle and the orbiting mother ship.

The results from the trajectory analysis were then passed on to the propulsion specialist. Given this information, the propulsion specialist was required to determine the sizes of the rocket motors necessary for orbit maneuvering, deceleration, and ascent. The process of sizing of rocket motors includes propellant selection, estimation of propellant weight, nozzle sizing and design, and grain shape design (if solid propellant rockets are selected).

The thermal control engineer was responsible for the management of energy and for the thermal environment of the spacecraft. Aeroheating during atmospheric entry, internal temperature maintenance on the martian surface, and heat dissipation of electrical components were some of the major problems. The thermal specialist had to develop schemes of insulation, select appropriate batteries as power source, and analyze the heat transfer at various stages of the mission.

RESULTS OF ANALYSIS

Mechanical Design

General configuration. The general configuration of the MSP is developed to provide structural support of the propulsion system, the instrumentation required for the mission, and to withstand the landing impact. It also serves as the launch platform for the ascent rocket, which propels the payload into the rendezvous orbit (see Fig. 1).

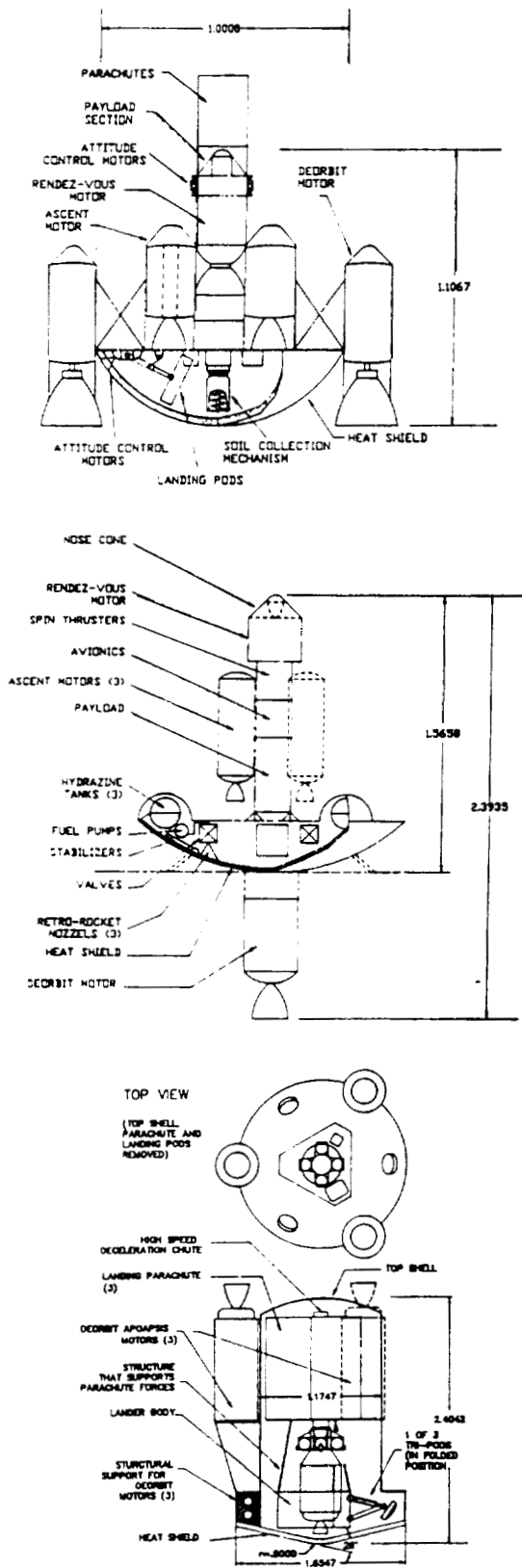


Fig. 1. Three Possible Configurations of the MSP

Vehicle deceleration system. For mechanical simplicity, parachutes are selected as the deceleration system. A high-speed deceleration chute, with a 4.52-m diameter cruciform canopy, is deployed at an altitude of 20 km. A second parachute, which has a flat circular canopy (39.4 m in diameter), is used for terminal descent. The combination of the two parachutes enables the MSP to land on the martian surface at a vertical speed of 10 m/sec.

Landing gear. Even though the MSP does not have any ultrasensitive instrumentation on board, it is still necessary to provide a reasonably soft landing to prevent possible damage to the subsystems. Collapsible aluminum honeycomb materials and oleo-pneumatic-type hydraulic shock absorbers are implemented in the landing gear/shock absorption system design for this purpose. Calculations show that this design is capable of withstanding about 8000 N, which is approximately equivalent to a load factor of 5 g (see Fig. 2).

Sample collection mechanism. The soil sample collection mechanism takes advantage of the atmosphere on Mars. The device consists of a drill, an aspirator, and a 200-W DC motor that drives both the drill and the aspirator. Dust particles generated by the drilling action are collected into the payload canister by suction, which is generated by the aspirator (see Fig. 3). The mechanism is expected to be operating for at most 15 min.

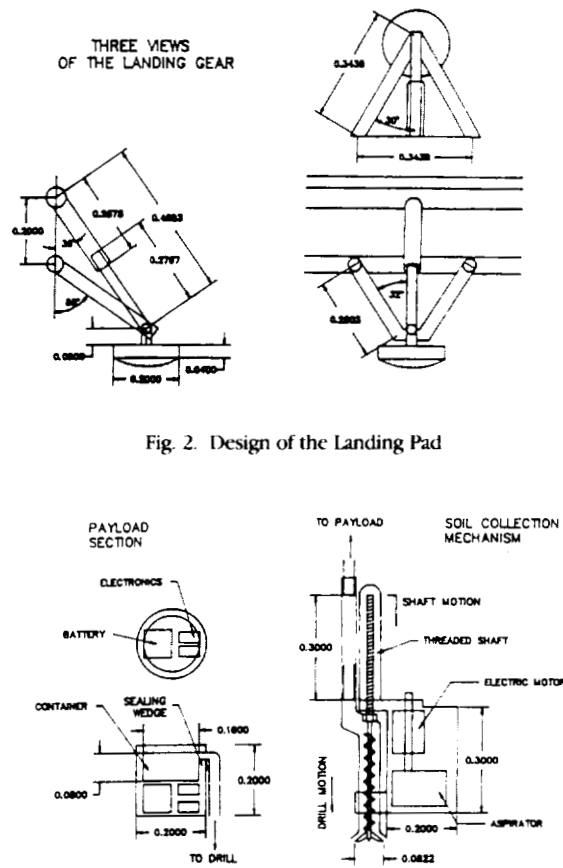


Fig. 2. Design of the Landing Pad

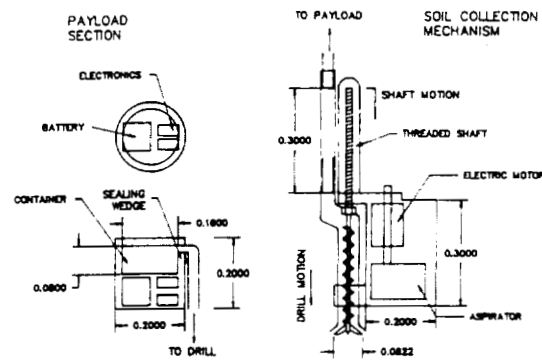


Fig. 3. The Soil Sample Collection Mechanism

Table 1. Summary of Mass Properties of the MSP

No.	Item Name	Mass (kg)	Vertical		Horizontal		Lateral	
			Arm z	Inertia Mz^2	Arm x	Inertia Mx^2	Arm y	Inertia My^2
1	Payload	10	22	4,840	0	0	0	0
2	Power supply (upper stage)	5	5	125	0	0	0	0
3	Power supply (lower stage)	2 × 10	5	250	0	0	0	0
4	Parachute System	60	54	174,960	0	0	0	0
5	Structure	40	0	0	0	0	0	0
6	Heat shield	100	26	67,600	0	0	0	0
7	Sample acquisition system*	3.6	14	706	0	0	0	0
8	Deorbit motor and fuel	4 × 28	6	4 × 1,008	16	2 × 7,168	16	2 × 7,168
9	Ascent motor and fuel	4 × 16	12	4 × 2,304	18	2 × 5,184	18	2 × 5,184
10	Rendezvous motor and fuel	1 × 4	22	1,936	0	0	0	0
	Totals (kg-cm ²)	403.6	—	263,665	—	24,704	—	24,704

*Sample acquisition system includes 1.36-kg Motov and 2.27-kg drill assembly.

MSP/MOV interface. A mechanism that allows the reattachment of the MSP and MOV at the final stage of the mission is also conceived. The design will permit a 7° angular misalignment and a 20-cm linear displacement during the rendezvous process (see Fig. 4).

Moments of inertia. The moments of inertia of each major components of the MSP are summarized in Table 1.

Trajectory Analysis

The trajectory analysis was broken down into several steps. First, an outline of the various stages of the mission was developed. Second, given the landing site, the minimum relative velocity change required and time of separation of the MSP were determined. With this information, more detailed calculations were performed, taking into account aerodynamic drag and the deceleration mechanism to determine more precisely the path for landing the spacecraft. Finally, the ascent trajectory and the ΔV required for rendezvous orbit injection were calculated in a similar fashion. The results are summarized in the following sections.

Outline of the mission scenario. Prior to trajectory analysis, the major stages of the MSP mission were identified. These stages are listed in Table 2.

Table 2. Mission Scenario

0	MSP and MOV orbit Mars
1	MSP separates from MOV, injection into descent orbit
2	De-orbit rockets jettisoned
3	Deceleration parachutes deployed
4	Terminal decent parachutes deployed
5	MSP touch down on Mars
6	MSP collects soil sample
7	The ascent rocket motor is fired
8	The ascent rocket is jettisoned
9	Rendezvous rocket firing; injection into rendezvous orbit
10	MSP/MOV rendezvous

Delta-V determination. Since the MSP and MOV are originally in a circular orbit around Mars, the MSP must be injected into a new orbit that intersects the vicinity of the designated landing site with minimum fuel consumption. However, the MSP's angle of approach must be greater than 15° because of the geological features of the surface. Given this constraint and knowing the mass of Mars and the original orbit of the MSP/MOV, both the new orbit and the minimum change in velocity required to achieve the new orbit can be determined using the equations of orbital mechanics (see Fig. 5).

Similar analysis can be performed for the ascent trajectory. The minimum change in velocity required to boost the payload to the proper altitude and injection into the rendezvous orbit were determined.

Descent trajectory. As the MSP approaches the surface, the resistance of the martian atmosphere becomes more significant. Further, the deployment of the deceleration systems affects the final stages of the trajectory greatly. Thus, the results of the previous section provide the initial condition of a more detailed trajectory calculation, taking into account various perturbations, to the ideal solution (Fig. 6). The equation to be solved is Newton's second law of motion in two dimensions; in our case, this is a system of nonlinear, second-order differential equations. These equations were solved numerically by Euler's method (Table 3).

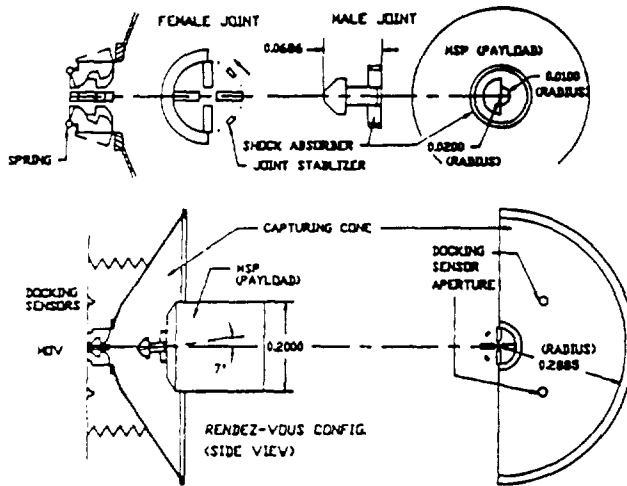


Fig. 4. MSP/MOV Interface Mechanism

ORIGINAL PAGE IS OF POOR QUALITY

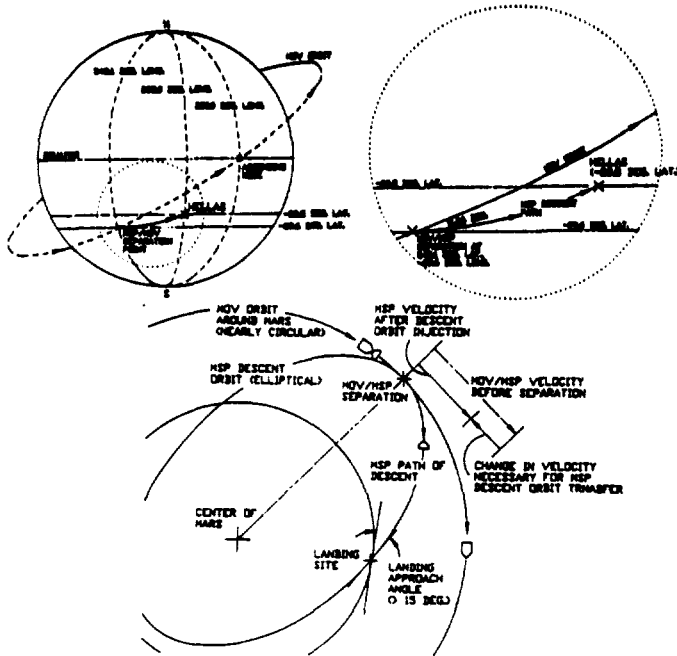


Fig. 5. Schematic Diagrams of the MSP Descent Path

Table 3. Summary of Trajectory Analysis

Separation occurs at:
 -29.6° latitude, 341.1° longitude, 600.0 km altitude

Velocity after separation:
 MOV: 3.281 km/sec
 MSP: 2.790 km/sec
 V: 795.0 m/sec

Descent elliptical orbit:
 major axis length: 3134 km
 eccentricity: 0.277

Descent Trajectory:
 range: 3372.6 km
 duration: 1524.5 sec

Time on Hellas: 57249 sec

Ascent Trajectory:
 max. velocity achieved: 3407 m/sec
 Range: 3420.1 km
 duration: 1323.5 sec
 circular orbit injection ΔV : 0.917 km/sec

Total mission time: 60096 sec = 16.69 hours

Propulsion

Based on the mission scenario and the required ΔV at various stages of the MSP mission, the types of propellant used for each of the rocket motors were selected. In addition, the size and shape of the exhaust nozzle and the requirements of the various subsystems were determined.

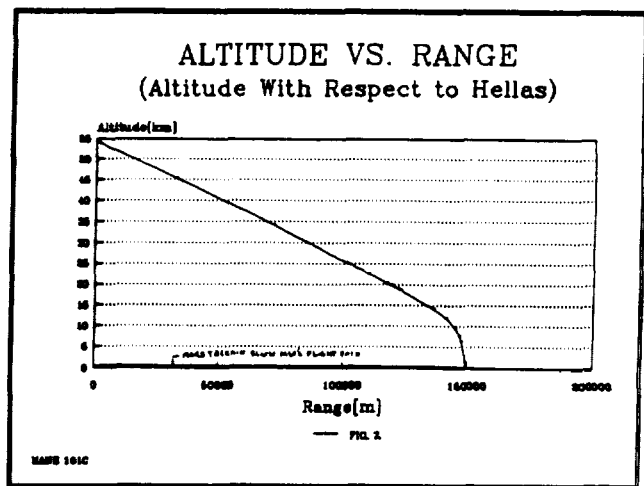
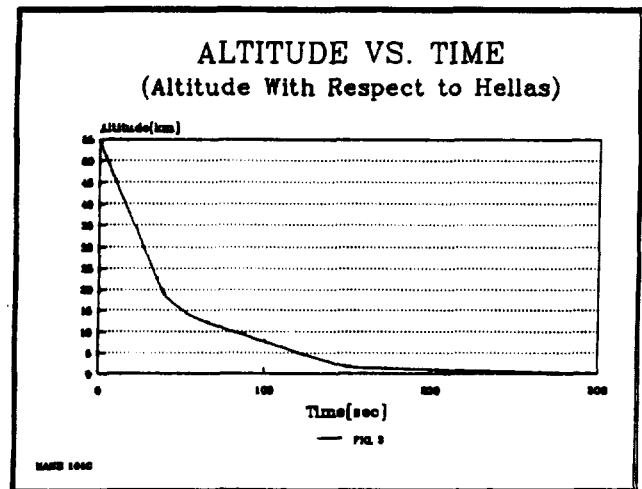
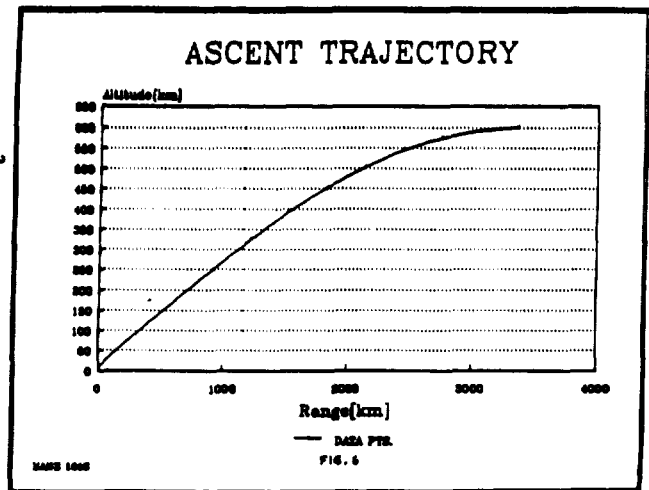


Fig. 6. Results of the Descent Trajectory Analysis

Propellant mass estimation. Given the change in velocity necessary at each stage of the mission and the estimation of total weight of the rest of the spacecraft by the mechanical designer, the propulsion specialist could estimate the mass of propellant needed. Given the mass and velocity prior to rocket firing and the final velocity, the mass expended to achieve the change can be calculated by conservation of momentum. A summary of a sample calculation is listed in Table 4.

Table 4. System Mass at Different Phases of the Mission

Event	Mass (kg)	Structure Dropped (kg)	Propellant Used (kg)
0	427.37		101.79
1	325.58	11.51	
2	230.07	60	
3	170.07		
4	170.07	93.63	
5	76.44		57.70
6	18.74	5.06	
7	13.69		3.69
8	10.00		

Rocket nozzle design. The exhaust nozzles must be carefully designed so that the performance (particularly the specific thrust) of each rocket engine can fulfill its function. For example, the ascent motor must have total thrust greater than its total weight in order to propel the payload into orbit. Ideal gas behavior is assumed throughout this analysis. The thrust force can be related to the nozzle throat area, exit area, and mass flow rate of the fuel/oxidizer mixture by 1-D compressible flow equations and thermodynamics laws. Since the exit area of the nozzle is essentially fixed by the physical size of the rocket itself, mass flow rate of the propellant and the throat area become the main variables. These variables are selected via iterative processes to yield the optimal thrust. Sample results are shown in Table 5.

Propulsion subsystems (gimbal, skin thickness, and grain design). A nozzle gimbaling scheme is also developed to maintain the stability of the ascent. For solid rocket applications, propellant grain shape is also determined to ensure an approximately constant generation of thrust in time (see Fig. 7).

Thermal Control

Thermal analysis for MSP during eclipse. When solar radiation to the MSP is blocked by the planet, the internal temperature of the spacecraft must be maintained so that temperature-sensitive instrumentation (battery, for example) will function properly. Steady-state energy conservation analysis shows that about 23 W of power is required to maintain a 20°C internal temperature.

Heat shield/aerobeating. During supersonic atmospheric entry, a large quantity of heat is generated by friction and the presence of a shock wave. Thermal analysis was performed on a graphite heat shield with thermal blankets (made of aluminized Mylar, separated by dacron mesh) on the inside of the shield. The calculation shows that the inside graphite shield will reach a temperature of 390 K. With the help of thermal blankets, the heat flux into the MSP itself will not cause any damage to the instruments.

MSP heat transfer characteristics at the martian surface. The major contributors of heat transfer during the MSP's stay on the martian surface are convective heat transfer due to winds, solar radiation, and the radiation of the martian surface (black body radiation). Analysis shows that, in order to maintain the 20°C internal temperature, 26 W is needed during daytime, and 48 W when solar radiation is absent.

Thermal environment maintenance scheme. The power requirement of the thermal control and the electrical components provides the basis for selecting a battery (Table 6). A zinc/silver battery, which is capable of an output of 28 V at 20 amp/hours, was chosen because of its superior energy density and weight among the available off-the-shelf selections.

Thermal control was achieved by an adaptive feedback-control system with heating coils and electrical grids. A block diagram of such a system is shown in Fig. 8.

Tolerable wind speed. An analysis was also performed on the maximum surface windspeed tolerated by the MSP before it tips over. Using simple but conservative assumptions about the drag coefficient of the MSP, it is shown that winds of up to 600 m/sec can be tolerated.

DISCUSSION AND CONCLUSION

Due to the time constraint of the course and shortage of test data of various components, many assumptions had to be made in the preceding analysis. Some of the more important ones are discussed in the following paragraphs.

Mechanical Design/Weight Estimate

Since a detailed structural analysis was not performed, the weights of the various structural members of the MSP were estimated based on comparison with other spacecraft with similar missions. However, conservative estimates are used throughout the process, and a large margin of safety was kept.

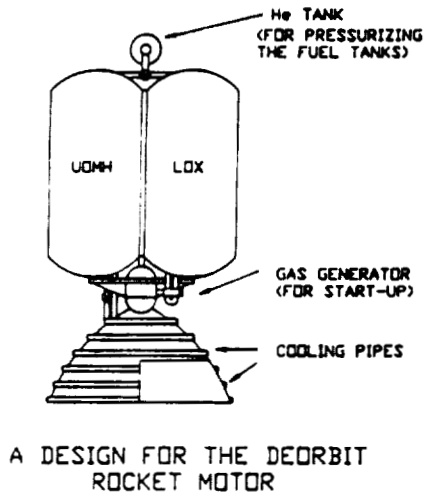
Trajectory Analysis

The actual atmospheric entry aerodynamics are quite complex, as chemical species are generated and dissociated under the intense heating of hypersonic flow speed. A more

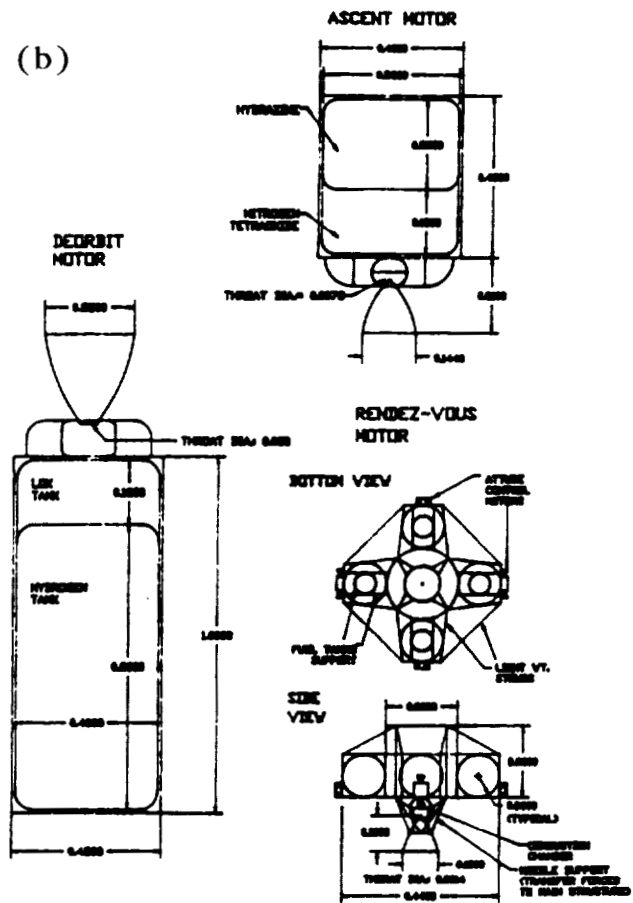
Table 5. Specifications of the Rocket Motors

Rocket Motor	Propellant Type	I_{sp} (sec)	Max. Thrust (N)	Flow Rate (kg/sec)	Throat Diameter (m)	Exit Diameter (m)
Deorbit	Liquid	298.0	3558.4	1.2	0.028	0.254
Ascent	Solid	234.3	2902.7	1.22	0.0008	0.180
Rendezvous	Liquid	298.3	1170.1	0.40	0.0146	0.188

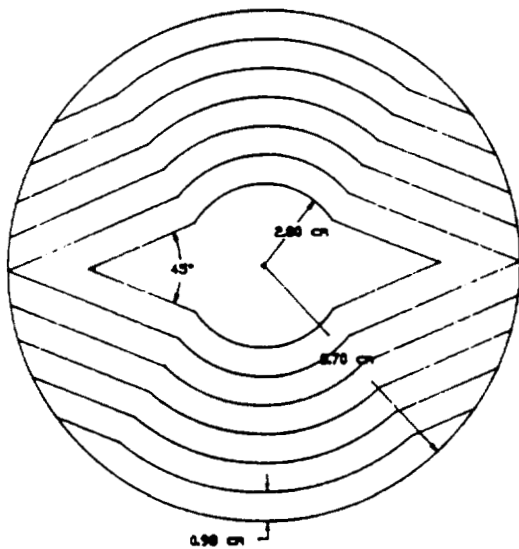
(a)



(b)



(c)



(d)

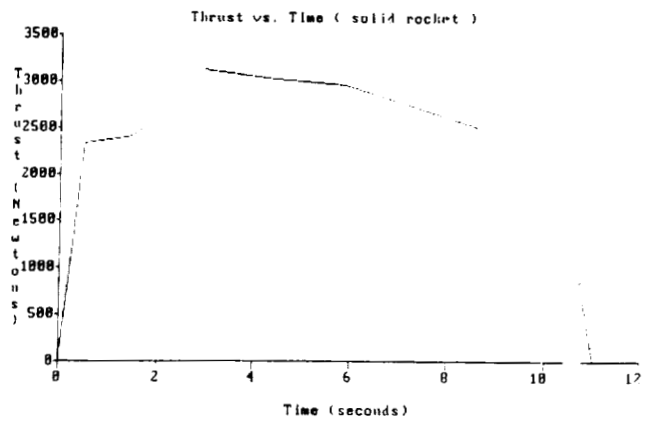


Fig. 7. (a) and (b) Dimensions of some of the rocket motors; (c) Proposed grain shape for a solid propellant rocket; (d) Thrust vs. time for the grain shape proposed in (c).

Table 6. Power Requirement and Battery Selection

Phase of Mission	Power Required to maintain at 293 K (W)	Control Power (W)	Time (min)	Energy Required (J)
Descent to 1	25.0	30	20.47	67,551
1 to 3	10.0	30	4.90	11,760
On the ground	Day: 25.76	30	490.00	1,639,340
	Night: 47.78	30	490.00	2,286,730
Drill	200.0	15		180,000
Ascent 5 to 8	12.6	30	22.00	56,236
Total Energy Required:				4,241,616
Battery Selected: EPI 4445 with 20 amp/hr at 28 V				
SZHR 7.0 with 7.0 amp/hr at 1.5 V/cell				
Total Battery Weight: 20.75 kg				

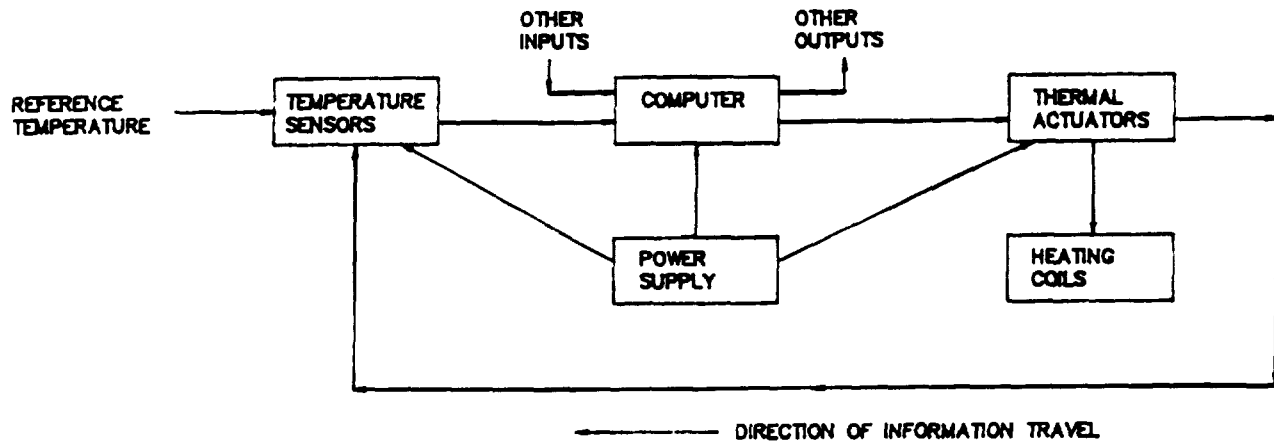


Fig. 8. A Block Diagram of the Thermal Control System

detailed computational fluid dynamics analysis could provide much better insight.

Propulsion Systems

As mentioned before, ideal gas assumptions are used throughout the analysis.

Thermal Control

In nearly all calculations performed on the MSP thermal environment, steady-state is assumed. Thus, thermal inertia and transient response of individual components of the MSP were neglected.

Conclusion

This preliminary study of an interplanetary exploration mission has shown the feasibility of such a mission. The students have learned valuable lessons about the complexity of spacecraft design, even though the mission is relatively simple.

ACKNOWLEDGMENTS

Participating students included Kevin S. Scott, James K. Dawson, Gordon M. Eichhorst, Arun J. Jain, Daniel A. Klotz, Li-Ming Lee (Report Editor), Marygrace R. Literatus, Sanjay S. Patel, Stewart G. Rydman, and Steven E. Woo. The instructor was R. X. Meyer, Adjunct Professor.

FB 13
p. 5 35

POSTLANDING OPTIMUM DESIGNS FOR THE ASSURED CREW RETURN VEHICLE

N91-18126

UNIVERSITY OF CENTRAL FLORIDA

The optimized preliminary engineering design concepts for postlanding operations of a water-landing Assured Crew Return Vehicle (ACRV) during a medical rescue mission are presented. Two ACRVs will be permanently docked to Space Station *Freedom*, fulfilling NASA's commitment to Assured Crew Return Capability in the event of an accident or illness. The optimized configuration of the ACRV is based on an Apollo command module (ACM) derivative. The scenario assumes landing a sick or injured crewmember on water with the possibility of a delayed rescue. Design emphasis is placed on four major areas. First is the design of a mechanism that provides a safe and time-critical means of removing the sick or injured crewmember from the ACRV. Support to the assisting rescue personnel is also provided. Second is the design of a system that orients and stabilizes the craft after landing so as to cause no further injury or discomfort to the already ill or injured crewmember. Third is the design of a system that provides full medical support to a sick or injured crewmember aboard the ACRV from the time of separation from the space station to rescue by recovery forces. Last is the design of a system that provides for the comfort and safety of the entire crew after splashdown up to the point of rescue. The four systems are conceptually integrated into the ACRV.

INTRODUCTION

For years, America's journey into space has demonstrated the benefits associated with working in the unique environment of microgravity. Continuing in this tradition, humans will soon launch an ambitious and far-reaching program to further the advancement of space technology. With the advent of Space Station *Freedom*, the U.S. will enter an era marked by a permanent presence in space. Moreover, the space station will allow continuous rather than intermittent operations to be conducted in orbit. The space station will open doors to many new methods of research and experimentation. Furthermore, humans will have a better opportunity to observe the Earth and forecast future trends from a vantage point only partially exploited by previous shuttle missions.

Space Station *Freedom* will eventually be permanently manned by a crew of eight. The crew will be rotated and resupplied by flights of the orbiter on an interval currently planned for three months⁽¹⁾. Due to the isolation and potentially hazardous conditions involved in space operations, NASA is committed to the policy of Assured Crew Return Capability for Space Station crews in the event: (1) a medical emergency occurs and an ill, injured, or deconditioned crewmember must be rapidly transported from the Space Station to a definitive health care facility on Earth; (2) a Space Station catastrophe forces a rapid evacuation of the crew from the station; or (3) the National Space Transportation System becomes unavailable, and an orderly evacuation of the crew from the Space Station becomes necessary. These events, or Design Reference Missions (DRMs), can be met by a concept known as the Assured Crew Return Vehicle (ACRV). Currently, NASA is considering three classes of ACRVs: water landers, runway landers, and open land, or nonrunway, landers.

The task objectives detailed in this report, will be limited to those required for a water-landing ACRV, medical and crew support subsystems, and postlanding operations. Some of the

medical and crew support subsystem designs will also support in-flight operational requirements. All designs presented follow the performance requirements and operational constraints supplied in JSC-31017 "CERV Systems Performance and Requirements Document."

DESIGN CONSIDERATIONS

The ambulatory nature of returning an ill, injured, or deconditioned crewmember back to Earth aboard a water-landing ACRV requires new technologies and operational procedures. The possibility of further injury or illness would compromise the mission. Following are general design considerations associated with the Apollo-based ACRV from the point immediately after splashdown to rescue by recovery forces.

The first major concern is providing crew egress and rescue personnel support subsystems. These subsystems include an emergency egress couch (EEC), a mechanism for removing the couch safely, and the necessary hardware for the assisting rescue personnel.

The EEC plays a vital role in the medical portion of the ACRV mission. The EEC must insure the safety of the sick or injured crewmember throughout all phases of the return mission. The design provides for the immobilization of the injured crewmember in a fully supine position from the hips up. Provisions are made to incorporate the necessary equipment in the couch to sustain the injured crewmember throughout the mission. The design insures the sick or injured crewmember is protected from the sea environment during egress.

The mechanism required to safely and quickly remove the EEC is termed the Rapid Egress System (RES). It must insure the minimum trauma removal of the sick or injured crewmember from the ACRV without endangering the rest of the

crew or rescue personnel. The RES is designed to include features that allow the couch and the injured crewmember to be safely transferred to a rescue vehicle. The design must provide the means for displacing the couch a safe distance from the ACRV.

The incorporation of a rescue personnel support (RPS) system is mandated by the necessity to provide for the safety of the rescue personnel and crewmembers. Strategic placement and accessible design of handholds, supports, and platforms used by the rescue personnel facilitates the successful manipulation of the craft and medical couch during recovery operations.

The second major concern is the proper orientation, attitude control, and stabilization systems required for the ACRV in the marine environment. Experience gained from previous Apollo water landings has shown that some sea and weather conditions cause severe discomfort to the crew. In the case of an injured crewman, this could cause further aggravation of an already existing injury, or even death. Instabilities of yaw, pitch, and roll motions of the ACRV also cause the attending crewmember to be ineffective. A more serious problem arises if the ACRV lands in an inverted position. Rescue is impossible if the craft remains in this orientation.

The objective of the ACRV orientation system is to ensure an upright postlanding orientation. ACRV vehicles may have multiple stable positions, with only one being the preferred. The Apollo craft had both Stable-1 (upright) and Stable-2 (inverted) positions during its postlanding mission phase. The Apollo landed approximately 50% of the time in the Stable-1 (preferred) position and, therefore, required a change of orientation nearly 50% of the time.

The attitude system is more than an extension of the orientation system. It provides an assisting buoyant force to counter the weight of the ACRV, which is approximately 10,000 lb. The system raises and maintains the ACRV high enough above the water to allow safe crew egress and rescue support. The planform area of the craft (the total area as seen from above) increases as it assumes the postlanding position. This increases the moment required, through wave action, to tip the ACRV over to an undesirable position. The attitude system also furnishes an area on which rescue personnel can safely work on the craft and place any necessary equipment.

The objective of the ACRV stabilization system is to provide for the stabilization and damping of the rotational and linear motions induced through sea and weather conditions. These motions are roll, pitch, and yaw for rotational motions and heave, surge, and sway for linear motions. Considering the circular symmetry of the Apollo design, roll and pitch can be considered the same motion.

The range of motion to be stabilized is characterized by the frequency of the disturbance. Vibrations due to ocean-wave excitation of a hull occur primarily at fundamental frequencies between 1 and 3 Hz. The resonant frequency of a human is approximately 2-5 Hz⁽²⁾. This places the frequency range of the disturbances within the resonance frequency range of a human, which may tend to stimulate motion sickness of the crewmembers.

The circular symmetry of the proposed ACRV presents a problem that is not encountered with typical ocean vessels. The roll in a ship only manifests itself in one direction, a plane normal to the deck. The motion of an ACRV is characterized by roll and pitch and may occur in any plane normal to the craft planform area. The stabilization systems developed for the control of ship roll only work for one direction⁽³⁾. The ACRV needs systems to dampen motions in all directions. This requirement limits the feasible choices for an effective ACRV stabilization subsystem.

The third major concern is associated with providing full medical support to an ill, injured, or deconditioned crewmember aboard the ACRV from the time of separation from the Space Station to rescue by recovery forces. While living and working on the Space Station, the astronauts will be involved in extravehicular activities and other demanding jobs. It is likely an injury may occur that requires emergency medical care available only at a hospital on Earth.

Since the ACRV must bring an injured crewmember back to Earth safely, it must be designed and equipped to handle any possible medical emergency. It must provide full medical support to a seriously ill or injured crewmember and partial support to a crewmember with minor injuries during the time period between separation from the Space Station to crew recovery on Earth.

The medical support subsystems must be as simple and easy to use as possible. In the case of an emergency, the astronauts should not spend time making the medical systems work properly. If the crew has been in space for an extended period of time, they will be deconditioned and not function well in the gravity of Earth without assistance. Another major requirement is that the medical support subsystems be capable of operating without adverse effects on other ACRV subsystems or the ACRV crew compartment and environment.

The medical equipment for the ACRV consists of the devices needed to maintain and/or monitor the crewmember's condition. The minimum medical equipment to be incorporated into the ACRV includes defibrillator/heart monitor, IV pump, ventilator, blood pressure monitor, portable suction, and blood oxygen monitor.

Since the EEC is a self-contained system, the administration, control, and removal of oxygen will be emphasized at the seat locations. The seat locations differ from the couch location in that a crewmember may need only pure oxygen administered at the seat and not require use of the EEC.

Finally, the fourth major concern is providing for the comfort and safety of the entire crew from splashdown to the time of rescue. The rescue team may not arrive at the craft for an extended period of time. Therefore, maintaining the comfort and health of the crew within the ACRV is necessary. If the ACRV and its crew must remain on the water for 24 hours, then food, water, and waste management systems need to be incorporated. An atmospheric and environmental control system to maintain a shirtsleeve environment also needs to be incorporated.

Providing a food supply for the ACRV system is important. Although humans can survive for weeks without food, ill,

injured, or deconditioned crewmembers may suffer if proper nutrition is not provided. Factors used in choosing ACRV food supply systems include shelf life, nutritional value, weight, size, taste, and system complexity.

Water is important to the crew for consumption and washing. Requirements for the amount of drinking water vary. Factors used in choosing water systems candidates are size, weight, complexity, and existence of the needed technology.

Waste management is important to the ACRV systems to provide for crew comfort and to prevent contamination. Factors used to choose the system types are weight, size, complexity, simplicity, and existence of required technology. Convenience is also considered since experience has shown that inconvenient waste elimination systems encourage the desire to avoid these systems by not eating or drinking.

The atmosphere inside the ACRV will conform to conditions present on Earth at sea level. This means the O₂-N₂ mix will be 20-80%, and the cabin pressure will be set at 14.7 psi. Systems used can be modeled after the atmosphere systems of the Skylab, space shuttle, and Hermes (European Space Plane) vehicles.

The contaminant control system removes known contaminants, odors, and CO₂ from the atmosphere aboard the ACRV. A most challenging task is the postlanding control of temperature, humidity, and ventilation. The regulation of these environmental components is a crucial factor in the success of the ACRV in the ambulatory mission.

When the craft lands, it is assumed that all avionics systems will be turned off except for a position beacon and local two-way communications equipment. The life support electronics are all solid-state low-power systems. Therefore, the initial thermal model will only include the body heat generated by a crew of two, which can be estimated using ASHRAE tables⁽⁴⁾. Body heat production is highly dependent on the activity level.

The primary problem with postlanding spacecraft temperature controls is that the mode of heat expulsion used in space will not work on the Earth's surface. The heat expulsion system in space takes advantage of the low temperature in the shade from the sun and near-vacuum air pressures. The radiators are usually mounted on the inside of the craft's skin to route the coolant fluid as close as possible to the radiative surface, the craft's outer skin. The coolant leaves the radiators and flows through the flash evaporators. When the radiators cannot expel the total heat load, the flash evaporator is activated. Cooling is accomplished by throttling liquid water to the near-vacuum pressure of space. The water boils and the steam is expelled from the craft. The latent heat of steam and the mass transfer from the craft completes the heat expulsion process.

During reentry, the radiators become less effective due to the heating of the craft's skin and the increase of the atmospheric temperature. In addition, the flash evaporator becomes less effective since the atmospheric pressure increases as the ship descends. At 100,000-ft elevation, the space cooling system becomes ineffective.

The time period of concern for this section of investigation begins when the craft has landed. However, some consideration will be given to the cooling system design for the several

minutes before landing when the space cooling system is inoperable. Although flash evaporation does not occur below 100,000 ft, it is recommended that the primary thermal control system in the atmosphere be provided with an alternative heat sink.

DESIGN SOLUTIONS

Crew Egress and Rescue Personnel Support

The design solutions associated with rapidly and safely removing a sick or injured crewmember from the ACRV and providing rescue personnel support will be addressed first. The hardware involved consists of an EEC, a mechanism to facilitate the removal of the couch, and the associated rescue support.

EEC is a specially designed couch for the ACRV medical mission and is termed the Special Purpose Couch (Fig. 1). The portion where the injured crewmember's legs reside is elevated with fully supine positioning from the hips up to aid in trauma cases. A hard cover with access ports encloses the structure providing a self-contained environment within. Provisions are made within the couch to accommodate medical equipment and data transmission devices. Material considerations ensure that the couch attains a positive buoyant nature should a mishap occur where the couch escapes into the water.

To facilitate the safe and rapid removal of the couch, the Four Link Injured Personnel Mechanism (FLIPEM) has been designed. The FLIPEM is a set of four bar linkages connected on both sides of a horizontal platform used to support the couch (Fig. 1). Once initiated, retaining latches release the

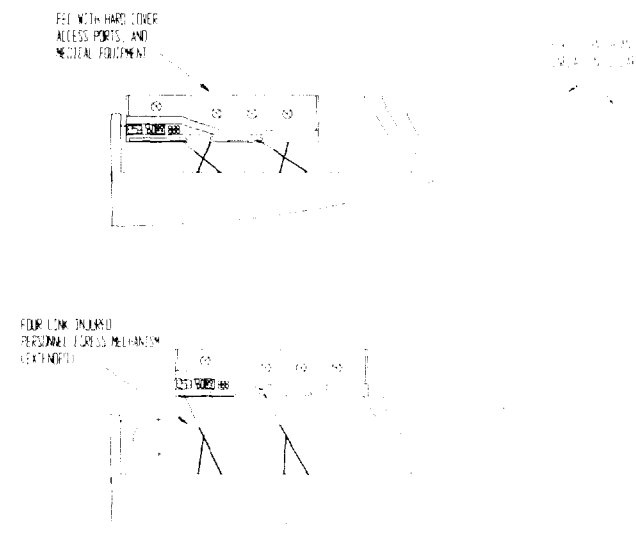


Fig. 1. Four-Link Injured Personnel Egress Mechanism and Emergency Egress Couch System

FLIPEM where nitrogen-charged piston cylinders drive the mechanism a set distance to the hatch opening. Ratchet locking systems are incorporated to prevent retraction. After removal of the couch to the rescue ships, the platform used for the couch aids the remaining crewmembers in their egress.

The rescue personnel system configuration consists of a set of handholds and footholds to provide a source of secure footing, and D-rings to provide points for safety line attachments to aid the rescue personnel. Retractable tethers are also incorporated to support both the divers and couch with a safety line for use during rough sea conditions.

Orientation, Attitude, and Stabilization Systems

The three-balloon orientation system utilized during the lunar program is chosen to attain the proper orientation of the Apollo craft after splashdown. Three 6.2-ft diameter balloons, deployed from the top of the ACRV, upright the craft and provide double redundancy in case of single balloon failure. Individual canisters, activated manually or automatically, provide the 375 cu ft of CO₂ needed for inflation.

Attitude control is accomplished by a system consisting of three multichambered segments. Each segment extends a third of the way around the perimeter of the craft. One segment of the ring resides under the egress hatch and has a 6 × 6 × 3-ft rectangular appurtenance. This appurtenance acts as a platform on which to place the couch before removal by the rescue ship, and as a platform for use by the rescue personnel. Individual canisters of CO₂ are used to inflate the rubberized woven Kevlar ring system.

The stabilization of the ACRV during adverse sea and weather conditions is accomplished by a deployable underwater parachute system. The basic premise of this system is that damping occurs through a weight force creating a moment. As the craft oscillates, the parachutes are forced to move large volumes of water. As the energy of the motion is dissipated by overcoming the inertia of the water and through shear and drag forces, the craft will be stabilized.

The parachute system is housed in the same compartment as the attitude ring system and deploys in conjunction with it. The parachutes are attached to cables that are weighted with segments of the ACRV skin. Three long cables are extended approximately six feet below the water line to avoid the wave action zone. The possibility of entanglement increases if more cables are added or their length increased.

Three additional parachute-cable systems are deployed to a depth just below the water line. These act to resist the heave and pitch motions of the craft, while the longer cables reduce the yaw and surge motions. The entire orientation, attitude, and stabilization systems can be seen in Fig. 2.

Medical Support Systems

This portion of the report addresses solutions to the partial medical support package, necessary medical equipment and monitors, and the oxygen administration and control systems. The Thomas Transport Pack was determined to be sufficient for use as the partial medical support package. This system is

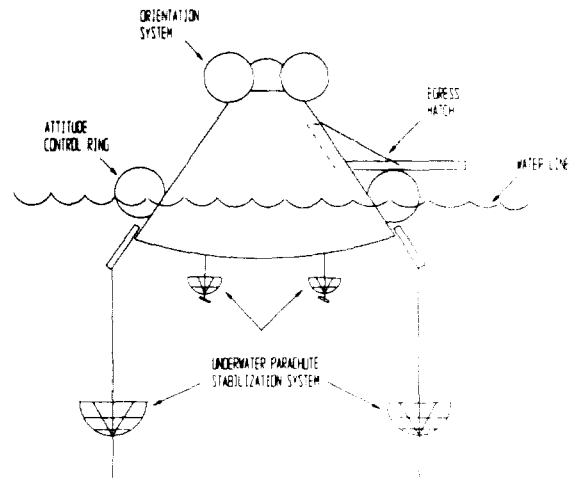


Fig. 2. Complete Orientation, Attitude, and Stabilization System

similar in configuration to the full-sized backpacks used by hikers. Currently, the Thomas Pack is employed aboard the shuttle fleet for the same type of application.

Extensive research was performed to evaluate suitable, "off-the-shelf" medical support equipment and monitors. As a result, several brand names were selected that conformed to the ACRV program requirements. Selections were also made for a defibrillator/heart monitor, IV pump, ventilator, blood pressure monitor, portable suction, and blood oxygen monitor. For all the selected equipment rubber isolators and honeycomb pads are incorporated to provide reduction to the loadings encountered during splashdown.

Each piece of equipment operates off a standard DC, 12-V source. The Apollo craft supplies both an AC and DC power source to run all flight systems. The Apollo DC source runs at a higher voltage; therefore, a modification is required to run the 12-V equipment. After the couch is removed from the FLIPEM, two 12-V Ni-Cad batteries function to supply power (for six hours) to the equipment. If all equipment is functioning the required power is approximately 80 W.

A deconditioned crewmember positioned on a normal flight couch, requiring only pure oxygen, will use a nasal cannula device to administer the oxygen. The nasal cannula is made up of one tube that separates into two tubes. The two tubes reside in the nostrils of the crewmember and are held in place by friction. The excess oxygen that is released from this system is filtered out by an air-dump device that captures the additional oxygen and expels it to the exterior of the craft or stores it in tanks.

Crew Comfort and Environmental Control Systems

Design solutions for the food, water, and waste management, atmosphere, contaminant/odor, and environmental control systems are addressed.

Food systems rely on space shuttle contingency bars for their proven application and low volume and weight. Water supply systems utilize plastic squeeze bottles for their ease of use and storage. The waste management system stems from a derivative of the Apollo-style waste bag system. Slight modifications to this system are necessary to qualify for use by both men and women.

Atmosphere and contaminant/odor control systems are derived from existing systems already in use. The atmosphere control system is based on the Skylab atmosphere system. This system uses oxygen and nitrogen tanks, stored at 3000 psi and regulated through valves, to provide the appropriate atmosphere. ACRV program requirements specify that a 14.7 psi (Skylab: 5 psi) atmosphere be maintained throughout the mission. Charcoal and lithium-hydroxide filters, used aboard the shuttle, will be used to scrub the air for odors and CO₂.

Maintaining environmental control within the ACRV throughout the mission is accomplished by flash evaporation with water above 100,000 ft and flash evaporation with ammonia below 100,000 ft. Below 100,000 ft, the primary heat source runs through an ammonia boiler system that has been pre-cooled at the space station, instead of through the radiator used in space. Though a pre-cooled system is more efficient than a non-pre-cooled system, the added complexity of interfacing with the space station coolant system will demand greater costs and design time. It is estimated that 116 lb of ammonia in a spherical tank would be required to maintain a comfortable temperature within the ACRV for a calm crew of two with no equipment (other than medical) running for a period up to 24 hours.

SUMMARY

This report addresses and provides solutions to the design considerations associated with the postlanding crew and medical support for a water landing ACRV. After splashdown has occurred, the orientation balloon system deploys, righting the ACRV (if needed) and maintaining it in the proper orientation. Then the attitude control ring is activated. The inflation of the ring forces the arms of the underwater parachute stabilization system to rotate out of their compart-

ments and deploy the parachutes. The parachutes are attached to segments of the discarded ACRV skin, which forces the tension in the cables. Six parachute-cable systems are deployed in all. Three parachute-cable assemblies drop to 6 ft under the surface of the water to control the motions of yaw and surge. The remaining assemblies drop to approximately 1 ft under the surface to control the motions of heave and pitch.

The medical support equipment and monitors will function throughout the entire mission from separation to recovery. The ammonia boiler environmental control system that is used to maintain a shirtsleeve environment inside the craft after splashdown is activated passing through 100,000 ft and functions until recovery. Food, water, and waste management systems are incorporated in case rescue is not immediate. Following hatch opening by the rescue personnel, the FLIPEM releases to deliver the medical couch to the hatch opening. The rescue personnel remove the couch along rails in the hatch and extension to a safe distance for attachment to cables used to lift the couch to the recovery ship. The remaining crew members exit using the platform left by the use of the FLIPEM.

ACKNOWLEDGMENTS

The authors of this design synopsis are Kenneth C. Hosterman, Graduate Teaching Assistant, and Professor Loren A. Anderson. Appreciation is expressed to the senior design students in Aerospace and Mechanical Engineering, who contributed to the work. A special note of appreciation is due NASA and USRA, whose sponsorship made this work possible.

REFERENCES

1. D. Herman, "Space Station Architectural Concepts and Functional Capability," *Space Applications at the Crossroads: 21st Goddard Memorial Symposium* ed. J. McElroy and E. Heacock (San Diego: Univelt, Inc., 1983) p. 257.
2. H. von Gierke and D. Goldman, "Effects of Shock and Vibration In Man," *Shock and Vibration Handbook*, 2nd ed., ed. C. Harris and C. Crede (New York: McGraw-Hill Book Company, 1976) Ch. 6, p. 23.
3. S. Blagoveshchensky, *Theory of Ship Motions*, trans. T. and L. Strelkoff under editorship of L. Landweber (New York: Dover Publications, 1962) p. 508.
4. ASHRAE Standard 55 - 1985, p. 375.

METHODS FOR THE DEVELOPMENT OF A BIOREGENERATIVE LIFE SUPPORT SYSTEM

N91-18127

UNIVERSITY OF COLORADO

INTRODUCTION

This paper is the result of a phase zero design project conducted for NASA Ames Research Center. Its goal is to establish the basis for the development of bioregenerative life support systems. This was accomplished through the specification of a comprehensive methodology that follows the process from basic research through implementation. However, before getting into the specifics of the methodology developed, a few points in understanding the driving forces of the space program being considered by NASA are necessary.

As an agency, NASA is designed to promote and embrace the fields of aerospace sciences and technologies. NASA does this by advocating and soliciting public support for its many programs. One aspect of this promotion involves outreach programs to educate students. The space program is full of imaginative possibilities that stimulate many students who may one day become scientists or engineers. Other people become advocates through sharing in NASA's achievements and the resulting national pride. Some of the most effective supporters are of course the myriad researchers, scientists, and astronauts who have performed the experiments that make up a large portion of the space program. These have added greatly to the nation's understanding of space, as well as our home planet, Earth.

Currently, NASA is undertaking the new task of the Space Exploration Initiative. This is a bold program to expand humankind's presence in space as well as to increase understanding of this unique environment. Since astronauts will be subject to this environment, it is hoped that many lessons will be learned about the way humans adapt and behave. Such fields as human physiology and psychology may be greatly enhanced. Away from Earth, the unique environment also enables specialized manufacturing for precision materials and pharmaceuticals. Applications of these technologies may then be used by industry and people on Earth, thus the benefits from the research and development in space are brought back home.

LIFE SUPPORT HISTORY

With the benefits of a manned space program in mind, the requirement to provide adequate life support measures becomes evident. Initially, manned space program efforts were concentrated on putting the first astronauts in space as quickly as possible. Consequently, the life support systems that were developed were little more than storage systems designed to supply astronauts with the minimum of air, food, and water that, once used, would be discarded or stored for return to

Earth, but not reused. For the early missions of short duration this approach was successful; yet as mission length increased, sending expendable supplies proved to be expensive. Some efforts were made to remove carbon dioxide from the cabin atmosphere with lithium-hydroxide "scrubbers." While this did not recycle carbon dioxide back into oxygen, it did extend mission duration capabilities.

Surprisingly, the technology now used on the shuttle has changed little from its predecessors on the Apollo missions. A simple projection of future requirements for a mission such as a 1000-day expedition to Mars with a crew of 10, shows that the mass of expendable supplies alone would be more than 100 metric tons. A way to resolve this problem is to utilize systems that recycle or reuse all or part of their mass.

PHYSICOCHEMICAL VS. BIOREGENERATIVE SYSTEMS

There are two basic approaches that can be taken to develop such systems: physicochemical and bioregenerative. The first of these is a system that uses physical or chemical methods to perform a particular life support task. The latter is a system that integrates physical and chemical methods to perform multiple life support tasks. In order to better understand these two approaches, we should examine their basic characteristics (see Fig. 1).

Physicochemical systems are in general more widely understood than their bioregenerative counterparts. The reason for this lies partly in the fact that most physicochemical devices are serial processors. These devices perform simple

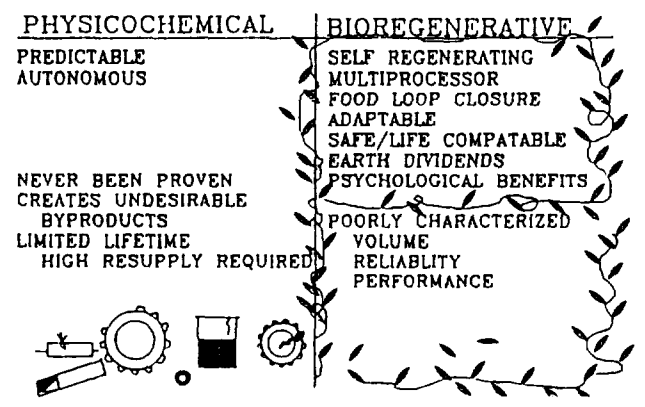


Fig. 1. Basic Characteristics

operations that are highly predictable and maintain constant performance characteristics. These systems are also relatively autonomous in that they do not necessarily rely on other systems to continue operation. However, this should not be interpreted to mean that physicochemical systems are either completely understood or better suited to space applications.

In fact, no closed physicochemical system has ever been proven on Earth or in space. Nor are all the characteristics of such a system desirable. Several components of proposed systems produce hazardous byproducts. Furthermore, because of the manmade nature of the components, repair and replacement of parts is inevitable.

Unfortunately, bioregenerative systems have been poorly understood by the engineering community. Much of the reason for this lies in the multi- or parallel-processor characteristics of living organisms. Additionally, organisms do not have constant, predictable performance characteristics; rather, they operate within a range of performance characteristics that may differ between individuals, as well as between organisms.

Interestingly enough, it is this very characteristic of wide ranges of performance that makes biological systems ideal for use in life support activities. Furthermore, as the term bioregenerative suggests, the system is always rebuilding itself. In effect, new processors are continuously available, thus minimizing the need for repair and spare parts.

Having selected a mostly bioregenerative system, one of the major characteristics to take advantage of is the similarity of the system to the system that supports life on Earth. Earth has supported life in a robust manner for millennia and the problems that are significant in the environment today might prove to be either disastrous or no more than a "hiccup" in the long term. One way of understanding these problems is the development of an independent and closely monitored model of the Earth's system. This model could be in the form of the bioregenerative system proposed.

CHARACTERIZATION

The main problem in understanding and developing bioregenerative systems is that there exists no standard, systematic way of dealing with them. At first glance, biological systems appear to be too complicated and ambiguous to be of any practical value within a standard engineering system, let alone something as crucial as a life support system. Upon closer inspection, it becomes clear that, with some initial simplifications, it is quite possible to control and manage these systems. As a starting point, it is possible to circumvent the inherent complexities of biological systems by introducing the concept of the "black box."

With this approach, any organism can be treated as a black box. As a black box, the contents and processes that occur within the organism cannot be determined through direct observation. Thus, the only way to characterize the contents of this box is through the description of the box's inputs and outputs. By characterizing only the inputs and outputs of an organism, the extremely difficult process of describing the various biological functions that occur within is avoided. As with any simplification, some degree of detail will be lost

depending on the magnitude of the simplification. Besides losing information on the internal processes of the organism, we also lose detail on the temporal aspects of the organism. It will be shown later that the information lost is either integrated at a later time or can be considered to be essentially unimportant when dealt with from a systems standpoint.

To describe the inputs and outputs, an initial breakdown into the three major categories of gases, liquids, and solids is made. This breakdown is used because, with the exception of energy inputs, it is able to handle all the input/output requirements of biological systems. It should be noted that, due to multiple inputs and outputs, this "black box" organism is not simply a serial processor but a highly integrated parallel processor.

To provide further detail the general categories of gases, liquids, and solids are each given more specific subdivisions. Gases may be broken into oxygen, carbon dioxide, and nitrogen, liquids into tissue water (water contained within the organism at time of harvest) and excreted water. Solids may be subdivided into carbohydrates, proteins, fats, nitrogen compounds, and others (vitamins, minerals, etc.). While these subdivisions were sufficient for the characterization of our organisms, other subdivisions may be required for more "exotic" organisms. The characterization of certain types of bacteria, for instance, may require the addition of a hydrocarbon input/output category.

This box can also be examined from the three different levels of a function, a process, and an operation (see Fig. 2). A function deals entirely with the nontemporal aspects of the inputs and outputs. The functional view of an organism is that, given certain inputs, the organism will produce certain outputs, without respect to time. A process, on the other hand, concerns itself with the fact that inputs and outputs occur over a timespan that is dependent upon the organism in question. Finally, the operation component takes into account the power, mass, and volume requirements that are necessary to support each organism.

There are two basic categories of organisms that can be used in the development of a bioregenerative system: plants and animals. Plants can be classified by a few general character-

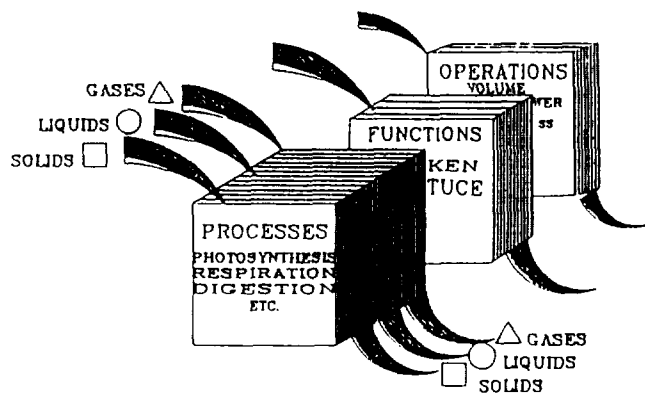


Fig. 2. Biological Characterization of Input/Output

istics: they consume carbon dioxide, water, protein, fat, and nitrogen compounds while producing oxygen and carbohydrates. Animals consume oxygen and carbohydrates while producing carbon dioxide, water, protein, fats, and nitrogen compounds. In addition, while plants store energy in a useful chemical form, animals convert chemical stores back into free energy. As a result, it can be seen that plant and animal systems are complementary when viewed from this production/consumption standpoint. The fact that plants and animals complement each other suggests the possibility of finding a correct balance of organisms whose characteristics allow for system closure.

There are three major steps required to accurately characterize the inputs and outputs of biological systems. The first, of course, is researching the appropriate sources for information concerning the inputs and outputs of these organisms. This is by no means trivial. After having gathered all relevant data, the second step is to consolidate and transfer it into a form that is both easily understood and readily applied. The next step is data comparisons that evaluate data for accuracy and establish relationships between organisms.

It is now possible to choose organisms for integration into the bioregenerative system. How much accurate data are available on each organism is primarily considered. Organisms that tend to have the most accurate and extensive amounts of information are used in agriculture and aquaculture. These organisms seem the most likely to be used in a life support system as they have been tried and tested for thousands of years. For this system, the following organisms were chosen: catfish, chickens, eggs, wheat, lettuce, potatoes, algae, bacteria, and man.

When trying to characterize the inputs and outputs of biological systems, it becomes apparent that many of the data are either inconsistent, incompatible, and/or incomplete for use in engineering. Almost all data available are based on organisms in open, 1-g systems. It is difficult to find data on inputs or outputs that are not easy to track. Exact rates of excretion and gas consumption need to be determined. For instance, how much water does a fish drink? Obviously extensive research, cross-referencing and hands-on experimentation is required. With this done, it becomes necessary to put all relevant data into a common metric.

There are a vast number of possible metrics that could be used to compare inputs and outputs (and hence find a system balance) but very few are of a form that can be readily understood and applied. After consideration of several possible metrics, it was decided to put all data into a mass (kg) format. Thus all data (water and feed consumption, carbon dioxide output through respiration, water output through transpiration, etc.) are converted to a mass value. With all inputs and outputs for each organism expressed in this common metric, it is possible to begin direct comparisons between organisms.

EVALUATION

Even though all the different inputs and outputs for each organism are defined with the same metric, it is still difficult to perform a direct comparison and evaluation between organisms. Data on organism A may state that 124 kg of mass

ELEMENTS	INPUT%	OUTPUT%	DIFFERENCE%
GASES:			
O ₂ :			
CO ₂ :			
N ₂ :			
CO :			
hydrocarbons:			
LIQUIDS:			
H ₂ O (lissue):			
H ₂ O (external):			
SOLIDS:			
carbohydrates			
protein:			
fat:			
fixed N			
compounds:			
other:			
TOTAL	100%	100%	0
	(100% is equal to 1 kg)		

Fig. 3. Data Sheet

is input and output over the lifetime of that organism. At the same time, data for organism B may state that the input/output mass is 30 kg over the course of its lifetime. Thus, it is necessary to normalize all data to its simplest form: 1 kg into the system and 1 kg out of the system.

In conjunction with the normalization of data into standard input/output units, a standardized data sheet was developed (see Fig. 3). This sheet defines the relative amount of inputs and outputs of an organism and defines them as a percentage of total output. By comparing inputs and outputs in this form it is possible to track elements the organism has a tendency to produce in surplus and those that it tends to consume or create a deficit. This data sheet allows consistent, comprehensive characterization of the inputs and outputs for any organism.

Checks on the validity and accuracy of the data must be performed. A fundamental concept in the validation of these functions is the conservation of mass. All mass going in must be accounted for in the mass output.

After having defined each organism's inputs and outputs, the organism can be treated simply as a set of transfer functions (see Fig. 4). A certain mass is input and the resulting output

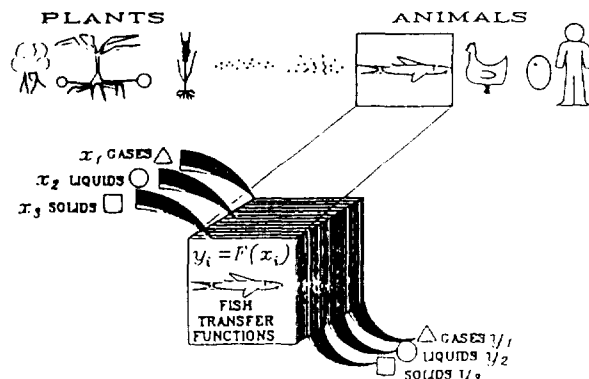


Fig. 4. Transfer Functions

of the substance is determined by the organism transfer function. Thus every biological system within the CELSS can be interpreted as a prepackaged set of transfer functions. Now these organisms can be handled using well understood control systems methods rather than from less understood (for the average engineer) biological approaches.

INTEGRATION

Now that any organism can be treated as a transfer function, it is possible to integrate multiple organisms into a closed system. Integration refers to the use of an organism's outputs as the inputs for any number of other organisms and thus input requirements can be balanced with output production.

As an example we will consider two ideal organisms in a closed system, the first of which (organism A) has a characteristic pattern of inputs and outputs given by its transfer functions. If we take a second organism (organism B) that is entirely complementary in terms of its inputs and outputs to organism A, it becomes possible to match inputs to outputs between the organisms and achieve a mass balance. If organism B has three times the amount of inputs and outputs (in kg) as compared to organism A, a mass balance can be achieved by creating a system composed of three organism As and a single organism B.

Since the organisms being dealt with are not ideal, it is nearly a given that after matching inputs and outputs, there will be some amount of mass left over (surplus) or still required (deficit), without which a perfect balance will not be attainable.

For our system, the nine previously mentioned organisms were integrated with a spreadsheet program (see Fig. 5). By summing the amounts of production (+) and consumption (-) of any single element across all nine organisms, it is possible to determine whether there is an overall surplus or deficit of this element. After determining the total surplus or deficit of each element, the absolute values of each of these quantities are summed to find a total system error or mass mismatch.

Although it appears that the mass mismatch within each element would cause a complete system failure, in actuality, this is not the case. Manmade physical systems are designed with singular, discrete performance characteristics. A car has a specific minimum turning radius, a plane has a maximum rate of climb, and a microwave oven requires a specific energy input. Both the inputs and outputs of these physical systems are specific, essentially nonvarying values, and a mismatch of inputs or outputs to these physical systems is unacceptable.

Biological systems, on the other hand, have a range of performance characteristics. Through training, an individual can improve his or her performance in a specific activity (time to run the 40-yard dash, for instance) by a significant percentage. As another example, nutritional inputs to a person can be varied through a remarkable range with little or no serious effects. Thus, for biological systems, mass mismatch does not render the system unfeasible because of its adaptability or range of performance characteristics. Biological organisms have an innate flexibility and robust quality that is normally not found in physical systems; hence, biological systems have their own inherent "safety net" that is different

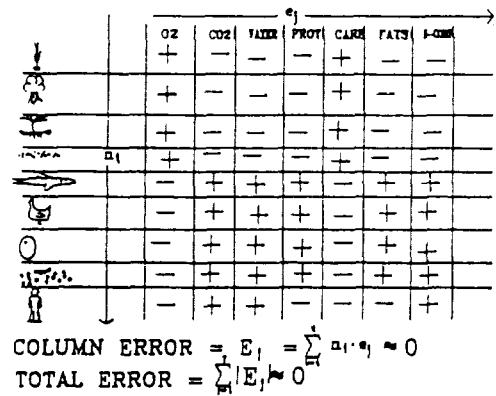


Fig. 5. System Mass Balance

from physicochemical systems (see Fig. 6). Through inherent control mechanisms and ranges of performance organisms are effectively self-regulating. If the carbon dioxide input into a plant is slightly reduced, for instance, the plant does not die but merely adapts to the new condition. It may not grow as quickly or as large, but it will live. Thus the attributes that make organisms difficult to work with (range of performance characteristics, etc.) are the same attributes that make biological systems worthwhile.

PROCESS DESCRIPTION

Any process takes place over time. This is certainly true for organic "devices" such as a plant or animal. For example, the time to maturity for lettuce is 30 days. Wheat and potatoes take 80 days. Single-celled organisms such as algae and bacteria have very short doubling times of 4 hours and 2 days, respectively. Animals, however, have longer times; chickens take 120 days and catfish, 180. Eggs, a special case in that they are produced by another organism, are laid daily (see Fig. 7).

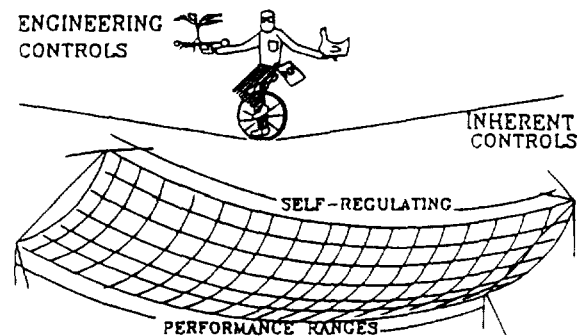


Fig. 6. Safety Net

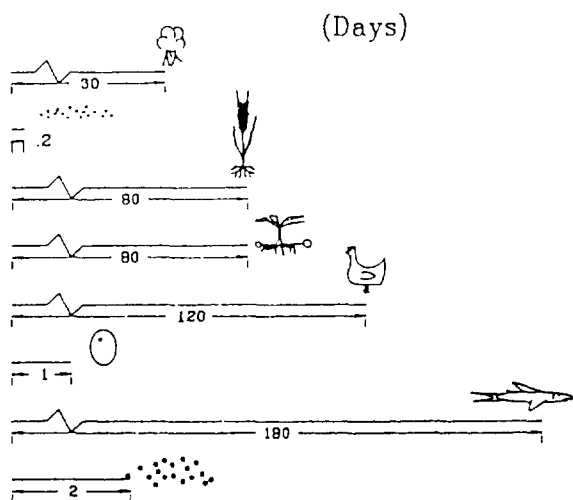


Fig. 7. Time to Maturity, Days

Each of the organisms selected, all of which are multiprocessors, also has an associated growth curve that dictates its performance characteristics over time. This curve can be used to determine the flow rates of inputs and outputs over time. All input flow rates are thus directly proportional to the organism's mass. So too, all outputs, with the exception of the tissue of the organism itself, will be directly proportional. The remainder of the outputs, in the form of the tissue mass, will manifest itself as a spike in the output portion of the performance curve (see Fig. 8).

It is possible to integrate the mass balance over time. To do this in terms of supporting one human per day, the scalar for human input/output data must be multiplied to account for the average inputs and outputs of one human on a daily basis. This factor must then be used to multiply the scale factors of the other organisms. These modified scale factors are the number of organisms produced daily to achieve the desired balance. Based on these calculations, an example of a system balance to support one human per day was achieved (see Fig. 9).

Within this process description it is of great importance to have a sound understanding that the resultant configuration is dependant upon the time characteristics of each organism. In other words, further multiplication of the system balance figures by each organism's respective time to maturity will determine the number of organisms on average that must be growing at any one time. With this understanding one can then begin the operation and implementation phase.

OPERATION AND IMPLEMENTATION

After achieving a mass balance, based on transfer functions and the integration, the next step is to determine the possible configurations that could support such a balance. In so doing, one should examine the implications of performance characteristics; mass, volume, and power requirements; and the sensitivity of the overall system.

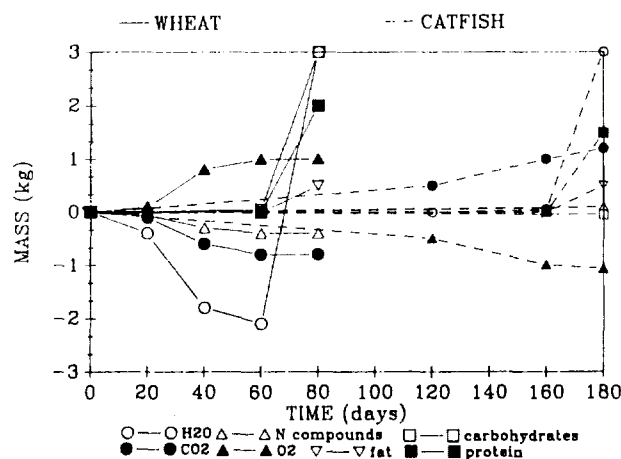


Fig. 8. Performance Curves for Wheat and Catfish: Surplus and Deficit of Throughput Elements

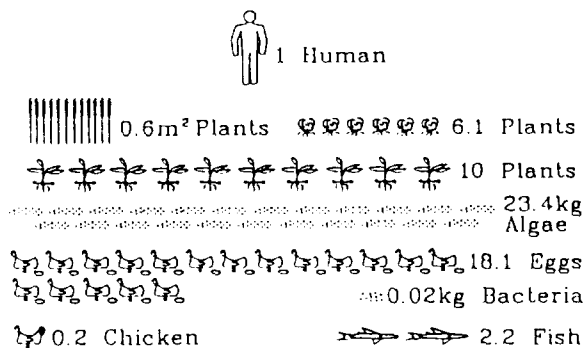


Fig. 9. System Balance to Support One Human per Day

To understand the overall performance characteristics of the system the performance curves may be integrated with the system balance to understand the fluctuations in surpluses and deficits that occur for the whole system over time. This is accomplished by the superposition of the curves based on the organisms' performance scaled to the number achieved in the system balance and their subsequent summation to create a system performance curve. It is important to note that this curve will be a reflection of whether a continuous production system or a batched system is chosen, and that it is based on single design points, while the system operates in a range of characteristics (or points). Thus, a large portion of these surpluses and deficits will be absorbed by the organisms due to adaptive responses in their performance. This feature of performance flexibility can be thought of as an inherent buffer on the system. As long as the surplus or deficit for each element remains within the buffer zone for the continued function of the organisms, the system will support itself. It is also possible to accommodate a larger surplus or deficit

through the use of additional buffers in the form of storage systems. A thorough understanding of both inherent and additional buffers will increase the range of possible configurations.

Once the system performance curves have been determined, the next step is to consider operational parameters. As with physicochemical systems, bioregenerative systems have certain characteristics in terms of system mass, power, and volume. With the system balance, it is possible to determine the overall system values for these parameters by multiplying the number of each type of organism in existence at one time by that type of organism's respective mass, power, and volume requirements on a per organism basis. The values for all organisms are then summed to reach the system mass, power, and volume requirements. These values should be inclusive of all support requirements such as lighting, circulation, pumping, ventilation, growing space, and structural materials. However, in the category of power requirements, creative phasing between batches and between organism type may reduce the load on the power system at any given time and should be carefully examined.

Definition of operational parameters will then lead to the tradeoff analysis. This phase weighs the degree of closure achieved in the mass balance against the requirements for system mass, power, and volume. At this point it may become obvious that certain aspects of the system are unacceptable for mission requirements (see Fig. 10).

An example might be that the mass to support one organism might be heavier than the mission's launch capabilities. If this is the case, several options are available. One is to rescale the mass and system balance to achieve a smaller system mass while accepting the subsequent decline in system closure. Should this be the outcome, provisions for extra supplies or physicochemical supplementation of the biological components could be made. The decline in closure may not occur, however, if the resulting performance remains within the inherent buffer zone and no additional adjustments are necessary. Another option to reduce system mass is to replace the organism in question with one that has more favorable characteristics. This will likely require extensive research to attain sufficient data on the organism, which must be considered before choosing this option. A point of interest here, is that when attempting these adjustments, the results are often counterintuitive. Thus the aid of computer modeling is essential for ease of performing tradeoff studies.

The final aspect of the tradeoff study is to perform a sensitivity analysis. This should be done for both minor perturbations, such as a decreased power supply, introduction of pathogens, or the removal of humans, to catastrophic failures of subsystems such as the elimination of one or several species of organism. The results should be weighed and further iterations may be required. On the other hand, it is likely that the system will prove sufficiently robust, requiring no adjustments.

CONCLUSION

What is presented here is a rudimentary approach to designing a life support system based on the utilization of plants and animals. The biggest stumbling block in the initial phases of developing a bioregenerative life support system is encountered in collecting and consolidating the data. If a database existed for the systems engineer so that he or she may have accurate data and a better understanding of biological systems in engineering terms, then the design process would be simplified. Also addressed is a means of evaluating the subsystems chosen. These subsystems are unified into a common metric, kilograms of mass, and normalized in relation to the throughput of a few basic elements.

The initial integration of these subsystems is based on input/output masses and eventually balanced to a point of operation within the inherent performance ranges of the organisms chosen. At this point, it becomes necessary to go beyond the simplifying assumptions of simple mass relationships and further define for each organism the processes used to manipulate the throughput matter. Mainly considered here is the fact that these organisms perform input/output functions on differing timescales, thus establishing the need for buffer volumes or appropriate subsystem phasing. At each point in a systematic design it is necessary to disturb the system and discern its sensitivity to the disturbance. This can be done either through the introduction of a catastrophic failure or by applying a small perturbation to a the system. One example is increasing the crew size. Here the wide range of performance characteristics once again shows that biological systems have an inherent advantage in responding to systemic perturbations.

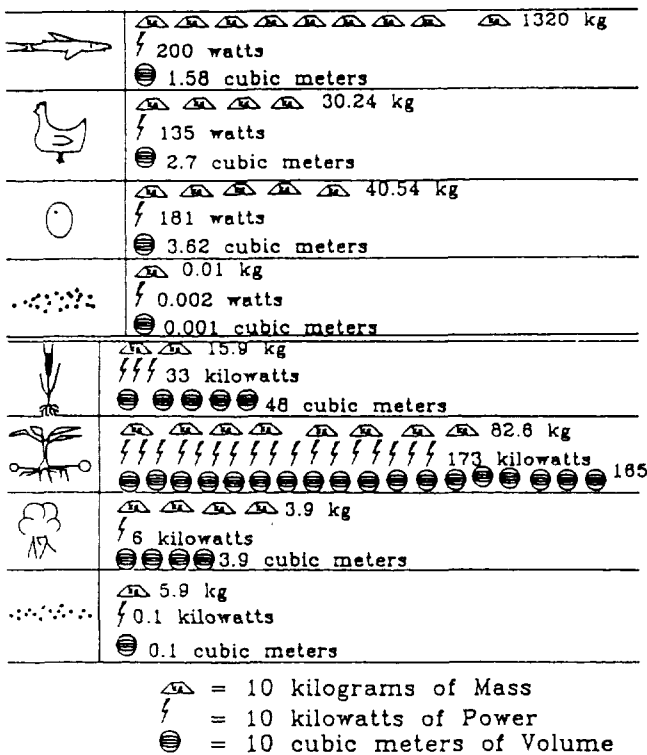


Fig. 10. Operational Parameters

Since the design of any space-based system depends on mass, power, and volume requirements, each subsystem must be evaluated in these terms. While one system, such as the catfish, proved itself to be mass (including support hardware) intensive, another system, the potatoes, proved itself to be power intensive. The ultimate design of a closed life support system will balance these criteria (mass, power, volume, closure, etc.) through the use of appropriate weighting factors based on mission constraints. This is an iterative process that also weighs these system design criteria against the system mass balance until all requirements are satisfied. These requirements are satisfied because bioregenerative systems operate within characteristic ranges. The mass balance is considered throughout the design process because this balance insures the closure of the system.

Phasing is another issue that must be addressed. Some systems are more suited for continuous harvest (daily egg collection), while for others, batch harvesting will be preferred (catfish or wheat). Storage facilities may be required to store system outputs to ensure the availability of needed inputs.

Since this is only a rudimentary analysis of a complex system, many other critical issues were not analyzed. Examples of these are labor requirements and the integration of bioregenerative with physicochemical systems. What has been shown, though, is that developing a bioregenerative system is possible from the design engineer's perspective once the approach has been adequately defined. Indeed, implementation can begin presently, and must do so in order to be utilized for the Space Station, the Moon, or eventually, Mars.

RECOMMENDATIONS

As was mentioned earlier, the compilation and consolidation of information on biological systems was a major obstacle to overcome. This obstacle could be minimized if a centralized

database with information on biological organisms were in place. This information might exist, but often in places or forms which are unusable to the systems engineer.

Another related problem is that a significant amount of data on closed and well-monitored systems does not exist. Research and development of these systems is within our reach today and is not only of significance to NASA and the space program but to other entities, such as the planet Earth.

While bioregenerative-based systems are complex, their development is not unattainable or unreasonable. The basic methodology that has been provided has several steps, and in order to make a bioregenerative system a reality, one of the safest and most comprehensive ways would be to utilize each of these steps, coupled with support activities such as experimentation, modeling, and testing. With such a program, closed bioregenerative life support systems will soon be a reality, and manned missions to Mars will become feasible through self-reliance and less dependence on Earth resources.

ACKNOWLEDGMENTS

Special thanks to the students of the Space Habitation classes, Steve Johnson and Alex Hoehn, TAs, Dr. Marvin Luttgies, and NASA/USRA. This paper was prepared by Michelle Goldman, Shawn Gomez, and Mike Voorhees. We thank Dr. Robert MacElroy and Dr. Mark Kliss of NASA ARC for support.

7-24
2007
p. 4⁴⁹

IMPLEMENTATION OF SENSOR AND CONTROL DESIGNS FOR BIOREGENERATIVE SYSTEMS

UNIVERSITY OF FLORIDA

N91-18128

The EGM 4000/4001 Engineering Design class is an interdisciplinary design course that allows students to experience the design process. The projects involved the design of sensors and subsystems of a closed-loop life support system (CLSS) with special emphasis on the Controlled Ecological Life Support System (CELSS) currently being developed at Kennedy Space Center (KSC) by NASA. This year's class comprised students majoring in Engineering Science, Aerospace Engineering, Agricultural Engineering, Mechanical Engineering, and Computer and Information Sciences. Consequently, the projects received support from students with many different interests and areas of expertise.

To understand the work performed by the students, one must understand the purpose and concept of a CLSS system. In the years to come, NASA will be constructing Moon bases and sending astronauts to other worlds on extended space missions. In order to support the crews, unreasonably large quantities of supplies would have to be sent from Earth. These supplies would be difficult to transport and require large holds. To remedy this problem, NASA plans to incorporate crops into the spacecraft. These crops would supply food for the crews, as well as provide beneficial psychological side effects. In addition, the plants would recycle the air and human waste and provide oxygen and water for the humans.

The students in the design class were to work on supporting this project. In order to do this successfully, the course was separated into two phases. The first semester involved studying the various aspects of a CLSS to determine sensing needs and develop ideas. The second semester involved first determining which of the ideas were most promising. Specific sensors were then designed and tested under laboratory conditions with promising results. Finally, recommendations for further development were proposed.

CLSS REQUIREMENTS

Since an operational CLSS system would incorporate many different engineering and scientific disciplines, the class was divided into subgroups that would study the different areas of the system. The five areas of concentration were atmosphere and temperature control, nutrient delivery systems, plant health, plant propagation, and solids processing. The group investigating atmosphere and temperature control focused on the temperature distribution within the growth chamber as

well as the possibility for sensing other parameters such as gas concentration, pressure, and humidity. The Nutrient Delivery Group investigated the sensing needs for monitoring the solution level in a porous membrane material and the requirements for measuring the mass flow rate in the delivery system. The Plant Health Group examined the causes and symptoms of plant disease and explored the various techniques for sensing these health indicators. The group investigating sensing needs for plant propagation and support focused on monitoring seed viability and measuring seed moisture content as well as defining the requirements for drying and storing the seeds. The Solids Processing Group covered the areas of harvesting, food processing, and resource recycling, with a main focus on the sensing possibilities for regulating the recycling process.

Atmosphere and Temperature Control

This group determined that one possible sensor is a relative humidity sensor that incorporates fiber optics. Another promising area is temperature or gas profiling of a growth chamber. This could provide needed information on the temperature gradients, as well as the gas flows within a chamber. This information would allow the determination of the ideal location for the various sensors that would be incorporated within the chamber.

Nutrient Delivery

This group found a crucial need for a wetness sensor that would determine the wetness of a porous medium on which the plants would be growing. This is an area of great importance since a saturated medium could cause the roots to rot, and a dry medium could destroy the plants. Consequently, a wetness sensor was proposed for semester two.

Plant Health

The sensing need found by this group was obviously a plant health sensor. Therefore, the majority of the work conducted was directed toward disease symptoms and available sensing technologies. The technologies studied included both destructive and nondestructive techniques including Mossbauer spectroscopy, fluorescence spectroscopy, visual imaging,

PRECEDING PAGE BLANK NOT FILMED

ORIGINAL PAGE IS
OF POOR QUALITY

PAGE 48 INTENTIONALLY BLANK

nuclear magnetic resonance, and various others. Also, expert systems were studied to help control the sensor system to be developed.

Plant Propagation

This group studied seed quality testing, seed moisture sensing, seed drying, and seed storage. Quality is important in order to insure that the seeds will germinate. The moisture content is critical to prevent rotting of the stored seeds and growth of fungi. Seed drying and storage techniques must be developed to minimize damage to the seeds.

Resource Recycling

This group concentrated mainly on recycling the byproducts of a CLLSS. This included harvesting, food processing, and waste recycling. The most promising projects were determined to be harvesting and food processing. These systems would need to be automated to relieve the crew from tedious work and allow them to concentrate on matters more directly associated with the mission.

CLLSS DEVELOPMENT

Based on the studies conducted during the first semester, the class proposed various projects for development. These were rated and compared to determine which were most needed and feasible. This resulted in the selection of a seed moisture content sensor using infrared diffuse reflectance, a porous medium wetness sensor, a plant health sensor using infrared digital imaging, and a controlling system for a robot arm and the plant health sensor using neural networks.

Seed Moisture Content

Moisture content of soybean seeds was chosen as the property that could best be sensed for three reasons: (1) the test is nondestructive to the seeds; (2) the process of varying moisture content in the seeds for testing purposes is a simple procedure; and (3) the method is easily automated. A moisture content sensor is important in a CLLSS for several applications. If the device could be constructed to sense the moisture of seeds or seed pods while they were still attached to the plant, the optimum harvest time may be determined. If not used to determine harvest time, a moisture content sensor could be used to determine whether a seed batch is retained for storage and replanting or sent to food processing, based on extremes in moisture content. Seeds too high in moisture may cause problems in storage as they are conducive to growth of mold and fungi and are more susceptible to mechanical damage during harvesting and handling. Seed batches of low-percent moisture may have dried on the plant too long, reducing their vigor and storage life. The measurement of seed moisture content may also be instrumental in controlling the drying times of seed batches before storage.

The concept of using infrared reflectance as a means to determine the moisture content of a seed batch is a technique based on the property of water to absorb certain wavelengths

in the infrared spectrum. The band most widely used in on-line moisture determination is the 1.94- μm band within the infrared spectrum. Because light rays that interact with a rough surface are scattered, the best method of sensing absorption properties is by diffuse reflectance.

In the design of this sensor system, two filters must be used—one that passes a water absorption band and another that passes a reference wavelength. The passed wavelengths interact with the surface of the seed sample producing a reflectance inversely proportional to the amount of infrared energy absorbed. Collecting the reflected energy and focusing it on a detector produces a corresponding voltage output. The signal produced by the detector for each filter is recorded, and the ratio of the two reflectances is recorded. The two filters chosen were a 1.8- μm reference filter and a 1.94- μm bandpass filter. The detector type is lead sulfide, which is capable of detecting both wavelengths of interest for the system.

Seed batches of 250 g were prepared for testing. Oven drying, microwaving, and sun baking created seed samples of relatively low moisture content (approximately 6%). To obtain high moisture contents, seed batches were soaked in liquid water for different time intervals to achieve samples ranging from 20-35% moisture. The moisture content of each 250-g batch was then measured by a Burrows Model 700 digital moisture meter and the values were used as the basis for test validation. The final tests performed under the optimal conditions resulted in reflectance measurements of seed samples that successfully differentiated between batches of different moisture contents.

Porous Medium Wetness

In order to maintain an efficient nutrient delivery system in a CLLSS, the ability to monitor the amount of nutrient solution available to a plant through the porous medium is necessary. The most important factor in plant growth and productivity is soil water, which controls the uptake of most of the nutrients required for plant growth. Nutrient uptake of a crop varies throughout the crop season, as well as daily. Monitoring the wetness of the porous plate will provide data necessary to help control the amount of nutrient solution available to the plants throughout their growth cycle. This control can help to maintain healthy plants, prevent leakage to the CLLSS atmosphere due to excess solution in the medium, and prevent air from entering into the delivery system due to a lack of solution in the medium.

The degree of wetness pertains to the relative concentration of water in a porous body, independent of the body size. Two sensing methods were developed for monitoring the wetness of the porous medium; one that uses infrared reflectance and one based on heat dissipation. The infrared technique is similar to the approach used by the Seed Moisture Content Group. This technique is especially suited to sensing porous plate wetness since it measures surface moisture. The thermal technique was developed to exploit the fact that the thermal properties of water differ quite significantly from those of air or ceramics. The technique of measuring heat dissipation to

sense the degree of wetness in the porous medium is based on the fact that the rate of heat dissipation in a porous medium of low conductivity is sensitive to water content. As the water decreases, a larger temperature gradient is needed to dissipate a given quantity of heat. The wetness of the porous medium can be correlated with the temperature gradients measured by the sensor for a given heat dissipation. These techniques allowed the wetness trend within the plates to be determined, though the exact moisture content was not quantified.

Plant Health Sensing

In order to maintain an extended space mission, it may be necessary to grow crops to support the astronauts physically and psychologically. The plants should be grown efficiently, with minimal interaction with the crew. This requires a number of automated systems to care for the crops. One such system should be able to monitor the health of the plants. This could be accomplished using three different levels. The first of these levels would consist of a primary health sensor that could scan the entire crop in order to identify trouble areas. The secondary sensor would be able to examine a trouble area more in-depth to specify the location and extent of damage. Finally, the tertiary system would be able to analyze the trouble area for a specific cause and a possible solution for the problem. The primary and secondary sensors would be noninvasive, while the tertiary sensor may be destructive; however, the extent of the destruction could be minimized by the information gathered by the secondary system.

This project centers upon the design and fabrication of a primary sensor system. To sense the plant health, various factors may be examined. In this case, the amount of chlorophyll located in the plant tissue provided a direct correlation to plant health. It may be seen that health decreases as the chlorophyll concentration decreases. This may be readily seen in chlorotic and necrotic tissue. Chlorotic tissue shows a deficiency in chlorophyll through a yellowing of the tissue. Necrotic tissue is dead tissue, which is brown and dry in appearance.

Chlorophyll is detected through the use of IR radiation absorption. Absorption is measured through the use of a digitizing camera system. Light is reflected off the leaf and collected by the camera. The light is first passed through a bandpass filter in order to pass a wavelength of 671 nm, which corresponds to the peak absorption of *chlorophyll-a*. As the amount of chlorophyll decreases, the amount of 671-nm light reflected will increase. This will be observed by the camera and recorded by a computer within an array of integers. This array represents the light intensities located within an image. Each number in the array represents a grey level and as the numbers increase, the intensity of light increases. Using the 671-nm filter to analyze the chlorophyll content of the plant tissue, it was possible to obtain data that clearly displayed unhealthy regions on the leaf.

Neural Networks

The main purpose of this project is to try to adapt neural network theory to CLLSS applications, or more specifically, to plant health. In order to do this, sequential programs are used

to simulate the parallel distributed processing of a neural network. This project was separated into two phases. The first consisted of using neural networks to control a robot arm. The second consisted of using neural networks to determine the health status of a plant based on the data accumulated by the Plant Health Group.

The robot arm was to be trained to grasp an object. This object was assumed to be the stem of a soybean plant approximately 2 in above the growing surface. The first preliminary step was to design and train a network to transform two-dimensional Cartesian coordinates to polar coordinates. Networks for polar-to-Cartesian coordinate transformations were also developed. Therefore, coordinates could be entered in either form. The team found that by giving the network more information by increasing the number of input elements, the network's ability to generalize was enhanced.

Phase two of the project involved using neural network techniques to determine the state of health of a plant leaf in an automated fashion. The goal was to develop a program that would read in a file containing data on the infrared reflectance of a leaf and prepare the data for use by a neural network that would be trained to distinguish between a healthy and a sick leaf. Although the neural network was trained on a very limited number of unhealthy conditions, the purpose was to demonstrate the feasibility of the process.

The Plant Health Group provided 28 usable images. All the images were taken in one sitting, so the lighting intensity was constant. Twelve of the leaves appeared healthy, and 16 appeared unhealthy. The Plant Health Group looked at a color graphic computer display of each leaf that was consistent with the leaf's visual appearance. One of the apparently healthy leaves, however, showed a spot of some kind and was thus graded as suspicious. Arbitrary values were then assigned to each category of leaf. Healthy leaves were assigned 0.9, and unhealthy leaves were assigned 0.1. The suspicious leaf was not assigned a value. A training set was created, consisting of 8 healthy leaves and 12 unhealthy ones. The other eight leaves, including the suspicious one, were saved for testing. After training, the network output values were within about 0.001 of the expected values for the training set.

For the test set, every leaf, except for two, was graded by the network to within 0.017 of the expected value based on visual classification. Of the other two, one which had been visually graded unhealthy was graded by the network at 0.761 and thus labeled suspicious. Visually, this leaf was healthy looking except for a brown edge. The other leaf, which had been visually classified as suspicious, was assigned a value of 0.898 by the network, which was considered reasonable.

CONCLUSION

In conclusion, all the design projects were at least partially successful in producing a working prototype. Further work is recommended as follows: The Seed Moisture Content Group recommends that the system developed should be interfaced with a computer and integrated with fiber optic technology

to further enhance the system. Also, infrared-light-emitting diodes could be used in order to eliminate the need for fragile filters. Currently, several members of the Porous Medium Wetness Group are designing a self-contained unit that will be flown on a KC-135 microgravity flight to further test the

sensor. The Plant Health Group recommends continued development of the project by incorporating three-dimensional analysis and background distinction into the health sensor. Neural networks could be designed to distinguish the edge effects and the three-dimensional problems of visual imaging.

7/11
P. 2 53

CONCEPTUAL SECOND-GENERATION LUNAR EQUIPMENT

FLORIDA A&M UNIVERSITY/FLORIDA STATE UNIVERSITY

N91-18129

INTRODUCTION

The spring 1990 *Introduction to Design* class was asked to conceptually design second-generation lunar vehicles and equipment as a semester design project.

The basic assumption made in designing second-generation lunar vehicles and equipment was that a network of permanent lunar bases already existed. The designs were to facilitate the transportation of personnel and materials. The eight topics to choose from included flying vehicles, ground-based vehicles, robotic arms, and life support systems. Two teams of two or three members competed on each topic and results were exhibited at a formal presentation.

A CLEAN-PROPELLANT-POWERED LUNAR FLYING TRANSPORT

The existence of lunar bases at different points of interest across the lunar surface would call for transportation means much more demanding than the original simple lunar rovers. A flying craft capable of traveling point-to-point distances in the range of 50-500 km is developed in order to shorten mission time and overcome inhospitable terrain. This report concerns the conceptual development of a cleanly fueled lunar flying vehicle to meet the second-generation requirements of material and personnel transportation between lunar bases. The possibility of exploration of remote areas by the same craft is also pursued. Three basic modes of operation are performed by modifications made at the lunar bases. The final design was named the Multi-Purpose Flying Vehicle (MPFV).

Modes of Operation

A lunar flying vehicle should be designed to be as versatile as possible, and to perform a number of functions by means of modifications performed at lunar bases. The lower unit of the MPFV resembles a lunar lander design and remains the same for all modes. This unit contains the control, fuel, and propulsion systems for vehicle operation in all modes. The top sections are different for each of the modes. Through these modifications, the design should perform three basic functions: (1) the transportation of materials from a main base or depot to other bases or construction sites; (2) the transportation of personnel from base to base; and (3) the exploration of specific points on the lunar surface.

Propulsion Systems

The requirement of clean propellants effectively limited the choice of fuels and oxidizers to one combination. With the exception of cold jets and electrical propulsion, the hydrogen-oxygen reaction is one of the cleanest forms of combustion

known. Fortunately, the hydrogen-oxygen rocket engine also has one of the highest specific impulses known. The MPFV uses a centrally mounted LH₂-LOX rocket for main thrust and oxygen cold jet rockets for stabilization during ballistic flight.

Conclusion

The MPFV represents a second-generation conceptual design for a multipurpose flying transport to operate on the Moon during the years 2010-2030. The MPFV can be operated in three basic modes with conversions made at appropriately equipped bases. Cryogenically stored hydrogen and oxygen are used as fuel to reduce the emission of toxic materials. Transportation from point to point is accomplished through the use of ballistic flight techniques consisting of short bursts of power followed by long periods of free parabolic flight.

EVA LIFE SUPPORT SYSTEM

The goal of the second-generation EVA suit is to increase operating time, safety, and efficiency without sacrificing the flexibility and geometrical character of the current Extra Mobility Unit (EMU). The basic design addressed to meet this goal has three distinct parts: (1) the redesign of the current EMU life support system; (2) the adaptation of an EMU oxygen rebreather and cooling system permanently affixed to a lunar vehicle; and (3) the interfacing of the two above systems to work in concert.

The new extended life support system will allow the crew member maximum flexibility and safety while performing extravehicular activities. The advantages of the suit for typical missions great distances from the lunar base are (1) the crew members do not expend the EMU's consumables while riding in the lunar vehicle to and from a destination and (2) the possibility of a system failure resulting in a fatality is greatly decreased.

The new EMU design is basically a technological update of the current design's computer, oxygen delivery, and cooling systems. New features include the use of cryogenically stored oxygen, the ability to operate from an external life support system (LSS), liquid refreshment, and waste management.

System Redundancy

The safety of the crew member using the EVA suit is the primary concern of the life support system. A failure of one of the suit systems should not result in a life threatening situation. The linear architecture of the current EVA suit presents many such cases, even with the use of in-line redundancy. The new EMU design will correct this deficiency

ORIGINAL PAGE IS
OF POOR QUALITY

by using a doubly redundant bilinear cross connect (BLCC) architecture developed for cave diving. Though this system is more complex, the use of improved technology and materials should allow the overall geometry of the existing system to remain the same. The improved system can be shown to be 14 times less likely to have a failure that would cause a fatality.

Conclusion

The redesigned EMU suit incorporates double redundancy in both separate systems and computer controllers. Three onboard computers can be used with a "majority rules" decision making process for diagnostic decisions during suit operation. A full manual operation mode can also be used if all control systems fail completely. The suit increases distance traveled and reduces the chance of failures resulting in fatalities.

PRESSURIZED LUNAR ROVER FOR GREATER DISTANCES

The goal of this project was to design a ground-based vehicle that will travel for longer distances than a 37.5-km radius from a lunar surface base. The existing design is limited to a 37.5-km radius due to the limitations of current EVA suits. Designing the pressurized vehicle would eliminate these restrictions and would allow for much more comfortable operation in the vehicle. The manned vehicle would operate on a three-day mission, traveling within a radius of 150 km at a speed of 10-15 km/hr, with a four-member crew. The primary function would be of an exploratory nature, involving experiments, photography, and computer analysis. Primary design considerations were structural, power, and control components.

Structural Design

The vehicle consists of a pressurized cabin that contains the life support for the crew members. It accommodates up to four crew members for an average mission time of three days. The windows are similar to those used on the space shuttle in that they consist of three separate structural members. A transparent film covers the outside glass and is periodically rolled over it in order to clear dust-impaired vision, with the rolls of plastic to be cleaned at the lunar bases.

Power System

The power source used in the design is the Isotope Brayton Cycle, which transfers thermal energy into shaft work by turbines. The closed loop Brayton power cycle consists of four separate loop systems involving argon gas, sodium-potassium, freon, and propylene glycol. The isotope fuel may be either Pu²³⁸, Po²¹⁰, or Cm²⁴⁴. These isotopes can be packaged into convenient fuel modules that can be shielded to prevent crew exposure to radiation and configured to eliminate the possibility of combining into a critical mass. The power load is maintained at as constant a level possible by the use of battery arrays to even the load. The power system is

transported in a separate trailer behind the main vehicle in order to reduce the dangers presented to crew members by this energy source.

Conclusion

The first goal of the second-generation pressurized lunar rover will be to establish itself on lunar bases and to develop a database on the lunar surface such that the accuracy of the topographic mapping can be confirmed for future development of unmanned missions. Based on present studies, the lunar vehicle will be feasible, but further development and research is needed to verify assumptions.

ROBOTIC ARM DESIGN PROJECT

This project represents a group effort to explore the possibility of deploying a robotic arm on the Moon. The arm was originally conceived as a specimen-gathering device to be fitted on a lunar vehicle, but it has been revised to satisfy a wider range of tasks. The design of the Extendable Robotic Collection System (ERCOS) incorporates key issues of compactness, versatility, reliability, accuracy, and weight. The arm can be used on both lunar vehicles and at lunar bases for a variety of functions.

Arm Structure

The robotic arm is composed of 9 links and attains 6 degrees of freedom. It combines the concepts of both revolute and cylindrical robots. A telescoping tower assembly is used for the majority of the arm's movement with revolute and cylindrical joints at the extremity for detailed motion. The telescoping assembly has the ability to collapse into a compact sealed structure when the arm is not in use. The material used throughout the arm is aluminum 2014-T6. With the material and structure known, computer modeling was then used for stress and deflection measurements.

Environmental Considerations

The environmental condition that would have the greatest effect on the ERCOS system would be the variation of temperatures causing expansions and contractions. This problem is overcome by placing thermal sensors at even increments along the links and using their output in the controller program to actively compensate to assure positional certainty.

Conclusion

The ERCOS system is a direct descendant of the robotic arm on the Viking lander used on the surface of Mars. The primary mission of the ERCOS design is similar in the respect of soil gathering operations, but it can provide a wide range of services to both stationary and mobile platforms. Different end effectors can be used with the basic robotic arm to provide the different functions as needed.

LUNAR ARTICULATED REMOTE TRANSPORTATION SYSTEM

FLORIDA A&M UNIVERSITY/FLORIDA STATE UNIVERSITY

N91-18130

The students of the FAMU/FSU College of Engineering continued their design from 1988-1989 on a first generation lunar transportation vehicle for use on the surface of the Moon between the years 2010 and 2020. Attention is focused on specific design details on all components of the Lunar Articulated Remote Transportation System (Lunar ARTS). The Lunar ARTS will be a three-cart, six-wheeled articulated vehicle. Its purpose will be the transportation of astronauts and/or materials for excavation purposes at a short distance from the base (37.5 km). The power system includes fuel cells for both the primary system and the back-up system. The vehicle has the option of being operated in a manned or unmanned mode. The unmanned mode includes stereo imaging with signal processing for navigation. For manned missions the display console is a digital readout displayed on the inside of the astronaut's helmet. A microprocessor is also on board the vehicle. Other components of the vehicle include a double wishbone/flexible hemispherical wheel suspension; chassis; a steering system; motors; seat restraints; heat rejection systems; solar flare protection; dust protection; and meteoroid protection. A one-quarter scale dynamic model has been built to study the dynamic behavior of the vehicle. The dynamic model closely captures the mechanical and electrical details of the total design.

OVERVIEW

It is inevitable that humans will venture beyond the Earth's boundaries and into space. Permanent habitation of the Moon is the first step towards future exploration. First-generation exploration (year 2010-2020) will include a base inhabited by approximately 15 astronauts (scientists, engineers, and doctors) whose purpose will be to explore the lunar surface and begin the building of permanent bases for lunar colony habitation. It will be necessary for the astronauts to have a reliable transportation system during their lunar stay whose operation is independent on the time of day it is being used (except in the case of solar-flare activity). This transportation system must be able to provide adequate transportation for two astronauts for a maximum excursion time of 10 hours. There must also be the capability of carrying additional payload such as additional people or large amounts of lunar regolith. The Lunar Articulated Remote Transportation System (Lunar ARTS or LARTS) is designed for this purpose.

This vehicle consists of three carts. The first cart carries the astronauts, the navigation equipment, the cameras, directional lighting and backup communication system hardware. The second cart houses the power system, the solar-flare protection blanket, and the heat rejection system for the power system. The third cart will be used for carrying cargo or for two additional astronauts. The vehicle will also have the capability of being operated in an unmanned mode. Using the concept of articulation and detachable hitches, the vehicle will be able to operate with either two carts or three carts. The first two carts will be permanently hitched together, while the second and third cart will be joined together with a flexible, removable hitch that will allow the astronauts to detach the third cart.

DESIGN REQUIREMENTS FOR THE LUNAR ARTS

The design constraints for the Lunar ARTS include operation, performance, and configuration requirements. The design requirements were set in accordance with the purpose of the

Lunar ARTS vehicle, which is to transport astronauts and material on the Moon between the years 2010 and 2020.

Operation Requirements

This vehicle will be in operation between the years 2010 and 2020. Design criteria for the vehicle include (1) reliability and simplicity; (2) maximum payload capacity of 750 kg; (3) ease of operation; (4) maintainability; and (5) mobility.

The vehicle is assumed to operate in recent lunar sites of interest characterized by data from previous landings. Two of the four sites lie on flat mare surfaces surrounded by mountains (Lacus Veris and Taurus Littrow), one lies purely in flat mare (Nubium), and one is a rugged highlands region (South Pole).

Performance Requirements

1. The vehicle will perform missions of 60 km (30 km radius from base) with passengers and 75.0 km (37.5 km radius from base) without passengers per day. There is a maximum of 10 hours per mission, which includes extra vehicular activity (EVA) time. The vehicle will travel with speeds up to 10 km/hr on a 0° slope.

2. The maximum slope angle is 30° while fully loaded.

3. The vehicle will provide controllable forward (0-10 km/hr) and reverse continuously variable speed.

4. The vehicle will provide a maximum steering turn radius of 30°.

5. There will be at least three displays that show total distance traveled for a mission, total mileage of the vehicle, and a variable-control travel display able to reset the display of distance traveled to zero. There will also be time displays that include total mission time, and a variable time with the capability of being reset to zero.

6. There will be three-dimensional vision capability for the navigation system. Two dimensions will be incorporated by stereo vision and the third dimension will use a laser range finder.

7. Protection must be provided to the astronauts for (a) dust accumulation, (b) solar reflection off Lunar ARTS surfaces, and (c) solar flare protection.

8. Design of the Lunar ARTS shall include the following safety features: (a) no sharp protuberances; (b) a restraint system to prevent astronauts from being ejected from the vehicle; (c) provision of adequate handholds for ride stability; (d) comfort; (e) no hot electrical components should be in contact with the astronauts; and (f) back-up system will be used so that no single failure of a component will endanger crew or will cause an inoperable vehicle.

9. When Lunar ARTS is brought back to lunar base, the dust will be removed.

10. The vehicle will provide materials for drilling and storage.

Configuration Requirements

1. Each wheel will have the following characteristics: elastic, solid wheels; rigid or semirigid chassis.

2. Maximum mass: 2700 kg loaded; 1480 kg unloaded.

3. Minimize operation impedance due to dust.

4. Structural system factor of safety is 1.5.

5. Provide storage space, protection, and means of attaching the Lunar ARTS tools for lunar operation.

6. House and protect cable and wiring.

7. Each wheel will must have a separate driving motor.

8. Provide display and control console.

9. Structure should be optimized for lowest weight.

10. Provide accommodations for two astronauts with EVA suits and a payload of 750 kg. Payload can include either lunar regolith or two additional astronauts with EVA suits.

11. The power source will be no more than 25% of the vehicle weight. This includes a back-up power system for locomotion and communication, as well as the heat rejection systems for the vehicle.

12. Astronauts traveling on the vehicle will have a switch on the vehicle to override automated control of vehicle.

13. Provide thermal and micrometeoroid protection.

14. Provide device to remove lunar dust and debris from Lunar ARTS while away from base.

15. Provide shock absorbers.

16. The chassis of each cart shall not exceed the overall dimensions of a length of 2.73 m (9 ft), a width of 1.83 m (6 ft) and a depth of 1.37 m (4.5 ft).

POWER

The first analysis to be performed on the vehicle is the power system. This is extremely important, as all other systems designs are dependent upon the power system. In deciding on a power system for the Lunar ARTS, it was necessary to calculate the power that was required for locomotion as well as the other components on the vehicle. This was done using two programs. The first was written to calculate the amount of power needed for locomotion when the vehicle is operating fully loaded. Wheel condition had to be specified in order to calculate the locomotion energy of the vehicle. The value obtained for locomotion was then entered into the power

program in conjunction with all other components' power requirements to obtain a total power requirement for the vehicle.

Fuel Cells

When a total power requirement was obtained it was necessary to decide on what power system to use. Batteries were ruled out as a power system. Fuel cells were chosen as the means for propulsion for the Lunar ARTS vehicle. Fuel cells are a technology that has already been proven successful in many space applications. NASA experts expect to have a lunar base established by the year 2005 that will use regenerative fuel cells and photovoltaics to serve as the primary power source for the base. This system can provide a continuous supply of hydrogen and oxygen for the Lunar ARTS.

Fuel cells are classified according to type of electrolyte, type of electrode, type of fuel, temperature, and type of catalyst.

The reactants that are used in the fuel cell stacks are hydrogen and oxygen with the by-products being heat and water. The reactants can be stored either as pressurized gases or as cryogenic liquids. Storing the reactants as cryogenic liquids reduces the size, weight, and meteoroid vulnerability of the storage tanks. Reactants will be stored as cryogenic liquids and will be heated upon leaving their storage tanks to be vaporized prior to entering the fuel cell stacks (the hydrogen and oxygen must enter the stacks as a gas for operation of the vehicle). After being cooled the water is stored as a liquid.

MOBILITY

Mobility of the Lunar ARTS incorporates five sections: suspension system, wheel design, hitch design, chassis design and modeling, and center of mass. The design and analysis of each was performed by independent groups, with system integration incorporated throughout the design process. This was accomplished by having all design personnel working on the mobility section meet weekly to discuss integration issues of the mobility components.

Suspension System

The suspension system is composed of three major components: flexible hemispherical wheels, a four-bar double-wishbone linkage, and a compound spring shock absorber. The double-wishbone linkage limits the spindle assembly to vertical motion, thus keeping the tracking of the wheels in contact with the lunar surface. The compound spring in the shock absorber is coupled with flexible hemispherical wheels, and the system was modeled in DADS to determine the damping constant.

The spindle assembly at the end of the control arms holds the driving and steering motors as well as the gearing and linkages used to transmit the power effectively. The primary steering is accomplished by electronic servomotors that rotate a spindle plate. The secondary, or backup, steering is an open-loop on/off switch control operated from a power bus by means of a control stick or joystick.

Wheels

The wheels of the Lunar ARTS are a hemispherical Kevlar polymer composite shell supported on the inside by a polar array of geometrically curved ribs and protected on the outside by a Mylar cover. Of utmost importance to the wheels is their dynamic flexibility during day and night operation. The deformation of the shell as it rolls will be supported by the rib array, and protection against lunar dust buildup will come from the Mylar cover. This design offers a large ground-contact area to provide adequate traction on the lunar surface while minimizing the problem of lunar dust.

Chassis

Each of the three carts is a "shoebox" frame with wall supports and mounting beams for the suspension system. An open top was chosen instead of a closed truss design to allow an easier entry and/or loading of the mass around the center of the cart. This would reduce the task of balancing the center of mass from mission to mission. Lightweight material with radiation "shields" conducive to the needs of the heat rejection group will make up the walls of the carts.

The first cart is primarily for transportation of astronauts; navigation equipment and computers are also kept in a rear storage compartment. This is permanently fixed to the second cart, which holds the power system. The third cart is for transporting hand tools, regolith accessories, and soil samples. Because the first cart is designed to carry the astronauts, its design will vary slightly from the basic design of the second and third carts.

Spindle

The third component in the four-bar linkage is the spindle assembly. This assembly houses the servomotors and steering mechanisms, as well as serving as a mounting for the spindle plate. It is made of two parallel plates welded one on top of the other by connecting rods that keep them vertically aligned with each other. The connecting points to the control arms are therefore vertically aligned to keep a constant relative distance between the ends of the control arms and to maintain a vertical parallelogram.

A vertical plate is mounted on the outer face of the housing with its normal parallel to the x-axis. This plate, referred to as the spindle plate, has bearing blocks located at the top center and the bottom center to allow rotation in the x-z plane. Holes are drilled in the top and bottom plates to create the vertical axis, about which the spindle plate rotates. The hub of the hemispherical wheels is mounted on the spindle aligned along the x-axis.

Hitch

The degrees of freedom constitute the major constraint in the hitch design. While the rolling motion takes place between the second cart and the shaft, the pitch and yaw motions take place at the ball and socket joint on the first cart. The orientation, or line of action, of the springs must be such that

the motion of the ball and socket causes pure compression of the spring. In addition, the springs must have different spring constants for two loading scenarios:

1. The vertical springs must be designed to balance moments caused by a displaced c.m. as determined by the center of mass constraints, plus a 200-Earth-pound astronaut boarding the passenger cart.

2. The side springs must not cause skidding of the carts during a turn. Note that if the first two carts are in a turn to the right, then the starboard springs will be in compression and port side springs will be in tension and vice versa, so the spring constant is one-half for each spring.

The motion of the hitch has to allow for 30° of yaw, turning, in the horizontal plane between consecutive carts. In addition, it must allow for a maximum of 25° pitch in the vertical plane and a final constraint of 45° roll between carts.

Primary Steering

The steering is accomplished by electric servomotors that rotate the spindle plate. Each wheel is turned by a separate servo that is controlled by the onboard computer. The steering servo is mounted to the housing and is connected to the spindle plate by a four-bar linkage. When the servo is actuated it will rotate the first link, which takes the rotational input, resulting in a translational output via the second link. This in turn will push or pull the third link, or spindle plate. The spindle plate will then rotate about the y-axis created by the two sealed bearings located at the top and bottom of the spindle plate.

Secondary Steering

The secondary steering or backup system is an open-loop on-off switch control operated from a power bus by means of a control stick or joystick. The power bus is wired directly from the steering servos through the joystick to the power source. It will bypass all onboard systems (i.e., onboard computers, monitoring and control devices) in case of failure. The joystick and power bus are located in the center of the forward bench seat and will allow operation from either the left or right side. Steering is accomplished by switching the power on and pushing the control stick in the desired direction of turning, left or right. Once the desired wheel angle is obtained, the stick is then returned to its center upright position.

This backup system is only effective for onboard system, wiring, or communication failures. Because this vehicle has four-wheel steering, if a steering servo fails, the vehicle can be steered by a single cart. The steering servos for the damaged or affected cart will be locked in the forward position by an auxiliary pin that secures the steering linkage to the nonrotating spindle. This will be done by a handcrank that fits into the steering servo. Once the wheels are locked, the cart with working systems will steer like a two-wheel steering vehicle. The problem of complete steering servo failure (all four wheels) was not considered because it would be highly improbable.

DISPLAY CONSOLE

On the previous lunar expeditions one of the problems that arose was the inability of the astronauts to clearly see the display information presented on the Lunar ARTS due to lunar dust. It is of the utmost importance that the astronaut be able to clearly see the display information at all times. It was, therefore, necessary to design a system to solve these problems.

In the display of information the astronaut must be able to call up various selections of data as needed for the completion of the mission goals. This could range from Lunar ARTS system information to scientific tools information status. To accomplish this task the display system must easily integrate with not only the Lunar ARTS systems but also with the numerous instruments and vehicles that could be put into use on various systems. To accomplish all the desired functions, it was decided that an inner-helmet device be used. This device consists of a fiber optics system that displays its information on a holographic medium. The display of information is accomplished in the following manner: holographic film is placed within a 30° radius of the astronaut's right eye; this film is where the information is projected. The astronaut sees the information projected at infinity, which means that the information would seem to be floating in space. When the brain sees this image it superimposes it on the image that the left eye sees; this gives the astronaut the sense that only one true image is being seen. The display system contains no high-voltage supplies and is totally fiber optic. This is preferred because there is little power drain and the astronaut is exposed to no high voltages. Since the display system is simply a means of displaying information, it may act as a display for other instrumentation as well. In the case of a helmet failure, a backup hand-held display could be plugged into the system to take the helmet display's place.

NAVIGATION AND COMMUNICATIONS

The object of the navigation system is to direct and control the movement of the Lunar ARTS from one lunar base to another, or to any point in between. In designing the system many factors concerning and relating to this purpose must be taken into consideration. Not all can be addressed here, so we will deal mostly with a description of the system and how some of these factors relate to the system.

Every control aspect of the Lunar ARTS incorporates communication systems. These systems transmit various signals including voice, data, video, and control signals. All these signals assist in the navigation of the vehicle. The following sections suggest processing and modulation schemes best suited to each of the information types. In optimizing the design, each discussion considers minimizing conversions and reducing noise effects.

The lunar environment dictates the materials of electronic equipment. Lunar radiation affects the performance of the electronic component, and for this reason, the design necessitates the use of radiation-hardened components. These components reduce the noise caused by radiation. The environmental effects of temperature also create undesirable

effects in the transmission of data. Therefore, not only must the components be radiation hardened, but should be relatively temperature insensitive through a broad range of temperatures to produce predictable electronic systems. Aside from component considerations, solar effects on radio waves need be reduced. Through the use of relatively high carrier frequencies, such effects can be minimized.

The navigation system of the Lunar ARTS is required to enable the user to have remote or manual control of the vehicle. It will have the ability to determine precise distances of nearby objects for remote operations and to send three-dimensional images to a remote station, along with relevant parameters such as velocity, fuel level, and distance to target object. It also will employ a heads-up display (HUD) and interhelmet optical aid (IHOA) inside the astronaut's helmet.

Navigation

The core of the system is the central processing computer located at the lunar base. In normal operation it will coordinate and prioritize system functions. A less comprehensive back-up system will be operational on the cart. Another key element of the system is the heads-up display (HUD), a device much like the ones employed in jet fighters today. It serves as the primary link between the pilot, the Lunar ARTS, and the lunar base. A stereo vision system provides a three-dimensional image for the pilot. A computer grid map of the lunar surface, in conjunction with the relay antennas, enables precise point-to-point navigation. In designing subsystems, emphasis is placed on minimization of mass and power requirements on the Lunar ARTS, consolidation of as much hardware as possible at the lunar base, and maximum utilization of cutting-edge technology.

There are three different modes of operation: on site, remote, and programmed. The primary mode is on site. In this mode the pilot is with the Lunar ARTS on the mission, connected to and controlling the Lunar ARTS via the HUD. At any time the pilot may elect to control the Lunar ARTS manually, and be guided by the lunar base or by eyesight. The remote mode consists of the pilot using the HUD to operate the Lunar ARTS from the lunar base. The HUD provides a visual environment that is indistinguishable from on site operation. This mode is useful for missions where a human presence is not necessary, or when the on-site pilot is unable to operate the Lunar ARTS. The programmed mode consists of the central processor control operating the Lunar ARTS from software, normally without direct human intervention. It is capable of real-time adjustment to changing mission conditions. It relies on a grid map whose grid points are the locations of the communication relay antennas. A path can be learned and stored for later use. The HUD can be used in parallel to monitor the mission or for minor intervention. This mode is most often used for routine missions like resupply and raw materials transfer.

Communications

Voice and video signals sent between the cart and the base utilize the standard practices for transmitting such signals. However, the other signal types require a more specific design.

The data signals, transmitted from the cart to the base, transmit sensor values through analog FM signals. When reaching the base, a computer processes the data signals. Control signals, sent from the base to the cart, incorporate a digital FM transmission. Special byte-sized codes induce the desired changes.

Voice transmission. Although FM transmission produces clear signals, amplitude modulation (AM) produces a clarity in the transmitted signal widely acceptable for voice transmission. The AM transmitter encodes the message signal in the amplitude of the carrier signal, a standard, high-frequency sine wave. In studying the frequency response of voice signal, few frequencies are found in the near-zero range. Therefore, a single sideband (SSB) scheme for transmission is desired. In using SSB transmission, advantages include conservation of bandwidth as well as reduction in the power consumption due to the suppressed carrier.

Video transmission. Because stereo vision is incorporated in the design, two video signals need transmission. These signals, along with the data signal related to the range finder, present the required knowledge for processing the 3-D signal at the base.

Standard video transmission incorporates AM for broadcasting. The recommendation for modulation is through vestigial sideband modulation (VSB) since, unlike voice signals, video signals contain a significant amount of low-frequency information. VSB modulation includes all the data of one sideband and part of the other sideband in its transmission. Thus, the transmission insures no loss in frequencies near zero and yet uses the same bandwidth as SSB transmission. In addition, the carrier signal should be included in the transmitted signal to aid in the detection and demodulation of the signal.

HEAT REJECTION AND PROTECTION

The Lunar ARTS vehicle has to be equipped with a means of protecting the vehicle from the environment it will encounter on the Moon and a means of rejecting heat from the power system and the electrical equipment. The heat

rejection system for the power system will incorporate a continuous loop of water originating in the water storage tank to reject the heat from the fuel cell stack. The water will pass from the water tank, through the stacks (to take away the by-products of water and heat), to a heat rejection system or storage system, and back to the water tank to be used again. The vehicle will be protected from meteoroid impact, solar flares, and dust accumulation. The protection and heat rejection systems depend greatly upon each other and were designed accordingly.

Worst-case scenario is taken into account for all calculations. This will occur when the sun is directly over the vehicle causing a lunar surface temperature of 230°F or 383 K. During a lunar night, the temperature of the surface is at 4 K.

Heat Rejection

Both the fuel cell system that powers the lunar rover and the electronic equipment give off heat that has to be rejected. Several different means of rejecting the heat were studied and the system that optimized the weight, amount of space, and amount of heat rejected was chosen. The system chosen to reject heat from the power system uses both active and passive cooling. This system uses a combination of a radiator and storage system during the lunar days and only a radiator during the lunar nights. Multilayer insulation blankets will be used on those components that must be kept at a constant temperature.

The heat rejection system is dependent upon the environment on the Moon. The incident radiant flux from the sun is 1360 W/m². The surrounding temperature is assumed to be that of deep space or -269°C (4 K). The heat rejection system must be capable of delivering 400 W of heat from the fuel cell stacks. The temperature of the water entering the heat rejection system will be 96°C or 369 K, while the temperature leaving the system is required to be 85°C or 358 K. The amount of heat that has to be removed from the electrical components is 43.2 W. The systems chosen also have to provide for both meteoroid and dust protection. It is assumed that the temperature at the lunar base will be kept at 22°C or 295 K.

LUNAR SURFACE VEHICLE MODEL COMPETITION

GEORGIA INSTITUTE OF TECHNOLOGY

During Fall and Winter quarters, Georgia Tech's School of Mechanical Engineering students designed machines and devices related to Lunar Base construction tasks. These include joint projects with Textile Engineering students and are listed here by project title.

Fall Quarter (32 students):

- Lunar Environment Simulator via Drop Tower Technology
- Lunar Rated Fasteners
- Lunar Habitat Shelter
- Design of a Lunar Surface Trenching Machine
- Lunar Support System
- Lunar Worksite Illumination (Daytime)

Winter Quarter (45 students):

- Lunar Regolith Bagging System
- Sunlight Diffusing Tent for Lunar Worksite
- Service Apparatus for Lunar Launch Vehicles
- Lunar Communication/Power Cables and Teleoperated Deployment Machine
- Lunar Regolith Bag Collection and Emplacement Device
- Soil Stabilization Mat for Lunar Launch/Landing Site
- Lunar Rated Fastening Systems for Robotic Implementation
- Lunar Surface Cable/Conduit and Automated Deployment System
- Lunar Regolith Bagging System
- Lunar Rated Fasteners and Fastening Systems

A special topics team of five Spring quarter students designed and constructed a remotely controlled crane implement for the SKITTER model that has been on exhibit at Atlanta's science and technology museum, SCITREK.

LUNAR SURFACE VEHICLE MODEL

Five other teams of Spring quarter students (51) designed entries for the "Lunar Surface Vehicle Model" competition that was held on May 31, 1990. These remotely controlled vehicles, each loaded a given payload, transported it over an obstacle course, unloaded it, and returned to the starting point. Their report titles are:

- Lunar Surface Vehicle Model - Team Mars
- Lunar Surface Vehicle Model - Team Mercury
- Lunar Surface Vehicle Model - Team Neptune
- Lunar Surface Vehicle Model - Team Pluto
- Lunar Surface Vehicle Model - Team Venus

The general rules of the judging and events along with the points distribution are outlined in the following sections and Table 1. In terms of lessons learned about system design methodology and project management, this competition proved to be extraordinarily effective. The event was covered by both the local and national news media. The crane implement model and the winning vehicle are to be exhibited at the NASA/USRA Summer Conference.

LUNAR SURFACE VEHICLE MODEL COMPETITION

General Rules

Remote Control. By radio, infrared sound, etc.

Mobility. 6 identical wheels, all-wheel drive, 3 axle centers, 3 wheels on each side, same trace, axle-to-axle centers greater than 1.5 times wheel diameter.

Power. Direct current, 50 V maximum, self-contained.

Speed. 5.0 km/hour maximum (level paved surface).

Size. Width 0.5 m maximum; Height 0.5 m maximum; Length 1.0 m maximum.

Turning. 3.0-m-diameter circle, (wall-to-wall), (level paved surface).

Drawbar Pull. Static force to be measured at axle height on centerline of vehicle, (level dry sand).

Ownership. Complete system is the property of Georgia Tech.

Cost. Less than \$1,000 fair market value; \$500 maximum available from NASA/University Advanced Design Program.

Payload. Mass: 0.5 kg ± 5%; Material: Aluminum; Size: Largest overall dimension 15 cm maximum; Passive.

Demonstration. Start vehicle at least 1.0 m from payload, drive to payload, load payload on vehicle within vehicle's length and width, transport payload over obstacle course, unload payload and return vehicle to starting point. 10 minute time limit. 3:00 Thursday, May 31, 1990 on the Ga. Tech. Campus.

Slope. Uphill and downhill in dry sand, 10%, 20%, and 30%. Sidehill in dry sand, 10%, 20%, and 30%.

Judged.

- Innovation in structure, power transmission, control, kinematics
- "Lunar" appearance
- Quality of workmanship
- Safety

Obstacle Course Events

1. Place the payload and vehicle at their designated places.
2. Start the timer.
3. Drive the vehicle to the payload.
4. Load the payload.
5. Set the pull scale at axle level.
6. Connect the vehicle to the pull scale.
7. Measure the drawbar pull capacity in sand.
8. Disconnect the vehicle.
9. Drive through the .5 m by .5 m opening.
10. Stop against the barricade for the length check.
11. Drive close to curb.
12. Stop momentarily.
13. Turn around a full circle between curbs.
14. Drive through the speed trap.
15. Turn around the pylon.
16. Drive through the speed trap.
17. Drive up, down and sidehill on the 10% slope sand.
18. Drive up, down and sidehill on the 20% slope sand.
19. Drive up, down and sidehill on the 30% slope sand.
20. Drive along the route to the unloading point.
21. Unload the payload.
22. Drive along the route to the starting point.
23. Stop the timer.

Table 1. Competition Points Accumulation

Category/ Criteria		Place or Award				
		1st	2nd	3rd	4th	5th
Judging: Innovation	Structure	200	100	50	0	0
	Power Transmission	400	200	100	0	0
	Control System	400	350	300	200	100
	Kinematics	200	150	100	50	0
Judging: Aesthetics	"Lunar" Appearance	300	200	100	0	0
	Workmanship	300	200	100	0	0
Judging: Safety	Very Safe	300				
	Reasonably Safe		200			
	Unsafe			0		
System Cost:	Less than \$400	500				
	Less than \$500		400			
	Less than \$600			300		
	Less than \$800				100	
	Less than \$1000					0
Speed: (Fastest = 1st)		400	300	200	100	0
Size: (Smallest = 1st)	Width	200	100	0	0	0
	Height	200	100	0	0	0
	Length	200	100	0	0	0
	Volume (WHL)	500	400	200	0	0
Turning Radius: (Least = 1st)		300	200	100	0	0
Drawbar Pull: (Greatest = 1st)		800	500	300	200	0
Weight:	Lightest (W_1)	1200				
	$\leq 1.05 W_1$		1000			
	$\leq 1.20 W_1$			800		
	$\leq 1.50 W_1$				600	
	$\leq 2.0 W_1$					400
Time Over Course: (Least = 1st)		700	600	500	200	0
Slope:	30%	500				
	20%		300			
	10%			100		
Sidehill:	30%	500				
	20%		300			
	10%			100		

2007
P.5 63

BAGGING SYSTEM, SOIL STABILIZATION MAT, AND TENT FRAME FOR A LUNAR BASE N91-18132

GEORGIA INSTITUTE OF TECHNOLOGY

Georgia Tech's School of Textile and Fiber Engineering and School of Mechanical Engineering participated in four cooperative design efforts this year. Each of two interdisciplinary teams designed a system consisting of a lunar regolith bag and an apparatus for filling this bag. The third group designed a mat for stabilization of lunar soil during takeoff and landing, and a method for packaging and deploying this mat. Finally, the fourth group designed a sunlight diffusing tent to be used as a lunar worksite. Following are summaries of these projects.

LUNAR REGOLITH BAGGING SYSTEM 1

This project encompasses the design of a two-part system consisting of a bag-filling apparatus and a bag. This system is designed to be used in construction applications on the Moon. The apparatus must not require more than 10 kW of power; it should fill bags for a given operating time and then recharge. The system should also be robotically controlled and must withstand harsh lunar environmental constraints. Some of these constraints include a temperature range of -250°F to 250°F, absence of a protective atmosphere, high levels of ultraviolet and gamma radiation, and abrasive regolith. These bags should provide adequate protection for a lunar habitat; they should also provide structural support. However, the bags must be small enough to be transported by an astronaut should a structural repair of the habitat be necessary.

The bag-filling machine is designed to be used in conjunction with the lunar SKITTER (which is currently in development). This bag-filling apparatus will operate 8 hours per day and fill 120 bags per day, with each bag having a capacity of 1 cu ft of regolith. The 5.5 ft x 12 ft, 1984-lb machine will be made of boron/epoxy and graphite/aluminum composites. The projected operating life is five years. Bags will be supplied to the machine on a prefabricated roll.

The bags will be constructed of Clark-Schwebel Fiber Glass Corporation's ECG 75-1/0 glass fiber in a plain weave fabric. Glass was selected on the basis of its high strength, elastic recovery (almost 100%), outstanding dimensional stability, excellent temperature use range, and excellent radiation resistance. Following is a list of bag/fabric specifications.

Ends per inch:	44
Picks per inch:	32
Fabric thickness:	0.0068 in
Fabric warp breaking strength:	250 lbf/in
Fabric fill breaking strength:	200 lbf/in.
Warp yarn:	ECG 75-1/0
Fill yarn:	ECG 75-1/0
Bag stitching yarn:	ECG 75-1/0
Stitch density:	40 stitches/in
Yarn diameter:	0.00036 in
Yarn linear density:	1 lbm/7500 yd

A schematic of the lunar regolith bagging system is shown in Fig. 1. Following is a list of bagging machine specifications.

Brush length:	5 ft
Brush diameter:	2 ft
Brush mass:	6.21 lb
Brush rpm:	150 rpm
Brush drive:	#40 chain and sprocket
Drive composition:	graphite/epoxy composite
Interior shroud coating:	Teflon
Machine length:	12 ft
Machine height:	6.56 ft
Machine width:	5.5 ft
Bag capacity:	1 cu ft
Funnel capacity:	10 bags of soil
Funnel height:	3.28 ft
Funnel top diameter:	3.67 ft
Funnel bottom diameter:	0.98 ft
Roll capacity:	975 bags
Full roll diameter:	3.18 ft
Roll shaft composition:	boron/aluminum composite

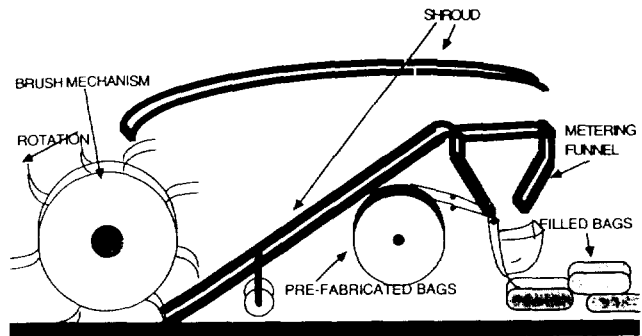


Fig. 1. Schematic of Lunar Regolith Bagging System 1

The bag-filling machine will operate by brushing small particles of regolith into the shroud. The shroud is designed to guide the flying debris through a calculated trajectory to the metering funnel. Prefabricated bags containing small metal strips in their mouths are opened electromagnetically. Shown in Fig. 2 is the bag opening method. A strain gauge is used to monitor bag volume. When a bag is full, the electromagnet is deenergized, thus allowing the bag to close. The closing mechanism consists of a continuous loop Kevlar drawstring

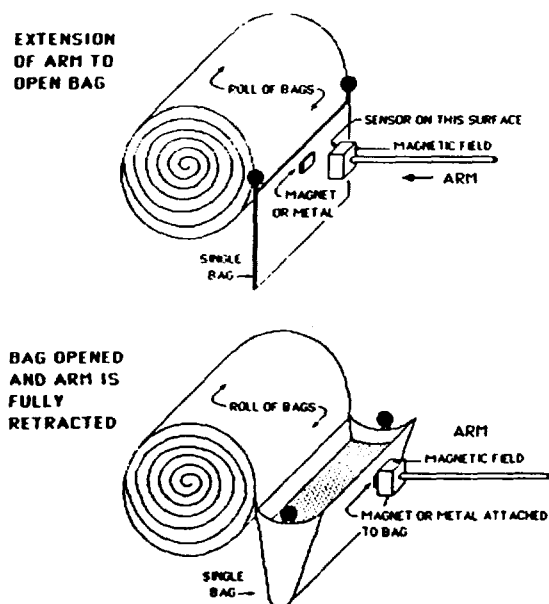


Fig. 2. Bag Opening Method for Bagging System 1

with raised barbs along its length, and two boron/aluminum composite balls mounted on the loop and adjacent to bag sides (as shown in Fig. 2). When a bag is full, it is cut away from the remainder of the roll with a diamond blade. As the bag drops from the machine, the composite balls slide into clutch slots. Meanwhile the barbed loop is pulled irreversibly through bag eyelets. The clutch then releases the balls, and the full, sealed bag drops to the lunar surface. The drawstring is a convenient feature that a recovery team might exploit in retrieving and transporting these lunar sandbags.

LUNAR REGOLITH BAGGING SYSTEM 2

As in the previous project, the goal of this design is to provide a satisfactory system for containing lunar regolith and for filling this container (bag). These bags are to be used in lunar construction applications. This system must operate under minimal power (less than 10 kW), and must withstand lunar environmental constraints such as severe temperature gradients, ultraviolet and gamma radiation, and abrasion by regolith. These bags also should provide protection and structural support for a lunar habitat. Additionally, the bag size should facilitate ease of transportation for either an astronaut or a transporting device.

The bag will be constructed of Kevlar 149 in a ripstop weave. Though a Dupont scientist indicated that this fiber is suitable for this application, its behavior under gamma radiation is questionable. This fiber does, however, have many advantages that suggest its suitability for this application; among these are low density, high strength, good cut resistance, good puncture resistance, and good ultraviolet and electron radiation resistance. The proposed bag configuration is analogous to the geometry of a pillowcase. This shape offers

maximum packing potential (ratio of regolith volume to unfilled bag volume), good stackability, and low seam requirements. Following are bag specifications.

Bag fabric weight:	6 oz/yd ²
Bag temperature range:	-300-800°F
Bag seams:	flat felled
Stitch density:	7-12 stitches/in
Bag width:	36 in
Bag length:	72 in
Bag fabric thickness:	0.0076 in
Bag fabric volume:	39 in ³
Maximum regolith volume:	29702 in ³
Bag mass/regolith mass:	0.001554

For Earth-to-Moon transportation and for bag-filling purposes, unfilled bags will be stacked one inside the other in "Dixie cup" fashion. This stacking configuration will facilitate accuracy in mechanical bag placement for filling. A magnetic thread to be used for bag opening will be woven into the mouth of the bag. Four 8.75-in long magnetic buttons to be used for fastening a full bag will be sewn into a lip in the mouth of each bag.

The proposed bag-filling mechanism is analogous to a "french fry scoop." The scoop will be attached to a lunar truck by an electronic arm whose motions are controlled by an electronic microprocessor. In filling, the scoop will be inserted into a bag opening. An electromagnet will activate the magnetic thread in the bag mouth, and will withdraw the bag from the bundle. As the lunar truck moves forward, it will drag the scoop and the bag through the regolith at a depth of 2 in. Electronic weight sensors will monitor the amount of dirt in the bag and eventually activate the magnetic closure system. The proposed closure system consists of hooks that will draw the inner bag lip out and cause the button magnets to snap together and thus seal the bag. Advantages of this bag-filling system are minimal disruption of regolith, minimal contact between moving parts and airborne regolith, and valid sealing mechanism for lunar temperature range.

This system is designed to operate for 8 hours per day and to fill approximately 16,000 cu ft of soil in 8 days.

SOIL STABILIZATION MAT FOR LUNAR LAUNCH/LANDING SITE

Presented in this project is a method for providing soil stabilization for a lunar launch/landing site. Flying debris (i.e., unrestrained soil) associated with lunar landers has the potential to damage equipment and to injure personnel associated with future lunar colonies. The proposed mat is large enough to compensate for landing errors; its expected life span is 10 years (assuming quarterly use). A schematic of this mat is shown in Fig. 3. Design constraints include light weight, adequate heat resistance for takeoff, sufficient impact resistance (for landing), ease of transportation and deployment, and low mat porosity.

The mat is to be constructed of Fiberite Corporation's PAN-based carbon fiber in a 2 × 2 basket weave. This structure will provide good tear strength, good crease resistance, and good

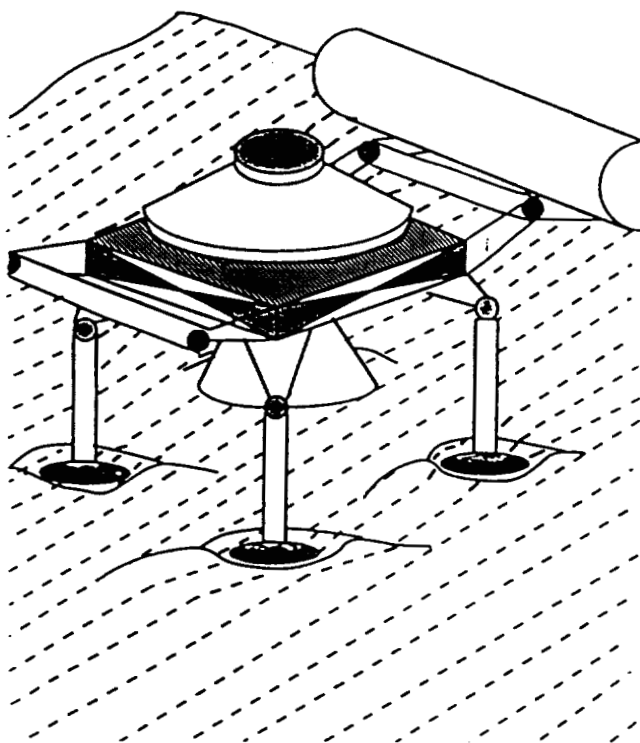


Fig. 3. Schematic of Soil Stabilization Mat for Lunar Launch/Landing Site

abrasion resistance. The mat will be double layered and 0.066 in thick. Forty panels measuring 100 m by 2.5 m each will be double stitched together using carbon thread and flat felled seams to form a square mat covering an area 100 m by 100 m. This mat will weigh 30,500 lb, including seams.

Heat resistance for takeoff is a key requirement for this mat. Exhaust gases associated with takeoff reach a maximum temperature of 1500°C. Exposure time is, however, only a few seconds. With a maximum usage temperature of 2000°C, carbon is appropriately heat resistant.

The mobility of yarns with respect to one another within a basket weave imparts good tear resistance to the mat. It is not feasible to clear a landing site of sharp rocks. It is, however, feasible to employ a fabric whose structure retards tear propagation.

Carbon fibers also resist ultraviolet and gamma radiation that cause organic fibers to degrade.

The stowage form of the stabilization mat is shown in Fig. 4. The 100 m by 100 m mat is folded in accordion style over 10-m widths. The resulting form is then 10 m wide and 100 m long. This form is then rolled along the lengthwise direction to form a cylinder measuring 1.46 m in diameter and 10 m in length. Thus the mat will fit into the shuttle's cargo bay (12 m x 6 m x 6 m). The mat's weight (30,500 lb) will also be within the shuttle's 60,000-lb capacity. The mat deployment method is shown in Fig. 5. Metal strips in the mat will serve

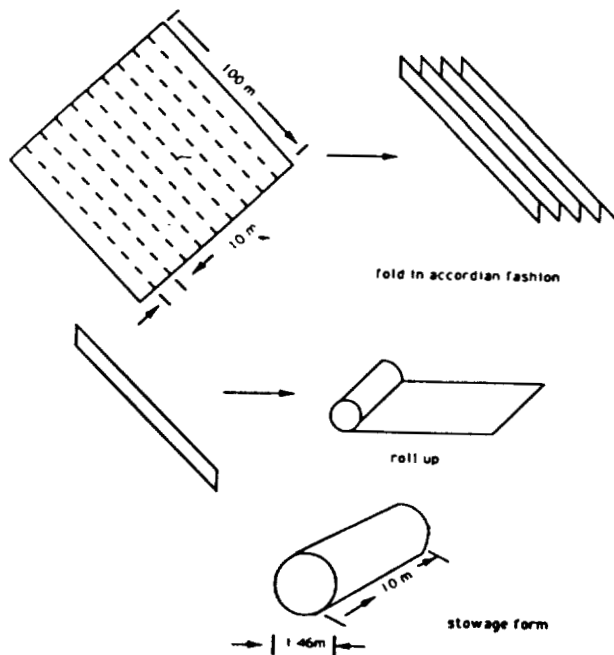


Fig. 4. Stowage of Soil Stabilization Mat

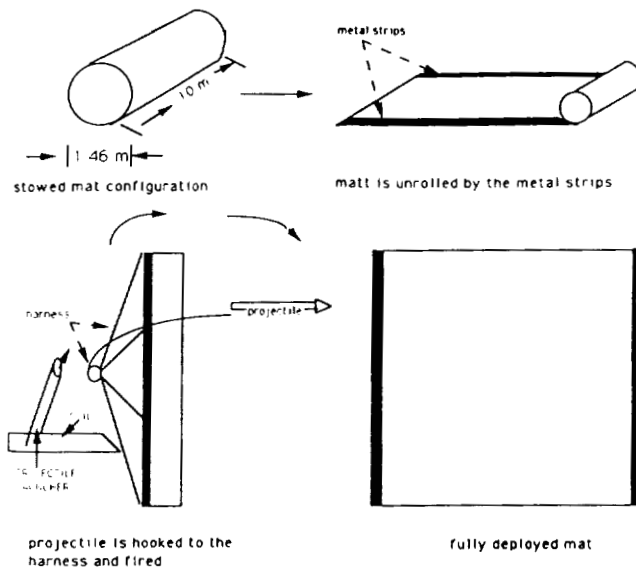


Fig. 5. Deployment of Soil Stabilization Mat

as coil springs that will unroll the mat. A harpoon-like device will be attached to the edge of the accordion fold and fired. This harpoon, when fired, will complete mat deployment.

This mat is designed to accommodate landings and launches of space vehicles measuring up to 18.9 m (62 ft) in length, 6.1 m (20 ft) in diameter, 27,216 kg (60,000 lb) in vehicle weight, and 15,876 kg (35,000 lb) in cargo weight. Following is a cost breakdown for the lunar mat.

Carbon fibers, \$1000/lb	31,000,000
Weaving cost	100,000,000
Transportation to Moon, \$25000/lb	775,000,000
Deployment	2,000,000
Total	908,000,000

Total estimated cost of production, transportation, and deployment of the lunar soil stabilization mat is \$908 million, with transportation comprising the bulk of the cost.

SUNLIGHT DIFFUSING TENT FOR LUNAR WORKSITE

Sunlight on the Earth has an intensity range of 100-1000 footcandles. Because the Moon lacks an Earth-like protective atmosphere, sunlight on the Moon is not diffused. Lunar sunlight has an intensity of 120,000 footcandles. Also, lunar sunlight is unidirectional. This unidirectionality causes objects on the Moon to be either extremely bright or extremely shadowed. These characteristics of lunar sunlight may cause severe distortion of an object's color and contrast on the Moon. Because many tools are color coded, light distortion may be a problem in the astronauts' working environment. Presented in this project is a means of overcoming this difficulty. The proposed solution to this problem is a structure with an umbrella-like frame and tent cover.

A schematic of the tent frame is shown in Fig. 6. The proposed hexagonal structure consists of a tripod frame with three rafters. The three legs will provide stability on uneven surfaces, and attached wheels will provide mobility. Rafters connected to the three legs plus the three additional rafters will form a hexagonal frame for the fabric cover and provide a large work area. Torsion springs incorporated in the frame will enable the structure to be folded compactly and to be self-assembled.

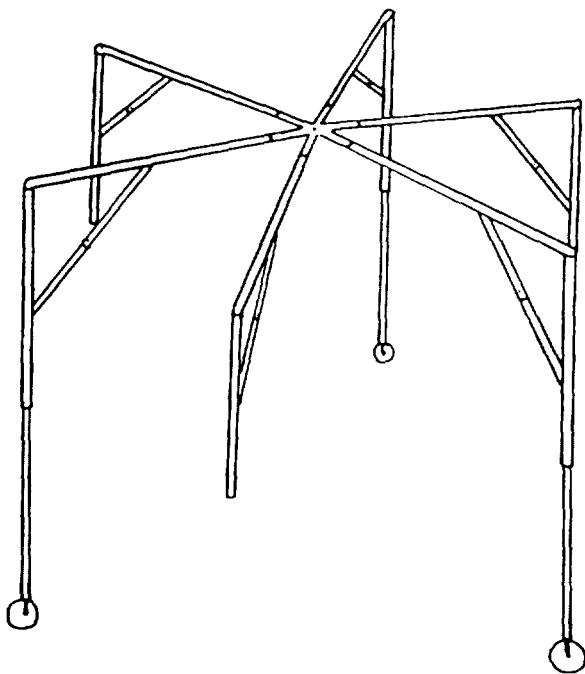


Fig. 6. Sunlight Diffusing tent Frame

Compression springs and extensional legs will reduce tent height for transportation requirements. The fabric cover, fixed tightly to the frame, will provide additional structural support.

Construction materials for this tent must withstand previously described harsh lunar conditions. Specific requirements of the apparatus are low weight to minimize transportation cost, minimal cargo space occupancy, ability to self-assemble, ability to both reduce light intensity and diffuse light, mobility, and structural integrity.

The primary frame will be constructed of titanium and the springs of chrome silicon. The tent and cover will be constructed of Clark-Schwebel Fiber Glass Corporation's eight-harness satin weave Style 7781 glass fabric. Fabric specifications are as follows.

Ends per in:	57
Picks per in:	54
Fabric weight:	8.95 oz/yd ²
Fabric thickness:	0.0090 in
Ends breaking strength:	350 lbf/in
Picks breaking strength:	340 lbf/in

This fabric will allow uniform light intensity of approximately 350 footcandles. Manufactured in 8-ft widths, panels of fabric measuring 43 ft in length will be sewn together in pairs. Measuring 15 ft in width, these double panels will form the sides of the structure. Panels will be attached to the frame by means of Teflon-coated fiber glass loops.

A diagram of tent deployment is shown in Fig. 7. In stage one, the structure will be fully compact. Restraining cords connecting the stand and the leg base will ensure that the wheels land precisely 15.4 ft from the tent center. In stage two, legs will be released while rafters are held stationary. In stage three, rafters will spring down and correctly position wheels. In stage four, both center-to-rafter and rafter-to-leg torsion springs will push the center sections upwards. In stage five, extensional leg latches will be released. The entire structure will "pop up" and fabric will drop over the legs. All locks and supports will be fully engaged at this stage.

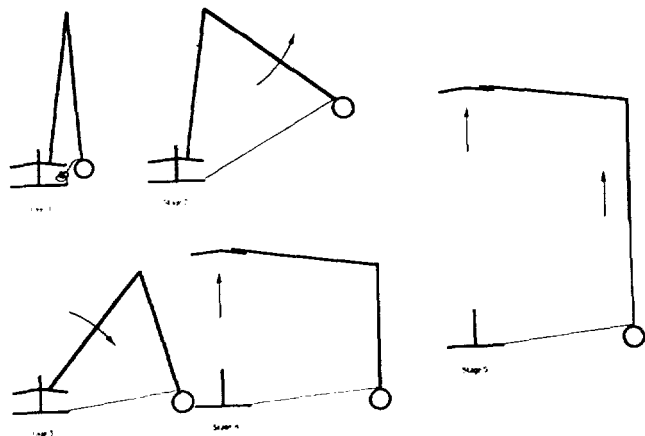


Fig. 7. Tent Deployment

Astronauts may enter and exit the work tent via slits in the fabric. Slits will measure 15 ft in length. Zippers will allow the slits to be opened an additional 13 ft. Large openings will allow the tent to be moved over large objects.

Listed below are structural specifications for the tent frame.

Lower leg section outer diameter	2.75 in
Lower leg section wall thickness	0.063 in
Upper leg section outer diameter	3.25 in
Upper leg section wall thickness	0.063 in
Rafter section (legs) height	4.00 in
Rafter section (legs) width	1.00 in
Rafter section (legs) thickness	0.063 in
Rafter section (extensions) height	3.00 in
Rafter section (extensions) width	1.00 in
Rafter section (extensions) thickness	0.031 in
Hanging extensions outer diameter	1.50 in
Hanging extensions thickness	0.031 in
Center locking device section height	2.00 in
Center locking device section width	1.00 in
Center locking device section thickness	0.063 in
Weight at center (springs and plate)	10.0 lb
Estimated weight of wheel assembly	5.0 lb
Estimated horizontal force at wheels	100.0 lb
Estimated compression spring weight	4.2 lb
Stress on upper leg at hinge	4.69×10^3 psi
Stress on upper leg at lateral support	-6.13×10^3 psi
Stress on rafter at lateral support	-6.70×10^4 psi
Stress on main rafter at center	8.4×10^4 psi
Minimum compression spring force	22.2 lbf
Minimum rafter to leg torque	2.29×10^3 in lb
Minimum center to rafter torque	4.76×10^3 in lb
Total weight	105 lb
Volume	787 yd ³



SPACEPORT AURORA: AN ORBITING TRANSPORTATION NODE

UNIVERSITY OF HOUSTON COLLEGE OF ARCHITECTURE

With recent announcements of the development of permanently staffed facilities on the Moon and Mars, the national space plan is in need of an infrastructure system for transportation and maintenance. A project team at the University of Houston: College of Architecture and the Sasakawa International Center for Space Architecture, recently examined components for a low Earth orbit (LEO) transportation node that supports a lunar build-up scenario. Areas of investigation included: identifying transportation node functions, identifying existing space systems and subsystems, analyzing variable orbits, determining logistics strategies for maintenance, and investigating assured crew return systems. The information resulted in a requirements definition document, from which the team then addressed conceptual designs for a LEO transportation node. The primary design drivers included: orbital stability, maximizing human performance and safety, vehicle maintainability, and modularity within existing space infrastructure. For orbital stability, the "power tower" configuration provides a gravity gradient stabilized facility and serves as the backbone for the various facility components. To maximize human performance, human comfort is stressed through zoning of living and working activities, maintaining a consistent local vertical orientation, providing crew interaction and viewing areas and providing crew return vehicles. Vehicle maintainability is accomplished through dual hangars, dual work cupolas, work modules, telerobotics and a fuel depot. Modularity is incorporated using Space Station *Freedom* module diameter, Space Station *Freedom* "standard" racks, and interchangeable interior partitions. It is intended that the final design be flexible and adaptable to provide a facility prototype that can service multiple mission profiles using modular space systems.

INTRODUCTION

Background

President Bush has stated the goals for the United States space program. This national plan includes establishing permanently staffed facilities on the Moon and Mars. These facilities will provide the foundation for extensive research on human response to longterm missions and the observation of our evolving solar system through astronomical instruments.

The first phase of the nation's space plan is Space Station *Freedom*, which is a scientific facility conducting experiments in microgravity. It does not, however, encompass the functions necessary to assist and maintain a lunar base in the near future. Phase two of the national space plan is a permanently staffed lunar facility within the first decade of the twenty-first century.

Research at the University of Houston College of Architecture and the Sasakawa International Center for Space Architecture has been in progress to develop a facility that can provide mission support for lunar and Mars initiatives. Because lunar and Mars support missions differ, the project team concentrated on a transportation node that could support a lunar base. It is intended that the final design be flexible and expandable to provide a facility prototype that can service single and/or multiple mission profiles using modular space systems and subsystems.

Problem Statement and Options

An orbiting facility is necessary for the construction and support of a lunar base. This facility will serve as a stepping stone for space exploration and advancement.

First option. S. S. *Freedom* should be redesigned and re-evaluated as a transportation node. This is costly, time

consuming and alters its present function as a microgravity research facility⁽¹⁾.

Second option. Phase in S. S. *Freedom* as a transportation node. This modification would delay projected phases of the national space plan (e.g. lunar facility)⁽¹⁾.

Third option. A separate transportation node is designed and developed to advance space initiatives. This option does not interfere with S. S. *Freedom* and provides a concentrated effort in the second era of space travel.

Options and Choice

The project team weighed all three options and chose to design a separate transportation node. The project team agreed that to redesign S. S. *Freedom* as a transportation node would be in conflict with its present international research mission. Therefore, it was decided to design a second facility that would complement S. S. *Freedom* and support a lunar base. The project was given the name Spaceport *Aurora*, which signifies a new dawn, a new beginning in space exploration.

Assumptions

- S. S. *Freedom* will remain a pure scientific experimental facility.
- All facility components limited to orbiter payload bay size and mass capabilities.
- Shuttle and Orbital Maneuvering Vehicle (OMV) required for transportation and construction of spaceport.
- Heavy Lift Launch Vehicle (HLIV) not required.
- Low Earth Orbit (LEO) facility; orbital altitude within proximity to S. S. *Freedom*.

• Crew Size:

Permanent Crew	Lunar Transfer Crew
Commander	Commander
Pilot	Pilot
Flight Surgeon; FS	Crew Medical Officer, CMO
Crew Medical Officer; CMO	Lunar Specialist - 3
Intra vehicular activity; IVA - 2	
Extra vehicular activity; EVA - 4	
Technician Specialist - 2	
Subtotal: 12	Subtotal: 6
Total: 18	

- International crew
- Two split six-hour work shifts, six crewmembers per shift, six-day work week.
- Crew rotation every six months.
- "Dirty" microgravity environment.

Phases of Spaceport Aurora Configuration

Phase I: Initial configuration. The initial configuration for Spaceport *Aurora* begins with the launch and deployment of the "power tower" truss, power beam truss, fuel depot truss, and docking ring. Once this is completed, truss hardware is added (power lines, communication lines, fuel lines, solar arrays, solar dynamics, radiators, antennas, remote manipulator system (RMS), mobile transporter, and reaction control modules (RCM)).

After the structure is assembled, initial pressurized modules (with partial racks) are launched. They include one habitation and one common module along with interconnecting nodes. Once the modules and nodes are connected and attached to

the structure, a logistics module (with supplies) is transported. The modules are completed with the installation of the remaining racks. The final step is occupation of the facility by the initial crew (4) (see Fig. 1).

Phase II: Assembly configuration. The assembly configuration consists of the launch and deployment of two rigidized inflatable hangars with door hardware and two rotating fixtures. Two work modules are launched along with a command module, control module, cupolas, two hyperbaric/airlocks and interconnecting nodes.

Once the assembly area is completed the remaining modules (with partial racks) are launched and connected. They include: a second habitation module, hotel (crew transfer) module, and the health maintenance facility (HMF)/experimental plant growth module. The modules are attached to interconnecting nodes and completed with the installation of the remaining racks. The final step is the launch of two assured crew return vehicles (ACRV) each capable of supporting a crew of 8. At the completion of this phase the facility has a permanent crew of 10 (see Fig. 2).

Phase III: Lunar mission configuration. The lunar mission configuration consists of the launch and installation of the fuel depot (8 propellant tanks, propellant management device and micrometeoroid protection) that will store and transfer fuel for the lunar vehicles. Once the fuel depot is completed the third and final ACRV is launched to accommodate a permanent crew of 18.

The final step is the launch of lunar vehicle components for assembly. This will be a gradual process that coincides with the development of the lunar facility. As lunar initiative activity increases so will the assembly of vehicles aboard Spaceport *Aurora* (see Fig. 3).

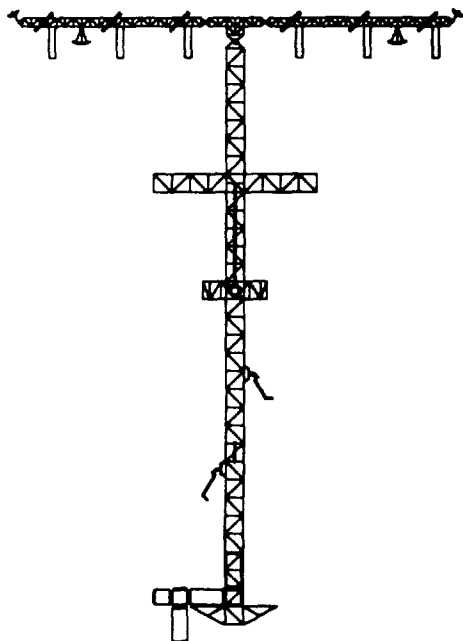


Fig. 1. Initial Configuration

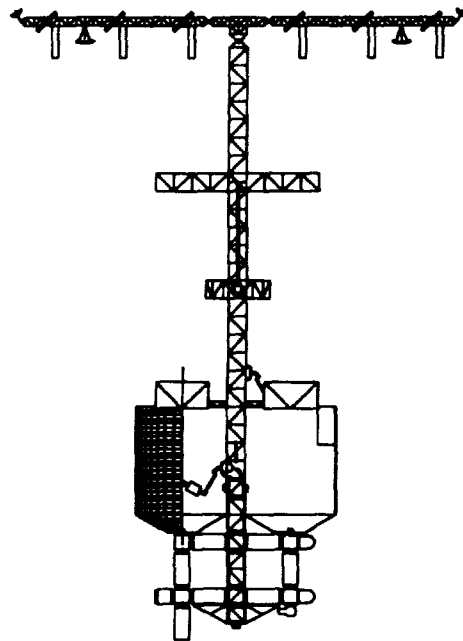


Fig. 2. Assembly Configuration

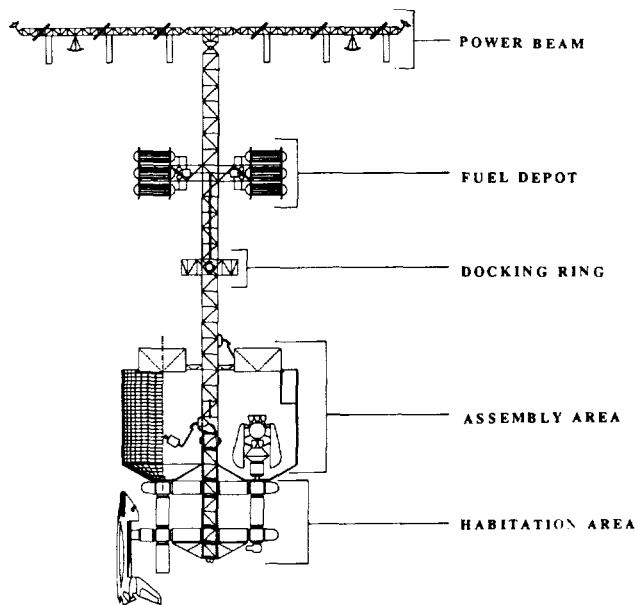


Fig. 3. Lunar Mission Configuration

Refer to Fig. 4 for total mass transported and total shuttle flights required per completion of phase.

DESIGN

The research on individual components provided a guideline for the overall configuration of the spaceport as well as the components themselves.

Facility Configuration

Goals. Spaceport *Aurora* is an orbiting transportation node with a hands-on environment involving routine and risk. With such operations occurring on a continuous level certain goals become apparent:

- Provide a productive working and living environment
- Provide redundant systems for safety and maintainability
- Provide for servicing of vehicles
- Provide a configuration that reduces orbital surface drag
- Provide for modularity within existing space infrastructure

Concepts. To provide a productive working and living environment a separation of the two activities is necessary. Both activities (working and living) require zoning of spaces as private or public.

To reduce orbital drag the components with the largest frontal surface area should be positioned parallel with the orbital path (x-axis)⁽²⁾. To reduce fuel consumption the mass of the spaceport should be balanced along the z-axis, creating a gravity gradient stabilized facility⁽³⁾.

Design solution. The "power tower" configuration is chosen because it provides a gravity gradient stabilized facility (which will assist in the transfer of propellant) with minimal orbital surface drag. The power tower provides an efficient structure using a modular construction system that will accommodate components of the existing space infrastructure. The power tower truss measures 560' (170.7 m) in length using a 17'6" (5.3 m) by 17'6" (5.3 m) bay module and the power beam measures 400' (121.9 m) in length using an 8' (2.4 m) by 8' (2.4 m) bay module. The power tower serves as the spine supporting the various facility components of Spaceport *Aurora*

PHASE I: Initial	PHASE II: Assembly	PHASE III: Lunar Mission	
Subtotal: 8	Subtotal: 12	Subtotal: 32	Total Flights: 52
138,900 kg*	240,200 kg*	744,400 kg*	Total Mass: 1,123,500 kg*

Fig. 4. Spaceport *Aurora* Configuration; Shuttle Flights and Mass

Assembly

Goals. Because of hazardous working surroundings and continuous monitoring, the assembly area must be a productive environment. The following goals are essential:

- Provide a safe working area in space
- Provide service and assembly capabilities
- Provide expedient construction
- Minimize EVA

Concepts. To ensure crew safety and minimize EVA time, redundant automated systems and telerobotics are necessary. In order to maintain EVA productivity during vehicle assembly, the hangar should be completely enclosed. Another safety factor within the hangar is protection from micrometeoroids. A double-insulated skin made of aluminum and Kevlar is necessary to keep meteoroid penetration at a minimum⁽⁴⁾.

A clear unobtrusive viewing area for EVA and telerobotic observation is required. This IVA station should be in close proximity to the vehicles serviced. Communication and monitoring throughout the facility is accomplished through audio/visual equipment.

Design solution. Rigidized inflatable hangars are incorporated to reduce shuttle flights, construction time and EVA time. The hangars are compact and placed within the orbiter cargo bay. Two hangars 85' (25.9 m) in diameter by 120' (36.6 m) in length are incorporated rather than one to increase the number of vehicles repaired and to reduce turnaround time. The control module 14'6" (4.4 m) in diameter by 25' (7.6 m) in length is located perpendicular to the two hangars providing dual, separate work cupolas on opposite sides for telerobotics supervision and observation. The assembly cupolas are located 10' (3 m) from the vehicle which is under repair within the hangar, providing a clear unobstructed view for IVA personnel. The command module, adjacent to the control module, 14'6" (4.4 m) in diameter by 34' (10.4 m) in length is the control center for the entire facility. The command

module monitors facility communications, navigation, energy levels, environmental systems and propellant supplies. The command module also provides a (EVA repair) viewing area within the hangars. The work modules 14'6" (4.4 m) in diameter by 34' (10.4 m) provide IVA repair of components which are too small and/or tedious for EVA within the hangars (see Fig. 5).

EVA access to the hangars is accomplished through the rotating drums or through the hyperbaric airlock. This provides direct access for EVA personnel into the hangars (an enclosed volume) reducing safety risks.

Both pressurized and unpressurized docking is needed. A docking ring 60' (18.3 m) in diameter with a hard dock is used for transfer of propellant and replacement parts. A pressurized docking node is used for transfer of lunar and spaceport crews. Thus, the cargo delivery does not disturb the habitation modules.

Habitation

Goals. The habitation area is the central meeting place for group interaction. Positive psychological and physiological environments are desirable. The habitation goals are:

- To increase productivity
- To utilize space efficiently
- To provide a safe environment

Concepts. The habitation area supports various functions which are inter-related yet different. Activities within the habitation modules include:

- | | |
|---------------------|----------------------|
| Sleeping | Personal Hygiene |
| Recreation | Eating |
| Drinking | Meetings |
| Studying | Personal Storage |
| Relaxation | Training |
| Meal Clean-Up | Communications |
| Private Conferences | Clothing Maintenance |
| Dressing | |

Separation of the habitation activities is important. Zoning from private to public is necessary.

To utilize space efficiently, interchangeable partitions for accommodating transfer crews provide flexible interiors. The permanent crew has sleeping quarters 28 ft² (8.5 m²) which are larger than the transfer crew 14 ft² (4.3 m²) who are on board for a shorter period of time⁽⁵⁾.

A consistent local orientation throughout the facility is an important factor to consider⁽⁶⁾. This will assist the permanent crew in performing daily activities, provide the transfer crew in adapting more quickly to their surroundings and, therefore, increasing productivity.

Design solution. All pressurized modules within the facility are 14'6" (4.4 m) in diameter by 34' (10.4 m) in length. This length is based on: (1) minimizing visibility distance from assembly cupola to vehicle in hangar; (2) configuration of modules within the power truss bays 17'6" (5.3 m); and (3) modularity for maintenance. Although the modules are shorter than standard S. S. *Freedom*, their length is consistent throughout the facility (for flexibility) and they are transported with partial racks preassembled.

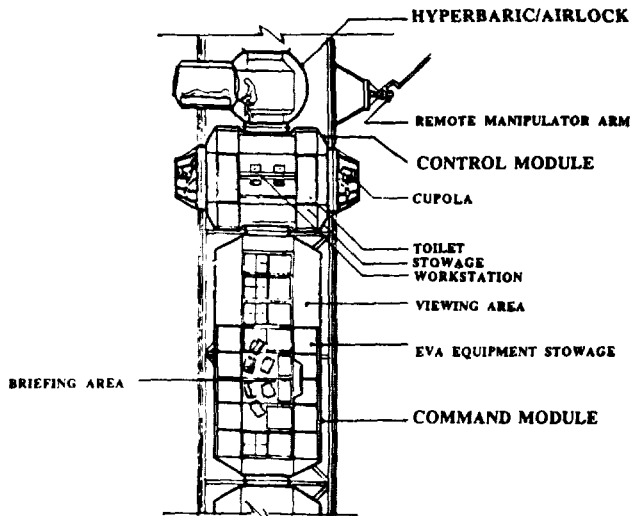


Fig. 5. Command Module, Control Module and Hyperbaric Airlock



Fig. 6. Habitation Module (Permanent Crew)

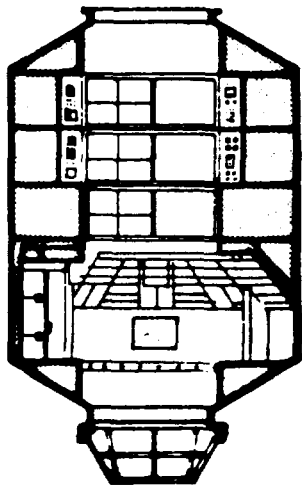


Fig. 7. Earth Viewing Wardroom Cupola

Because of split work shifts, dual habitation modules for crew sleeping quarters provide privacy and redundancy. Each module has a separate hygiene facility that serves as a backup (and improves maintainability) in case of malfunction (see Fig. 6).

A common module is centrally located to accommodate crew activity such as dining, housekeeping, recreation, etc. A hotel module accommodates transfer crews (lunar and spaceport) and serves as a backup for common module house-keeping activities (cooking, laundry, dining, etc.).

A consistent orientation is maintained throughout the facility except when entering the Earth viewing wardroom cupola and the control module. Both the Earth viewing cupola and control module are unique spaces that require a change in orientation for maximum viewing capabilities. The Earth cupola is an area where "sharing a unique experience can relieve some of the stress of a confined environment"⁽⁷⁾ (see Fig. 7).

Health Maintenance Facility (HMF)

Goals. The HMF provides the crew with physiological and psychological treatment. When compared to S. S. *Freedom*, the following goals for Spaceport *Aurora* HMF are:

- Assured crew safety and health
- Increased function of airlocks
- Increased privacy
- Improved patient care

Concepts. The HMF requires a large separate facility because of the large crew and the split work shifts. The flight surgeon is trained for preventive care, diagnostic care and therapeutic care⁽⁸⁾. The flight surgeon will monitor and record crew behavior, which will serve as a data bank for future long term missions (lunar and Mars). Because of the diverse medical functions, the health facility is zoned according to

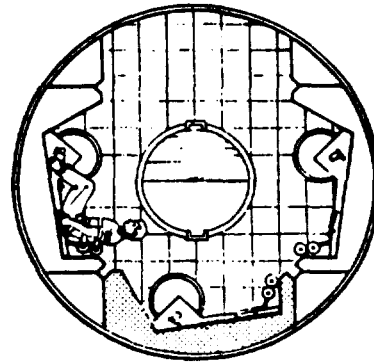


Fig. 8. Exercise Area

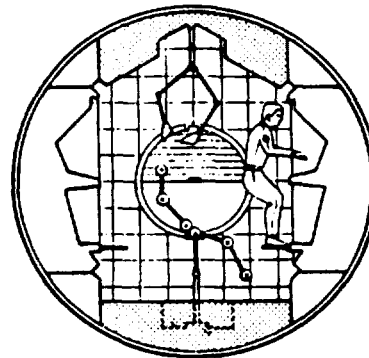


Fig. 9. Medical Area

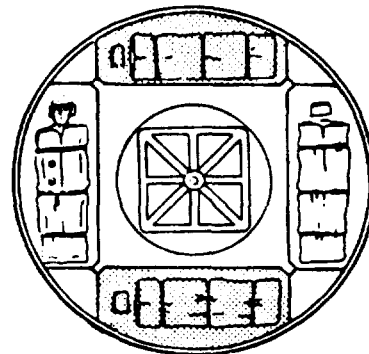


Fig. 10. Quarantine/Recovery Area

activity level to provide improved individual patient care and increased privacy.

Design solution. The HMF is a separate module shared with the experimental testbed. The HMF occupies 65% of a habitation module 14'6" (4.4 m) in diameter by 22' (6.7 m) in length. It is located adjacent to an assured crew return vehicle (ACRV) for expedient patient evacuation.

The HMF facility is zoned according to activity function: (1) exercise adjacent to the entrance of the module (most active); (2) medical and health monitoring located at center of the module (moderately active); and (3) recovery and/or quarantine adjacent to testbed (inactive) (see Figs. 8, 9, and 10).

Exercise as preventive care is particularly stressed. The bicycle ergometer and treadmill are cited as the most efficient devices. The exam table is redesigned as a restraining apparatus for improved patient comfort in microgravity. The airlock adjacent to the HMF also serves as a hyperbaric chamber in case of EVA decompression.

Because of the dangers of a hands-on environment in space, a fatality may occur. Preparation for such an event is neither pleasant nor predictable. In order to maintain crew safety, a rack system in the recovery area is designed as a temporary morgue using refrigeration techniques (to preserve the deceased crewmember and contain the spread of disease) until the body is transferred to Earth.

Assured Crew Return Vehicle (ACRV)

Goals. The goals for ACRV are to provide a simple, reliable vehicle that requires minimum crew training. The vehicle should be volume efficient, provide buoyancy (for water landing), reasonable loiter time (return trip time), and minimal g-stress upon reentry (for a deconditioned or injured crewmember).

Concepts.

- Apollo
- Station crew return alternative module (SCRAM)
- Reference configuration, Discoverer shaped
- Langley lifting body (see Figs. 11-14).

Design solution. Based on ACRV comparisons the "Reference" Discoverer design is chosen. It is 13'6" (4.1 m) in diameter by 11'6" (3.5 m) in length based on passenger capacity (6) with injured crewmember (8) uninjured crewmembers, 24-hour loiter time, single flotation point for buoyancy, minimal g-stress upon reentry and minimal crew interface⁽¹¹⁾. A total of three vehicles are necessary for complete evacuation of facility personnel (see Figs. 15 and 16).

Power Systems

Goals. The power systems' goals are to provide high output, reliability, efficiency, low weight and volume, and regulation of heat build up.

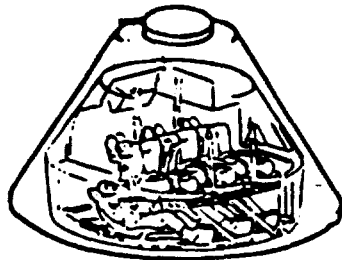


Fig. 11. Apollo-derived Vehicle⁽⁹⁾

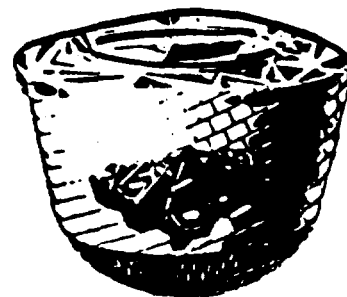


Fig. 13. Reference/Discoverer-Shaped⁽⁹⁾

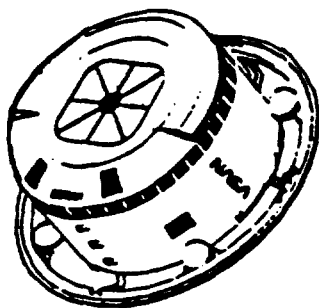


Fig. 12. SCRAM Vehicle⁽⁹⁾

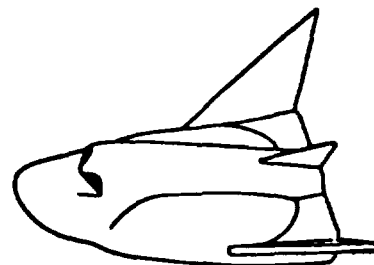


Fig. 14. Langley Lifting Body⁽⁹⁾

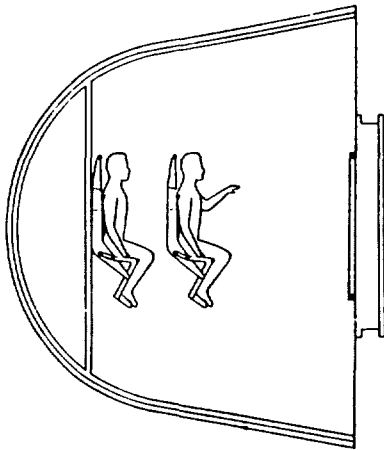


Fig. 15. Discoverer Longitudinal Section⁽¹⁰⁾

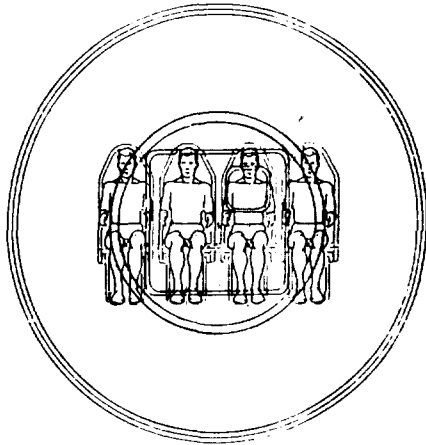


Fig. 16. Discoverer Cross-Section⁽¹⁰⁾

Concepts.

- Photovoltaics: (a) silicon cells (b) gallium arsenide cells
- Solar dynamic
- Electrochemical storage: (a) nickel cadmium batteries (b) nickel-hydrogen batteries
- Fuel cells
- Power management and distribution (PMAD): a system converting power from the solar arrays and distributing it to specific jobs.

Design solution. Spaceport *Aurora* requires a hybrid power system to ensure safe and efficient operation. Photovoltaic arrays (6 power modules; 20' (6.1 m) in width by 95' (29 m) in length) are used as a primary source of power with solar dynamics, 50' (15.24 m) in diameter, as the secondary system⁽¹³⁾. Nickel-hydrogen battery packs provide the backup system low mass and weight requirements⁽¹⁴⁾. A power management and distribution (PMAD) unit is required to control and distribute incoming power. Radiators are required to eliminate excess heat and are located near solar arrays and habitation area (see Figs. 17 and 18).

Fuel Depot

Goals. The fuel depot goals are to provide safe, efficient, stowage and transfer of propellant, while using minimal EVA and maximum telerobotic operation. The fuel depot is an important component for mission success, yet dangerous to crew safety. The immediate environment adjacent to the depot is prone to pollution from transfer of propellant and boiloff gases. Safety, therefore, is an important goal. The fuel depot should be remote from the habitation modules, yet easily accessible from the assembly area.

Concepts:

- Attached fuel depot
- Tethered fuel platform
- Co-orbiting fuel platform

Design solution. Based on a comparison of the three concepts, an attached fuel depot is chosen to reduce propellant transfer time. The depot is located opposite the habitation area to reduce risk of pollution (from fuel spill) and to provide a gravity gradient stabilized facility. The fuel depot

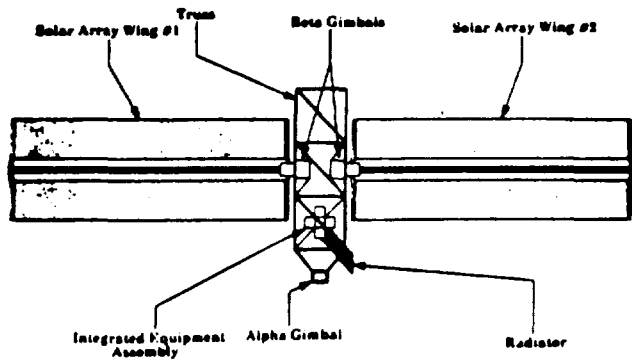


Fig. 17. Photovoltaic Module⁽¹²⁾

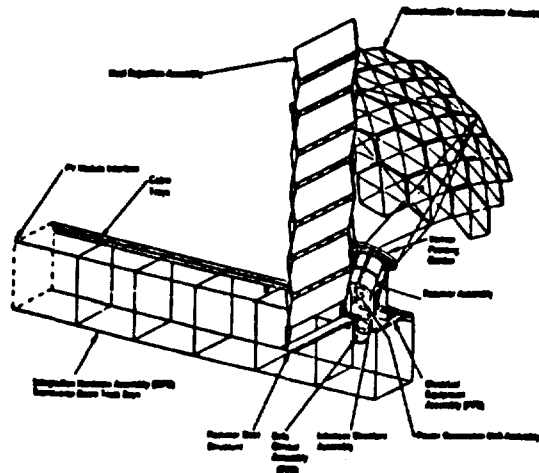


Fig. 18. Solar Dynamic System⁽¹²⁾

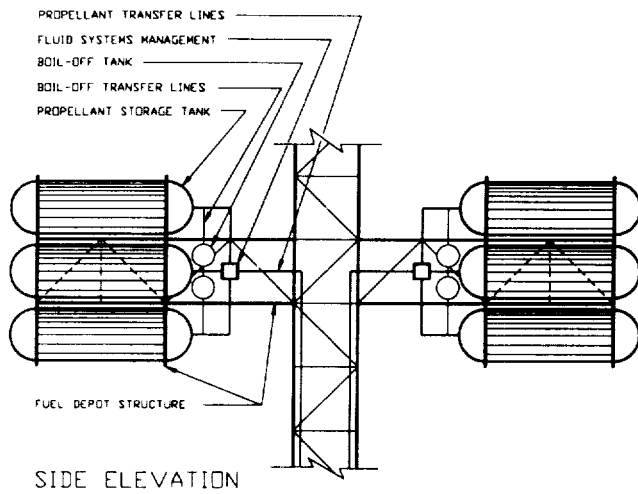


Fig. 19. Fuel Depot

consists of 8 propellant tanks (each containing an oxygen and hydrogen tank) 14'6" (4.4 m) in diameter by 44' (13.4 m) in length each containing 100,000 lb of propellant. The depot also contains a propellant management device (on either side of the truss), fluid transfer lines (refrigeration and heat lines), and is enclosed with a Kevlar micrometeoroid double skin⁽⁴⁾ (see Fig. 19).

The propellant tanks will be partially filled for the initial launch, since the orbiter's maximum cargo capacity is limited to 55,000 lb. Once connected to the fuel depot structure, each propellant tank will require two shuttle trips for maximum stowage capability (100,000 lb). The orbiter will transport a reusable transfer propellant tank to LEO, where the shuttle will rendezvous with Spaceport *Aurora*. Once the shuttle is

attached to the docking ring, transfer of propellant to the fuel depot occurs through transfer lines which connect to the transfer propellant tank. This operation is automated and monitored by a fuel specialist from within the command module; there is no need for EVA supervision for this activity. After the process is complete, the orbiter returns the transfer tank to Earth where it will be inspected and replenished with propellant.

Refueling of vehicles occurs after the vehicle has been serviced and repaired in the hangar. Vehicles within the hangars will contain no fuel to reduce risks to EVA personnel and to reduce pollution to nearby viewing cupolas. The RMS transports the vehicle toward the docking ring, where it is connected to a hard dock with propellant transfer lines. Once the vehicle is fueled, it is deployed with an attached OMV (acting as a space tug) and launched within the vicinity of Spaceport *Aurora*.

Experimental Plant Growth Facility

Goals. The primary goal of the plant growth facility is to gather data on the effects of microgravity on plants. A second goal is to provide an Earth-like environment to serve as a morale booster.

Concepts.

- Hydroponics: root is grown in nutrient solution⁽¹⁵⁾
- Aeroponics: root is grown in air⁽¹⁶⁾

Design solution. The plant growth facility is adjacent to the HMF occupying 35% of a habitation module 14'6" (4.4 m) in diameter by 12' (3.7 m) in length. Two standard racks are incorporated for growing plants using the aeroponic method. The aeroponic method consists of a nutrient solution line that sprays the plant root area within an enclosed membrane. A nutrient solution collector and return line

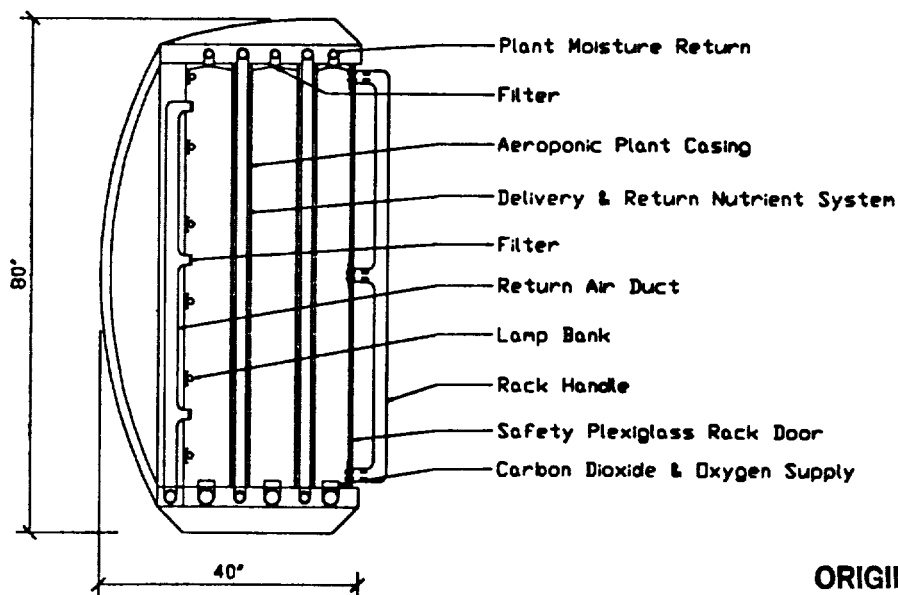


Fig. 20. Plant Growth Rack: Aeroponic Method

**ORIGINAL PAGE IS
OF POOR QUALITY**

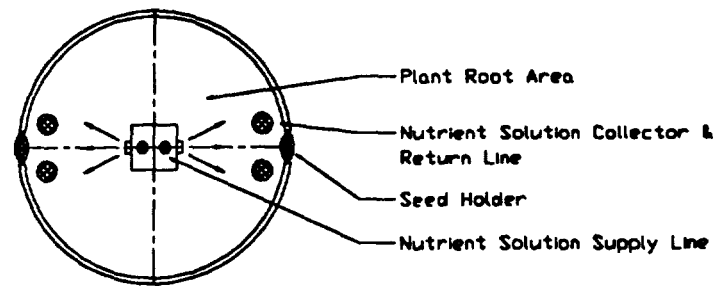


Fig. 21. Aeroponic Membrane Section

transfer the remaining solution to the storage tanks using pumps⁽¹⁷⁾. The plants within the racks will be grown in continuous artificial light cycles. A major concern is the heat that the lights generate. To reduce heat buildup, fiber optics are incorporated that provide the same light intensity and maintain low heat levels within the racks and module (see Figs. 20 and 21).

Along with the hardware above, management devices to monitor and operate the plants are necessary: (1) Atmosphere management: air revitalization, atmosphere pressure, module temperature and humidity control; (2) Water and waste management: water reclamation, water quality monitoring and solid waste management; (3) Food management: record edible biomass, food preparation and reclamation of inedible biomass⁽¹⁸⁾.

CONCLUSION

Spaceport *Aurora* is a low Earth orbit (LEO) gravity gradient stabilized transportation node, which provides support missions for the construction and maintenance of a lunar facility. All spaceport components are constructed and supported through the orbiter and OMV. Deployable truss systems and rigidized inflatable hangars are used to minimize EVA and expedite construction. Modularity and flexibility is enforced using existing space systems and subsystems (standard racks, airlocks, environmental controls, etc.) used in S. S. *Freedom*. Dual hangars, habitation modules and hyperbaric chambers serve as a backup in case of malfunction, which provides redundancy.

A total of 52 shuttle flights is necessary for full configuration of Spaceport *Aurora*. Estimating shuttle operation at peak capacity (10 flights per year), the time frame for full configuration is estimated at five years and six months. Total orbiter flights is calculated using mass of components transported, and an additional two flights (per phase of configuration) in case of unexpected logistics problems. Total mass transported at completion date of configuration will be 1,123,500 kg.

Safety, through enclosed hangars, evacuation vehicles (ACRV) and a remote fuel depot reduces risk to crewmembers. A productive environment is accomplished through zoning of the two different activities: working and living. Human comfort is achieved through the use of large crew quarters, private

spaces, and Earth viewing cupolas, which improve living conditions within a confined environment.

The configuration for Spaceport *Aurora* is based on a defined mission profile: to support a lunar facility and its space transfer vehicles. It is intended that the design for *Aurora* can be modified and adapted depending on the mission profile. Using existing space systems and subsystems, Spaceport *Aurora* can vary in configuration to accommodate different profile scenarios as space activity increases and a need for maintenance arises.

In conclusion, Spaceport *Aurora* will provide a convenient service route to the Moon. It is not intended as an end in itself but as a milestone along this journey. The spaceport is the logical rest stop to change the modes of space transportation. Much like an aircraft carrier the spaceport will act as a mobile landing strip to many space vehicles.

ACKNOWLEDGMENTS

Project Team Members were David Gutierrez, Mike Kennedy, Tina Mason, Paul Morin, David Mullican and Ramon Patino. Faculty advisor was Deborah J. Neubek.

REFERENCES

1. Covault, Craig. 1989. Space station changes for lunar base would cost NASA more than \$1 billion. *Aviation Week & Space Technology*, October 9th.
2. Bond, Victor. 1990. Interview by author, February 6. University of Houston: Clear Lake.
3. Livingston, Lewis. 1989. Interview by author, October 10. University of Houston - SICSA: Houston.
4. Eagle Engineering, Inc. 1988. Transportation node space station conceptual design. NASA contract NAS9-17878. Eagle Engineering report no. 88-207. Houston: Eagle Engineering, Inc.
5. Bedini, Dr. Daniele. 1988. Space station habitation module: privacy and collective life. IAF-88-080.
6. NASA. 1989. Man-systems integration standards. Revision A. NASA-STD-3000.
7. Thornton, Dr. Bill. 1989. Telephone conversation with author. October 16.
8. Bueker, Richard. 1989. Interview by author, October 4. KRUG International: Houston.
9. NASA. S-87-00431, 1987.
10. NASA. ACRC CERV Option Reference Concept. J. O. 052-PA-301, 1988.
11. NASA CERV Office, New Initiatives Office. 1988. ACRC - CERV Phase A Report. JSC-23321. NASA Johnson Space Center. Houston.

12. NASA. Space Station Freedom Media Handbook, 1989.
13. Baraona, Cosmo R. 1986. The space station power system. Cleveland, Ohio.
14. Cochran, T.H. and T.L. Labus. 1987. Space station electrical power system. 38th Congress of the International Astronautical Federation. IAF-87-234. 10-17 Oct., at Brighton, United Kingdom.
15. Greene, Joseph. 1989. Bioregenerative life support systems and space flight. NASA Educational Publication.
16. Robbins, Jim. 1987. Second nature. The Sunday Times Magazine London. June 28th.
17. Schwartzkopf, Steven H., Mel W. Oleson, Hatice S. Cullingford. 1989. Conceptual design of a closed loop nutrient solution delivery system for CELSS implementation in a micro-gravity environment. 19th Intersociety Conference on Environmental Systems. 24-26 July, at San Diego, CA.
18. Henninger, D. L. 1989. Life Support Systems Research at the Johnson Space Center. *Lunar Base Architecture: Soils for Plant Growth*, Madison, WI. ASA-CSSA-SSSA.

IN-SITU RESOURCE UTILIZATION IN THE DESIGN OF ADVANCED LUNAR FACILITIES

P. 9
N 91 - 18134

UNIVERSITY OF HOUSTON COLLEGE OF ARCHITECTURE

Resource utilization will play an important role in the establishment and support of a permanently manned lunar base. At the University of Houston - College of Architecture and the Sasakawa International Center for Space Architecture, a study team recently investigated the potential use of lunar *in-situ* materials in the design of lunar facilities. The team identified seven potential lunar construction materials: concrete, sulfur concrete, cast basalt, sintered basalt, glass, fiberglass, and metals. Analysis and evaluation of these materials with respect to their physical properties, processes, energy requirements, resource efficiency, and overall advantages and disadvantages lead to the selection of basalt materials as the more likely construction material for initial use on a lunar base. Basalt materials can be formed out of *in-situ* lunar regolith, with minor material beneficiation, by a simple process of heating and controlled cooling. The team then conceptualized a construction system that combines lunar regolith sintering and casting to make pressurized structures out of lunar resources. The design uses a machine that simultaneously excavates and sinters the lunar regolith to create a cylindrical hole, which is then enclosed with cast basalt slabs, allowing the volume to be pressurized for use as a living or work environment. Cylinder depths of up to 4-6 m in the lunar mare or 10-12 m in the lunar highlands are possible. Advantages of this construction system include maximum resource utilization, relatively large habitable volumes, interior flexibility, and minimal construction equipment needs. Conclusions of this study indicate that there is significant potential for the use of basalt, a lunar resource derived construction material, as a low cost alternative to Earth-based materials. It remains to be determined when in lunar base phasing this construction method should be implemented.

INTRODUCTION

With the announcement of President Bush's plan to return man to the Moon permanently, it will be important to identify new and innovative technologies that will insure the success, sustainability, and eventual growth of a lunar base. Many of these technologies involve the use of lunar resources. Lunar resources can be used to supply needed replenishables for a lunar base, replenishables that would otherwise have to be brought from Earth, a more costly alternative. Lunar resources contain abundant supplies of oxygen for life support systems and rocket propellant, and less abundant but significant supplies of volatile gases. Additionally, lunar resources can be used to supply construction materials for the growth of a lunar base. The use of lunar-derived construction materials will be one of the most significant steps toward self-sufficiency and independence from terrestrial resources.

In view of this important step, research at the University of Houston-College of Architecture and Sasakawa International Center for Space Architecture has been undertaken to identify and analyze potential lunar-derived construction materials, and apply the findings to the design of an advanced lunar facility. This paper presents a summary of these findings and a summary of the final design concept that was developed as a NASA/USRA advanced design project.

Project Goals

The four primary goals of this project are:

- To develop a structural system using products derived from lunar resources;
- To design pressurized and unpressurized structures that exploit the use of lunar resources;

- To discover economical and practical uses for lunar resources in support of lunar structures; and
- To establish self-sufficiency and independence from terrestrial resources.

Project Assumptions

In general, it is assumed that the use of lunar-derived construction materials would begin at an advanced phase of a lunar base, not at its initial phase. Because of the dynamic character of lunar base planning at present, the design team chose not to assume any single scenario, preferring instead to concentrate on the development and organization of a structural system that is both functionally flexible and adaptable to many lunar base scenarios.

LUNAR RESOURCES

Of the potential resources, the lunar regolith is the most accessible and easily converted into lunar construction materials. It is, on average, 80 μm in diameter, and contains oxygen, silicon, magnesium, iron, calcium, aluminum, and titanium as its seven primary elements⁽¹⁾. It can be divided into two groups, the mare basalts and the anorthositic highland rocks. The mare basalts are relatively higher in iron, magnesium, and titanium content, and have a surface depth between 4 to 6 m. The anorthositic highland rocks are relatively higher in aluminum and calcium content, and have a surface depth between 10 to 12 m. Figure 1 shows the average elemental compositions of lunar surface regolith for both the mare and the highlands.

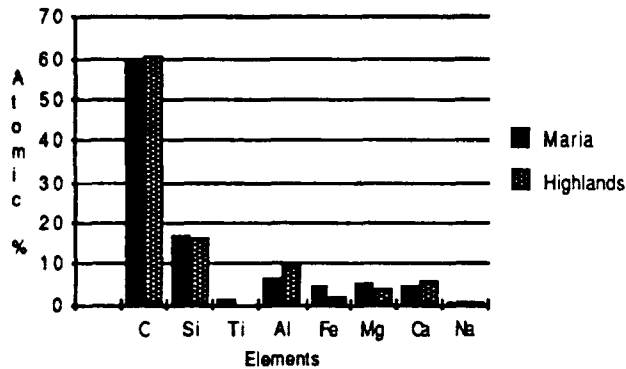


Fig. 1. Average Elemental Compositions of Lunar Surface Regolith

CONSTRUCTION MATERIALS

The research team identified seven possible construction materials that can be derived from lunar resources. These materials include two varieties of basalt, cast and sintered; two varieties of glass, cast and fiber; concrete; sulfur-based concrete; and metals. Each construction material was evaluated on criteria that included physical properties, production processes, energy requirements, material resource yields, products, applications, and miscellaneous requirements of the material such as dependence on terrestrial resources. A very brief overview of each construction material is given below.

Basalt

Basalt can be formed in two different ways, casting, a process by which regolith is heated until molten, poured into molds, and then cooled in a slow, controlled manner, and sintering, a process by which regolith is heated under pressure (below the melting point), causing the regolith material to bind together. Basalts, in general, have high compressive strengths, involve simple processing techniques, are resistant to chemicals and abrasion, have good resource yields, and are easily cast. Disadvantages of basalt include its brittleness, low tensile strength, and the need for metal molds in precision casting.

Glass

Glass can be cast into blocks and panels, or it can be spun into fibers. The primary difference between glass and basalt

processing is that the cooling rate of glass is much higher. Glass, when manufactured in the anhydrous vacuum conditions of the lunar environment, attains extremely high compressive and tensile strengths. Unfortunately, it loses much of its strength when exposed to air, has very high energy requirements for processing, is very brittle, and requires organic bonding agents when produced as fiberglass.

Concrete

Lunar concrete is very similar to Portland cement concrete used here on Earth. Advantages of this construction material include its relatively simple production, low energy requirements, high abrasion resistance, and easy castability. The major disadvantage of lunar concrete is that it requires water, or in the case of lunar oxygen production, hydrogen to be supplied from the Earth. Additional disadvantages include its low tensile strength, long curing time, and the requirement of pressurized processing.

Sulfur-based Concrete

As the name implies, sulfur-based concrete uses sulfur as the binding agent. Advantages include its high early strength, resistance to corrosion, and its independence from terrestrial resources. Disadvantages include material deterioration at lunar daytime temperatures, low sulfur yields from the lunar regolith, and flammability of the sulfur.

Metals

As was shown earlier, a number of metals exist in the lunar regolith including iron, magnesium, aluminum, and titanium. These metals, because of their high tensile and compressive strengths and their ability to be formed into small, intricate parts, would be ideal for construction materials for lunar applications. Unfortunately, extraction of metals on the Moon is an extremely complicated and high energy process, with relatively low yields. Only if metal extraction were linked with another process, such as the reduction of ilmenite for oxygen, would the process approach effectiveness.

Table 1 shows the physical properties of candidate construction materials. Iron was chosen as a representative metal because it is easier to extract than other metals and, therefore, a more likely candidate for a lunar construction material.

Figure 2 presents a summary of candidate construction materials. Each material was given grades for processing

Table 1. Physical Properties

	Glass	Basalt	Concrete	Sulfur Con.	Iron
Compressive Strength (MPa)	620	540	76	55	—
Tensile Strength (MPa)	3000	35	—	7.1	270
Modulus of Elasticity (GPa)	870	110	21	—	196
Density (g/cm ³)	2.7	2.9	2.4	2.4	7.8
Melting point (°C)	1500	1300	600	115	1537
Cooling point (°C)	760	800	—	—	—
Thermal Expansion (cm/cm°C)	4.2×10^{-6}	7.8×10^{-7}	1.19×10^{-5}	1.44×10^{-5}	1.2×10^{-5}

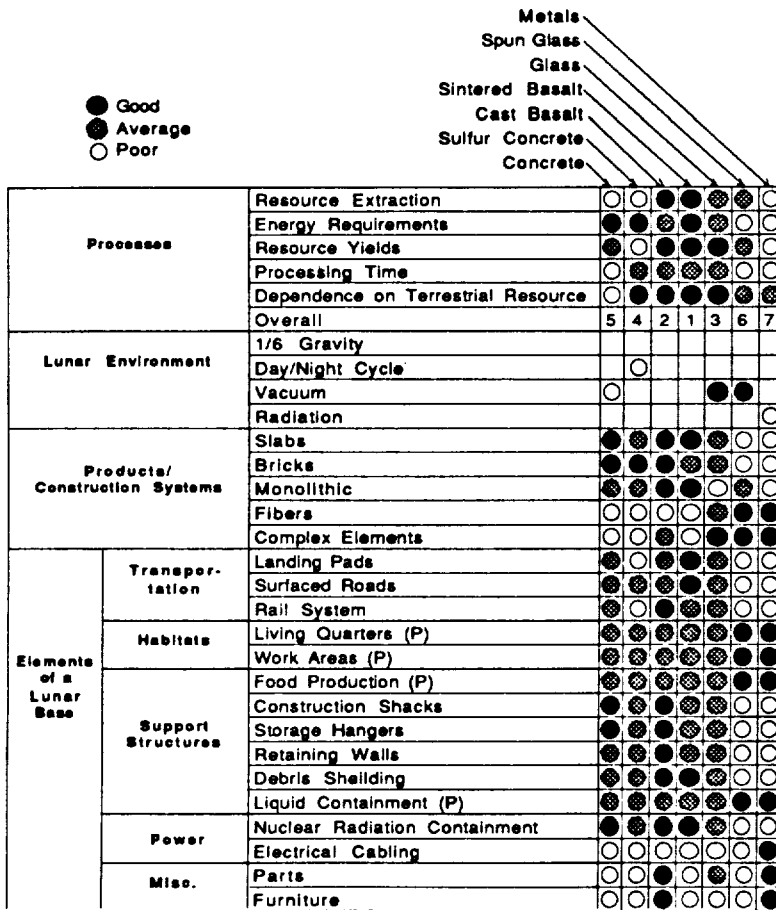


Fig. 2. Material Summary

according to characteristics of resource extraction, energy requirements, resource yield efficiency, processing time, and dependence on terrestrial resources. An overall process ranking was then given to each construction material. Effects of the lunar environment on each construction material were positively or negatively noted, and possible products were identified. Finally, applications of each construction material were evaluated according to various elements of a lunar base. Thus, it was easy to identify the construction material or materials that would meet the goals of the project and would be more appropriate for initial use on a lunar base.

Basalt materials were chosen for use on this project because of their high yield efficiency, simple process, short processing time, independence from terrestrial resources, variety of potential products and applications, and the lack of negative lunar environment effects.

DESIGN

The design of a lunar facility that uses lunar-derived construction materials as its primary component is a difficult and highly complicated task. The design team chose to simplify this process somewhat by taking a systems integration approach to the problem. This approach emphasizes the articulation of various construction components, how they fit

together, and how they are constructed. Additionally, the facility is seen as the initial application of lunar-derived construction materials to a pressurized structure, a prototypical facility that offers proof of concept. The design team, therefore, concentrated on determining the most effective conceptual approach to constructing pressurized structures on the Moon with emphasis on system flexibility, modularity, simplicity, ease of production, and adaptability to automation.

DESIGN CONSIDERATIONS

Before continuing with a description of the final design concept, it may be useful to briefly discuss some of the design considerations unique to the lunar environment and the effects they may have on the design of basalt structures.

Gravity Level

The most obvious difference between the Moon and the Earth is the gravity level. With the gravity level of the Moon approximately 1/6 that of the Earth, lunar structures will be able to carry a dead load six times the mass of a comparable terrestrial structure. Spans can be increased with a significant savings in construction materials, or, as with pressurized structures, additional regolith for thermal and radiation

protection can be supported. Lunar basalts can be cast in sizes and shapes that will be optimal for lunar construction. Additionally, construction equipment can be downsized because of the lower gravity level, which will offer significant savings in transportation costs.

Radiation Shielding

Protection from the harmful effects of radiation will play an important role in the design of lunar structures. It has been shown that 0.5 meters of lunar regolith is needed to reduce radiation dosages to safe and acceptable levels for short-term stays⁽²⁾. Long-term missions will require additional protection. The lunar basalt structure must be able to support this additional mass in case of depressurization. Definition of high use areas, both pressurized and unpressurized, must be made in order to determine which structures should receive radiation shielding.

Thermal Shielding

In some situations, such as habitats and equipment storage structures, thermal shielding should be provided. Measured temperatures on the lunar surface range between 111°C and -171°C⁽³⁾. Lunar basalt is capable of handling these extremes in temperature without physical or structural degradation.

Vacuum

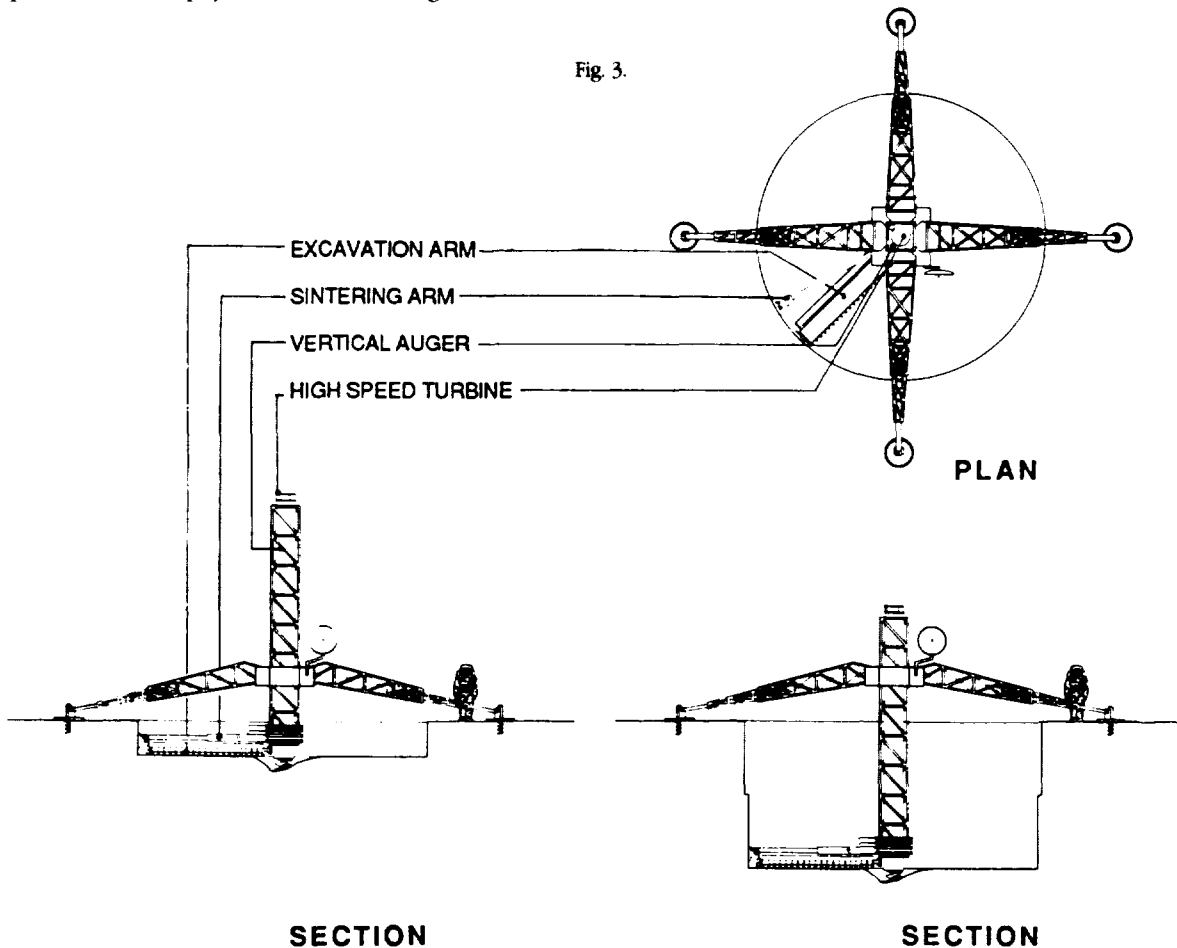
Besides affecting lunar basalt fabrication processes and product strength⁽⁴⁾, vacuum conditions also affect long-term structural properties. Without an atmosphere, the Moon is devoid of most of the harmful effects of terrestrial weathering. This, combined with the fact that basalt is highly resistant to corrosion and abrasion, will give lunar structures extremely long lifespans, and will alleviate many of the problems of continued maintenance.

Lunar Dust

Lunar dust is a highly abrasive, electrostatically charged material. As was shown by the Apollo program, the lunar dust has a negative effect on operations and could present a serious threat to astronaut safety through degradation of equipment and hardware. Cast basalt, because of its high abrasion resistance, is an ideal structural material for the lunar surface.

Automation

Considering the harsh conditions of the lunar surface, automated and teleoperated capabilities will need to be maximized for lunar construction. EVA time will be limited,



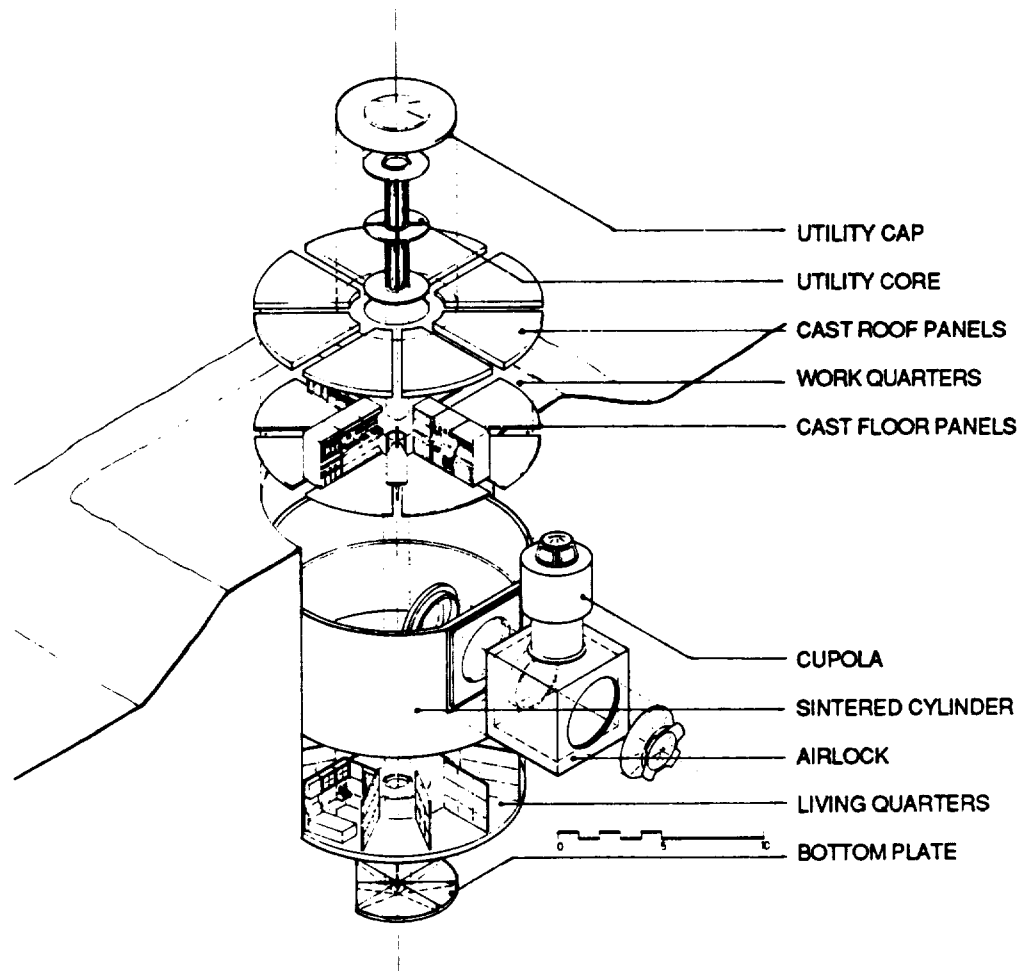


Fig. 4.

therefore expanding the need for robotic and telerobotic construction techniques. Systems should be developed that can easily adapt to different shapes and sizes of lunar basalt materials. In pressurized structures, joints should be minimized to ease assembly and accelerate the construction process. Manufacturing and construction systems should allow for quality control testing of construction materials and joints.

Auxiliary Systems and Interfaces

Auxiliary systems, such as environmental control systems, will need special attach points and interfaces allowing penetration through the structural cavity. There may be a need for modular inserts that can accommodate a number of different systems. Pressurized structures will require additional support around penetrations, increasing the size and mass of the basalt materials.

DESIGN DESCRIPTION

Numerous design concepts were considered before the final solution was realized. These design concepts were classified

into one of three types: monolithic systems, panel systems, or block systems. Monolithic systems, in general, are built-up in a single step process, forming an integral shell-like structure. Block and panel systems, on the other hand, are built from prefabricated pieces, which are then assembled on site, the only difference between the two being the size of their pieces. The final design solution incorporates construction processes from monolithic and panel systems.

The key ingredient of the final design solution is the Regolith Excavation and Sintering Machine (RESM) which, as the name implies, excavates and sinters a cylindrical hole in the lunar surface. Figure 3 shows a plan and two sections of the machine. The RESM's excavation arm first sweeps up the regolith in a circular pattern transferring it to a vertical auger that moves the regolith to the top of the machine where a high speed turbine throws the regolith out and away from the construction site. As the excavation arm continues removal of the regolith, the sintering arm follows closely behind turning the walls of the excavated hole into sintered basalt. The final output of the machine is a cylindrical hole with walls of sintered basalt, 10-15 m in diameter and 6-12 m in depth, depending on the location of the construction site.

The RESM is an easily deployable structure (the legs retract and fold during transport) that has been designed to fit into the cargo bay of the current Space Transportation System. Operation has been automated as much as possible, reducing EVA time and construction expense. Additionally, the RESM, as a primary reusable component of the construction system, significantly reduces continuing construction costs.

Advantages of constructing a subsurface facility are numerous. The surrounding regolith helps to equalize the internal forces of a pressurized structure relieving loads on the shell structure. A subsurface facility also reduces the amount of surface area that must be protected by transferred regolith from cosmic and solar radiation. Regolith that is removed in the construction process is simply piled back on top of the completed structure, alleviating the need for the complicated processes and equipment of above surface protection systems. Additionally, subsurface facilities utilize the regolith *in-situ*, transforming the regolith into a primary building component, which in turn minimizes energy usage and EVA time.

Figure 4 shows an exploded isometric of the completed facility. This cylindrical facility, designed for an unspecified lunar mare site, is 10 m in diameter and 6 m in depth, and consists of 2 floors, the upper configured as work quarters, and the lower as living quarters. The middle floor and roof are comprised of precast, pie-shaped basalt panels that rest on a prepackaged utility core. The utility core, shipped from Earth as a single package, provides the necessary structural rigidity

for the pressurized facility, while allowing complicated utility systems to be packaged as a single unit. Two airlocks are provided (Fig. 4 shows only one for visual clarity) for requirements of dual egress. The airlocks are constructed from six equally sized cast basalt panels to minimize formwork, each containing metal inserts for necessary interfaces, such as hatch doors, etc.

The design team concentrated on a systems approach to the problem. Interior layout and functionality of the presented concept is only one of many possible configurations. Flexibility is a key aspect of the design. Configuration of the interior building systems lends itself to manipulation for changing uses of the facility. Organization around a central utility core maximizes the amount of usable space, and provides a degree of geometric modularity. Modular cast basalt partitions can be used to separate individual crew quarters and work areas, reducing the amount of interior components that must be brought from Earth. Additionally, these interior partitions can be designed and cast to support a variety of attachable fixtures.

Figure 5 shows a section/elevation of the completed facility. Cupolas have been placed above the airlock to allow viewing of the lunar landscape and observation of telerobotic and automated systems. Circulation between floors is provided by a simple ladder, and equipment can be lowered into the first level by a mechanical pulley system. A modular rack system can be used to simplify equipment changeout, much like what is planned for use on the Space Station *Freedom*.

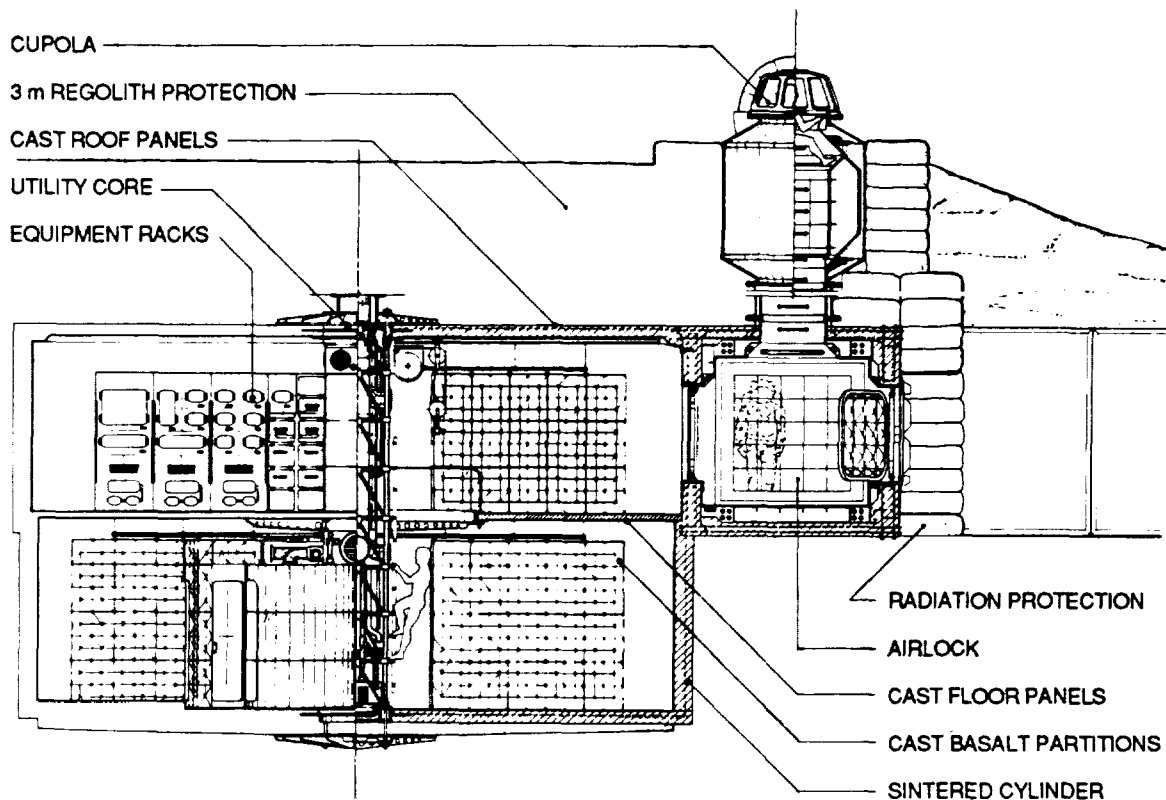


Fig. 5.

FACILITY ASSEMBLY

Step 1

The first step in the construction of the advanced lunar facility is the digging of trenches for the airlocks. In the final design configuration, these are set at an angle of 180° to each other, allowing minimum distance to egress in emergency situations. Regolith is moved by bulldozing equipment that is already present on the lunar base for mining of oxygen, thus improving the cost efficiency of the equipment and the facility. The cast panels adjacent to the cylinder walls are set in place. This will allow the RESM to structurally integrate the cast panels with the finished sintered walls of the cylinder, forming a monolithic structure, (Fig. 6a).

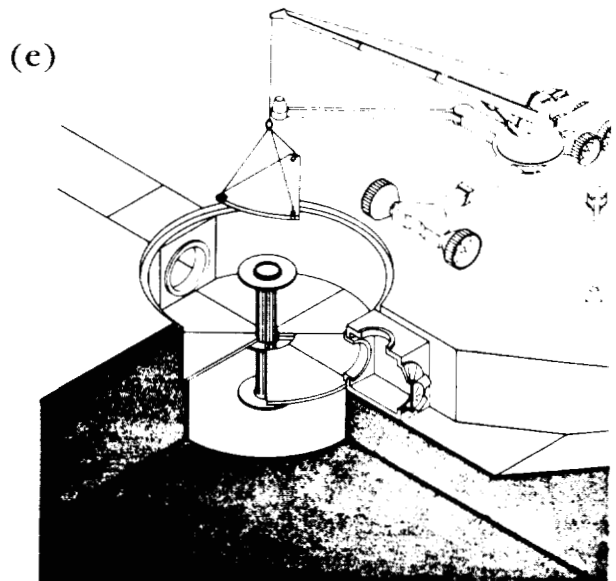
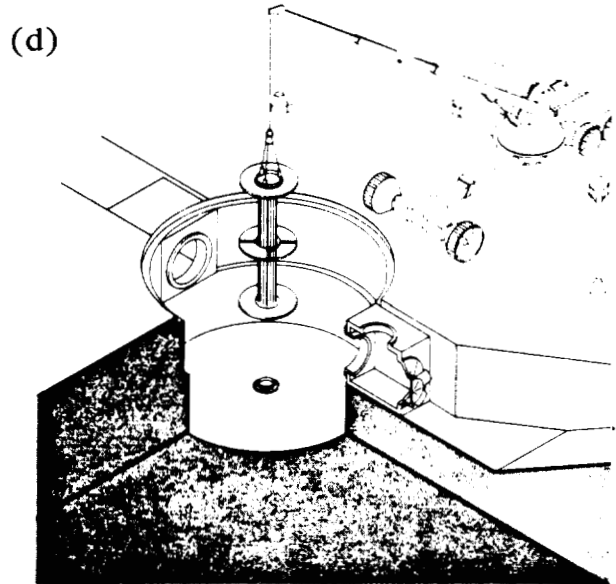
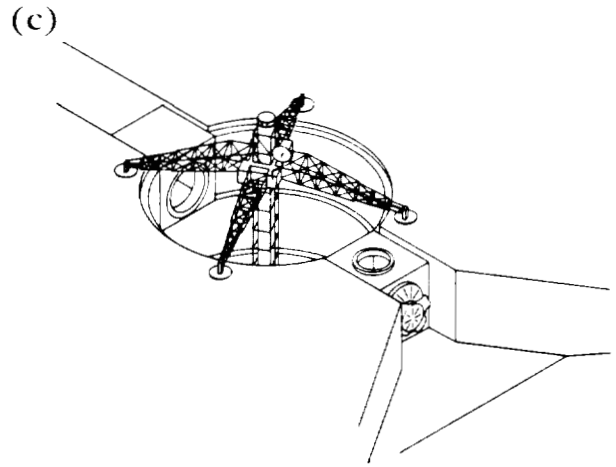
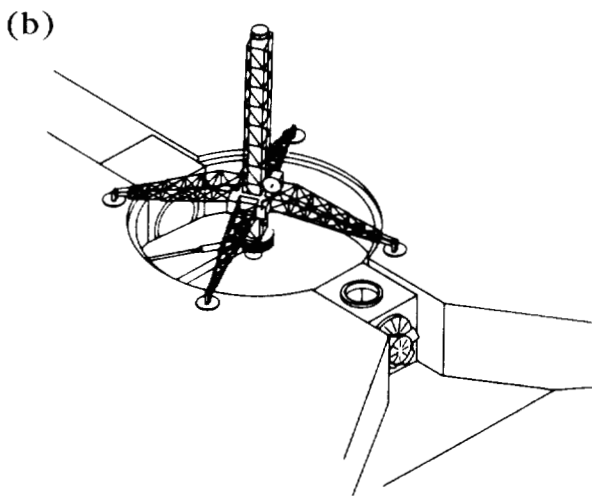
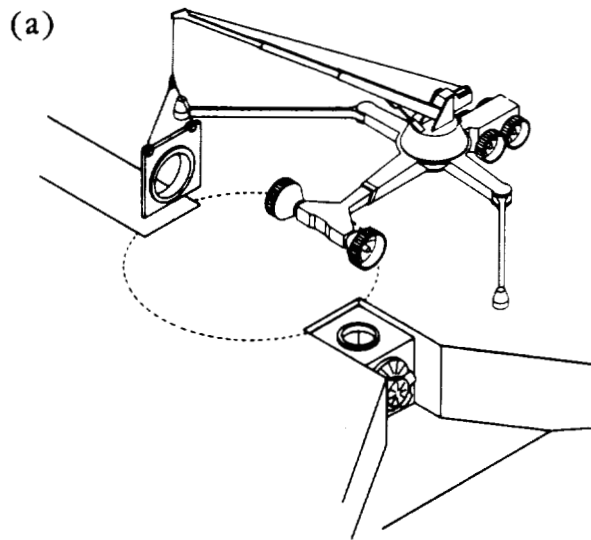
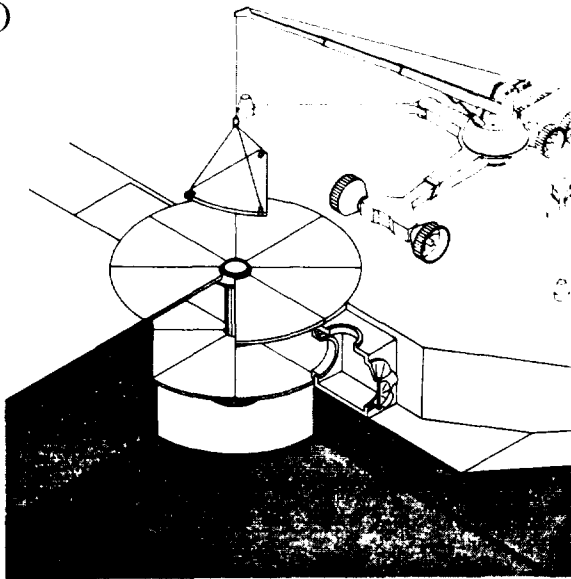


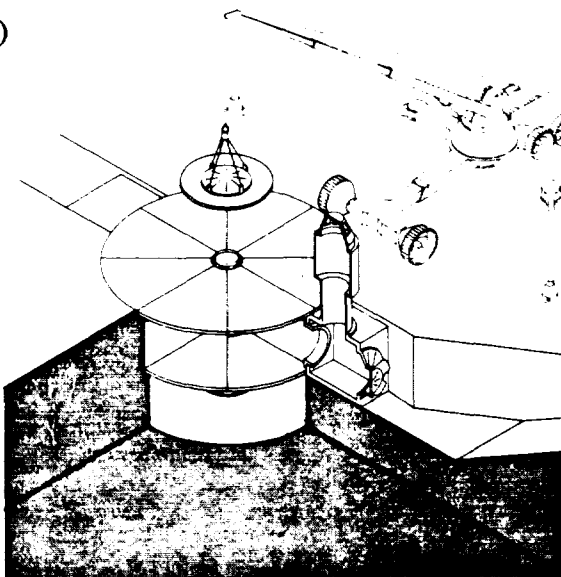
Fig. 6. (a)-(h) Facility Assembly

(f)

**Step 2**

The Regolith Excavation and Sintering Machine is lowered into place by the lunar base crane. The legs are unfolded and extended to the proper length, and the excavation and sintering arms are attached. The machine begins the excavation of the cylinder, transferring the removed regolith to the surrounding landscape. The removed regolith will be eventually used to cover the facility for radiation and thermal protection required for human habitats. The sintering arm follows closely behind the excavation arm, applying heat and pressure to the regolith walls forming a 10-20 cm crust of basalt. Ledges are sintered in place, allowing easy placement and support of the cast basalt floor and roof slabs by the lunar base crane (Fig. 6b).

(g)

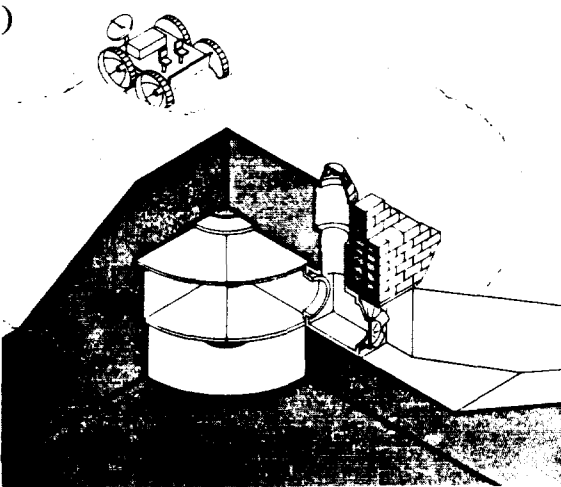
**Step 3**

Excavation and sintering continues. If a large object is encountered, teeth on the excavation arm simply move the object to a basket located behind the arm. The design team chose a facility depth of 6 m, allowing accommodation of a two-level facility, the upper serving as crew work area and the lower serving as crew living area. After the walls are sintered, a bottom structural plate is buried in the regolith. This plate will serve as an attach point for the utility core. The floor of the cylinder is then sintered, integrating the bottom plate into the monolithic structure. The arms are then detached and brought out of the hole, and the crane moves the RESM to the next construction site (Fig. 6c).

Step 4

Next, the utility core is brought to the site by a lunar utility vehicle, hoisted by the lunar base crane, and lowered into the cylindrical cavity. The utility core is carefully attached to the bottom plate. The utility core, a pre-packaged system brought from Earth, contains all essential systems for the facility, including the life support, air handling, electrical, communications, and heat control systems. The utility core is also a primary component of the facilities structure. The utility core will be wrapped in a protective covering (not shown), keeping the equipment from the damaging effects of lunar dust (Fig. 6d).

(h)

**Step 5**

The middle floor pieces, eight total, are then lowered into place. The floor pieces are made of pie-shaped cast basalt and are set into preconstructed notches in the sintered wall and the utility core. This enables easy installation, requiring minimal EVA time for crane operation. Additionally, the basalt floor pieces are the same size and shape, allowing one metal mold to cast all pieces, thus saving additional transportation costs and eliminating unnecessary waste. The middle floor is separate from the structure enabling, if necessary, the removal of pieces for other interior configurations (Fig. 6e).

Step 6

The cast basalt roof panels are then placed into the preconstructed notches located on the top of the utility core and the side of the sintered cylinder wall. The cast panels contain grooves on abutting edges, which allow the pouring of superheated molten regolith to join the panels together. The superheated regolith partially melts the surrounding cast basalt, fusing the panels together into a single unit, thus allowing the completed facility to act as a monolithic structure. The surrounding regolith helps alleviate much of the stress on the structure, and outward forces on the cylinder top are held in check by the structural integrity of the utility core (Fig. 6f).

Step 7

The utility core and the cylinder top are then capped with a prefabricated metal piece which is the final structural component of the utility core and the lunar facility (Fig. 6g). The observation cupola is also set in place at this time. The cupola, delivered from Earth, will allow for the monitoring of telerobotic systems and the viewing of space and the lunar environment. Exterior viewing will meet some of the psychological needs of the crew and eliminate many of the negative characteristics of subsurface structures. The structure can now be pressurized and interior systems can be delivered and assembled in a shirtsleeve environment. If necessary, an interior vapor barrier can be applied at this time.

Step 8

Covering the facility with regolith is the final step in the assembly process. The regolith, which was excavated from the cylinder, is pushed by a bulldozer over the top of the facility to a depth of at least three meters giving more than adequate protection from both solar and cosmic radiation to the inhabitants below (Fig. 6h). Final assembly and checkout of the interior systems occurs, and the facility is ready for use. Additional facilities can be constructed with the same equipment and the necessary prepackaged systems shipped

from Earth. Other facilities may require less equipment, depending on their function, saving additional transportation cargo space for other needs.

CONCLUSIONS

Lunar resource utilization will play an important and ever-increasing role in the sustainability and growth of a lunar base. After lengthy analysis, the design team determined that basalt, a construction material that can be derived from lunar regolith, will best support the needs of both pressurized and unpressurized structures. The design solution presented in this paper offers a system of simplicity, modularity, and flexibility, achievable in an economic and cost effective manner.

Further research is necessary on basalt structures, in general, and the effects of the lunar environment on basalt processing. Additionally, research must begin on joining techniques, especially between sintered and cast components. Eventually, more accurate studies will need to be conducted on the proper phasing of basalt structures into a lunar base scenario.

ACKNOWLEDGMENTS

Study team members were M. G. Fahey, P. C. Spana, and T. K. Wise. Faculty advisors were L. Bell, G. Trotti, and D. Neubeck with Dr. A. Binder, consultant.

REFERENCES

1. Binder, Alan B. 1988. Lunar Resources: What is known and expected. *Engineering, construction, and operations in space*. Johnson, Stewart W. and Wetzel, John P., editors. American Society of Civil Engineers, New York, New York. pp. 48-54.
2. Nealy, John E., John W. Wilson, and Lawrence W. Townsend. 1988. *Solar-flare shielding with regolith at a lunar-base site*. NASA Technical paper 2869.
3. Schmitt, Harrison. 1988. Constraints on lunar base construction. *Engineering, construction, and operations in space*. Johnson, Stewart W. and Wetzel, John P., editors. American Society of Civil Engineers, New York, New York. pp.35-45.
4. Dalton, Charles and Edward Hohmann, editors. 1972. *Design of a lunar colony*. Report prepared by the University of Houston, NASA Manned Spaceflight Center and Rice University under NASA grant NGT44-005-114.

PRELIMINARY GREENHOUSE DESIGN FOR A MARTIAN COLONY: STRUCTURAL, SOLAR COLLECTION AND LIGHT DISTRIBUTION SYSTEMS

UNIVERSITY OF IDAHO

N91-18135

The design of a greenhouse that will be a component of a long-term habitat on Mars is presented. The greenhouse will be the primary food source for people stationed on Mars. The food will be grown in three identical underground modules, pressurized at 1 atm to allow a shirt-sleeve environment within the greenhouse. The underground location will support the structure, moderate the large environmental variations on the surface, and protect the crops from cosmic radiation. The design effort is concentrated on the outer structure and the lighting system for the greenhouse. The structure is inflatable and made of a Kevlar 49/Epoxy composite and a pipe-arched system that is corrugated to increase stiffness. This composite is pliable in an uncured state, which allows it to be efficiently packaged for transport. The lighting system consists of several flat-plate fiber optic solar collectors with dual-axis tracking systems that will continually track the sun. This design is modeled after the Himawari collector, which was designed by Dr. Kei Mori and is currently in use in Japan. The light will pass through Fresnel lenses that filter out undesirable wavelengths and send the light into the greenhouses by way of fiber optic cables. When the light arrives at the greenhouse, it is dispersed to the plants via a waveguide and diffuser system.

INTRODUCTION

The greenhouse is intended to be the primary food source for a Mars-based habitat. The food will be grown in three identical modules that are located underground. The design effort is concentrated on the outer structure and a lighting system for the greenhouse. The structure is inflatable, made of a Kevlar 49/Epoxy composite that is corrugated to increase stiffness. The lighting system consists of several flat plate fiber optic collectors with dual-axis tracking systems that continually follow the sun. The light passes through Fresnel lenses that filter out undesirable wavelengths and send the light into junction boxes in the top of the structures by way of fiber optic cables. The light is then taken from the junction boxes and dispersed to the plants by a waveguide and diffuser system.

STRUCTURAL DESIGN

The design of the outer structure of the food production system consists of three identical modules, each having the capability of producing 50% of the food required by the Mars colony. The modules will be located at a depth of 4 m below the martian surface. This underground location will shield the plants and colonists against harmful radiation, support the structure, and assist in moderating the extreme environmental variations that occur on the surface of Mars. The structure will be pressurized at 1 atm, or 101.3 kPa, in order to maintain a shirt-sleeve environment in which the colonists can work without requiring the use of a pressurized spacesuit.

The structure of the greenhouse is inflatable and is made of prepreg composite material that can be cured to a permanent, solid structure. An inflatable structure has several advantages over a rigid design including the ease with which it can be packaged and transported, as well as the reduction of workload associated with the construction of the greenhouse. Most importantly, however, is the fact that an inflatable structure made of a composite that is pliable in an uncured state can be inflated and tested on Earth, and then deflated and packaged for transport to Mars.

The composite chosen for the structure of the greenhouse is Kevlar 49/Epoxy. Kevlar 49/Epoxy has excellent material properties, including its specific tensile strength, specific stiffness, and impact strength. This composite also has a high potential for structural use as well as a high repairability rating⁽¹⁾. The structural properties of Kevlar 49/Epoxy compare well to other structural materials (see Table 1).

Table 1. Materials Comparison

Material	Density (lb/in ³)	Spec Tensile Strength (× 10 ⁶ in)	Spec Stiffness (× 10 ⁸ in)	Repara- bility	\$/lb (88)
Stainless Steel	0.29	0.86	1.03	moderate	2.46
Al 2024-T6	0.10	0.57	1.05	moderate	1.87
Ti-6Al-4V	0.16	0.81	0.99	low	20
Graphite/Al	0.09	1.14	2.33	moderate	1000
Kevlar 49	0.05	5	2.2	high	15

Growing Area

The growing area that is required for this application has been determined by an USRA-sponsored design team at the University of Florida⁽²⁾. In that study, the food supply was to support a colony of eight people. The current design is to support 10 colonists, so the growing area has been increased proportionally. The total growing area required is 534 m². This area incorporates a safety factor of 1.5 into the design.

Dimensions

Three separate modules are required for food production, each with dimensions of 7.62 × 15.24 m. Because of the excellent load-carrying ability as both a pressure vessel and an underground structure, a domed-shaped cylinder is used for the modules. The ends of the structures are also domed, yielding a total floor area of 136.66 m². The domed ends

provide area for activities not accounted for in the growing area estimation, such as germination and harvesting. The total internal volume of each module is 463.26 m³.

The walls of the structure are corrugated to increase rigidity and stability in a loss-of-pressure situation within the greenhouse. Before inflation of the structure is completed, an internal floor frame is inserted to help the structure retain its shape during the installation process. The internal flooring provides space for irrigation, heating, electrical, and other greenhouse-related systems.

In determining a suitable wall thickness for the structure, two loading scenarios are considered. For the first condition, the greenhouse is modeled as a pressure vessel⁽³⁾. This analysis is applicable under normal operating conditions; however, a second approach must be considered in the event of a loss-of-pressure situation in the greenhouse. For the second condition, the greenhouse is modeled as an underground culvert. This analysis involves two procedures for culvert design: (1) a culvert design code⁽⁴⁾ and (2) a soil-culvert interaction method⁽⁵⁾. From these analyses it was determined that the loss-of-pressure situation is the limiting factor in the design. Using a 15.24 cm × 5.08 cm corrugation, as shown in Fig. 1, and incorporating a safety factor of 2, the required wall thickness is 0.89 cm.

Thermodynamic Analysis

The steady-state heat losses were determined by modeling the greenhouse as a cylinder without ends, having the same surface area as the greenhouse. When the structure is buried 4 m beneath the surface, the natural insulation of the martian regolith holds the steady-state heat transfer to 1.1 kW. Because of the foreseen difficulty of burying the structure at a depth of 4 m, the heat loss has been analyzed at different depths. Figure 2 shows the plot of the steady-state heat transfer vs. the depth at which the structure is buried. At a more practical depth of 2 m, the heat loss is still remarkably low at a value of 1.7 kW.

The large temperature gradient across the wall of the structure and the depth at which the structure is buried make the transient heat losses an important part of the heat transfer

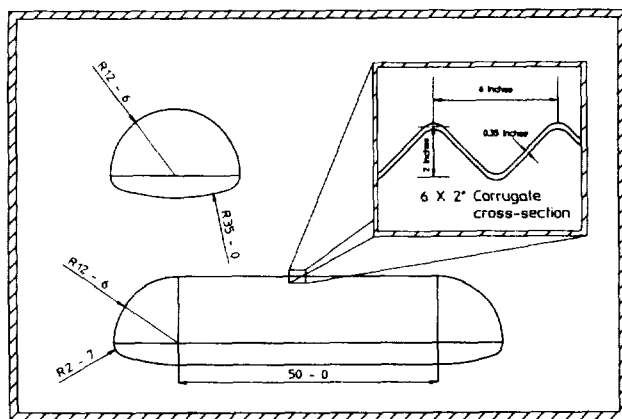


Fig. 1. Structure Configuration and Cross-Section

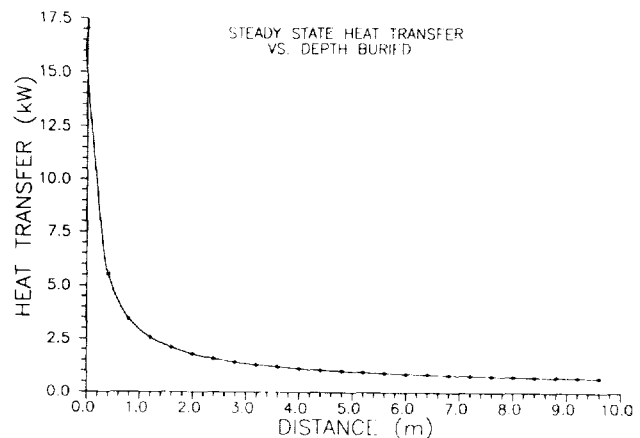


Fig. 2. Steady-state Heat Transfer vs. Depth Buried

analysis. To approximate the time required for the soil to reach steady state, the soil around the structure is modeled as a semi-infinite slab with a sudden wall temperature change. Figure 3 shows that steady-state conditions are reached in approximately 25 weeks, but the losses are less than 2 kW after only 6 weeks. At a depth of 2 m, steady-state heat loss, which is 1.7 kW, is reached in only 8 weeks. The steady-state heat loss is 55% higher at the 2-m depth, but takes only one-third of the time to reach steady state. The tradeoffs between power requirements for heating and the difficulty in burying the structure need to be examined to determine the optimal depth for the greenhouse.

SOLAR COLLECTION UNIT

The greenhouse is supplied with natural light that is collected on the surface and transported to the underground modules via fiber optic cables and light waveguides. The growing environment within the greenhouse is maintained at 30°C with a carbon dioxide concentration approximately 4

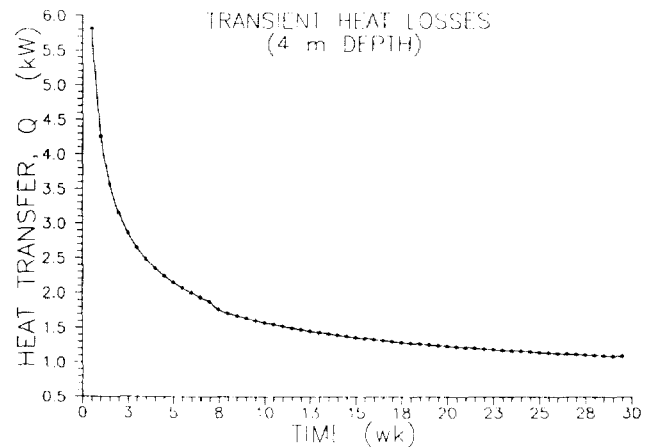


Fig. 3. Transient Heat Losses at 4-m Depth

times greater than Earth levels. This improves photosynthetic efficiency, which reduces the amount of light required for plant growth from 300 W/m^2 to 100 W/m^2 ⁽⁶⁾.

The amount of collector surface area and the shape of the collector are dictated by the latitudinal location on Mars. A conceptual study conducted by an USRA-sponsored design team at the University of Wisconsin determined that a location 20° North of the martian equator is optimal⁽⁷⁾. The seasonal intensity is much more uniform at this latitude, and martian dust storms occur less frequently in the northern hemisphere.

The solar light collector is modeled after the Himawari collector that is currently in use in Japan. The Himawari collector has a honeycomb configuration of light-collecting cells. The light is concentrated through Fresnel lenses onto the ends of fiber optic cable bundles. The ends of the collection unit are supported by bearings attached to a base that swivels for two axes of tracking. The entire unit is enclosed in an acrylic dome, which aids in filtering ultraviolet radiation and protects the system from weather and dust.

To meet the lighting requirements of the greenhouse, 119 m^2 of collector area is needed for each growing module. Six collectors are required for each module, with each having an incident collection surface area of 20 m^2 . The shape of the collector is trapezoidal, as shown in Fig. 4, with the skewed edge parallel to the ground at sunrise and sunset. The shape of the design is specific to a martian location of 20° N .

Using a two-axis equatorial tracking system, a $20^\circ - 0^\circ$ (horizontal) motor axis will follow the daily solar movement. The annual motor axis will make small daily adjustments to complete 50° of rotation between seasonal extremes.

Sensors are positioned in the panel of the collectors to provide feedback to a central computer system in each growing module. The motorized system makes small adjustments to the daily schedule when misalignment occurs, and automatically resets the collector after sunset.

Hybrid stepper motors are coupled to harmonic gear drives for adjustments to both axes. The characteristics of this motor make it ideally suited for high-torque applications requiring incremental motion and holding capability. When this type of motor is supplied from an electronic drive, accurate position control and precise speed control is maintained. The harmonic

gear can have as much as a 400:1 gear reduction for high torque loads. Harmonic gears have long life cycles and require little or no maintenance.

The collector and tracking axis are mounted on a 40-cm-diameter support column that houses the optic cables and computer link to the controls. The plate is constructed of a rigid honeycomb composite and reinforced by four radial flange beams.

The maximum stresses were approximated by modeling the worst-case loading conditions in a finite element analysis. The collector was modeled as turned on its side and perpendicular to a 100-m/sec wind. A model of the lower hinge showed a maximum stress of 26.2 MPa, which yields a factor of safety of 8. The maximum stresses in the support column are 5.5 MPa.

LIGHT DISTRIBUTION SYSTEM

Light enters the greenhouse via bundles of fiber optic cables that extend from the light collector on the planet surface. The fiber bundles enter through the top of the greenhouse at six junction boxes. Light emanating from the end of the 317.5-mm-diameter fiber bundle is channeled into a 60-mm-diameter, hollow dielectric pipe. This pipe, precisely machined into an optical waveguide, is made of tempered, low-expansion borosilicate. The light travels through the waveguide and is sent into a light-diffusing pipe that is placed over the plant beds. The diffuser is a hollow dielectric tube made of clear, fused silica. The upper section inside the tube is coated with magnesium oxide. As the light passes through the diffuser, it strikes the coating and is reflected downward to the plants.

Waveguide Theory

Light entering the optical waveguide is transmitted down the pipe by way of small angle reflections. The light enters the pipe at an acceptance angle of 1° . If the light comes in at an angle greater than 10° , it suffers high losses down the waveguide. Any light entering at less than a 10° angle travels through the pipe until it hits the reflective material, then it is reflected down the pipe.

The hollow waveguide used in this design is made of borosilicate glass tubing that is honed to a uniform diameter. The inside of the pipe is a vacuum, which allows light to travel without any of it being absorbed or scattered. The outside of the pipe is coated with a thin aluminum oxide film that will serve to direct light that radiates into the glass back into the tube. A webbed sheathing, which protects the tube, is placed over this film while allowing adequate ventilation for heat dissipation.

Light Diffuser

The light diffuser is designed to distribute the light from the pipe down to the plants in a uniform and efficient manner. For this application, a downward light diffuser is used in

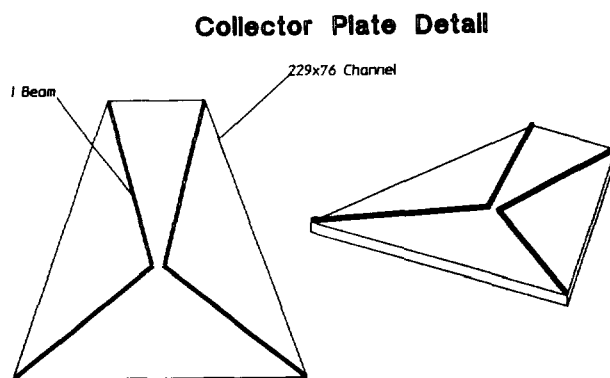


Fig. 4. Collector Plate

conjunction with a reflector panel that is placed above the pipe to capture any light that may be lost through the top or sides of the pipe.

The diffuser is made of clear, fused silica, which has very good transmission characteristics at all wavelengths⁽⁸⁾. The upper inside surface of the tube is coated with magnesium-oxide powder, which is 98% efficient for diffuse light reflection⁽⁹⁾.

In order to get an even intensity of light over the entire plant bed, the coating is placed at a 30° arc at the point where light enters the diffuser. The arc increases linearly down the length of the pipe, reaching a 180° arc at the end of the diffuser. The coarseness of the powder increases as it is applied down the length of the pipe in order to reflect more light.

The diffuser consists of two pieces of hollow dielectric tubing, each piece being 7.62 m long. The pipes are coupled together, and the ends of the pipes are sealed with lenses that allow the light to pass through while keeping a vacuum inside each portion of the diffuser. The upper diffuser is connected to a support above the upper plant bed and the lower diffuser is connected to the bottom of the upper plant bed.

CONCLUSION

The inflatable structure serves as an ideal greenhouse while being feasible to transport and easy to assemble on Mars. Locating the structure underground protects it from the

extreme environmental variations on the surface. The proposed lighting system provides all the necessary light for photosynthesis with little external power demand. These considerations make the proposed greenhouse design a viable means of providing an ongoing food supply for a martian colony.

REFERENCES

1. Adams, D. E., "Descriptions of Candidate Materials of all Types," University of Wyoming, 1987.
2. Nevill, "Design Study of a Prototype Closed Loop Life Support System," University of Florida, Dept. of Aerospace Engineering, Mechanics and Engineering Sciences, Dec. 1988.
3. Megyesy, E. E., *Pressure Vessel Handbook*, 6th edition. Pressure Vessel Handbook Publishing Co., July, 1983.
4. American Iron and Steel Institute, *Modern Sewer Design*, 1985.
5. Duncan, J. M. "Soil-Culvert Interaction Method for Design of Metal Culverts," University of California, Berkeley, 1978.
6. Milthorpe and Moorby, *An Introduction to Crop Physiology*, Cambridge University Press, London, 1974.
7. Graf, J., Leroy, S., Monyette, T., and Myrhum, M. "Providing Light for a Mars Plant Growth Module," University of Wisconsin, 1985.
8. McLellan and Shand, *Glass Engineering Handbook*, McGraw-Hill, 1984.
9. Smith, W. J., *Modern Optical Engineering: The Design of Optical Systems*, McGraw-Hill, 1966.

AN UNMANNED PROBE TO PLUTO N 91 - 18186

UNIVERSITY OF ILLINOIS, URBANA-CHAMPAIGN

Now that Voyager II has completed its grand tour of the solar system, all the planets in the solar system, with the exception of Pluto, have been studied. Even now, missions to return to Mercury, Venus, Mars, Jupiter, and Saturn are currently flying or are planned. However, a mission to explore Pluto is not, at the present time, being considered seriously. The design problem presented to the students was very general, i.e., design an unmanned mission to Pluto with a launch window constraint of the years 2000-2010. All other characteristics of the mission, such as mission type (flyby, orbiter, lander, penetrator), scientific objectives and payload, and the propulsion system were to be determined by the design teams. The design studies exposed several general problems to be solved. Due to the extreme distance to Pluto (and a corresponding travel time in the range of 10 to 25 years), the spacecraft had to be lighter and more robust than current spacecraft designs. In addition, advanced propulsion concepts had to be considered. These included the new generation of launch vehicles and upper stages and nuclear electric propulsion. The probe design offered an abundance of synthesis and analysis problems. These included sizing trade studies, selection of subsystem components, analysis of spacecraft dynamics, stability and control, structural design and material selection, trajectory design, and selection of scientific equipment. Since the characteristics of the mission, excluding the launch window, were to be determined by the design teams, the solutions varied widely.

INTRODUCTION

Although missions to return to Mercury, Venus, Mars, Jupiter, Saturn, and comets are planned or currently flying, a mission to Pluto is not planned until after 2010. The first step in the exploration of Pluto will occur when Hubble Space Telescope becomes active. This instrument should provide clearer pictures of Pluto and Charon than currently exist. However, even this clarity will not be sufficient to perform the analyses necessary to answer the current questions about Pluto and Charon.

To provide scientists with the data required to perform those analyses, a mission to Pluto and Charon is necessary. There are three classes of missions that can be flown: (1) flyby, (2) orbiter, and (3) lander. Flyby missions have an inherent limitation in the amount of time spent in the vicinity of the area of interest. However, they are the easiest to design and the least expensive to build and fly.

Orbiter missions are inherently more costly than flyby missions because of the requirement to enter orbit about the body of interest. However, this type of mission provides more time to study the body of interest, allowing additional and more exact experiments to be performed. Because of the distance from Earth to Pluto, this type of mission must be able to adapt to the environment the spacecraft encounters.

The most costly mission class is the lander. There exist two subclasses of landers: a lander, which lands softly on the surface of the body in question, and a penetrator, which explores the area under the surface of the body. A lander mission provides the most accurate and largest quantity of data about another body. For this type of mission, an important question is which body to land on, Pluto or Charon?

PROJECT BACKGROUND

Forty-two undergraduate students, divided into seven groups, were enrolled in the spacecraft section of Aeronautical and Astronautical Engineering (AAE) 241, Flight Vehicle Design, in

the spring 1990 semester. This paper summarizes the work of those student groups as submitted in their final design reports.

Today, little is known about plutonian space and current discoveries raise more questions than they answer. The Hubble Space Telescope should be able to answer some of the questions, but the only way to answer most of the questions is to send a spacecraft to Pluto to take data first hand.

Pluto, the ninth planet in our solar system, was discovered in March 1930, using photographic plates taken in January of that year. Charon, Pluto's only known satellite, was discovered in July 1978, but not recognized until 1985. With an eccentricity of 0.25 and a perihelion of 29.6 A.U., Pluto has an orbital period of 248 years.

Pluto itself is estimated to weigh about 1/400 of the mass of the Earth, with a diameter of approximately 2300 km. The composition of the planet is estimated to be about 70% rock and 30% water ice and methane ice. The atmosphere is believed to be composed mostly of methane, which is sublimating from the surface, with traces of heavier gases such as argon, neon, and nitrogen. Due to the large eccentricity of the orbit and the distance from the sun, the atmosphere of Pluto is thought to form and collapse cyclically as a function of the orbital period. The next collapse is expected to occur around 2025.

PROJECT OBJECTIVE

The project objective was to develop a conceptual design for a spacecraft to perform an unmanned scientific study of plutonian space to be launched sometime in the first decade of the 21st century. Performance, weight, and cost are very important to the acceptance of this type of mission, so approaches were taken that optimize these parameters in design tradeoffs. The spacecraft had to be reliable and use off-the-shelf hardware whenever available. The use of materials or techniques expected to be available after 1999 was prohibited.

SYSTEM REQUIREMENTS

A thorough preliminary design study was conducted by the students to determine major design issues, establish the size of, define subsystems for, and describe the operation of the spacecraft that satisfies the following requirements:

1. The amount of on-orbit assembly should be identified and minimized.
2. The following subsystems are identified for the purposes of system integration: (a) science instrumentation; (b) mission management, planning, and costing; (c) attitude and articulation control; (d) command, control, and communication; (e) power and propulsion; and (f) structure (including materials and thermal control).
3. The usage of the space shuttle should be identified. If the space shuttle is used for launch, the payload/shuttle interfaces must conform to NASA standards.
4. Nothing in the spacecraft's design should preclude it from performing several possible missions.
5. The spacecraft should have a design lifetime sufficient to carry out its mission plus a reasonable safety margin, but nothing in its design should preclude it from exceeding this lifetime.
6. The vehicle should use the latest advances in artificial intelligence where applicable to enhance mission reliability and reduce mission costs.
7. Mission science objectives must be described and justified.
8. The design should stress reliability, simplicity, and low cost.
9. For cost estimating and overall planning, it should be assumed that four spacecraft will be built. Three will be flight ready, while the fourth will be retained for use in an integrated ground-test system.

SCIENCE INSTRUMENTATION

The students working in this area were to determine the science objectives for the mission. In addition, they were to select the instruments necessary to fulfill these objectives. Some of the selected objectives were (1) determine the composition and structure of Pluto's atmosphere; (2) study the dynamics of the Pluto/Charon system; (3) determine the mass, composition, and structure of Pluto; (4) determine the mass, composition, and structure of Charon; (5) determine the surface characteristics of Pluto; (6) determine the existence and structure of the magnetic field of Pluto; (7) study Jupiter (during a gravity assist maneuver); and (8) search for other satellites in the Pluto/Charon system.

The instruments chosen to meet these objectives can be divided into two major groups, remote sensing and fields and particles. The remote-sensing instruments were determined to be the most important, with all seven groups selecting both narrow- and wide-angle cameras and ultraviolet spectrometers. These instruments provide information to help determine the composition and structure of the bodies and the atmosphere, and provide for the search for additional satellites in the Pluto/Charon system. Pictures of the system taken by the cameras will help determine its dynamics.

The fields and particles instruments will be used for interplanetary science experiments during the voyage to Pluto and will be used to study the magnetic field of Pluto, if one exists. The instruments selected include magnetometers, selected by six groups, and plasma particle detectors, selected by six groups. Figure 1 shows the layout of a representative science platform.

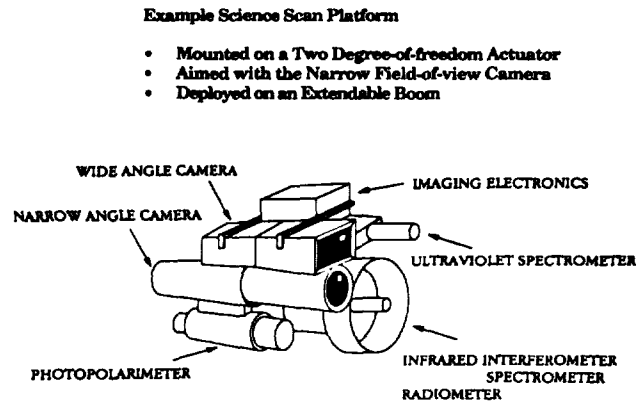


Fig. 1. Example Science Scan Platform

MISSION MANAGEMENT, PLANNING, AND COSTING

Mission management was responsible for the selection of a trajectory to Pluto and a launch vehicle for the spacecraft. Table 1 shows the types of missions chosen and the duration of the missions. Five of the seven groups selected a flyby mission, like Voyager, whereas the other two felt the additional data-gathering capabilities provided by the orbiter were important. The duration for the flyby missions ranged from 13 to 19 years, while the orbiter missions were 22 and 15 years respectively. Note that Group 7 utilized a nuclear-electric propulsion system. Note also that all seven spacecraft are expected to arrive in plutonian space prior to the predicted collapse of the atmosphere of Pluto.

Table 1. Mission Type and Duration Summary

Group	Mission Type	Launch Date	Arrival Date	Mission Time (yrs)
1	Flyby	09/2000	05/2018	18
2	Flyby	02/2002	02/2017	15
3	Flyby	01/2002	09/2020	19
4	Orbiter	12/2004	01/2025	22
5	Flyby	01/2003	02/2019	16
6	Flyby	05/2009	12/2021	13
7	Orbiter	04/2004	04/2019	15

For the six groups using the classical chemical propulsion systems, a tool call MULIMP was used to help determine a trajectory for the spacecraft. As shown in Table 2, a variety of trajectories were selected. These include a Jupiter Gravity Assist (JGA), where the spacecraft leaves the Earth and performs a gravity assist maneuver at Jupiter in order to increase the speed of the spacecraft and shorten the trip time.

Another trajectory was the Earth-Jupiter Gravity Assist (EJGA) where the spacecraft leaves Earth's sphere of influence, performs a gravity assist maneuver at Earth, and then performs another gravity assist maneuver at Jupiter before proceeding on to Pluto. One group chose to fly directly to Pluto without any interplanetary flybys or gravity assists in order to get to Pluto before the atmosphere collapsed. The final chemical trajectory performed gravity assist maneuvers at both Jupiter and Saturn on the way to Pluto (JSGA).

Table 2. Trajectory and Launch Vehicle Summary

Group	Launch Vehicle	Trajectory	Delta V (km/sec)	Propulsion Type
1	Titan IV/Centaur	JGA	11.2	Chemical
2	Titan III D/Centaur	EJGA	7.5	Chemical
3	Titan Commercial/TOS	EJGA	5.9	Chemical
4	Shuttle C/STV	JGA	12.1	Chemical
5	Ariane IV	DIRECT	8.6	Chemical
6	Titan T-34D/Centaur	JSGA	12.4	Chemical
7	Shuttle C	JGA	N/A	Nuclear Electric

N/A - Not Available; E - Earth; J - Jupiter; S - Saturn; GA - Gravity Assist

Group 7 uses a nuclear-electric propulsion system. The analysis of this trajectory was performed using a tool called CHEBY2. However, this program does not provide for gravity assist maneuvers. This spacecraft spirals out of Earth's sphere of influence beginning in nuclear-safe orbit. The spacecraft performs a gravity assist maneuver at Jupiter and finally spirals into an orbit about Pluto.

The total costs of the missions were determined using the Science Applications International Corp. Planetary Cost Model. This model includes design, development, testing and evaluation, the four flight vehicles required by the RFP, and the ground support personnel required during the entire mission. For the chemical systems, the estimated costs range from \$1.03 billion to \$2.11 billion in 1990 dollars while the nuclear-electric orbiter's estimated cost is \$4.21 billion.

ATTITUDE AND ARTICULATION CONTROL

For attitude determination, all seven groups chose to use a sun sensor and the ASTROS star sensor for determining attitude. Also, all the groups used the Fiber Optic Rotational Sensor (FORS) as the gyroscope to be used most of the time.

For control, all groups selected a three-axis active control system over spin-stabilized or dual-spin configurations. All seven groups chose to use thrusters as the method of attitude correction, with the electric propulsion group using reaction wheels, as well, for stability. For the attitude control thrusters, the six chemical groups used monopropellant hydrazine as the propellant, while the electric propulsion group used ionic mercury as the propellant.

In order to isolate the motion of the science instruments from the rest of the spacecraft, all seven groups chose to put the instruments requiring pointing on a scan platform. This

scan platform was gimbaled in two axes in order to provide the equipment with the widest field of view. The most common scan platform selected was the High-Performance Scan Platform (HPSP).

COMMAND, CONTROL, AND COMMUNICATION

This subsystem is responsible for selecting the communications equipment as well as the "brains" of the spacecraft.

For the communications portion, a large antenna is required in order to communicate over such a large distance. In addition, the distance necessitates a large power supply. Also, adequate storage for the scientific data obtained is required when the spacecraft is unable to communicate with Earth or when the data input is greater than the communications rate.

As shown in Table 3, the antenna sizes ranged from 1.5 m to 4.8 m with 4.8 m used most frequently. Also, most groups used the proposed upgrades in the deep space network (DSN) in order to improve communications capability. These upgrades included increasing the size of the primary receiver to 70 m and making the antennas Ka-band capable. For communications, the data rates ranged from 300 bps to 388,000 bps. Powers ranged from 6.3 W to 25 W, except for the nuclear-electric orbiter, which used a power of 1000 W.

Table 3. Antenna Sizing Summary

Group	Size (m)	Band	Transmitted Power (W)	DSN Receiver Size (m)	Data Rates (bps)
1	4.8	Ka	20	70	316,891
2	1.5	X	13	64	300
3	4.8	Ka	10	70	145,500
4	4.8	Ka	6.3	70	388,000
5	2.5	X	20	70	N/A
6	3.7	X	25	64	N/A
7	4.8	Ka	1000	70	N/A

POWER AND PROPULSION

The selection of the method for supplying electric power to the spacecraft was based on a combination of the mission length, the distance from the sun, and the peak power loads. For the power supply, Pluto is too far from the sun for practical use of solar radiation. The mission times are too long for batteries to be able to store energy for the entire voyage. This leaves a nuclear power supply as the only viable option. Of the different types of nuclear power sources, five groups chose the modular isotopic thermoelectric generator (MITG), one group chose a type of radioisotope thermoelectric generator (RTG), and one group chose a nuclear reactor.

Once the power supply has been selected, the size of the power supply must be determined. This is a function of the peak power required, and the duration of the mission. The power selections are summarized in Table 4. Again, the group using the electric propulsion has a vastly different power supply. They plan to carry two SP-100 nuclear reactors to supply all the power needs of the spacecraft.

Table 4. Power Supply Summary

Group	Mission	Mission Duration (yrs)	Peak Power (W)	Power Supply	Number of Slices	Mass (kg)
1	Flyby	18	297	MITG	13	29.1
2	Flyby	15	256	MITG	15	34.0
3	Flyby	19	165	MITG	2 × 11	49.9
4	Orbiter	22	237	RTG	1*	26.0
5	Flyby	16	373	MITG	23	44.4
6	Flyby	13	290	MITG	13	60.0
7	Orbiter	15	80,500	Reactor	2*	4600.0

MITG = Modular Isotopic Thermoelectric Generator.
 RTG = Radioisotope Thermoelectric Generator.
 * Indicates the number of power units where slices are not applicable.

The responsibilities in the propulsion area were propellant selection, propellant tank sizing, and orbit insertion propulsion for the two orbiters. For this mission, four chemical propulsion options were considered: cold gas, solids, monopropellants, and bipropellants. Cold gas and solids are not applicable to the mission. Three groups selected the monopropellant hydrazine because it is simple, reliable, storable, and has relatively low cost. The other three chemical groups chose the more complex, but higher I_{sp} , bipropellant, hydrazine and nitrogen tetroxide.

The nuclear-electric propulsion system is different. The propellant options investigated for this system include cesium, xenon, argon, and mercury. Of the four options, mercury was selected because it provides the best tradeoff between cost, storability, and I_{sp} .

For the chemical systems, the propellant mass ranged from 473 kg to 2000 kg for the flyby missions and 3120 kg for the orbiter. The nuclear-electric mission had a propellant mass of 12,000 kg.

STRUCTURES

This subsystem was responsible for locating the components, determining the mass properties, and thermal control. Figures 2 through 4 show the layout of three representative spacecraft: Fig. 2 is a flyby, Fig. 3 is an orbiter, and Fig. 4 is the nuclear-electric propulsion orbiter.

Locating the components and determining the mass properties must be performed together. The components should be arranged on the spacecraft to minimize the cross product of inertia about the axes of the thrusters. This is the principle reason for the arrangements shown in Figs. 2 through 4.

Thermal control is required in order to maintain the temperature within acceptable limits for all components within the spacecraft. Various methods were employed by the groups. The most widely selected method was the placement of thermal heaters throughout the interior of the spacecraft. Radioisotope heating units, where the energy from nuclear decay is used to heat nearby components, were also common. The nuclear-electric orbiter used high-temperature radiators to remove the waste heat from the nuclear reactor.

For the chemical flyby missions the structure (dry) masses range from 445 kg to 756 kg with the total masses ranging

from 1093 kg to 2500 kg. The chemical orbiter has a dry mass of 3243 kg and a total mass of 6363 kg. The nuclear-electric orbiter has a dry mass of 8914 kg and a total mass of 20,914 kg.

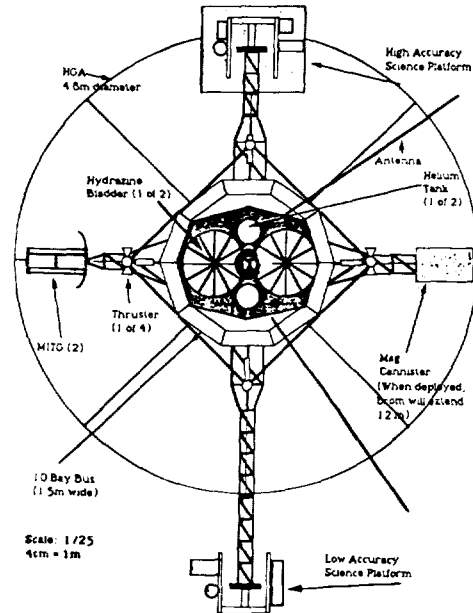


Fig. 2. Bottom View of an Example Flyby Spacecraft

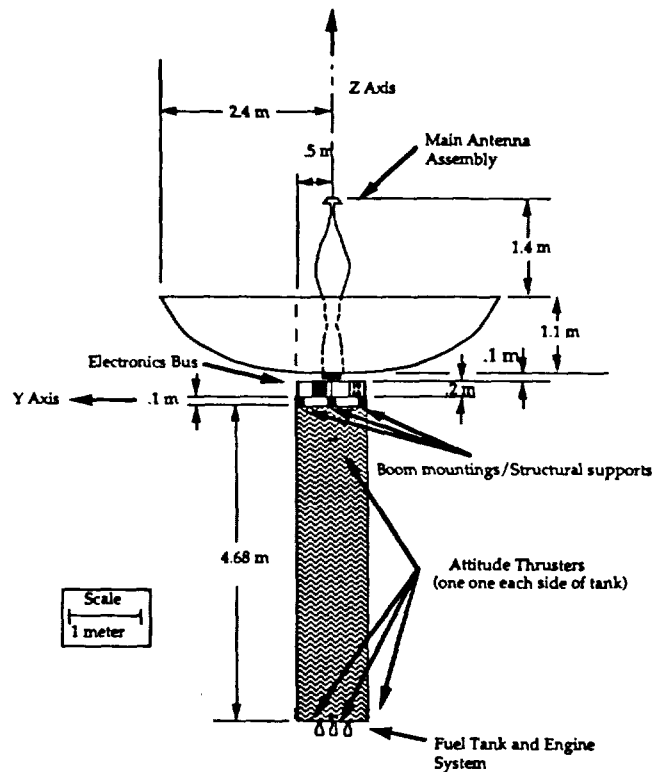


Fig. 3. Side View of an Example Orbiter Spacecraft

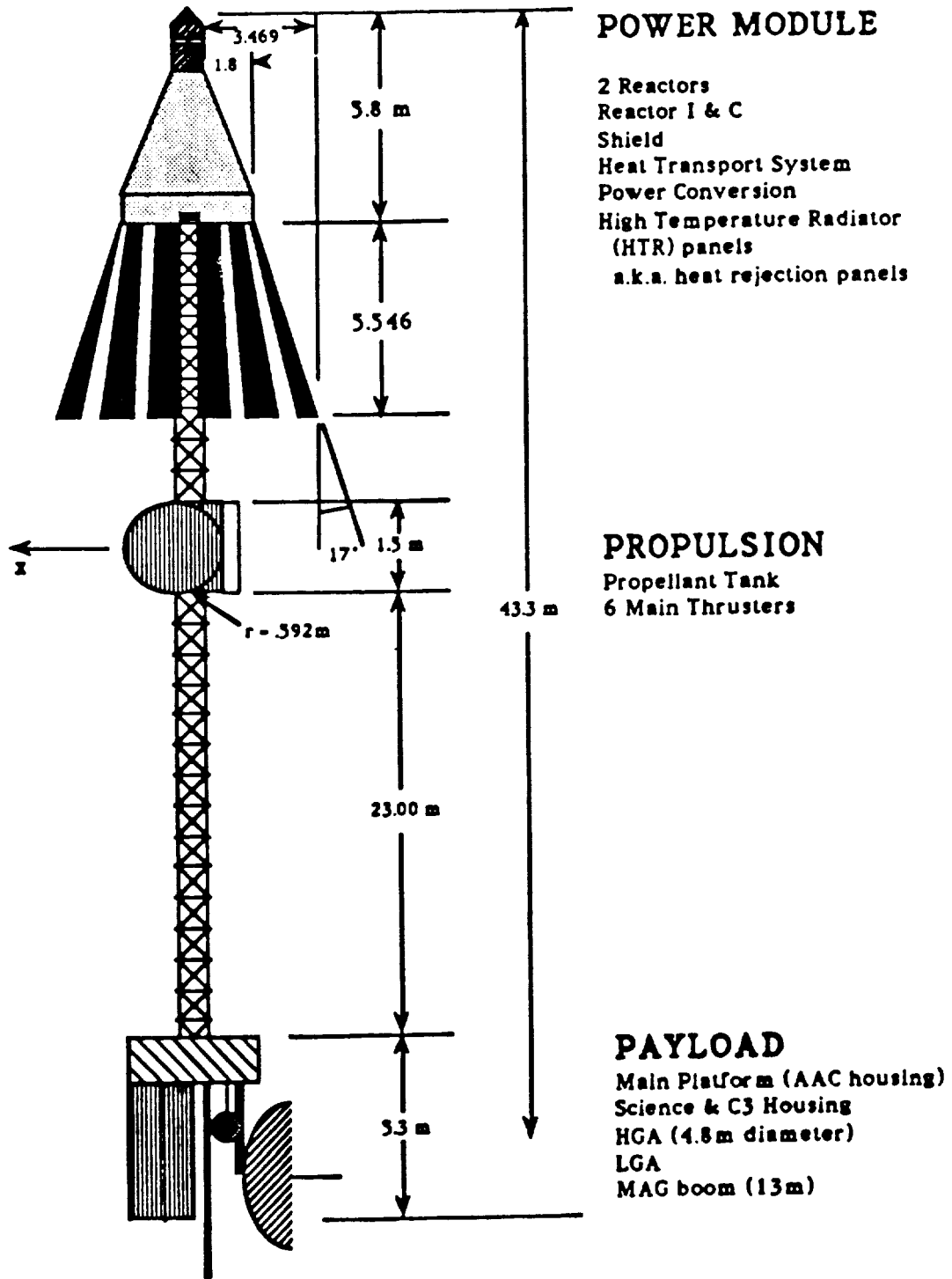


Fig. 4. Side View of the Nuclear-Electric Orbiter Spacecraft

72-14
22-101
P. 5 '99

AUTOMATION OF CLOSED ENVIRONMENTS IN SPACE FOR HUMAN COMFORT AND SAFETY

KANSAS STATE UNIVERSITY

N 91 - 18137

INTRODUCTION

Project Description

The Environmental Control and Life Support System (ECLSS) for the Space Station *Freedom* and future colonization of the Moon and Mars presents new challenges for present technologies. Current plans call for a crew of 8 to live in a safe, shirt-sleeve environment for 90 days without ground support. Because of these requirements, all life support systems must be self-sufficient and reliable.

The ECLSS is composed of six subsystems. The temperature and humidity control (THC) subsystem maintains the cabin temperature and humidity at a comfortable level. The atmosphere control and supply (ACS) subsystem insures proper cabin pressure and partial pressures of oxygen and nitrogen. To protect the space station from fire damage, the fire detection and suppression (FDS) subsystem provides fire sensing alarms and extinguishers. The waste management (WM) subsystem compacts solid wastes for return to Earth, and collects urine for water recovery.

Because it is impractical, if not impossible, to supply the station with enough fresh air and water for the duration of the space station's extended mission, these elements are recycled. The atmosphere revitalization (AR) subsystem removes CO₂ and other dangerous contaminants from the air. The water recovery and management (WRM) subsystem collects and filters condensate from the cabin to replenish potable water supplies, and processes urine and other waste waters to replenish hygiene water supplies.

These subsystems are not fully automated at this time. Furthermore, the control of these subsystems is not presently integrated; they are largely independent of one another. A fully integrated and automated ECLSS would increase astronauts' productivity and contribute to their safety and comfort.

THREE-PHASE DESIGN PLAN

The Kansas State University Advanced Design Team is in the process of researching and designing controls for the automation of the ECLSS for Space Station *Freedom* and beyond. The approach chosen to solve this problem is to divide the design into three phases.

The first phase is to research the ECLSS as a whole system and then concentrate efforts on the automation of a single subsystem. The AR subsystem was chosen for our focus.

During the second phase, the system control process will then be applied to the AR subsystem. To aid in the development of automatic controls for each subsystem and the overall

ECLSS, mathematical models are used for system simulation on a computer. Once the simulation has been completed, various methods of control can be tested. Using the AR subsystem control system as a "proof of concept," the other ECLSS subsystems will be automated.

Finally, during phase three, the six subsystem control systems will be combined to form a control system for ECLSS. The control system will perform routine control duties as well as provide fault diagnosis and isolation.

The Kansas State University Design Team has completed phase one and is currently in the midst of phase two. Mathematical models have been developed and numerous AR subassembly components have been simulated on a computer. Phase two development will continue through the next two semesters. Phase three will be initiated upon the completion of the second phase.

This paper describes a portion of the work done at Kansas State University during the 1989/90 academic school year. First, the components of the AR system are discussed. Then the paper focuses on the four-bed molecular sieve, which is described in detail along with a proposed control scheme. The mathematical models of the AR components developed by the group are not discussed in this paper, but can be found in the complete report. Similar work was done for the other components of the AR subsystem. That work also is discussed in the complete report.

DESIGN TEAM DESCRIPTION

The Kansas State University Advanced Design Team is composed of engineering students from several disciplines, a student from general science and education, a graduate student assistant, and engineering faculty members. Chemical, electrical, industrial, and mechanical engineering disciplines are represented by both students and faculty.

To complete the first semester's work, the design team appointed three lead engineers to work with the faculty and teaching assistant to organize and direct the activities of the group. Initial breakdown of the group assigned two or three students to each ECLSS subsystem to collect information. Once this preliminary investigation had taken place, the AR subsystem was selected for further study.

During the second semester, the design team was organized into three groups to study the AR subsystem in detail. One group focused on mathematical models, another group studied control strategies, while the third concentrated on physical operations.

PAGE 98 INTENTIONALLY BLANK

PRECEDING PAGE BLANK NOT FILMED

**ATMOSPHERE REVITALIZATION
CARBON DIOXIDE REMOVAL**

Figure 1 is a diagram of the AR subsystem. The subsystem's purpose is to produce oxygen for respiration. The AR subsystem removes water vapor, CO₂, and trace contaminants from the cabin atmosphere. It produces oxygen and potable water. The subsystem is composed of four parts, the CO₂ removal system, the CO₂ reduction system (CRS), the oxygen generation assembly (OGA), and the trace contaminant control system (TCCS). Only the CO₂ removal system is discussed here.

Metabolic CO₂ is removed from the cabin atmosphere by a four-bed molecular sieve. The sieve consists of two desiccant beds to remove water vapor from the incoming air, two CO₂ adsorption beds, a blower to force the air through the system, a CO₂ pump, a CO₂ accumulator, a precooler, and five multiple-flow selector valves.

Figure 2 is a diagram of the four-bed molecular sieve. During a typical adsorption cycle, air enters the four-bed molecular sieve from the temperature and humidity control (THC) subsystem (1). After passing through a directional control valve (2), the air enters the desiccant bed (3). Dry air leaves the desiccant bed and passes through another directional control valve (4) before passing through the blower (5). The air, which has been warmed by the desiccant bed and blower, then passes through a precooler (6). After leaving the precooler and passing through a third directional control valve (7), the air enters an adsorbent bed (8). The CO₂ adsorbent bed, which was heated to release CO₂ earlier, now cools as it adsorbs CO₂. Air leaves the adsorbent bed, passes through a check valve (9), then enters the second desiccant bed (10). This warm dry air evaporates water accumulated in the desiccant bed during its adsorption cycle. This humid, cool air passes through a final directional control valve (11) before returning to the THC subsystem (12).

While one bed is adsorbing CO₂ (8), the other bed (14) is desorbing CO₂. The desorbing begins with an initial pumpdown of the bed to draw off residual air. A check valve

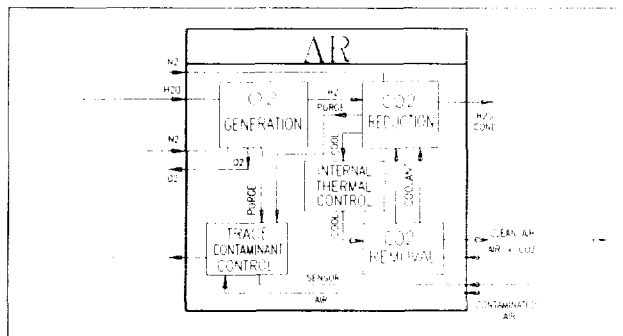


Fig. 1. Atmosphere Revitalization Block Diagram

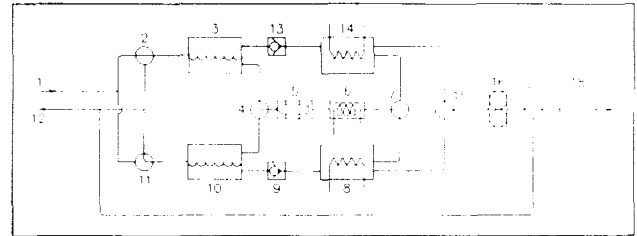


Fig. 2. Four-Bed Molecular Sieve

(13) prevents pumping air through the desiccant bed during the desorption cycle. The CO₂ pump (16) pumps air through a valve (15) and back to the THC subsystem through a directional control valve (17). After the initial pumpdown, the pump is shut off while heat is steadily applied to the CO₂ sorption bed by electric heaters. After the bed is sufficiently heated, the pump is restarted. Now the directional valve (17) is set to send CO₂ to the pressurized, fixed-volume accumulator (18).

After the desorption cycle is complete, the valves switch positions and the CO₂-free desorbing bed becomes the adsorbing bed, and the CO₂-filled adsorbing bed becomes the desorbing bed. Likewise, the now water-filled adsorbing desiccant bed becomes the desorbing bed, and the drier desorbing bed becomes the adsorbing desiccant bed.

Desiccant Bed

Each desiccant bed is filled with a water-adsorbent material. The adsorbent materials used in these beds are zeolite 13X and silica gel. Silica gel and zeolite 13X are placed in separate layers and the incoming air stream passes over both layers. These two layers are necessary because the silica gel adsorbs water vapor well at high relative humidities, but its efficiency decreases for relative humidities of less than 50%. Zeolite 13X, however, is more efficient for relative humidities of 35% or less. In tests performed by NASA, the combination of these two layers removed nearly 100% of the water vapor in the incoming stream. As a result of this water removal, the temperature of the air stream increases. These adsorbents readily desorb water when the warm air stream from the CO₂ beds pass over them.

Blower

The blower is a motor-driven centrifugal fan. The motor is designed to operate with 115/220-V AC, three-phase, 400-Hz power. Deswirl vanes help convert swirl energy into useful static pressure. The blower is made of corrosion-resistant material with bearings designed to isolate grease from working air.

Precooler

The precooler is a double-pass coolant and single-pass process-air-flow heat exchanger that is made of stainless steel.

Carbon Dioxide Removal Bed

The CO₂ beds contain heater cores as well as CO₂ adsorbent material. The adsorbent used to remove CO₂ is zeolite 5A. It was chosen because of its high CO₂ capacity, its good kinetic qualities, and its low water poisoning factor. Zeolite 5A can be poisoned by water, therefore it is necessary to use desiccant beds to remove water vapor from the incoming air stream. Since zeolite 5A must be heated to release CO₂, the beds contain heaters.

Carbon Dioxide Pump

The CO₂ pump is an electric-motor-driven rotary vane pump. Except for sealed shaft bearings, the pump is unlubricated to prevent air contamination. The rotor vanes are made of self-lubricating carbon graphite.

Carbon Dioxide Accumulator

The CO₂ accumulator is a composite fiber/metal tank. The tank's initial CO₂ pressure of 90 psia will provide 90 minutes of continuous CO₂ flow for the CO₂ reduction portion of the AR subsystem. If the accumulator ever becomes too full, the excess CO₂ is vented.

CONCEPTUAL CONTROLS OF FOUR-BED MOLECULAR SIEVE

Introduction

This section details the progress made by the Conceptual Controls Group toward the design of a control system for the four-bed molecular sieve of the ARS.

When formulating the control scheme, astronaut safety was paramount. However, factors such as control system complexity, reliability, cost, system efficiency, and power consumption were also taken into account.

This section contains a description of the current control scheme, the proposed control scheme, and a sensor layout detail. In addition, a comparison is made between the current and proposed control systems.

Current CO₂ Removal Control Scheme

The control scheme that is presently used is a two-cycle process based solely on time. The removal system runs continuously with the role of each pair of desiccant and adsorbent beds performing the opposite function of the other pair in each half cycle. Each half cycle is 55 minutes long. All selector valves and major system components are controlled using electrical signals and specific time increments. It is not known if there are any sensors in place to allow for failure detection. Figure 3 shows the state of each bed in the system vs. time.

During the CO₂ desorbing phase, three primary operations occur. These individual operations are sequenced in time. The first operation is the residual air pumpdown. The desorbing

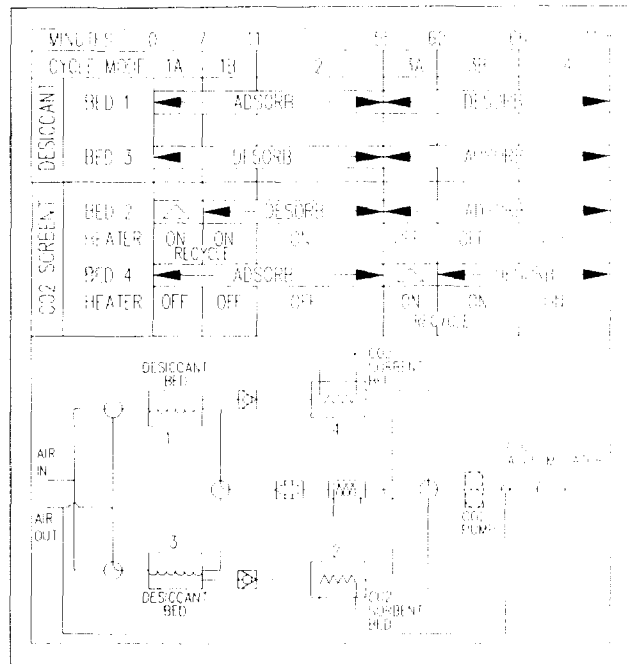


Fig. 3. Four-Bed Operation as a Function of Time

bed is pumped down using the CO₂ pump. Residual air is removed and routed to the cabin via the THC subsystem. Next the CO₂ pump is turned off and the heater in the adsorbent bed is activated. Finally, the CO₂ pump and heater are activated for the remainder of the half cycle and the CO₂ concentrate is channeled into the fixed volume CO₂ accumulator.

Proposed CO₂ Removal Control

This new control system will be based on the current concentration of CO₂ in the cabin. The control will be achieved by using the signals from several CO₂ gas detectors placed throughout the cabin. Using these signals, an average CO₂ concentration will be determined. Each gas sensor will sample the cabin air once every 10 seconds. Once the CO₂ concentration has been obtained, the microprocessor will determine what action is necessary. There are three primary modes of operation: CO₂ maximum removal mode, power efficiency mode, and off mode.

CO₂ removal mode. When the concentration of cabin CO₂ exceeds the high level (Table 1), the computer will direct the removal system into the CO₂ maximum removal mode. This mode uses a fixed half-cycle time increment similar to the current control system. However, this cycle-time will be derived with the idea of removing CO₂ from the cabin at the fastest rate possible. Because the ability of the desiccant bed system to remove CO₂ over time is an exponentially decaying function, it would be best to have a short cycle time and switch the functions of the pairs of beds as rapidly as possible.

This time interval will be obtained using our math modeling techniques, and information about switching lags and set-up times. In particular, the CO₂ adsorbent bed cool-down time

as it relates to efficiency, will be important. The goal will be to remove the greatest amount of CO₂ per unit time.

This mode would be used when large amounts of CO₂ are present in the cabin, for example, during emergency situations of increased astronaut numbers.

Table 1. CO₂ Operating Modes

Level	Mode	CO ₂ Concentration (ppm)*
Hi	CO ₂ Removal	≥ 1000
Lo	Power Efficiency	300 < x < 1000
Off		< 300

* Concentration levels were formulated using standard threshold limit values and information from Dr. Stephan Konz, Kansas State University.

Power efficiency mode. When the level of cabin CO₂ is between the Hi and Lo levels indicated in Table 1, the power efficiency mode would be activated. This mode uses a fixed half-cycle time that allows for adequate CO₂ removal, but minimizes the amount of electrical power used per unit of CO₂ removed. This time interval will be determined in a fashion similar to the manner in which the time internal for the CO₂ removal mode was found.

This mode will be useful when electrical power is limited on the station, for example, when a solar panel is damaged or a power shortage occurs.

Off mode. During this operation the removal system will not be operating. This would allow astronauts to make repairs on the system.

System Monitoring Scheme

Below is a list of all the major system components in the CO₂ removal subsystem. A sensor is described for each component. This monitoring scheme will allow the system to be controlled, as outlined above, and also allow component failures to be detected. For each component, the output of the sensor(s) will be compared with a desired output and an error signal will be generated. The monitoring microprocessor, using an artificial intelligence program, will determine if a component failure has occurred. In the event of failure, the astronauts would be alerted via a computer terminal. Figure 4 is a pictorial of the system monitoring scheme.

Cabin. CO₂ gas sensors will be placed throughout the cabin to obtain an average CO₂ gas concentration. Using this information the microprocessor will select the appropriate operating mode for the CO₂ removal system.

Air selector valves. These valves have end-of-position switches that can be used to determine if they have been completely switched into a valid position. This also allows the current position of the valve to be known.

Desiccant bed. A humidity sensor will be placed just in front of the blower to measure the water content of the air stream. The system requires that a dew point of -70°F be maintained for air entering the adsorbent. This sensor will indicate if a desiccant bed has malfunctioned.

Blower. A pressure sensor will be placed in front of the blower and directly downstream from the blower to measure the pressure drop. A power sensor will be used to monitor

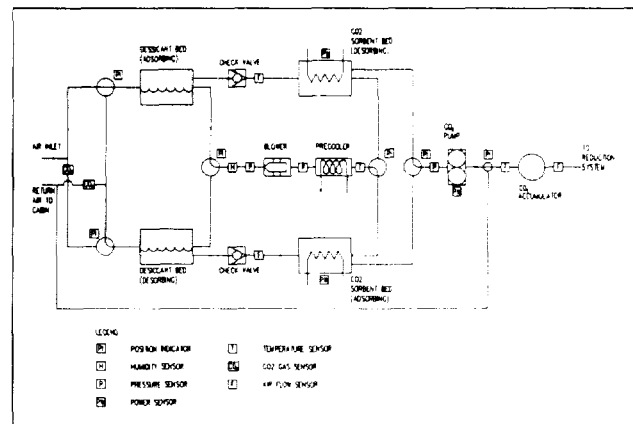


Fig. 4. Proposed CO₂ Removal Sensor Locations

the power consumed by the blower. Using the information from these sources it will be possible to determine if the blower is friction dragging, turning too slowly, or otherwise failed.

Precooler. A temperature sensor will be placed on the airstream line after the precooler to determine if the air entering the adsorbent bed is cool enough to allow for effective adsorption.

CO₂ adsorbent bed. A CO₂ gas sensor will be placed on the air-return-to-cabin pipe. By comparing the gas concentration at the bed exit with the gas concentration in the cabin it will be possible to determine if the bed is saturated or malfunctioning. A sensor will be used to monitor the power consumption of the adsorbent bed heater.

Check valve. An air-flow-rate sensor will be placed between the check valve and the CO₂ adsorbent bed to determine if the valve is leaking. The check valve assures that cabin air is not drawn directly into the system and stored in the CO₂ accumulator.

CO₂ pump. A pressure sensor will be placed between the pump and the CO₂ selector valve. This sensor will allow leaks to be detected in the CO₂ selector valve, check valve, post-precooler air select valve, and adsorbent bed. This sensor will also aid in monitoring the pump. The pump's power consumption will also be monitored using a sensor.

CO₂ accumulator. An air-flow-rate sensor will be placed directly on both sides of the CO₂ accumulator to allow leaks to be detected.

Comparison of Control Schemes

The newly devised control scheme has several advantages over the current method. The primary advantage is that the new system has feedback. It operates on measured cabin CO₂ gas concentration. This allows the system to operate on a situational basis. The addition of three operating modes allows the new system to respond to different levels of CO₂ in the most effective manner. When CO₂ levels are high and threaten crew safety, the system will operate to remove CO₂ as rapidly

as possible, with power consumption by the removal system being of secondary importance. When cabin CO₂ concentrations are between high and low, (Table 1) the CO₂ removal system will focus on power efficiency, freeing up power for higher priority needs. Finally, the CO₂ removal system will be completely shut down if the cabin CO₂ level is very low.

The proposed control scheme has two main disadvantages over the old: it will be more complex and costly to implement. The new method will require a study to determine the cycle times for the CO₂ removal and power efficiency modes. The cost of the new system monitoring scheme may also be a drawback.

17-12
P.6
105

PROJECT EXODUS

UNIVERSITY OF MARYLAND

N91-18138

"In 1492, Columbus knew less about the far Atlantic than we do about the heavens, yet he chose not to sail with a flotilla of less than three ships . . . so it is with interplanetary exploration: it must be done on the grand scale."

—Wernher Von Braun
Das Marsprojekt, 1952

INTRODUCTION

In 1952, Von Braun envisioned the first mission to Mars. He compiled a document entitled *Das Marsprojekt* that called for passenger and cargo ships as well as a landing craft. His idea was that the first mission would require many ships to reach the Red Planet.

Project Exodus is an in-depth study intended to identify and address the basic problems of such a mission. The most important problems concern propulsion, life support, structure, trajectory, and finance. Exodus, which means "mass migration" or "mass departure," will employ a passenger ship, cargo ship, and landing craft for the journey to Mars.

Project Exodus is scheduled for the year 2025. Construction of the vehicles will be performed at the Space Station. First, the cargo ship will be launched and then the passenger ship, known as the waverider, will be launched depending on the arrival of the cargo ship. The waverider, carrying 10 astronauts, will use the Venus atmosphere to perform an aerogravity assist for deflection angle and delta velocity savings for the trip to Mars. It will dock in low Mars orbit (LMO) with the cargo ship and the astronauts will descend to the martian surface using the landing craft, the Nuclear Rocket Using Indigenous Martian Fuel (NIMF shuttle). After three to five months on the surface of Mars the astronauts will again use the waverider to return to Earth and dock with the Space Station.

The cargo ship will transport the unassembled martian base, NIMF shuttle, surface life support, and return fuel and engine to LMO. The cargo ship is a very long truss to which the payload is attached. It is propelled in a spiral trajectory to Mars using a Nuclear Electric Propulsion (NEP) system.

The NIMF shuttle is used to transport the astronauts to the martian surface as well as around the planet. It is powered by a solid core nuclear engine that can use CO₂ as a propellant. The NIMF shuttle has a range of 650 miles, and will be used to bring the astronauts back to LMO with the waverider.

While on the surface the astronauts will construct a dome base that will be mostly underground to help shield against solar radiation. They will explore the planet, perform experiments, and attempt to extract useful substances, such as water, from the planet. The base will be the start for possible colonization.

This report presents the three major components of the design mission separately. Within each component the design characteristics of structures, trajectory, and propulsion are addressed. The design characteristics of life support are mentioned only in those sections requiring it.

WAVERIDER

The waverider is the hypersonic, manned vehicle designed to transport astronauts to Mars. It will use an aeroassist maneuver at Venus and then return them to Earth via a sprint mission.

The design process for the waverider begins by placing a generic shape such as a cone or wedge in a flow field to create a shock wave. The waverider leading edge is then created so that it is everywhere attached to the shock. Subsequently, the lower surface is designed along the streamlines present in the flow field. Finally, the upper surface is constructed along the freestream streamlines so that the pressure acting along the upper surface is simply the freestream pressure. Since each leading edge design corresponds to a unique waverider, an infinite number of waveriders are possible for each shock. However, software written at the University of Maryland can generate specific, optimized waveriders for a particular condition. Generally, these conditions are maximum lift-to-drag ratio, minimum coefficient of drag, and volumetric efficiency.

The particular shape chosen was optimized for a maximum L/D while also considering volumetric efficiency. The waverider has a L/D of 8.47, a length of 60 m, a maximum height of 6.01 m and maximum width of 16.43 m (Fig. 1).

The waverider will approach Venus with a velocity (relative to Venus) of 14 km/sec. This corresponds to a local Mach number of 71 (based on freestream temperature). It will experience intense aerodynamic heating effects during its passage through the Cytherean atmosphere. Designing an integrated structure and thermal protection system capable of withstanding the severe heating conditions represents a major technical hurdle.

Three-dimensional Advanced Carbon-Carbon (ACC) was chosen as the waverider structural material. ACC outperforms all other materials above 1250 K. It has a high emissivity, which

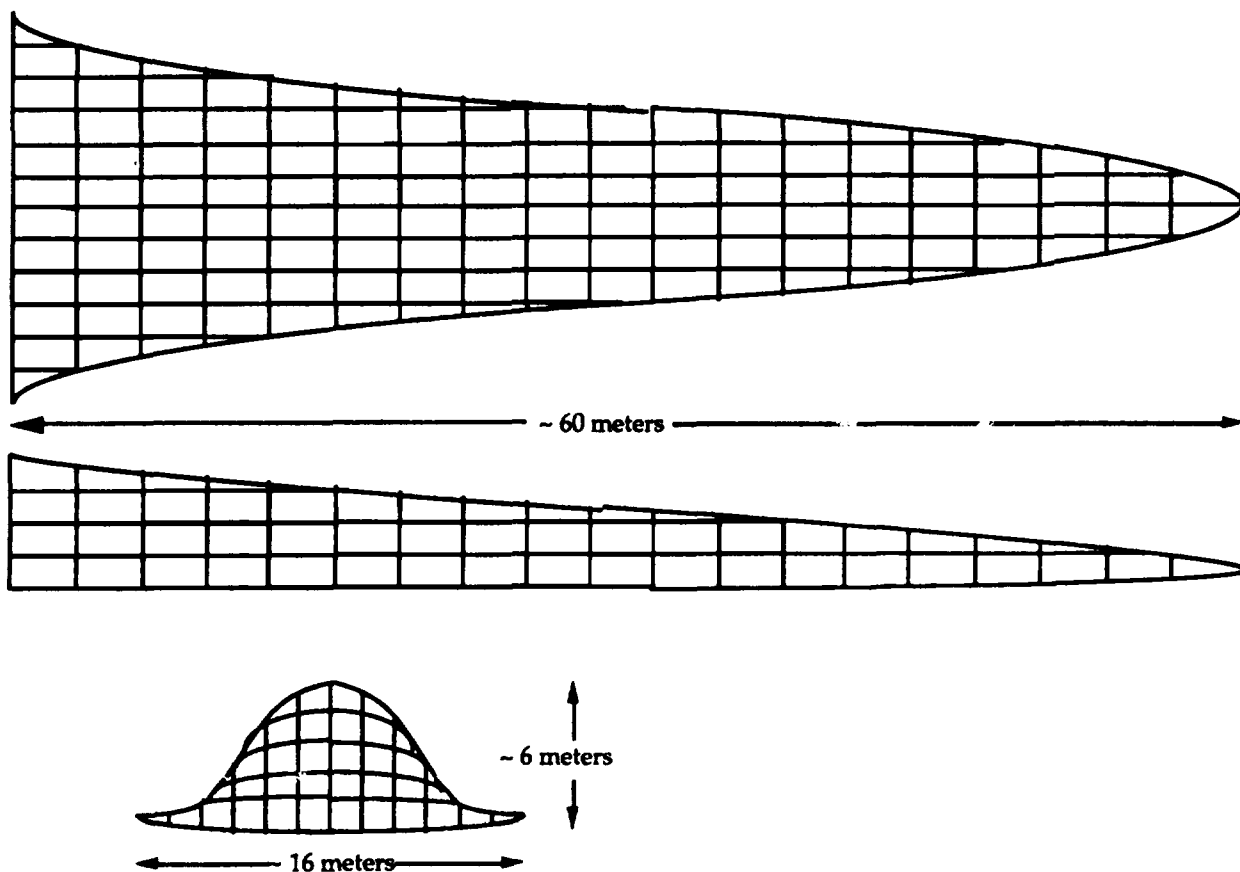


Fig. 1. Waverider Configuration

is a key in reducing surface temperature. ACC is extremely lightweight, with a density of about 1.7 g/cm^3 . To maintain aerodynamic integrity of the vehicle, ablation will not be used to control the temperature. Instead, a combination of chemistry effects, radiative energy, and conduction (active cooling) will be employed. An active, heat pipe design will be integrated into the leading edge. The heat pipes are extremely thin tubes of tungsten with the liquid metal, lithium, as the working fluid.

The waverider will have a double leading edge design (Fig. 2). The original leading edge will conform to the computer-generated waverider shape. This leading edge will comprise the the first 25 m of the waverider and will have its own heat pipe system. In essence, the waverider's first 25 m will simply be a shell to provide the proper waverider configuration. This original leading edge will perform the aeroassist maneuver at Venus and the aerobrake at Mars. While in LMO, this leading edge will be pyrotechnically separated from the remainder of the vehicle. The new vehicle will consist of the new leading edge, complete with its own heat pipe system and the life support module. Several reasons exist for using a double leading edge design. While performing two atmospheric maneuvers, the original leading edge could conceivably suffer some damage that would affect its aerodynamic capability. Thus the waverider will have a new

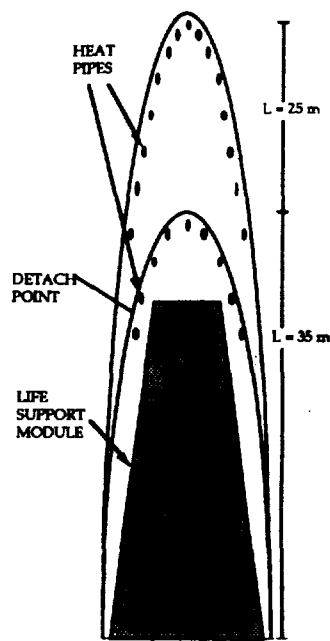


Fig. 2. Waverider Double Leading Edge with Heat Pipe Configuration

leading edge for its return trip to Earth, which is particularly important for aerobraking. In addition, the new leading edge will be more blunt than the original. This will not only reduce the maximum temperature and heating values, but will also increase drag, thus reducing the amount of time needed to slow down in Earth's atmosphere. Finally, by separating the original leading edge, the waverider mass will be greatly reduced. This will reduce the amount of fuel that must be transported by the cargo ship to Mars for the return trip to Earth.

With regard to the manned Mars mission project, a new approach must be considered: the aerogravity assist (AGA). Gravity-only assists rely simply on celestial mechanics, whereas an AGA also depends on aerodynamics. This maneuver incorporates a vehicle with high aerodynamic lift such that this lifting force augments gravity in balancing the centrifugal force on the vehicle by flying upside down. This equilibrium allows the vehicle to fly through the planetary atmosphere at a constant altitude. With a high lift-to-drag ratio, the amount of time in the atmosphere can be maximized as desired. This aspect of the maneuver is particularly applicable to the waverider configuration. Lift-to-drag ratios of 7-10 have been demonstrated and an L/D of 15 has even been exhibited for the Cytherean atmosphere. Such a maneuver can reduce the ΔV required or the time of flight to a given destination.

Since the shortest time to Mars was desired, the fastest trajectories possible were selected as candidates for the flight out. These were subjected to the constraints that a maximum ΔV of 9 km/sec is available for LEO departure and a maximum ΔV of 14 km/sec can be achieved with an aerobrake at Mars (the g -forces for higher speeds become intolerable). The time of flight (TOF) for the trip out is 108 days with a stay time of 0-220 days on the surface of Mars. The TOF for the return trip is 178 days.

The waverider will be propelled to Mars by a chemical engine using LOX and LH₂ as fuel and it will be propelled back to Earth by a solid-core, nuclear engine using LH₂ as fuel. The nuclear engine has an I_{sp} of 1150 sec and requires 89,101 kg of fuel to power a 50,000-kg waverider, while a chemical engine, with an I_{sp} of 450 sec requires 436,262 kg of fuel to power the same waverider. Because of volume restrictions, the waverider propulsion system has to be external to the ship (Fig. 3) and must be detached before entering the atmosphere of Venus. Even though the nuclear engine outperforms the chemical engine, the chemical engine was chosen for the flight to Mars because it would cost less to discard one, instead of two nuclear engines. The nuclear engine is the better choice for the return trip because it requires less fuel, an amount within the limits of the cargo ship payload capacity.

A major concern for any mission in space is providing enough food, water, and oxygen for the astronauts to survive the mission. To provide these life support supplies, an integrated regeneration system, also known as a closed loop system, is proposed. An integrated regeneration system is very complex. It involves carbon dioxide removal and concentration, carbon dioxide reduction, oxygen generation, water reclamation, solid waste removal and processing, nitrogen generation, and storage for all of these processes. Storage is



Fig. 3. Waverider with Chemical Booster

very important because the output of one subsystem is the input to another. Matching flow rates will be very difficult. Providing storage for each subsystem helps to eliminate this problem. The same type of regeneration systems used on the waverider will be used on the martian base. The power supply for these systems and all other systems on the waverider will be a 300 W/kg solar array.

During a manned Mars mission the astronauts will require shielding from Van Allen belt radiation, galactic cosmic rays, and solar cosmic rays (also known as solar flares). Shielding for radiation from the nuclear engine will be incorporated in the design of the engine. A bunker area will be incorporated into the waverider design to protect the astronauts during solar flares.

CARGO SHIP

The cargo ship, as its name implies, is an unmanned, interplanetary vehicle that carries supplies and equipment needed by astronauts on the surface of Mars (Fig. 4). It will be assembled at the Space Station with several components that will be constructed in the space environment near the Space Station. The waverider will leave low Earth orbit when the cargo ship successfully arrives at Mars where it will remain in LMO until rendezvous with the waverider. At this juncture, the astronauts will disassemble the components of the cargo ship needed on Mars and send them down to the surface.

The cargo ship is made up of several components including the nuclear reactor, radiation shield, heat radiator, argon fuel for magnetoplasmadynamic (MPD) thrusters, six ion attitude control thrusters, and seven MPD main thrusters. Payload includes the return hydrogen fuel and nuclear engine for the waverider, the NIMF shuttle, and two cargo capsules containing martian base supplies and surface life support.

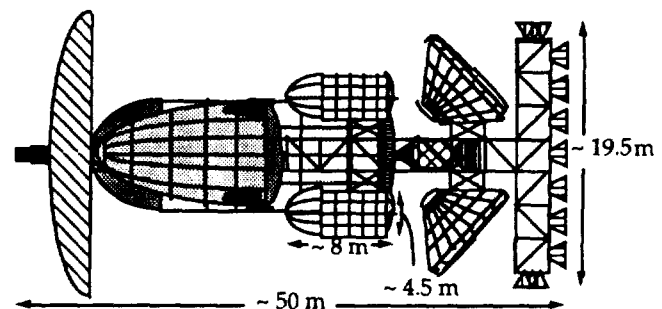


Fig. 4. Cargo Vehicle

The cargo ship is a vehicle connected by a truss to give flexibility in the arrangement and accessibility of each component. It is a desirable structure because of the loads that it sustains. Its main force of action is along its axis, which allows for a design to withstand optimal tensile and compressive stresses. Buckling loads on the members are more significant than tensile and compressive loads, thus the design is to disallow buckling (and axial stresses).

The materials considered for truss members are titanium and graphite epoxy. Titanium is used for nodes (connection elements) of the truss. In using the composite, graphite epoxy, for the individual truss members, strength increases while density decreases, therefore weight decreases. The members are also clad with aluminum to prevent erosion.

The cargo capsules that will be sent down to the surface of Mars will have the configuration of the Apollo capsules. This shape offers several desired characteristics. It has a high drag coefficient, which is required for the rapid deceleration in thin martian atmosphere. It decreases heating on the undersurface of the capsule because of the large radius of curvature, which increases the distance between the surface and the shock. Also, if designed correctly, the structure will be stable about one orientation only. This means that during initial reentry, no matter what the attitude of the vehicle is, it will stabilize about the nose forward orientation without an attitude control system.

Reentry will utilize two decelerators: parachutes and retrorockets. The parachutes will be stowed in a small compartment at the apex of the capsule. After deployment of the chutes, the landing gear will be extended and the heat shield for the retro rockets will be discarded exposing the nozzles, which will fire to decelerate to a soft landing velocity.

The materials considered for the capsules are carbon-carbon composites and aluminum alloys. The composites are used for the undersurface of the capsule, which experiences the greatest heat. It was calculated that 1400 K would be reached, which can be easily withstood by the composite material. The infrastructure of the capsules will probably be made out of materials such as boron-aluminum.

The purpose of the cargo ship is to deliver a maximum payload both efficiently and inexpensively to Mars. Since mission time is not of great importance, a low-thrust orbital maneuver can be considered for this cargo vehicle. A nuclear-electric propulsion system was compared to both advanced chemical boosters and a nuclear-thermal rocket as possible options for this mission.

A nuclear-electric propulsion (NEP) system was determined to be the most attractive propulsion option. It consists of a multimewatt nuclear power plant that generates electricity necessary to operate the MPD thrusters. The MPD thrusters generate an electrical arc between an anode and a cathode that ionizes the propellant. The resulting plasma is then electromagnetically accelerated through the MPD nozzle to create thrust. The resulting exhaust velocity is extremely high, and specific impulse values ranging from 3000 to 9000 sec can be attained.

Since fuel mass is related exponentially and inversely to specific impulse, large fuel savings can be achieved by using

an NEP system. In order to transport a 200,000-kg payload from LEO to martian parking orbit, only 134,000 kg of fuel would be required. This is significantly less than the fuel required for chemical (855,770 kg) and nuclear-thermal (235,406 kg) propulsion systems.

The spiral trajectory consists of three separate legs: Earth escape spiral, outbound coast, and martian capture spiral. The transfer begins with the 52-day Earth escape spiral during which the cargo vehicle slowly escapes the Earth's gravitational well by making many spiraling orbits. The spacecraft then coasts for several months until it refires its engines to straighten its orbit. When the cargo vehicle approaches Mars, it begins to spiral over a period of 39 days until it reaches martian parking orbit.

Since the spiral trajectory is a low-thrust maneuver, the total mission time is 601 days, or 1.65 years. This is significantly longer than a high-energy Hohmann transfer. A faster trip is not required, since the payload is only cargo; it is only necessary for the cargo ship to reach martian parking orbit before the waverider vehicle.

The main component of the nuclear-electric propulsion system is the nuclear power plant, which generates all the power necessary for the MPD thrusters and the onboard power systems. The nuclear reactor is a 5 MW_e/20 MW_t distributed heat transport design. This type of reactor is favored over conventional solid-core reactors for safety reasons. The absence of a core pressure vessel increases the chances of core burn-up in case of an accidental atmospheric reentry. Also, in case of land impact, the core reactor will be in a subcritical configuration. The curved structure of the reflector prevents core compression in the case of impact.

The main engines for the cargo ship will be MPD thrusters. These engines ionize propellant and electromagnetically accelerate the resulting plasma to very high speeds. The plasma is then expanded out through a nozzle to produce thrust. Although MPD thrusters are presently still in the development stages, the prospect of using them in cargo-type, low-thrust missions is extremely attractive.

Exhaust velocities have been measured ranging from 15,000 to 80,000 m/sec in laboratory conditions. These can provide extremely high specific impulse values on the order of 1500 to 8000 sec. Thus the required fuel mass is significantly less than comparable chemical or nuclear-thermal systems. For this mission, seven MPD thrusters will be fired individually in succession. This will provide the necessary ΔV for a constant, low acceleration necessary to complete the spiral trajectory. A thrust of 115 N will be assumed for an I_{sp} of 4000 sec. The MPD thrusters will use argon as a propellant.

SURFACE MISSION

The major components of the surface mission are the NIMF shuttle, the 5-MW nuclear reactor power supply, the main dome, the two landing capsules, the life support and recycling equipment, the scientific payload, the rover, the extraction equipment, and miscellaneous piping, wiring, and tankages. The surface mission will last about three months. It will entail a large number of short-range, 2-5 km missions around the

main base and multiple long-range missions to several sites of interest. During these missions, experiments will be set up and samples will be collected at the various sites.

A geodesic dome was chosen for the martian base (Fig. 5). The most volume-efficient structure was sought so that interior living space could be maximized while minimizing total surface area. Therefore, the material mass required to be transported to the martian surface will be minimal. The sphere is the most volume-efficient shape and this can be conveniently represented by a geodesic dome. To achieve the volume necessary to house 10 astronauts, required life support, and miscellaneous equipment, a 5/8 dome of 7.62-m (25-ft) radius was selected (5/8 refers to a dome larger than a hemisphere). The dome will be partially buried and sandbags will be used to hold the upper portion in order to shield against radiation. Shell construction can be completed by 10 people in 1-3 days.

A vehicle using indigenous fuel as a propellant in a nuclear thermal engine is a NIMF (Fig. 6). The NIMF shuttle will have three primary functions. First, it will be used to transport the 10 astronauts from LMO to the martian surface. Second, the NIMF will be used for exploratory missions, traveling about the martian surface refueling itself with liquid CO₂. When the surface mission is over, the NIMF will transport the 10 astronauts back to LMO to rendezvous with the waverider.

COST ANALYSIS

The costing model for this mission was broken up into two parts: waverider and cargo mission. This model generates a bottom-line cost based on the mass of the two interplanetary vehicles. Personnel costs are derived from the bottom-line cost. Since the vehicles for this mission will be constructed and launched from the Space Station, cost estimates had to be calculated for Earth-to-Space-Station launches, construction at the Space Station, and fuel storage costs. All cost estimates are added to the bottom-line cost and the values are inflated to the year 2012 values.

The waverider is estimated to cost \$92.56 billion and the cargo ship is estimated to cost \$101.243 billion. Total cost of the mission is estimated at \$193.803 billion for the year 2012.

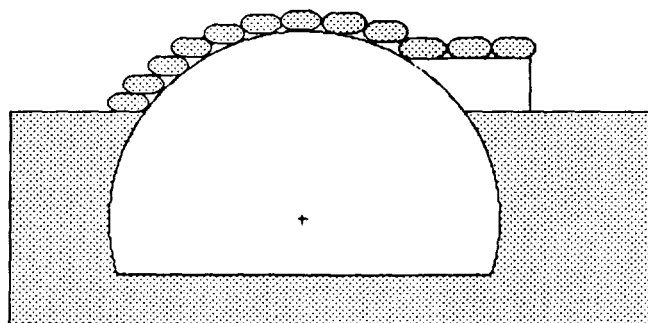


Fig. 5. Geodesic Dome for the Martian Base

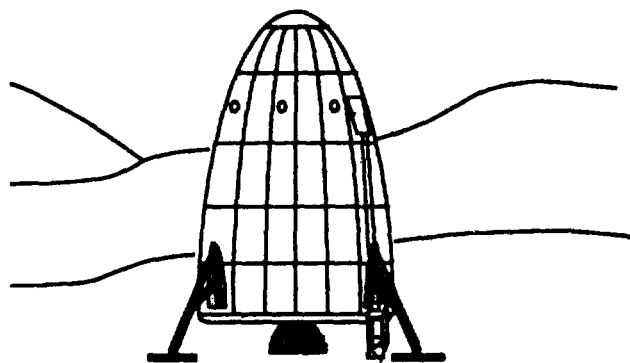


Fig. 6. NIMF Lander

CONCLUSION

The Request For Proposal called for the use of a hypersonic waverider to transport 10 astronauts to Mars for a 3 to 5 month exploratory mission by the year 2025. It also called for using the waverider for an aerogravity assist through the atmosphere of Venus. Other criteria for the Request For Proposal were minimum time of flight, minimum cost, minimum launch mass from Earth, maximum payload delivery to Mars, safe human environment, and practicality of accomplishment with projected technology in the desired timeframe.

The waverider will be constructed entirely of advanced carbon-carbon (ACC), which is lightweight but very durable. The waverider will experience extreme temperatures in the atmospheres of Venus, Mars, and Earth because of very high relative velocities. ACC was chosen as the best material to handle all loads encountered and keep the vehicle mass at a minimum. By performing the aerogravity assist through the atmosphere of Venus, the waverider achieves a deflection angle and ΔV increase for the trip to Mars, as well as a launch window for a return trip, which is open for 7.5 months. The Venus gravity assist also allows for sequential launches of the cargo ship and waverider that will not require the cargo ship to stay in orbit for a couple of years before the waverider can dock with it. The waverider will be constructed with a double leading edge so that the outer portion can be removed after the Mars aerobrake maneuver. Removal of the outer leading edge reduces the vehicle mass and therefore reduces the return trip fuel mass requirements. The return propulsion system will be a nuclear solid core engine that uses H₂ as a propellant. The engine performance characteristics far outweigh those of a chemical engine and the fuel mass requirements are considerably less. The aerobrake maneuvers at Mars and Earth eliminate the need for a propulsion system for deceleration. Life support aboard the waverider will incorporate an integrated regeneration system instead of all stored supplies. Life support also includes the design of an artificial gravity centrifuge to help counteract the effects of microgravity.

The cargo ship, which is a long truss with all the payload attached to it, travels to Mars on a spiral trajectory using a nuclear electric propulsion system. The NEP system consists

of a nuclear electric power plant, MPD thrusters, and ion attitude control engines. The MPD thrusters and ion engines both use argon for a propellant. The NEP system requires a longer mission time than any of the other propulsion systems considered; however, it also requires the least fuel mass. The nuclear electric engine that powers the cargo ship has an operating lifetime of seven years. This engine will also be the power plant for the Mars base.

The Mars base will be constructed mostly underground to shield from solar radiation. It is also constructed from ACC. The base is a 5/8 dome that can be constructed in 1-3 days. It will provide a shirtsleeve environment for the astronauts as well as a permanent structure for future missions. The NIMF shuttle, which is propelled by essentially the same engine used to return the waverider to Earth, will be used to transport the astronauts to and from LMO as well as around the planet. The

shuttle uses CO₂ as a propellant, which will be extracted from the martian atmosphere and compressed into liquid form. The NIMF shuttle makes it possible to study a wide range of locations on the planet, allowing extensive search for useful extractable materials that could lead to possible colonization of Mars.

The effort to reduce cost began by keeping mass at a minimum. With production scheduled to begin by the year 2012, financing a mission of this size will have to be done on an international scale. Much of the new technology such as the waverider, nuclear solid-core engine, MPD thrusters and total regenerative life support systems will require more research. Pushing technology is the key to reaching the point that the first stone can be laid for a mission like this. Without a tremendous push for more research and development, man may never set foot on Mars.

MANNED MARS MISSION

UNIVERSITY OF MARYLAND

12
13
III
P.6
N91-18139

INTRODUCTION

Terrapin Technologies is pleased to propose a Manned Mars Mission (M³) design study. The purpose of M³ is to transport ten people and a habitat with all required support systems and supplies from low Earth orbit (LEO) to the surface of Mars and, after an eight-man surface expedition of three months, to return the personnel safely to LEO. The proposed hardware design is based on systems and components of demonstrated high capability and reliability. The mission design builds on past mission experience but incorporates innovative design approaches to achieve mission priorities. Those priorities, in decreasing order of importance, are safety, reliability, minimum personnel, transfer time, minimum weight, and minimum cost. The design demonstrates the feasibility and flexibility of a waverider transfer module.

MISSION OVERVIEW

The M³ begins with the departure of the Landing/Launch Vehicle Module (LLVM) from LEO on a transfer trajectory to Mars. The LLVM is comprised of three submodules: (1) the LLVM Departure/Return Stage, (2) the Lander/Launcher/Habitat Submodule, and (3) the Supply Stage (SS). The Departure/Return Stage provides propulsion and control for the burn out of LEO, as well as propulsion and control for primary burns to achieve a low Mars orbit (LMO) and propulsion and control for the burn to return the waverider to LEO. The Lander/Launcher/Habitat Submodule provides all life support, logistics, and equipment for the surface expedition as well as propulsion, thermal protection, parachute braking system, and control for descent to the Mars surface and propulsion and control for liftoff and rendezvous with the Departure/Return Stage in LMO. Finally, the SS carries supplies for the Waverider Orbital Personnel Module (WOPM) return to LEO.

Following departure of the LLVM from LEO and checkout of all systems in Mars orbit, the WOPM departs LEO for Venus. The WOPM is composed of two submodules: (1) the WOPM Departure Stage, which provides propulsion and control for the burn out at LEO and separates after that burn is complete, and (2) the waverider, which provides propulsion and control for transfer into LMO, thermal protection for an aeroassist maneuver in the Venus atmosphere, guidance for all phases of the mission, and accommodations for the ten passengers on both departure and return legs of the mission. After separation

from the WOPM near Venus, the Departure Stage, with propulsion produced by a nuclear generator, will return autonomously to LEO to be reused for future missions. The LLVM Departure/Return Stage and the WOPM Departure Stage are of the same design, and, for generic discussions, will be referred to as "the booster."

After transferring from Venus to LMO, the WOPM performs an aerobrake maneuver and carries out a rendezvous with the LLVM, already in Mars parking orbit at 170 km. Systems are checked out, and the waverider, SS, and Return Stage, now docked together, are separated from the Lander/Launcher, which then descends to the martian surface with eight of the ten crewmembers. The other two crewmembers remain on board the waverider to monitor the habitat on Mars and maintain frequent communication with the ground stations on Earth. They will also be responsible for performing scientific experiments and transferring supplies for the return voyage from the SS portion of the LLVM.

After the three-month expedition is complete, the Liftoff Submodule rejoins the WOPM in LMO. Personnel transfer to the waverider, and the empty SS is jettisoned. This allows the WOPM to return to Earth without the added weight of the SS, thereby decreasing the necessary amount of return fuel. Finally, the WOPM departs for Earth with the Return Stage providing propulsion.

VEHICLE DESIGN AND FUNCTION

The LLVM is designed to carry all necessary supplies for the surface mission and return voyage since the crew would not have need of them until LMO is achieved. In addition, the thin, aerodynamic structure of a waverider of reasonable proportions is not capable of transporting such large volumes and still achieving the high values of L/D required for the Venus fly-by portion of the mission.

As noted previously, the boosters for the WOPM and the LLVM are of identical design and will be recovered at the end of the mission.

The Launcher/Lander/Habitat is a blunt, lifting cone and thus provides a compact, efficient volume for the crew dwelling on the surface.

The WOPM is designed to carry the ten-person crew and all the supplies and equipment needed to reach LMO from LEO. When the Liftoff Subsystem returns to LMO for

rendezvous, the WOPM must be capable of adjusting its trajectory to meet that of the Liffoff Module. Once the remaining crew reenters the waverider, it will dock with the booster portion of the LLVM in the proper configuration for the return trip.

TRAJECTORY

The trajectory of the waverider consists of leaving Earth orbit on an elliptical transfer orbit to Venus, performing an aero-gravity assist (AGA) maneuver at Venus, and then traveling to Mars on a new, elliptical orbit. After the three-month surface mission, the waverider is placed on an elliptical transfer orbit back to Earth, where a velocity increment is applied to slow the vehicle down and place it into orbit about the Earth.

The advantage of using the waverider for this application lies in the fact that it is a lifting body. A waverider is a vehicle built so that it can create a shock wave that does not separate from the leading edge. Because it "rides" on its own shock wave and avoids the usual pressure losses, the vehicle can achieve much better aerodynamic performance for a given high-speed condition.

Since its structure is tailored to "ride" the shock wave at a certain flight condition, the waverider can enter and fly through the planet's atmosphere without experiencing excessive velocity loss due to drag. Also, it can remain at a constant altitude during the atmospheric passage, thus allowing almost any desired angular deflection. Thus an AGA maneuver can be used to provide a high angular deflection about Venus with minimal loss in velocity.

Considering all the variables, the Earth-Venus-Mars trajectory was then determined by trial and error runs of a computer code. This trajectory allows the waverider to reach Mars in 135 days, with a required deflection angle of 82° through the atmosphere of Venus. An elliptical transfer orbit with a duration of 137 days was selected for the return trip to Earth. The manned mission totals only 362 days. This trajectory meets the requirements of the Request for Proposal, in that it provides the minimum time of flight to Mars within two years of the specified year, 2025. Table 1 describes the final trajectory for the entire mission of the waverider.

Table 1. Final Trajectory of Waverider

Launch Date	Planet	V_{∞} *	Bend angle
8/22/2026	Earth	6.6 km/sec	—
10/28/2026	Venus	16.0 km/sec	82°
1/02/2027	Mars	-13.2 km/sec†	—
4/02/2027	Mars	6.0 km/sec	—
8/17/2027	Earth	5.0 km/sec†	—

* V_{∞} is given as the relative velocity to the corresponding planet.
 † The negative sign indicates the velocity is to be lost at the given planet.

The SS trajectory will consist of placing the vehicle on a Hohmann transfer orbit to Mars, where it will then be placed in a circular orbit about Mars and remain there until it docks with the waverider. The time of flight to Mars via a Hohmann transfer is 258 days.

The entry phase of the landing trajectory was chosen for moderate entry velocity and heating alleviation. A shallow flight path at entry is maintained to reduce heating and increase range to permit drag to reduce velocity. As a means of reducing propellant required for landing, parachutes will be deployed. The final profile chosen involves a moderate entry initiated from a 170-km circular parking orbit, entry velocity of 3.61 km/sec at 90 km, guidance for thermal control and velocity reduction from 90 km until conditions are reached to allow parachute deployment, three-stage parachute deployment beginning at Mach 2.6, and a final powered flight, hover/landing phase initiated at 0.5 km.

The Launcher Submodule is contained within the Launcher/Lander Module and provides the transfer from the martian surface to a parking orbit where it will rendezvous with the waverider to transfer personnel and scientific samples for the return to Earth. The final launch trajectory determined iteratively by computer requires a gravity turn of 200 sec after an initial period of 0.4°/sec constant turn rate to gain altitude.

WAVERIDER STRUCTURES AND MATERIALS

Design of the size and shape of the waverider was done by computer generation. A program written at the University of Maryland allows the user to input the expected flight conditions and desired physical characteristics (i.e., length, size constraints) for a vehicle and will output the size, shape, and aerodynamic characteristics of a corresponding waverider. In order to accomplish our trip in the shortest possible time, volume optimizing and designing for an L/D of at least 7 was found to produce the best final design. The final design for the waverider is shown in Fig. 1. The vehicle had a L/D of 6.89 and an internal volume of 5300 m³.

The waverider will experience severe heating rates, temperatures, and structural loading when it passes through the atmospheres of Venus, Mars, and Earth. These will vary on different surfaces of the waverider, so different parts of the waverider are designed accordingly.

The upper surface of the waverider will experience relatively low temperatures, since it is parallel to the freestream air flow. It will be protected with a hot structure system.

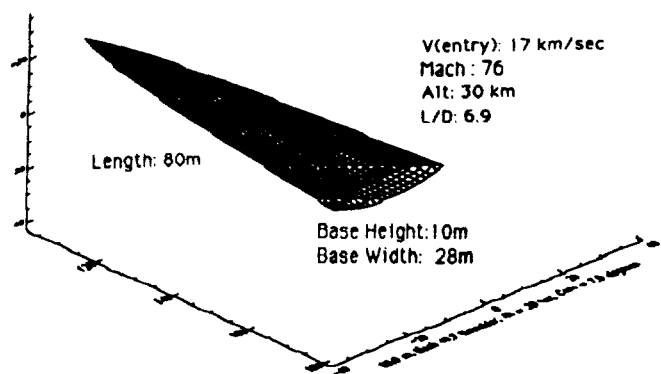


Fig. 1. Waverider Design

The lower surface of the waverider will experience different temperatures and heating rates at different locations. The inner part of the surface that experiences temperatures below 2500 K will be covered with a thermal protection system consisting of thermal tiles made of three-dimensional carbon-carbon composites, the structural material with the highest specific strength above 1200 K.

Since carbon-carbon can only withstand temperatures up to 2500 K, the area behind the nose and leading edges will need an active cooling system. The structure will consist of carbon-carbon composites surrounding refractory metal heat pipes. Liquid hydrogen will pass through these pipes, absorbing heat from the structure and carrying it to the rear where it can be expelled out of a nozzle to provide a propulsive thrust to help overcome some of the drag. To protect the structure during the encounter with Venus, 5000 kg of hydrogen will be needed and an additional 5000 kg will be needed for Mars. The hydrogen will be heated to a temperature of 1000 K and expelled through two nozzles at a mass flow rate of 13.89 kg/sec. This will provide an extra 75,000 N of thrust.

The nose and the leading edges of the waverider will experience heating rates of up to 33,500 W/cm². This corresponds to a temperature of 9000 K, the highest experienced anywhere on the vehicle. Carbon phenolic, the ablative material used on the Galileo probe, was selected to protect the vehicle because it can withstand temperatures over 11,000 K. During the martian encounter, the last of the ablative material will burn away, exposing the active cooling system. This will reduce the L/D ratio for the martian aerobraking, which will allow for a quicker reduction in speed.

The hot structure making up the upper surface of the waverider will have a mass of 19.6 kg/m². The thermal protection system and active cooling system on the lower surface will have a mass of 34.2 kg/m². The total structural mass of the waverider will be 93,050 kg.

WAVERIDER PROPULSION

In order to meet mission requirements, our propulsive system—embodied in a booster—can be used for both the SS and the waverider by changing the amount of fuel. Since the main showcase of this mission will be the use of the waverider, it is in this area that development costs will be the highest. To counterbalance this, our propulsion systems emphasize cost and development efficiency over risky technologies.

The propulsion requirements for this mission are primarily safety, reusability, and low development cost. Because we are using nuclear engines, it is extremely important that the mission be safe and successful for the future of space exploration.

Our final engine choice was a solid core nuclear rocket. The major safety hazard of this system is from radiation, which is easily shielded by use of a shadow shield—a barrier of shield material that is between the reactor and the endangered areas. The reactor will be of bimodal design, i.e., the engine generates electricity as well as thrust, but does not do so simultaneously. Such an output would require 3500 kg of helium. The

specifications for the waverider booster are given in Table 2. The acronym NEBIT refers to Nuclear Engine Booster for Interplanetary Travel, and WR stands for the waverider.

Table 2. Waverider Booster Specifications

Booster Length	40 m	Tank Length	30 m
Booster Width	22 m	Truss Length	35 m
Booster Mass (fueled)	556,440 kg	Miscellaneous Mass	15,000 kg
Fuel Mass (maximum)	426,440 kg	Reactor Mass	15,000 kg
Thrust	2,352,000 N	Tank Mass	20,000 kg
Specific Impulse	1,200 sec	Tank Diameter	8.7 m
Delta V (with WR)	10,523 m/s	Truss Diameter	4 m
Total Mass (NEBIT + WR)	856,440 kg		

A CerMet (ceramic metal) fuel element was selected for our reactor. The mass of the core, pressure vessel, and reflector will be approximately 20,000 kg. The specifications of the supply ship boosters are given in Table 3.

Table 3. Supply Ship Booster Specifications

Booster Length	40 m	Tank Length	30 m
Booster Width	35 m	Truss Length	35 m
Booster Mass (fueled)	1,032,880 kg	Miscellaneous Mass	15,000 kg
Fuel Mass (maximum)	852,880 kg	Reactor Mass	15,000 kg
Thrust	2,352,000 N	Tank Mass	20,000 kg
Specific Impulse	1,200 sec	Tank Diameter	8.7 m
Delta V (with SS)	5,621 m/sec	Truss Diameter	4 m
Total Mass (NEBIT + SS)	1,332,880 kg		

WAVERIDER LIFE SUPPORT

One of the major problems that the astronauts on the Mars mission will have to overcome is the effect that a zero-gravity environment will have on the human body. The effects of prolonged weightlessness on the human body include: decalcification of bones, shrinkage of the heart, decrease in blood volume, and loss of muscle mass.

As a solution to the problem, the crew will make use of both an exercise program (interactive) and an artificial gravity system (passive).

For the exercise program, each astronaut will be scheduled for up to 2 hr of strenuous exercise per day. The familiar treadmill and exercycle will appear on the ship, as well as fluid resistance workout machines.

For the artificial gravity system, the Terrapin Technologies gravity-bed system is being planned. This device is essentially a rotating disk to which the astronaut will be strapped while sleeping. An 8-hr sleep shift while strapped to the gravity bed will provide the needed stress on the bones. This stress will be an axial force acting primarily on the long, load-bearing members (arm, leg bones, and spine). In addition to the bones, the heart and other muscles will gain benefit from the pull of gravity. The primary design of the gravity bed calls for all parts to be made of aluminum.

Another of the major problems that will have to be dealt with is the exposure of the astronauts to radiation. This radiation will come from several sources: radiation from the nuclear engines on the ship, radiation from primary cosmic rays, and radiation from solar flares. This radiation could be of four main types: energetic protons, fast neutrons, X-rays, and gamma rays.

The fast neutron radiation from the nuclear engines on the ship is taken care of by means of a shadow shield discussed above. According to our radiation model, no additional shielding is required to protect the waverider crew from cosmic rays.

The problem of solar flares is slightly more complicated to deal with, since the only way to protect against these high-energy protons is to have a large amount of shielding. By orienting the waverider so that the reactor (with its own shielding) is between the sun and the astronauts, the amount of lead shielding needed to protect the astronauts would be reduced. A protective wall that the astronauts can hide behind during a solar flare was also designed.

SUPPLY STAGE STRUCTURES

The size of the SS was based on supply volumes and the need to accommodate the ascent/descent module. However, the SS was designed to be as low in volume and weight as possible to facilitate the transport from LEO to LMO and to minimize costs.

Since the SS must dock with the waverider in LMO, the configuration was developed in conjunction with the waverider and booster systems. The supply ship must be 25 to 30 m long. Since nothing large will be brought back from the surface of Mars, it is sufficient that the entrance/exit of the ascent/descent module be 2 m. The SS configuration is shown in Fig. 2.

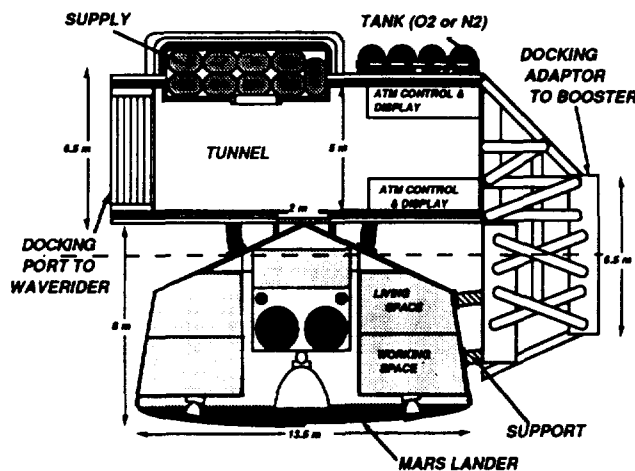


Fig. 2. Supply Vehicle Configuration, Cross-Sectional View

LANDER/LAUNCHER STRUCTURES

During the planning phase of the landing segment of the mission, a decision was made to perform only one landing. This was based on the need to keep all the supplies centrally located on the planet surface. A low-mass structure is also desired since the lander must be transported to Mars. Since fuel requirements and overall cost increase with mass, lightweight, composite materials will be used.

Atmospheric entry at hypersonic speeds will produce high heating due to the viscous effects of atmospheric molecules interacting with the surface of the vehicle. An aeroshell similar to that used on the Viking spacecraft will be employed to protect the lander from the heat loads. Carbon-carbon composites will be used for the aeroshell, eliminating the need for an ablative material. The aeroshell will be designed as a lifting body that will decelerate the lander until parachutes can be used to further slow the descent.

A single atmospheric entry dictates the need for the lander to contain an ascent module as well as the supplies for the three-month stay and the necessary living and working space within the habitat. The fuel tanks for the ascent module are placed above the combustion chamber and nozzle. The design employs the ascent engine during the descent phase of the mission.

The ascent stage has a mass of 1150 kg. The radius of the module is 2.1 m. While the eight astronauts may be cramped, they will be able to fit into this module for the duration of its flights. The astronauts will lie on their backs such that they will radiate from the center of the craft like spokes on a wheel.

The lander vehicle will be utilized as the crew's living quarters for the three-month stay on the surface of Mars. The power system will consist of GaAs solar arrays during daylight hours in tandem with regenerative fuel cells and NiH₂ batteries

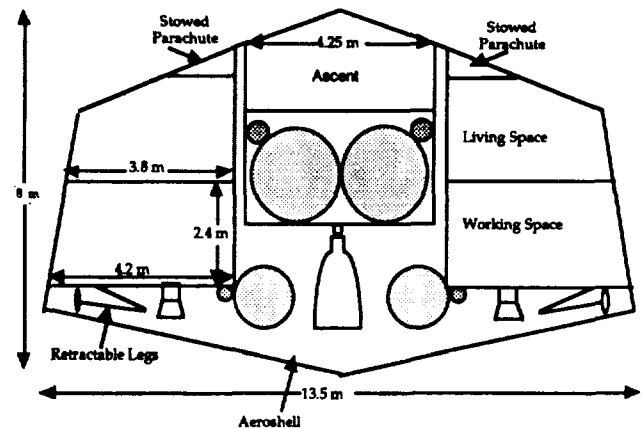


Fig. 3. Lander/Launcher Module, Cross-Sectional View

at night and during dust storm periods. The entire system will weigh 196.5 kg (Fig. 3).

LANDER/LAUNCHER PROPULSION

The primary design goal of the ascent and descent module propulsion systems is reliability. In propulsion systems, the pumps are the most common and likely failure. This weak link is eliminated by using a blowdown system.

The lander and ascent module will be aboard the supply ship for up to a year and a half before being used. Therefore, storable fuels like hydrazine or its derivatives [specifically a 50-50 mix of unsymmetrical dimethylhydrazine (UDMH) and hydrazine] are utilized. Because of its relatively high freezing point, the oxidizer tanks will have to be temperature controlled by a heater/thermal blanket. There will be three small descent engines as well as one large ascent/descent engine included in the configuration.

Since this engine is used for descent deceleration, some maneuvering to adjust the landing site is desirable. This requires variable thrust capabilities; therefore, thrusters are included in the design.

LANDER LIFE SUPPORT

Life support concerns for the Mars lander are simplified due to the 0.38-g martian environment. Even though the duration of the visit to the surface will be short, an emphasis on regenerative systems, particularly for water, is still critical. These and other requirements were considered in developing a life support system to accommodate the needs of the crew.

Two types of radiation are present on the surface of Mars: ultraviolet and ionizing. Since the astronauts will never be exposed directly to the atmosphere, ultraviolet radiation is not a major concern. However, ionizing radiation in the form of solar flares is a major problem. Equipment will be placed on the waverider to constantly monitor the sun to warn of threatening solar activity.

Mars has a weak electromagnetic field and a thin atmosphere, so most of the incident radiation due to a solar flare will arrive at the surface. Shielding to protect against solar flares would make the lander too heavy to fly (and land safely). The only reasonable solution seems to be to abort the mission in case of a solar flare that would affect the lander. The lander would boost to orbit and dock with the waverider, which would be in the safety configuration.

The lander will have two levels. The upper deck will be the private quarters and contain the bathroom; the lower deck will have work stations and the galley. The galley unit will contain a washer, dryer, microwave oven, sink, trash compactor, refrigerator, freezer, and storage space. This level will contain the airlock for outside excursions as well as work space, an exercise area, and storage space for the EVA suits. Total life-support weight for the lander and ascent modules is 3904 kg.

While on Mars, the astronauts will collect rock and soil samples from different depths to determine composition and water content. The trip to Mars will most likely be a precursor to a permanent base, and this mission will show how well people can adapt to the environment. Therefore, the need to assess resource potential is the most critical for this mission.

COMMUNICATIONS

Terp Tech's philosophy is to keep the ground crew in contact with the flight crew as long as possible. The LLVM will be directed by Mission Control and thus needs to be in contact with Earth at all times. Communications with the waverider will be lost during the AGA at Venus and during aerobraking at Mars.

LLVM

The LLVM must carry a sophisticated communications system. It will be used as a platform to do in-depth studies of martian geology, meteorology, and atmosphere to be transferred to Earth before the waverider arrives.

Waverider

Communications, the only link between crew and Earth, will be fundamental to completing the mission. Especially before the critical maneuvers, AGA and aerobrake, the crew will compare instrument readings with ground control. Lag time is a significant problem. The maximum lag time will be 20 min, but the combination of lag and AGA blackout time will result in longer periods without communication.

The M³ system must be light, low in power consumption, able to handle large amounts of data, transmit with minimal error, and be reliable.

COST

Cost for the M³ was estimated from costs for a Mars reference mission with similar hardware complexity (all costs in 1990 dollars). The waverider and hardware costs were determined by scaling the STS orbiter development cost by mass. Costs of the LLVM and the WOPM Departure Stage were determined by scaling costs from the reference mission by mass. The WOPM and LLVM would be launched into LEO by a large, expendable vehicle. The STS/Centaur G' was selected as the most cost effective. In summary, the total program cost is \$105 billion. This compares to \$96 billion development cost for the Apollo program.

SUMMARY

In summary, Terrapin Technologies has met the requirements of the RFP, as demonstrated by the following key features of the proposed design:

Minimum time of crew flight. The waverider trajectory selected allows the crew to reach Mars in 135 days, 125 days earlier than the arrival time for a Hohmann trajectory.

Minimum cost. The boosters for both the LLVM and WOPM vehicles are of the same design, and both return to Earth so that they may be reused in future missions. The dual flight design, with the WOPM and LLVM flying separately to Mars, allows reduction in the size and volume of the more complex, manned waverider. Regenerative life support systems reduce the amount of life-support supplies needed on the mission.

Feasibility in the time scale proposed. The mission has been planned as if it were the *first* Manned Mars Mission. A nuclear engine will be proven technology in the early 21st century. Composites will be sufficiently advanced and affordable for these types of missions.

Journey compatible with humans. The guiding principle behind the entire mission design is the safety and comfort of the crew. Sleeping, eating, resting, and working habits of the

crew were considered carefully. The design focuses on the facts that this is a manned mission and that it is crucial that the crew return safely.

Stretching the technology envelope. Terrapin Technologies has proven that a waverider can be built, flown, and equipped for a crew and that solid reactor rockets can be used to explore the inner solar system. With these two technologies, the exploration of the planets lies within our grasp.

117
p. 6

WALKING ROBOT: A DESIGN PROJECT FOR UNDERGRADUATE STUDENTS

UNIVERSITY OF MARYLAND
DEPARTMENT OF MECHANICAL ENGINEERING

N 91 - 18140

The design and construction of the University of Maryland walking machine was completed during the 1989-1990 academic year. It was required that the machine be capable of completing a number of tasks including walking in a straight line, turning to change direction, and maneuvering over an obstacle such as a set of stairs. The machine consists of two sets of four telescoping legs that alternately support the entire structure. A gear-box and crank-arm assembly is connected to the leg sets to provide the power required for the translational motion of the machine. By retracting all eight legs, the robot comes to rest on a central "Bigfoot" support. Turning is accomplished by rotating the machine about this support. The machine can be controlled by using either a user-operated remote tether or the onboard computer for the execution of control commands. Absolute encoders are attached to all motors (leg, main drive, and Bigfoot) to provide the control computer with information regarding the status of the motors (up-down motion, forward or reverse rotation). Long- and short-range infrared sensors provide the computer with feedback information regarding the machine's position relative to a series of stripes and reflectors. These infrared sensors simulate how the robot might sense and gain information about the environment of Mars.

INTRODUCTION

The University of Maryland walking machine, Prototerp IV, was designed to be a martian planetary rover. Among the design requirements were that the machine be able to support itself on a set of movable legs and not depend on rollers or wheels for its maneuverability. In addition, it was required that the machine be able to "walk" in a straight line and turn to change the direction of motion. These requirements allow the machine to follow any path as well as walk over an irregular surface. The University of Maryland Planetary Rover has the capability to obtain control feedback information regarding its immediate environment and thus can autonomously compute any desired and obtainable path.

The machine was designed and built by the senior Mechanical and Electrical Engineering students of ENME 408 over the two-semester period of the 1989-1990 academic year. The motivation behind building Prototerp IV was to provide the students with practical experience to improve and refine their engineering skills by combining their talents as they worked toward a common goal. In addition, this project aimed to provide an environment where the students learn about robotic systems and apply their creativity to construction of their walking machine.

Prototerp IV required two semesters to evolve. The machine was designed in the fall of 1989, and construction was completed in the spring of 1990. For both semesters, the students were divided into groups that were to address a particular aspect of the project.

In the first semester, the students proposed the initial design. There were four groups: (1) the chassis group, which was responsible for the chassis, drive-line, and the Bigfoot; (2) the leg group, which was responsible for the designing of the legs; (3) the control group, which was responsible for the control hardware and software as well as the selection of all motors; and (4) the sensors group, which was responsible for the selection of rotation, position, and vision sensors.

In the second semester, the students were responsible for the actual construction of the walking machine. As in the first semester, the students were split into groups that were responsible for reviewing the design proposal of the previous semester and suggesting changes to improve the overall design of the machine. There were five groups involved during the second semester: (1) the chassis and Bigfoot group; (2) the leg group; (3) the drive-line group; (4) the control hardware group; and (5) the control software group.

CHASSIS AND BIGFOOT

The chassis of Prototerp IV provides a rigid support to which all other components are attached. Primary considerations for the chassis design include durability, functionality, weight, balance, and safety.

Many materials were considered for the design of the chassis. Preliminary calculations indicated that the robot would weigh approximately 150 lb. In order to prevent bending or flexing along the length or width of the chassis, it was determined that a 2" x 3" 1024 aluminum box channel would be best suited to fulfill the requirements⁽¹⁾. The advantages of using aluminum include its high strength-to-weight ratio and the ease with which it can be machined to proper dimensions.

The overall shape of the body resembles a composite I-beam. To allow for the placement of the gearbox, crank assemblies, computer, and power-packs, the web of the composite I-beam is made of two sections of box channel separated by a distance of 11". Mounted on the outer edge of each web section, near the center, are two leg assembly slider rod support brackets (Fig. 1). Initially, these support brackets were to be a single piece of aluminum channel that bisected the web at the midpoint. This effectively cut the chassis into two pieces. It

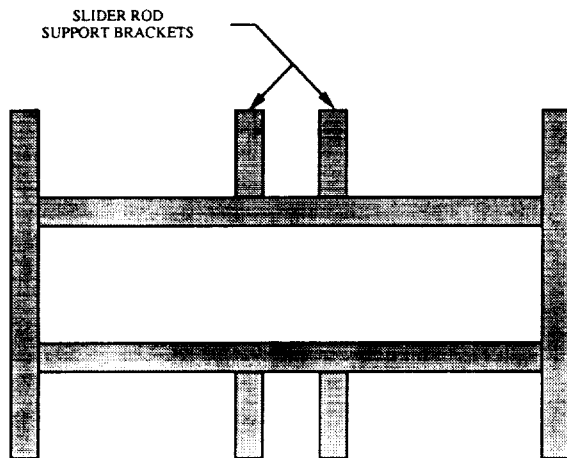


Fig. 1. Chassis

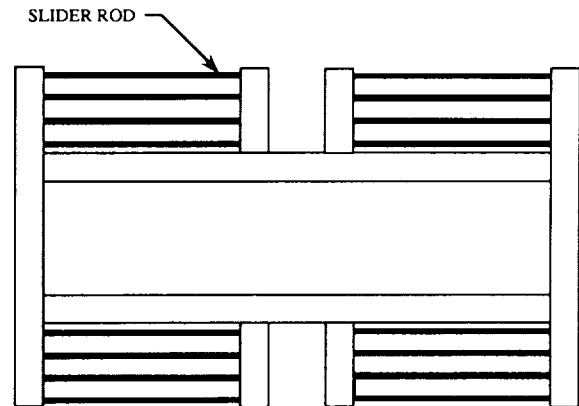


Fig. 2. Slider Rods

was then determined that this design would significantly reduce the rigidity of the robot, which could result in buckling and failure. Upon review, it was decided that the best approach was to make web sections continuous, and mount the slider rod support brackets and slider rods directly to them.

It is important that the chassis remains properly aligned with 90° angles at each corner. Further, a crucial requirement for the leg assembly slider rods is that they should be parallel to one another to reduce drag during each stride (Fig. 2). To ensure that these conditions are met, connections between the sections of the chassis must remain rigid. Therefore, a $3'' \times 3''$ aluminum angle was used as a brace at the inside of each section with four bolts at each leg of the brace. The junctions were tested with a design factor of safety of 5 to ensure that the supports would hold under the repetitive torsional and bending loads.

There are many components that will ride on the chassis including the onboard computer, main-drive gearbox, Bigfoot motor, eight leg motors, photo-interrupter, encoders, infrared sensors, and battery packs. The gearbox is the heaviest component and is located as close as possible to the center of gravity. The remainder of the free-floating parts are positioned carefully to distribute the weight as evenly as possible throughout the chassis and to locate the center of gravity of the robot close to the ground for stability. For safety in the design, all components are securely fastened to the chassis and all sharp edges are rounded off. The powerful crank arms and gearbox are covered with a plastic shell to prevent them from catching anything as they move the connecting rods.

The design of Prototerp IV incorporates the use of a centrally located "Bigfoot" on which the robot pivots when executing a turn. Because of this design feature, the body is required to be symmetric about the centroidal axes to ensure balance and reduce friction. This Bigfoot consists of a fixed shaft on which a geared collar rotates. The "legs" of the Bigfoot are two $1/2''$ -square, 2"-long pieces of aluminum channel that are connected directly to the bottom of the collar. At the ends

of each channel are threaded posts that act as "feet." They have rubber caps attached at the ends to provide a nonslip contact with the floor as the robot is turning. The Bigfoot motor shaft is geared directly to the Bigfoot assembly by a collar. The Bigfoot is capable of turning the robot 90° in 5 sec.

DRIVE-LINE

It is the function of the drive-line to provide the forward locomotive force for Prototerp IV. Several different designs were considered throughout the evolution of the machine. The final design consists of a gearbox and crank-arm assembly that transmit force from a single motor to the leg groups.

The prime mover of the drive-line is the gearbox assembly. The driving force of the gearbox is provided by a $1/20$ -hp electric motor. This motor operates on 12 V DC, and has a built-in 36.7:1 gear reduction transmission. Attached to the output shaft of the motor is a $3''$, 72-tooth spur gear that meshes in line with two identical spur gears. The second and third gears were each connected by a shaft and key to a chain sprocket (Fig. 3).

A length of chain was used to transmit the motive force from the gearbox to the $5.41''$ -long crank arms through the use of sprockets. Using this configuration, it was possible to create

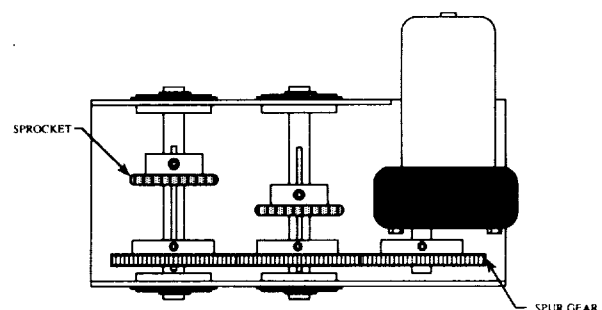


Fig. 3. Gearbox

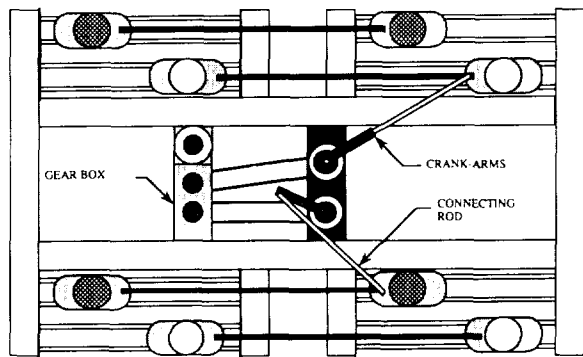


Fig. 4. Crank Arm and Connecting Rod Replacement

opposing rotation of the crank arms. Connecting rods were then attached between the crank arms and each of the forward, innermost leg support brackets. This design translates the rotational motion of the crank arm to linear motion of the legs (Fig. 4).

To achieve the goal of moving the eight legs in two groups of four, a series of connecting rods, pulleys, and cables was used. The connecting rods were attached between forward and rear leg brackets in such a way that the inner and outer sets of legs move independently, but in tandem. Cable was then routed around pulleys so that the inner group of legs on one side of the robot was connected to the outer group of legs on the other side (Fig. 5).

LEGS

Prototerp IV's leg assembly has been designed on the premise that the machine will always be resting on four of its eight legs while walking. This approach to the walking problem provides excellent stability during all phases of maneuvering. During a typical walk maneuver, the first set of the machine's four legs is supporting all the weight while the second set of four legs is transitioning to the next position. Once this position is reached, the second set of legs supports the machine while the first set then moves to the next position. Since all eight legs are coupled together, and are horizontally translated by one motor, the horizontal motion of the machine is continuous.

The transitioning set of legs remains above the supporting set of legs due to the vertical telescoping leg design. This vertical telescoping motion is adjusted by a single motor that is attached to the top of each leg. The vertical and horizontal drive mechanisms achieve the lift and translate motion that enable the machine to walk.

The following description contains the basic sequence that constitutes a step. The typical walk cycle has the machine initially supported by one set of legs. The other set is moving horizontally relative to the body at a level of about three inches

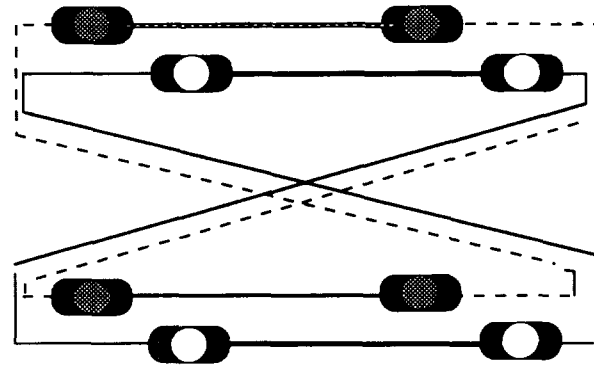


Fig. 5. Pulley Arrangement

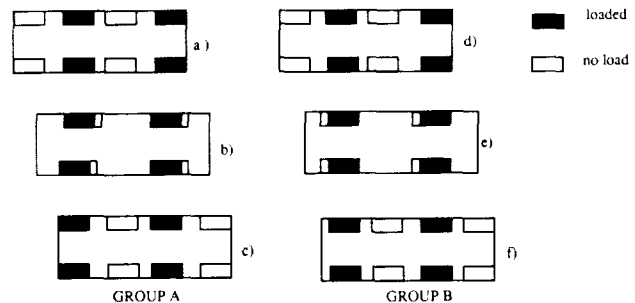


Fig. 6. Walk Routine

above the floor. When the machine reaches the desired horizontal position, the transitioning legs are lowered and the supporting legs are then raised and begin to transition to the next desired horizontal position (Fig. 6).

Vertical translations of the legs are made possible by a telescoping design that incorporates the lower, keyed part of the leg to be driven either into or out of the upper, slotted part of the leg. A motor fixed to the top of the leg rotates a ball screw through a worm gear assembly. The ball screw, supported by bearings, drives a ball nut vertically along the screw. This ball nut is fixed to the lower portion of the leg, the inner tubing, which is keyed to fit into the slotted upper portion of the leg. The key, a delrin strip fixed to the lower part of the leg, and slot, the linear bearing of the upper leg, allow for the ball nut to remain fixed with respect to the ball screw. Thus, the leg is driven in a telescoping fashion.

The exploded diagram (Fig. 7) of the entire assembly illustrates the mechanisms that are involved in the above process. At the top of the assembly, a Pitman motor, operating at 12 V, drives the worm. An aluminum couple joins the motor shaft to the worm shaft. The other end of the worm shaft is supported by a bearing mounted on the inside of the aluminum gear box. The gear box is screwed to the top of the bearing housing. The worm drives a worm gear that is fixed to the ball screw and is supported by two bearings that are contained

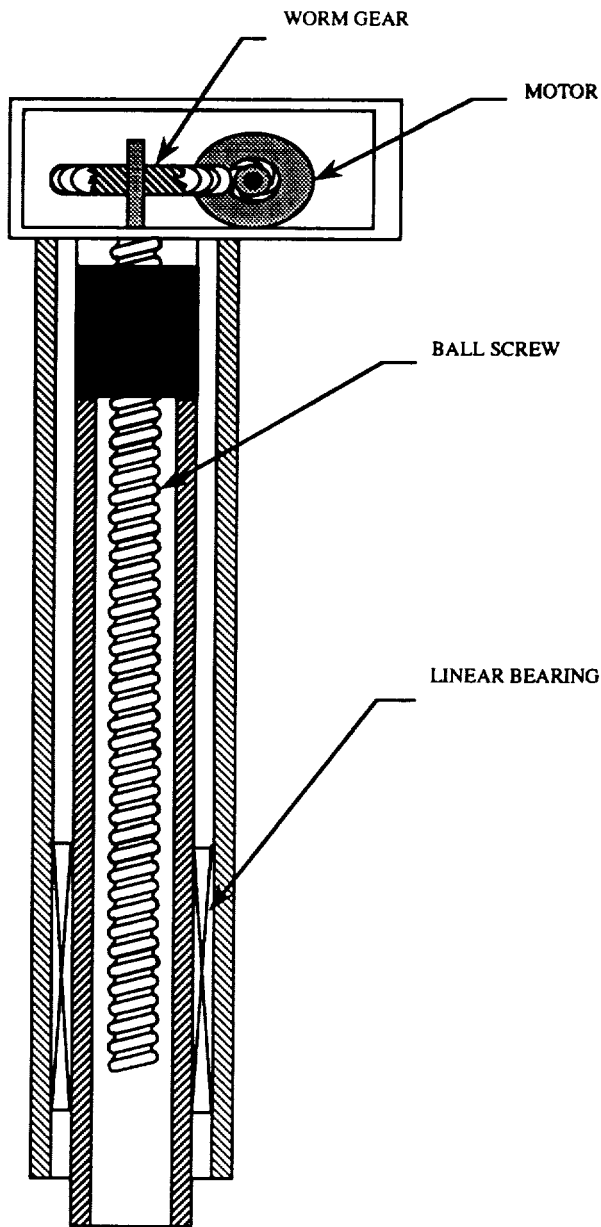


Fig. 7. Leg Assembly

in the aluminum bearing housing. This bearing housing is screwed inside the top of the outer tubing. The smaller inner tubing of the lower leg holds a linear bearing that forms a slot in which the delrin key of the lower leg slides. This key/slot of the upper and lower parts of the leg prevents rotation with respect to the upper and lower parts of the leg as the ball screw rotates. This allows the ball screw attached to the lower leg to move vertically as the ball screw rotates. The ball screw is attached to the lower part of the leg via an aluminum couple. And finally at the bottom of the lower leg is the foot, which holds the contact sensors.

CONTROL HARDWARE

The Prototerp IV walking robot control system is based on the 87C196KB 16-bit embedded microcontroller from Intel. The system is composed entirely of high-speed Complementary Metal Oxide Semiconductor (CMOS) integrated circuits. The advantage to using these circuits is that they require less current for operation and therefore conserve power. The control hardware utilizes a power source separate from that which supplies the motors. This prevents a possible voltage fluctuation from affecting the operation of the chips. A separate power source is needed because when a motor initially starts, it can cause a large power drain that in turn could cause the voltage to drop to an unacceptable level (below 3.7 V).

The control system has the capability of obtaining information on the robot's current configuration through the use of closed-loop feedback. This monitoring capability is achieved through a wide variety of sensors placed in several locations throughout the robot. The types of sensors used include encoders, short- and long-range infrared sensors, photo-interruptors, and switches (Fig. 8). Encoders are connected to each motor. They provide information pertaining to the configuration of specific components such as the height of each leg or the position of the crank arms. Infrared sensors provide information on the position of the robot relative to a specific object when the emitted infrared beam is reflected back to the sensor. Leg position is determined through the use of a photo-interruptor, which directs a light beam toward a sensor and sends a signal to the computer any time the beam is crossed. On the robot, the photo-interruptors are activated any time a leg crosses a certain position. This provides a means with which to count the number of strides taken. Finally, double position (momentary on-off) switches are located at the bottom of each leg and are used to sense when a leg makes contact with the floor.

The information from all sensors is gathered by the 87C196KB processor and is used to analyze the current status of the robot and its surroundings. Once the analysis has been completed the control system directs the machine to make any necessary adjustments.

It is the purpose of the control system to vary the robot's motors according to specific demands; to operate in either direction, at a certain speed, or to shut down. The voltage for

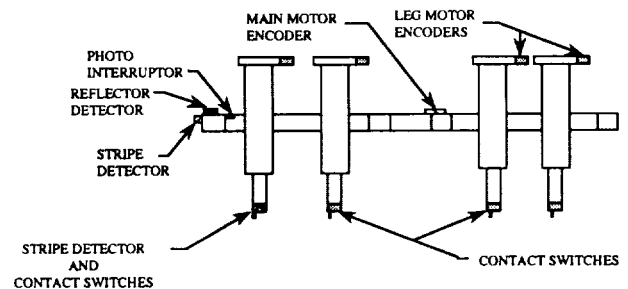
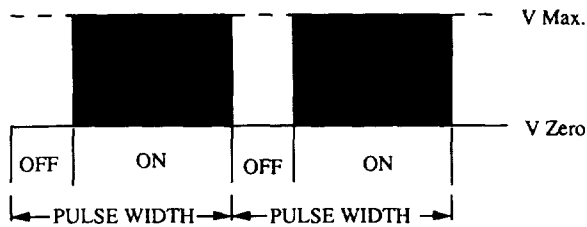


Fig. 8. Sensor Location



$$\text{PROPORTIONAL VOLTAGE} = [1 - (\text{time off}/\text{time on})] \times V \text{ Max}$$

Fig. 9. PWM Waveform

the motor is controlled by a pulse-width-modulated (PWM) wave created by the control system. An illustration of a PWM wave form is shown in Fig. 9.

The PWM hardware achieves the variable speed control of a motor by adjusting the time on/time off ratio of each period of the wave form. These adjustments are repeated thousands of times per second. As the motor is incapable of reacting to these fluctuations, it interprets the signal as a percentage of the maximum voltage where the percentage is proportional to the on time of the PWM wave form.

CONTROL SOFTWARE

It is the purpose of control software to regulate all motors of the robot. These motors include (1) the main drive motor, (2) the Bigfoot motor, and (3) each of the eight leg motors.

An absolute encoder is mounted onto each motor to provide positional information about the motor. The resolution of each encoder varies from motor to motor (the resolution is 2400 counts per inch of movement of the telescoping legs, 1024 counts per revolution of the main drive motor, and 365 counts per revolution of the Bigfoot). This is an important consideration as far as control software is concerned. The different encoder resolutions imply separate yet interactive software routines for integrated operation of all motors.

There are four separate software routines designed to control the motors and coordinate their operation in performing various tasks that a planetary rover might need, such as walking, turning, or climbing.

The first-level routine is the most basic of the four. Its function is to control the operation of the motors. This is accomplished by varying the cycle time of the Pulse Width Modulators. The PWM can be varied from 0% (totally off) to 100% (full speed operation).

The second-level routine is dedicated to the interpretation of the closed-loop feedback information. This feedback information is provided through all the sensors including the infrared sensors, the motor encoders, and the leg stride photo-interruptor. Information from these sensors will be used to determine motor regulation.

The third-level routines are dedicated to the execution of the walk routines. This software incorporates all information gathered by the sensors (second-level software) and coordinates the operation of the motors (first-level software).

The fourth and final level of software is designed to control the robot during autonomous operation. This routine has programmed into it a series of commands that will allow the robot to walk through a figure eight or walk up stairs thus demonstrating autonomous roving possibilities.

As previously stated, the robot walks on two groups of four legs. At any one time, only four legs are in contact with the ground. As each leg is mechanically linked to the drive motor, the horizontal leg location is a function of the angular position of the crank arms, and thus the horizontal position of the leg assembly, is provided by the main drive motor encoder and the information regarding the vertical position of the foot is provided by the leg motor encoders. Therefore, the vertical and horizontal position of the base of the legs can be calculated at any time.

The path of the leg foot as it transitions from the nonsupporting return stroke to the supporting walk stroke was designed to follow a form based on a second-degree equation (Fig. 10). There are benefits to using a second-degree equation for the travel path of the leg feet. At some point all feet are simultaneously on the ground and by using an asymptotic approach trajectory for the foot as it finishes the return stroke, a smooth transition between stride changes is assured. Since the leg groups travel with different relative velocities most of the time, it becomes important to keep the time spent on the ground by all legs at a minimum. A second-degree decay fulfills two requirements: (1) the vertical foot positioning is at ground level for the transition; and (2) the vertical foot velocity is at a minimum when contact is made.

The control of the Bigfoot turning motor incorporates a slightly different approach to that of the legs. A proportional feedback system acts to determine the appropriate Bigfoot motor speed based on the actual and ideal robot position. By calculating the maximum angular acceleration and deceleration of the robot as it is turning, it is possible to calculate the

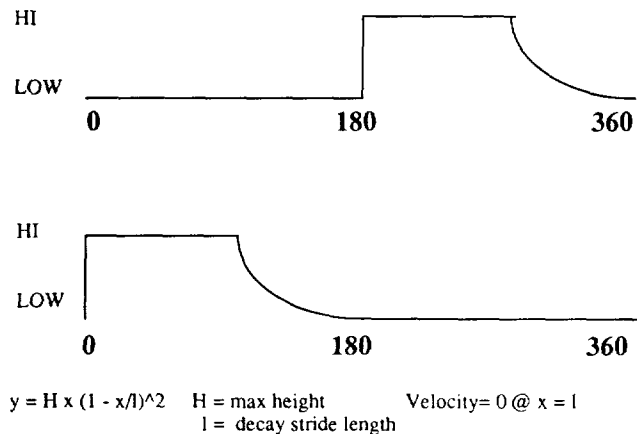


Fig. 10. Leg Height vs. Angular Position of Crank Arm

time required to power the Bigfoot motor to achieve the desired rotational acceleration. Then, proportional feedback is used to calculate the time when the polarity of the Bigfoot motor is to be reversed so as to decelerate the robot and stop rotation at the desired angular position.

Upon testing the machine, a backdriving problem was encountered with the telescoping legs. Because the legs can move freely in the vertical direction when no driving voltage is applied, the leg motors tend to spin backwards under the weight of the robot and the machine falls to the ground. Software control had to backdrive the legs in order to keep the vertical motion steady during the walk routines. Located in the foot of each leg is a switch that closes when it comes in contact with the floor. The status of the contact switches and the intended leg speeds developed in other routines are considered by the software routines before control voltages are sent to the motors. If the situation warrants backdriving the motors, then the lowest level routines instruct motor-control hardware circuits to send sufficient voltage as to prevent the backdriving of the motors.

CONCLUSION

The experience of designing and building Prototerp IV was unique for every person involved in the project. From the initial conception through all phases of the design, to the final details of construction, Prototerp IV has proven to be both challenging and rewarding. As an interdisciplinary experience for the students, this project has excelled. It has provided an excellent opportunity for Electrical Engineering students to learn about mechanics, and for Mechanical Engineering students to further their knowledge of electronics. The project has given these students a glimpse of the real world with all

of the joys and sorrows that await them as they enter the job market as junior engineers. This experience has also shown the students the value of working harmoniously in groups; arguments don't get the job done! In addition, during the course of construction, each group was required to deal with vendors for supplies. We were often required to plead for quick delivery or bargain for donated parts, a new experience for many of the students. In short, every member of the Prototerp IV team was required to learn and grow along with the robot.

ACKNOWLEDGMENTS

Support for the University of Maryland Walking Machine project was given through a grant from NASA/USRA Advanced Design Program. This support is gratefully acknowledged. The students of EMNE 480 would also like to thank Bob Anders, of the University of Maryland Engineering Machine Shop, and Bob Lincoln, of the University of Maryland Electronics Laboratory, for their technical advice and unending support of our efforts. Finally, we would like to thank Mark Uebel, our teaching assistant during this project, for without his direction, concern, and all those sleepless nights toward the end, Prototerp IV would not be a reality.

REFERENCES

1. Shigley, Joseph Edward. *Mechanical Engineering Design*. McGraw-Hill Book Company, New York. 1989.
2. Willems, Nicholas, John T. Easley and Stanley T. Rolfe. *Strength of Materials*. McGraw-Hill Book Company, New York. 1981.

MASSACHUSETTS INSTITUTE OF TECHNOLOGY

Nearly 30 years after John F. Kennedy expressed his desire for an expansion of the space program of the U.S.A., we have been given an even greater opportunity. President George Bush, in July 1989, expressed his desire to once again expand the space program of the U.S., as well as that of other nations around the world. The challenge: "To return man to the Moon, this time to stay." And then, to journey to another planet—a manned mission to Mars. Certainly, the challenge is tremendous, and the obstacles great. However, prepared to achieve this incredible goal is Project Artemis, the project that when complete will turn the dream of permanent manned presence in space into reality.

Why is this challenge, with all its complexity, worth pursuing? The list of reasons begins with the fact that the expansion of human presence in space is an exciting and intriguing opportunity. In addition, the opportunities for scientific and technological advancement are great, as are the opportunities to explore and investigate our closer neighbors in our solar system. The educational benefits and the new employment positions necessary to support such an extensive and long-term project are innumerable. There is also the potential to develop and utilize the resources of the bodies that we explore, possibly resulting in economic benefits for the nation as a whole. Finally, as a nation, we have much to gain in security and pride in being the first country to establish permanent human presence on another celestial body. Meeting this will result in benefits that the U.S.A. and the world will enjoy for many years to come.

The goals of Project Artemis are designed to meet the challenge put forth by President Bush. The first goal of the project is to establish a permanent manned base on the Moon for the purposes of scientific research and technological development. The knowledge gained from the establishment and operations of the lunar base will then be used to achieve the second goal of Project Artemis: establishment of a manned base on the martian surface. Throughout both phases of the program, crew safety will be the number one priority. In addition, commonality will be emphasized whenever possible to reduce costs and increase reliability. Vehicles and modules for the lunar portion of the program will be adapted to suit the different needs of the martian phase; subsystems will use as many common components as possible.

The ground rules for Project Artemis are those considerations that have driven the design of the vehicles, bases, and the overall mission. There are four main issues that have governed the entire mission: crew safety and mission success, commonality, growth potential, and costing and scheduling.

The safety of the crew will be the top design priority. In all portions of the mission, the safety of the crew will be maximized. This will govern the following aspects of the

mission: testing, reliability, and abort considerations. No mission involving the transport of crew members will be considered successful unless the crew is returned safely to Earth once the objectives of the mission have been accomplished.

The second design priority will be commonality between systems. Wherever possible, comparable systems in the lunar and Mars missions will be designed to maximize commonality. This includes entire vehicles, bases, and subsystems. Commonality will also be maximized between vehicles in the same mission. Commonality has an added importance as the lunar mission will be used to learn about the technology for the martian mission.

Since permanent bases will be established on both the lunar and martian surface, growth potential is also an important issue. The bases should be designed to promote future growth. Likewise, the vehicles and ground facilities should also allow for the long-range growth possibilities of the mission.

The final design consideration concerns the costing and scheduling of the entire mission. Without compromising the previous considerations, the cost of the mission should be minimized. Similarly, the scheduling of the entire mission should minimize the timespan of the mission and costing peaks.

The first step toward the success of Project Artemis is the establishment of an advanced space launch system that will include an Earth launch system and an orbital transfer node (OTN). The need for these two components is driven by the large amount of cargo necessary to begin both the lunar and martian phases of the project. The transportation of this cargo from Earth to low Earth orbit (LEO) in a timely manner will require a rigorous launch schedule, as well as Earth launch vehicles that are capable of carrying extremely large payloads. Once in LEO, the amount of orbital vehicle assembly and storage space required makes it virtually impossible for Project Artemis to proceed without an OTN designated exclusively for project use. A schematic of the Project Artemis space launch system is shown in Fig. 1.

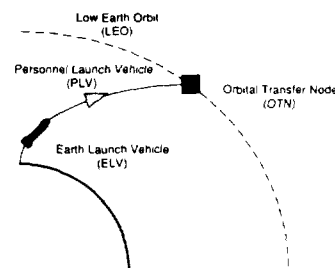


Fig. 1. Project Artemis Space Launch System

A typical mission begins with the launch of cargo from Earth. The Earth launch vehicle (ELV) (shown in Fig. 2) is designed to meet the Project Artemis Earth launch requirements. The ELV is a hybrid liquid/solid multistage rocket capable of carrying a nominal payload of 125,000 kg to LEO. Eight solid rocket boosters comprise the first stage of the ELV. A liquid core using liquid hydrogen and liquid oxygen as fuel makes up the second stage. The upper stage is liquid as well, and it also uses liquid hydrogen and liquid oxygen propellents.

Personnel are transported to LEO in the personnel launch vehicle (PLV), which will be boosted into orbit on a Titan IV. The PLV is capable of carrying a crew of eight to LEO and back again to Earth. A schematic of the PLV is shown in Fig. 3.

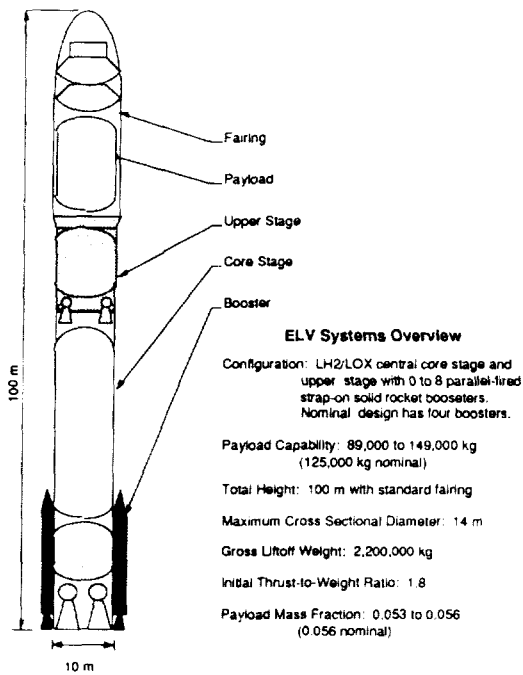


Fig. 2. Earth Launch Vehicle

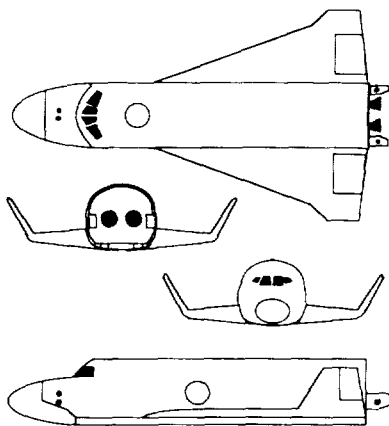


Fig. 3. Personnel Launch Vehicle

Once in LEO, both the cargo and the PLV can be picked up by one of two orbital maneuvering vehicles (OMVs) situated in LEO. The OMVs are NASA vehicles, designed for Space Station *Freedom*, and will not be described in depth within the context of this report.

Once it has picked up its cargo (either mission cargo or the PLV) the OMV transports the cargo to the OTN. The OTN is essentially a space station orbiting the Earth at an altitude of 470 km, and an inclination of 28.5°. Included in the configuration of the OTN are a habitation module, a command module, a vehicle assembly area, a cargo "warehouse," and three vehicle docking interfaces. The OTN is illustrated in Fig. 4.

All Project Artemis vehicles are equipped with common docking interfaces (CDIs). The CDIs ease the docking operations between vehicles and provide a location where the crew can exit one vehicle and enter another.

Once the Project Artemis space launch system is established, the first phase of the lunar mission will take place. The purpose of the lunar mission is to establish a permanently manned base on the Moon. Commonality between the lunar and martian missions is stressed at all times during this process. Since the lunar program will be functional before the martian program, evaluation of the progress of the lunar mission will enable the implementation of necessary modifications to the martian mission.

The lunar mission commences in LEO with necessary vehicles and materials provided by the Earth launch system discussed previously. Figure 5 shows the lunar mission profile.

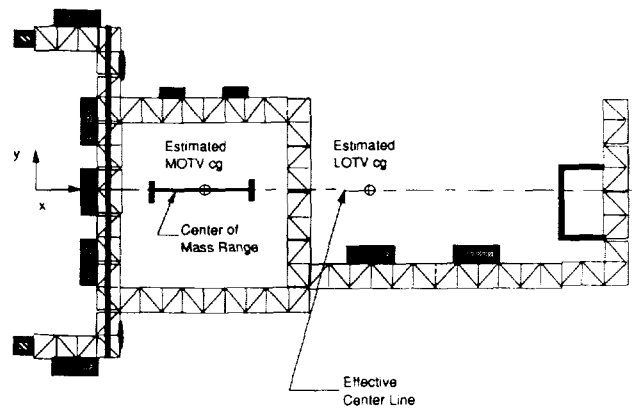


Fig. 4. Orbital Transfer Node

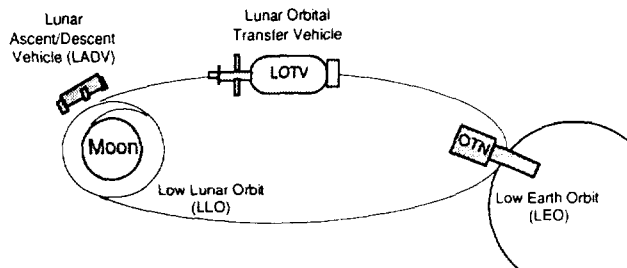


Fig. 5. Lunar Mission Profile

Vehicles used for the lunar phase are the lunar orbital transfer vehicle (LOTV), crew transport module (CTM), and the lunar ascent/descent vehicle (LADV).

The transfer from LEO to low lunar orbit (LLO) will be made in one of three identical LOTVs. Each of these vehicles is propelled by a particle bed reactor (PBR) engine and is capable of carrying a payload of 47,000 kg. Figure 6 shows a more detailed LOTV. The first 10 LOTV missions, each taking about 4 days to reach LLO, will transport necessary cargo. Then, the LOTV will begin its manned journey, transporting a crew of five astronauts to LLO. During transit, the crew will travel in the CTM, which is attached to the LOTV in the payload section.

After firing the LOTV engine to insert into LLO, the cargo or crew will be transferred to the LADV through use of a common docking interface. The LADV is shown in Fig. 7. Each of the three reusable LADVs is propelled by hydrazine and is capable of transporting a payload of 13,000 kg to the lunar surface, and a payload of 9,000 kg off the lunar surface. After a successful transfer, the LADV will transport the crew or cargo to the lunar surface and preparations for assembly of the lunar base will begin.

The lunar base consists of four prefabricated modules connected together providing habitation, communication, health maintenance, and laboratory research facilities. The

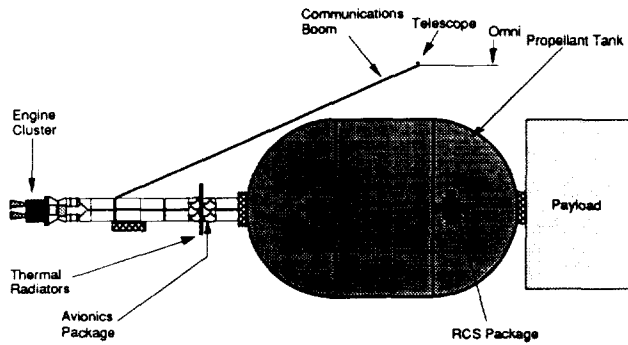


Fig. 6. Lunar Orbital Transfer Vehicle

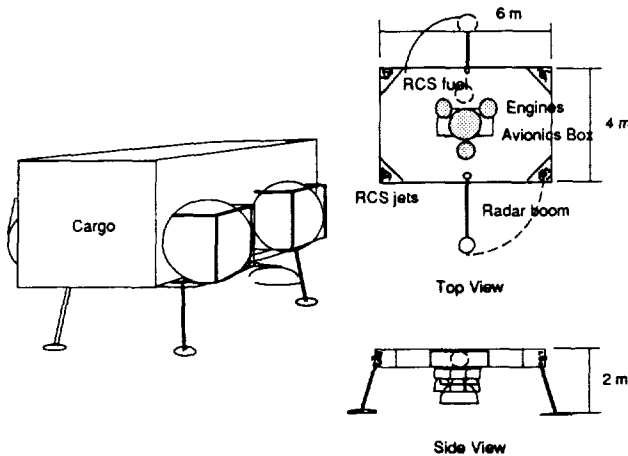


Fig. 7. Lunar Ascent/Descent Vehicle

modules are cylindrical, measuring 6 m in diameter and 10 m in length. The layout of the lunar base is shown in Fig. 8 and will be fully constructed within two weeks of the astronauts' arrival on the lunar surface.

In order to provide support for the base, resupply missions must carry 13,000 kg of supplies to the base every 6 months. In addition, crew rotation will occur every four to six months with an overlap of some crew members to insure familiarity with base operations. During the first operational stage, the base will support 5 to 15 crew members at one time. After the lunar base becomes fully operational, approximately five years into the program, the Mars portion of Project Artemis will begin. The Mars mission will incorporate improvements deemed necessary for project success from the evaluation of the lunar mission program.

The purpose of the Mars portion of Project Artemis is to use the technology developed for the lunar mission to establish a permanent manned base on Mars. In order to meet this goal, commonality with the lunar mission will be maximized in every area possible. As a result, the phases of the Mars mission closely parallel the phases of the lunar mission. A schematic of a typical Mars mission is shown in Fig. 9.

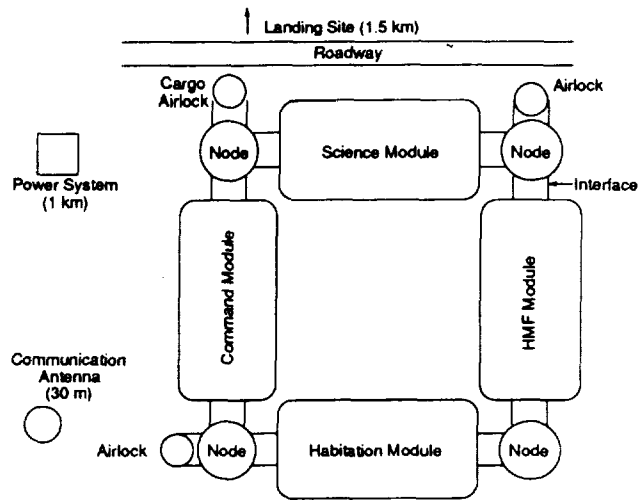


Fig. 8. Lunar Base

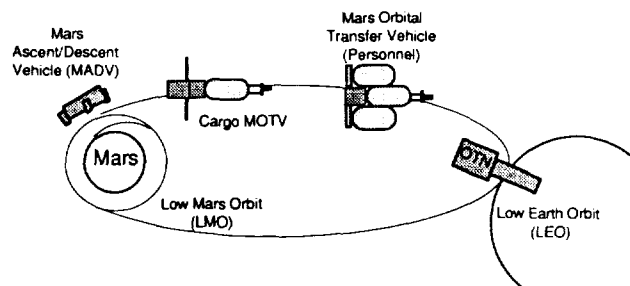


Fig. 9. Mars Mission Schematic

The mission begins in LEO at the OTN. At the commencement of the mission, cargo is carried to low Mars orbit (LMO) on the cargo version of the Mars orbital transfer vehicle (MOTV). This vehicle is shown in more detail in Fig. 10. The transfer of cargo from LEO to LMO takes approximately 280 days. The MOTV is propelled by the same PBR system utilized by the LOTV in the transfer portion of the lunar mission, and is capable of transporting a payload of up to 44,000 kg.

In order to transport all the necessary start-up cargo to LMO, Project Artemis will use six cargo MOTVs, which are expendable. Personnel will be transported to LMO on the personnel MOTV, which is shown in Fig. 11. The personnel MOTV can transport a crew of five, uses a PBR engine, and is reusable.

Once it arrives in LMO, the cargo MOTV will aerobrake in order to attain an acceptable parking orbit. Initial payloads of the cargo MOTV will include the Mars ascent/descent vehicles (MADVs), which are the vehicles that transport cargo and personnel to and from the martian surface. The cargo MADV is shown in Fig. 12. Both MADVs are liquid chemical engines. The cargo MADV can carry a payload of 13,000 kg, and is fueled by liquid hydrogen and liquid oxygen. The personnel MADV can carry five people, and is fueled by monomethylhydrazine and nitrogen tetroxide. The 11 cargo MADVs are expendable, while the 2 personnel MADVs are reusable. As

soon as the payload of the MOTV has been transferred to the appropriate MADV, the MADV begins its descent to the martian surface.

Once the initial cargo is on the surface and trenching and leveling operations have been completed by the unmanned rovers, base assembly can begin. Like the lunar base, the Mars base consists of prefabricated modules, which are attached to one another by common nodes. The Mars base modules are identical in size and structure to the lunar modules shown in Fig. 8; only the interior layout differs, due to the increased storage needs of the Mars base. Like the lunar base, the Mars base includes areas for habitation, communication, laboratory research, and health maintenance.

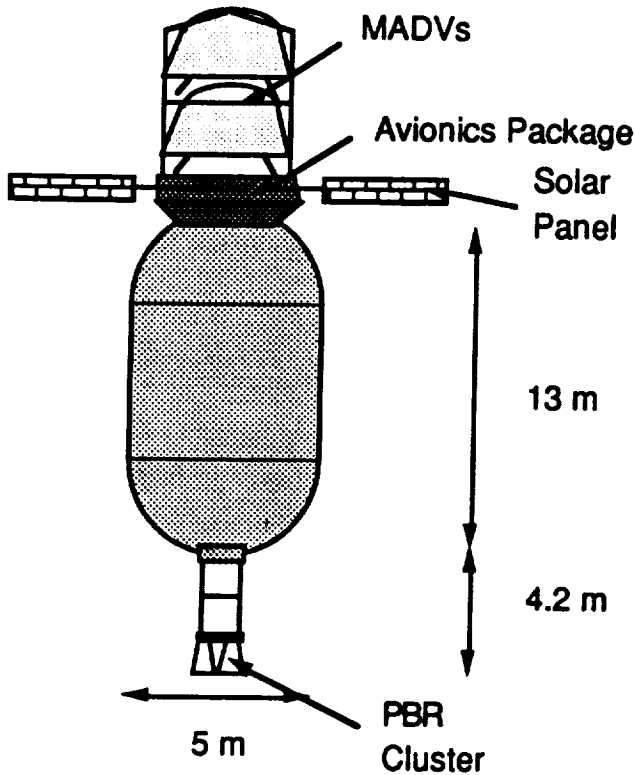


Fig. 10. Mars Orbital Transfer Vehicle - Cargo

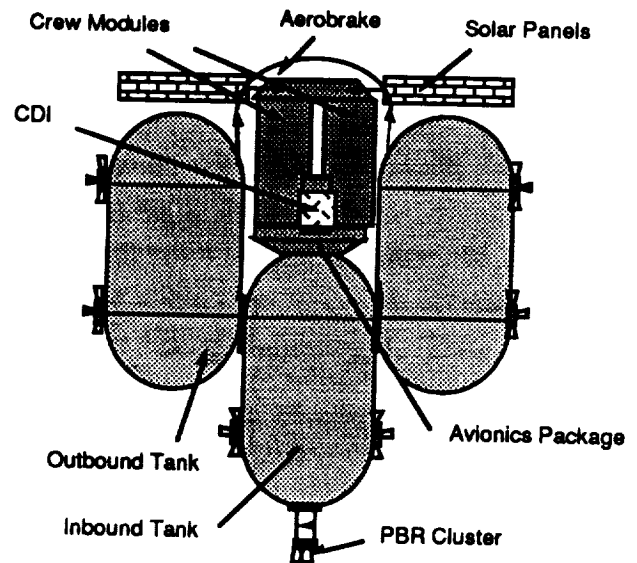


Fig. 11. Mars Orbital Transfer Vehicle - Personnel

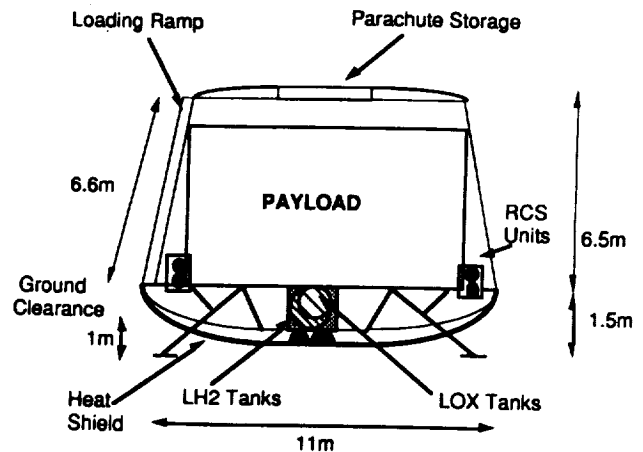


Fig. 12. Mars Ascent Descent Vehicle - Cargo

Initially, a crew of five will construct and operate the Mars base. Crew rotations and resupply will occur every 14 months. The long duration of each rotation is because launch windows only occur every two years. Also, the transfer time for the personnel MOTV takes approximately six months. Eventually, the crew size will increase from 5 to 10, and the base will be at its full operational capacity.

Project Artemis presents technological and logistical problems. Questions of availability of necessary technology, in addition to the cost and time commitments demanded from a single nation for success of this project, need to be addressed before a national endeavor is begun. The project requires the

nation's interest, priorities, and resources for a long period of time. Although in this respect the demands of this project are great, the value of the advancement of human knowledge of our solar system through the completion of Project Artemis would be tremendous.

ACKNOWLEDGMENTS

This report was prepared by Shawn Birchenough, Denise Kato, and Fred Kennedy with Professor David Akin who thank Professor Joseph Shea, Professor James Mar, and Teaching Assistant, Howard Eisen.

10
P. 7 129

PROJECT EGRESS: THE DESIGN OF AN ASSURED CREW RETURN VEHICLE FOR THE SPACE STATION

UNIVERSITY OF MICHIGAN

N 9 1 - 1 8 1 4 2

Keeping preliminary studies by NASA and industry in mind, including the official Request for Proposal (RFP) published by NASA Johnson Space Center, a conceptual design of an Assured Crew Return Vehicle (ACRV) has been developed. The system allows the escape of one or more crewmembers from Space Station *Freedom* in case of emergency. The design of the vehicle addresses propulsion, orbital operations, reentry, landing and recovery, power and communication, and life support. In light of recent modifications in Space Station design, Project EGRESS (Earthbound Guaranteed ReEntry from Space Station) pays particular attention to its impact on Space Station operations, interfaces and docking facilities, and maintenance needs. A water-landing, medium-lift vehicle was found to best satisfy project goals of simplicity and cost efficiency without sacrificing the safety and reliability requirements of the RFP. With a single vehicle, one seriously injured crewmember could be returned to an Earth-based health facility with minimal pilot involvement. Since the craft is capable of returning up to five crewmembers, two such permanently docked vehicles would allow a full evacuation of the Space Station. The craft could be constructed entirely with available 1990 technology, and launched aboard a shuttle orbiter.

INTRODUCTION

NASA has a longstanding dedication to the concept of Assured Crew Return Capability (ACRC). The first trajectories of the Mercury and Gemini programs assured the return of the capsule into the atmosphere. The dedication to ACRC continued during the Apollo missions, which flew in a "free return" trajectory. This trajectory allowed the capsule to circle the Moon and return to Earth automatically in the event of an emergency. Furthermore, the Lunar Module had the capacity to serve as an emergency vehicle. On November 13, 1970, the explosion of an oxygen tank aboard the Apollo 13 Service Module mortally damaged the tanks and systems inside the vehicle, and forced the crew to use the Lunar Module for the return to Earth.

NASA continued to assure the return of any space-based crew during the Skylab missions. Crew return was assured by the Apollo capsule, which transported the crew to Skylab and remained docked at the orbiting lab throughout the mission. In addition, NASA configured an Apollo capsule to carry five crewmembers (the normal capacity of an Apollo capsule was three crewmembers) so that two crewmembers could travel to Skylab and return to Earth with the Skylab crew.

However, unlike the Apollo capsule on Skylab, the crew transportation vehicle for Space Station *Freedom* (the space shuttle) will not remain docked at the station during the crew work cycle (approximately 90 days). NASA originally planned for the space shuttle to assure the return of *Freedom's* crew. However, the tragic explosion of the Space Shuttle *Challenger* over the Atlantic Ocean on January 28, 1986, forced NASA to reevaluate the means of assuring the return of any or all of *Freedom's* crew. In order to assure the safe return to Earth

of the Space Station crew, NASA proposed and issued a Request For Proposal (RFP) for an Assured Crew Return Vehicle (ACRV).

MISSION OVERVIEW

The ACRV will serve as an alternative return vehicle from the Space Station. The ACRV will be permanently docked at Space Station *Freedom* and will serve *Freedom* in three primary design reference missions: (1) The return of the entire Space Station crew (eight crewmembers) in the event that the space shuttle is unavailable; (2) the return of the entire Space Station crew in the event rapid evacuation from Space Station *Freedom* is required; and (3) the return of an injured or ill crewmember in the event that rapid return is required.

The goal of the EGRESS team was to design a vehicle that would be simple, reliable, and would minimize impact on existing programs. Simplicity and reliability are always goals in the design of a space vehicle, but even more so for an emergency vehicle. In order to reduce impact on existing programs the design of the vehicle would need to minimize both crew training and maintenance requirements and maximize independence from the Space Station.

Keeping in mind the old adage "what goes up must come down," the EGRESS design team needed to determine how the vehicle would return to Earth. The primary concerns were the lift-to-drag ratio (L/D) and the vehicle's landing mode. Initially, a high lift-to-drag, such as the shuttle or an aeroplane, was researched by the team. A high lift-to-drag vehicle encounters low forces during reentry and is very maneuverable; however,

it would require wings to generate lift. The RFP requires that the ACRV fit into the space shuttle cargo bay, which has a diameter of 15 ft. This stipulation would require a winged ACRV to have retractable wings, which are both mechanically and structurally complicated. In addition, such a vehicle configuration would require complicated control surfaces to control yaw, pitch, and roll maneuvers. Finally, a high L/D would require extensive initial training and continuous refresher training for pilots of the vehicle. On the other hand, a low L/D vehicle is simpler to operate and requires less training time. Since the Mercury, Gemini, and Apollo vehicles were all low L/D vehicles, a low L/D vehicle uses flight-proven hardware. However, low L/D vehicles encounter high reentry forces and have limited, if any, maneuverability. Thus, the design team chose a medium L/D for the EGRESS vehicle. This configuration will encounter mild reentry forces and have modest maneuverability, while still being simple to operate.

After the decision to design a medium L/D vehicle was made, the team needed to determine the landing mode of the EGRESS vehicle. The two possible places for a vehicle to land are on land or in the water. A land landing vehicle would allow for landing site selection in close proximity to a health care facility allowing rapid transportation of an injured or ill crewmember to the facility. In addition, a land landing vehicle would be reusable since it would not suffer the corrosive effects of salt water. However, since the vehicle was to have a medium L/D it would not be capable of gliding to a landing site as the space shuttle does. Instead, the vehicle would need to deploy parachutes to slow its descent, and then use an impact system (such as retro rockets or airbags) to minimize its impact with the ground. This configuration would still encounter large impact loads at touchdown. Since the EGRESS vehicle must have the capability to return an injured or ill crewmember, it is desirable to minimize the impact loads experienced by the occupants of the vehicle. Furthermore, a land landing vehicle would require extensive training in order to complete the precise maneuvers required for an accurate landing.

The impact loads encountered during a water landing are less than those of a land landing, which makes the water landing more desirable for the return of an injured or ill crewmember. Furthermore, a water landing does not require the accuracy of a land landing, and will not require the extensive training for landing procedures. Thus the EGRESS team chose to design a medium lift-to-drag vehicle that will land in the water.

The specific locations of the landing sites were determined from the availability of recovery forces and health care facilities, and the groundtrack. The limiting factor in the recovery forces proved to be the availability of a heavy lift helicopter capable of lifting 10,000 lb, the weight of EGRESS. In addition to the weight constraints of the recovery forces, the groundtrack imposed further constraints on the landing site selection process. Only a small portion of the groundtrack goes over the United States or coastal areas with nearby U.S. military bases. The second Design Reference Mission requires the craft to leave with relatively short notice; therefore it is desirable to have the craft land at a primary landing site from any of its

orbits. With these criteria in mind, Pearl Harbor (Hawaii), Okinawa (Japan), and Kennedy Space Center (Florida) were chosen as the primary landing sites, and Guam was chosen as a secondary site. The health care facilities available at the landing sites are Pearl Harbor Naval Hospital, Kadena Naval Hospital, Patrick Air Force Hospital, and Anderson Air Force Hospital, respectively. Two vehicles will be stationed at *Freedom*, while four vehicles will be on the ground to provide both support and redundancy. In addition to replacing used vehicles, the ground-based vehicles will allow the spacecraft to be updated. The two vehicles aboard the Space Station will be placed at nodes 1 and 2 of the Space Station, resulting in ease of departure from the station and minimum interference to the Space Station operations.

The remainder of this report discusses the structure of the EGRESS vehicle, the internal configuration, mission analysis, and training requirements.

VEHICLE STRUCTURE

The design of the vehicle structure consisted in consolidating the varied requirements of a space vehicle. After the design process leading to the final configuration is presented, the two additional components of Project EGRESS are described.

Design Process

To adhere to the design goals of simplicity and reliability, a vehicle based closely upon the Apollo reentry capsule was envisioned. However, the Apollo provided only a low L/D. The EGRESS vehicle needed to feature medium-lift capabilities. This was accomplished with the use of a bent-nose biconic reentry vehicle. The Apollo module was a conic vehicle. A biconic would be formed if the nose cone of the Apollo were stretched into a longer cone, with the rest of the vehicle unchanged, and then bent at an angle to the rest of the vehicle. EGRESS was designed to be a medium-lift vehicle thus capable of a cross-range travel much greater than that of an Apollo vehicle. In addition, EGRESS will have better thermal emissivity characteristics and lower reentry accelerations than Apollo.

To achieve the desired aerodynamic characteristics, the vehicle required certain shape constraints and a minimum wetted surface area. One of the shape constraints imposed by atmospheric reentry was that the vehicle's hatch be protected from reentry burn-up by placing it behind the vehicle's nose from an angle of impingement of 60°. The shape of the vehicle was designed to meet all these requirements, as well as to fulfill the mission guidelines. EGRESS was first transformed into a flattened bent biconic and then slowly transformed into what was referred to as a "raft" shaped vehicle.

The final configuration developed from an amalgamation of existing and experimental reentry vehicles. The EGRESS vehicle is squat with a rounded, triangular body that is 13.5 ft long, 6 ft high, and 9 ft wide, that weighs 8018.83 lb, and that has an exterior volume of 355 cu ft and an interior volume of 250 cu ft. In addition to the reentry vehicle, the EGRESS system has a deorbit propulsion package that is detachable from the vehicle. These components are shown in Fig. 1. An airlock was also designed.

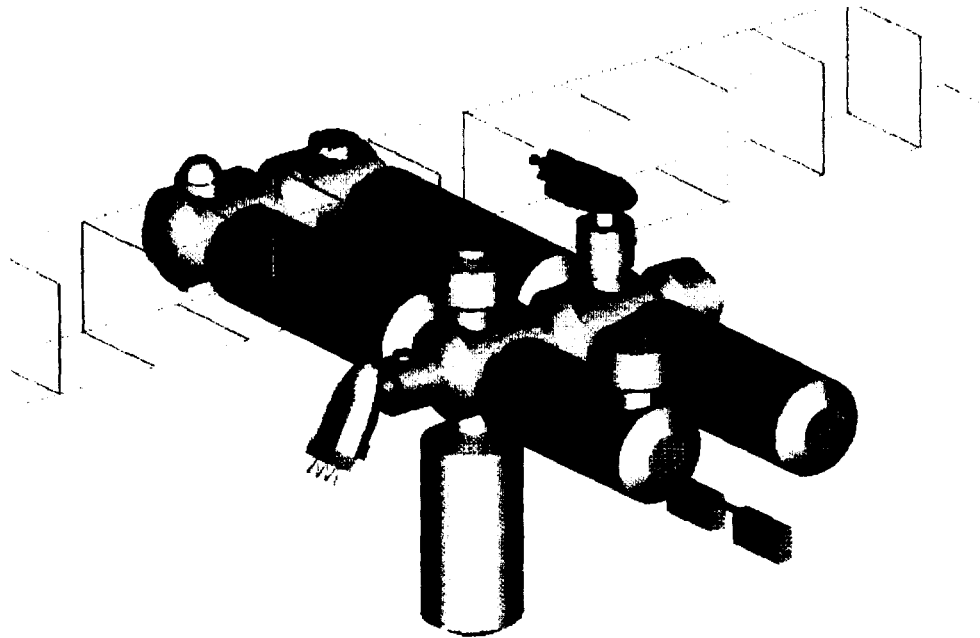


Fig. 1. Components of Project EGRESS

Airlock

During normal Space Station operations, astronauts will be conducting regular Extra Vehicular Activity (EVA) missions in pairs. The EVA astronauts can enter the Space Station through designated EVA airlocks at only a few nodes. If a Space Station catastrophic failure terminates either the Space Station power system or any nodes between the astronauts' entrance airlock and the EGRESS, the EVA astronauts will not be able to enter the EGRESS. In order to assure that EVA astronauts will be able to enter the EGRESS during a station integrity failure, EGRESS must have its own airlock.

The airlock is a short cylinder with length 6.25 ft and diameter of 8 ft, an inner volume of 332 cu ft, a total mass of 3282 lb, and the ability to contain and to sustain two spacesuited astronauts. The airlock is double-hulled to protect it from meteoroid impact that would cause habitable airlock lifetime to diminish.

Propulsion Package

EGRESS's engines, fuel, and pumping systems will be contained in a jettisonable structure separate from the main body of EGRESS, as shown in Fig. 1. This structure will be jettisoned following the deorbit burn for two reasons. First, dumping the propulsion pack will decrease both the mass and the drag of the vehicle. Second, placing the propulsion pack in a safe orbit will allow the pack to be reused. EGRESS will perform a small separation maneuver after which the structure will use some of the remaining fuel to put itself in a safe orbit where it will be retrieved later.

The propulsion package consists of three rocket engines and a box framework. EGRESS will use three R-40 engines in a straight line to accomplish the deorbit burn. With this arrangement a normal burn would be performed with all three engines. In the event that the center engine fails, the two outside engines would be ignited. In the event that one of the end engines fails, two options exist: burning only the center engine or burning the center and remaining engine while compensating for induced moments by RCS jets. The framework houses two sets of fuel and two sets of oxidizer in four spherical tanks, two sets of helium propellant-feed also in spherical tanks, and four reaction control system thruster clusters. The box framework is 7.8 ft tall, 7.4 ft wide, 3.4 ft thick, and weighs 108 lb. The total weight of the propulsion package is 2275 lb.

INTERNAL CONFIGURATION

Since the EGRESS vehicle must transport humans, the internal configuration of the craft is as important as the external structure. Internal configuration consists of design and layout of the crew cabin, determination of crew size, and design of life support systems.

Crew Cabin Design

Each EGRESS vehicle will be configured to return up to five crew members. The crew size is based upon both the basic configuration requirements and the duties of the different crewmembers. The primary crew of a pilot, a patient, and a medical technician will be seated in the rear "top row" while

the secondary crewmembers will sit in the jump seats in the "bottom row" of the cabin. These configurations will allow easy access to necessary controls and provisions, easy entry and exit of the vehicle, and maximum center of gravity stabilization during the flight. The crew configuration in the EGRESS vehicle is shown in Fig. 1.

Pockets on the sides of the cabin will carry pressurized pens, clipboards, notepaper, and "cue cards" outlining flight and medical procedures for use during an EGRESS flight. Food will also be stored in these pockets. Flashlights and penlights will be provided for use during systems checkouts, EGRESS flights, and recovery. Waste management equipment and supplies are stored under the medical technician's seat on the floor of the crew cabin. The majority of the critical care medical equipment, including one package of ventilator tubing, two liters of lactated Ringers solution, and intravenous lines, will be stored in a medical supply kit on the floor of the crew cabin when not needed. "Trauma pants" with inflatable leg chambers, also stored in this kit, will allow a patient to better withstand the g forces of reentry. General-use medical supplies, including bandages, alcohol prep-pads, needles, and syringes, are located in pockets on the wall of the crew cabin next to the medical technician. Two fire extinguishers, one located within reach of the pilot and another in the rear of the craft, will give the crewmembers the ability to quickly control and put out fires in the crew cabin. An emergency supply kit will carry five automatically inflatable life jackets, a flare gun with flares, and other provisions needed to ensure the safety and survival of the crew during a wait for recovery. In addition, an automatically inflatable five-person raft, stored behind the jump seats at the front of the crew cabin, will allow the crew safe exit from the EGRESS vehicle if required.

Crew Size

EGRESS is capable of returning three to five crewmembers from the Space Station. For the return of an injured or ill crewmember, at least two crewmembers are needed to support the injured crewmember as stated previously. After such a mission, five crewmembers would be left aboard *Freedom* to continue normal operations; thus a second EGRESS vehicle must be capable of returning the remaining five crewmembers to avoid the need for a third vehicle. All crewmembers must be evacuated from the station on the two EGRESS vehicles attached to the Space Station. Assuming a Space Station crew of eight, three crewmembers will ride in one vehicle and five in the other. The EGRESS spacecraft carrying three crew members will be used to transport critical experiments and equipment back to Earth, if necessary.

Life Support Systems

Absolutely essential to the successful utilization of the EGRESS spacecraft is the presence of a simple but efficient Environmental Control and Life Support System (ECLSS) on the vehicle. The EGRESS ECLSS is composed of two main systems: an environmental and atmospheric control system, and

a life support system. Other supporting systems included a waste management system and a crew water and food provisioning system.

The Atmospheric Supply and Pressurization System will provide a cabin pressure of 14.7 psi and a 21% oxygen, 79% nitrogen atmosphere in order to provide a safe, comfortable environment for the crew during a normal flight of the EGRESS vehicle. In addition, the system contains redundancy and emergency features to allow environmental support in emergency situations. Constant monitoring of the total cabin pressure and oxygen partial pressure will be done by the Main Environmental Control System. In addition, EGRESS will provide a patient a higher oxygen concentration through a Patient Environmental Control System, a separate environmental loop that processes exhaled air for up to 48 hr.

The life support system will meet all the physiological requirements of up to five crewmembers for 24 hr. Medical systems will allow advanced life support for one ill or injured crew member on board the EGRESS for up to 48 hr. The interior systems, including the seats, control panels, windows, and general provisions, were all designed and placed within the EGRESS crew cabin according to the basic physiological, ergonomic, and psychological requirements of five crewmembers.

Because space travel and reentry into the atmosphere inherently involve risks to human life, criteria for use were developed to ensure that the EGRESS vehicle will only be used when remaining on the Space Station would pose greater risks than would returning to Earth. These criteria were also used as a basis for defining the necessary crew systems and provisions according to the use of the vehicle.

MISSION ANALYSIS

If the EGRESS vehicle were to be used, its mission would follow an established sequence of events. The mission would consist of startup, orbital maneuvers, atmospheric reentry, and landing and recovery. After the recovery and processing of the vehicle, a new vehicle will be launched into orbit. Like the original two vehicles aboard the Space Station, any new vehicles will enter the established maintenance cycles.

Startup

EGRESS is powered by primary, nonrechargeable batteries during its operations. Power will also be provided to EGRESS from Space Station *Freedom* using a rechargeable nickel-hydrogen battery system as a reservoir. Power will be distributed to EGRESS systems using four main buses. Two major interface areas are present in the power distribution system, one between EGRESS and the propulsion module, and the other between EGRESS and the Space Station. Power will be distributed and monitored using state-of-the-art software in order to help detect problems before they develop, and isolate problems that may surface.

The communication system is primarily based on S-band radio transmissions. This system will use the Tracking and Data Relay Satellite System (TDRSS), which is currently used by the

space shuttle, to relay signals to the ground. EGRESS will also use a Very-High Frequency (VHF) system to communicate with search and rescue forces. The VHF system could serve as a backup for voice communications if there are problems with the primary S-band system. L-band communications will also be used to receive signals from the Global Positioning System satellites in order to accommodate the navigation system described below.

The EGRESS computer system, which is in control of most of the EGRESS subsystems throughout a crew return mission, is designed for reliability. The processing units, high-powered space-rated IBM AP101S general purpose computers, are linked in a triple redundant configuration. The computers are connected to an optical disk mass storage device and the rest of the vehicle's subsystems, through a 24-bit data bus. Under control of the EGRESS Automated Software Environment, the system is responsible for regulating the power and life support systems, as well as serving as the flight management system and controlling most of the vehicle's operations.

In order for the EGRESS vehicle to accomplish its various missions, it is important that the vehicle have accurate navigation and guidance for control. The navigation system consists of an inertial navigation system (INS) that is augmented by the Global Positioning System (GPS). The Honeywell CG1320 INS, based on a ring laser gyroscope, is used to provide highly accurate attitude information. By incorporating GPS into the system, a precise position can be determined to within 15 m. Though the system is normally initialized while the EGRESS vehicle is docked, initialization can take place after separation in the rapid evacuation scenario.

Orbital Maneuvers

The EGRESS vehicle's mission will begin with separation from the Space Station. This separation will consist of two phases. The first phase is a 1 ft/sec positive radial burn that will last approximately three minutes. EGRESS will use a gaseous nitrogen system to separate from the station. Two clusters of two 1-lbf cold gas thrusters will be placed on either side of the vehicle to allow separation at 1 ft/sec from either node 1 or node 2.

When EGRESS reaches a height of 150 ft above the station, the second phase of separation will begin. This maneuver will consist of a 2 ft/sec retrograde burn that will put the EGRESS in proper position for the deorbit burn after approximately 40 min. For on-orbit maneuvers, EGRESS will be equipped with 42 reaction control jets. There will be one cluster of 16 across the nose of the vehicle and two clusters of 11 each in the aft section of EGRESS.

The deorbit burn will be a retrograde burn, and the transfer will resemble a Hohmann transfer. The retrograde motion will allow the EGRESS vehicle to transfer from the station's orbit to the 400,000-ft atmospheric boundary. The time and velocity change required for the maneuver depends on the station's altitude. At the minimum altitude of 140 n.m., the required ΔV is 227 ft/sec, and the maneuver will take 24.4 min. At the maximum altitude of 270 n.m., the required ΔV is 391 ft/sec, and the maneuver will take 36.6 min. EGRESS will use three

Marquardt R-40 engines to deorbit. The R-40 is a liquid bipropellant engine using monomethyl hydrazine as the fuel and nitrogen tetroxide (N_2H_4) as the oxidizer. The vehicle will have three engines, but will be capable of deorbiting using only one, as stated previously.

In order to insure proper fuel flow to the engines, a rubber bladder pressurization system will be used. This system employs rubber "bags" inside spherical tanks in order to separate the fuel (or oxidizer) from the pressurizing gas. This design will allow up to 99% fuel expulsion from the tanks in a zero-g environment.

Reentry

The EGRESS vehicle must be protected from the intense heat generated as the vehicle's kinetic energy is imparted to the atmosphere. The primary concerns were the rate of heat transfer to the vehicle and the maximum temperature experienced during reentry. A ceramic thermal protection system will be employed by EGRESS. The TPS of the EGRESS will consist of HRSI tiles covering the underbelly and nose area of the craft with an AFRSI blanket covering the remaining areas. This type of ceramic TPS is lightweight, has a high-temperature capability, will not degrade in orbit, and would be reusable if not damaged on impact with the ocean.

Additional concerns include calculation of the aerodynamic flow field about the EGRESS vehicle and the aerodynamic forces exerted by that field on the vehicle. A computer program to calculate Newtonian flow was written to provide this information. As a result of computer analysis, the EGRESS vehicle was shown to be statically stable, have a L/D of 0.7, and reenter the atmosphere at 40° angle of attack.

The attitude control system of the vehicle guides the EGRESS to its landing location. Attitude control is provided by two 65-lbf thrusters. The effects of attitude control were analyzed by another computer program that integrated the flight trajectory of the EGRESS vehicle. This trajectory analysis shows that the vehicle is capable of a cross-range of 500 n.m., which guarantees the ability of the vehicle to land at any primary landing site on either of two successive orbital passes. Furthermore, a simple flight algorithm was created that kept the g loads throughout reentry below 4 g, the g-loading limits of the RFP.

Landing and Recovery

The EGRESS vehicle uses a conventional deceleration system of two drogue parachutes and three flat circular parachutes that are deployed by means of three smaller pilot parachutes. An attenuation system that would provide increased deceleration right before impact is not needed since the conventional parachutes will slow the craft to an impact deceleration within the specifications of the RFP, which allows a maximum impact loading of no more than 10 g through the chest of an injured crewmember.

When the EGRESS splashes down, a self-righting system will automatically deploy to right the vehicle. The uprighting system will use air bags to change the center of buoyancy,

causing the craft to right itself. A manual backup switch is available in the event that the automatic system fails. The self-righting system will provide additional dynamic stability to the EGRESS in heavy seas beyond the static stability of EGRESS. The center of buoyancy of the vehicle was positioned to provide a natural stability to the EGRESS vehicle allowing it to sit "nose up" in the water after landing.

Design Reference Mission 3, return of an injured crewmember, requires the crew to be removed and rapidly transported to a health care facility (HCF). For this reason, the Coast Guard was selected to remove the crew using either the HH-65A (Dolphin) or the Huey (Bell UH-1H). The Navy was selected to recover the EGRESS craft using the CH-53E (Super Stallion). The Navy would also retrieve the crew if the Coast Guard is unavailable. The EGRESS vehicle will be able to land at night with minimal changes to daylight procedure, while extremely poor weather would force a landing at another site. In the event that the only available landing sites have poor weather, a modified recovery procedure would be used in which the entire EGRESS would be lifted out of the water and transported to a HCF, with the crew inside. This procedure would avoid the possibility of the craft being swamped once the hatch is opened.

Post-Recovery Processing

Ground operations are needed to support the craft while on-orbit. Areas of ground operations include storage of replacement vehicles, mission control, and post-recovery operations. Since there will be four on-ground spares for the EGRESS vehicle, an EGRESS operations center is recommended to house the ground fleet as well as any spare parts and official documentation pertaining to the EGRESS project.

Ground control for an EGRESS mission will be handled from the mission control center for the Space Station. All EGRESS mission control personnel positions will be filled from either normal Space Station ground operations staff or any backup personnel stationed at ground control. In the event an EGRESS vehicle is used and a replacement needs to be sent in its place, the issue of replacing the ground spare was also considered. Research showed that the most cost effective alternative for replacement for the ground spare would be the construction of a new EGRESS vehicle that would reuse any properly functioning subsystems from the used vehicle. Although most of the EGRESS spacecraft will not be salvageable, certain systems inside the vehicle could be reused. However, since the craft will sit low in the water, water may spill into the cabin compartment damaging many of the systems inside the cabin area. To minimize water entry the hatch can remain closed until the crew must exit the vehicle. Attitude thrusters and separation burners will not be reusable due to salt water contamination. The displays and readouts may be damaged by salt water contamination; however, the main computers, which contain the navigation, flight operations, communications and ECLSS, will be sealed from the pressurized interior of the vehicle and will thus be protected from water damage. The parachutes used in the landing will be reusable with only minimal cleaning required. Testing and verification will need

to be performed on all reusable systems to insure no damage was sustained during landing. If the systems check out then they will be used in the construction of a new EGRESS vehicle.

Launching System

The primary launch system for the EGRESS craft was specified by the RFP to be the Space Transportation System. This requirement placed certain constraints on dimensions and possible exterior configurations for placement in the payload bay. If the space shuttle were unavailable, a backup system in the form of an expendable booster was also considered. The Martin-Marietta Titan III was the most cost effective alternative and met all the necessary specifications.

The spacecraft will be attached in the space shuttle payload bay by means of a frame. This frame will attach to the payload bay by means of a longeron and keel attachments using a seven-point attachment scheme due to the weight of EGRESS. The attachment points will be connected to hard points on EGRESS's frame accessible by indented handholds so that EGRESS may be freely removed from the bay with the space shuttle's or with the Space Station's Remote Manipulator System (RMS). The frame will be made from aluminum with a diameter of approximately 2 in. The keel and longeron trunions will be made from chrome-plated steel with diameters of 3 and 3.25 in, respectively. The total frame weight is 1050 lbm. The airlock for EGRESS cannot be mounted to the vehicle while the vehicle is in the shuttle bay; therefore, it too will be mounted within the shuttle bay in a separate framework assembly. Like EGRESS, the airlock will be mounted by means of a seven-point attachment scheme using longerons and keels.

Placement

Since the EGRESS vehicle will be docked on Space Station *Freedom*, the vehicle will impact the station and crew in many ways including docking/berthing, crew training, and station drills. The procedure for docking the EGRESS vehicle will be handled completely by remote manipulator arms of the Space Station. The vehicle will be extracted from the shuttle cargo bay by the Space Station's Remote Manipulator System (RMS), which will place the vehicle in its proper location on the station.

The first step in determining a location for the vehicles was the identification of ports on the Space Station that were already occupied. Ports 3 and 6 are reserved for space shuttle docking, and port 8 is an alternate location for *Freedom's* logistics module. Ports 1, 2, 4, and 5 were considered less desirable due to their proximity to the shuttle docking locations. Vehicles placed on these ports might interfere with the loading and unloading of payloads from the shuttle's cargo bay. In addition, vehicles placed at these locations would interfere with the field of vision from the cupolas, which will be the workstations from which *Freedom's* remote manipulator system will be operated. Thus ports 7 and 9, on nodes 1 and 2, were chosen for EGRESS placement. The vehicles are shown in their proper locations in Fig. 2.

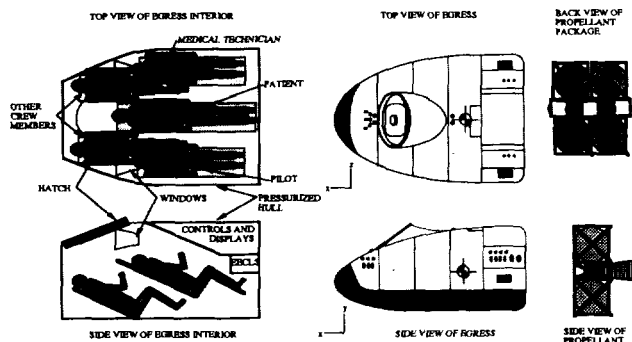


Fig. 2. Placement of EGRESS vehicles on Space Station *Freedom*

Maintenance

To minimize the effects of contaminants in the environment aboard the vehicle, as well as other primary sources of failure in equipment, the vehicle will be placed in a dormant state with its hatch closed while on-orbit. Remote-controlled diagnostic tests will be run periodically to detect any failure in the systems and results will be sent to ground control for analysis. Extensive maintenance check-ups will be performed semiannually for a complete inspection of all the components aboard EGRESS.

TRAINING

In order to minimize crew training aboard Space Station *Freedom*, all initial training will be performed on the ground with a proposed mock-up of an EGRESS to familiarize the pilot and crew with the vehicle systems and its internal configuration. Training will include piloting and navigation as well as use of all other systems onboard the EGRESS vehicle. Pilot training will also include familiarization with the back-up manual system. Basic repairs of the vehicle's main systems, maintenance, and checkout procedures will also be covered.

The space shuttle crew will undergo Apollo-type simulator training in addition to normal training in order to learn the EGRESS procedures. Each phase of Apollo training consisted of 1-hr oral briefings and 3-hr simulator exercises. The total training time was 200 hr of simulator exercises and 60 hr of briefings. The simulators were used for entry, rendezvous, and docking practice and were also used to simulate emergency situations. Thus, an EGRESS simulator environment must be designed and constructed for this training.

In order to properly utilize the EGRESS medical systems and supplies, the medical technician must be properly trained in both general medical procedures and in the use of the EGRESS equipment. Because present plans do not include a physician on Space Station *Freedom*, NASA will require the following medical training for the space station crewmembers: (1) All Space Station crewmembers shall be trained in basic first aid and Basic Life Support, including CPR; (2) Two crewmembers will have extensive medical training, such that one crewmember has specialized training equivalent to that of an emergency medical technician and an anesthetist/surgical assistant, and one crewmember has at least 100 hr of general medical training.

In the event that the EGRESS vehicle is used to transport an ill or injured crewmember to Earth, an EGRESS medical technician will be chosen from the two Space Station crewmembers who have had the most medical training and experience. Periodic on-orbit training will also be needed for the crew to maintain a basic knowledge of the operational procedures of the EGRESS vehicle. Subsequent pilot training will also be needed to insure proficiency in the manual backup system and maintain pilot familiarity with the cockpit. A simulator for piloting the vehicle should be provided aboard *Freedom*. Manuals and configuration drawings of the vehicle will also need to be available on the station for maintenance checkout and simple repairs.

CONCLUSION

Project EGRESS has designed a craft that meets the requirements of Johnson Space Center's Request for Proposal. The design was simple, reliable, and provided means for the evacuation of the Space Station or the return of an injured crewmember.

Three primary areas have been identified as needing further research. First, since the EGRESS will spend at least two years in the space environment, the effects of long-duration exposure on structural strength and life support systems must be determined. Second, procedures must be developed for retrieving the jettisonable propulsion pack after the deorbit burn. Third, the dynamic stability of the EGRESS within the supersonic flight regime must be addressed.

ACKNOWLEDGMENTS

The authors acknowledge the students of the Aero 483 Space System Design class at the University of Michigan for their hard work and dedication. Special gratitude is due Prof. Harm Buning and teaching assistant Laura Kistler for their guidance in the design process.

3-20-77
p. 8 137

BICONIC CARGO RETURN VEHICLE WITH AN ADVANCED RECOVERY SYSTEM

N91-18143

UNIVERSITY OF MINNESOTA

The current Space Exploration Initiative is focused around the development of the Space Station *Freedom* (SSF). Regular resupply missions must support a full crew on the station. The present mission capacity of the shuttle is insufficient, making it necessary to seek an alternative. One alternative is a reusable Cargo Return Vehicle (CRV). The design suggested in this report is a biconic-shaped, dry-land recovery CRV with an Advanced Recovery System (ARS). Liquid rocket boosters will insert the CRV into a low Earth orbit. Three onboard liquid hydrogen/liquid oxygen engines are used to reach the orbit of the station. The CRV will dock to the station and the cargo exchange will take place. Within the Command and Control Zone (CCZ), the CRV will be controlled by a gaseous nitrogen Reaction Control System (RCS). Alternatively, the CRV will have the capability to exchange the payload with the Orbital Maneuvering Vehicle (OMV). The bent biconic shape will give the CRV sufficient crossrange to reach Edwards Air Force Base and several alternative sites. Near the landing site, a parafoil-shaped ARS is deployed. The CRV is designed to carry a payload of 40 klb, and has an unloaded weight of 35 klb.

ACRONYMS

ARS	Advanced Recovery System
CCZ	Command and Control Zone
CRV	Cargo Return Vehicle
FRCI	Fibrous Refractory Composite Insulation
HABP	Supersonic/Hypersonic Arbitrary Body Program
L/D	Lift-to-Drag Ratio
LRB	Liquid Rocket Booster
OMS	Orbital Maneuvering System
OMV	Orbital Maneuvering Vehicle
PLOG	Pressurized Logistics Module
RCS	Reaction Control System
SSF	Space Station <i>Freedom</i>
SSRMS	Space Station Remote Manipulator System
TABI	Tailorable Advanced Blanket Insulation
TPS	Thermal Protection System
UPLOG	Unpressurized Logistics Module

INTRODUCTION

Between the years 2000 and 2010, space station *Freedom* (SSF) is projected to be fully operational. Currently, the space shuttle is the only way to resupply the Space Station. However, SSF requires a yearly resupply of 214,000 lb, and since the shuttle can only support 5 missions a year, with a total upcargo of 178,185 lb, NASA is looking at Cargo Return Vehicles (CRVs) as a way to augment the shuttle's capacity. This report outlines the design of a biconic CRV proposed to fill this mission.

Requirements

1. The primary operational period will be between the years 2000 and 2020.
2. The CRV will be unmanned.

3. The primary mission will be to meet the resupply/return needs of SSF (in orbit at 220 n.m. and 28.5° inclination).
4. All payload supplied or returned from SSF will be transported in a Pressurized Logistics Module (PLOG) or Unpressurized Logistics Module (UPLOG).
5. The CRV will use shuttle-compatible payload interface methods.
6. The CRV will have an upcargo capability of 40,000 lb.
7. The CRV will be partially reusable.
8. The CRV will have a dry-land recovery using a runway of not more than 10,000 ft.
9. The primary landing site will be Edwards Air Force Base.
10. The CRV will be able to transfer cargo both by direct docking and using the Orbital Maneuvering Vehicle (OMV).

Design Criteria

The design of the biconic CRV took place in three stages. First a trade study was conducted, then a conceptual design, and finally models were built and tested to verify the conceptual design's results.

As a result of the trade study, it was decided that the the CRV would consist of a bent-axis biconic (see Figs. 1a,b), with a two-stage reentry phase.

The main objective is to achieve a highly reusable vehicle, minimizing weight and size.

During the first stage of reentry, the CRV will be reentering the atmosphere. The split axis serves to provide enough lift to allow the biconic to come to within a few miles of the landing site. At this point the parafoil is deployed.

To minimize the weight, size, and drag, it was decided that the ARS would be nonrigid and internally stored.

Design considerations in the area of propulsion sought to integrate the CRV with an already existing, or planned, launch vehicle. The design of launch boosters was beyond the scope of this project.

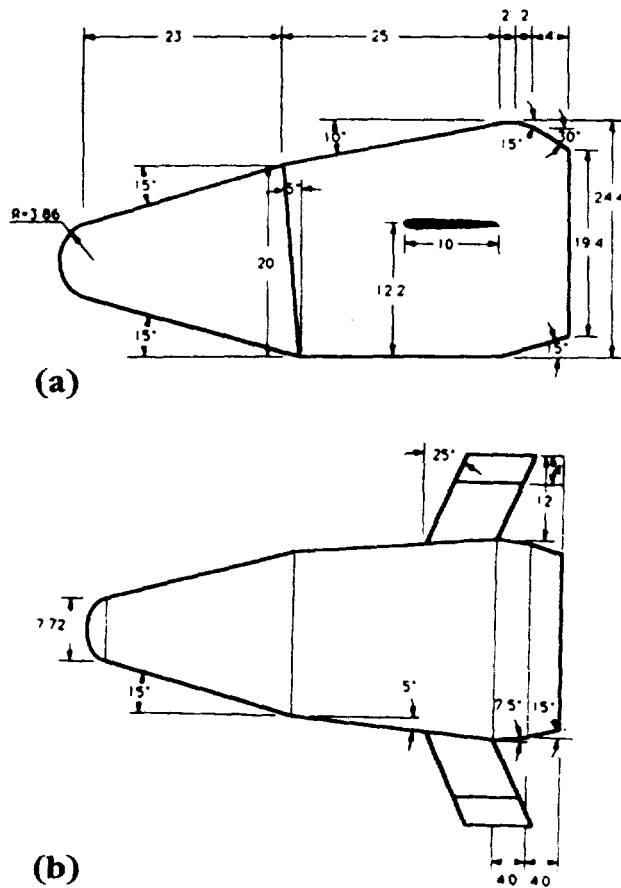


Fig. 1. Dimensions of the CRV. (a) Side View of the CRV; (b) Top View of the CRV

MISSION OPERATIONS

The nominal mission scenario for the CRV is a rendezvous and cargo exchange with Space Station *Freedom* at its orbit of 220 n.m. with an inclination of 28.5° . The CRV will launch from Kennedy Space Center.

The Launch

A number of assumptions about the dynamics of the CRV had to be made. The Earth-to-orbit phase was modeled as a standard two-body problem. Further, the assumption that velocity changes (ΔV s) are instantaneous, was made. Since the burn times are small compared to the duration of the maneuvers achieved, the assumption is legitimate.

In determining the magnitude and time of the ΔV s necessary to reach the station's orbit, two factors had to be weighed against each other: mission time vs. fuel consumption. Because fuel is heavy and one of the CRV design objectives is to minimize weight, minimizing the ΔV s at the expense of time is a good trade in most cases (if the time is too long the weight of the batteries required to maintain the vehicle may offset the benefit derived from the reduced fuel consumption).

With this in mind, the Hohmann transfer was selected for this mission. While it is a lengthy transfer operation, it is also most energy efficient. Here the craft is set into an elliptical orbit. When this orbit brings the CRV closest to a circular orbit, a burn takes place to reach and maintain the latter orbit. The problem with time, then, is that in order to enter the desired orbit at the appropriate place, there has to be a certain waiting period while the two orbits are out of phase.

The liquid rocket booster (LRB) will deliver the CRV into a 50×100 -n.m. elliptical orbit; then four more burns, using the CRV's Orbital Maneuvering Systems (OMS) engines, will bring it to the SSF (see Table 1).

Table 1. Orbit Burns.

Maneuver	ΔV (ft/sec)
50×100 -110 transfer	100
110-210 transfer	180
210 circularize burn	180
210-220 transfer	20
220 circularize burn	20
Proximity maneuvers (non-OMV)	58
Proximity maneuvers (OMV)	40
220 deorbit	317
Total	895 (non-OMV) 877 (OMV)

To avoid out-of-plane burns, the CRV will have phasing waits. Ignoring phase delays, there is one launch opportunity for the CRV every day. This window offers a minimum phase delay (0 hr) every fourth day or 62 orbits. At most, the delay is 33 hr. Coupled with a reentry phasing delay of 0 to 20 hr, the total mission time varies between 18.35 and 75.35 hr non-OMV, and 19.85-76.85 hr OMV. It is assumed that small out-of-plane perturbations can be corrected by the CRV's Reaction Control System (RCS).

Proximity Operations

All operations close to the Space Station are carefully monitored and avoided if possible. Surrounding the SSF is what is known as the Command Control Zone (CCZ), which extends 5 n.m. above and below the station, and 20 n.m. all around it. Any object entering this zone can endanger the safety of SSF, and is therefore required to follow many safety guidelines. For the sake of simplicity and safety, original NASA requirements stated that the CRV would not be allowed to enter the CCZ, making cargo transfers possible only using the Orbital Maneuvering Vehicle (OMV).

To transfer payloads with the OMV, the CRV would park itself behind SSF outside the CCZ. The OMV would then retrieve the cargo module from the CRV and tow it back to the station. To save orbit time, while the OMV is towing the PLOG/UPLOG, the CRV would reposition itself in front of the SSF, remaining outside the CCZ. Then, the OMV would bring the return cargo to this new position while the CRV is phasing for the deorbit burn.

Since the OMV program has been scaled back, it has become important that the CRV be able to venture safely into the CCZ and dock to SSF. This is accomplished with two short jumps inside the CCZ, that can be modeled as Hohmann transfers (see Fig. 2).

In order for the CRV to dock directly to SSF, a special docking mast was designed (see Fig. 3).

Requirements of the docking mechanisms include the ability to physically support the CRV and interface monitoring with SSF systems, and compactness. Also to be considered is the positioning of the mast such that the Space Station Remote Manipulator System (SSRMS) be able to reach the cargo bay and effectuate a transfer while the CRV is soft docked at the cupola node (see Fig. 4).

In the biconic CRV, the docking mechanism is located in front of the cargo bay. This is to allow the latter to dock to SSF vertically (Fig. 4), thereby insuring not only a good reach by the SSRMS, but also good stability characteristics. Mechanism design resulted in a short mast that rotates back into the CRV for storage when it is not docked to the Space Station (Fig. 3).

Contingency Plans

Contingency plans have been developed in case any of the on-orbit maneuvers should fail to be completed on schedule. This might occur in the event of engine malfunctions or systems failure.

Only one maneuver requires significant correction: the 110-210-n.m. transfer, which is timed to bring the CRV behind the Space Station. The ΔV s required to reposition in such an event are shown in Fig. 5. Any other errors can be resolved by either waiting for the phase difference to correct itself, or by small perturbations methods.

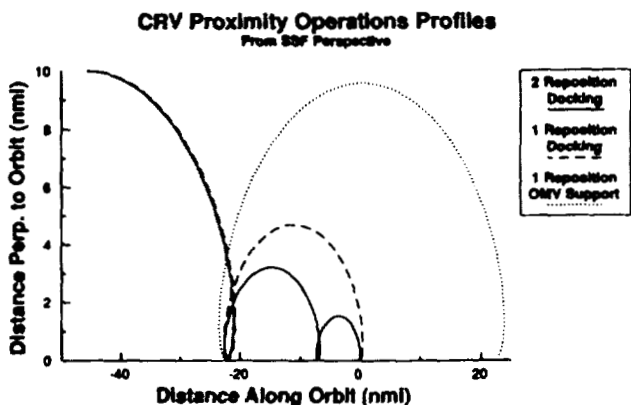


Fig. 2. CRV Position Relative to SSF During Proximity Operations

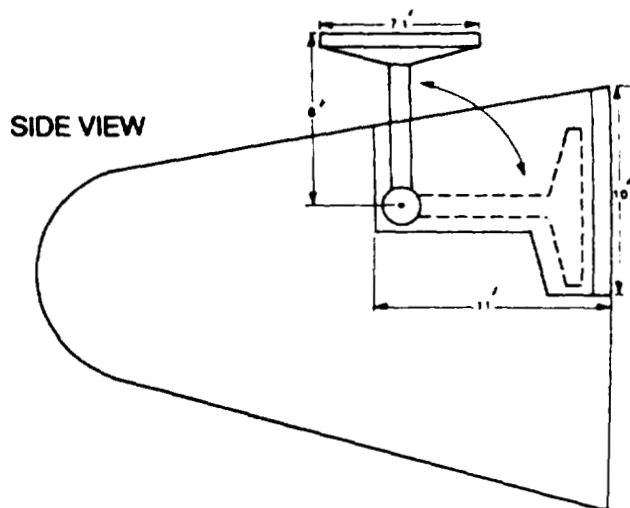


Fig. 3. The Docking Mast

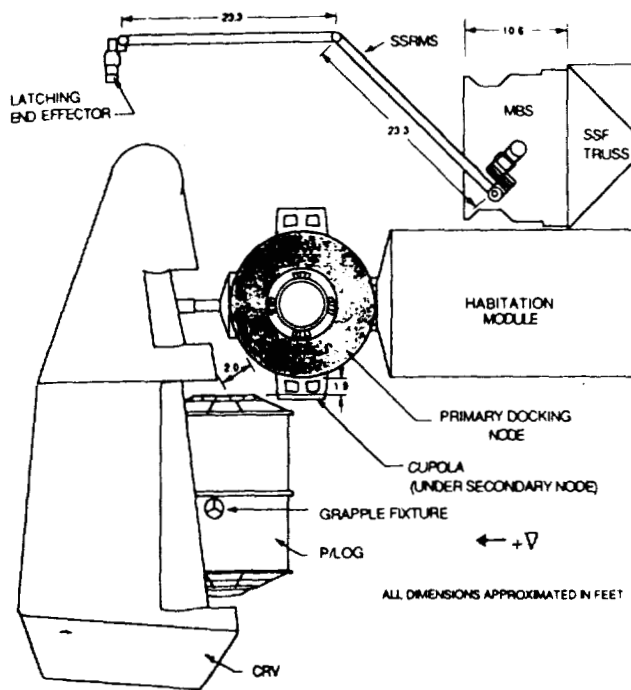


Fig. 4. Vertical Docking of the CRV at SSF

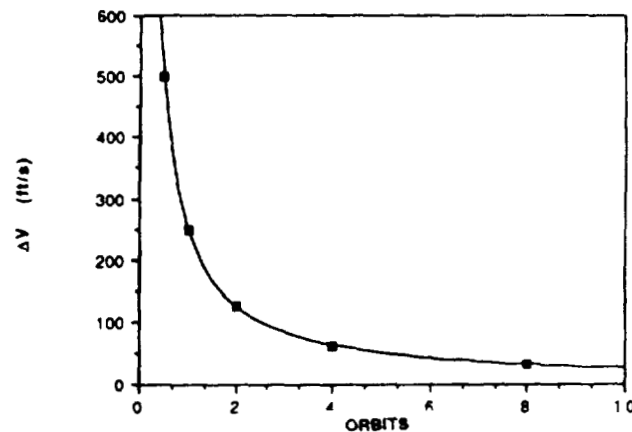


Fig. 5. Phase Correction Burn

Reentry

The initial deorbit burns require a 0-20-hr phase delay. After this initial burn, the dynamics of the CRV are governed by the atmosphere during an unpowered reentry. More detail on this phase is offered in the aerodynamics section of this report.

Ground Operations

While on the ground, the CRV has been designed to be compatible with all space shuttle processing facilities except the launch pad vertical payload integration bay.

The primary landing site is Edwards Air Force Base, while the launch site is Kennedy Space Center. This raises the problem of transporting the CRV back to KSC after landing. One of the objectives of design dealt with this problem. The CRV was designed to be as small as possible, and as a result it is possible to fit the CRV inside the Boeing Superguppy's cargo bay.

The processing scenario of the CRV has been modeled to follow that of most unmanned spacecraft, with a few minor changes. The predicted maintenance operations for the CRV are estimated to require 23 days, with a processing turnaround time of 66 days and a 7-day layover for transportation back to KSC, making the landing-to-takeoff turnaround 73 days.

PROPULSION

Propulsion is a part of almost all the CRV's phases of operation. It starts with the launch, continues with on-orbit transfers and proximity operations, and ends with the deorbit burn; after which the reentry is supported by aerodynamic lift only.

The CRV has been designed to launch vertically integrated with single-core expendable LRBs (see Fig. 6). As has already been specified, designing a launch vehicle was beyond the scope of this project. Instead, a choice was made from already existing systems. Design considerations include a 4.0-g maximum acceleration due to PLOG constraints.

The LRBs used for the launch are being designed by NASA and, while not yet in existence, are planned for service well ahead of time of the CRV's operational period. These rockets have a booster-out capability in excess of 85 klb. Since the CRV has a maximum takeoff weight of 74 klb, its safety is assured.

The boosters will insert the CRV at a 50×100 -n.m. orbit and then reenter the atmosphere.

The CRV also has three Orbital Maneuvering System (OMS) engines, which are capable of producing the large ΔV s needed to move the CRV from the low Earth orbit up to its $220 \times 220 \times 28.5^\circ$ final orbit. The OMS engines are fueled by a liquid hydrogen/oxygen mixture, and weigh only 86.65 lb each, with a specific impulse (vac) of 414.4 sec.

The amount of fuel needed to support the burns was a very important factor in choosing the OMS. The propulsion system is designed with a 20% fuel reserve.

REENTRY AERODYNAMICS AND CONTROL

Reentry of a biconic CRV cannot be aided by a fixed rigid wing, so an Advanced Recovery System (ARS) is needed. Trade studies conducted early in the development of this biconic's

conceptual design showed that a ram-air parafoil would make a very efficient ARS in terms of size and weight. The ram-air parafoil also showed good control characteristics and soft landing capabilities. Its low range, however, made a two-stage reentry a must.

Stage 1—Atmospheric Reentry

During the first stage of reentry, the CRV enters the atmosphere. It is in this stage that the CRV is expected to cover most of its range. To help the CRV meet its crossrange

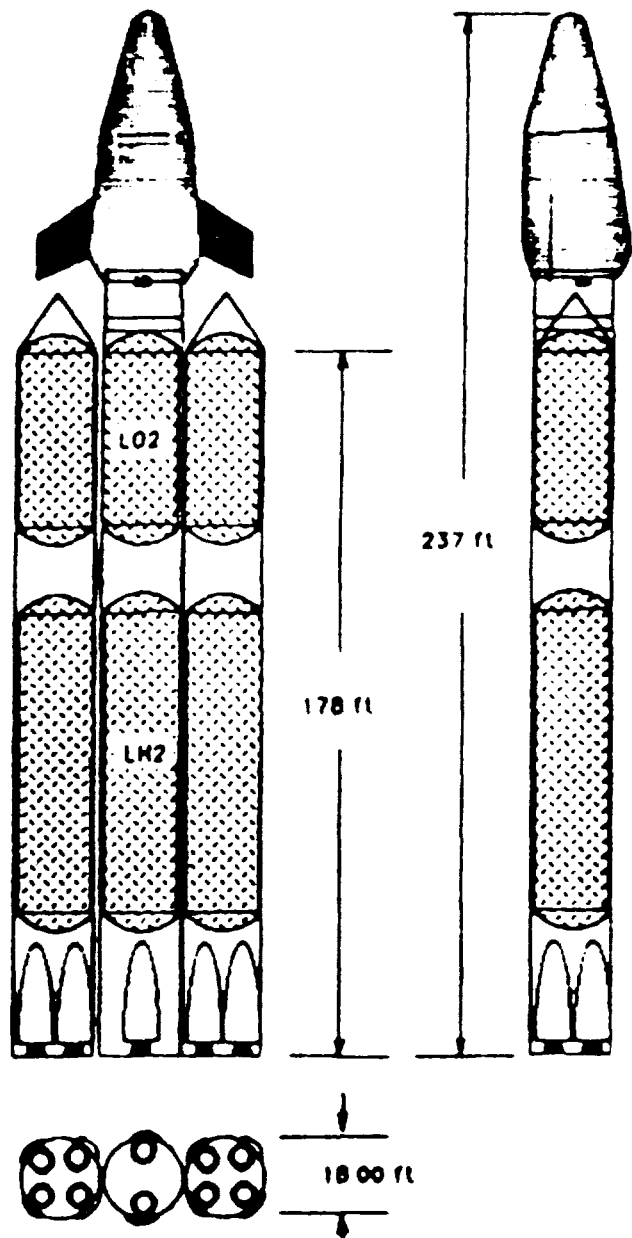


Fig. 6. Launch Configuration

requirements, it was designed with an axis bent with respect to the fore and aft cones. The result of the bend is aerodynamic lift.

At first, the bent biconic body was modeled after a previously designed biconic interplanetary vehicle (see Fig. 7), because a large amount of wind tunnel data was available for that configuration, allowing the design team to validate several analytical aeroprediction codes.

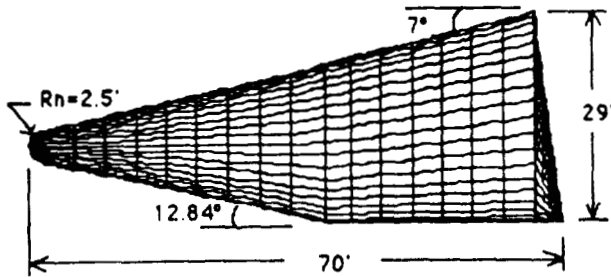


Fig. 7. HABP Model of the Baseline Configuration

The Supersonic/Hypersonic Arbitrary Body Program (HABP) was the main tool used in determining the aerodynamic characteristics of the body and understanding how each change affected the vehicle performance. The HABP accepts several methods to determine the pressure distributions around the vehicle. Using the baseline configuration as a reference, it was found that the Modified Newtonian and the Van Dike methods yielded the best results, compared to wind tunnel data. The former method was chosen as the standard for calculations, and was applied to the initial model to reshape the biconic in order to make it an efficient CRV.

Aerodynamics played the greatest role in shaping the CRV. Other considerations included providing good interior volume efficiency and acceptable heat load distributions. For example, during the design, the nose radius was increased from 2.5 ft to 4 ft. During reentry, heating is greatest around sharp edges. Therefore, increasing the nose radius lowered the heating levels in the nose making the use of lighter heating tiles in that area possible. Another advantage of the increased nose radius is that it allowed placement of onboard systems a lot closer to the front of the vehicle (see Fig. 8), not only improving the volumetric efficiency of the vehicle, but allowing a forward shift of the vehicle's center of gravity, a needed element in vehicle control.

CONTROL

During this stage of reentry, early versions of the vehicle displayed unacceptable instabilities (see Fig. 9). The lack of control surfaces made the Reaction Control System (RCS) the only means of controlling maneuvers. This was not only a costly proposition in terms of weight, but also did not yield good control characteristics. One of the biggest instabilities of the early versions was in the yaw direction, while its longitudinal axis symmetry makes it completely roll stable.

To render the CRV more stable, control fins were added. These consist of two tail-mounted horizontal fins, which have zero camber and can deflect $\pm 30^\circ$ to provide the needed longitudinal control. Further, the outer third of the fins can fold upwards 90° to function as winglets. Yaw control is achieved by staggering the deflection of the left and right fin, making either the left or right "rudder" more effective, thus creating the appropriate yaw moment (see Fig. 10).

CRV stability was tested longitudinally in both the Phugoid and Short period modes. Laterally, it was tested in the rolling, spiral, and Dutch roll modes. The biconic CRV is satisfactorily stable in all these modes.

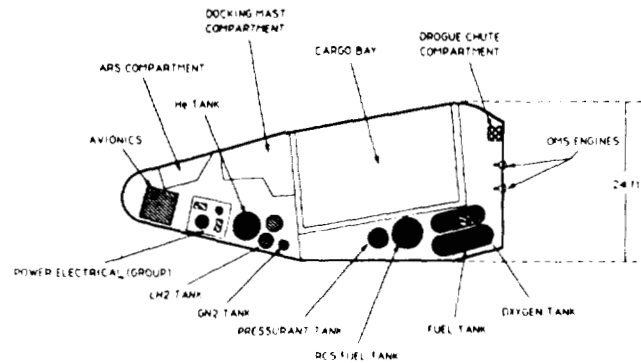


Fig. 8. System Placement (side view)

Pitching Moment Coefficient vs. Angle of Attack

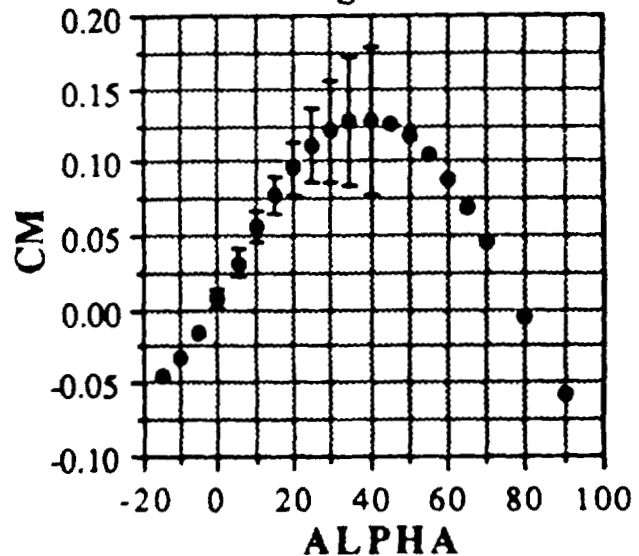


Fig. 9. Early Versions of the CRV Showed Instabilities

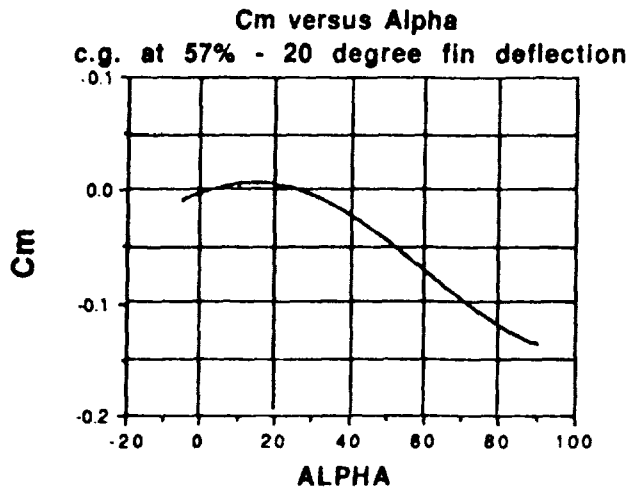


Fig. 10. Stability Characteristics

Stage 2—Advanced Recovery System

During this stage, the Advanced Recovery System (ARS) is deployed. Just prior to its deployment, a drogue shoot is deployed to bring the dynamic pressure down to less than 100 lb/ft². This allows the ARS to be deployed safely.

The ARS is a ram-air parafoil with a planform area of 22,250 sq ft, with a wingspan of 250 ft and a chord length of 89 ft. A modified Clarke-Y-17 airfoil section was chosen for the parafoil, as this type of section is most widely used on ram-air parafoils. The Clarke-Y-17 is shown in Fig. 11.

The ARS is made entirely of fabric with no rigid structures and is packed in a manner similar to a conventional parachute. It is deployed at an altitude of 10,000 ft. The parafoil is designed to be deployed and disreefed with 75% flap retraction. The flaps are actually the trailing edge of the parafoil and can be retracted to provide additional lift and directional control. The retractions occur by reeling in the lines attached to the trailing edge.

The parafoil is made up of 51 cells. The midspan reefing technique is used and is accomplished by folding and stowing a number of cells two places for each reefing stage. After deployment, the parafoil is disreefed in three stages, as shown in Fig. 12. During the first stage, the 11 center cells are opened. The five outer cells on each side are then opened during the second stage. The remaining 30 cells are disreefed in the final stage.

Wind tunnel tests of similar airfoils lead to the following aerodynamic characteristics:

Trim Angle of Attack	7°
Lift Coefficient	0.84
Drag Coefficient	0.22
Moment Curve Slope	-0.005
Lift-to-Drag Ratio	3.8

The flare maneuver just prior to landing is performed by cutting the lines connecting the parafoil to the rear of the CRV. The weight of the CRV is shifted forward until a "lazyleg," or

piece of cable that lengthens each line connected to the rear of the CRV, is tightened. The CRV touches down immediately after this maneuver.

THERMAL ANALYSIS

The Thermal Protection System (TPS) is designed to protect the CRV from the excessive heat loads during reentry. It is necessary to protect not only the structure itself, but also the avionics, the cargo bay area, and the control surfaces.

The avionics are cooled by placing them on a freon-cooled cold plate inside a pressurized (air) container. The freon is pumped through a radiator with approximately 117 sq ft of area placed on the inside of the cargo bay doors. In tandem with the radiator system, an evaporative system provides direct cooling to the freon system. In the lower atmosphere, where evaporative and radiative cooling cannot take place, freon and water are circulated through a heat exchanger. The water absorbs some of the heat.

The cargo carrying PLOG and UPLOG were designed to withstand a heating load of approximately 440 Btu/hr/sq ft. This is the value chosen to be a maximum constraint on the heating of the cargo bay. The insulation chosen is a low-weight Q-fiber insulation lining the cargo bay in a layer 0.375 in thick.

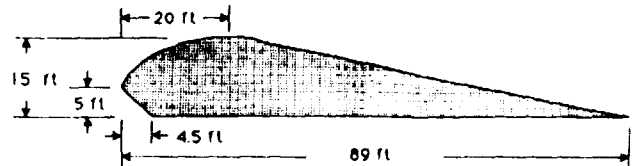


Fig. 11. Clarke-Y-17 Airfoil

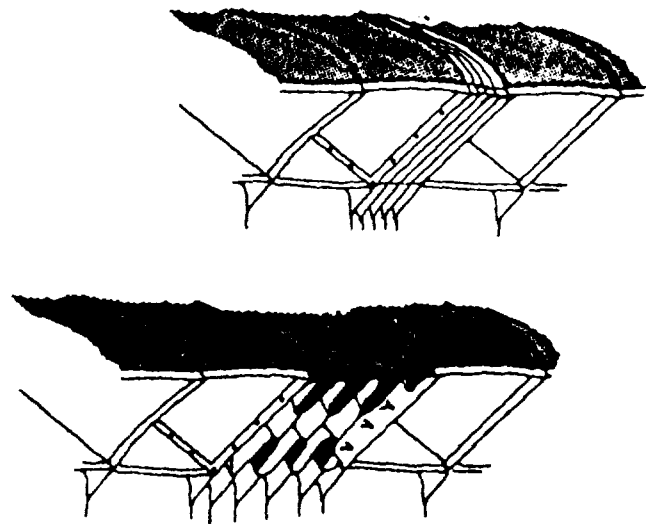


Fig. 12. Disreefing of the Parafoil

The program MINIVER was used to determine the external heating loads along the surface of the vehicle and on the control surfaces. Using this program, the maximum temperature was found to be 2775°F in the nose of the vehicle and along the leading edges of the control surfaces. These areas are covered by LI-2200 in 6-in by 6-in tiles at an angle of 18° to the airflow. The tiles were put at an angle to prevent them from being ripped off the way they are on the space shuttle. The tiles vary in thickness from 2.5 in near the flow stagnation area to 2 in toward the rear of the vehicle.

The underside of the vehicle experiences the next highest heating loads. Fibrous Refractory Composite Insulation (FRCI) will cover this area as well as the remainder of the control surfaces. These tiles are also 6 in by 6 in at an angle of 18° to the flow. The thickness decreases from approximately 2 in to 1.5 in moving towards the rear of the CRV.

The rest of the vehicle is covered by Tailorable Advanced Blanket Insulation (TABI). These tiles are approximately 2 ft by 2 ft and decrease in thickness from 1.5 in to 0.75 in moving toward the rear. The different insulations are shown on the CRV in Fig. 13.

The tiles are attached to the CRV by two different methods. All tiles are directly or indirectly connected to the outer skin of the structure by the cost-effective adhesive, RTV-560. However, due to the frequent replacement of tiles, a "hook-and-loop" method is used to attach the TABI tiles. Fig. 14 shows the three types of insulation and their attachments.

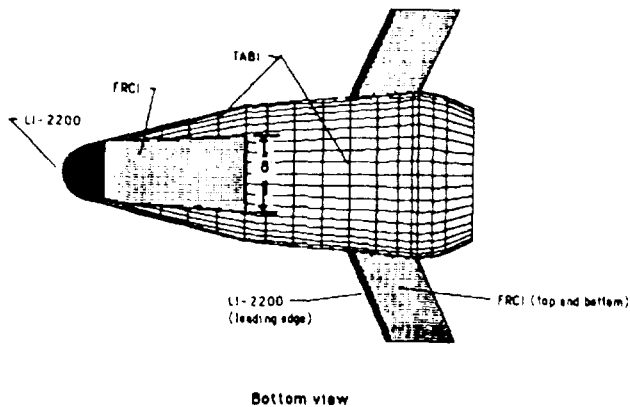
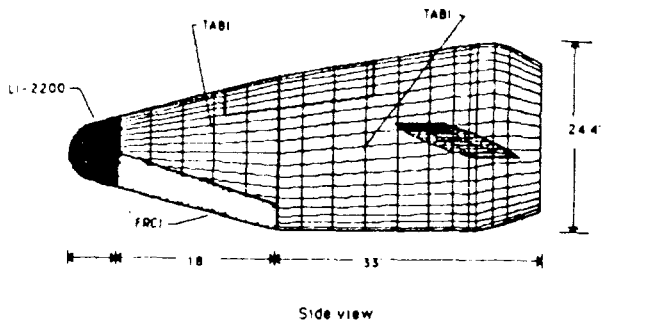


Fig. 13. CRV Insulated Tiles

STRUCTURAL DESIGN

The fuselage substructure, the cargo bay support structure, the outer skin, and the ARS Docking Mechanism and Drogue Chute compartments were some of the substructures designed by the structural design team. This was a very critical part in the design of the CRV. All substructures must be designed to withstand any applied load.

The fuselage support structure consists of a system of ring frames and stringers. There are 32 box-shaped ring frames spaced 22 in apart from the nose to the rear. There are 74 Z-shaped stringers surrounding and supporting every ring frame, except for the first 6 rings, which only require 37 stringers. The stringers are spaced approximately 12 in apart at the largest diameter of the CRV and converge slowly as the diameter decreases.

The cargo bay support structure designed to support the PLOG or UPLOG is a series of half rings just over 15 ft in diameter. There are 14 of these half rings coplanar with outside rings numbers 15-28 from the front, also spaced 22 in apart. The inside rings are all box shaped and are arranged as shown in Fig. 15.

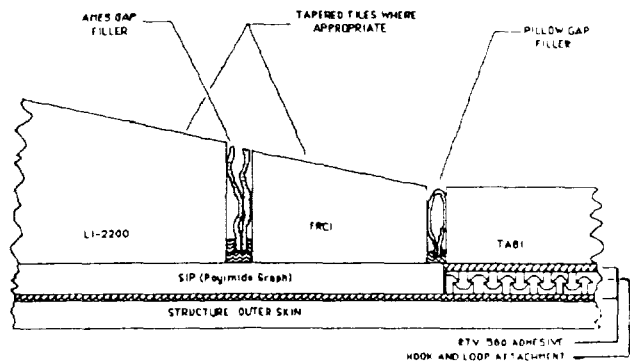


Fig. 14. TPS Materials and Attachment Methods

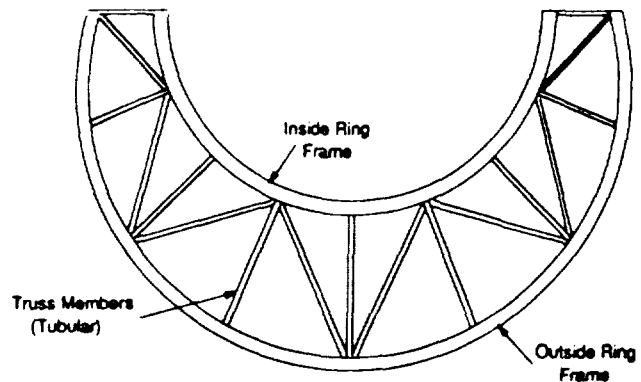


Fig. 15. Payload Bay Support Structure

The outer skin is made of HRH-327 honeycomb with aluminum 2219 facing material on each side. The reason for using the honeycomb structure is that it is the most efficient way to get the maximum strength out of the lightest material. The honeycomb panel consists of five layers of material, as shown in Fig. 16. The layers consist of an aluminum face sheet on the inner and outer surfaces attached to the HRH-327 honeycomb by an adhesive, as shown in Fig. 16. Each aluminum face sheet is 0.02 in thick and the honeycomb is 0.05 in thick.

With the given ARS design, a 69.05-cu-ft compartment would be necessary to pack the chute. A 25% margin of error and an additional 10 cu ft for the deployment chute were also added, making the necessary volume of the ARS storage compartment 96.3 cu ft. Due to the location and size of the cargo bay, it was necessary to place the compartment in the fore cone of the vehicle. The compartment is 3.2 ft deep, 4.5 ft wide, and has a maximum length of 8.3 ft on the surface, tapering off towards the center of the CRV to 5.1 ft. The taper is at a 45° angle.

The drogue chute compartment is placed near the rear of the CRV on the top surface just behind the cargo bay. Its volume is 15 cu ft, including a 50% margin of error. The compartment is 3.42 ft wide with a depth and length of 2.17 ft.

The docking mechanism compartment was uniquely designed to fit the shape of the mechanism. It is also placed in the fore cone of the CRV between the ARS compartment and the cargo bay. The compartment is 8 ft wide, 11 ft long, and has a maximum depth of 10 ft, as shown in Fig. 3.

CONCLUSION

Worthy of mention is the absence of a backup recovery system to the ARS. A design for such a system was actually carried out, but it was decided not to include it as part of the design for several reasons. First, the extra weight would

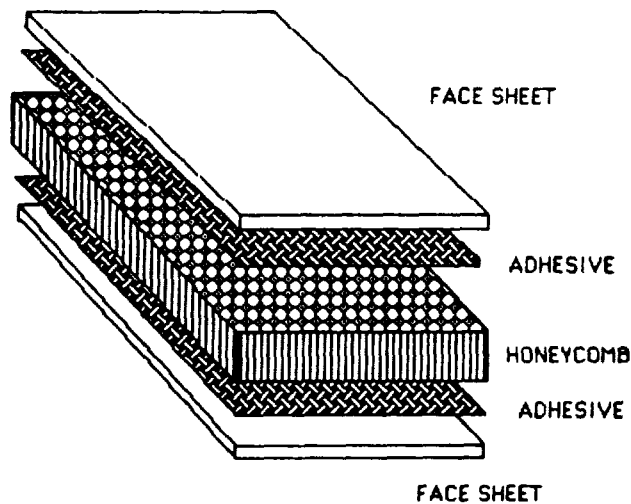


Fig. 16. Honeycomb Structure

necessitate downscaling the maximum payload. This is undesirable. Second, volume constraints in the backup system bay are such that the size of the secondary chute would have to be limited; given these limits, the touchdown velocity of the CRV, in case of main system failure, would have to be greater than desired, causing some systems to be damaged on impact. Third, the high reliability of the ram-air ARS does not warrant the penalty weight of a back-up system.

INFORMATION SUMMARY

Bent-axis biconic with a ram-air inflated parafoil ARS

- $(L/D)_{\text{Hyper}} = 1.5$
- $(L/D)_{\text{Subsonic}} = 3.8$ -ARS
- Weight Unloaded = 34.06 klb
- Cargo Capacity = 40 klb
- Crossrange \approx 700 n.m.

The advanced recovery system

- Planform Area = 22,250 ft² (250 ft \times 89 ft)
- Deployed at 10,000 ft altitude
- Midspan reefing in three stages

Vehicle dimensions

- Length = 59 ft
- Diameter nose = 7.7 ft
- Diameter max = 24.4 ft

Supersonic reentry control is via tail-mounted adjustable deflection fins, with folding winglets.

The CRV will be capable of docking directly to SSF as well as being OMV compatible.

- Mission time with OMV = 19.85-76.85 hr
- Mission time non-OMV = 18.35-75.35 hr

Propulsion

- Top-mounted launch on dual-booster/single-core LRBs
- Orbit insertion at 50 n.m. \times 100 n.m. at 28.5°
- Three OMS engines
 - LH₂/LO₂ propellant and oxidizer
 - Weight = 86.65 lb (each)
 - $I_{sp, vac} = 414.4$ sec
 - Thrust_{vac} = 1600 lbf
- The RCS system uses LH₂/LO₂ outside the CCZ and GN2 inside, as specified by SSF requirements.

Transportation of the CRV back to KSC will be via the Boeing Superguppy. CRV turnaround time is 66 days.

WINGED CARGO RETURN VEHICLE CONCEPTUAL DESIGN

UNIVERSITY OF MINNESOTA

N 91 - 18144

NASA is committed to placing a permanent space station in Earth orbit in the 1990s. Space Station *Freedom* (SSF) will be located in a circular 220 n.m. orbit at 28.5° inclination. The *Winged Cargo Return Vehicle's* (CRV) primary mission is to support the SSF crew by flying regular resupply missions. The *Winged CRV* is designed to be reusable, dry-land recoverable, and unmanned. The CRV will be launched inline on three liquid hydrogen/oxygen rocket boosters with a payload capability of 113,000 lb. The three boosters will take the CRV to an orbit of 50 × 110 n.m. From this altitude the orbital maneuvering engine will place the vehicle in synchronous orbit with the Space Station. The *Winged CRV* will deliver cargo modules to the Space Station by direct docking or by remaining outside the SSF command zone and using the orbital maneuvering vehicle to transfer cargo. The CRV will be piloted by SSF crew while in the command zone. After unloading/loading, the CRV will deorbit and fly back to Kennedy Space Center. The *Winged CRV* has a wing span of 57.8 ft, a length of 76.0 ft, and a dry weight of 61.5 klb. The cargo capacity of the vehicle is 44.4 klb. The vehicle has lift/drag ratio of 1.28 (hypersonic) and 6.00 (subsonic) resulting in a 1351-n.m. cross-range. The overall mission length ranges between 18.8 and 80.5 hr. The operational period will be the years 2000-2020.

NOMENCLATURE

AFSRI	Advanced Flexible Reusable Surface Insulation
CCZ	Command Control Zone
CRV	Cargo Return Vehicle
FRCI	Fibrous Refractory Composite Insulation
GLOW	Gross Lift Off Weight
GPS	Global Positioning System
HABP	Hypersonic Arbitrary Body Program
IMU	Inertial Measuring Unit
L/D	Lift-to-Drag Ratio
LEO	Low Earth Orbit
LM	Logistics Module
LRB	Liquid Rocket Booster
MSBLS	Microwave Scan Beam Landing System
OMS	Orbital Maneuvering System
OMV	Orbital Maneuvering Vehicle
RCC	Reinforced Carbon Carbon
RCS	Reaction Control System
SPDS	Stabilize Payload Deployment System
SSF	Space Station <i>Freedom</i>
SSRMS	Space Station Remote Manipulator System
TPS	Thermal Protection System

71,929 lb of payload per year. It is with this basic requirement that the project was undertaken. The project was conducted in three parts: Trade Study, Conceptual Design, and Testing and Analysis. The first phase, the trade study, considered a lifting body, a biconic, and a winged configuration based on performance, reliability, and availability of technology. The trade studies were also used to determine major vehicle systems, and preliminary mission profile. The configurations chosen were the winged and biconic configurations.

The second phase of the project was a conceptual design of the vehicle. To conduct this the class was divided into two design teams, one for each configuration considered. The remainder of this summary will focus primarily on the design and testing of the winged configuration. The winged configuration design team was further broken down into eleven discipline groups: System Integration, which oversaw the design process of the vehicle as well as the overall management of the design team; System Layout, which was responsible for the placement of systems, vehicle drawings, and the mass properties of the vehicle; Mission Operations, which was responsible for the orbital mechanics, mission profile, space station operations and ground operations; Reentry Dynamics, which was responsible for the flight profile from reentry to ground; Aerodynamics, which was responsible for the analysis of the vehicle aerodynamically, including the various control devices considered such as winglets, canards, and the vertical tail; Stability and Control, which calculated the stability derivatives as well as examining the control requirements on orbit and in the atmosphere; Thermal Protection and Control, which was responsible for thermal analysis of the vehicle and the placement of thermal protection; Avionics and Power, which was responsible for the choice of avionics and power systems needed by the vehicle; Propulsion, which selected the number of engines, engine type, and the launch system; Structures, which determined the overall layout of structural members; and Cost and Optimization, which

INTRODUCTION

The Cargo Return Vehicle Design project was performed by students in the senior design class at the University of Minnesota. The project is intended to help supply Space Station *Freedom* (SSF) with its logistics needs. With development of the SSF, NASA has calculated that there will be logistic problems in supplying the station with enough to support a permanent manned contingent. It is with this shortfall in mind that a new vehicle was proposed. Currently NASA predicts that the SSF will need 8 flights per year and 250,709 lb of payload to support it. Currently the space shuttle can only be committed to 5 flights per year and 178,285 lb of cargo. This leaves the Space Station with a shortfall of three flights and

examined optimization of some of the systems on the vehicle. The disciplines each met individually twice each week; the team as a whole met once a week. There was also a weekly meeting of the configuration control board whose responsibility it was to define the vehicle design and to settle all disputes between discipline groups over the final design of the vehicle. The overall vehicle designed by the group had physical characteristics as given in Table 1.

Table 1. Vehicle Physical Characteristics

<i>Overall Dimensions</i>		
Length		76.0 feet
Span		57.8 feet
Height		19.8 feet
<i>Cargo Bay Dimensions</i>		
Length		30.0 feet
Width		19.8 feet
Height		19.8 feet
<i>Vehicle Weights</i>		
Weight (dry)		61,596 lb
Weight (launch)		113,000 lb
Consumables		5,568 lb
Weight (landing)		106,012 lb
Max. Payload		44,416 lb

Major systems on the vehicle are given in Table 2.

Table 2. Major Systems

<i>Propulsion</i>	
Launch system	Liquid Rocket Booster system
Main Orbital	1 OMS Engine
RCS (normal)	28 NTO/MMH thrusters
RCS (special)	24 Cold Gas Thrusters (for use around SSF)
<i>Avionics Systems</i>	
Guidance and Navigation	Global Positioning System (GPS), Star Tracker, IMU
Communications and Tracking	Tracking and Data Relay Satellite System (TDRSS)
Autoland Control	Microwave Beam Scan Landing System Electro-Servo Actuators
<i>Power Systems</i>	
Avionics Controls	Fuel Cells Ni Cad Batteries

The vehicle contains many other subsystems that will be explained later in the summary. The final vehicle configuration can be seen in Fig. 1. The configuration features a delta-wing planform with a strake and winglets for lateral stability and control. The cargo bay is similar in design and length to the space shuttle so as to be compatible with all the same cargo handling systems. There is a docking ring bay located ahead

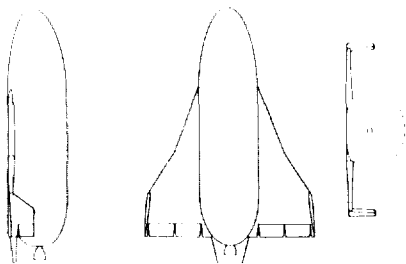


Fig. 1. Three View Drawing of Vehicle

of the cargo bay to facilitate docking of the vehicle to SSF without affecting payload capability or placement in the cargo bay. The vehicle will glide in to land on cyclical landing gear (not shown).

The third stage of the Project was the Testing and Analysis Stage. The class was again broken into eleven discipline groups: System Integration, Integration Staff, Modeling, Wind Tunnel Testing, Wind Tunnel Data Analysis, Water Tunnel Testing, Structural Analysis, Cost and Optimization, and Marketing and Promotion. The main function at this stage was to analyze more completely the design of the vehicle. The System Integration group acted as the project managers while the Integration Staff primarily worked on editing the contractor reports. The Wind Tunnel groups worked on analyzing the vehicles' lift-to-drag ratio and some of the stability derivatives to determine if they coincided with the calculated ones found during the design phase. The Water Tunnel group examined qualitatively the flow around the vehicle examining the effects of the strakes and winglets. The Modeling group worked with both testing groups building the test models as well as building a display mock-up for the Marketing group. The Structural Analysis group worked on analyzing the structure of the vehicle using the program NASTRAN in order to finalize the size of the structural members. The Marketing group was responsible for the promotion, public relations, and the displays of the vehicle for the ADP Summer Conference as well as at the university. Cost and Optimization examined the feasibility of the overall concept as well as performing a justification study. The testing and analysis confirmed much of the work done earlier.

SYSTEMS LAYOUT

The systems layout discipline's major responsibilities were to keep track of the placement of the various systems through vehicle drawings, and to calculate the mass properties of the vehicle. The vehicle final weight statement can be seen in Table 3.

Table 3. CRV Finalized Weight Statement

Body	11,693 lb
Wings	8,809 lb
Thermal Control System	250 lb
Propulsion System	1,353 lb
Avionics and Power	12,000 lb
Landing Gear	3,200 lb
Docking Module	250 lb
Growth	5,000 lb
Dry Weight	61,596 lb
Payload	44,416 lb
RCS Propellant	241 lb
OMS Propellant	4,627 lb
Cold Gas Propellant	700 lb
Adapter	1,420 lb
Total Launch Weight	113,000 lb
Less Consumables	5,568 lb
Less Adapter	1,420 lb
Total Landing Weight	106,012 lb

MISSIONS OPERATIONS

The total mass in orbit will increase approximately 833% from 1998 to 2006. The SSF must receive approximately 115,000 lb of cargo per year. Of this cargo, 76% would be returnable and the other 24% would be trash. The SSF will need fluids for continued growth and for use in experiments to be conducted on the station. For growth to occur there is a need for 12 flights per year by the year 2004. The U.S. will be responsible for carrying 42% of the cargo to the SSF. The CRV must have the ability to meet SSF cargo requirements. The station will have of 275 KW of power, 24 crewmembers, and 5 or more modules. Cargo transfers must be of the order of 200 metric tons per year, which can be provided by 9 enhanced CRV flights per year.

The CRV will be capable of performing the required mission utilizing one of two possible mission plans—denoted nominal (primary) and alternate (secondary).

In the nominal mission, the CRV would leave a 110-n.m. injection orbit, en route to a stabilized "parking orbit" at the rear edge of the Space Station *Freedom* Command and Control Zone (CCZ). An Orbital Maneuvering Vehicle (OMV) would be dispatched from the SSF and perform two round-trips in the process of transferring and exchanging the Logistics Modules (LM). LM pickup and dropoff at the CRV would take approximately 30 min each and would be simplified by the inclusion of a Stabilized Payload Deployment System (SPDS). LM exchange at the SSF would nominally be performed solely by the OMV (~1 hr exchange time) and contingently by the OMV with the aid of the SSRMS (~2-3 hr exchange time). The overall nominal mission would be completed in 18.8 hr.

In the alternate mission plan, the CRV would leave the injection orbit and proceed directly to the SSF and dock with the help of the SSRMS. The SSRMS would berth and de berth the CRV and perform all LM exchange maneuvers. The CRV would be required to stay docked to the SSF for at least 6 hr, until a launch window opens. As a result, the alternate mission plan would take considerably longer to perform.

In either mission plan, the flight would be directed by several ground control centers and the SSF crew. Any vehicle inside the CCZ would be controlled by the SSF crew and any vehicle outside the CCZ would be controlled by ground crews.

REENTRY GUIDANCE AND DYNAMICS

The main purpose of the discipline was to define the CRV's flight profile, determine the g -loading, maximum dynamic pressure on the vehicle, and cross range requirements. They were also responsible for defining the minimum lift-to-drag ratio for the vehicle to reach the primary landing sites and determining the cross range. The cross range was calculated using standard empirical approximation. The cross range was determined to be 1351 n.m. The maximum g -loading was found to be 2.25 g and occurs during S-turn maneuvers used to decelerate the vehicle. The flight profile is shown in Table 4.

Table 4. Flight Profile

Event	Time to Touch-down	Altitude (ft.)	Velocity (ft/sec)
De-orbit Burn	1 hr	220 n.m.	Mach 26
Blackout	30 min	300,000	23,900
Maximum Heating	20 min	230,000	19,350
Exit Blackout	12 min	180,000	13,500
Begin Energy Management Systems	5 min	80,000	1,900
Initiate Autoland System	1.5 min	14,000	650
Initiate Preflare	30 sec	2,000	580
Complete Flare	15 sec	135	450
Landing Gear Down	10 sec	100	400
Touchdown	0 sec	0	320

AERODYNAMICS

The aerodynamics discipline group was in charge of defining the wing shape, camber, and essential body surface designs. The group used a Hypersonic Arbitrary Body Program (HABP) to evaluate the winged CRV's aerodynamic characteristics in the hypersonic and supersonic regions (Table 5). The HABP program is capable of calculating aerodynamic characteristics of arbitrary 3-D shapes in both the hypersonic and supersonic regions. For the subsonic aerodynamics the Boeing computer program AIREZ was used to estimate characteristics of all flight regimes, from subsonic to supersonic. Another program, developed at the University of Minnesota, ULTIMATE, was employed to reveal flight qualities that AIREZ was not capable of performing. Also studied was the possibility of employing canard surfaces for longitudinal control.

Table 5. Maximum L/D Characteristics

Mach	AIREZ	HABP Fins and Tail	HABP w/Strake
1.2	1.83	N.A.	N.A.
1.5	1.66	N.A.	N.A.
2.0	1.58	1.36	1.66
5.5	1.39	1.29	1.58
10.5	1.50	1.28	N.A.
20.5	1.52	1.28	1.28

Sweep = 47°	Nose Length = 27 ft
Wing Taper = 0.28c	Nose Dia. = 19.9 ft
S = 1888 ft ²	Effect Dia. = 21.6 ft
Fin Taper = 0.34c	Nose Droop = -2 ft
Fin S = 170 ft ²	Nose Radius = 1.8t
Strake = 70.76°	Thick Ratio = 1.1

Throughout the trade study and conceptual design phases the CRV body was continually changed and redefined. The CRV began with vertical tail, deployable canards, and variable winglets. Based on the determination that a subsonic L/D of 6 would be adequate for approach and landing, a variable winglet option was eliminated. The performance of the winglet-only and vertical-tail-only configurations in the hypersonic and supersonic regions were found to be comparable. Therefore, use of both wing fins and a vertical tail was redundant, and the vertical tail was dropped from the body design. Theoretically the use of fins should increase the L/D

favorably in the subsonic region due to a reduction in induced drag. Fins also are less susceptible to blanketing during reentry. Finally, the use of fins allows flexibility in docking with the Space Station. As a result of these benefits the winglet-only configuration was chosen to be the final form for the CRV.

STABILITY AND CONTROL

The stability analysis of the vehicle was performed using two main computer programs, the MINNEMAC program for computation of root loci for different stability modes and the Stability Analysis Program, which computed the aerodynamic derivatives. The analysis was performed in hypersonic/supersonic and subsonic flight regimes. The neutral and maneuver points for the different flight regimes are listed in Table 6.

Table 6. Neutral and Maneuver Points*

Regime	Neutral Point (ft)	Maneuver Point (ft)
Subsonic	45.05	46.08
Hyper/Supersonic	53.40	54.43

* All points measured from the nose of the vehicle.

From the calculation of the neutral points and the center-of-gravity envelopes from the system layout discipline it was determined that the vehicle would be stable throughout the hypersonic and supersonic ranges but would be unstable in the subsonic regime. This was decided to be acceptable since current fly-by-wire technology exists to control unstable flight.

The other function of the group was to examine control systems and size the control surfaces. The overall control of the vehicle would be accomplished by the RCS engines while on orbit and during reentry until the dynamic pressure on the CRV reached 10 psf. At this point the aerodynamic control surfaces would begin to be used and the RCS would be phased out. The vehicle would rely totally on aerodynamic surfaces by the time the dynamic pressure reached 170 psf. The control surfaces were sized using both a scaled-down space shuttle approximation, and deflection and moment constraints for refinements.

POWER AND AVIONICS SUBSYSTEMS

Power Supply

The power system on the CRV must satisfy several requirements. The most crucial aspect of any power supply for the Winged CRV is reliability. Power supply must be flexible regarding length of operation and must be cost effective. Of the power systems available, fuel cells satisfied the requirements.

Avionics have a peak usage of approximately 2.0 kW during thrusting maneuvers. If a pressurized logistics module is on board then an additional 1.5 kW would be required. This produces a peak power need of about 6 kW depending on the type and number of other components in use. Current fuel cells produce 7 kW continuous and 12 kW peak. One fuel cell could supply all the power required for the vehicle, but the

design incorporates three fuel cells for system redundancy. The fuel cells are self-cooling units with their own oxidizer and fuel supply. They are located in the bottom of the vehicle along with their fuel and oxidizer tanks. (A separate fuel supply is required because fuel cells need a much higher grade of fuel than that used for propulsion.) The hydrogen/oxygen fuel exits the cells as water at about 140°F. This water could be used for heating or cooling other components.

Servo Actuator Power Supply

The servo power supply comes from a separate battery system because these servos require too high a peak load to be powered by the fuel cells. The type chosen were NiCad batteries because of their weight, volume, and performance characteristics.

Guidance and Navigation

The major components of this subsystem are the Global Positioning System (GPS) receiver, Inertial Measuring Units (IMU), and a star tracker. The GPS system determines the position of the vehicle relative to the Earth and SSF. The GPS works in either an arbitrary three-axis system or with latitude, longitude, and altitude. By giving a continuous update of the position, the GPS also provides a constantly updated velocity vector. The IMUs are the primary sensor for the guidance and navigation system. They sense both lateral and longitudinal rotational acceleration and detect rotational velocity. The CRV would incorporate 2-4 IMUs. The star tracker mounts directly on the hull of the CRV and would have a small view port. Each component feeds into a digital integration unit and then is sent to the main data handling computers.

Automatic Landing System

The main components of the auto landing system are the Microwave Scan Beam Landing System (MSBLS), a radar altimeter, the landing gear, steering and braking systems, and television cameras for remote control. The main functions of this subsystem are to capture and track lateral guidance path, capture and track the vertical guidance path, provide sideslip maneuvers prior to landing, drop landing gear automatically, and steer and brake while on the ground. The MSBLS is the primary navigation device. It is activated at 10,000 to 14,000 ft when the vehicle is parallel to the runway and provides azimuth angle, elevation angle, and distance during final approach and landing. The on-board radar altimeter provides height above the ground up to 5480 ft.

THERMAL PROTECTION SYSTEMS

The following materials were selected: Reinforced Carbon-carbon (RCC), Fibrous Refractory Composite Insulation (FRICI), and Advanced Flexible Reusable Surface Insulation (AFSRI). Approximate thermal calculations were made to justify the TPS placement on the vehicle.

The TPS for the Winged CRV is based primarily on the effective protection of the substructure while considering weight penalties. The aeroheating effects were defined from a computer program, MINIVER, approximate calculations, and space shuttle data. The protection materials chosen were RCC, carbon-carbon tiles, Fibrous Refractory Composite Insulation-8, and Tailorable Advanced Blanket Insulation (for the shuttle-type heat sink and hot structure system). The placement of the materials can be seen in Fig. 2. The total weight is 11,609 lb. Future use of an active cooling system appeared promising for use in connection with improved hot structures.

Aeroheating Analysis

To effectively apply thermal protection to the CRV accurate analysis of the temperature and heating rate along a trajectory is required. To fulfill this requirement, the program MINIVER was used. Using the trajectory established by the Reentry Dynamics group, and models for the various body sections, the thermal environment encountered by the CRV was estimated. The CRV was split into five sections for modeling purposes. These sections consisted of the nose, body, wing tips, wing section one (sweep = 68°), and wing section two (sweep = 54°). The models for each of these sections were input into MINIVER and analyzed twice; once, at laminar flow, and once, at turbulent flow. From the Reynolds number data in the MINIVER output, it was found that the air flow would remain laminar for this trajectory. This was based on transition beginning at $Re = 3 \times 10^5$, and fully turbulent flow at 4×10^8 . From this methodology the TPS was chosen and placed in each of the five regions. From Fig. 2 and Table 7 an accurate idea of the vehicle protection regions can be analyzed.

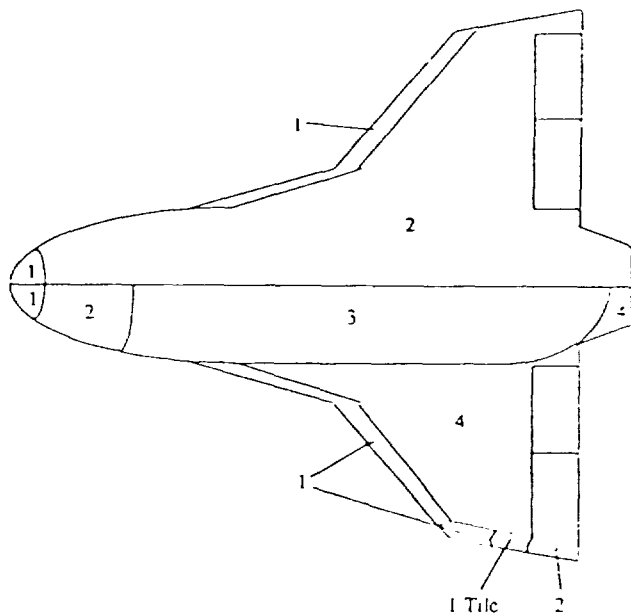


Fig. 2. TPS Placement

Table 7. Material Key

Region	Temperature	Material
1	2000-3000°F	RCC
1-Tile	2000-2700°F	Carbon-Carbon Tile
2	1500-2300°F	FRCI-8
3	800-1500°F	TABI
4	<800°F	TABI

PROPULSION

The objective of the propulsion discipline was to design a propulsion system for the CRV to meet all the mission requirements. The primary design inputs were thrust level, ΔV requirements, and total dry weight of the CRV. The two possible propulsion configurations for the CRV include a system with SSF control zone capabilities, and one without.

Orbital Maneuver System Engine Selection

The Orbital Maneuvering System (OMS) of the CRV serves two main purposes. First the system must produce the necessary thrust to propel the CRV from a 100-n.m. to a 210-n.m. orbit after booster shutdown. Second, the system must produce sufficient ΔV for de-orbit.

Based on a theoretical engine, it was concluded that the current space shuttle OMS would satisfy all the requirements. The Aerojet AJ10-190 was chosen for the use in the CRV. The dimensions of the engine are given in the following sections.

Reaction Control System

The Reaction Control System (RCS) for the Winged CRV is responsible for fine orbital and attitude adjustments in space and will not be used in the lower atmosphere. The system consists of 52 thrusters positioned as shown in Fig. 3.

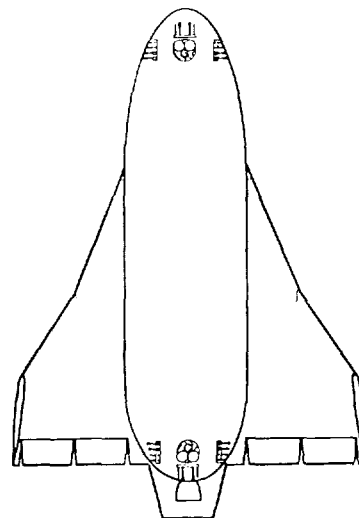


Fig. 3. RCS Placement

RCS Auxiliary

SSF regulations prohibit all but the use of cold gas propellents within the SSF control zone. To meet this requirement an auxiliary RCS system was designed to be used within the SSF control zone. The system was designed with the possibility of hard-docking to SSF.

Number of RCS Thrusters and Placement

For effective six-axis control, 24 cold gas and 28 NTO/MMH thrusters were placed as shown in Fig. 3. Each main thruster will produce 400 lb of thrust. All thrusters will be fired individually except in emergencies. This number of thrusters allows for at least one degree of redundancy for each axis of motion. The thrusters will also be located to allow for paired-thruster operation if needed.

Launch System

The launch system must deliver the loaded CRV to a 100 n.m. insertion orbit. The launch system was chosen on the basis of payload to low Earth orbit, the mounting procedure of the CRV and the fuel type. The final decision was a delivery system consisting of two liquid rocket boosters (LRB) mounted on each side of one core unit, each with its own engines and fuel (Fig. 4). The core would also carry all of the avionics and controls. The fuel used for this system is liquid hydrogen (LH₂) and liquid oxygen (LOX). The engines for this application would be space shuttle main engines (SSME).

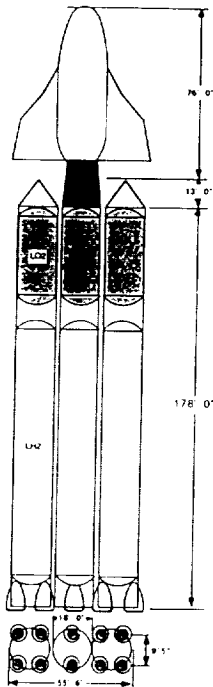


Fig. 4. Launch System

Table 8. Launch System Data*

Height (w/o CRV)	178'
Payload to LEO	125,000 lb
GLOW	2,600,000 lb
Engines	10-SSME

* For further description see System Mass Comparison.

STRUCTURAL DESIGN AND ANALYSIS

The structural design was completed during the design phase of the project. The vehicle was intentionally over-designed so that the elements would not fail. The main structural materials chosen for the vehicle were aluminum TA2219 for the construction of the frames, aluminum TA2024 honeycomb for the skin of the vehicle, and a Graphite/Epoxy composite was chosen for the cargo bay doors, since they do not contribute to the overall strength of the airframe. The design was divided into four sections, front, middle and aft fuselage, and the wing. The fuselage sections were connected by means of two main structural bulkheads fore and aft of the mid fuselage section (see Fig. 5).

The front fuselage was based on a semi-monocoque design similar to conventional aircraft. This design utilized TA2219 for the majority of the structure. The front fuselage houses the front landing gear, the avionics bays, and the docking module bay.

The wing is a conventional wing design consisting of spars, webs, and honeycomb skin. The wing is constructed from aluminum TA2219 except for the skin, which is TA2024. The aft landing gear base was placed within the wing structure.

The mid fuselage consists of a 30-ft-long primary load-carrying structure housing the payload bay. The mid fuselage is a truss frame construction of aluminum TA2219 that includes a wing carry-through structure and the payload bay doors. The payload bay doors are constructed entirely out of a graphite epoxy composite.

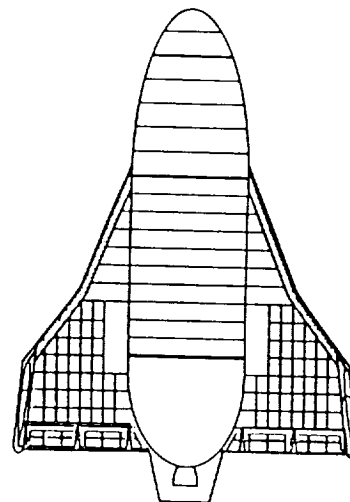


Fig. 5. Structural Layout

The aft fuselage consists of an external shell structure and an internal thrust structure. Both are constructed primarily out of aluminum TA2219 along with boron epoxy laminates and titanium reinforcements. The section houses the OMS engine and was designed to transfer the thrust and launch loads to the mid fuselage.

The analysis phase involved using the NASTRAN program to examine the design from the previous quarter. The program used finite element methods to determine forces and stresses on the different elements in the vehicle. To perform the analysis the vehicle was divided into two main sections, the fuselage and the wing. Dynamic pressure data from HABP runs were used as input for the program. The stresses were then used to determine which of the elements failed and which were overdesigned so that the crosssections and shapes of the materials could be refined.

DESIGN OPTIMIZATION AND COST ANALYSIS

During the second phase of the project the optimization group worked on the optimization of two systems on the CRV, the CRV/Booster interface and the propulsion system.

The optimization of the interface focused on defining the material used on the structure, the crosssection of the members in the structure, and the number of vertical members in the structure. The most important parameter to optimize was weight. The propulsion system optimization, sizing of fuel tanks and feedlines, was done by determining the ideal sizes and then looking for existing hardware.

During the second phase of the project, optimization focused on the overall justification of the CRV project as well as deciding which vehicle to go ahead with. Optimization groups from both the Winged and Biconic teams worked together, and examined reusable and expendable launch vehicles. The primary vehicles examined were Atlas Centaur, Shuttle C, both the Winged and Biconic CRVs, and increasing the shuttle's commitment to the Space Station. Criteria were cost per pound to orbit, reusability, reliability, and availability. Conclusions were that the CRV and, more specifically, the winged version, was the most viable option.

MODELING

The primary responsibility of the Modeling Group was to build models for physical testing of the vehicle. The testing group entered surface location coordinates into a CAD/CAM system and models were milled on a numerically controlled milling machine.

Two models were made for the testing of the vehicle. A wooden model was constructed for wind tunnel testing, and an aluminum model was used for water tunnel testing. The group also worked on constructing a display model for the ADP Summer Conference.

WIND TUNNEL TESTING

The Wind Tunnel Testing Group was responsible for developing and implementing the test plan. The group constructed and instrumented the setting and conducted the testing.

The primary purpose of the testing was to find the lift/drag ratio of the vehicle as well as various aerodynamic derivatives. Testing was conducted in the University of Minnesota's Aerospace Engineering Department subsonic, continuous flow tunnel. The test plan included running the model in the tunnel at two different velocities and at six different angles of attack (between 0° and 25°). The vehicle was also tested at three different sideslip angles.

WIND TUNNEL DATA ANALYSIS

The objective of the Wind Tunnel testing group was to calculate stability derivatives from data obtained from the wind tunnel testing group. The stability derivatives calculated included the lift-to-drag ratio, L/D ; lift curve slope, $C_{l\alpha}$; C_{ma} ; and weathercock stability, $C_{n\beta}$.

The results were compared with computed values from aerodynamics and stability studies performed during the design phase of the project. Table 9 gives a comparison between the tested values and computed values.

Table 9. Test Results

	Testing	Computed
L/D	5.846	5.96
$C_{l\alpha}$	0.1055	1.929
C_{ma}	-0.1158	-0.3968
$C_{n\beta}$	0.09071	0.07106

The two sets of values compare fairly well, particularly, the lift-to-drag ratio. The lack of correlation in the other values probably results from the very low speeds at which the tests were conducted.

WATER TUNNEL TESTING

The Water Tunnel Group was responsible for a qualitative analysis of the flow around the vehicle. Tests were conducted at the St. Anthony Falls Hydraulics Lab at the University of Minnesota. The tests were made at several different angles of attack, Reynolds numbers, and sideslip angles. The vehicle was pulled through a stationary water tank. The flow was examined to determine the effect of the winglets, strake, and the rest of the vehicle. From the tests no unusual effects were found. The flow behaved as expected; the angle of attack at stall was approximately 25°. This closely matches what was predicted by the Aerodynamics Group.

CONCLUSIONS

The Winged CRV met all the specifications and requirements that were set out for it. The conclusions of the design project were that the Winged CRV could easily provide the necessary cargo to supply Space Station *Freedom* with its logistics needs. The CRV also appears to be the most cost effective option available to accomplish this task.

153
P. 11

HIGH-LATITUDE COMMUNICATIONS SATELLITE (HILACS)

NAVAL POSTGRADUATE SCHOOL

N 91 - 18145

The Naval Postgraduate School in the AE 4871 Advanced Spacecraft Design course has designed a communications satellite (HILACS) that will provide a continuous UHF communications link between stations located north of the region covered by geosynchronous communications satellites. This area (above approximately 60° N) will be served via a relay net control station (NCS) located with access to both the HILACS and geosynchronous communications satellites. The communications payload will operate only for that portion of the orbit necessary to provide specified coverage. The satellite orbit is elliptic with perigee at 1204 km in the southern hemisphere and apogee at 14,930 km with 63.4° inclination. Analysis and design for each of the subsystems was done to the extent possible within the constraints of an 11-week quarter and the design and analysis tools available. Work was completed in orbital analysis, the reaction control subsystem (RCS), attitude control subsystem (ACS), electric power subsystem (EPS), telemetry, tracking, and control (TT&C), thermal control subsystem, and the structures subsystem. The design team consisted of 12 students. Additional support was provided by the Jet Propulsion Laboratory and the Naval Research Laboratory.

SPACECRAFT DESCRIPTION

The High-Latitude Communications Satellite (HILACS) will provide a continuous UHF communications link between stations located north of the region covered by geosynchronous communications satellites, i.e., the area above approximately 60° N latitude. HILACS will also provide a communications link to stations below 60° N via a relay net control station (NCS), which is located with access to both the HILACS and geosynchronous communications satellites. The communications payload will operate only for that portion of the orbit necessary to provide specified coverage.

The satellite orbit is elliptic with perigee at 1204 km in the southern hemisphere and apogee at 14,930 km. The orbit inclination is 63.4° to eliminate rotation of the line of apsides. The orbit period is 4.8 hr, during which each spacecraft will be operating approximately 1.6 hr. The complete constellation will consist of three spacecraft equally spaced in mean anomaly.

The reaction control subsystems (RCS) and the stationkeeping propulsion subsystem is a monopropellant hydrazine system. There are four 38-N thrusters for the initial apogee adjustment and twelve 2-N thrusters for the RCS and stationkeeping. The propellant is contained in four tanks with internal pressurant bladders.

The satellite is three-axis-stabilized by four reaction wheels with thrusters providing redundancy and reaction wheel desaturation. The spacecraft is nadir-pointing with antenna-pointing accuracy of $\pm 0.5^\circ$. The satellite rotates about its yaw axis so as to maintain the solar panel axis (roll axis) normal to the sun line, providing maximum solar power efficiency. The attitude control subsystem (ACS) will utilize four sun sensors, two Earth sensors, and a three-axis rate-sensing gyroscope. The orientation of the four reaction wheels provides redundant operation.

The electric power subsystem (EPS) is a single bus, fully regulated system with bus voltage of 28 V. The EPS consists of two solar array panels, a 16-cell, 12 amp-hour nickel-

hydrogen battery, power control circuitry, and a shunt resistor bank. The EPS provides 343 W at end-of-life (EOL) at aphelion with a 10% margin. The solar array is comprised of GaAs solar cells, selected for their superior radiation tolerance.

The telemetry, tracking, and control (TT&C) subsystem design provides for both autonomous operations and direct control by a midlatitude ground-control station. The NCS will also be able to perform some TT&C functions.

The thermal control subsystem is primarily a passive system, with radiators on the satellite faces mounting the solar array panels, which will always be oriented parallel with the sun line. The other surfaces of the spacecraft will be insulated to maintain internal temperatures within acceptable limits. The passive system is augmented by heaters for equipment/locations requiring unique treatment.

The primary spacecraft structural support is the central tube, which provides the load-bearing structure for the equipment panels and fuel tanks. The central tube is also designed to provide for the design loads resulting from stacking of three satellites for launch.

Launch and Orbit Sequence

Figure 1 shows the launch configuration. All three satellites will be launched simultaneously on a single Delta/STAR 48 launch vehicle. The launch will take place from the Kennedy Space Center, and will place the three satellites initially into a 15,729 km \times 1204 km orbit at the desired inclination (Fig. 2). The launch vehicle final stage will provide active control for stabilization for the three stacked spacecraft while in ascent, elliptical parking orbit, and prior to each spacecraft's separation. As each satellite is separated from the final stage it will be spinning about a stable axis, eliminating the need for additional stabilization during the sun/Earth acquisition phase. Again, attitude stability is provided by the final stage of the launch vehicle for the still attached spacecraft. In this initial

PAGE 152 INTENTIONALLY BLANK

PRECEDING PAGE BLANK NOT FILMED

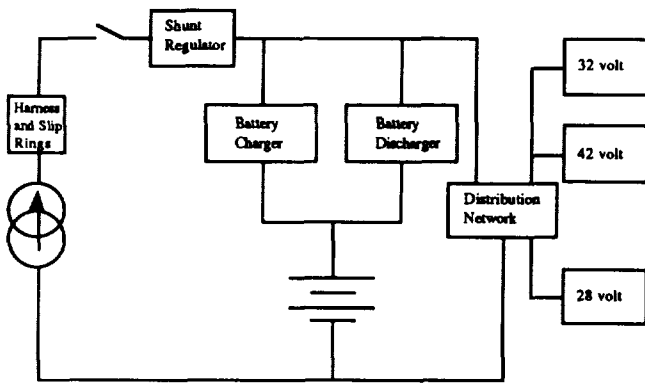


Fig. 1. Launch Configuration

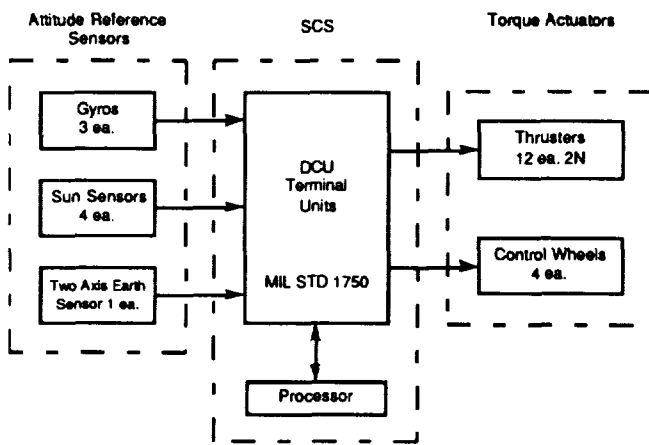


Fig. 2. Transfer Orbit Sequence

orbit, each spacecraft will acquire the sun and then the Earth to assume their Earth-pointing, three-axis stabilized configuration. The following sequence will then occur: solar arrays deploy, allowing electrical and thermal stability; the trailing satellite in the launch orbit will be reoriented and perform a perigee burn of 1.73 min using the four 38-N thrusters (-42.2 m/sec ΔV); orbit insertion of spacecraft into the 14,933 km \times 1204 km mission orbit. Since the mission orbit has a 4.8 hr period compared to the 5.0 hr period of the launch orbit, the second spacecraft will be aligned for insertion 8 orbits later, with the final spacecraft aligned following an additional 8 orbits. This sequence will put the entire plane of satellites in position 80 hr after the initial spacecraft is inserted into the mission orbit. This relatively long period between the insertion of each satellite also provides for the accurate determination of orbital parameters of the preceding spacecraft and adjustment on subsequent insertions as needed. The spacecraft on-orbit configuration is shown in Fig. 3.

Station Keeping/Orbit Perturbations

The time rate of change of inclination due to the gravitational effects of the Moon and the Sun were computed. In both cases, the rate is periodic in the right ascension of the orbit-

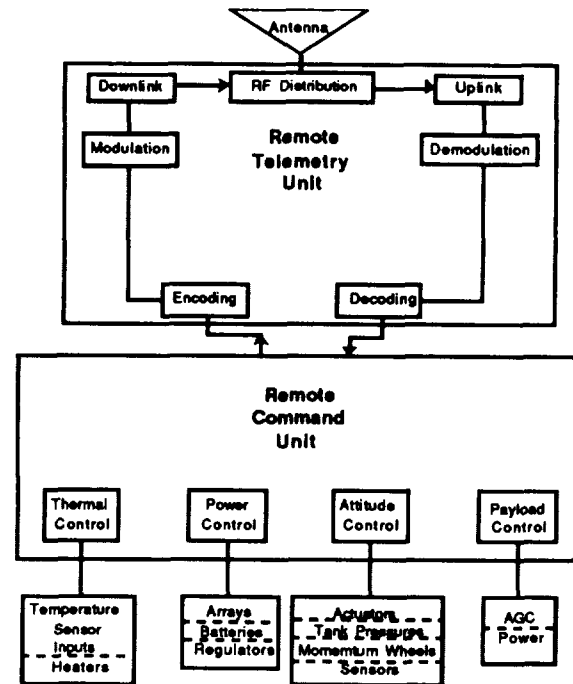


Fig. 3. On-Orbit Configuration

ascending node, which is decreasing at the daily rate of -0.425° . This causes the inclination rate to cycle completely in 847 days, with a maximum value of $0.1175^\circ/\text{yr}$ throughout the 3-year lifetime of the satellite. Since this represents the worst case alignment of the sun and the Moon during the mission, the actual values should be computed for these bodies based on their true positions for a given launch date recognizing that the resulting perturbation would actually be no larger than $0.1175^\circ/\text{yr}$. The error in inclination that would accumulate would only be that which represents the satellite life beyond one of the 847-day cycles. With this small change in inclination there is no need to budget propellant for station keeping due to inclination drift.

Argument of Perigee

Even though the satellites will be placed at the critical inclination, there will be drift of the argument of perigee due to higher-order effects. The long-period dynamic equations (normalizing the system to remove those short-period terms dependent only on mean anomaly) of the mission orbit were numerically integrated using a Runge-Kutta 4th-order fixed-step integrator. The analysis included perturbations to a Keplerian orbit due to the J₂, J₃, J₄, J₅ zonal harmonics. Although the mission orbit proves to be very stable in argument of perigee having drift through 360° with a period of 1100 yr, $0.33^\circ/\text{yr}$, the orbit is very sensitive to errors in inclination. A 0.1° error in inclination increases circulation of the argument to a rate of $1.44^\circ/\text{year}$. There is no need to budget propellant to correct for this small amount of drift for

the three-year lifetime. Propellant has been budgeted to correct drift of the argument of perigee through four years since the solar array has the capacity to provide power for more than the planned three-year satellite life. This station keeping will require a change in direction of the spacecraft velocity vector of 1.44° each year, representing a change in velocity of 133.7 m/sec. Using the attitude control thrusters, this will require a total of 81.8 kg (180 lbm) of propellant over 4 years. The current satellite design provides adequate capacity for this requirement as well as approximately 50 kg of additional propellant as margin.

The satellite is required to be Earth pointing and have solar array in direct view of the sun. The amount of yaw required each orbit is a function of the angle β between the solar orbit plane and the satellite orbit plane. This relationship is given in the following equation⁽¹⁾

$$\beta = A(B \sin \gamma \cos \Omega - \cos \gamma \sin \Omega) - C \sin \gamma$$

where β = orbit plane illumination angle; $A = \sin(i)$; i = orbit inclination = 63.435° ; $B = \cos(\epsilon)$; ϵ = solar orbit inclination = 23.44° ; $C = \cos(i) \sin(\epsilon)$; γ = sun central angle (measured ccw from vernal equinox to current position of sun relative to Earth); Ω = right ascension of the satellite orbit ascending node.

The angle between the solar array normal and the incident sunlight is given by the following equation⁽²⁾

$$\cos \theta = (\cos \alpha \cos \rho \sin \beta + \sin \alpha \cos \tau \cos \beta - \cos \alpha \sin \rho \sin \tau \cos \beta)$$

where $\cos \theta$ = angle between array normal and incident sunlight; α = array articulation angle between the array normal axis and the local horizontal, measured positive away from the Earth; ρ = spacecraft yaw angle measured ccw from inertial north; β = orbit plane illumination angle (see above); and τ = angle from solar noon, measured in the direction of the satellite orbit from the point on the orbit closest to the sun (local noon).

Solar Eclipse Periods

Batteries will be needed to provide power during solar eclipse. With a perigee of 1204 km, this will occur when orbit plane illumination angles are less than 57.3° ($\arcsin(\text{Re}/(\text{Re} + 650))$). Starting at zero for the orbit right ascension (Ω), and 180° for the sun central angle (γ), there will be 901 days out of the 1095 day planned lifetime during which the spacecraft will experience an eclipse of some duration. The resulting maximum solar eclipse period is 37.5 min during which the solar arrays are not illuminated. At 5 orbits per day, this specifies the need for batteries that can provide spacecraft bus power for up to 37.5 min through 4500 or more cycles.

SPACECRAFT CONFIGURATION

Equipment Layout

The primary considerations involved in developing the HILACS configuration were (a) to size the satellite for the Delta launch vehicle; (b) to shape the satellite and distribute masses to achieve the proper moment of inertia ratio for stability during a transfer orbit phase if required; (c) to use the east and west faces as equipment panels for thermal considerations since these faces will always be oriented parallel to the sun vector; and (d) to maintain as much modularity in the equipment layout as possible (see Figs. 4-7).

Four fuel tanks were used to achieve redundancy and to distribute the fuel mass. The basic shape of the satellite (1.9 m \times 1.3 m \times 0.7 m) was driven by the geometry of placing the four fuel tanks around the center tube within the Delta payload envelope. A fuel tank is mounted in each corner along the center line in height. The panels and component distribution are configured as shown in the figures for the spacecraft configuration.

Structures Subsystem

The spacecraft structural design is required to support the weight of three spacecraft under design loads for a Delta II (Table 1). The spacecraft employs identical designs for all three spacecraft, which forces an oversized structure for two of the three. Aluminum 6061-T6 was chosen for ease of machining and a favorable strength-to-weight ratio. The design supports loads through the central support assembly consisting of a frustum cone shell attached to the Delta II 3712B interface, a central cylindrical shell, and a similar frustum cone shell at the top of the spacecraft that attaches to the interface between each spacecraft.

Table 1. Design Constraints for Delta II Launch

Natural Frequencies	Lateral	Axial
Spacecraft	15 Hz	35 Hz
Equipment Panel	25 Hz	35 Hz
Solar Panel	35 Hz	-
Limit Loads		
Max. Lateral Condition	3.0 g	2.2 g
Max. Axial	-	6.0 g
Lateral Dynamic Loads	30 g	-
Factor of Safety = 1.5		
Margin of Safety = 10%		

A majority of the equipment mass is located on the east and west panels, which are designed to withstand 30 g and have a fundamental frequency above 25 Hz. The panels were designed to support 92.2 kg each of equipment mass. Load paths are provided to the central support assembly by means of panels attached to the north and south ends of the equipment panels. These support panels are also used to secure the four propellant tanks for axial loads. The panels are made of aluminum honeycomb material with core thickness 9.525 mm, and face thickness 0.912 mm. The same honeycomb

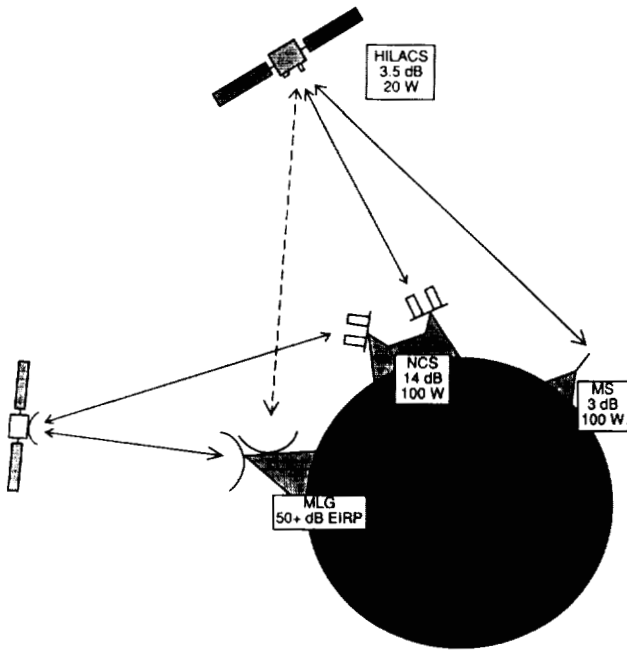


Fig. 4. East-Facing Panel

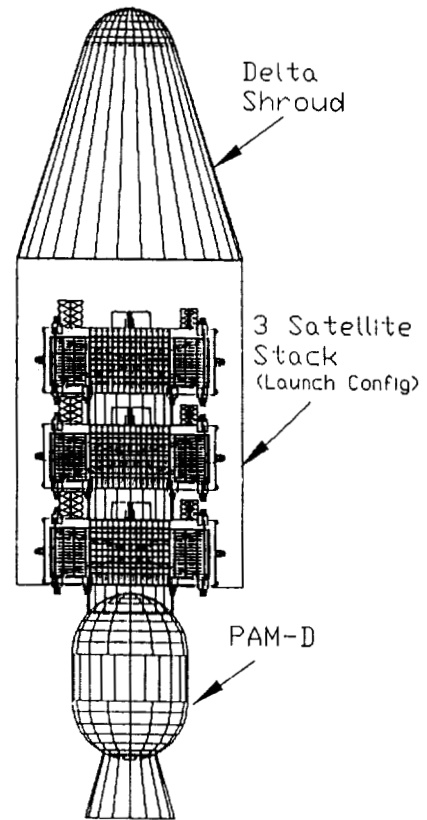


Fig. 5. View of Major Interior Elements

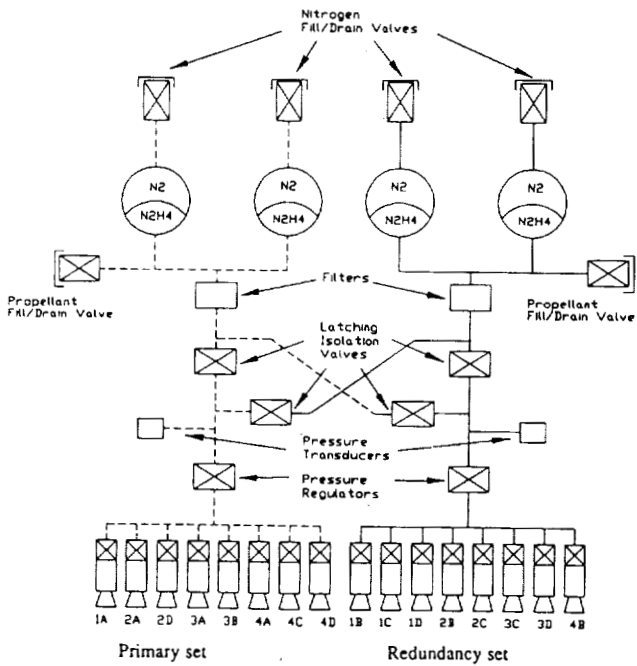


Fig. 6. Earth-Facing Panel

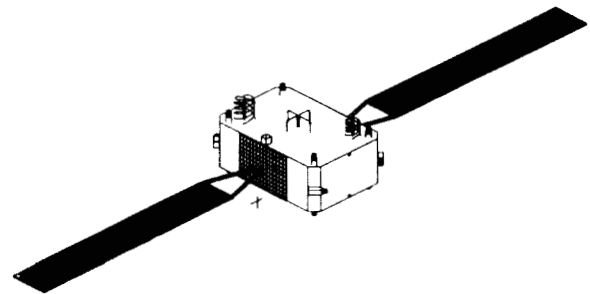


Fig. 7. West-Facing Panel

material is used for the equipment panels, propellant support panels, and spacecraft cover panels. Lateral load support for the propellant tanks is provided by struts attached to the top and bottom of the tanks and to the central support assembly.

The fundamental frequency estimated for the stacked configuration in lateral bending (6.22 Hz) was found to be well below the required 15 Hz for the Delta II launch. Because of this, the thickness values for the central support assembly were increased to raise the fundamental frequency for lateral bending. However, in the time of the course, the frequency issue was not resolved. The frequencies given from finite element analysis are shown in Table 2.

Table 2. Frequencies and Eigenvalues for Spacecraft

Mode	Frequency (cps)	Eigenvalue
1	42.71	7.2004D + 04
2	42.99	7.2946D + 04
3	68.02	1.8264D + 05
4	68.12	1.8318D + 05
5	80.69	2.5706D + 05
6	81.47	2.6201D + 05
7	103.99	4.2690D + 05
8	119.52	5.6391D + 05
9	129.11	6.5813D + 05
10	129.39	6.6095D + 05

Mass Summary (Tables 3-5)

Table 3. Mass Budget

Subsystem	Mass (kg)
TT&C	13.712
Payload	21.871
Attitude Control System	17.130
Electrical Power System	48.550
Reaction Control System	34.666
Thermal Control System	42.634
Structure	46.622
Dry Mass	225.185
Propellant	145.212
Wet Mass	370.397
Margin	41.520
Total Mass	411.917

Table 4. Propulsion Mass Breakdown

Item	Mass (kg)
Propellant (station keeping)	136.77
Propellant (ΔV change)	7.21
Propellant (desaturation)	1.00
Twelve 2-N Thrusters (12 \times 0.319 kg)	3.83
Four 38-N Thrusters (4 \times 0.735 kg)	2.94
Tanks (4 \times 5.897 kg)	23.59
Tubings, Valves, and Fittings	4.31
Nitrogen Pressurant	0.23
Total	179.88

Table 5. Structural Mass Summary

Structural Element	Mass (kg)
West Face Equipment Panel	0.918
East Face Equipment Panel	0.918
Lower Frustum of Cone	9.082
Cylindrical Support	8.192
Upper Frustum of Cone	5.221
(4) Propellant Support Panel	0.162
(8) Short Hollow Circular Strut	0.271
(8) Long Hollow Circular Strut	0.383
(4) Attachment Panel	0.086
North Face	0.624
South Face	0.624
Earth-Facing Panel	1.670
Anti-Earth-Facing Panel (with hole)	1.179
Structural Fasteners/Brackets	1.840
(2) Conical Support Ring	0.274
(2) Cylinder Support Ring	0.163
(4) Tank Ring	1.180
Support Structure Assembly Fittings	4.536
Total	46.622

Power Summary (Tables 6 and 7)

Table 6. Satellite Power Summary

Power Requirements	Power (W)
Payload	101.05
TT&C	11.22
EPS	20
ACS/RCS	70
Thermal Control	50
Wire Losses	7.05
Total Loads	259.32
Battery Charge Power	52.5
Total Sunlight Load	311.82
Ten Percent Margin	31.18
Total Design Power	343.00

Table 7. Eclipse Loads

Eclipse Power Requirements	Power (W)
EPS	20
ACS/RCS	70
Thermal	50
Total Eclipse Loads	140

PAYLOAD

System Description

The communications operations are shown in Fig. 8. The mission dictates a highly elliptic orbit at a 63.4° inclination. The ground stations are assumed to be located anywhere above 60° N latitude. To link these stations with a geosynchronous satellite, a central station acting as a hub must be located within the footprint of a geosynchronous satellite and HILACS. The location of this net control station (NCS), must be approximately 60° N latitude. A fourth site must be considered as well. This site is the source for data transmitted to the geosynchronous satellite and is assumed the ground control

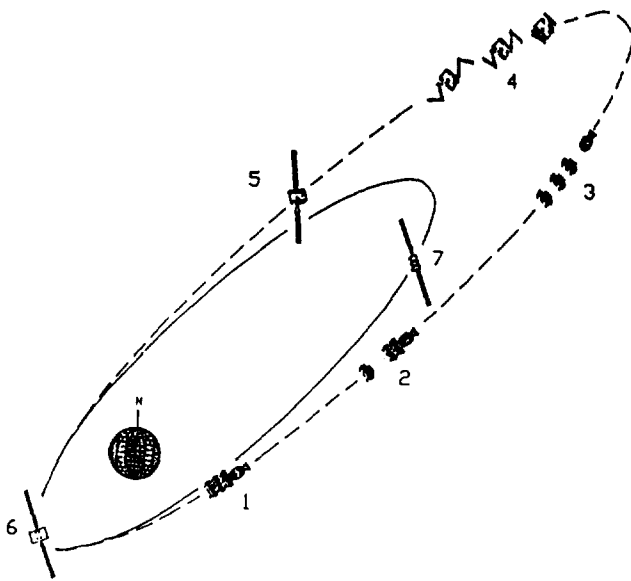


Fig. 8. Schematic of Communications Operations

site for its net of satellites including HILACS. It will be assumed that this station is located approximately 40° N (maximizing the number of locations on the Earth) and will be designated the midlatitude ground station (MLG).

The communication system operates at UHF with an uplink frequency of 350 MHz and a downlink frequency of 253 MHz. The link will operate at a data rate of 4800 bps using coherent BPSK modulation. A linear block error correction coding scheme is used resulting in a coded bit rate of 9600 bps.

The net operates in a hub-polling scheme in which the NCS controls access to the net in accordance with the needs of the users. This style of operation permits a variable number of users and maximizes the channel's data rate for this simplex link. The NCS polls each station prior to transmit to ensure it is ready to receive data and to find out whether they have any data to transmit. The NCS then relays data from the MLG (via a geosynchronous satellite) and from other stations on the net to the specific station. It then receives data from the station and readdresses these messages for further relay. It then repeats the process for each station on the link.

The NCS monitors satellite positions and ephemeris and predicts the position of the next ascending satellite. It establishes a link with the ascending satellite and performs a systems check prior to its activation. The NCS then determines the optimal altitude to introduce this satellite into the net and to release the descending satellite. It is conceivable that the NCS could operate two satellites simultaneously to ensure the most reliable communications throughout the region above 60° N latitude. The NCS also monitors the satellite health transmitted via the link.

The mobile ground stations, having a wide beamwidth and low-gain antennas, need only turn on their receivers to the default position and wait to be polled. Once polled, they establish link and move to an allocated slot for the remainder of their time on the link.

Design and Hardware

A bit-duration bandwidth product of 2.0, resulting in a bandwidth of 19.2 kHz is used as a compromise between minimizing the noise bandwidth and the intersymbol interference for this link. The MLG is assumed to be an established site with a high-gain helical antenna array with 25 dB of gain, transmitter with up to 1000 W (30 dBW) capability [so it will be optimally adjusted to maintain an EIRP ($P_t G_t$) just below saturation for the satellite system], and a receiver system with an effective temperature (T_e) of 150 K.

The NCS has two sets of helical arrays with 14 dB of gain. The station will require two of these antennas to provide a link with the active descending satellite and the ascending satellite in preparation for its activation. The effective noise temperature (T_e) at the receiver front end is computed to be 290 K for a noise figure of 3 dB relative to 290 K. It will be assumed that this station can transmit with a power of 100 W (20 dBW). The ground stations are assumed to be mobile, limiting their antenna to a crossed dipole design with a gain of 3 dB. The receivers' noise figure is 6 dB causing them to have T_e s of 865 K. The station's transmit power is also assumed to be 100 W (20 dBW). The satellite antennas have gains of 3.5 dB with a transmit power of 20 W (13 dBW). The receiver's noise figure is assumed to be 2 dB.

The system temperature is calculated after the antenna cable and at the receiver front end. The receiver noise figures relative to 290 K were listed earlier; the coaxial cable temperature is also assumed to be 290 K for each system. The antenna temperature (T_a) is dependent upon the gain of the antenna and the direction it is pointing. The MLG, with its relatively high-gain antenna, pointing away from the Earth has an assumed temperature of 150 K. Because the NCS and the mobile stations have low-gain antennas with a correspondingly wider field of view, their T_a is assumed to be approximately the temperature of the Earth, or 290 K. Since the satellite's antenna is pointing at the Earth, its T_a is also equal to 290 K.

The losses associated with the link equations are atmospheric loss, which is negligible for UHF, and free space loss, which is approximately 190 dB for the ranges in this link. Since this link is operated at a relatively low channel capacity, a relatively large bandwidth of twice the bit rate, or $2R_b$, is used minimizing the effect of intersymbol interference (ISI). Because the geometry will be changing due to the relative motion of the satellite and ground stations, the effect of fading will be time varying. Terrain effects can be minimized by optimizing the location of the ground station. To decrease the effect of the fading, which will appear in the form of a "burst error," a linear block code is used in the signal. This block code with a code rate of twice the data rate is effective when fades last for short periods of time. If long-term effects plague the ground station, modifications may be necessary such as elevating the ground plane to limit multipath, adding a second antenna to create spatial diversity, installing a directional, tracking antenna, or moving the ground station to a site less susceptible to the effects of multipath. Interference effects will be due to harmonics of military UHF voice communications.

These effects will be more transient than the fading effects, so the block coding should effectively minimize this interference effect.

For ideal stacking of the satellites on the launch vehicle, a maximum separation of 0.3 m was required. A resonant quadrifilar helix antenna was chosen since it is compact, has a wide beamwidth (approximately 110°), is simple in design, and has circular polarization. Analysis results in determining that quarter-turn, half-wavelength antennas with dimensions of approximately one-quarter wavelength for axial length and diameter are optimal for the dimensional constraints.

A crossed dipole antenna is used as a backup for the quad-helices and as the transmit and receive antenna for the TT&C system. It is composed of two orthogonal, center-fed, half-wavelength antennas⁽³⁾. The antenna is sized for the downlink frequency of 253 MHz, for a length of 0.593 m. It has a resonating circuit (a trap) that electrically shortens the antenna for the higher uplink frequency of 350 MHz or 0.429 m. The antenna is placed at 0.15 m above the ground plane to create the required radiation pattern⁽⁴⁾.

ELECTRICAL POWER SYSTEM DESIGN

The electrical power system (EPS) performs the functions of electrical power generation, storage, conditioning, and distribution for the on-orbit operation of the satellite. The majority of the generated power is consumed by the communications payload, with the balance used for the general operation of the spacecraft bus, attitude control, thermal control, TT&C, and the electrical power system itself. The communications payload system will operate only when the satellite ground track is above 50° N latitude. The TT&C system will operate only during sunlight periods of the cycle. The remaining systems will require power throughout the orbit.

The subsystem will be arranged as shown in Fig. 9. The shunt regulator will maintain the bus voltage at 28 V during sunlight periods and the battery charge/discharge unit is

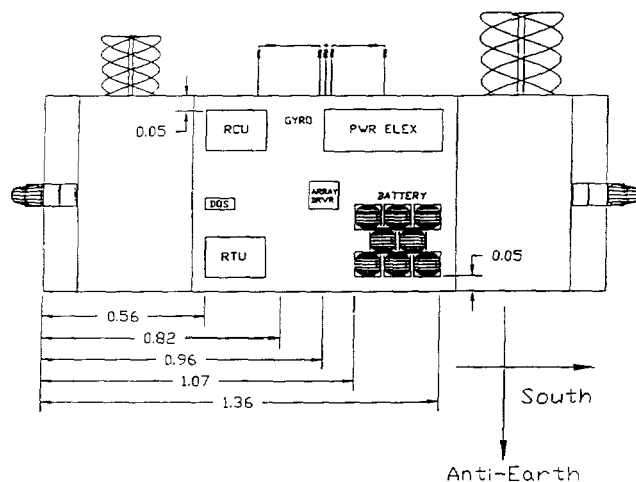


Fig. 9. Functional Block Diagram of EPS System

responsible for maintaining eclipse loads and charging the battery. The arrays are switchable to allow for single array operation during periods when the required power is less than one array can supply. Auxiliary voltage levels of 32 and 42 V for use by the propulsion and attitude control subsystems will be generated from the 28-V bus using DC-DC converters.

EPS Design and Hardware Description

The solar arrays maintain normal incidence to the sun by having two degrees of freedom in the system: (1) satellite rotation about the yaw axis, and (2) solar array rotation about the array longitudinal axis. The arrays will be split into two independent, switchable systems with one array switched off-line until bus voltage demands. The cells used in the array have the following capabilities under AM0 conditions:

- $I_{sc} = 232.0 \text{ mA}$
- $V_{oc} = 1014.0 \text{ mV}$
- $I_{mp} = 219.5 \text{ mA}$
- $V_{mp} = 876.0 \text{ mV}$
- $P_{mp} = 192.3 \text{ mW}$
- Efficiency = 17.83%

Radiation effects on the solar cells are extreme due to passage through the lower portion of the Van Allen belts and represent the primary limiting factor of the satellite lifetime. Radiation received by the cells was calculated using tabulated data prorated for the fraction of time spent in orbit altitudes and summing the amounts received from the panel front and back over the three-year period. The array substrate thicknesses and shielding effectiveness are listed in Table 8⁽⁵⁾.

Table 8. Array Substrate Radiation Effects

Structure	Thickness (cm)	Shield Effectiveness (mm)
Thermal Paint	0.0043	0.03
Al Facesheet	0.013	0.16
Core Adhesive	0.007	0.06
Al Core	1.6	0.19
Core Adhesive	0.007	0.06
Al Facesheet	0.013	0.16
Epoxy/Glass	0.01	0.08
RTV-118	0.007	0.03
Total Thickness	1.6613	0.77
Back Shield Thickness (in ml)		30.315

For an expected on-orbit life of three years, the total radiation received in one-MeV-equivalent electrons for front and back exposure is $5.14E + 15$ for voltage and power and $2.82E + 15$ for current. This equivalent radiation exposure results in degradation percentages for 12 ml liquid phase epitaxy (LPE) GaAs solar cells listed in Table 9. The radiation degradation experienced by 6-ml cells will be lower-resulting in higher EOL performance.

Table 9. Radiation Degradation Results

Cell Parameter	Final Parameter Percentages
V_{oc}	0.892
V_{mp}	0.86
I_{sc}	0.77
I_{mp}	0.768

An advantage of the GaAs cells over silicon cells is their stability at higher temperature. This stability becomes important as the array temperatures increase toward the end-of-life with decreasing array efficiencies. The design was iterated until the required EOL output power was achieved at an operating temperature consistent with the design array area. Worst case solar flux at aphelion with an array pointing error of 8.5° (0.15 rad) was assumed. The final design results are given in Table 10.

The power values for the satellite if launched at perihelion vice aphelion are a BOL power of 540 W and an EOL power of 382 W.

Table 10. Final Array Design

Cells in Series	44
Cells in Parallel	80
Total Number of Cells	3520
Total Array Area with Intercell Spacing	30,307.2 cm ²
Panel Dimensions (2.5 cm boundary on all sides)	0.487 m × 3.305 m × 1.74 cm
Array Mass	12.19 kg
Worst Case Operating Temperature	46.68°C
Minimum Eclipse Temperature	-117.88°C
Max. Power Output at 30.9 V	504 W
Minimum Power at EOL	357.53 W

Battery Design

The battery for eclipse power is a 12 amp-hour nickel-hydrogen battery manufactured by Eagle Picher. This battery is provided in a two-cell common pressure vessel (CPV) configuration. The battery voltage per CPV cell varies from 2.2 V to 3.2 V at full charge. For the bus configuration of a buck converter for constant current charge and a boost converter to maintain the line voltage, the number of CPV cells is limited to 8 for the 28-V bus. This gives a maximum battery voltage of 25.6 V and a minimum of 17.6 V.

The battery requirements are obtained from the eclipse load requirement of 140 W. With the boost converter efficiency of 85%, the actual power supplied by the battery during the eclipse period will be 164 W. The maximum eclipse period is 37 min of the 4-hr-48-min orbit. This gives a minimum recharge time of 4 hr 11 min. For the three-year projected mission lifetime, the satellite will experience a maximum of 4500 eclipse periods. Nickel-hydrogen batteries provide the highest capability of withstanding a large number of discharge cycles while still able to undergo large depths of discharge.

For a LEO satellite for which the charge and discharge cycles are numerous, the amount of energy that is removed from the battery must be replaced by an additional 10%. The charge rate chosen for this satellite is C/7. At this rate, the charging current is 1.7 A, and the maximum power required for charge,

including charger efficiencies, is 52.5 W. The time required for charging the battery after a discharge of 164 W at 17.6 V minimum for 37 min is determined by calculating the number of amp hours removed and adding 10%. For this design, 5.74 amp hours have been removed and will be replaced by 6.32 amp hours. Charging at 1.7 A yields a required charge time of 3.7 hr.

The power electronics control section of the power subsystem is responsible for maintaining the proper level of voltage for the satellite bus. The bus will be a fully regulated bus at 28 V. This regulation is accomplished by employing a shunt regulator for periods when the solar array is powering the spacecraft and by using a boost regulator for periods when the battery system is supplying the power. The bus voltage regulation accounts for a 1.3-V drop from the array slip ring and 0.8-V diode drops on each array and on each series string. A desired 30.9 V is then achieved at the array.

ATTITUDE CONTROL

The requirements for attitude dynamics and control (ADCS) are that the satellite be nadir pointing and three-axis stabilized. The communications system requires ±2° pointing accuracy. The ADCS system configuration (Fig. 10) is designed for a pointing accuracy of ±0.5°. A monopropellant propulsion system is used that affects despin and desaturation, and sun-sensing capability to maximize solar array efficiency. The system is designed to be single-fault tolerant.

The ADCS performs in two modes, transfer orbit and on-orbit. The satellite will be ejected from the Delta launch vehicle with between 30 and 100 rpm during transfer orbit. The system will then despin the satellite after ejection, acquire the sun with sun sensors, despin completely, and acquire the Earth. After despin, the solar cells will deploy, and the reaction wheels and gyros will activate. The ADCS will maintain three-axis stabilization during transfer orbit burn to maintain solar power. Once on orbit, the ADCS will reacquire the Earth with the Earth sensor, and the satellite will be oriented for full operation.

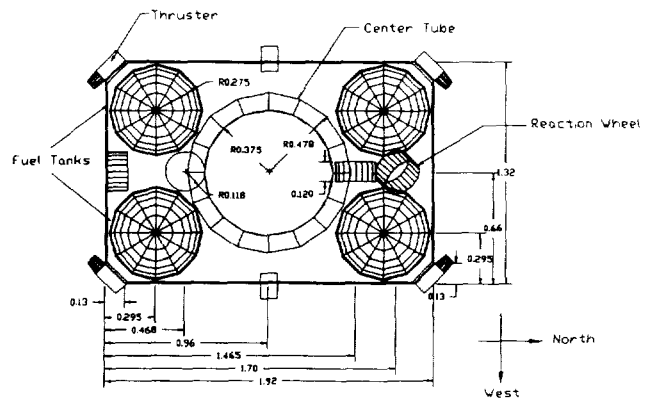


Fig. 10. ADCS Block Diagram

A four-reaction-wheel control actuator was chosen with three wheels along the roll, pitch, and yaw axis (initial spacecraft coordinates) and one wheel at a 45° angle for redundancy. The spacecraft will have additional redundancy for the control actuators provided by the thruster. The 2-N thrusters will be fired to desaturate the reaction wheels, despin the satellite and provide redundancy. The ADCS senses disturbance torques, due either to internally generated, solar pressure, or magnetic/gravitational torques, and provides the necessary attitude corrections. Internal torques are the dominant forces in wheel saturation. The internally generated torques arise from internal friction and instabilities. Thrusters will be able to desaturate the wheels quickly, with minimum pointing error.

The sensors for HILACS consist of an Earth (horizon) sensor, sun sensors, and rate gyros. The Earth sensor is a two-axis scanning conical-horizon sensor located near the antenna on the Earth face. Accuracy for a worst case pitch and roll error of $\pm 0.07^\circ$ at 1204 km can be achieved. Four two-axis sun sensors are mounted two each on the Earth and anti-Earth faces. The sun sensors provide yaw sensing with worst case error of $\pm 0.01^\circ$. One sun sensor will be able to give an accurate sun angle independent of the other sensor. This allows for nearly 4π steradians of coverage for the satellite. The redundant element is a three-gyro inertial-reference unit mounted inside the spacecraft. The outputs from the sensors are fed into the control computer for onboard processing. Commands are then sent to the actuators.

Components chosen for the ADCS are space qualified parts with pedigree characterized by previous flight performance. The sun sensors used are the coarse sun sensors flown on the INTELSAT VII satellite. The Earth sensors are manufactured by Barnes and well hardened for radiation tolerance. The rate measuring assembly was flown on INTELSAT V. The reaction wheels are made by Honeywell and were flown on DSCS III. The computer is a Mil Standard 1750 that is capable of providing autonomous control of the spacecraft.

TT&C

The highly elliptic orbit with inclination of 63.4° prevents continuous control of the satellite from the MLG station. The TT&C must, therefore, be capable of controlling the satellite operations for a significant part of its life (see Fig. 11). When the satellite is in line of sight with the MLG it must be able to downlink its telemetry as well as respond to commands. These commands include initial maneuvers into operating orbit, modifications to current functions, and modifications to onboard programs to adapt the satellite to changes in operating conditions. Since the satellite cannot be continuously controlled by ground for many of its orbits, it will have the ability to link to the NCS during its operating cycle. During the time that it is linked to the NCS it will be polled as any other mobile station (MS). Once polled, it will downlink telemetry data specific to its operations such as transponder status and power system information.

The RTU interfaces with the telemetry antenna and the remote command unit (RCU). It performs all the functions of

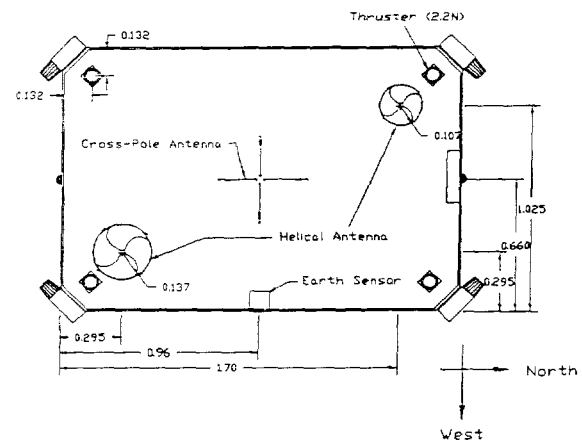


Fig. 11. TT&C Block Diagram

a transceiver including RF distribution to the single antenna, modulation, demodulation, and encoding/decoding of the telemetry data. The RTU uplink is at 350 MHz and its downlink is 253 MHz. The information is transmitted at a 1200-bps data rate, resulting in a 2400-bps transmission rate after encoding.

The RCU performs satellite control operations through the use of coded algorithms resident in memory. Dual microprocessors perform redundant operations based on these algorithms and their commands are correlated to remove the possibility of destabilizing operations due to single-event upsets (SEU). The RCU formats and relays telemetry to the RTU and acts on this telemetry in performing autonomous control of the satellite. The RCU also receives command signals from the RTU and performs these operations, which have priority over onboard generated commands.

The RTU uses a crossed-dipole hybrid antenna resonant at 350 MHz and 253 MHz. The RTU receives formatted commands from the RCU that are then encoded to modulation to the downlink frequency and transmitted. The RTU also demodulates and decodes uplinked telemetry commands to the acceptable format for the RCU. The RTU sends limited telemetry data to the NCS while performing transponder operations.

The RCU receives analog information from various sensors. It samples and performs pulse code modulation on the signals and then relays this data to the microprocessors for control functions.

The RCU commands heater operation based on temperature sensor data, and monitors voltages and currents to control the array drives, battery charging, solar array switching, and current regulation via the shunt regulator. The RCU also monitors the attitude control system and propulsion system operations by receiving data from the momentum wheels, Earth/sun sensors, thruster actuators, and propellant tank pressure sensors. The automatic gain control for the receiver and the transmit power of the transponder are monitored by the RCU.

PROPULSION SUBSYSTEM

The propulsion subsystem is a catalytic monopropellant hydrazine subsystem. The subsystem consists of four propellant

tanks with positive expulsion elastomeric diaphragms separating the pressurant from the propellant as shown in Fig. 12. The tanks are manifolded to two redundant sets of thrusters. The two sets of thrusters are interconnected and isolated by latching valves to provide redundancy for all on-orbit control functions.

After Delta II separation, the first of the three satellites will be slowed down to achieve the final orbit. Four 38-N thrusters and four 2-N thrusters will be fired at perigee to slow down the first satellite. The same procedure is repeated for each of the remaining two satellites for orbit insertion. Then only the 2-N thrusters will be used for roll, pitch, yaw desaturation, and despun.

The entire propulsion subsystem consists of four 38-N and twelve 2-N thrusters, four propellant/pressurant tanks made of titanium alloy, fill/drain valves for propellant and pressurant, latching isolation valves, filters, pressure regulators, pressure transducers, and lines made of titanium alloy.

The Delta II launch vehicle was chosen primarily because of its adaptability and cost. The Taurus and Atlas II launch vehicles will also satisfy the launch requirements.

The Delta II 7925 upper stage consists of the Morton Thiokol Star 48B solid rocket motor, a cylindrical payload attach fitting with clamp assembly and four separation springs, a spin table with bearing assembly, and motor separation system. The upper stage also contains a nutation control system (NCS).

The Delta II 3712B attach fitting is the interface between the upper-stage motor and the spacecraft. It supports the clamp assembly that attaches the spacecraft to the upper stage and allows the spacecraft to be released at separation. It mounts the four separation springs, two electrical disconnects, even sequencing system, upper stage telemetry, and the NCS.

THERMAL CONTROL

Passive thermal control techniques are used throughout the satellite. Two radiators made of optical solar reflector material, each $0.9 \times 0.7 \text{ m}^2$ are placed on the east and west faces of the

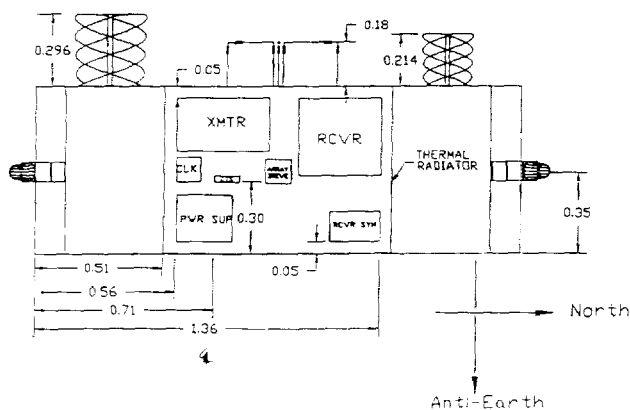


Fig. 12. Propulsion Subsystem

spacecraft. These faces are always edge on to the sun, thus receiving albedo and Earth radiated flux, but no solar flux.

All electronic modules are located on the equipment panels that are mounted back-to-back with the OSR to minimize conductive paths. The equipment panel is of aluminum honeycomb construction with aluminum heat sinks as required. No detailed thermal analysis of the substrates was attempted.

Multilayer Insulation (MLI)

MLI is used throughout to thermally isolate components. "Low" temperature applications use MLI with outside layers of aluminum kapton (spacecraft sides, etc.). "Hot" temperature locations use MLI with outside layers of titanium kapton (thrusters). A nominal thickness of 10 layers was used throughout. Temperature ranges for components are given in Table 11.

Table 11. Temperature Ranges for Components

Component	Operating Temp. (°C)
Electric power	
Control unit	-25/ + 30
Solar array	-160/ + 80
Shunt	-45/ + 60
Battery	0/ + 40
Payload	
Receiver electronics	-20/ + 45
Transmitter electronics	-15/ + 45
Antenna	-170/ + 90
Attitude control	
Earth/sun sensors	-25/ + 60
Angular rate assembly	-10/ + 60
Reaction wheels	-10/ + 55
Propulsion	
Tank	-5/ + 60
Valves	-5/ + 60
Thrusters	-5/ + 60

Two basic types of heaters are used: redundant and replacement. Redundant heaters are used as additional sources of thermal dissipation to maintain certain equipment (tanks, lines, valves, etc.) above minimum operating temperature. These consist of heat filament elements wound in layered material such as kapton. The other type of heater is the replacement heater, which is turned on when certain equipment (payload transmitter) is turned off in order to minimize thermal excursions. The former require additional power requirements whereas the latter do not. Thrusters have their own heaters for their catalytic beds. Heater control is either by enable/disable command from the ground, or once enabled, automatic control by thermistor to maintain temperatures within the allowed range.

Thermal design encompasses four phases of a satellite's life, namely prelaunch, launch, transfer orbit, and on-orbit. Only the on-orbit case was considered for this report. Analysis involved the two hot and cold steady-state cases. Internal sources include electronic equipment and soak-back from engine firings. External sources include solar, albedo, and Earth radiation. A thermal model was created identifying locations

of extreme temperatures for the satellite. Only a few iterations were done due to time constraints and availability of software tools.

ACKNOWLEDGMENTS

The project team would like to thank Prof. B. Agrawal for his guidance and support throughout this effort. We also want to thank Profs. R. Kolar, R. W. Adler, G. A. Myers, and A. Kraus, of the Naval Postgraduate School for their assistance. The following personnel from the Naval Research Laboratory also contributed to the success of the project: Mike Brown, Shannon Coffey, Chris Garner, Marv Levinson, and Tom Kawecki. Finally, we would like to thank Mr. J. D. Burke, our NASA center representative from the Jet Propulsion Laboratory (JPL), and Dr. J. H. Kwok also from JPL.

REFERENCES

1. *NASA Solar Cell Array Design Handbook*, Vol. I, equation 9.10-18, October, 1976.
2. *NASA Solar Cell Array Design Handbook*, Vol. I, equation 9.10-27, October, 1976.
3. John D. Kraus, *Antennas*, 2nd Ed., USA, McGraw-Hill, 1988.
4. Bruce S. Hale, *The ARRL Handbook for the Radio Amateur*, Sixty-sixth Ed., CT, American Radio Relay League, 1988.
5. JPL and NASA, *Solar Cell Array Design Handbook*, Volumes 1, p. 12.2-1. JPL Publication SP 43-38. October 1976.



165
p. 4

PROJECT WISH: THE EMERALD CITY

OHIO STATE UNIVERSITY

N91-18146

INTRODUCTION

When Project WISH (Wandering Interplanetary Space Harbor) was initiated as a multi-year project, several design requirements were specified. The space station must have a lifetime of at least 50 years, be autonomous and independent of Earth resources, be capable of traveling throughout the solar system within a maximum flight time of three years, and have a population of 500-1000 people. The purpose for the station is to provide a permanent home for space colonists and to serve as a service station for space missions.

In the process of designing the Emerald City, given the stated design requirements, the following systems were studied: Orbital Mechanics, Propulsion, Vehicle Dynamics and Control, Life Support, Communications, Support Systems, Power, Thermal Control, and Configuration. The travel times and necessary velocity changes to move throughout the solar system were determined in orbital studies. The Propulsion System Study then focused on the necessary impulse and thrust levels to provide the velocity changes derived by the Orbital Mechanics group. Vehicle Dynamics and Control considered the station's flexible dynamics and rigid attitude behavior. This analysis provides information for orbit selection, body shape and configuration, and propulsion requirements for station keeping in a nominal orbit. The Life Support System must satisfy all the physical needs of the inhabitants. It will provide the air, water, waste management, and food requirements for the crew and passengers. The Support Systems are communication, shuttles, and maintenance. The Communication system will provide the colonists with a means of talking to other colonists and sending valuable scientific data to earth. Shuttles will move people and supplies to and from the station. Repair and upkeep of the various systems on the station will be provided by the Maintenance Subsystem. All the electrical power used to run and maintain the station will be supplied by the Power System. The temperature ranges required by the people and equipment will be controlled by the Thermal Control System. Finally, everything is put together and an initial configuration of the station, the Emerald City, is described.

ORBITAL MECHANICS

Orbital mechanics determined whether the Emerald City could travel anywhere throughout the solar system within the mission requirement of three years. Using a trajectory optimization computer program obtained from NASA Lewis Research Center, velocity changes (ΔV s) for many orbital transfers were calculated. Adjusting for gravitational effects by roughly multiplying by a factor of two, the highest mission ΔV s were compared and checked against propulsion feasibilities.

From this, an outer limit was chosen to be the orbit of Saturn. This came from comparing the worst cases of planet to planet transfers. The ΔV from Saturn to Jupiter is about 100 km/sec, and from Uranus to Saturn is about 200 km/sec. The propulsion system cannot reach numbers of 200 km/sec, in general, for the anticipated mass of the ship.

Also, a nominal orbit was selected. A variety of orbital shapes and uses were examined. A circular orbit at 3.2 A.U. was chosen because it put the ship close to both the asteroid belt and Jupiter, so that raw materials for resupply and repair could be reached. It was located on the ecliptic plane to minimize z-directional velocity changes.

The nominal orbit will also serve as a place to do maintenance and to rest between missions. It will also be advantageous for communications, since colonies that need the ship will know its approximate location. There may be other reasons for having a nominal orbit and work continues in finding an optimized place for the ship to stay.

PROPULSION SYSTEM

The propulsion system of the Emerald City was one of the major subsystems that has been studied during the first year of Project WISH. It should also be one of the key areas of development in the project because, without an effective propulsion scheme, the Emerald City will be unable to accomplish its mission of supporting colonies on distant worlds and gathering data from previously inaccessible sources.

The propulsion system study for the Emerald City was divided into five phases. In the first phase, the mission requirements of Project WISH were broken down and studied in order to determine their effect on propulsion. Two influences on the selection of a propulsion unit were the three-year flight time and the mass of the station. These will determine the specific impulse that must be generated to accomplish the missions.

In the second phase, equations were developed that could relate how much of an effect the demands of the mission would have on the propulsion system. Equations relating the payload mass ratio, propellant mass ratio, and impulse to important design criteria such as the specific impulse and specific power were then used to compare the capabilities of different propulsion systems for given missions.

The third phase consisted of system comparisons for four propulsion concepts: chemical, electrical, nuclear, and antimatter. Only nuclear and antimatter were found to offer the combination of high thrust and high specific impulse that would be required for Project WISH.

In the fourth phase, an in-depth study of the two promising systems was performed. From this investigation, antimatter propulsion was chosen because of its higher thrust and specific impulse potential. Even though the nuclear systems are far more developed than antimatter, the thrust and specific impulse were simply too low for the more demanding missions.

The fifth phase was to carry out mission analysis using concepts specific to antimatter propulsion. One of the most important concepts is the mass ratio (initial to final mass) that will result in the minimum use of antimatter. This ratio was found to be 5:1 and has been used to determine the impulse and antimatter mass required for the mission of Project WISH.

VEHICLE DYNAMICS AND CONTROL

A system the size of the Emerald City is structurally too complex to be considered rigid. Therefore, some analysis of the flexibility effects was warranted. An initial longitudinal dynamic model was developed in order to perform parameter studies to determine crew station location and acceleration levels. Relationships among the structural parameters, propulsion system parameters, mass ratios, and propulsion time were established. Some model analysis is presented and some simulation is discussed.

A three dimensional lumped-mass model of the crew compartment was introduced in order to further study its in-plane and out-of-plane flexible dynamics. Out of these systems, some design constraints will be imposed. This study is in its infancy but is very important to the overall design.

Attitude dynamics covered analysis of the Emerald City as an uncontrolled, rotating, rigid body representing a gyroscopic system. By obtaining the configurations at which the space station may be stable, minimum control power will be used to maintain attitude stability. After determining the positions of equilibrium for a generic spinning body in a heliocentric orbit, a control system study is done in order to analyze the body disturbed from equilibrium.

By studying the nonlinear equations of motion, it is shown that the stability of the Emerald City is dependent on body shape, rate of spin, and orbital radius. These parameters translate into astronomical terms as structural configuration, artificial gravity, and parking orbit. Equilibrium analysis identified a unique orientation relative to the orbit plane for the Emerald City to insure non-diverging attitude.

The Emerald City, a spinning body in its steady-state configuration was then studied for control of small perturbations from its equilibrium conditions. The control system study used a linear quadratic regulator solution to estimate the amount of control power that might be needed for a number of configurations and artificial-g spin rates.

LIFE SUPPORT SYSTEM

The Environmental Control and Life Support System (ECLSS) for the Emerald City will be a nearly closed loop system. All life requirements will be met by the six integrated subsystems: Air Revitalization (ARS), Atmosphere Control (ACS), Temper-

ature and Humidity Control (THCS), Water Waste Management (WWMS), Solid Waste Management (SWMS), and Nutritional Supply (NSS).

The ARS is responsible for carbon dioxide reduction, oxygen generation, and air composition regulation. The ACS will circulate air and filter out or absorb any dust particles or harmful chemicals. THCS will remove humidity during the oxygen regeneration process and through the use of water separators. All equipment within the station will be maintained at proper working temperatures through the use of a water-based transport media heat rejection system. Due to the large volume of water used in the station per day, a WWMS must have an efficiency of recovery in excess of 99%. The WWMS for this ECLSS will use a thermopervaporation process that can achieve this efficiency. The SWMS is responsible for retrieving all reusable resources from both plant and human waste. The NSS will provide all the food requirements for the crew through the use of a hydroponics system.

COMMUNICATION SYSTEM

For the Project WISH scenario, a communication system capable of extremely high data rate and long range capability was required. To meet these design parameters, both microwave systems and laser systems were examined. Due to the substantial advantages in available bandwidth and diffraction limits, the laser system was chosen over the microwave system.

The smallest laser beam width that can be produced for use in communications is one microradian. From this, the transmitter antenna size was determined by performing a simple calculation involving wavelength.

For complete laser communication system characteristics, the range equation was used. This equation relates the range, transmitter power, antenna diameters, noise, and receiver power. Sample calculations for an optimal communication system showed that a 500 kW laser transmitter could easily send 12500 Mbits/sec of digital data across 12 A.U. of empty space using a 61-cm transmitter. The receiver antenna would require a diameter of at least 71.6 cm.

Problems with the communication system centered around having direct line of sight to the receiver and concern about the accuracy of assuming an "optimal" system. The first problem can be solved by incorporating relay stations in the form of satellites or planetary colonies. The second problem can be alleviated by reserving extra electric power for the system should factors such as modulation techniques, noise considerations, and beam capture prove to be more degrading to system performance than assumed in the optimal system.

POWER SYSTEM

A power budget was required to design a system that can produce the needed amount of electrical power. From the subsystems, the following preliminary budget estimates were obtained.

Estimated Power Budget:

1.	Propulsion (storage)	several	GWe
2.	Life Support	3	MWe
3.	Communications	10	MWe
4.	Dynamics and Control	several	GWe
5.	Heat Transfer	0.6	GWe
6.	Shuttle and Maint.	5	MWe
7.	Misc. Power	5	MWe

The parameters of fission and fusion reactors were reviewed to identify a power system that would provide the electrical power required by the Emerald City. Based on mass, specific power, and stability, the power source for the Emerald City will be a rotating particle bed reactor. However, if the power budget does increase to the tera-watt range, a fusion reactor would then be needed since these reactors have the potential of supplying an essentially inexhaustible source of energy. In this case, the considerations of mass and specific power will not be important compared to total power achieved.

THERMAL SYSTEM

The thermal control system of the Emerald City will use active and passive systems to control the temperature of the station. An active thermal control system employs radiators or a mass conversion system to dissipate waste thermal energy. On the other hand, a passive thermal control system uses paints, coatings, and insulations to control the station temperatures.

The Emerald City will use a radiator to control most of the waste heat produced by the power system and other subsystems. A radiator, similar to the Rotating Bubble Membrane Radiator (RBMR), was chosen. It differs from a RBMR in that it wraps around the cylinder of the station forming a torus rather than a sphere. The radiator will use nozzles to spray molten metal on a surrounding envelope or bubble. As the droplets hit the envelope, they radiate thermal energy. Since the bubble will be attached to the spinning section of the station, the centrifugal force will move the droplets to a trough where they are collected and recirculated.

This type of radiator was chosen over other types because of mass and meteoroid protection. The tiny droplets of fluid and the bubble will provide the needed surface area to dissipate the waste heat. Because the droplets are so tiny, they have very low mass and the mass of the total system is much lower compared to conventional heat pipes. In addition, meteoroid protection is provided by the bubble. If a meteoroid hits the radiator, it passes through the bubble and continues on its course. However, the bubble is made of a self-sealing material, so that any rips or tears repair themselves and there is little loss of the circulating fluid. This type of meteoroid protection provides additional mass savings because armoring, typical in convention systems, is not needed.

CONFIGURATION

To determine a feasible configuration, all of the subsystems had to be accommodated. Not only does each of the subsystems have to be in an appropriate place with respect to the others, but the entire unit has to meet the stability and control requirements. At this stage in development, the requirements are very general. This configuration is a place to start rather than a final design.

The systems that need to be integrated are the shuttle, communications, habitat, power, thermal control, and propulsion. These systems must be pieced together so that the stability requirements are met and construction is feasible.

The habitat must protect the crew from the hazards of space. These hazards include micrometeors, solar and cosmic radiation, and near-vacuum conditions. Besides being a protective shelter, the habitat must also accommodate agriculture and life support systems in an architecture that will avoid unnecessary stresses for its human occupants.

The propulsion system must be able to access the large amounts of hydrogen it will use as a working gas. The drive will emit large amounts of gamma rays, which are lethal to living organisms without shielding.

The design will be composed of various section roughly correlating to the subsystems. These sections include the habitat, power and propulsion, fuel tankage, radiator, de-spun platform, and the connecting pieces. This configuration is pictured in Fig. 1.

At this point in the project, the habitat is conceived as a torus with an outside diameter of 600 m and a tubular radius of 60 m to provide 0.8 g at a spin rate of 1.6 rpm. However, larger torus diameters such as 1850 m with 1-g at 1 rpm may have to be considered when all subsystem designs are to be integrated optimally for the overall system. If this structure is made of a medium grade aluminum alloy, then the minimum thickness of the shell will correspond to radiation shielding of 3000 kg/m², just over the 2800 kg/m² required for galactic radiation protection. Certainly, psychological considerations

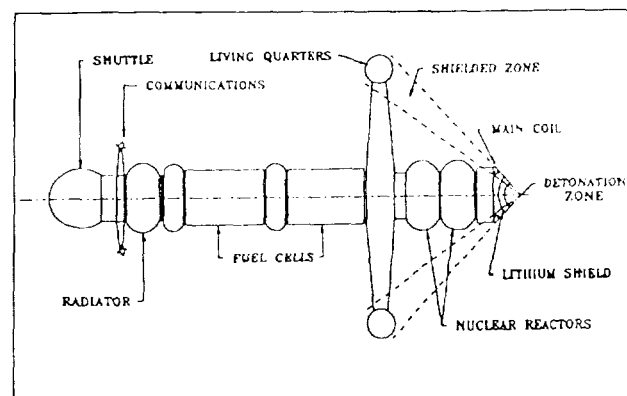


Fig. 1. Configuration

will play a large role in designing the interior architecture of the torus.

The propulsion system is placed on one end to transfer all of the thrust force through the axis of the spacecraft. Each set of fuel tanks will be connected to a main, load-carrying structure. Each fuel section will also have plumbing for the fuel, power transmission, heat pipes, and communication capabilities.

On the very end will be the radiator and the de-spun section containing the shuttle and the communications platform. The connections between the de-spun and spun sections are mechanical, power, fuel, and personnel transport. The connections are not complex and can be produced reliably.

The main support structure that runs through the fuel cells will connect directly to the radiator. This structure will also run through the nuclear reactor and connect to the propulsion system. Although the structure could be made out of any strong material, it may be advantageous to make it out of reinforced concrete. This material has a very large compressive strength to weight ratio.

The torus will be connected to the main structure with a large number of spokes, similar to a bicycle wheel. There will also be two pressurized tubes connecting the habitat with similar tubes in the main structure. These tubes will be the means of transportation between the habitat and the shuttles.

CONCLUSION

Hard work in researching and performing parametric studies to make the Emerald City of Project WISH realizable has taken place by starting from scratch and creating a sketch of a possible design for the space oasis. With such an undertaking, the more that is learned merely reveals how much more needs to be learned. Since Project WISH began, an initial decision on propulsion and power systems has been made, parameters for life support systems have been established, various subsystems have been analyzed, and necessary orbital restrictions have been determined. An initial configuration has been produced and work on detailed subsystem studies has begun. Project WISH will continue over the next two years, refining studies begun this year and incorporating additional aspects not yet considered.

P.5 169

DESIGN OF AN AUTONOMOUS LUNAR CONSTRUCTION UTILITY VEHICLE

N 91 - 18147

OLD DOMINION UNIVERSITY

In order to prepare a site for a manned lunar base, an autonomously operated construction vehicle is necessary. In this report, a Lunar Construction Utility Vehicle (LCUV), which uses interchangeable construction implements, has been designed conceptually. Some elements of the machine have been studied in greater detail and are the focus of this report. Design of an elastic loop track system has advanced to the testing stage. A standard coupling device has been designed to insure a proper connection between the different construction tools and the LCUV. Autonomous control of the track drive motors has been simulated successfully through the use of a joystick and computer interface. A study of hydrogen-oxygen fuel cells has produced estimates of reactant and product requirements and has identified multilayer insulation needs. Research on a 100-kW heat rejection system has determined that it is necessary to transport the radiator panel on a utility trailer. Extensive logistical support for a 720-hr use cycle requires further study.

INTRODUCTION

President George Bush has made human missions to the Moon and Mars national goals. He has directed the National Aeronautics and Space Administration to develop the necessary technologies and planning that will ultimately lead to permanent bases on the Moon and Mars. A lunar base will likely evolve first because of its relative closeness to Earth. Regardless of the evolution, initial construction of these bases will rely on autonomous and teleoperated construction vehicles to reduce hazards to humans.

A rugged and reliable construction vehicle capable of performing a range of construction tasks is needed. Old Dominion University has investigated a lunar construction utility vehicle during the last two years as part of the USRA program. This vehicle is designed to perform several construction tasks by interchanging tools autonomously. The evolution of the LCUV has proceeded from a conceptual design of the overall system to a more detailed design of the coupling system for interchangeable construction implements, power generation trade-off studies, a heat rejection system design, control system strategies, and tracked locomotion design refinements. The report that follows is a current overview of the LCUV design.

AUTONOMOUS COUPLING DESIGN

One of the major purposes of the LCUV is to prepare a lunar base site for construction. To complete this task, several different operations need to be performed. However, it is advantageous to use one type of vehicle for many construction activities so that the number of machines required on the Moon is minimized. It is therefore necessary to have a vehicle (the LCUV) that is able to interchange tools for specified functions. To do so, a standard coupling device is needed for proper connection between the tools and the LCUV.

Initially it was assumed the coupling would be attached to a robotic arm mounted on top of the LCUV. However, after

consideration of the dynamic and static loadings that will occur, it was determined that resulting reaction forces and torques would be too great for robotic arms using current technology. Thus the coupling system design that has evolved anticipates mounting implements on the front of the LCUV.

The coupling design is configured as a three-point system. The receiving end of the coupling is located on the tool implement. The receiving end consists basically of a shell-like triangular box. The face of the box is open to facilitate the insertion of the locking mechanism. The locking mechanism, which is located on the front of the LCUV, attaches to an implement by rotating three levers into the tool receiving box. Each of the three levers will be driven by worm gears. Worm gears were chosen over linkages because of their ability to move the arms through greater angles. The ability to rotate the arms through an angle greater than 180° is necessary to allow for large positioning tolerances. The coupling device will be able to lift a tool vertically by raising three linkages that attach the coupler to the LCUV. The coupling will be able to rotate about the fore-and-aft axis to make the coupling and tool movement more dexterous. After the three locking levers are inserted into the box, they rotate outward and around the outside of the box, grasping pins at the outermost corners of the implement's receiving box (see Fig. 1). As the levers swing around, they pull the implement up to the coupler that is attached to the LCUV. It is then locked into position. A picture of the coupling as it would look mounted on the LCUV is shown in Fig. 2.

Provisions are made for connecting cooling fluid, data links, and electrical power lines to the implement via connections within the implement box. An interface located centrally on the coupling device mates with a female socket on the implement receiving box. A feasible design can be derived from the quick-disconnect coupling as shown in Fig. 3⁽¹⁾. With further investigation, this design may be the start of an appropriate power connection lead.

C-3

14

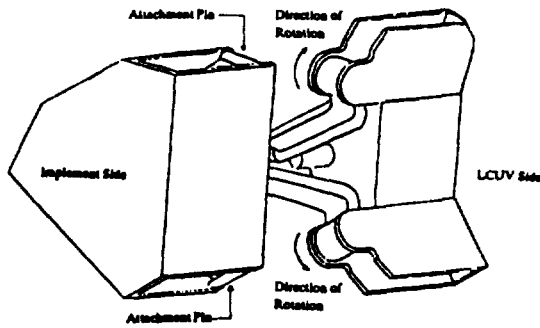


Fig. 1. Autonomous Coupling Device

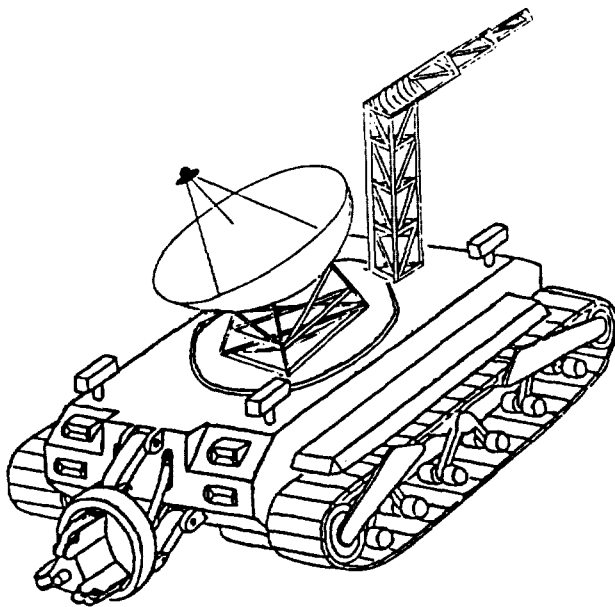


Fig. 2. LCUV with Coupling Mechanism

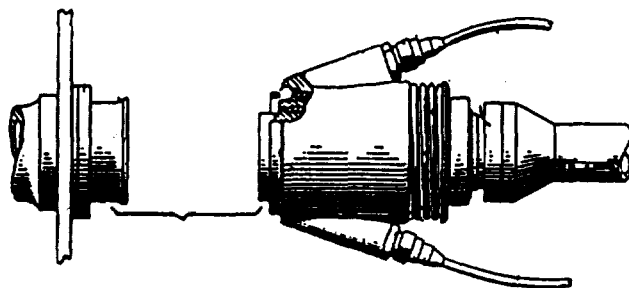


Fig. 3. Quick Disconnect Coupling

LOCOMOTION SYSTEM

The Elastic Loop Mobility System (ELMS) was originally designed by Lockheed Missiles and Space Company⁽²⁾ in the early 1970s for use on a Mars Explorer. The elastic loop system uses a continuous track that is designed to deflect when loaded. The advantages of the elastic loop system arise from its ability to deflect during dynamic loading and from its simple overall design. As the load on the track is increased, the deflection of the track results in greater contact area with the ground, thus increasing the traction of the LCUV. Probably the most important advantage of the ELMS is the built-in shock absorption provided by the track deflection. The track acts like a spring when it deflects, making the suspension system less complicated. The track design uses few moving parts, a prime objective for an unmanned vehicle in the harsh lunar environment. The configuration of the current design is shown in Fig. 4. Some design areas that needed to be addressed were loop design, telemetry box design, pivot plate construction, chassis connection, and testing procedures.

The construction of one loop, to test the mechanism of the ELMS, has been completed. Evaluation of this first loop revealed some problems that were not addressed in the initial stages of construction. Once the first loop has been debugged, a second loop can be constructed to take advantage of the modified plans. A preliminary conceptual design for the chassis connection has also been completed but work has not begun on the construction of this connection. Once construction of the connection system is completed the tracks can be attached to the LCUV chassis and testing can begin.

CONTROL SYSTEM

The research and development of an autonomous lunar construction utility vehicle requires a Locomotion Control System (LCS). The LCS is an integral part of the overall LCUV control system. The purpose of the LCS is to ensure that the drive motors are performing what the navigation control system requires, i.e., each motor rotates at the specified angular velocity.

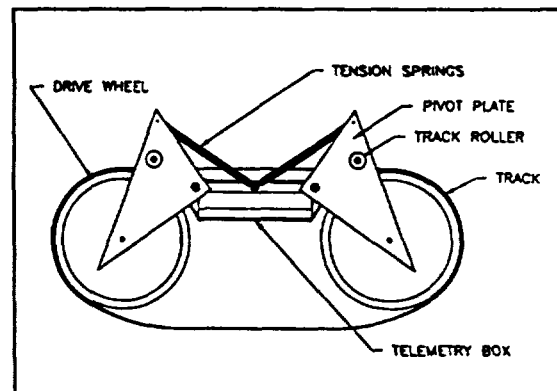


Fig. 4. Elastic Loop Track System

The LCS must operate under the lunar environmental extremes and maintain the vehicle's autonomy of operation as efficiently and reliably as possible. The task of developing this control system is explained in this section. Also, the areas of command input, control mode, output mode, and feedback measurement have been analyzed and modified. The project covers five major areas: system constraints, control system research, hardware requirements, software requirements, and problems and solutions.

The use of digital control was determined to be the best in accuracy, versatility, and cost effectiveness. A standard 286 personal computer interfaced with a Keithley 570 D/A and A/D conversion board was used as the primary control hardware. A visual representation of the control model is available in Fig. 5.

To simulate the autonomous operation of the drive motors, a joystick was used as the source of navigational information. The joystick information is scanned by the computer and the control software operates from this information in the following manner:

1. The joystick information is scanned by the computer.
2. This information is then translated into the desired angular velocity for each motor.
3. The desired angular velocity is then transferred to the Keithley board and sent to each respective motor in terms of voltage.
4. Once this voltage is applied to the motors, they rotate at a specific angular velocity, thus rotating the tachometers mounted on the drive shaft of each motor.
5. The rotation of each tachometer causes them to create a voltage.
6. This voltage is then input to the computer via the Keithley board.

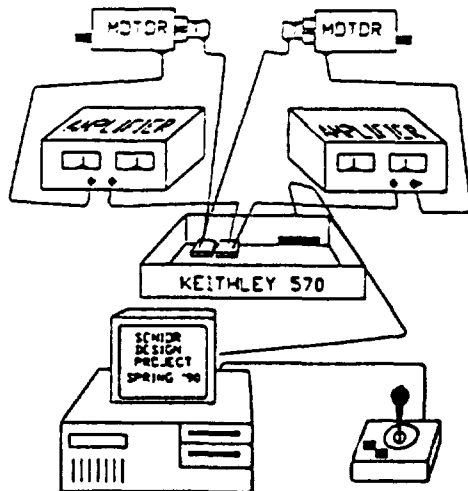


Fig. 5. Motor Controller Diagram

7. The relationship between angular velocity and voltage is linear. This relationship is described below (for a tachometer)

$$\omega = \frac{\text{Voltage}}{K_t}$$

$$K_t = 0.022$$

8. Now the computer has the values of the desired angular velocity and the actual angular velocity. The control error is then calculated. The error is the difference between these two values.

9. The control effort, U, is then determined from the error reading found by the computer. This effort is determined through the relationship

$$U = K_p \cdot \epsilon$$

$$\epsilon = (\omega_{\text{desired}} - \omega_{\text{actual}})$$

10. Step 3 is resumed by the control program until there is no error or until the computer receives new navigational information, in which event the processor would start with step 1.

POWER SUPPLY

The proposed LCUV requires a sustainable source of power for 720 hr of continuous operation. Analysis must be performed on the LCUV's requirements to determine the kind of power supply available using existing technology. When a power system for the LCUV is determined, the limitations and resources of the environment within which it operates must be taken into account. Energy from hydrogen-oxygen fuel cells was considered in the present study.

The fuel cell is a fairly simple electrochemical device. Its primary parts consist of an anode, a cathode, and an electrolyte⁽³⁾. The energy conversion occurs at the anode where the fuel (hydrogen) enters and is ionized. As this occurs, electrons are removed and travel across a load, which generates a current. The hydrogen ions then diffuse across the electrolyte. At the cathode, oxygen enters and combines with the hydrogen ions and the electrons that traverse the load. This recombination forms water, which is removed from the system. Each fuel cell can be placed in series to form a fuel cell stack which delivers a desired combined power output and voltage.

The design chosen for the reactant and product storage tanks consists of having the containers with several layers of radiation insulation mounted around their surfaces, as shown in Fig. 6. With this set-up, the outermost layer will absorb the radiation from the sun and will increase in temperature. The outer layer will radiate energy to the layer beneath it. In this process, every layer will transfer heat to the layer directly below it. This process continues until the heat reaches the surface of the tank. Therefore, by selecting the number of layers and the emissivity of the shielding material, heat transfer can be controlled. Some heat gain can be tolerated by allowing

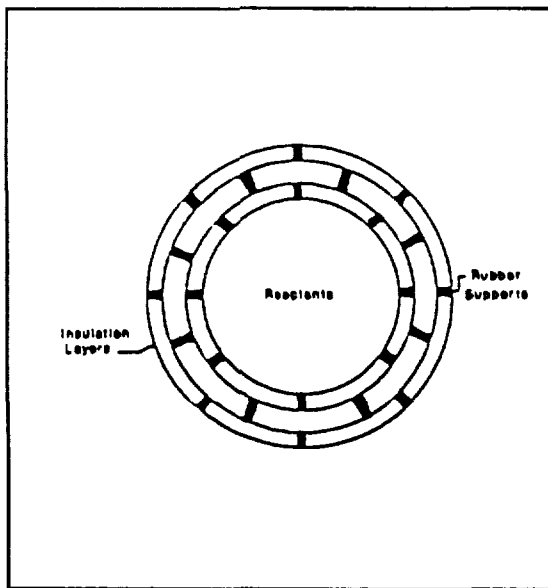


Fig. 6. Multi-Layer Insulation (Sectional View)

the liquid inside the tanks to boil. Specifically, a background or baseline rate of power generation becomes an insulation design constraint.

The insulation shield would be composed of highly polished aluminum film having low emissivity values. Low emissivity is required because resistances associated with the radiation shield become very large when emissivities are small. This would mean that lower heating rates are received by the cryogenic fluid⁽³⁾. Also, polished aluminum is currently available with high solar reflectance, good durability, and high flexibility.

HEAT REJECTION SYSTEM CARRIAGE

The only effective way to release heat in a lunar environment is by a radiator. To optimize the operation of the LCUV, a logistics trailer is designed to be used for housing the power supply and the heat rejection system. In order to supply coolant fluid and power to the LCUV from the carriage, a telescoping truss structure is incorporated to support the lines.

The heat rejection carriage was determined to be twice the size of the LCUV. This assumption of a 6 m by 6 m by 3-m deep vehicle was to allow for added stability.

Another major assumption was that when the radiator is fully deployed, its support platform will remain stationary in a predetermined location during a particular operation. This stationary configuration requires a collapsible truss type system to couple the radiator to the LCUV. This collapsible truss system will allow the LCUV to operate in a predetermined radius around the radiator and will also provide protection for the lines that carry the fluid and power to the radiator and its carriage.

The design of the truss selected for further consideration was a variation on a fire truck extension ladder. The ladder design possessed many of the qualities that are necessary to satisfy the design requirements that apply to the LCUV and heat-rejection unit.

For a 110-ft-long Emergency-One ladder at full extension and 0° inclination (horizontal) under an 800-lb point load at the free end, the maximum deflection was 18 in⁽⁵⁾. For application to the heat-rejection unit, distributed loads are more of a concern than point loads. The distributive loading consists of the structure's own weight, along with the weight of the fluid and power lines. Also for the LCUV, the extension unit will be supported at each end, thus deflection will occur in the center and not at the end. Due to this fact, greater extension lengths may be achieved and the extension unit can serve as an overhead crane.

HEAT REJECTION SYSTEM RADIATOR

The LCUV has a major problem with its ability to reject excess thermal energy. The solution to this problem is not an easy one; however, it is attainable through the use of a radiator. This radiator would need to be of considerable size and complexity in order to meet the heat rejection needs of the LCUV operating in the harsh lunar environment. The goal of this group has been to research the problems associated with the development of a daytime heat rejection unit that will meet the requirements of an LCUV working under the worst possible conditions on the lunar surface.

The research and design for the heat rejection unit has been carried out subject to limiting assumptions. The first assumption was that the LCUV should have the ability to perform heavy construction in the hottest lunar environment. This means that the heat rejection unit will be designed to operate at noon on the lunar equator and reject sufficient thermal energy to allow for productive LCUV operation.

The amount of thermal energy that realistically needs to be rejected is assumed to be 100 kW. This is a generous assumption and is intentionally large to prevent design shortfalls.

It is desired to operate the radiator at the lowest possible return temperature, which was determined to be approximately 340 K. This requires a radiator that is 50 ft (15 m) in length and 50 ft high. Operating the radiator much below this temperature is not feasible because it was determined that it was not possible to assume radiator surface temperatures below 340 K at lunar noon.

The radiator's large size will require it to be collapsible. It will be collapsed when the heat rejection unit is being transported along the lunar surface. If the radiator were not collapsible, considerable vibration problems would arise during transportation. The envisaged radiator can unfold in five hinged vertical panels. This will require pipe connections between the panels that can pivot to allow for this motion. The panels will be lifted from the top by one solid member that is hoisted by a cable and pulley system.

Two sides of the radiator will have vertical truss sections similar to the collapsible truss discussed for use between the LCUV and the heat rejection unit. When this truss is fully de-

ployed after being unloaded onto the lunar surface, the vertical trusses will extend upward to approximately 55 ft (17 m) and will remain fixed. These members will carry the radiator panel's load and will also act as guides for the radiator as it is raised and lowered.

A pulley system will be placed on top of each truss system that will be used to deploy the radiator. The cables will run from the panels up through the vertical trusses and into the carriage body where a hoist mechanism will either release or reel in the cable.

CONCLUSIONS

An autonomously operated 35-kW_e lunar construction utility vehicle (LCUV) design has been studied. The vehicle is intended for unmanned, heavy construction operations that will occur during the establishment of permanent lunar facilities and during many types of mining activities. The LCUV design study assumed continuous vehicle operation for 30 terrestrial days between refueling. Hydrogen-oxygen fuel cells were chosen as the 30-day power source, assuming a central solar-cell or nuclear power plant system is available to collect water (produced by the fuel cells) and to resupply the vehicle with liquid hydrogen and liquid oxygen.

A three-point coupling system was designed that could enable autonomous coupling of heavy construction implements without requiring precise positioning. An estimated mating tolerance of 10 cm in all directions appears feasible.

A continuous, elastic loop track design has progressed to the preliminary testing phase. Individual components have been subjected to preprototype design and testing as they have been developed. The track system continues to show desirable attributes for heavy construction operations. Interactions between the track system and control system teams produced the conclusion that only one drive motor should be used per

track, rather than the original assumption of two. A control system design has evolved that uses a joy stick to generate digital signals that can simulate the command stream that will occur during lunar operations. Successful control of two motors has been demonstrated.

The heat rejection system was designed under a worst-case scenario. It was determined that the LCUV could generate 100 kW of heat on the Moon's equator. A radiator that could reject this heat would have to be approximately 50 ft long by 50 ft high. A separate logistics trailer has been conceptualized to house the heat rejection unit because the radiator's large size would restrict the LCUV's capabilities. A truss type of structure was incorporated in the design to support the power and coolant lines between the trailer and the LCUV.

More research is needed in the power and heat rejection systems. The large size of the fuel tanks and radiator require an independent, self-contained unit to support the LCUV. One way to reduce the size would be to use a solar power system, operated only during lunar daytime, instead of continuous operation with fuel cells. This would reduce the overall weight of the vehicle by eliminating the large fuel tanks as well as remove the central power station requirement. However, a solar panel of nearly the same dimensions as the radiator would be needed. This alternate design needs further investigation.

REFERENCES

1. Paine, Thomas, Allan McDougal, and Douglas Davis. "Quick-Disconnect Coupling," US Patent No. 3,656,781, Apr. 18, 1972.
2. Trautwein, W. "Design, Fabrication, and Delivery of an Improved Single Elastic Loop Mobility System (ELMS)," Lockheed Missiles and Space Co., NASA Contractor Rpt, NASA-CR-123841, July 1972.
3. Parrish, M. A. "Fuel Cells—A Survey," *Materials in Engineering*, Vol. 2, No. 2, pp. 68-72, Dec. 1980.
4. Incropera, Frank P., and David P. Dewitt. *Fundamentals of Heat and Mass Transfer*, John Wiley and Sons, New York, 1985.
5. Aiken, Jeff, Project Engineer, Emergency-One Inc., Ocala, Fla., Personal Interview, March 30, 1990.

P. 7

PRELIMINARY SUBSYSTEM DESIGNS FOR THE ASSURED CREW RETURN VEHICLE (ACRV)

PENNSYLVANIA STATE UNIVERSITY N91-18148

Described herein is a series of design studies concerning the Assured Crew Return Vehicle (ACRV). Study topics, developed with the aid of NASA/Johnson Space Center's ACRV Program Office, include a braking and landing system for the ACRV, ACRV growth options, and the design impacts of the ACRV's role as a medical emergency vehicle. Four alternate designs are presented for the ACRV braking and landing system. Options presented include ballistic and lifting body reentries; the use of high-lift, high-payload aerodynamic decelerators, as well as conventional parachutes; landing systems designed for water landings, land landings, or both; and an aerial recovery system. All four design options presented combine some or all of the above attributes, and all meet performance requirements established by the ACRV Program Office. Two studies of ACRV growth options are also presented. Uses of the ACRV or a similarly designed vehicle in several roles for possible future space missions are discussed, along with the required changes to a basic ACRV to allow it to perform these missions optimally. The outcome of these studies is a set of recommendations to the ACRV Program Office describing the vehicle characteristics of the basic ACRV that lend themselves most readily to adaptation for use in other missions. Finally, the impacts on the design of the ACRV due to its role as a medical emergency vehicle were studied and are presented herein. The use of the ACRV in this manner will impact its shape, internal configuration, and equipment. This study included the design of a stretcher-like system to transport an ill or injured crewmember safely within the ACRV; a compilation of necessary medical equipment and the decisions on where and how to store it; and recommendations about internal and external vehicle characteristics that will ease the transport of the ill or injured crewmember and allow for swift and easy ingress/egress of the vehicle.

LIST OF ACRONYMS

ACLS	Air Cushion Landing System
ACRC	Assured Crew Return Capability
ACRV	Assured Crew Return Vehicle
CERV	Crew Emergency Rescue Vehicle (former designation for ACRV)
JSC	Johnson Space Center
MSFC	Marshall Space Flight Center
NSTS	National Space Transportation System (Space Shuttle)
SPRD	System Performance Requirements Document (JSC-31017)
SSF	Space Station <i>Freedom</i>
TPS	Thermal Protection System

INTRODUCTION

Since the beginning of the space program, NASA has been dedicated to the design philosophy of assured crew return capability (ACRC). This philosophy has meant that every manned program in NASA's history has had some method of returning the astronauts safely to Earth in the event of a failure of the primary return system. The commitment to ACRC continues in the design of Space Station *Freedom*. The primary return method for the space station's crew is the National Space Transportation System (NSTS), but NASA has foreseen the need for a dedicated, space-based return vehicle at *Freedom* to act as a "lifeboat" in at least three circumstances: (1) a catastrophic event occurs on the space station, the crew is forced to evacuate immediately, and the shuttle is not at *Freedom*; (2) there is a medical emergency that exceeds the capability of the space station's facilities, and the shuttle cannot

respond in time; and (3) the NSTS is forced to halt flights for any reason, meaning it is not available to resupply or transport the station's crew. NASA has begun the design of the Assured Crew Return Vehicle (ACRV) to meet these contingencies.

Through USRA's Advanced Design Program, Penn State became associated with the ACRV Program Office at Johnson Space Center in 1989. Prior to the 1989-90 academic year, several ACRV design topics were identified by Penn State faculty and ACRV Program Office personnel. During the past academic year, 49 seniors in Penn State's Aerospace Engineering Department were divided into 7 project groups and pursued 3 of these topics: the design of a braking and landing system for the ACRV, the investigation of ACRV growth options, and the investigation of the ACRV's role as a medical emergency vehicle and how this impacts its overall design. This report summarizes the results of these three studies.

ACRV BRAKING AND LANDING

For the purposes of this investigation, the braking and landing system of the ACRV was defined as those devices and vehicle characteristics that slow the vehicle upon atmospheric reentry and allow it to land safely on the Earth's surface. This did not necessarily include a propulsion system for a deorbit burn or an attitude control system, but some of the project groups felt it necessary to examine these systems also.

The braking and landing system of a reentry craft provides an interesting design challenge due to the large variety of alternatives available to the designers. It also involves some of the most important design decisions, since this system may impose size, shape, and weight constraints on the vehicle's other systems.

The project groups had certain restrictions imposed on their design by the ACRV System Performance Requirements Document (SPRD; JSC 31017). This document, written by the ACRV Program Office, was developed to provide guidelines for the ACRV design, but was intentionally left as vague as possible to allow for the maximum creativity on the part of the designers. Several of the more important requirements are

1. The fully constructed ACRV must be able to be launched in the shuttle payload bay.

2. In its role as a medical emergency vehicle, the ACRV system (including recovery forces) must be able to deliver the returning astronauts to a suitable medical care facility on the ground within 24 hours of the decision to leave the space station. Of this time, no more than six hours may be spent in transit. This allows for up to 18 hours to be spent on-orbit awaiting an appropriate reentry window.

3. Reentry accelerations must be limited to 4 g for all crewmembers. Impact accelerations and total impulses upon landing must be limited to 15 g and 3 g-sec for healthy crewmembers, and 10 g and 2 g-sec for an ill or injured crewmember.

4. The ACRV must be able to be operated by a deconditioned crew.

5. To maximize the reliability of the system, proven "off-the-shelf" hardware should be used whenever possible.

Four of the seven student project groups did preliminary and detailed designs of an ACRV braking and landing system, the first of which incorporates the use of a lifting body reentry shape, an expendable ablative heat shield, a parafoil gliding parachute, and an air cushion landing system (ACLS). The lifting body shape chosen was the M2-F3 configuration (see Fig. 1). This shape provides a number of advantages, including a high lift-to-drag ratio (approximately 1.2), high volumetric efficiency, and a tested prototype with a large database. The high L/D gives the vehicle a large crossrange, enabling it to

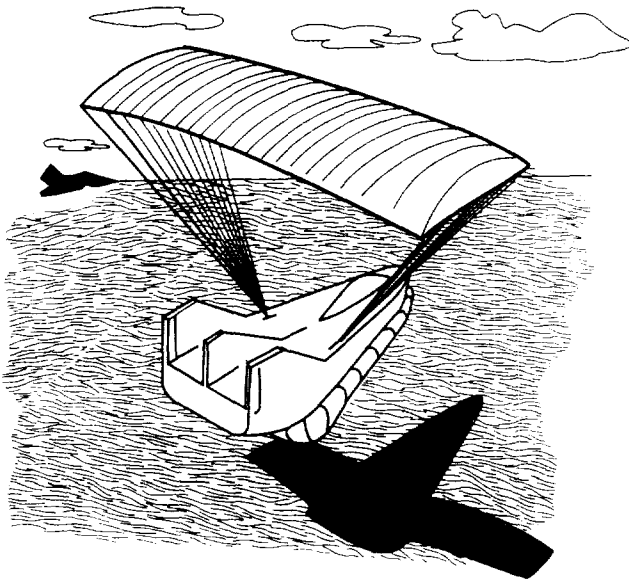


Fig. 1. An M2-F3 lifting body with air cushion landing system

reach the continental U.S. from a large percentage of its orbits, and also reduces the reentry g -forces to considerably below the limits set forth in the SPRD. The high volumetric efficiency means that even with the size constraints of the shuttle's payload bay, there will be sufficient room for up to eight astronauts (the crew complement of Freedom). The fact that the M2-F3 shape has been extensively tested in the past and has proven reliable also gives it a distinct advantage over other configurations because this reduces the amount of prelaunch flight testing required.

The chosen thermal protection system (TPS) is an expendable, ablative heat shield. The M2-F3 configuration experiences sufficiently high temperatures at its stagnation points to require the higher temperature resistance of an ablative TPS (as compared to ceramic tiles). Additionally, the curved lower surface of the M2-F3 shape, which experiences reentry temperatures low enough to allow the use of the reusable tiles, could not easily be integrated with the tiles' flat surfaces. For these reasons, an ablative TPS was chosen. The desired landing system, described below, required that the heat shield be detachable. While this limits the choice of landing sites, the advantages of the landing system were deemed sufficient to merit a detachable TPS.

A high-payload ram-air inflated parafoil was chosen as the preferred aerodynamic decelerator. High-payload parafoils are currently being researched by Pioneer Aerospace Corporation and NASA's Marshall Space Flight Center; flight tests have already been conducted with a 10,000-lb payload. These tests have proved successful, even when the parafoil suffered minor canopy and suspension-line damage. Further tests will increase the payload to 60,000 lb. The landing system chosen imposed a sink rate at landing of 12 ft/sec. This rate can be achieved for a vehicle weighing 12,500 lb (the estimated weight of the ACRV) by using a 300-ft parafoil wing span. Parafoils of this size have successfully been deployed by Pioneer and MSFC.

The chosen landing device is an air cushion landing system (ACLS). This system is composed of an inelastic cushion that is inflated from the underside of the ACRV. When inflated, it forms an isosceles triangular shape along the perimeter of the ACRV's lower surface, with the tip of the triangle at the front of the vehicle and the base at the rear. After inflation, air flows out of small holes in the lower surface of the cushion, creating a clearance height (typically 1 in). When in ground effect, this flow creates a higher pressure within the cushion cavity, supporting the vehicle and reducing friction between the trunk and the ground. This device has been tested and proven reliable on aircraft weighing up to 41,000 lb and over a large variety of landing surfaces (water, sand, concrete, grass, and rough land with small tree stumps).

Additionally, the ACLS has also proved able to perform satisfactorily with significant damage to the cushion (tests were performed by cutting a 3500-sq-in hole in the cushion surface).

The second proposed design differs from the first in several ways. First, it does not impose a vehicle shape on the ACRV, but instead suggests a heat-shield shape. The heat shield suggested is ablative, and its shape is the same as an aerobrake being studied at Johnson Space Center (JSC) as part of an Aeroassist Space Transfer Vehicle. This shape was chosen due

to its design for a low heating rate and integration into the shuttle's payload bay. Additionally, researchers at JSC have already performed experiments on the aerobrake, so its aerodynamic and heating effects have already been studied, and a future test flight on the shuttle is planned. Since a vehicle shape is not imposed on the ACRV, the shape can be optimized for the other onboard systems, providing a significant advantage. Using this shield, the ACRV will reenter using a hybrid lifting-ballistic trajectory similar to that used by the Apollo spacecraft. This means the crew will experience g-forces near but below the SPRD requirements mentioned above.

After reentry, a set of drogue parachutes is deployed to slow and stabilize the ACRV, after which the heat shield is separated from the vehicle proper (see Fig. 2). The shield is connected to the main body of the craft by four aluminum struts that are joined using pyrotechnic bolts. These allow the heat shield to be detached from the rest of the vehicle at the appropriate time. The heat shield has its own parachute, which is deployed after separation, allowing a more controlled descent into the ocean.

Once the heat shield has been separated, the ACRV deploys a high-payload parawing. This device works similarly to a hanglider, and allows the ACRV to have a slow, controlled

descent to a runway landing. Such a device has already been tested using a Mercury capsule for a payload. The parawing will be triangular, with a length of 86 m and a width of 75 m.

On approach to the runway, landing gear will be lowered from the bottom of the craft to allow for a conventional-type landing. The landing gear is similar to that used on a Learjet 24. A study was performed to show that parawing velocities and estimated vehicle weight would allow the use of such gear. To accommodate a deconditioned crew, the ACRV will have a control system that can be remotely piloted throughout its flight.

The third braking and landing proposal comprises a lifting-body design with a lift-to-drag ratio near 1.0, a thermal protection system, a set of conventional canopy chutes, and a water landing. Rather than employing a previously used shape for its vehicle, this design contains a new lifting body shape with an L/D near 1.0 (see Fig. 3). The aerodynamic characteristics of this shape are defined such that it will meet all SPRD requirements with regard to size and g-loading.

While a specific thermal protection system was not included in the design, the desired properties of the vehicle's TPS were specified as high specific heat, high emissivity, and low thermal conductivity. Given these desired characteristics, a TPS can be designed that is adequate for the ACRV's needs.

The lifting characteristics of the chosen shape for this design will slow the ACRV to approximately Mach 1.5 before any supplemental braking devices are used. After this velocity has been achieved, two conical ribbon drogue parachutes will be deployed to slow the ACRV to subsonic speeds; then, three 88-ft triconical canopy chutes are used to slow the vehicle for landing. This design calls for a water landing, which greatly simplifies the design and lowers the cost.

The fourth and final braking and landing proposal differs in several ways from the others. The proposed system is composed of a lifting body, ceramic tiles for thermal protection, conventional parachutes for further deceleration, and an aerial recovery. Additionally, this project group

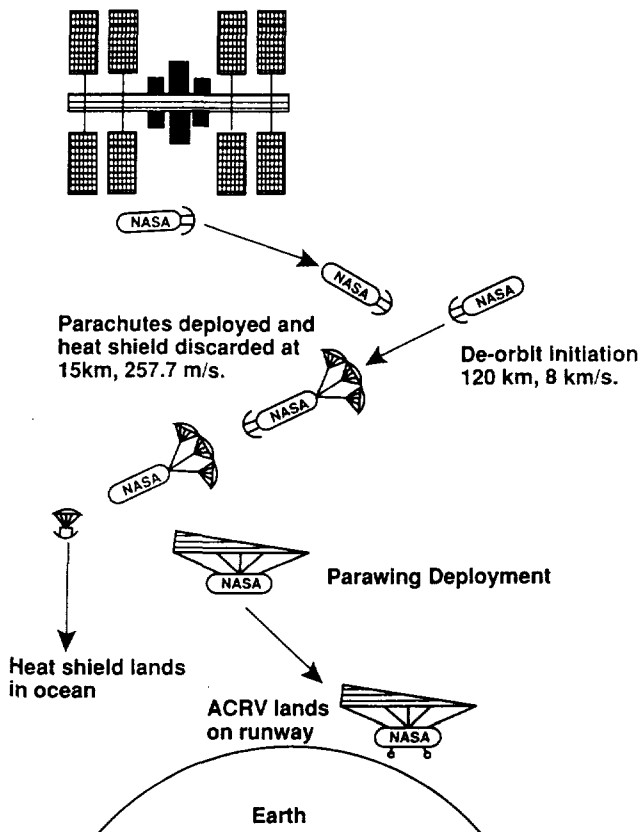
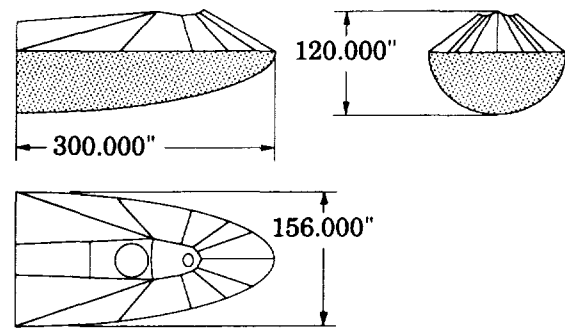


Fig. 2. A parawing and detachable heat shield configuration



Approximate Surface Area:	800 (ft ²)
Approximate Volume:	1500 (ft ³)
Predicted L/D:	1.0
Predicted Ballistic Coefficient:	55 to 75 (lb/ft ²)

Fig. 3. An alternative lifting body shape with L/D ≈ 1

investigated the use of a tether to aid in the deorbit maneuver. While a tether proved not to be sufficiently effective in reducing required propellant mass to justify the additional complexity, it did provide an interesting design challenge.

One difference between this proposal and the rest is that no shape was specified for the vehicle or its heat shield. Instead, a rather extensive analysis was performed to find an optimal lift-to-drag ratio given the desired g-loadings, crossrange, heating effects, time of flight, and velocity at 10 km altitude. The recommendation is for an L/D of 1.8. This L/D will result in g-loads less than 1.3 g, reentry heating rates and temperatures low enough to allow the use of shuttle tiles, a velocity below Mach 0.5 at 10 km altitude, sufficiently high crossrange to reach a large number of landing sites in the continental U.S., and a reentry flight time under the three-hour limit imposed by NASA.

After reaching 10 km altitude, the parachute system is deployed. The first chute is a ringslot drogue parachute. This will further slow and stabilize the vehicle for the deployment of the main chute, a ringsail parachute with a surface area of 2410 m². This combination of parachutes will allow the ACRV to achieve a velocity of less than 10 m/sec at 5 km altitude. This value was desired for the recovery system detailed below.

Rather than use a conventional landing, this design calls for an aerial recovery of the ACRV (see Fig. 4). This method has been used in the past to recover unmanned satellites, but a modified system should be able to safely recover and transport the ACRV before it reaches the ground. This design uses a modified Sikorsky CH-53E helicopter to retrieve the ACRV after it has slowed to a descent rate under 10 m/sec. Using an aerial recovery will greatly reduce the time needed to get the crew to land facilities without increasing the complexity of the ACRV itself. When performing a medical emergency mission, the ACRV could be flown directly to a hospital helipad and detached from the helicopter there, providing swift transport to medical facilities for an ill or injured crewmember.

ACRV GROWTH OPTIONS

Growth options are the future missions that an ACRV or a similar vehicle might undertake. A study of ACRV growth options includes investigating proposed or suggested future

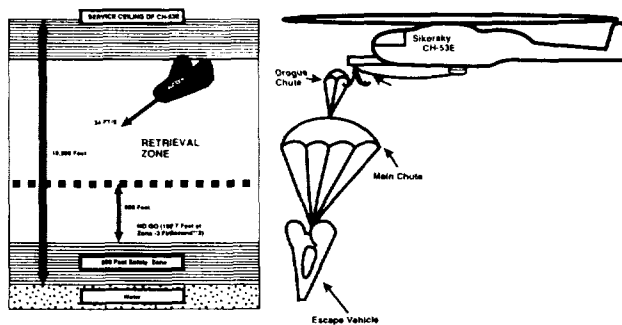


Fig. 4. Aerial recovery of the ACRV using a modified CH-53E helicopter

missions in space to determine whether an ACRV-based vehicle might be able to perform or contribute to these missions. Once this preliminary investigation is done, modifications to the ACRV enabling it to perform these missions optimally are determined, and these modifications are then used to recommend the vehicle characteristics of the basic ACRV that lend themselves most readily to adaptation for use in these future missions. A growth options study is essential for good design in this sort of circumstance, where planning now could mean significant cost reductions in the future due to the availability of a vehicle that can be easily modified to perform many tasks.

Two of the seven project groups participating in this program chose to examine growth options for the ACRV. The two groups were able to determine some fundamental characteristics of an ACRV by knowing about its mission and by examining the SPRD (for example, the structure of the ACRV must be designed to take the high stresses of an atmospheric reentry). From these characteristics, they were able to perform a growth options study. In addition, both groups examined a more detailed aspect of the ACRV growth options. A summary of the results of these two studies is presented below.

The first growth options study proposes the use of a modified ACRV to perform the following missions: shuttle and international space vehicle rescue; space station crew rotation; space station cargo transfer; satellite boosting; satellite servicing; and lunar operations. The report also investigates using a modified ACRV boosted on an expendable launch vehicle (ELV) to accomplish some of these missions. The shuttle and international space vehicle rescue would be a mission to rescue the crew of a disabled spacecraft in Earth orbit. The modified ACRV would leave *Freedom*, rendezvous with the spacecraft, transfer the crew to the ACRV, and transport them either back to *Freedom* or down to Earth's surface. The growing number of existing and proposed manned spacecraft make this a viable mission. Figure 5 shows the increasing levels of structural complexity and subsystem requirements for these missions.

Space station crew rotation and cargo transfer missions are fairly self-explanatory. Using the ACRV for these missions would help reduce the station's dependence on the shuttle. The satellite boosting and servicing missions are also fairly self-explanatory. Having an on-orbit vehicle to aid satellite operations in this manner could greatly extend the life of many existing satellites, significantly reducing replacement costs.

Lunar operations cover a variety of topics. The modified ACRV could be used as a "command module," similar to that used during Apollo missions, for transferring either crew or cargo to the Moon when U.S. space activities turn in that direction. It could also act as an ACRV for a Moon base, giving the crew of the base the same benefits as it does the space station's crew.

As part of a more detailed look into how these growth options might be executed, this project group examined the necessary hardware infrastructure to accomplish the above missions. The resulting options were (1) to build an individual, ACRV-based spacecraft to accomplish each mission; (2) to

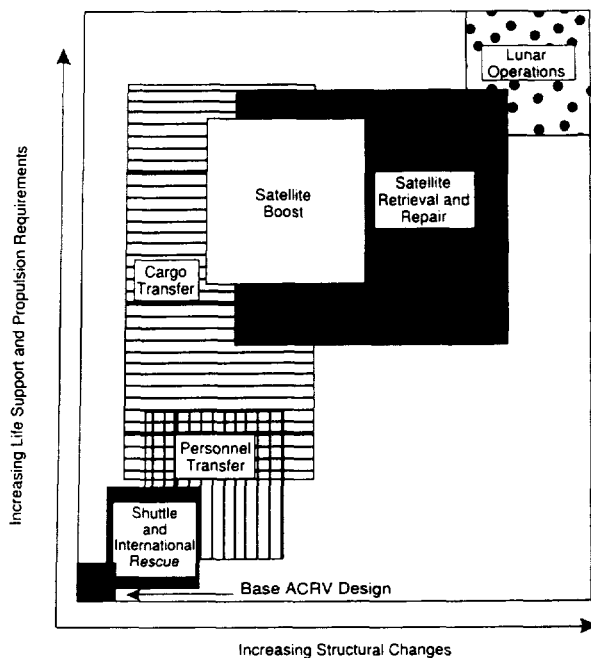


Fig. 5. Increasing structural and subsystem complexity for alternative ACRV missions

build multimission spacecraft, still ACRV-based, which could perform two or more of these missions; and (3) to build a modular ACRV. The recommendation was to use the third option—a modular ACRV (see Fig. 6). This means that the ACRV would be designed with the ability to be attached to modules that would enhance its systems. For instance, there might be a propulsion module that provides extra fuel and a larger thrust engine. When performing its mission of crew return, the ACRV would have no modules attached, but when traveling to geosynchronous orbit to repair a spacecraft, the propulsion module would be attached due to the increased fuel and thrust requirements of the mission.

A modular design would have several advantages over the other solutions. First, the basic ACRV, whose only mission is space station crew return, can be designed and built now, with a little modification to allow for expansion. As other missions

become desirable, modules can be designed and built to be compatible with the ACRV's systems. This allows the basic vehicle to remain relatively simple, with the added complexity coming in the form of modules, not revisions to the old design. This type of system also provides for future, unforeseen needs. If an unforeseen mission becomes necessary, a new module can be built to allow the ACRV to perform it. Also, a breakdown in a module may cause the ACRV to be unable to perform a specific mission, but it would not disable the entire vehicle. The modular design does have its disadvantages, though, such as the need for storage space at Freedom and the necessity of connecting and disconnecting all the modules needed for a given mission. It was felt, however, that the significant advantages of a modular design far outweigh the disadvantages.

To execute a modular design, several characteristics in the basic ACRV are desirable. First, a ballistic-type design more readily lends itself to exterior modifications and additions. For this reason, a ballistic ACRV is desirable. Second, a removable heat shield would allow large mass savings when the ACRV is performing missions not requiring atmospheric reentry. Additionally, an active life support system more readily lends itself to expansion, and will be required on some of the longer-duration missions mentioned above. While the basic crew return can be accomplished with a passive system, using an active system now will simplify changes in the future. It is also recommended that the power, life support, and computer systems be designed with the possibility of requiring external additions in the future. Some of the modules will augment these systems, so the current design must be done with expansion in mind. Lastly, the computer should have the ability to accommodate "black box" additions, where mission-specific commands can readily be added to the basic capabilities of the control mechanisms.

The second of the growth options studies had several similarities to the first. It also considered using a modified ACRV for the satellite servicing, lunar operations, space station crew and cargo transfers, and international rescue missions. In addition, this study examined the use of the ACRV as a portion of a Mars mission vehicle, and as an unmanned asteroid miner. On a Mars mission vehicle, the ACRV would serve much the same purpose as a command module. One proposed design for a manned Mars mission vehicle includes the use of a small

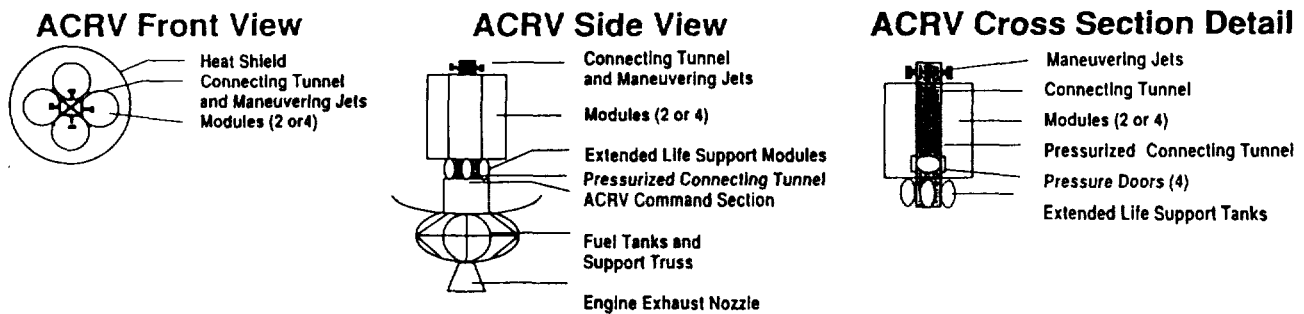


Fig. 6. A modular ACRV design for alternative missions

crew vehicle that would be detached from the main ship upon Earth approach and would decelerate using an aerobraking maneuver. A modified ACRV could perform well in this role. As an unmanned asteroid miner, the ACRV would fly to a near-Earth asteroid that was chosen for mining operations. There, it would load itself with ore mined from the asteroid and would return to Earth, reentering the atmosphere to deliver its cargo.

A quantitative approach was taken to assess the ability of an ACRV to perform each of the missions by estimating the deviation of the major subsystems from the norm of the crew return mission requirements. Using this method, the most compatible growth options were found to be the space station crew and cargo transfer missions, the international space vehicle rescue mission, and the lunar operations missions. Based upon this analysis, recommendations for the basic ACRV configuration include a ballistic shape, a detachable heat shield, and the ability of the subsystems to be readily expanded to handle long-duration missions. Figure 7 depicts the results of this study.

As part of a more detailed look into the growth option possibilities for the ACRV, this project group did a preliminary design of an ACRV-based lunar operations vehicle. The base ACRV is an Apollo-like command module, which is supplemented by a transfer vehicle and a landing platform. The crew remains in the command module for the entire mission. During trips between low Earth orbits and low lunar orbit, the unmanned transfer vehicle provides the propulsion for the command module. The landing platform stays in low lunar orbit. Following rendezvous of the command module/transfer module vehicle with the platform, the command module detaches from the transfer vehicle, attaches to the lander, and proceeds to the lunar surface. On the return trip, the lander transports the command module to lunar orbit, where it docks with the transfer vehicle, and then returns back to low Earth orbit, where it may either reenter Earth's atmosphere or dock with the space station. A preliminary design of the subsystems of the command module was also performed.

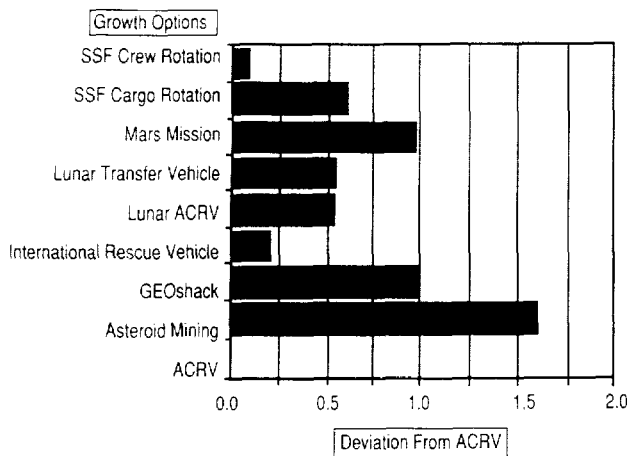


Fig. 7. Deviation of major subsystems from baseline ACRV design for alternative missions

ACRV MEDICAL MISSION

The medical mission of the ACRV arises if a space station crewmember becomes ill or injured requiring time-critical medical treatment beyond the capability of the space station's facilities, and the shuttle cannot respond in time to transport the crewmember. This mission places special restrictions on the ACRV design because, as stated earlier, the ACRV is required to perform this mission within 24 hours of the decision that the trip is necessary, and the portion of that time spent in transit cannot exceed 6 hours. Additionally, there are different impact impulse requirements for healthy and ill or injured crew. For the purpose of this analysis, it was determined that the ACRV itself met only the restrictions for healthy crewmembers, and that special equipment was necessary to protect the ill or injured occupant.

The assignment for the project group performing this study was to assess the impacts that the medical mission makes on the ACRV. This mission will affect the shape, internal configuration, and equipment of the entire vehicle. Additionally, the group was asked to design the actual stretcher-like system for transporting the crew member safely.

First, the decisions on what medical equipment to include were made by examining the current state of the art in medical emergency care and transportation. To this end, the group investigated the medical equipment currently used in ambulances and medical helicopter transports. This led to an extensive list of necessary medications and devices for proper care of an ill or injured individual. This list included special devices for dealing with the fluctuating gravity environment and devices that could transmit data on the ill or injured crew member to Mission Control for evaluation by the on-duty flight surgeon.

The next task was the design of the stretcher mechanism. It was decided that the optimal design would comprise two parts: a base and a sub-stretcher (see Fig. 8). The base is

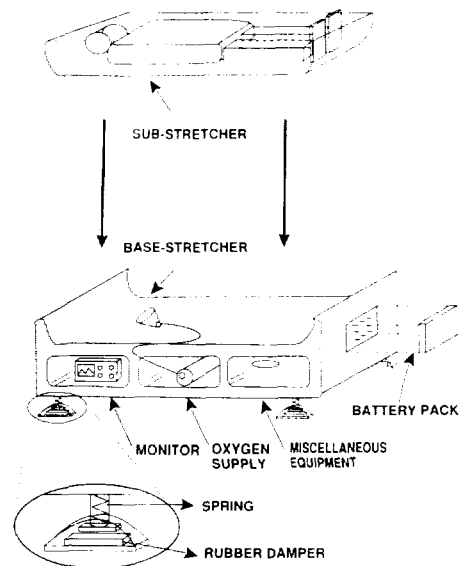


Fig. 8. Base and sub-stretcher for the medical mission

permanently mounted to the floor of the ACRV, and contains within it shock absorbing mechanisms to protect the patient during impact. Additionally, the base contains storage space for the above-mentioned equipment and pharmaceuticals. The substretcher consists of a device called a vacuum splint. This device is a bag filled with flexible beads. When inflated around a patient, the splint conforms to his or her shape. The air is subsequently evacuated, and the vacuum splint becomes rigid, immobilizing the patient's entire body. Most of the anterior side of the patient is still exposed, to allow for the connection of monitoring equipment and/or IV tubing. This procedure is performed on the space station, and the patient remains in the splint until reaching the ground-based medical facility. This allows easy, safe transport of the patient from the space station

to the ACRV, to the surface transport vehicle, and to the hospital. Onboard the ACRV, the vacuum splint is placed in the base, and a number of restraints will keep the splint firmly in place. The top of the base is concave to allow easy and secure positioning of the patient.

Several recommendations on the design of the rest of the vehicle were also made. Due to the low reentry forces, a gliding or lifting-body reentry shape was recommended. A runway or similar type of landing was also recommended due to the lower impact loads experienced by the crew in such a landing. Additionally, this study showed that a hatch should be installed on the top surface of the ACRV, and that this hatch should be large enough to allow an immobilized patient to be evacuated in a horizontal position.

P.4

REPLENISHABLE FOOD SUPPLY ON MARS

PRAIRIE VIEW A&M UNIVERSITY N91-18149

The design team's present objective is to design a facility which will provide an environment to grow plants on the surface of Mars for a continuous supply of food for a ten-member crew. The main focus of the project is the design of a greenhouse. Concentration of the current design effort is on the outer structure, internal layout, and construction methods. The project conducted by undergraduate students at Prairie View A&M University during Fall 1989 and Spring 1990 is presented in this report.

INTRODUCTION

Prairie View A&M University has been participating in the NASA/USRA Advanced Design Program since 1986 and is taking a lead in the design of a surface-based factory on Mars for the production of life-support products.

The Prairie View A&M University students conducted research on "Replenishable Food Supply on Mars" during Fall 1989 and Spring 1990. The names of the students and the report titles are given in Table 1.

Using simple systems of organic soil supported by native systems supplemented with nitrogen and other essential elements is being considered. Hydroponic growing is under investigation. (In hydroponics, plants are cultivated in water containing dissolved inorganic nutrients, rather than in soil.) The system will consist of a trough in which plants will be grown and a pumping system that will pump nutrient solution into the trough at regular intervals.

Table 1. Reports, 1989-1990.

Name	Title
<i>Fall 1989</i>	
Lisa Armstrong	Control Design for Vegetation on Mars
Raymond Hillis	Design of a Structural Facility on Mars
Garth Daley	Site Selection and Use of High Strength Plastics in Martian Facility
Raymond Hardemon	Layout for Greenhouse
Beverly Dixon	Crop Production Using Hydroponics on Mars
Victor Young	Construction Methods on Mars
Marcus Hines	Air Pressure and Temperature Control
Ogbonna Nnamdi	Food Production Techniques for Mars
Wazier Ajibola	Farming Methods on Mars
Terrance Jackson	Materials for Construction on Mars
<i>Spring 1990</i>	
Terrance Jackson	Construction Materials for Greenhouse on Mars
Charles Nickson	Radiation Shielding for Martian Structures
Noman Alyasin	Soil Investigation for Structural Foundation on Mars
Garth Daley	Soil Moving Device on Mars
Henry Ogoli	Construction of Structures on Mars Using Robots
Aaron Galloway	Mixing System for Hydroponic Cascade
Rosa Brice	Support Structure for a Hydroponic Cascade
Beverly Dixon	Storage Tank and Piping for a Hydroponic System on Mars
Toufic Nabbout	Greenhouse Conveyor Belt for Crop Rotation

DESIGN OF A MARTIAN GREENHOUSE

The greenhouse group's objective is to design a greenhouse pressurized at one atmosphere to allow for human habitation and plant growth. A dome-shaped greenhouse has been selected because of its ease of construction, sturdiness, and adaptability to a variety of construction materials (Fig. 1).

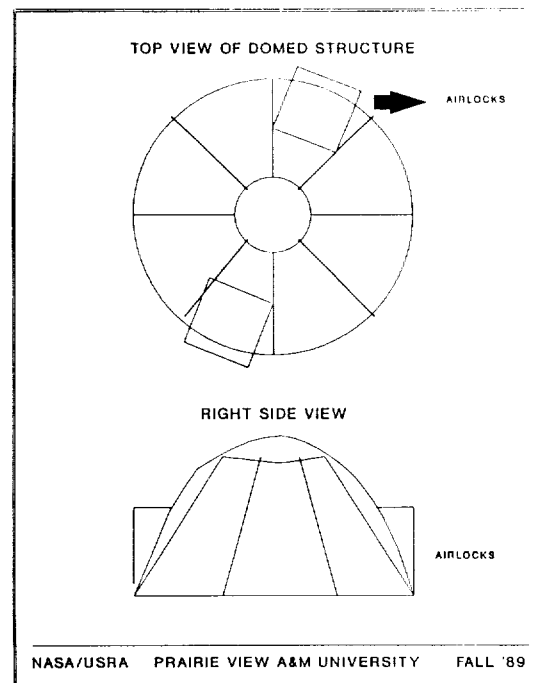


Fig. 1. Greenhouse Structure

FOOD PRODUCTION TECHNIQUES

A special focus of the present effort is to evaluate conventional and unconventional food production systems and plants, as well as to evaluate the potential for utilizing plants that are not currently employed in standard agronomic systems but appear to be useful if transferred to the martian surface environment.

SITE SELECTION

The site chosen for the greenhouse is the Tharsis plain on Mars. The site, located between latitudes 0° and 20° and longitudes 60° and 120° East, satisfies the criteria of soil stability, area for expansion, nonundulating terrain, and infrequent sandstorm activity.

MATERIALS OF CONSTRUCTION

Lightweight materials resistant to radiation with high strength and low deformability are criteria for construction materials for the greenhouse. The materials should also be able to withstand pressure differences between the interior and exterior surfaces of the facility.

Fiber reinforced plastics (FRPs) will be used. These are classified in five main groups: (1) nylons, which are long strands of amines and are formed by reacting a diacid with a diamine; (2) acetals, which are compounds formed from a diethyl aldehyde base, and polyester resins, which are produced by reacting phthalic acid with glycerol; (3) polycarbonates, which are formed from chains of carbonates; (4) blends of polystyrene, which are compounds formed from chains of styrene or phenylthylene and (5) polyphenylene oxides.

RADIATION SHIELDING

The objective is a feasible plan that will protect humans and plants from martian radiation.

Criteria

1. The shielding should protect humans and plants from radiation.
2. The shielding should be incorporated into the structure.

CONSTRUCTION METHODS

Another focus of this project was to investigate the methods that might be useful in the construction of the greenhouse. One method being investigated for lifting is via airbags. As illustrated in Fig. 2, a panel is laid across the airbag and air

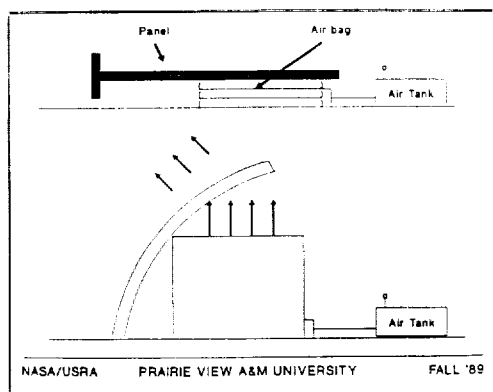


Fig. 2. Construction Method

is released from the tank into the bag. As the bag is inflated, the panel is slowly raised upward into position. Once the bag is filled, the air tank is removed and a support is added to hold the panel in place while it is being fixed into the foundation of the greenhouse. The procedure is repeated until all of the panels are in place.

Since there will be limited manpower during the building of the greenhouse and other habitation facilities on Mars, construction using robots is also being investigated. Robots will be able to perform such maneuvers as lifting, drilling, hammering, etc.

ENVIRONMENTAL CONTROL

The development of a conditioning system for soil-grown plants is one of the goals of the environmental controls group. Plants will be grown on a conveyor belt system, which will allow for easy rotation of crops into the room where they receive nutrients.

This system must have the capability to monitor and control environmental conditions in addition to light such as humidity, temperature, oxygen and carbon dioxide levels, pressure, water tension in the soil, and presence of metabolites or toxicants.

The entire system is composed of a recognition device, a computer, and an automated pumping system (Fig. 3). The recognition device was modeled after the bar coding technique currently used on packaged grocery items. The code for each crop will be different. The plant's moisture, nutrient, and light content requirements will be coded and stored by the computer.

Another element is a control feedback loop that will consist of the following components: a process, a measuring sensor and transducer, a controller, and a final control element with the associated electropneumatic converter and transmission lines for the process measurement and the control command signal.

The final stage of the conditioning process will be the activation of an automated pumping system to open the valves of the nutrient pipes. Once the crop has been properly

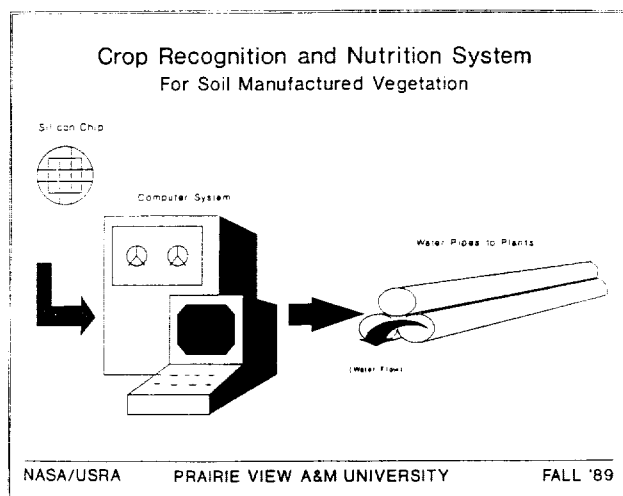


Fig. 3. Crop Recognition and Nutrition System

identified, the computer will instruct the valves of the pipes that contain the required nutrients to open, allowing the nutrients to flow into the water supply. The process will be timed according to individual crop needs. Once the nutrients have been dispersed, the system will shut itself off and prepare for the next crop on rotation.

SOIL INVESTIGATION FOR STRUCTURAL FOUNDATION

Subsoil explorations, referred to as site investigation, soil, and foundation investigation, are to determine the engineering properties and conditions of the soil and rock below the surface.

In order to provide economical construction and maintenance to minimize costly failures, overdesign, or overruns, a design based on an adequate foundation investigation and information about the nature of soil is necessary. The best way to obtain this information is to plan and execute a subsoil investigation to provide an efficient and cost-effective design.

The Planning Process

Soil explorations are conducted to verify information from surface examinations (see Fig. 4). The objectives of the soil investigation are: (1) to determine location, depth, thickness, and extent of each soil layer including description and classification of the soil and geology of the bedrock; (2) to determine the depth and characteristics of groundwater; (3) to determine the nature of soil and its stratification; (4) to obtain disturbed and undisturbed soil samples for visual identification and appropriate laboratory test; (5) to perform permeability tests, Van shear tests, and standard penetration tests; and (6) to make drainage calculations.

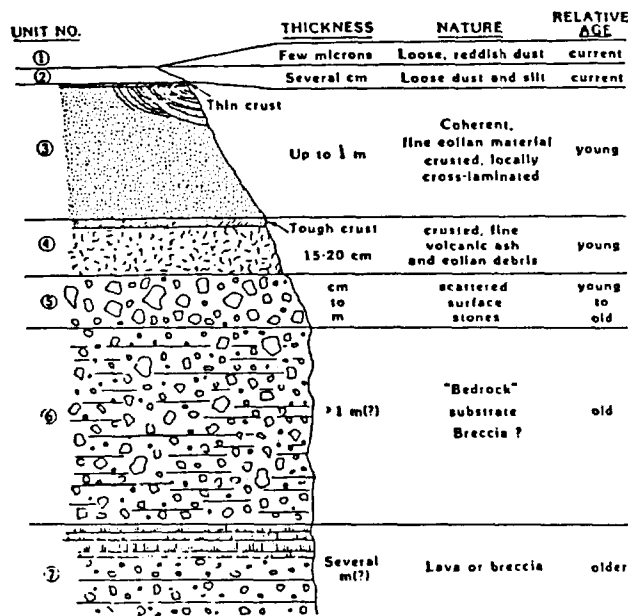


Fig. 4. Soil Profile of Mars

STORAGE TANK AND PIPING FOR HYDROPONIC SYSTEM ON MARS

The purpose of this design project is to investigate and analyze the design of a storage tank and the pipeline layout for a hydroponic system to be used on Mars. The objectives include: designing a piping system that will supply a flow of nutrients for each plant; designing a storage tank that can hold the volume needed; and selecting a pump that will provide adequate flow of water.

The project involves chemical, mechanical, and civil engineering. With the information and design analysis from all three, a functional hydroponic system can be designed for Mars.

Hydroponics

Hydroponics is a method of growing plants without soil. The plants are grown in an inert supporting medium, deriving their water and nutrients from a solution in the base of the container. The main benefit of the system is that the frequency of maintenance can be drastically reduced.

Plant Production

Plants can be grown in hydroculture from the earliest stage by germinating seeds or root cuttings in loose open materials like Perlite, frit, or cubes of polyurethane foam. The rooted cuttings are then placed into special plastic pots that have slitted or mesh sides to allow for the circulation of the hydroculture nutrient solution.

After planting, the pots are usually placed in raised troughs assembled from precast concrete units and lined with polyethylene sheets. The troughs contain about 50 mm of water circulated by pumps to aerate and mix the nutrient solution, as well as to control the water level.

The development of roots submerged in the nutrient solution is restricted by the low solubility of oxygen (8 ppm, by weight). Research has shown that growth is optimized at twice this level, which demonstrates the advantage of aerating the system. Jetting the circulated nutrient solution back into the production troughs can stimulate root growth in some species by up to 20%. Such an expensive procedure is not always necessary, as root development in many species is sufficiently rapid without the benefits of aerated water.

Hydroponic Systems

With large hydroponic systems, it is often necessary to pump the nutrient solution to different stories within a building. Pumps to achieve the necessary lift with a gravity cascade system for return may be used. Submersible pumps are proving to be of considerable advantage because of their ease of installation.

The time required to fill each trough completely will be one hour. The system is designed to continue to pump water in order to keep oxygen for the plants; however, the water level will remain stable.

The materials used for the design will be aluminum for the vessel pump, and PVC plastic for the pipe. These materials will allow for easy transportation because they are light and corrosion-resistant.

There is little chance of overflow because the design incorporates spillways, glove valves, and computer control (Fig. 5).

After six weeks, the system will be completely turned off for cleaning and restarted with fresh water as well as new soil medium.

This design will provide an efficient supply of food on Mars.

RECOMMENDATIONS FOR FUTURE RESEARCH

Plans for future research are the conceptual development and detailed design of all aspects of the colonization of Mars including the following:

1. Fish and poultry farm on Mars for life support
2. Mining of ores
3. Manufacturing of drilling tools
4. Use of robots for farming
5. Power generation system
6. Manufacturing of motors, batteries, and computers

ACKNOWLEDGMENTS

The College of Engineering and Architecture at Prairie View A&M University has been participating in the NASA/USRA Advanced Design Program since 1986. Recently, Prairie View was selected for continued participation in the program for the academic years 1989 through 1992. The university is also coordinating design activities through the new Texas Space Grant Consortium. The program, which is an interdisciplinary effort, involves students and faculty throughout the College of Engineering and Architecture. The students are actively involved in design projects related to space under the supervision of Dr. K.M.A. Rahman, Chairman of the Civil Engineering Department, Dr. R. Radha, Assistant Professor of the Civil Engineering Department, Dr. Ken Walter, Associate Professor of the Chemical Engineering Department, and graduate engineering student, Danette Willis-Reynolds.

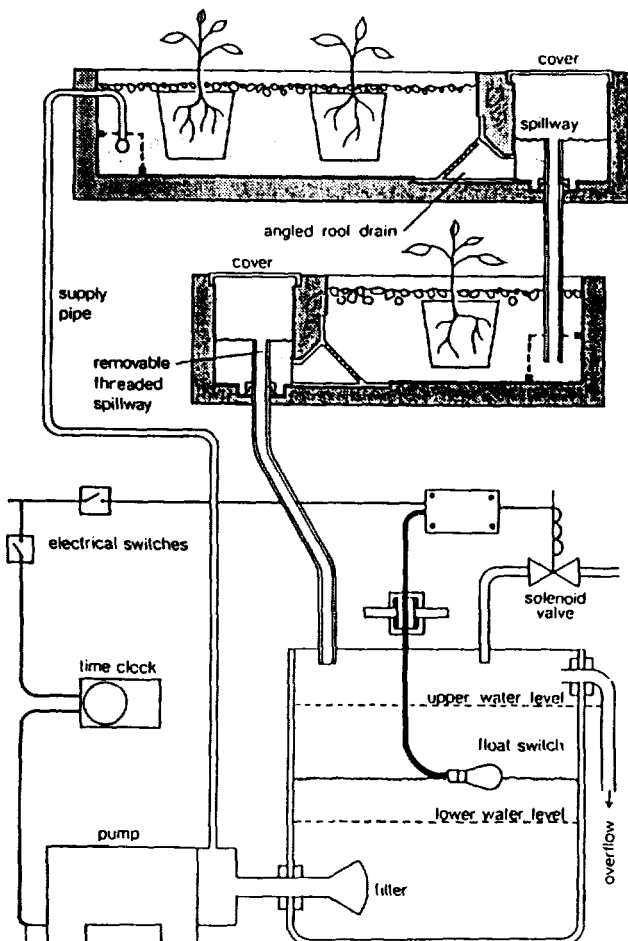


Fig. 5. Hydroponic System Design

HABITABILITY: CAMELOT IV

UNIVERSITY OF PUERTO RICO
SCHOOL OF ARCHITECTURE

N 91 - 18150

INTRODUCTION

Fifty years after the start of the Space Exploration Initiative there will be a permanent martian outpost in operation. Transporting personnel to it will be accomplished by sending passengers through a shuttle to a vehicle in a heliocentric elliptical orbit intersecting both Earth's and Mars' orbits, while it is in terrestrial proximity. Passengers will land on Mars a month and a half later through a transfer shuttle that will also exchange Earth-bound passengers to the vehicle reaching perigee again in 22 months.

Such a vehicle was originally conceived at the Aerospace Engineering Department of the University of Michigan in 1987 as part of the NASA/USRA Advanced Design Program. It was called CAMELOT, an acronym for Circulating Autosufficient Mars-Earth Luxurious Orbital Transport. It housed 17 passengers and a crew of 3 in a 3.6 m × 7.3 m rectangular cross-section toroid of 34.1 m radius, thus providing a volume of 284.8 m³ per person, including the Closed Environmental Life Support System (CELSS). It created an artificial gravity of 0.4 g by rotating the ring at a rate of 3.22 rpm.

During 1988-89 the NASA/USRA Advanced Design Program sponsored research and design efforts at the School of Architecture of the University of Puerto Rico aimed at developing habitability criteria and at defining a habitability concept as a useful tool in understanding and evaluating dwellings for prolonged stay in extraterrestrial space. CAMELOT was studied as a case in which the students would try to enhance the quality of life of the inhabitants by applying architectural design methodology. Thus, a process of transformation of the original CAMELOT took place and the CAMELOT III presented to NASA/USRA's Advanced Design Program evolved.

HABITABILITY CONCEPT DEFINITION

The study proposed 14 habitability criteria considered necessary to fulfill the defined habitability concept, which is "that state of equilibrium that results from the interaction between components of the Individual Architecture Mission Complex, which allows a person to sustain physiological homeostasis, adequate performance, and acceptable social relationships."

The habitability criteria can be summarized as follows:

1. Personal Identification: Refers to the possibility of allowing the individual to influence the arrangement of his/her personal areas.
2. Social Interaction: To satisfy the need for companionship.

3. Aleatoric Conditions: To avoid excessive routine, providing pleasant surprises.

4. Contact with Nature: Is a buffer to soften the impact of a totally encompassing artificial environment and developing a new sense of indoor-outdoor.

5. Mental Landscapes: To evoke memories, symbols, and experiences of terrestrial life.

6. Privacy: A private place for everyone on prolonged stay in an enclosed habitation is necessary to maintain harmony in interpersonal relationships and self-reliance.

7. Equalitarian Conditions: Differences among passenger facilities should reflect purpose and function, as well as individual preferences, rather than rank or hierarchy.

8. Variability: Environmental stress can be overcome by introducing a variety of elements, shapes, decor, color, materials, and textures.

9. Functionality: A "habitable" place must perform well in the physiological-quantitative sense for the sustenance of human life beyond the level of mere survival.

10. Sensorial Stimulation: Cognitive processes depend on all senses; therefore, visual stimuli are to be complemented by an environment rich in positive auditory, tactile, olfactory, and gustatory factors and enhancements.

11. Music and Environmental Sound: The problem of absolute silence in extraterrestrial space has to be dealt with to prevent travelers from being startled by their own visceral motions and by any minor unexpected noise, as well as to control access to communications.

12. Stability and Security: Muscle tone and visual-motor coordination developed under terrestrial conditions will find alien an environment where there are gravity gradients, Coriolis and gyroscopic forces, and constant torque on the anatomy. The environment must be designed to compensate for these conditions.

13. Comfort: Includes conditions such as illumination, temperature, humidity, pressure, and atmospheric composition, which can be quantitatively determined according to standards.

14. Sense of Orientation: The architectural design of floors, walls, and ceilings must create a new sense of up and down, east and west, north and south to reinforce orientation.

ARCHITECTURAL DESIGN DEVELOPMENT

A series of design factors and architectural strategies were considered in making the following changes to the original CAMELOT:

1. The single-level toroid ring of a 12' × 24' cross-section was changed to a two-level, true torus of 24' section diameter, keeping the 112' rotational radius.

2. Consequently, the volume increased by 41% to allow for quality of life enhancements.

3. The CELSS was reorganized by moving it to the lower level of the torus, which is also its outer level, and was compartmentalized in a system of drawers that ran along the sides of the main corridor of the vessel, providing for circumferential access and transportation.

4. The areas of the vessel were reorganized into three main sectors (instead of four), thus using only three spoke elevators to provide access to and from the central core. The areas were organized as the dwelling sector, which includes cabins for passengers and crew members; the work sector, which includes laboratories, torus control room, medical center, and a master CELSS; and the leisure sector, including a galley, dining-conference room, library-lounge, recreation-gymnasium, and a chapel.

5. Additionally, the three spoke elevators were placed in a lobby, under which the safe havens were located, containing facilities for dwelling while the vessel is under the influence of extreme radiation because of solar flare activity or some other hazardous condition that would require such protection. The Safe Havens consist of a series of cubicles measuring 8' × 4' × 4' high that are highly shielded, have food supplies for at least 24 hr, allow access to communications, computers, and entertainment, and contain supplies for clothing changes, a personal toilet, and a couch for sleeping or sitting.

6. The circumferential corridor provided a continuous means of circulation along the lower level of the entire torus, flanked on one side by a carousel-type transport for cargo or injured humans, and a means of reaching every room in the vessel. Access to rooms was always through vertical ladders and hatches on the ceiling to promote upper body tonification by requiring its use for locomotion.

7. Interior gardens were provided as an external CELSS feature in several two-story locations along the dwelling and leisure sectors.

REFINEMENTS AND REVISIONS TO IMPROVE QUALITY OF LIFE

Considering that several of the habitability criteria were dependent on qualitative, rather than quantitative factors, it was deemed necessary to develop them further in order to ensure and promote greater objectivity in evaluating habitats for prolonged stay in extraterrestrial space. CAMELOT III was also found underdesigned as far as (1) the nature of the enveloping membrane, which was required to withstand pressures of 2000 lb per sq ft to hold the required internal atmosphere of the vessel; (2) the assembly process in Earth orbit for such a vessel (robotics and EVA processes); (3) the security systems for emergency and accidental conditions of operation; (4) the need for a detailed example of lighting, texture, materials, and color scheme to illustrate the application of the habitability criteria; and (5) the design of its furniture, which was found to be still too prejudiced by 1-g living conditions.

These provided the working agenda for the Space Research and Design Studio during academic year 1989-90.

NEW INSIGHTS ON ARTIFICIAL GRAVITY

From the available data, it soon became evident that artificial gravity is necessary to overcome physiological and even anatomical deterioration of humans on prolonged stay in space. During research, however, further insight was gained regarding the architectural implications of such artificial gravity in environments, disclosing conditions such as (1) Coriolis and gyroscopic effects over all bodies in motion (north-south movements), which are 4000 times greater than those experienced on the surface of Earth; (2) weight gains and losses related to east-west movements of significant magnitude due to the addition or subtraction to the circumferential speed, which causes the centripetal force that creates the artificial gravity effect; (3) gravitational gradients due to upward and downward movements (toward or away from the center of rotation movements); in fact, due to the conditions of CAMELOT, the person who would experience 0.4 g on his/her feet, would also be experiencing 0.37 g on the top of his/her head; (4) discomfort due to dislocation of reflexes relating to normal visual input and its correlative input from the inner-ear fluid motion. (In the September 1962 issue of *Astronautics*, a chart was published relating the rotational parameters to a comfort zone for the design of artificial gravity manned space stations. CAMELOT was designed taking into account such parameters. However, more recent research has made corrections in relation to the rotational parameters, leaving CAMELOT just outside the comfort zone.); (5) excessive variations in local verticals that create confusion and disorientation; (6) unfamiliar behavior of objects and bodies that tend to move in straight paths, while the environment or the frame of reference is rotating. (It is conceivable that in CAMELOT a body suspended unrestrained for one second would not only experience a lateral displacement due to inertia, but could also rotate up to 58° relative to the envelope); and (7) large anatomical stresses as a consequence of such rotational and lateral displacements. For example, if the passenger were to rely on feet and balance alone to stand erect, assuming he/she has become accustomed to the moving environment, the torque exerted by the gluteus maximus over the trochanter bone in the sagittal plane would be 700 times that of normal anatomical stresses.

FORM AND CONSTRUCTION PROBLEMS

Additionally, construction and form difficulties were found, such as

1. Large periods of time and numbers of people will be needed for extravehicular activity (EVA) in low Earth orbit (LEO) for the assembly of the skin of the vessel.

2. It will be difficult to attain air tightness in the membrane assembled in orbit due to the great number of joints.

3. Due to fluctuations in the upper atmosphere, orbit decay is an ever-present danger during LEO assembly until the vessel has attained enough structural integrity to make orbital corrections possible.

4. A relatively small torus like CAMELOT (112' radius), cannot fulfill the promise of spatial continuity because floors curve up too steeply and are perceived as walls at a distance. Ceilings bend away in horizons, which seem to meet the floors, to visually enclose the volume, thus making it impossible to view really large expanses of areas.

5. The monolithic integrity of the toroidal form does not lend itself to the modular redundancy principle aimed at providing subsistence in case of failure of life support systems, fire, decompression, puncture of the membrane, fracture of the structure, or any other similar emergency or accident.

6. Extreme limitation of the capacity for passengers, while requiring 14,000 ft³ of volume per passenger (including CELSS), makes the vessel too luxurious or uneconomical.

7. The extreme Coriolis and gyroscopic effects on a passenger moving on the hallway, as mentioned before, would require design of handrails and other grab bars to ensure a means of personal locomotion, using the upper body and not only the legs as in terrestrial environments, in order to exert control over such a motion and to relieve the body of extreme anatomical stresses.

8. The period between the warning of solar flare radiation and its actual arrival can be as little as 20 sec. Therefore, Safe Havens cannot be concentrated in a given location, but must be dispersed throughout the vessel, so that they can be reached from any location in such a short time.

A NEW VESSEL, SIMILAR CONCEPT

To solve those problems, a new version, called CAMELOT IV, has been designed. It consists of 12 shuttle external tank (ET) envelopes on an array of 3 groups of 4, tethered from a common core. The passenger capacity has been tripled to 60 persons and therefore its volume has also increased. The array rotates at a 1-km radius (instead of 30 m) at a speed of 0.6 rpm (instead of 3.22 rpm). Thus, gravitational and locomotion conditions become 80-90%, similar to those experienced on Earth. The tether arms are built using Buckminster Fuller's concept of "tensegrity" and are 1 km long with a section 30.38 × 30.38 m supporting a solar energy collector array of 24,000 m². They carry up to four elevators to the microgravity sector in the central hub, which in turn houses laboratories, the nonrotating interface for passengers, supplies, and cargo access. That core also houses the observatory, the command bridge, part of the antenna, and an ejectable nuclear reactor array.

The idea of tensegrity was promoted by R. Buckminster Fuller, the inventor of geodesic geometry, as a means of achieving very versatile, lightweight structures in which the members in compression are minimized and are discontinuous, whereas the members in tension are continuous and very slender, giving the structures an appearance of floatability.

The solar energy collector array was arrived at after consideration of several alternatives. The first one was to place a dish with a radius of 87.4 m around the central core. It was discarded because it required additional structural support. For the same reason, the idea of a 4-m-wide ring at 1 km radius was rejected. The proposed solution of an 8-m-wide strip of

solar panels attached along the length of the tensegrity tether arms seemed to be the most practical solution.

The orbital trajectory design developed at Michigan was kept with two new enhancements proposed: (1) the requirement that the main plane of the vessel that contains the solar energy panel array will always be facing towards the Sun; (2) that a 24-hr precession motion be introduced to the axis of rotation to create a sense of daily cycles in the "natural" illumination through ceiling panels and windows. This would help maintain the circadian cycles of crew and passengers as they live on the vessel.

It is envisioned that an antenna array would allow 360° rotation so that some would always be facing Earth base, whereas the others would always be pointing toward the martian base.

Four shuttle liquid hydrogen external tanks have the equivalent volume of the original CAMELOT. Conceivably, they could be recycled and refurbished for use in such a vessel, rather than wasting their sturdy and airtight skin by burning it in the atmosphere, which is the current procedure. It is proposed that they be redesigned so that access be made possible to their interior for construction of habitable quarters in a higher orbit, where they could be stored until the time that NASA is ready to build CAMELOT.

Instead of using counterweights to balance the tethers of CAMELOT IV, it is proposed that the capacity of the vessel be increased in order to subdivide the community in modules similar in size to the original CAMELOT, so that instead of 20 people, there would be 60, or three arrays of four ETs for 20 people each. Each ET envelope will contain its own CELSS. Organization into three sectors, dwelling, work, and leisure, will be conserved to grant a sense of mobility to the passengers, even within their own particular array. Circulation between ETs of one array is accomplished through 12' × 12' cylinder connectors. Transportation between arrays and the central microgravity core is through the four tensegrity tether arm elevators.

The dwelling sector ET array now proposed consists of two ET envelopes (the recycling of a shuttle's liquid hydrogen tank). They would be organized in three floors. Each dwelling ET will house 10 cabins, and a meeting area on the center floor. There will be a torus control room in one of them. Safe havens will be located in the upper level and a CELSS along the lower level corridor.

The work sector will consist of only one ET envelope to be located north of the dwelling sector. It will house four laboratories, a medical center and a master CELSS, all of which will be distributed in the two upper floors. The lower floor will also house a CELSS along the corridor.

The leisure sector ET will also be one tank located south of the dwellings, containing galley, dining-conference room, library-lounge area, a double-height gymnasium-recreation room, and a chapel.

All sectors will have double- and triple-height gardens at the rounded ends of the envelopes. The recycled conical liquid oxygen tanks and the collar connectors of the shuttle ETs could be used for assembling the microgravity laboratories and other facilities in the core.

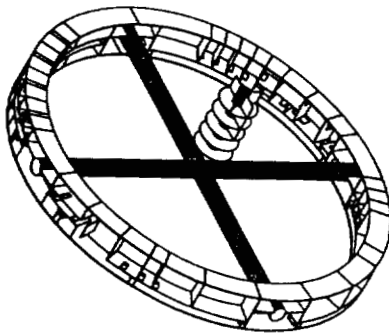
Spoke elevators will consist of 8-ft-diameter cylinders that will travel on cables located within the tensegrity tether structure between the ET arrays and the central core.

THE FINAL CAMELOT

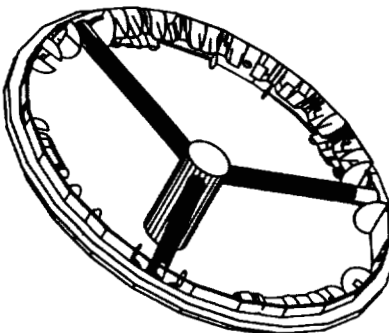
CAMELOT IV is presented here in a tripodal configuration, but conceivably it is a form that allows for growth and expansion. It could be exploded to a multiple-arm array, as long as there is means of counterbalancing the tethers and the spin is controlled to attach additional arms to reach eventual toroidal form of 1 km radius. By that time the start of the Space Exploration Initiative will be a subject of study for historians. CAMELOT would then have 108 arrays of 4 ETs and would be transporting a population of over 2000 people between Mars and Earth, two of the planets inhabited by a multiplanetary human species reaching for the stars.

APPENDIX

Illustrations pertaining to Camelot IV are included in this Appendix.



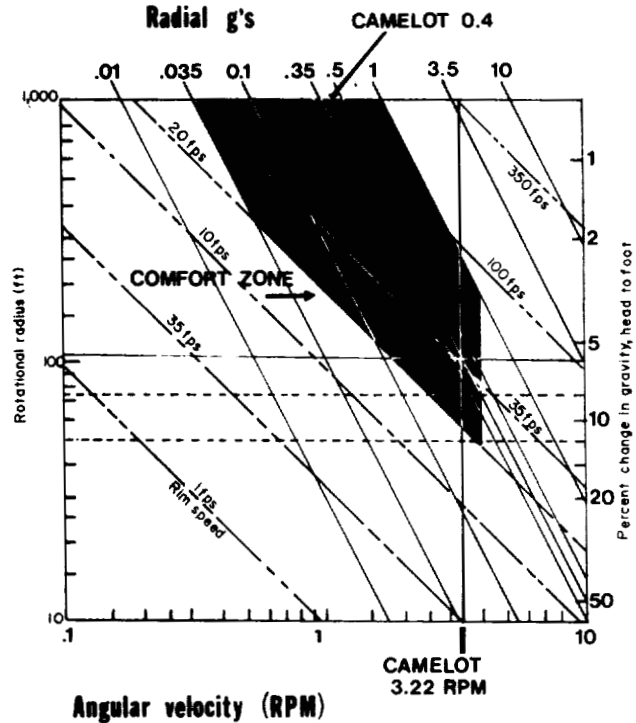
Camelot I. Axonometric



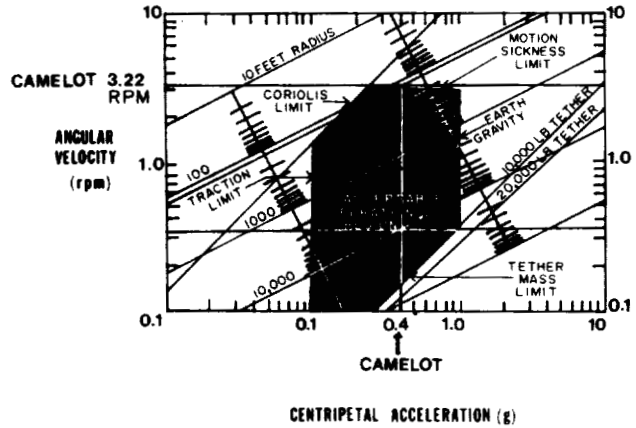
Camelot II. Axonometric

ACKNOWLEDGMENTS

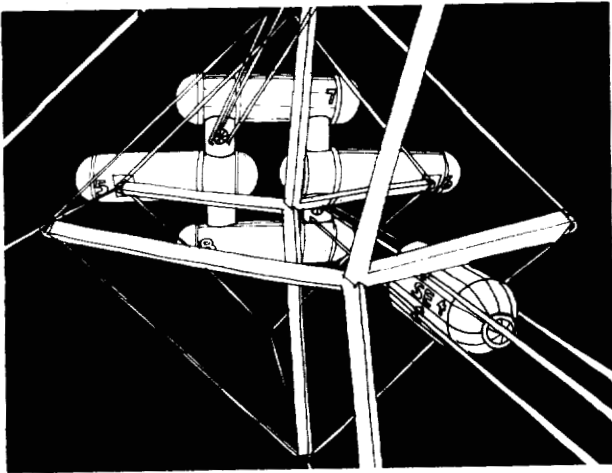
Principal authors included W. Alequín, A. Barragan, M. Carro, F. García, I. González, J.A. Mercado, N. Negrón, D. López, L.A. Rivera, M. Rivera, J. Rodriguez, O. Rodriguez, J. Sánchez, P. Soto, H. Torres, and F. Vizcaya. They were assisted by teaching assistants O. Budet and R. Mellado, and Prof. A.F. Andino.



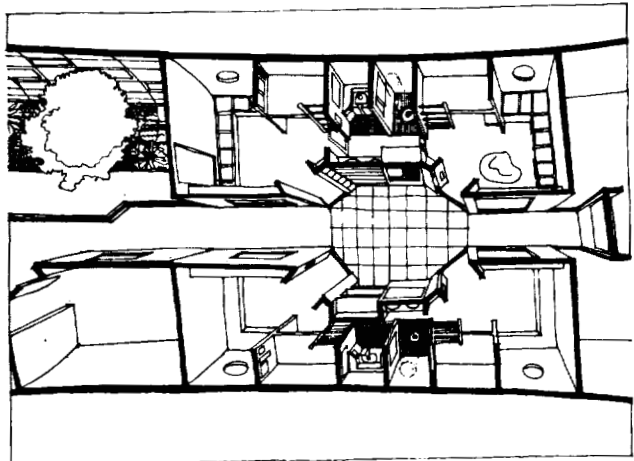
Rotational Parameters and Comfort Zone



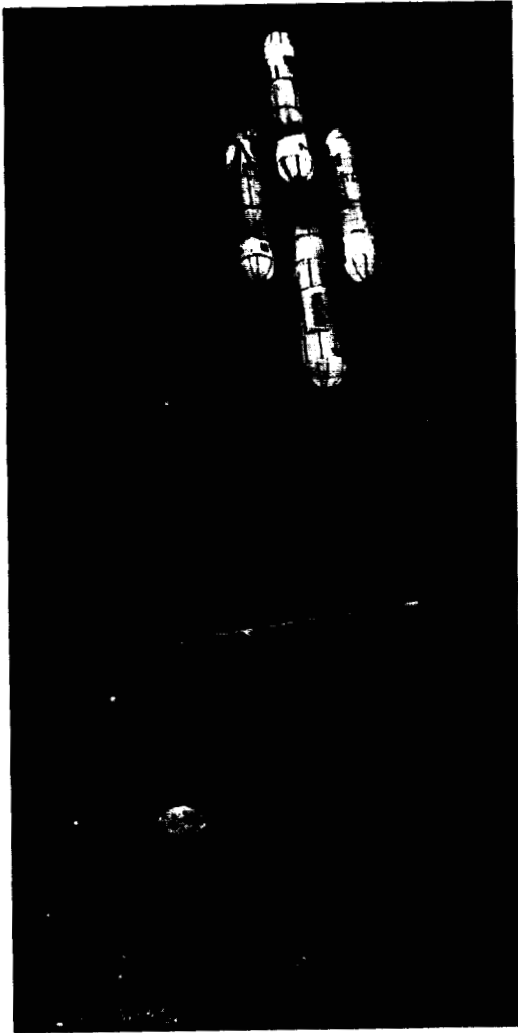
Artificial Gravity Parameters



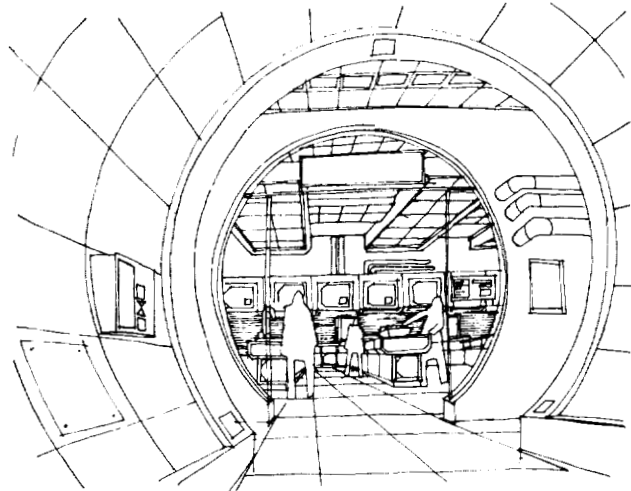
Camelot IV



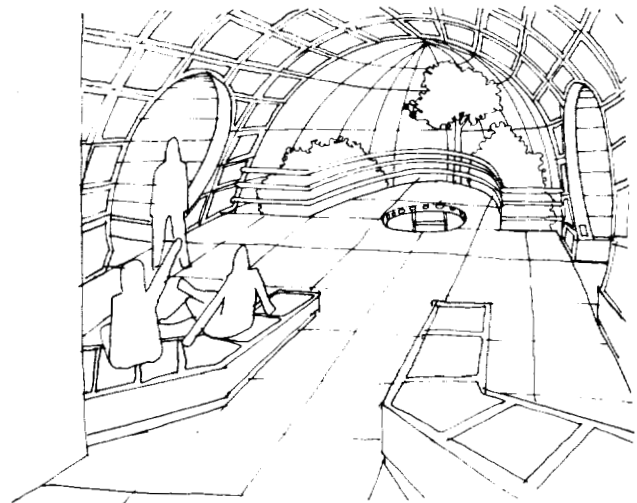
Dwelling Area Floor Plan



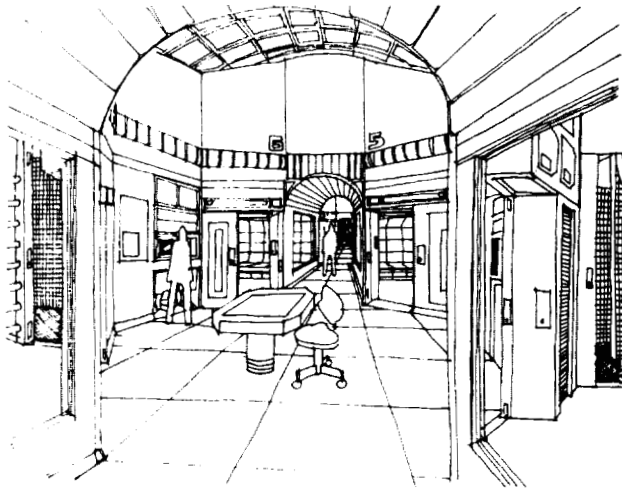
ET Array on Tether End



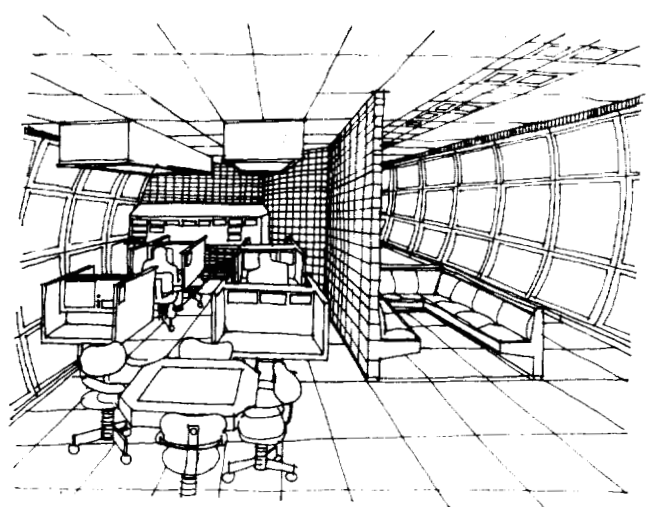
Master CELSS



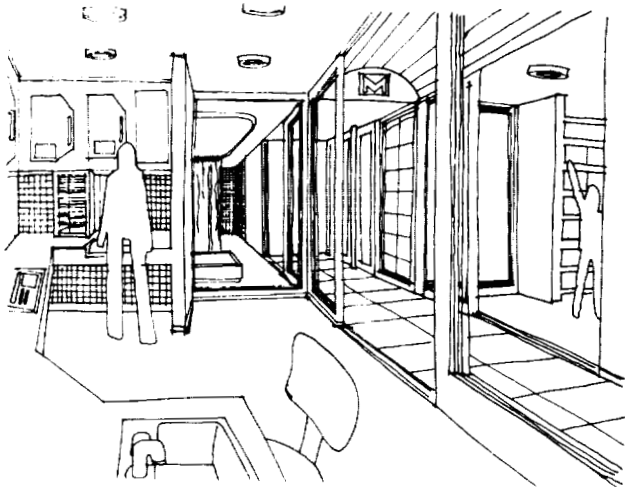
Meeting Area



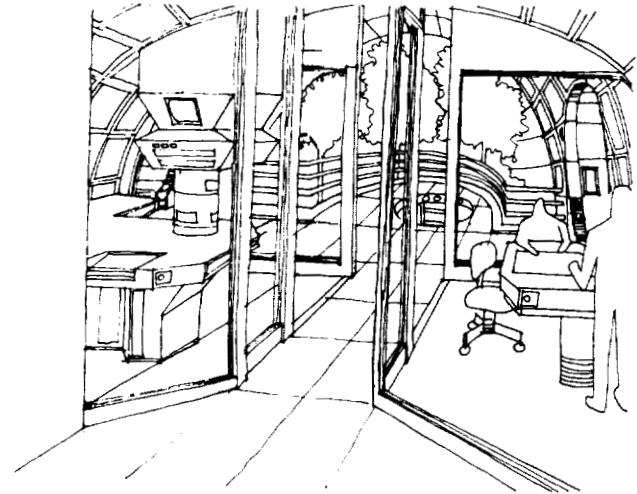
Dwelling Sector



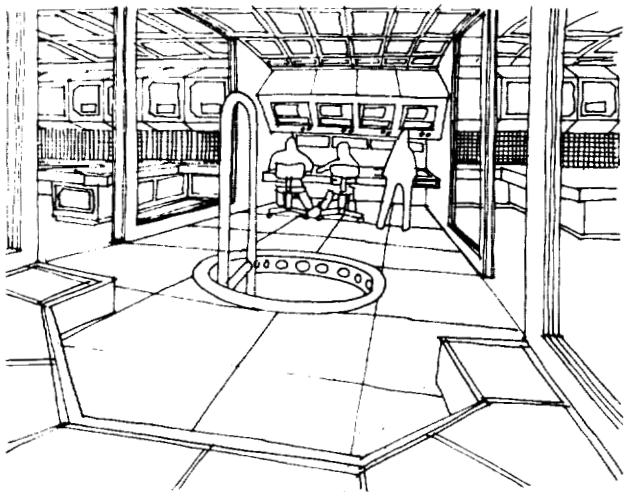
Library



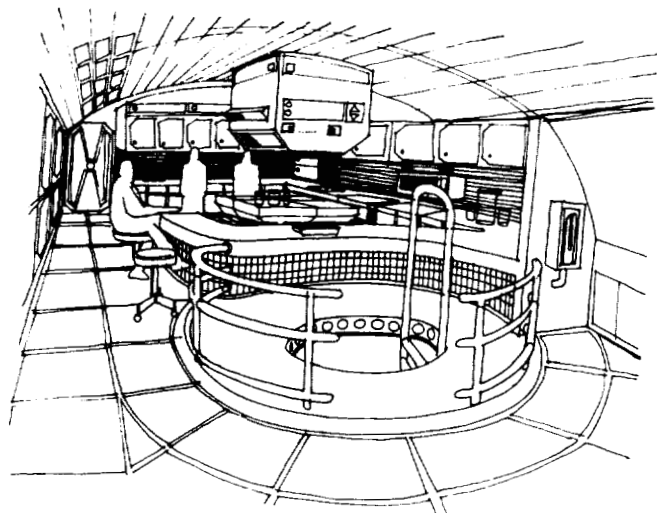
Laboratories



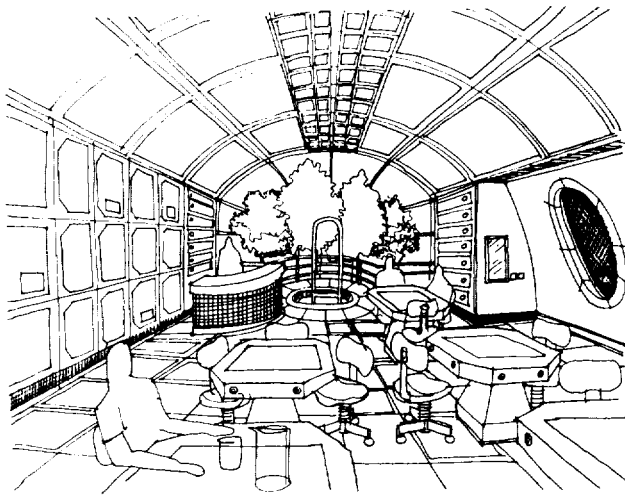
ET Control System



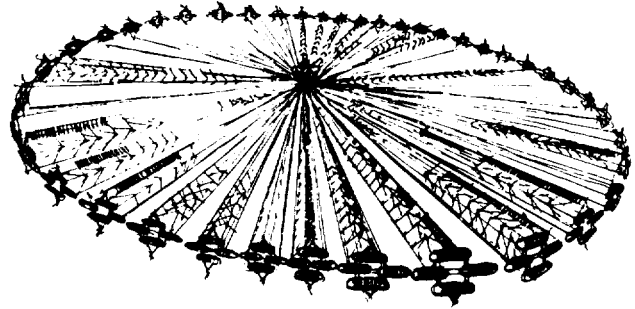
Lab Control Area



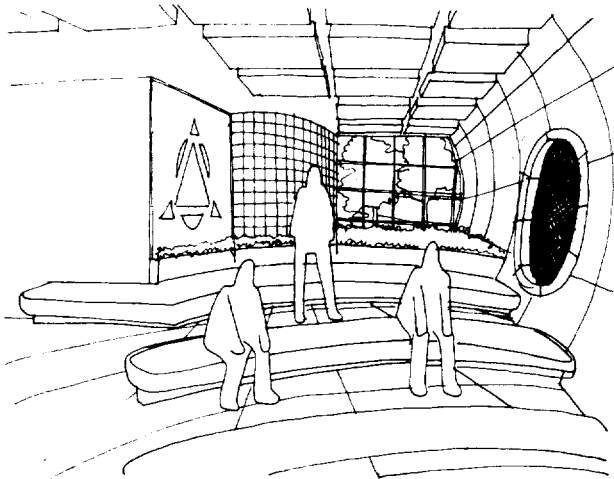
Galley



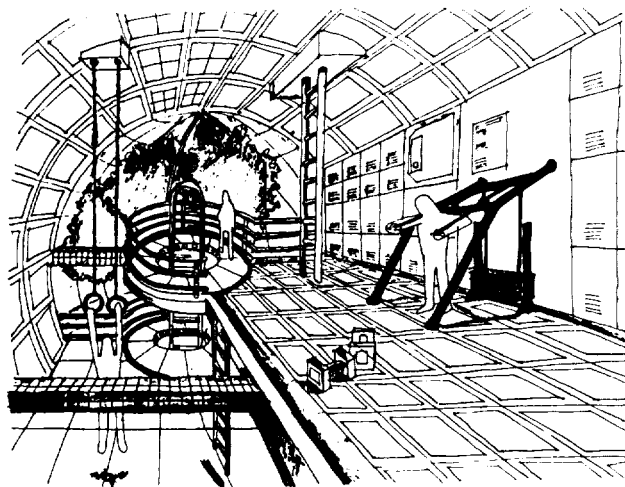
Dining-Conference Room



The Final Camelot



Chapel



Gym

P. 8

INVESTIGATIONS INTO A POTENTIAL "LASER-NASP" TRANSPORT TECHNOLOGY

N91-18151

RENSSELAER POLYTECHNIC INSTITUTE

In this fourth year of the "Apollo Lightcraft Project" at RPI, the following question is asked of laser-boosted spacecraft technology: Can this technology also be used to replace domestic and international jet flights? Clearly, if laser propulsion technology is less polluting than present jet transports, then it could become a major element in helping to reduce the problem of global warming. Also, if Lightcraft (or "laser-NASP") engines can be designed around solar satellite power sources and renewable propellants (e.g., air, LH₂, LN₂, H₂O, etc.), then an enormous savings in hydrocarbon resources would be realizable.

This 1989-1990 annual report on RPI's design project begins with a first-order economic analysis of just such a beam-powered global transport system—based upon a fleet of 10,000 Lightcraft, designed to carry one, two, or five passengers in minimum volume capsules. A detailed conceptual design is presented for an on-place Mercury Lightcraft; other designs are briefly explored for larger, 15-place Executive Lightcraft, and 150- to 350-passenger Jumbo Lightcraft.

Various other teams in the class conducted experiments or performed theoretical analyses on various aspects of the Lightcraft propulsive engine and vehicle technology. One group machined an accurate, 6" diameter model of the hypersonic air inlet (using a CNC lathe), instrumented it with PCB pressure transducers, and tested it from Mach 10 to 25 in RPI's hypersonic shock tunnel. Another group simulated the inlet aerodynamic performance with a computational fluid dynamic (CFD) code called PARC 2D. Analytically predicted shock positions and pressure distributions were then compared with Schlieren photographs and pressure data taken during the experiment.

One other group designed a laser propulsion experiment that will be carried out by the 1990-1991 design class. Another designed superconducting magnets for the laser-heated MHD-Fanjet engine, which accelerates a Lightcraft from Mach 10 to orbital velocity. Others built and tested a 1-1/4" diameter Lightcraft inlet in RPI's Mach 3 wind tunnel, and analyzed the performance of the primary optics of a Mercury Lightcraft. Perhaps the most profound analytical achievement was the analysis of a laser-heated, rocket-driven MHD generator using 20,000°K hydrogen as the working fluid; the method employed a combined simultaneous solution of a quasi-1D MHD code with a 3D radiation code.

In summary, the class design team made exceptional progress in continuing to climb the steep learning curve on laser-propelled flight/transport technology.

INTRODUCTION

Technological innovation has repeatedly caused drastic revolutions in world travel patterns. The schooner, steamship, dirigible, and airplane all had their profound effects. Here we present an economic analysis of yet another new transport mode that will make the advances of these former modes seem like microscopic progress. We are talking about the Apollo Lightcraft, a technology that will allow people to travel half-way around the world, essentially door-to-door in 45 minutes. It will make trips possible that simply cannot be made today except by astronauts. And our economic analysis tends to show that the operating and capital costs of this system can be recovered once the Lightcraft technology is mature.

BACKGROUND

It is well recognized that mankind's quest for increased speed has not yet abated, not even with the introduction of the supersonic Concorde. In fact, the Concorde has merely whetted our appetite for faster, futuristic flight. People want to reach their destination as quickly as possible. Two recent proposals have heightened our interest in travel time savings: the High Speed Civil Transport (HSCT) and the Hypersonic Aircraft (HA)⁽¹⁾. The HSCT is the next step in the development

of supersonic transports and the Hypersonic Aircraft is a jump beyond the HSCT. The HSCT is much closer to today's technology, and advanced studies have been conducted on the marketability of this technology in the growing international transportation market^(2,3,4,5,6,7,8).

But these advances in high speed transport technology have generated an interesting dilemma—namely, while the systems must be cost effective to be saleable, increasing speed also increases costs. This "Catch-22" is readily apparent when considering the HSCT. While it has been proposed that the HSCT needs a range of at least 7500 n.m. to be profitable (the range of current 747-400 technology), at this range and at Mach 2.5, it requires twice the fuel of the 747 to carry the same number of passengers, and at Mach 3.5 it needs nearly four times the fuel. It seems that as range increases, fuel requirements grow at an exponential rate (see Fig. 1)⁽⁹⁾.

Clearly the success of the HSCT and other super- or hypersonic transports is dependent on an ability to produce these travel-time savings. Fuel consumption is a major problem, but the real trouble is that the time savings can only be pushed to a certain limit, beyond which access and egress times (i.e., the times spent going to and from the airports) become the real liability. Also, since supersonic speeds are possible only

PAGE 194 INTENTIONALLY BLANK

PRECEDING PAGE BLANK NOT FILMED

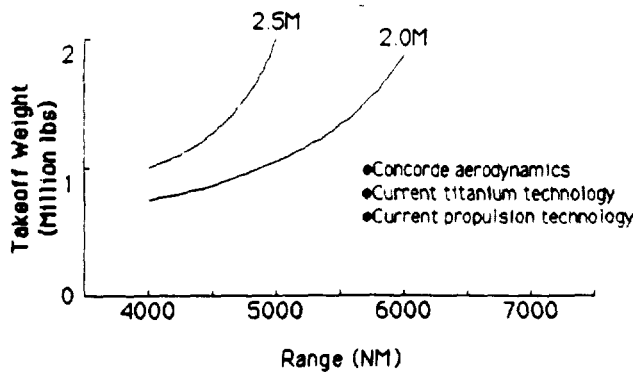


Fig. 1. HSCT Fuel Consumption (Weight) vs. Range⁽⁹⁾

over water, only certain city pairs can benefit from the time savings that can be achieved. The inability to fly supersonic over land also has serious impacts on flight paths. A flight from Paris to Tokyo, for example, requires either a subsonic track over land, or an extended diversion to fly completely over water. Moreover, travel becomes complicated as more changeovers at intermediate airports become necessary.

For these reasons, while the HSCT may increase flight speed over water by a factor of three, it may reduce overall travel time by only 50% or less. Note that the over-water flight time is not total travel time, but merely over-water air time; over-land air time and access and egress times are additional. This becomes quite important when one considers how many airports will be capable of supporting an HSCT system. If an HSCT network is only partially implemented, access and egress times to HSCT port cities could be quite long. This inability to effect major travel time savings will clearly limit the marketability of the HSCT and other such super- or hypersonic transport.

HSCT proponents hope to capture the top 25% of the international travel market in spite of these limitations. And they think they can do this in spite of what they expect to be a 30% differential in fares. Helping the HSCT is an assumption that the reduced travel times will stimulate demand. Historically, reduced travel times have stimulated travel by a factor of 1.25 to 1.5⁽⁵⁾.

APOLLO LIGHTCRAFT TECHNOLOGY

The real question is not whether the HSCT (or some other high speed transport) can be developed in the near term, but how much longer we will or should continue to base future air transport schemes on large aircraft and fossil fuels. This is where the Apollo Lightcraft technology fits in^(10,11,12). The Lightcraft (see Fig. 2) is not an extension of current aircraft into the next century, but a categorically different technology because of many unique features. First, and most obviously, a Lightcraft has a propulsion system that is not powered by fossil-fuels. It uses laser beams transmitted from satellite solar power stations (SPS)^(13,14), for the propulsive energy source (see Fig. 3). Size is another difference. A Lightcraft is designed to carry

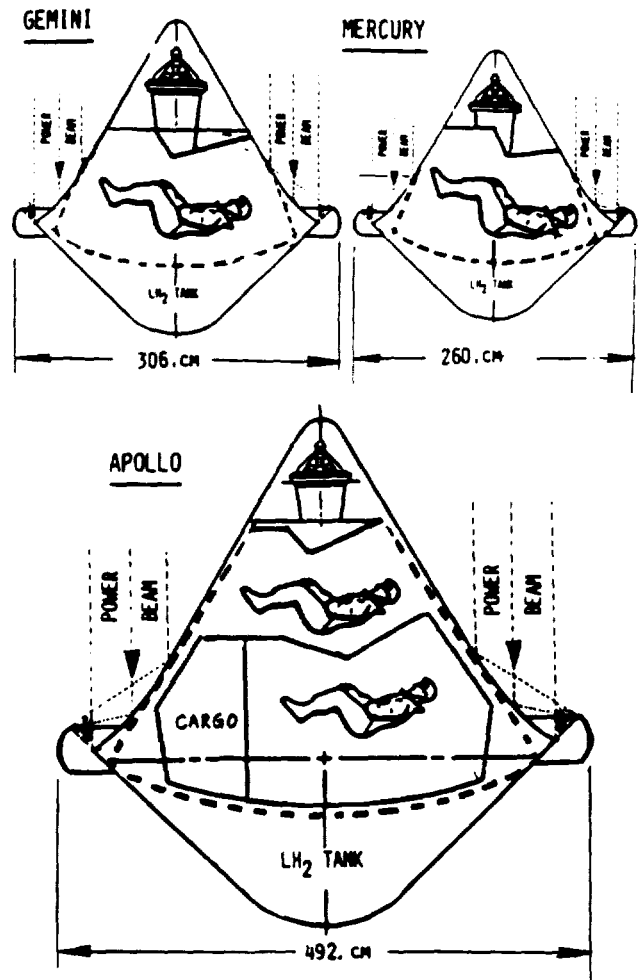
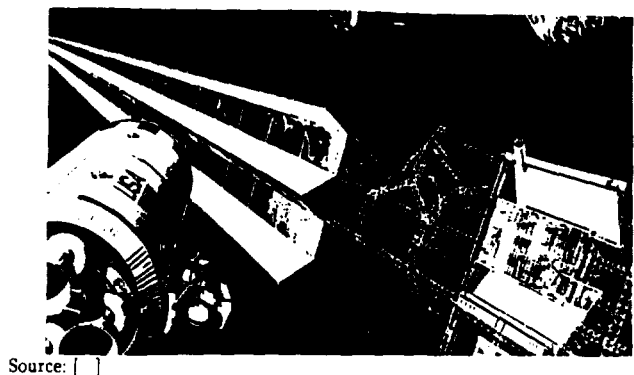


Fig. 2. Family of Laser Boosted Lightcraft⁽¹¹⁾



Source: []

Fig. 3. 7 GW_e Satellite Solar Power Station

only one to five persons. Second, it is designed to take off and land from any airport equipped with a Lightcraft landing pad (see Fig. 4). Third, its range is unlimited. In fact, it becomes more cost effective the further it travels. Unlike the HSCT and hypersonic aircraft, it does not carry its own energy source,

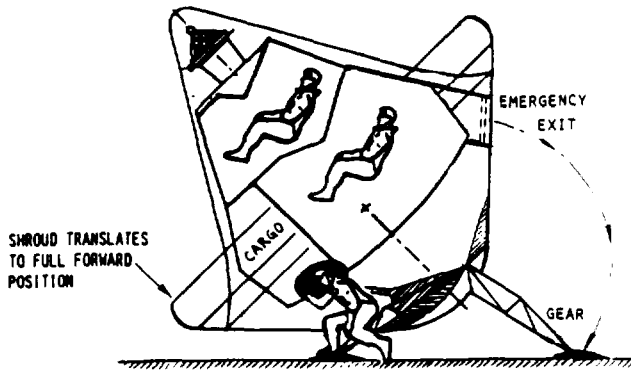


Fig. 4. Passenger Entrance and Egress (Gear Permits Pointing to Laser Power Satellite)

and does not need exponential fuel increases to increase range. Most of its flight is exoatmospheric, and its reentry is performed much like the shuttle (see Fig. 5). Fourth, a Lightcraft not only minimizes in-flight travel time, but also access and egress times. The result is that total travel time is dramatically reduced, so much so for long trips that no data presently exist to suggest how profound the effect will be. Fifth, a Lightcraft is not dependent on fossil fuels. Its electricity needs can be provided by large solar power stations (SPS) positioned in geostationary orbit.

PROJECTION OF FUTURE DEMAND

The projections of Lightcraft demand presented here assume that the technology will compete with the HSCCT and, over time, successfully capture a certain percentage of that marketplace. They also assume that Lightcraft system fares will be competitive with the HSCCT and that network travel times will be at least as short if not shorter.

We expect the rate of penetration will be slow at first (see Fig. 6) then grow more rapidly as the technology becomes accepted, and finally stabilize at 25% of the marketplace. We assume 20 years will be required to accomplish this, both because the Lightcraft is an entirely new technology that will

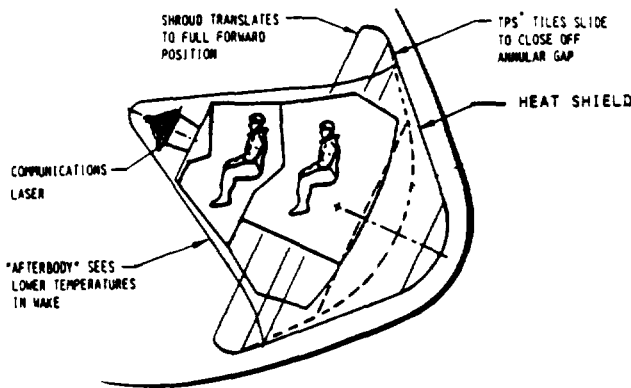


Fig. 5. Re-Entry Configuration

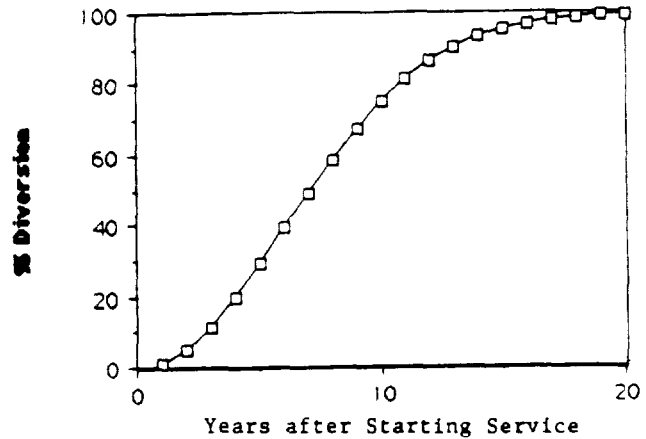


Fig. 6. Growth in the percent of HSCCT riders using Lightcraft during the first 20 years

require an extended public acceptance time and because the support infrastructure for the Lightcraft system will take time to complete.

Given this market penetration curve (i.e., Fig. 6) and projections of HSCCT demand, ridership for the Lightcraft system can be estimated (see Table 1). We have considered two scenarios. In scenario A, it is assumed that the Lightcraft system will capture 25% of the HSCCT ridership projected by Wasiuta⁽⁷⁾. (This HSCCT ridership projection calls for a compounded 4%/year growth in long-distance air travel until 2015. To be conservative we have assumed no growth thereafter.) In scenario B, an additional stimulation factor of 2.5 has been applied (to the total long-distance ridership estimate) based on the time savings the Lightcraft system will produce.

To ensure that the scenario B estimate is not unrealistic, a cross-check has been made, based on a top-down analysis starting from world population figures. Details on this scenario C are given in Table 2. The analysis year is 2015 (Year 0 for the market penetration curve) when the world population will be approximately seven billion. Table 2 first shows that about 1.56 trips over 4000 miles will be generated by a typical 4

Table 1. Lightcraft Revenue Estimates (1989 dollars)

	Pleasure		Business
	Long	Short	
Trips/year/household	3	10	30
Person/trip/household	4	2	1
Person-trips/yr/hh.	12	20	30
% over 4000 miles	3%	3%	2%
Person trip > 4000 mi/hh	0.36	0.6	0.6
Total person trips over 4000 miles per household	= 1.56 pass./family		
World population	= 7,000,000,000		
No. of households	1,750,000,000		
%-hh involved	2%		
Person-trip/yr over 4000 mi	54,600,000		
Person-trip/day over 4000 mi	149,600		
Implied trip expansion factor	2.5		

Table 2. Calculations for Scenario C

Year	Dvrsn (%)	Revenue A	PV of A	Revenue B	PV of B
1	1.38	\$217	\$20	\$543	\$50
2	5.39	\$850	\$71	\$2,126	\$178
3	11.73	\$1,849	\$141	\$4,623	\$353
4	19.89	\$3,136	\$217	\$7,840	\$544
5	29.18	\$4,618	\$291	\$11,544	\$728
6	39.28	\$6,194	\$355	\$15,486	\$887
7	49.29	\$7,773	\$405	\$19,432	\$1,012
8	58.81	\$9,274	\$439	\$23,184	\$1,098
9	67.46	\$10,637	\$458	\$26,592	\$1,145
10	74.99	\$11,825	\$463	\$29,562	\$1,157
11	81.31	\$12,821	\$456	\$32,052	\$1,141
12	86.41	\$13,625	\$441	\$34,063	\$1,102
13	90.39	\$14,253	\$419	\$35,632	\$1,048
14	93.39	\$14,726	\$394	\$36,814	\$984
15	95.58	\$15,071	\$366	\$37,677	\$916
16	97.12	\$15,314	\$338	\$38,286	\$846
17	98.18	\$15,481	\$311	\$38,702	\$777
18	98.88	\$15,591	\$285	\$38,978	\$712
19	99.33	\$15,662	\$260	\$39,155	\$650
20	100.00	\$15,768	\$238	\$39,420	\$595
Total		\$204,684	\$6369	\$511,709	\$15,923

person household. With world population at 7 billion (implying 1.75 billion such households), and with 2% of these households making such trips, the number of person-trips per year over 4000 miles is estimated to be 54.6 million. On a daily basis, this is 149,600 trips. Compared with the total long-distance air travel projections presented⁽⁷⁾, this implies a trip expansion factor of 2.5. While these estimates are crude, they do show that scenario B is not impossible, and, if the jumps in ridership seen in the past repeat themselves, a growth factor of 2.5 may occur, given the time savings that the Lightcraft system will produce.

To estimate annual revenues, we have taken the ridership estimates presented in Table 1 and multiplied by \$0.12 per passenger mile, a revenue estimate that has been used in the HSCT analyses⁽⁷⁾. We have also assumed an average trip length of 5000 miles.

To estimate the net present value of these revenues, for either scenario A or B, a discount rate of 210% has been used, as is typical for somewhat risky investment opportunities and/or programs involving the use of governmental funds. Under scenario A, the net present value of the revenues is thus \$204 billion in 1989 dollars; for scenario B, it is \$511 billion.

STRUCTURE OF THE LIGHTCRAFT INDUSTRY

We foresee a commercialization of the Lightcraft network similar to that of the present automobile rental industry for the following reasons. First, Lightcraft will tend to be used like rental cars. Small groups of people will use them on an occasional basis to make very long distance trips. Table 2 suggests that for scenario C (described earlier) only 1.566 passenger trips per year will be generated on average by the typical four-member Lightcraft-user household. At this rate, only a few households will use them enough to justify owning them privately.

Second, Lightcraft will be very different from existing wide body aircraft, more closely resembling the family car; thus airlines are not likely to be interested in them. Economies of scale due to vehicle size, to which the airlines have become accustomed, simply will not exist. In fact, since Lightcraft will be able to take off and land at virtually any airport, (i.e., any one equipped with a proper vertipad) the Lightcraft network will effectively become a long-distance, high-speed extension of the present private (auto) transportation system. Third, the capital cost of a Lightcraft will be high. Relative to the cost of a present-day commercial airplane, Lightcraft will be inexpensive, having a cost per pound about on par with corporate business jets (see discussion below), mainly due to the fact that a Lightcraft will not have to carry its own propulsion plant. (It will usually be a capsule moved by efficient beamed-energy engines around the planet and/or into space.) But, nonetheless, corporate, rather than private, individual financing will probably be required to purchase them, and rental companies will be well poised to arrange for such financing.

SUPPLY ANALYSIS

In the supply analysis, we have attempted to determine the net present value of the costs of creating and operating the Lightcraft system over a 20-year time horizon (2015 to 2035). This is the timeframe over which implementation of the system is expected.

We have assumed that remote energy sources (i.e., SPSS) will be available to power the Lightcraft system, that 500 will eventually be required, and that the vehicle technology will already be mature.

The cost analysis was accomplished by estimating capital expenditures and then analyzing operating costs. The operating cost of a Lightcraft depends basically on the beamed energy requirement plus a small quantity of liquid hydrogen needed for energy conversion during laser boost. It should be noted that very little hydrogen is needed on short endoatmospheric flights where the Lightcraft does not reach hypersonic velocities. In addition to the energy requirements, maintenance expenditures will be required, but this is covered in the capital costs. In theory, the Lightcraft should have a low maintenance cost because of its combined-cycle engine, which has no moving parts. One sensitive area is the large receptive laser mirror, which may require maintenance of its adaptive surface actuators, or repair of minor scratches or marring of the surface.

For purposes of this analysis, the assumed cost for the liquid hydrogen is \$975 for a five-person Lightcraft traveling half-way around the globe. This number is based on 1987 dollar values for liquid hydrogen. It has been suggested that liquid hydrogen prices will decrease with increased demand (especially if the "hydrogen economy" materializes). This is one of the founding philosophies behind the push for hypersonic transport, where it has been assumed that fuel prices will be cut in half. The present study assumes that liquid hydrogen prices will remain at their 1987 levels. The price used for electricity is \$.017/kWh, from estimates for the SPS electric power sources

mentioned previously. It includes price surcharges that would be added to the base kWh charge to account for fluctuations in demand.

Table 3 shows a chart of the energy and hydrogen costs for various trip lengths in the three different Lightcraft sizes. Obviously, these data are an estimation of costs at the prices mentioned above. The costs incorporate predicted losses in the conversion of electricity into laser light at the power source. Also, they represent a linear extrapolation of cost for a trip to the farthest point on Earth in the five-person Apollo Lightcraft. The linear reduction in cost with decreasing trip length is a conservative projection because the costs for the 12,000-mile trip are actually those required for the Apollo Lightcraft to achieve orbit; thus any of the shorter missions will not need more hydrogen, and will require considerably less electricity than a linear extrapolation. As far as the vehicle sizes are concerned, the two-person "Gemini" vehicle (see Fig. 2) is estimated to need 1/2 the energy of the five-person vehicle (as opposed to 2/5 based on the number of passengers). Similarly, the single-passenger Mercury unit is assumed to require 1/3, instead of 1/5. Obviously, these assumptions are based on the increased efficiency of carrying more passengers in a single vehicle, since the payload is only 9% of the takeoff weight for the largest Lightcraft. It should be noted, however, that this logic cannot be extended indefinitely. In fact, calculations have shown that a five-person Apollo vehicle is close to being the largest feasible craft due to the 2.5-GW propulsive laser beam needed from a 7-GW SPS with a 40% efficient laser and 90% beam transmission efficiency. Additionally, these direct operating costs include a \$100 landing fee per flight.

Table 3. Energy Costs for Various Trip Lengths

Trip Length (mi)	Lightcraft Capacity (passengers)		
	5	2	1
12,000	\$3530	\$1815	\$1243
10,000	\$2958	\$1529	\$1052
8,000	\$2387	\$1244	\$862
6,000	\$1815	\$958	\$671
4,000	\$1243	\$672	\$480

Figure 7 shows estimated group sizes for Lightcraft flights. These are used to calculate the number of vehicles required for each vehicle size. Distribution among the various craft sizes is based upon the above estimates plus additional conditions that 10% of the single passengers will team up to form doubles and that 5% of the doubles will group to form four- (or five-) member flights. Table 4 shows the number of daily revenue flights necessary to service the passenger groups shown above. These figures are based on 150,000 passengers per day, the number corresponding to scenario B, and must be upwardly adjusted to compensate for repositioning, spares, and peak demand. Then, the fleet size can be calculated. Finally, capital expenditures can be estimated to show investment in fleet according to traffic diversion, so that capital costs can be estimated on a per flight basis.

The first adjustment that must be applied is for repositioning. In our analysis, we have assumed that 50% of all flights must be repositioned. This is conservative in light of most

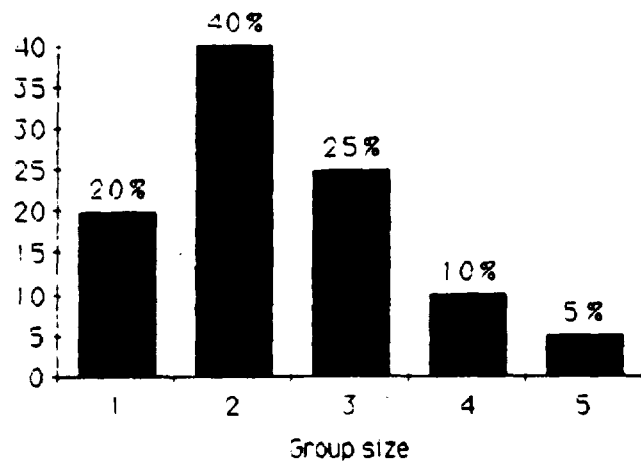


Fig. 7. Assumed Passenger Grouping

automobile rental company experience, but provides a reasonable worst-case scenario for estimating cost. As traffic increases, the repositioning factor will eventually diminish to a much smaller value (e.g., 5-10%), thus reducing costs with a greater number of flights (this has not been taken into account here). It is assumed that the energy costs for repositioning would be charged to the users. This will tend to encourage passengers to fly to well-traveled areas, while retaining the ability to fly nearly everywhere. The resulting flights are as follows: 40,500 singles, 47,250 doubles, and 29,500 quintuples.

After adjusting the number of flights for repositioning, a first estimate of the fleet size can be prepared, ignoring peaking in demand and spares. Since the longest flight will take approximately 45 minutes, Lightcraft should be able to fly every 2 hours, leaving the remaining time for loading, unloading, and any routine inspections or maintenance that must be done. This results in 12 flights per day per Lightcraft. The fleet size at this stage would be 3375 singles, 3938 doubles, and 2438 quintuples.

From this fleet size, the number of vehicles must be adjusted upward to account for peaking in demand. The first reason for doing so is that demand will be higher on some days than others. Day of the week and month of the year will both have an effect, let alone variations from year to year for a given day. Peaking due to religious and national holidays can be ignored

Table 4. Daily Flights by Lightcraft Size in Year 20*

Group size	No. of passengers	1 person craft	2 person craft	5 person craft
1	30,000	27,000	3,000	
2	60,000	28,500	1,500	
3	37,500			12,750
4	15,000			3,750
5	7,500			1,500
Revenue Flights		27,000	31,500	19,500

*These 78,000 flights per day represent 150,000 flights per year and 15,000 payload tons lifted into space each day.

because we are dealing with the entire world population. Peakings in such demand will tend to offset one another. Non-Christians, for example, will still be willing to travel on Christmas, while non-Americans will want to travel on Thanksgiving. The result will be that national religious holidays will not have a significant effect on Lightcraft travel. Rather than deal with these phenomena at a detailed level, a 300-day year has been assumed. This means adjusting the fleet size upward by a factor of 365/300, resulting in an approximate 20% increase. Once this number has been calculated, an adjustment must also be made for spares. A 10% spare ratio has been assumed. This means 10% of the fleet will be out of service for repair, implying the fleet size must be increased by another 9%.

Finally, estimates must be made for the cost of the Lightcraft vehicles. This is perhaps the most difficult task. In the long run, with mass production, Lightcraft might become quite inexpensive. For the time being, however, we have assumed that today's typical business jet and propjet prices will pertain (i.e., \$250/lb). At \$250/lb, the one-passenger Mercury Lightcraft would cost \$0.717 million, the two passenger Gemini, \$1.43 million, and the Apollo vehicle, \$3.06 million.

Given these assumptions and calculations, Table 5 shows that the five-person unit could actually become the cheapest means of transportation in the long-distance travel market. Even the single-capacity Mercury will be competitive with the HSC. If so, the implications are tremendous. The Lightcraft network might be capable of capturing the entire long-distance international market, rather than just the 25% of the HSC market as we assumed. This would considerably change the results presented here.

The final information presented in Tables 6 and 7 pertains to the total costs involved. This is useful not only for showing the capital expenditures required throughout the implementation of the Lightcraft network, but also for comparison to the revenue estimates made previously. Using the same discount rate of 10%, the values obtained from this table should hold the same present value as those derived from

revenue estimates. The present values are important because expenditures will precede revenues. Table 6 shows that capital costs will occur over a period of 16 years, 4 years less than the 20 years analyzed in the revenue estimates. The maintenance and operating cost expenditures given in Table 7, however, will logically coincide with revenue.

The total present value of costs for the Lightcraft system is \$12,982 million. This can be compared with net present value of \$15,923 million for the revenue estimate.

CONCLUSION

This paper has examined the economic prospects for a revolutionary new aerospace transport system based upon the Lightcraft technology, which, when operational, will enable people to fly half-way around the world in 45 minutes. Based on what we know to date, it appears the new technology will be able to cover both its operating and capital costs, with at least an 18% margin to spare, allowing ticket prices below any other Mach 1 or higher transport options. Developers should be encouraged to push Lightcraft prototype work through to completion in the next half decade, because it is simply a matter of time before this mode becomes the principal means for long-distance international travel.

POSTSCRIPT

Figure 8 shows the number of satellite solar power stations (SPSs) and launches per day needed to satisfy projected demands for the Lightcraft network. The calculations assume 50% repositioning and a five-minute boost duration, 7GW_c SPS capacity with 40% laser-to-electric power conversion efficiency, and 90% beam transmission efficiency for continuous global service. Note that in Year 20, 509 SPSs are required to provide this service, which represents 25% of the total world market. If the Lightcraft network captures the complete world market, roughly 2000 SPSs will be required by Year 20.

It is interesting to compare this result with current 1989 U.S. and world energy consumption. The present U.S. ground

Table 5. Development of Costs per Passenger per Flight, by Lightcraft Size (1989 dollars)

Trip Len	Veh. Cost	10%	Maint	Rev Fl/yr	Cap Cost Fl	Oper. Cost	Total/pax
<i>(a) Single passenger lightcraft</i>							
12,000	\$715,000	\$71,500	\$14,300	2,190	\$39	\$1,243	\$1,282
10,000	\$715,000	\$71,500	\$14,300	2,190	\$39	\$1,052	\$1,091
8,000	\$715,000	\$71,500	\$14,300	\$2,190	\$39	\$862	\$901
6,000	\$715,000	\$71,500	\$14,300	2,190	\$39	\$671	\$710
4,000	\$715,000	\$71,500	\$14,300	2,190	\$39	\$480	\$520
<i>(b) Two passenger lightcraft</i>							
12,000	\$1,430,000	\$143,000	\$28,600	2,190	\$78	\$1,815	\$947
10,000	\$1,430,000	\$143,000	\$28,600	2,190	\$78	\$1,529	\$804
8,000	\$1,430,000	\$143,000	\$28,600	2,190	\$78	\$1,244	\$661
6,000	\$1,430,000	\$143,000	\$28,600	2,190	\$78	\$958	\$518
4,000	\$1,430,000	\$143,000	\$28,600	2,190	\$78	\$672	\$375
<i>(c) Five passenger lightcraft</i>							
12,000	\$3,052,500	\$305,250	\$61,050	2,190	\$167	\$3,530	\$739
10,000	\$3,052,500	\$305,350	\$61,050	2,190	\$167	\$2,958	\$625
8,000	\$3,052,500	\$305,250	\$61,050	2,190	\$167	\$2,387	\$511
6,000	\$3,052,500	\$305,250	\$61,050	2,190	\$167	\$1,815	\$396
4,000	\$3,052,500	\$305,250	\$61,050	2,190	\$167	\$1,243	\$282

Table 6. Lightcraft Capital Costs

Year	Dvrsn (%)	Year (%)	Singles	Doubles	Five-man	Capital(\$Mil)	PV(\$Mil)
1	11.73	11.73	522	610	377	2,397	221
2	19.89	8.16	364	424	263	1,668	140
3	29.28	9.39	419	488	302	1,920	146
4	39.28	10.00	445	520	322	2,044	142
5	49.29	10.01	446	520	322	2,046	129
6	58.81	9.52	424	495	306	1,946	112
7	67.46	8.65	385	449	278	1,767	92
8	74.99	7.53	336	392	242	1,540	73
9	81.31	6.32	281	328	203	1,291	56
10	86.41	5.10	227	265	164	1,043	41
11	90.39	3.98	177	207	128	814	29
12	93.39	3.00	134	156	97	613	20
13	95.58	2.19	97	114	70	447	13
14	97.12	1.54	69	80	50	316	8
15	98.18	1.06	47	55	34	216	5
16	100.00	1.82	81	95	59	372	8
Total			4455	5198	3218	20,441	1235

Table 7. Lightcraft Maintenance and Operating Costs

Year	Dvrsn (%)	Maint(\$Mil)	PV(\$Mil)	Oper (\$Mil)	PV (\$Mil)
1	1.38	48	4	423	39
2	5.39	81	7	1,657	139
3	1.173	120	9	3,603	275
4	19.89	161	11	6,110	424
5	29.28	202	13	8,996	567
6	39.28	240	14	12,068	692
7	49.29	276	14	15,143	789
8	58.81	307	15	18,067	856
9	67.46	332	14	20,723	892
10	74.99	353	14	23,037	902
11	81.31	370	13	24,977	889
12	86.41	382	12	26,544	859
13	90.39	391	11	27,767	817
14	93.39	397	11	28,689	767
15	95.58	401	10	29,361	714
16	97.12	409	9	29,835	659
17	98.18	162	3	30,160	659
18	98.88	162	3	30,375	555
19	99.33	162	3	30,513	507
20	100.00	162	2	30,719	464
Total		5117	193	398,763	12,408

electric power grid supplies roughly 80 quadrillion Btu (i.e., QUADS), of which 85-90% comes from fossil fuel plants. This power could be provided by 150 SPSs (e.g., 7 GW_e each, at the SPS; 65% transmission efficiency to groundbased receiving antennae; 5 GW_e into each of the grids)⁽¹³⁾.

All U.S. energy needs (i.e., transportation, industrial, domestic, etc.) could be covered by 500 SPSs. Since world consumption is 4 times that of the U.S., 2000 SPSs, spaced 40 to 50 miles apart in geostationary orbit would be needed for the whole planet.

It is also useful to compare the total payload moved per day on the Lightcraft network, with that of the space shuttle orbiter (65,000 lb or roughly 30 tons maximum). Figure 8 shows that in Year 20, 15,000 tons of paying passengers and baggage will be moved daily on the Lightcraft network. This will be equivalent to 500 shuttle launches each day.

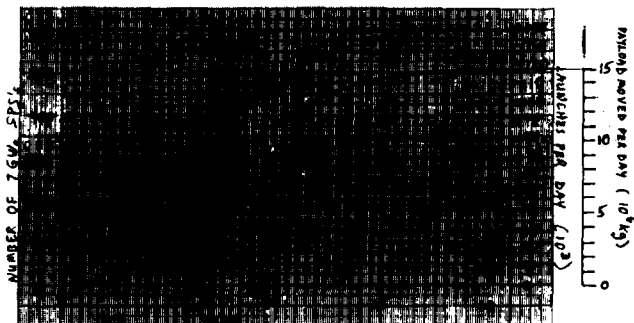


Fig. 8. Number of SPSs and launches per day vs. year

ORIGINAL PAGE IS OF POOR QUALITY

REFERENCES

1. Loomis, J. (ed.), *High Speed Commercial Flight: From Inquiry to Action*, Proceedings of the Second High Speed Commercial Flight Symposium, Columbus, OH, October 1988, Battelle Press, Columbus, OH, 1989, pp. 83-97.
2. Kaldahl, W., "Remarks Regarding Operations and Markets," in Loomis J. (ed.), *High Speed Commercial Flight: From Inquiry to Action*, Proceedings of the Second High Speed Commercial Flight Symposium, Columbus OH, October 1988, Battelle Press, Columbus, OH, 1989, pp. 77-82.
3. Koelle, D., "On the Optimum Cruise Speed of a Hypersonic Aircraft," in Webb, D. (ed.), *Proceedings of the First International Conference on Hypersonic Flight in the 21st century*, ISBN 0-9608700-1-6, Department of Space Studies, University of North Dakota, Grand Forks, ND, January 1989, pp. 278-283.
4. Lacalli, R. and H. Oman, "Economics of Hypersonic Flight," in Webb, D. (ed.), *Proceedings of the First International Conference on Hypersonic Flight in the 21st Century*, ISBN 0-9608700-1-6, Department of Space Studies, University of North Dakota, Grand Forks, ND, January, 1989 pp. 284-289.
5. Mizuno, H., "Remarks Regarding Operations and Markets," in Loomis, J. (ed.), *High Speed Commercial Flight: From Inquiry to Action*, Proceedings of the Second High Speed Commercial Flight Symposium, Columbus, OH, October 1988, Battelle Press, Columbus, OH, 1989, pp. 83-97.
6. Swihart J., *Cost Effective Transportation and High Technology*, Boeing Commercial Airplane Company, November 1984.
7. Wasiuta, H., "Hypersonic Flight - Future Commercial Potential," in Webb, D. (ed.), *Proceedings of the First International Conference on Hypersonic Flight in the 21st Century*, ISBN 0-9608700-1-6, Department of Space Studies, University of North Dakota, Grand Forks, ND, January 1989, pp. 301-306.
8. Wood, R., "Hypersonic Flight and World Tourism," in Webb, D. (ed.), *Proceedings of the First International Conference on Hypersonic Flight in the 21st Century*, ISBN 0-9608700-1-6, Department of Space Studies, University of North Dakota, Grand Forks, ND, January 1989, pp. 290-300.
9. Williams, L., "Remarks Regarding Aircraft Research and Development," in Loomis, J. (ed.), *High Speed Commercial Flight: From Inquiry to Action*, Proceedings of the Second High Speed Commercial Flight Symposium, Columbus, OH, October 1988, Battelle Press, Columbus, OH, 1989, pp. 40-52.
10. Myrabo, L. and W. Smith (ed.), *Apollo Lightcraft Project Annual Report* NASA/USRA 3rd Annual Summer Conference, Washington, DC, June 1987.
11. Myrabo, L. (editor), *Apollo Lightcraft Project Annual Report*, NASA/USRA 5th Annual Summer Conference, Marshall Space Flight Center, Huntsville, AL, June 1989.
12. Myrabo, L. (editor), *Apollo Lightcraft Project Annual Report*, NASA/USRA 5th Annual Summer Conference, Marshall Space Flight Center, Huntsville, AL, June 1989.
13. Brown, W., "Beamed Power Transmission and Transportation Systems in the Equatorial Plane," draft of paper prepared for presentation at the 9th Biennial SSI/Princeton Conference on Space Manufacturing, May 1989.
14. Walbridge, E., *Laser Satellite Power Systems*, Report No. ANL/ES-92, Argonne National Laboratory, Argonne, IL, January 1980.

1989-90 PROJECT SUMMARIES

P.6
N91-18152

THE UNIVERSITY OF TEXAS, AUSTIN DEPARTMENT OF AEROSPACE ENGINEERING AND ENGINEERING MECHANICS

There were two NASA/USRA-sponsored Advanced Design efforts at UT Austin during the 1989-90 academic year, both associated with space design. The aerospace engineering program is a sustaining program and the mechanical engineering program is a new effort. Interactions between the two programs are strong, with faculty from each department acting as consultants to students from the other department. Both programs are now coordinating their activities through the new Texas Space Grant Consortium, a consortium of universities across the state of Texas. The aerospace engineering space design program is now coordinating with the department's aircraft design course, and abstracts of the spring aircraft design projects are included in this document. Undergraduates in the spring undergraduate design courses used subsystem design notes developed by graduate students in a fall 1989 graduate spacecraft design course. The aerospace engineering program has expanded its outreach considerably, publishing a newsletter, involving Dr. Harlan Smith of the UT Department of Astronomy in a fall design, bringing in a high-school intern to work with an undergraduate design team, using an undergraduate student from the humanities as a member of a fall design team, and having a student from ENSAE (Sup'Aero) in France work as a member of a spring design team. A new aerospace engineering graduate level design course was taught in fall 1989 in which preliminary designs for five different spacecraft were developed. Student designs summarized here include two undergraduate space designs and five graduate space designs from fall 1989 plus four undergraduate space designs and four undergraduate aircraft designs from spring 1990.

GEOSTATIONARY SATELLITE SERVICING FACILITY UNDERGRADUATE, FALL 1989

The objective of this study is to create a preliminary design for a man-tendable orbiting servicing and repair facility for geostationary satellites. The facility is composed of two major elements: a habitation module and the satellite service bay. Satellite Retrieval Vehicles (SRVs) will be based at the facility and will rendezvous with satellites needing retrieval and repair. These satellites will be returned to the facility where their problems will be diagnosed telerobotically and then they will be stored. When several satellites have been retrieved and their problems analyzed telerobotically, a manned servicing vehicle will be sent, carrying the required parts, to effect the needed repairs. The repair crew will return to the Earth and the satellites will be returned to operational orbits.

The design features a nonpressurized service bay of octagonal cross-section connected to a pressurized cylindrical habitation module. The facility is powered by solar arrays on both sides of the station, mounted on long booms that also provide support for radiators. The design features a manipulator arm that is used in the repair and storage of satellites. Satellites awaiting repair can be stored outside the service bay.

LUNAR FAR SIDE OBSERVATORY AND SCIENCE BASE UNDERGRADUATE, FALL 1989

The objective of this study is to establish requirements for an observatory and science base on the farside of the Moon. A lunar observatory will allow highly accurate astronomical observations free from radio and atmospheric interference from the Earth. Such a facility will also serve as a base from which to conduct other scientific studies, thus allowing a nearside base to be designed for dedicated propellant

production. The lunar observatory is designed as a man-tendable facility that can be assembled using autonomous and teleoperated robotics.

The design features an Arecibo-type antenna array for radio astronomy, a VLF array, optical telescopes, a solar observation package, and selenographic experimentation package. The base includes a nuclear power plant and habitation modules for a crew of four. The base was designed to operate for a year in the untended mode. Crew visits would last 90 days once per year.

TEXAS EDUCATIONAL SATELLITE GRADUATE, FALL 1989

The goal of this study is to design a communication satellite, the Lone Star Satellite, to link universities, industry, research facilities, and high schools throughout the state of Texas. The services provided by this satellite could be expanded to include other southwestern states such as Louisiana, Oklahoma, and New Mexico to allow for cost sharing. Such a satellite would greatly enhance higher education by allowing universities and research centers to share lectures and seminars remotely via television. It would also provide an educational outreach program by allowing universities to broadcast lectures and programs to high schools. Communications capacity not used by the state and its agencies might be leased to the private sector to reduce the overall cost of the satellite. The primary requirement for the Lone Star Satellite (LSS) is to provide 24-channel capacity dedicated to TV signals only. An optional capability includes a steerable antenna to provide coverage of areas outside the main footprint. Another optional

capability is the inclusion of voice telecommunication channels for use by state agencies both from fixed bases and from mobile units.

The design features a three-axis stabilized, solar powered satellite similar to the commercial communications satellites currently in geostationary orbit. The satellite, on orbit, has a mass of about 680 kg. The satellite is powered by solar panels and is launched on a Delta-class booster.

ASTEROID RENDEZVOUS VEHICLE GRADUATE, FALL 1989

The primary objectives of the proposed Multiple Asteroid Rendezvous Tracker and Explorer (MARTE) are to analyze the composition and characterize the motion of five asteroids. To achieve these objectives, the spacecraft will be composed of two major components: a laboratory lander craft and five minispacecraft. The laboratory lander will be equipped with a complete sample analysis laboratory along with multiple external sensors. Each of the five minispacecraft will be much smaller than the main lab and contain only a few instruments. The minispacecraft will be targeted to five separate asteroids where they will land and perform a preliminary surface analysis. The laboratory lander will then proceed to and land upon the asteroid deemed to be the most interesting as a result of the minispacecraft's findings, where it will perform a much more detailed analysis, including sampling.

There were a number of design issues that required study in the design of MARTE. First, the asteroids in the asteroid belt are in dissimilar orbits with widely ranging orbital elements. For this analysis, an arbitrary group of about 30 asteroids with semimajor axes less than 3 A.U. and inclinations of less than 1° was chosen. Five asteroids were chosen from these 30 as a target group based solely on their relative positions during the three-year period between 1998 and 2000. Since the shape and rotation rates of most asteroids are unknown, cameras will be placed onboard the minispacecraft to provide visual identification of the shapes and to determine the rotation rates from pictures taken during the approach. Another design issue is the need for a semiautonomous control for these spacecraft. Since the roundtrip time delay for signals between the spacecraft and Earth can be over 20 minutes, control of the spacecraft from Earth would be impractical. The use of multiple minispacecraft was a major design decision. Since obtaining data on a number of asteroids is the primary objective of MARTE, and since transfer of a single spacecraft between asteroids would require large velocity changes, a single spacecraft that performs rendezvous with multiple asteroids was found to be impractical. Thus, the multiple minispacecraft scenario was adopted.

TITAN PROBE GRADUATE, FALL 1989

The objective of this study is to design a probe to study Titan, Saturn's largest moon. Titan possesses a significant atmosphere that is composed primarily of diatomic nitrogen; the surface pressure on Titan is 1.6 times that of Earth. Titan's

atmosphere is compositionally similar to Earth's early atmosphere—primarily nitrogen with traces of organic chemicals, some of which are thought to have played a significant role in the development of life on Earth. The mission objective is to gather information about Titan's meteorology, geology, and history. The spacecraft chosen for this mission consists of two portions: an orbiter and a lander. The orbiter is based on the Mariner Mark II design that will be used for the CRAF and Cassini missions. Because a design exists for the orbiter, most of our effort is directed toward developing the lander. The main constraints for this mission will be similar to previous planetary missions: total weight and trajectory limitations. Additional constraints will be imposed on the lander due to atmospheric reentry and Titan's extreme surface conditions. The Mark II probe is a modular design and our design for the lander is modular, with all subsystems broken into functional packages. This allows for the inevitable budget cuts and mission redefinition. Major subsystems present on the Titan probe include power, propulsion, thermal management, aerodynamic deceleration, landing (both soft landing and penetrators), sensors, guidance and control, attitude control, and structure. The design relies heavily on past JPL successes, but is flexible enough to incorporate current and near-future technology.

SUBSYSTEMS COMMONALITY ASSESSMENT FOR LUNAR/MARS LANDERS GRADUATE, FALL 1989

The focus of this project is to identify commonality in components of four different extraterrestrial lander vehicles that are likely to be used in the lunar/Mars program and to incorporate this information in common subsystem designs. The vehicles are the lunar piloted lander (LPL), the lunar cargo lander (LCL), Mars piloted lander (MPL), and Mars cargo lander (MCL). The LPL and MPL are both expected to carry four crewmembers from orbit to the surface and back. The MPL, however, will be expected to be a base of operations for several days on the first several missions to the martian surface. The LCL and MCL are similar in cargo capacity but differ in that the MCL is not expected to return to orbit.

The majority of the effort in this design project is directed toward the spacecraft subsystems since it is not expected that a single vehicle design will adequately handle all four missions. The subsystems examined are structures; propulsion; ECLSS; sensors; guidance, navigation, and control; computers; power; and thermal control. Commonality of subsystem design between the lunar/Mars program lander vehicles and the Earth-Mars crew transfer vehicle, which is the subject of a parallel study, are also examined. Cost savings in both the design and operations phases of a program can be achieved by setting commonality and maintainability goals early in a vehicle development program. In this study each lander vehicle's subsystem requirements and physical parameters are researched in detail and conceptual designs for the four landers are presented. Key enabling technologies are identified. By examining the four lander vehicles as a family of spacecraft constructed from common components, it is hoped that design considerations that affect program costs have been identified.

**NUCLEAR THERMAL ROCKET-PROPELLED
EARTH-MARS VEHICLE
GRADUATE, FALL 1989**

The goal of this study is to present a design for a cargo and/or crew-carrying Mars vehicle, the Mars Transfer Vehicle (MTV). This study deals mainly with hardware and systems integration rather than mission planning or trajectory analysis. Design features are (1) functional commonality; (2) propulsion system performance, reliability, and potential for further development; (3) crew safety; and (4) ease of construction. Functional commonality is important so that the vehicle can serve multiple purposes. The propulsion system chosen, a major driver in the design, will probably have far-reaching effects, since later vehicles may use derivatives of this system. Systems to protect the crew significantly affect the design of the MTV. Finally, construction and maintenance techniques must be chosen so as to reduce risks, cost, and complexity in overall vehicle operations. The overall design philosophy adopted is to use conservative estimates when dealing with projections of future technology.

The MTV is 110 m long and has an initial mass of 536 metric tons in Earth orbit. Propulsion is provided by two dual-mode 75,000-lb-thrust nuclear thermal rockets (NTRs) that supply 15 kW of electric power to the vehicle during nonthrusting operations. In the unmanned configuration, the vehicle would carry two 50-ton-capacity cargo landers. In the manned configuration, the MTV carries a habitation module with five crewmembers plus a lander. On a manned mission, the vehicle would return the habitation module and crew to Earth orbit, with the lander remaining at Mars. Typical mission length will be less than two years and the vehicle should be reusable for four or five missions. The projected vehicle lifetime is about 15 years, including layovers at Earth and at Mars.

Assumptions are that the MTV will be constructed in Earth orbit, relying on Space Station *Freedom* and large Orbital Transfer Vehicles (OTVs); nuclear propulsion will be politically feasible from a Nuclear Safe Orbit at about 800 km altitude; low-boiloff, advanced liquid hydrogen tanks will be available; landing sites will be selected using unmanned precursor missions; four major propulsive burns are made during the mission (trans-Mars injection, a braking maneuver at Mars, trans-Earth injection, and a final braking maneuver at Earth); a heliocentric near-Hohmann Earth-Mars transfer is used; and the final orbit is 900 km above the surface of Mars. The orbits of the planets are assumed to be circular and coplanar. The required velocity impulses are found using a patched conic approximation. Using these assumptions, the velocity impulse required for Earth departure is 3.49 km/sec and the velocity impulse at Mars arrival is 2.04 km/sec. The fuel budgets are increased by 10% to account for approximation inaccuracies and midcourse corrections. Under these assumptions, the one-way transfer time is about 260 days.

The spacecraft rotates slowly at about 0.5 rpm to provide uniform solar thermal loading to the vehicle exterior. The nuclear reactors each generate approximately 1556 MW of thermal power during propulsive burns. This heat is transferred to the hydrogen propellant and is rejected when the hydrogen

exits the nozzle. This method of heat rejection is also used during the reactor cool-down period. When operating in electrical power generation mode, a reactor will produce about 1 MW of thermal power. Radiators for the power generation system are located on the surface of the power module and on small fins attached to the surface. The masses of the thermal control systems are included in the mass estimates for the propulsion subsystem and the power subsystem.

The vehicle configuration chosen has a single truss surrounding the central tank. The primary structure is an axial truss of square cross-section. The truss is sized to surround a central fuel tank (7.5-m-diameter). Ten truss bays are used to sufficiently distance the radiation-sensitive crew and payload from the NTRs. There are five reusable titanium honeycomb fuel tanks, each 7.5 m in diameter, and 23 m long. Combined, they hold 365 tons of liquid hydrogen (LH₂). The central tank is sized to use the LH₂ to shield the habitation module and payload from the NTRs.

**COMPREHENSIVE ORBITAL DEBRIS
MANAGEMENT PROGRAM
UNDERGRADUATE, SPRING 1990**

Since the launch of Sputnik I in 1957, humans have placed over 19,500 objects into various orbits around the Earth. Of these objects, many unwanted ones have been removed through reentry, but over 7100 unnecessary items large enough for routine tracking remain in orbit. In addition, the North American Defense Command estimates that there are 40,000 to 55,000 residual orbiting objects that are too small to be tracked.

These remnants, commonly known as space debris, pose serious risks to space operations. A collision with space debris could result in the death of crew and/or destruction of property. In addition, there is also the possibility of a cascade (Kessler) effect. Originally predicted by Donald J. Kessler, space debris expert at NASA, the cascade effect theory predicts that debris could become self-generating in the near future. Kessler asserts that even if no new objects are placed in orbit, fragmentation from the collisions between existing objects will not only increase the amount of debris, but will result in more collisions causing an exponential growth of space debris.

Due to the dangers of space debris, viable long-term solutions must be developed and implemented before the situation becomes uncontrollable. Because of the cascade effect, solutions such as satellite shielding or debris avoidance systems provide no long-term help. Long-term solutions involving space debris removal are being studied in order to address the cascade effect and reduce the threat to current and future space endeavors.

The proposed debris management plan includes debris removal systems and preventive techniques and policies. The debris removal is directed at improving the current debris environment. Because of the variance in sizes of debris, a single system cannot reasonably remove all kinds of debris. No

effective system is currently available to remove the debris smaller than 10 cm in diameter. However, an active removal system, which deliberately retrieves targeted debris from known orbits, was determined to be effective in the disposal of the larger debris that can be tracked directly from Earth.

A roving debris-removal vehicle, based on the OMV, has been designed to rendezvous with large debris pieces, attaching deorbit propulsion modules. The roving debris-removal vehicle has two arms and "glues" the deorbit propulsion system to the debris pieces. Telerobotic control is used on the roving vehicle. The vehicle is periodically resupplied using a launch-on-demand refueling vehicle. The refueling vehicle deorbits itself after transferring the supplies and fuel to the roving debris-removal vehicle.

The second part of debris management is its prevention. This prevention program is intended to protect the orbital environment from future abuses. This portion of the plan involves various methods and rules for future prevention of debris. The preventive techniques are protective methods that can be used in future design of payloads. In order to encourage launching states to employ these preventive measures, several international treaties have also been proposed.

MICROGRAVITY FREE-FLYERS FOR SPACE STATION UNDERGRADUATE, SPRING 1990

The goal of this project is to design a spacecraft that will be used with Space Station *Freedom* to provide the best possible environment for microgravity experiments. Astronauts, pumps, and other vibration-causing entities onboard *Freedom* cause this environment to be degraded substantially. A free-flyer will be designed to overcome these disturbances by being removed from *Freedom* while microgravity experiments are running. The mass of the experiments will be up to 1000 kg, with experiment lifetimes up to 2 years. The free-flyer will automatically deploy, maintain stability, reboost when necessary, and return to *Freedom* for changing experiments.

A typical mission profile will consist of placing experiments onboard, performing a check-out of the systems, deploying the free-flyer, controlling the attitude and orbit, sending experimental data to *Freedom*, reboosting when necessary, returning to *Freedom*, docking, and changing experiments. Each aspect of the mission presents problems. The level of human interaction—that is, how much of the astronauts' time will be required—will have to be determined by the free-flyer. Experiments will have to be fitted to each free-flyer mission. Power requirements, communication requirements, microgravity tolerances, and duration requirements must be considered for each experiment onboard the free-flyer. Compatible experiments will then be fitted together. The free-flyer should be stabilized with minimum acceleration and vibration.

The free-flyer is designed to be placed in orbit by the space shuttle and to fly up to five experiment modules. The core vehicle contains one or more power modules, a variable capability propulsion module, a thermal management system, and an attitude control system. Any module can be replaced using the Space Station mobile manipulator arm.

ALL-TEXAS EDUCATIONAL SATELLITE SYSTEM UNDERGRADUATE, SPRING 1990

In an effort to unite educational resources throughout the state of Texas, the 1989 Texas Senate passed Senate Conference Resolution No. 23. This resolution directs the Automated Information and Telecommunications Council to study the feasibility of a state-sponsored educational satellite project. The objective is to design a satellite communications system (TEXSTAR) that will enhance the educational productivity in Texas. Such a system will enhance education at all levels throughout the state. The design team has designed TEXSTAR, an educational satellite communications system that will be considered a means of equalizing the distribution of educational resources throughout the state. TEXSTAR will be capable of broadcasting live lectures and documentaries, in addition to transmitting data from a centralized receiving-transmitting station. Included in the design of TEXSTAR are system and subsystem design for the satellite and design of ground stations. The launch vehicle used will be the Texas-built Conestoga 421-48. The TEXSTAR system incorporates a cluster of three small satellites in slightly inclined geosynchronous orbits. Because of the configuration and spacing of these satellites, the system will be accessed from ground stations as if it were one large, geostationary satellite.

To fulfill all service objectives, TEXSTAR must be able to relay 20 video signals simultaneously, providing uninterrupted coverage to the entire state 24 hours per day. Transponder number and size, however, must be weighed against the mass and cost of the satellite. This effort is designed to benefit not only the Texas educational system, but also the Texas economy. Therefore, satellite components and launch vehicles designed and built in Texas will be used as much as possible. The success of the TEXSTAR project will provide better services, create jobs, and attract national attention to this innovative solution to our educational dilemma.

LUNAR CORING LANDER SEARCHING FOR WATER AT THE LUNAR POLES UNDERGRADUATE, SPRING 1990

As a new era in manned space exploration of the solar system begins, NASA is turning its sight back to the Moon. Plans to build a lunar base are presently being studied. One of the most important considerations is qualifying and quantifying the presence of water on the Moon. The existence of water on the Moon implies that future lunar settlements may be able to use this resource to produce things such as drinking water and rocket fuel. Because of the very high cost of transporting these materials, *in-situ* production could save billions of dollars in operating costs of the lunar base.

Scientists have suggested that the polar regions of the Moon may contain some amounts of water ice in the regolith. This report suggests six possible mission scenarios that would allow lunar polar soil samples to be collected for analysis. The options presented are a remote sensing satellite; two unmanned robotic lunar coring missions (one is a sample return and one is a data return only); two combined manned and robotic polar coring missions; and one fully manned core

retrieval mission. Each mission has its own advantages and all are considered to be viable with little or no required advancement of the present state of technology.

One of the combined manned and robotic missions has been singled out for detailed analysis. This project proposes sending at least three unmanned robotic landers to the lunar pole to take core samples as deep as 15 m. Upon successful completion of the coring operations, a manned mission would be sent to retrieve the samples and perform extensive experiments in the polar region. The lander subsystems are descent propulsion, automatic landing site selection system, self-leveling landing gear, power, thermal management, drilling and core handling, sample module ascent propulsion, sample return vehicle guidance, sample landing propulsion, and sample package landing gear.

**ATLAS AIRCRAFT-BUSHWHACKER PROJECT
LOW-INTENSITY CONFLICT AIRCRAFT (LICA)
UNDERGRADUATE, SPRING 1990**

During the 1980s, the transition from emphasis on full-scale battles to localized low-intensity conflicts created a demand for a low-cost aircraft designed for close-air support against a lightly armed opposition. The Bushwhacker project focused on developing an aircraft that falls between the capability of a counterinsurgency aircraft such as the North American OV-10 developed in the 1960s and the present battlefield tank killer, the Fairchild A-10 developed in the 1970s. Its primary task will be forward air control, which consists of a defined loiter time combined with a series of attack runs to deliver rockets, machine-gun fire, and other antipersonnel ordnances. The low-intensity conflict aircraft (LICA) will be marketed for the U.S. Armed Forces and U.S. allies in the Central American region. The project trade studies are directed toward developing a maneuverable and agile aircraft whose cost does not outweigh its military worth.

The LICA is a straight-wing, twin-turboprop-powered aircraft with a maximum takeoff weight of 16,650 lb, a span of 46.6 ft, a length of 43 ft, and a wing area of 333 sq ft. It carries a payload of 1620 lb, has a maximum attack speed of 325 kt and a stall speed of 132 kt. The sea-level rate of climb is 3500 ft/min. Its takeoff distance is 1000 ft and its landing distance is 700 ft.

**THE "GATEKEEPER" MULTIMISSION
ANTI-DRUG AIRCRAFT
UNDERGRADUATE, SPRING 1990**

The flow of illegal narcotics has become an uncontrollable problem. Current drug interdiction methods are failing to curb large amounts of narcotics entering the U.S. onboard light aircraft. Drug-laden aircraft regularly elude radar and evade capture to deliver drugs. U.S. Customs relies on multiple aircraft to perform drug interdiction. Presently, Customs uses radar-equipped E-2C Hawkeyes to search for smugglers. The E-2C guides a Cessna Citation II to a potential target for identification and possible pursuit. If a drug drop is observed, a HU-60 Blackhawk helicopter is directed to apprehend smugglers on the ground.

The Gatekeeper will be a new drug-interdiction aircraft combining the drug-interdiction capabilities of the Citation II and the Blackhawk. Gatekeeper will be designed to intercept a wide variety of adversary aircraft. The DC-3, Cessna 310, and the Cessna 172 (all used to smuggle drugs) will be used to set Gatekeeper performance requirements.

Gatekeeper will have (1) sufficient payload to carry advanced radar for tracking illegal drug aircraft, (2) long endurance to allow sustained surveillance, and (3) a flight envelope wider than the composite envelope of the three competitor aircraft mentioned above. This will enable Gatekeeper to apprehend drug smugglers and should serve as a potent deterrent to the import of illegal drugs in the U.S. The Gatekeeper design features a span of 62 ft, a length of 42 ft, a cruise speed of 120 mph, with a maximum speed of 0.78 Mach. Its design cruise altitude is 7000 ft and its range is 1970 n.m. The Gatekeeper weighs 23,000 lb at takeoff, and carries 7300 lb of fuel and a payload of 2500 lb. It is powered by two 3300-hp turboprops with counterrotating propellers. It has an aspect ratio of 9 and a wing area of 429 sq ft. Specific fuel consumption is 1.36 lb/hr/lb at cruise.

**THE PEREGRINE I, A FUTURISTIC
COMPETITION SAILPLANE
UNDERGRADUATE, SPRING 1990**

In 2050, technological advancements in fields including metallurgy and aircraft design will allow new and innovative ideas to flourish in the public and private arenas. Soaring will replace yachting as the ultimate in international competition, spurring American industry to take the reins in an effort to gain superiority in the highly competitive sport. The goal of this project is to extrapolate the results of current research and use them to conceptually design the Peregrine I, a futuristic sailplane that will lead the United States to preeminence in international competitive soaring. Efforts are made to incorporate the vertical and horizontal tail configurations into the fuselage and wings. To soar competitively using this unconventional no-tail design, the sailplane will employ miniature onboard flight computers. Enormous strides in the study of engineering materials will allow the use of composites to reduce aircraft weight. Additionally, boundary layer control mechanisms and advanced airfoil and wing designs will be considered for the sailplane design. The availability of advanced technologies is being anticipated to conceptually design a futuristic sailplane that will bring the United States to dominance in international soaring competition.

**THE "BALLISTICO"—A PLATFORM FOR
MICROGRAVITY EXPERIMENTS
UNDERGRADUATE, SPRING 1990**

The objective of this study is to provide an alternative aircraft to the NASA KC-135 aircraft presently used to conduct parabolic microgravity flights. The purpose of this aircraft is to provide a limited microgravity environment for research applications such as biomedical and human-adaptation studies, materials processing, fluid physics, life sciences, and spaceflight hardware testing. The mission performed by the KC-135

consists of 40 parabolas with a microgravity time of 25 sec/parabola. The Ballistico's mission requirements are to conduct 72 parabolic maneuvers with a microgravity time of 28 sec/parabola. The aircraft is similar in design to the KC-135 with the capacity for 20-25 passengers and 20,000 lb of research equipment.

The Ballistico aircraft is a 230,000-lb (takeoff weight), four-engine aircraft with four Rolls Royce RB211-535C engines at 37,000 lb thrust each at sea level. The aircraft carries a 24,900-lb payload and has a ceiling of 37,000 ft. The wing area is 1716 sq ft, the span is 115 ft, and the length is 156 ft. The cruise speed is Mach 0.82 at 25,000 ft.

209
P.4

PROJECT SUMMARIES

N91-18153

THE UNIVERSITY OF TEXAS, AUSTIN

INTRODUCTION

The Mechanical Engineering Design Projects Program (MEDPP) at The University of Texas at Austin is the capstone engineering course in the Mechanical Engineering curriculum. Teams of three or four students work together for one semester on industry-sponsored engineering projects; projects are typically sponsored when the sponsoring company does not have the time or resources to solve a problem, wants independent verification of in-house studies, or wants a fresh and uninhibited approach to a design problem.

A number of NASA projects (sponsored by Johnson Space Center, Houston, Texas) were undertaken by student teams in the MEDPP from 1984 through 1987. Additional space projects were sponsored by USRA through the Advanced Design Program in a cooperative effort with the Aerospace and Engineering Mechanics Department at The University of Texas at Austin from 1986 through 1989.

In June 1989, the MEDPP became a participating member in the USRA Advanced Design Program. Four projects were completed during the first semester as a participating member and three projects were completed during the second. The first project discussed deals with the use of satellite data in managing the use of Earth resources. The remaining six projects focus on the design of vehicles and equipment for use in NASA's proposed lunar base. A discussion on the lunar base precedes the project descriptions to clarify assumptions used in the design process.

DEVELOPMENT OF A COMPUTER SIMULATION MODEL FOR PREDICTING VESSEL STATION-KEEPING REQUIREMENTS IN THE GULF OF MEXICO

Satellite data are currently used in a variety of ways, ranging from meteorology and weather forecasting, communications, and monitoring trends in the use of Earth resources. Satellites can also be used to accurately measure the distance from the Earth's surface (either land or water) to the satellite. Knowing the satellite's altitude at all points in the orbit allows satellite altimeter data to be converted into a height above or below a chosen reference level.

One use of satellite altimeter data is for the determination of wave heights in a body of water. Wave height data indicate water speed and direction, so they are useful in tracking major water currents (such as the Loop Current in the Gulf of Mexico) and eddies (large columns of rotating water spawned by major water currents). Wind velocity can also be determined from wave height data; therefore, weather predictions can also be made using the data from satellite altimeters.

Development of a computer simulation model for predicting vessel station-keeping requirements was the goal of this project. An existing code, used in predicting station-keeping requirements for oil drilling platforms operating in North Shore (Alaska) waters was used as the basis for the computer simulation. Modifications were made to the existing code to adapt it for use in simulating conditions found in the Gulf of Mexico (e.g., location of land masses, major water currents, etc.).

The input data to the model consists of satellite altimeter readings and water velocity readings from buoys stationed in the Gulf of Mexico. The satellite data consist of altimeter readings (wave height) taken during the spring of 1989. Each satellite image records wave height data in a 1-km² area of the Gulf of Mexico. In addition, the groundtrack of the satellite repeats every 16 days indicating that data taken during the current orbital pass is 22.5° west of the previous data. Therefore, smoothing techniques were used to account for the spatial and temporal separation of the satellite data in developing a complete input file for the computer model.

Buoys are periodically placed in the Gulf of Mexico to track the direction and speed of the water at various points. Available buoy data is used to verify the water velocity and direction predicted by the computer simulation.

The simulation model predicts water velocity and direction, and wind velocity. Knowledge of these parameters is used to determine vessel station-keeping requirements and weather forecasts. The simulation model can also be used as a resource-minimization tool. Fuel consumption can be greatly reduced through the proper location of vessels in areas of low water velocity.

LUNAR BASE PROJECTS

Background

The concept of a manned lunar base has intrigued mankind for many years. Current mission scenarios call for the establishment of a lunar base beginning soon after the turn of this century. The reasons for establishing a lunar base can be broken down into scientific, resource production, and technology development considerations. The primary lunar resource production effort is focused on the extraction of oxygen from the lunar soil. The production of lunar oxygen (LUNOX) is considered essential for manned exploration of the solar system and beyond.

While the designs were being developed, the following assumptions concerning existing facilities and technologies were made. First, it was assumed that an operational space

station is in low Earth orbit (LEO). A space station is needed as a staging point for the vehicles that will carry crews and cargo to the Moon. Crew cabs and cargo will be carried on lunar landing vehicles resembling the Lunar Excursion Module (LEM) used during the Apollo program. The landing vehicle will be propelled from LEO to low lunar orbit (LLO) using a transport vehicle. Once in LLO, the lunar landing and transport vehicles will separate, with the lander continuing on to the lunar surface.

Second, it was assumed that missions to the Moon will be scheduled approximately six months apart. Using this timetable, lunar cargo landers are required to sit unattended in the lunar environment for long periods of time until the next manned mission arrives to off-load the cargo. Under the present mission scenarios, the lunar landing vehicles are considered expendable until the lunar base becomes manned, at which point the vehicles can be designed with multimission capabilities.

Once the lunar base becomes somewhat developed, launch and landing facilities will be established at some distance from the habitation modules, laboratories, and power plant. This is necessary in order to minimize the danger of landing and launching vehicles in populated areas and because soil particles lofted by the lander engine blast can cause damage to equipment and vehicles.

All the structures and equipment making up the lunar base must be protected from the harsh lunar environment, which includes solar and galactic radiation, extreme temperature fluctuations, periodic micrometeorite impacts, and the constant presence of intrusive and abrasive lunar dust. In order for the lunar base to be a feasible project, innovative designs are needed that will minimize the weight, space, power consumption, manpower, and operation times of the structures, equipment, and vehicles for the lunar base.

Reconfigureable Lunar Cargo Lander

The establishment of a lunar base will require large amounts of equipment and material to be transported to the Moon. During the Apollo lunar missions and in the current lunar base scenario, much of the lunar vehicle is discarded after performing its intended function. The high cost of transporting equipment from the Earth to the Moon makes disposal of any equipment extremely undesirable. Therefore, a lunar landing vehicle that reconfigures into another machine will aid in minimizing the mass to be transported to the Moon during the establishment of a lunar base.

A lunar cargo lander has been designed that can be reconfigured to form the structure over a habitation module; the structure will support the regolith layer used for radiation and thermal protection of the crew and equipment. The lander consists of four legs attached to a central platform. The habitation module and associated internal payload are mounted along one centerline of the platform. Propellant tanks and instrumentation are mounted to the platform in the areas around the habitation module. The lander engines are mounted on the underside of the central platform; the platform

prevents damage to the vehicle components during firing of the engines by isolating them from the engine blast.

After the habitation module, propellant tanks, instrumentation, and engines have been removed from the lander, the legs and central platform are reconfigured such that the lander "straddles" the habitation module. The lander structure will be covered with a fine mesh or blanket and then covered with regolith. The design of the lander also permits multiplexing of the habitation modules in any array desired. Therefore, for every cargo lander sent to the Moon, a payload is delivered and a habitation module (complete with radiation and thermal protection) is produced.

Thermal and Micrometeorite Protection System

As mentioned in the background section, the assumption was made that lunar cargo landers will sit unattended in the lunar environment for long periods of time between successive missions. The lunar cargo lander and payload must be able to endure the lunar environment, which is characterized by large temperature changes and periodic impacts by micrometeorites. A system is required that will protect lunar cargo landers and payloads in these conditions.

A thermal and micrometeorite system that deploys after landing has been designed. The system consists of a composite blanket that is stowed in compact form during transport to the lunar surface. The composite blanket, in the deployed configuration, will provide thermal and micrometeorite protection for the lunar cargo lander. Compressed air "struts" are built into the blanket and are used to deploy the protection system and stiffen the blanket in the deployed position, so that it does not rest against any part of the lander.

Compressed air for the protection system is obtained by boiling off the liquid oxygen (LOX) remaining in the propellant tanks. Air pressure in the struts is maintained using a simple boiler device and valves that regulate the flow of air into and out of the struts. Pressure regulation is required since it is anticipated that the air pressure in the struts will change in response to changes in the ambient conditions.

Once the lander has been off-loaded and the protection system is no longer required, the system can be reconfigured for use as (1) the covering for the structure over the habitation module prior to the addition of the regolith or (2) the exterior covering for a lunar base garage, maintenance facility, or similar structure.

Versatile Lifting Machine with Robotic Capabilities

The establishment and operation of a lunar base will require machines with lifting capabilities for loading and unloading cargo, and robotic capabilities for dextrous operations. A single machine, capable of performing a variety of lifting operations as well as robotic activities, would increase the rate of lunar base development by minimizing the amount of equipment transported to the Moon.

A versatile lifting machine has been designed that is capable of heavy-lift and robotic operations. The machine consists of a chassis, telescoping boom attached to a rotating turntable, robotic manipulator, outriggers (stabilizing legs), and wheels.

The boom is a truss structure composed of three separate sections that telescope to suit the particular operation. The boom is equipped with a hook and cable assembly for general lifting operations similar to cranes on Earth. The robot manipulator is a serial mechanism with 7 degrees of freedom; the manipulator is attached to the end of the boom to aid in attaching the cable to payloads as well as for performing dextrous operations. Attaching the manipulator to the boom allows the manipulator to be positioned within a large work envelope. The manipulator end-effector is a simple three-jaw gripper that permits a wide variety of robotic tasks to be performed.

Four telescoping outriggers are attached to the chassis to stabilize the machine during lifting operations. The outriggers are retracted during transport (to the Moon and on the lunar surface) of the lifting machine. The wheels for the lifting machine are cone-shaped wheels selected for their good performance characteristics in the lunar soil. A hitch is mounted to the lifting machine chassis allowing it to be towed behind a drive vehicle.

Cargo Transport System

A lunar base will likely consist of a number of developed areas (e.g., habitation, laboratory, launch and landing facility, power plant) set apart from each other due to safety considerations. A point-to-point cargo transport system linking the various areas of the lunar base could reduce the power consumption and the manpower needed to move cargo and equipment from one part of the base to another.

A cargo transport system has been designed that consists of an autonomous vehicle that travels on a self-repositioning track. The vehicle consists of an enclosed cargo compartment attached to a chassis; the batteries, drive train, and instrumentation are mounted to the chassis beneath the cargo bay. A serial manipulator is mounted at each end of the vehicle with a conveyor belt running between the two manipulators.

The vehicle is driven by two wheel assemblies located beneath the vehicle. The direction of travel is controlled by guide wheels located on the wheel assemblies that are in contact with a guide rail at the center of each track section. The vehicle drives on a track that is made up of individual track sections connected by a coupling device; track sections are continuously repositioned using the procedure that follows.

As the vehicle moves forward, the rear robotic arm picks up the track section over which the vehicle has just passed and places it on the conveyor belt. At the same time, the forward robotic arm takes a track section off the conveyor belt and attaches it to the track sections already on the ground. The conveyor belt is used to transport track sections from the rear of the vehicle to the forward end.

Direction of travel for the vehicle is determined by the positioning of the track sections. Turning the vehicle is accomplished by laying successive track sections at an angle to the previous sections specified by the desired turning radius. The use of this design will permit energy-efficient transport of cargo and equipment between various areas of a lunar base without a developed roadway.

Design of a Road Construction System for a Lunar Base

The operation of a lunar resource production facility will require the transport of large amounts of raw and processed materials to different areas of a lunar base. In the event that an autonomous transport system (such as the one described above) cannot fulfill the transportation requirements, a system of roads and the associated construction machinery will be required to minimize the energy expended in transporting materials to different areas of the base. A design for a road construction system satisfying these needs is discussed below.

The first step in the project was to determine the road type best suited to the needs of a lunar base. Types of roads considered included concrete, paved, sintered-soil, gravel, and dirt. Consideration was given to the materials and energy required to build each type of road as well as the specific road maintenance requirements and ease of repair. A compacted-dirt road was determined to be the most suitable.

The next step was to identify the machine functions required to produce a compacted-dirt road. The functions identified were excavating and leveling of the regolith, distributing regolith in the excavated roadway, and compacting the regolith to produce a smooth, hard surface. Background research was performed to identify the existing terrestrial machines used to perform these functions as well as any conceptual designs proposed during lunar base studies.

The road construction system selected consists of a main drive unit, a grader attachment, and a vibratory compactor. The main drive unit is a general purpose vehicle that can be used for a variety of operations in addition to its intended use in road construction. Four dome-shaped wheels, a wide wheel-base, and a low center of gravity provide excellent stability for the vehicle while performing any number of operations. A ballast area is provided that can be filled with regolith to increase the vehicle traction forces. A hitch is mounted to the rear of the chassis for towing vehicles.

The grader attachment connects to the front of the main drive unit and the vibratory compactor is towed behind the drive unit. The grader is designed to permit easy adjustment of the cutting blade (e.g., depth of cut, bite angle, and orientation of blade with respect to direction of travel). Vibratory compaction is achieved using a roller and oscillating weight combination. All equipment is designed for operation by base personnel; however, provisions for teleoperation of the road construction system were made during the design of the system.

Design of a Device for Removing Lunar Dust from Material Surfaces

The Apollo lunar missions showed that lunar dust caused a variety of problems ranging from damage to equipment to endangering crew health. The dust was found to be extremely abrasive and to be selectively attracted to a number of materials. The first part of this project was devoted to the characterization of physical properties of lunar dust, and the second to the design of a device for removing the dust from material surfaces.

The dust attaches to material surfaces through mechanical bonding and electrostatic forces. In addition, the dust has a strong affinity for painted metal and plastics. Once the forces holding the dust on surfaces and the materials to which the dust has an affinity were identified, methods for breaking the bonds attaching the dust to a material were proposed.

Since the dust is held to a surface using primarily mechanical and electrostatic forces, three general methods (mechanical, electrostatic, and chemical) for removing the dust were identified. Mechanical methods for dust removal include vibration, scraping/brushing, air jet, and suction (for use in pressurized environments only). Electrostatic methods include both passive (grounding the material surface) and active (preferentially attracting the dust to a stronger electric field). Finally, chemical means for dust removal consist of breaking the bonds using a liquid solution.

The target application for the dust removal device is a spacesuit used in lunar base operations. This application requires that the device work on different materials as well as equipment with irregular geometries.

The final design consists of a brush-blower device designed for use in a nonpressurized environment. A brush, consisting of rows of flexible plastic bristles, is mounted on the end of the device. Gas nozzles are located such that the dust is blown away from the material surface once the brush has loosened

the dust. Small amounts of a waste gas (carbon dioxide) are needed for operation of the device.

The dust-removal device is designed for ease-of-use by personnel wearing spacesuits. Control of the gas flow is achieved using a variable-flow needle valve. In addition, a "dead man" feature is provided that prevents the accidental loss of gas in the event that the device is dropped.

CONCLUSIONS

One of the primary goals of the USRA Advanced Design Program is to foster student interest in space activities and engineering. Working on the space design projects allows students to understand the challenges of designing equipment and vehicles for various missions and environments. In addition, other activities of the USRA give students the opportunity to present their work to an audience outside their university through mid-semester reviews as well as the Summer Conference.

The benefits of the ADP are not limited to the students working on the project. The graduate Teaching Assistant and faculty members involved with the program also benefit through their contact with students, other faculty, and NASA researchers. The ADP undoubtedly creates an interest and excitement in space engineering extending far beyond the university campus.

P. 4 213

MIMES AND GEOSHACK
UNITED STATES NAVAL ACADEMY

N91-18154

**MULTIPLE INTEGRATED MICROSPACECRAFT
 EXPLORATION SYSTEM**

It is the goal of mankind to eventually visit Mars. Before such a visit occurs, it would be valuable to gain scientific information about the planet. The Multiple Integrated Microspacecraft Exploration System (MIMES) is designed for that very purpose. The MIMES mission will send to Mars a spacecraft carrying five probes, each of which will descend to the martian surface to engage in scientific experiments. There will be two types of probes: a penetrator that will embed itself in the martian surface, and a soft lander. The probes will transmit scientific data to the carrier spacecraft, which in turn, will relay the information to Earth.

Launch Vehicle

MIMES includes a 115-kg carrier spacecraft, or bus, and five 15-kg probes. Each probe is a microspacecraft, which can be defined as a space vehicle with a mass under 20 kg. The entire package will be carried by a Taurus launch vehicle (see Fig. 1), which is being developed jointly by the Hercules Aerospace Company, the Defense Advanced Research Projects Agency (DARPA), and Orbital Sciences Corporation. Its upper three stages are currently used on the Pegasus, an air-launched vehicle that uses a wing to provide lift. The first stage of the Taurus is the booster used on the MX Peacekeeper missile of the U.S. Air Force.

Propulsion

The MIMES bus will travel to Mars by means of a Hohmann transfer orbit. It will use a liquid bipropellant for the escape and capture burns. The fuel consists of monomethyl-hydrazine and nitrogen-tetroxide. The total mass of this fuel is 914 kg, and it is carried in four groups of tanks, with a primary and secondary group for each constituent (see Fig. 2).

Orbital Mechanics

The bus will enter a circular parking orbit about the Earth at an altitude of 460 km, maintaining three-axis stabilization with monopropellant hydrazine thrusters. It will then execute the escape burn, entering a Hohmann transfer orbit about the Sun. During this stage, the bus will communicate with a ground station on the Earth by means of four omnidirectional whip antennas. It will receive its power from solar cells attached to its sides. After the bus enters the sphere of influence of Mars, but before it executes the capture burn, it

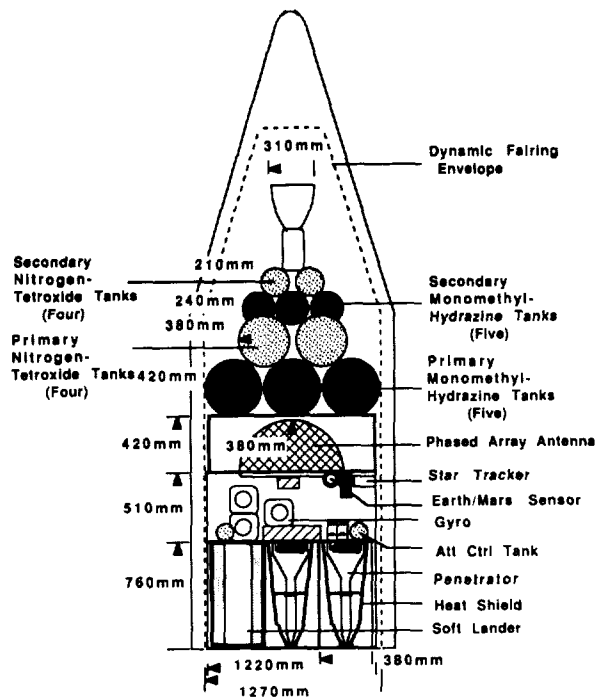


Fig. 1. Bus and Probes in Taurus Fairing

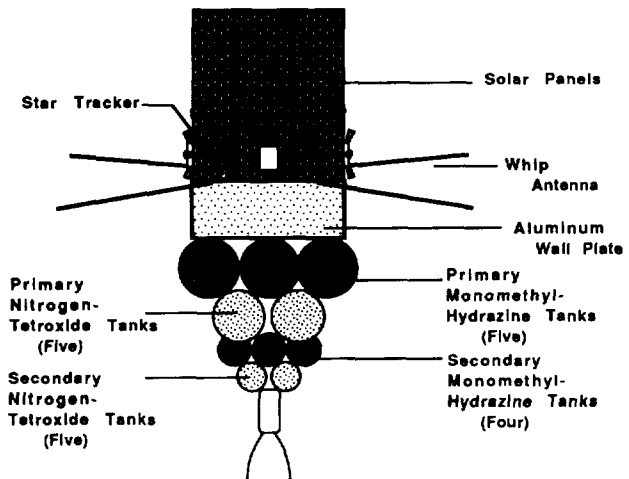


Fig. 2. Interplanetary Transfer Configuration

**ORIGINAL PAGE IS
 OF POOR QUALITY**

will deploy the five probes. Each probe will be ejected out the top of the bus by the use of a spring. This will occur at a distance of approximately 40,000 km from Mars.

Atmospheric Entry

After being deployed, the probes will approach Mars and descend into the atmosphere of the planet. The probes will have heat shields made of a flexible carbon fabric coated with an ablative material, which will provide protection and aid deceleration. Each probe will separate from its heat shield and deploy a parachute. The parachutes will be designed to allow the penetrators and the soft landers to descend at speeds of 135-165 m/sec (490-590 km/hr) and 18 m/sec (65 km/hr), respectively. The penetrators, which are built of titanium, will be able to survive an impact of up to 300 g. The soft landers, made of aluminum, will each have an airbag to dissipate energy on impact.

Penetrator Instrumentation

After embedding themselves in the martian surface, the penetrators will begin scientific experiments. Upon entry, accelerometers will be used to determine the deceleration profiles of the penetrators. In addition, gamma-ray spectrometers will be used to analyze the martian soil. Thermal probes will also be used, determining ambient temperatures, near-surface thermal conductivity, and ambient heatflow. Finally, seismometers will be used to determine the interior structure of Mars. Ultimately, an entire network of seismic stations may be established with additional MIMES missions.

Soft Lander Instrumentation

The soft landers will conduct a variety of experiments. Each will have an atmospheric descent package that will measure temperature, pressure, density, and high-altitude wind speeds. On the ground the soft landers will become meteorological stations that measure temperature, wind speed and direction, pressure, humidity, and atmospheric dust loads. The soft landers will be able to conduct more experiments than the penetrators because they have a larger volume, yet a lower structural mass.

Orbiter Operations

After deploying the probes, the bus will execute a capture burn to enter a polar circular parking orbit at a 4500-km altitude. This altitude is high enough to avoid aerodynamic drag and significant gravity-gradient disturbance torques. It is also low enough to accommodate data received from forty probes simultaneously. Initially, the bus will not be able to receive transmissions from the probes because its phased-array antenna will be blocked by the fuel tanks. After the capture burn, the tanks will be jettisoned by means of explosive bolts, uncovering the antenna (see Fig. 3). The bus will then maintain three-axis stabilization by means of monopropellant hydrazine thrusters, contained in four small tanks within the

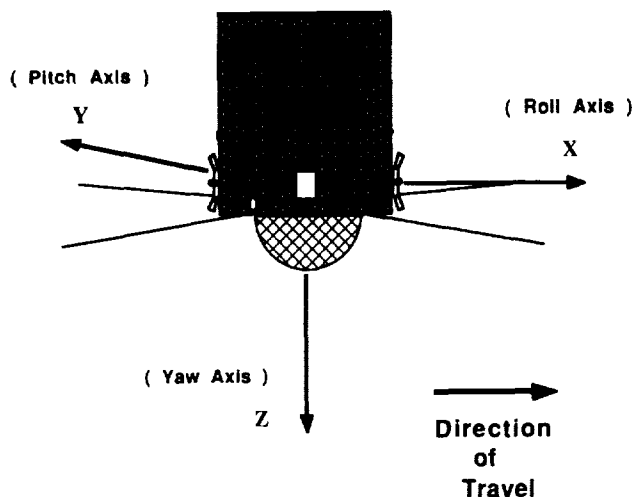


Fig. 3. Mars Orbital Configuration

bus. These thrusters will also be used to orient the phased-array antenna toward Earth, allowing stored data to be transmitted. Data will not be transmitted while the bus is in the shadow of Mars, as the bus will only be able to draw power from nickel-cadmium back-up batteries.

Summary

MIMES involves the use of microspacecraft for a mission that in the past has required vehicles with thousand-kilogram masses. While the MIMES penetrators and soft landers will not carry as many instruments as would such larger spacecraft, MIMES does provide the opportunity for multiple missions. Follow-on launches, with buses that do not require capture burns, would provide enough instruments on Mars' surface to collect as much data as the larger spacecraft. In addition, the MIMES probes would be carried aloft on several launches, reducing the risk of losing an entire system on a failed launch. These factors make MIMES an important consideration in the exploration of Mars.

GEOSHACK

GeoShack, the Geosynchronous Operations Support Center, is a manned spacecraft intended for use in geostationary orbit (see Fig. 4). Due to the high cost of satellites in geosynchronous equatorial orbit (GEO), their numerous and varied missions, and the heavy use of geostationary orbit, it would be beneficial to have a manned spacecraft with the specific purpose of servicing and maintaining satellites in that orbit. The spacecraft would be permanently stationed at GEO. In effect, GeoShack would be a small space station outpost. It would possess all standard crew support and servicing equipment needed for short duration missions. Astronauts would be transferred from the space station to GeoShack and return to the space station using a Space Transfer Vehicle (STV).

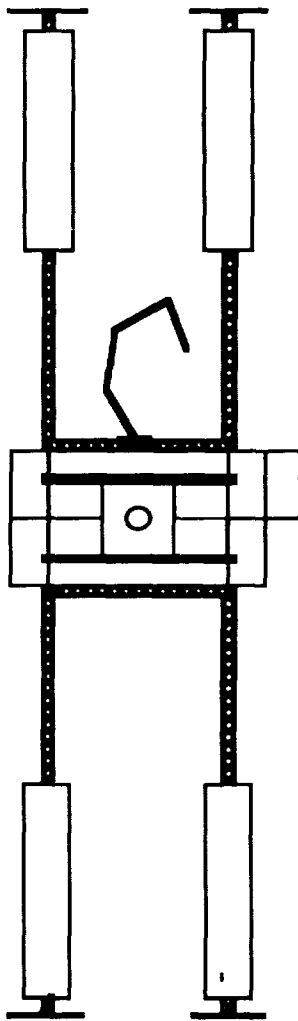


Fig. 4. GEOSHACK Orbital Configuration

Introduction

The mission of GeoShack is to service geostationary satellites and thus extend the lifetime of hardware in an increasingly crowded orbit. GeoShack was designed on the premise that it would be a long-life spacecraft that would begin functioning in the late 1990s. Imperative to this design is the presumption that the space station is manned and functional; a majority of GeoShack will be assembled at the space station.

In the design of this spacecraft, topics were divided into the following subsystems: structure, interior design, launch and assembly, propulsion, attitude control, power, thermal control, life support, communications, command and telemetry, rendezvous and docking, telerobotics and Remote Manipulator Arm (RMA), and Extravehicular Activity.

Major design constraints include:

1. Ability to rendezvous, capture, and berth spacecraft with an RMA.
2. Provide power and attitude control to the STV and attached satellites.

3. A lifetime of at least 25 years.
4. A maximum mission duration of twelve days.
5. A maximum of five EVA per mission.
6. A maximum of two satellites serviced per mission.
7. To remain unmanned for up to three years.
8. To support a maximum of four missions per year.
9. Provide a shirt-sleeve working environment.
10. Satellites will have docking interfaces and grapple fixtures.
11. Orbital transfers of the GeoShack/STV will be controlled by the STV.
12. The maximum difference in longitude of two satellites will be 30°.
13. GeoShack should not contribute to orbital debris.
14. Design should be modular with high growth potential.

Structure

Primary structure of GeoShack consists of exterior structural rings, walls of the two cylindrical modules, and four end caps. Secondary structure consists of the interior flooring and walls, which subdivide GeoShack. External structure is composed of all attachments, supports, booms, and trusses.

Interior Design

Interior design is composed primarily of the cylindrical habitat (see Fig. 5) and laboratory (see Fig. 6) modules, the major living areas. These spaces are designed with the consideration of astronaut comfort and hygiene, food preparation, growth potential, and accomplishment of the task of satellite servicing and repair.

Launch and Assembly

GeoShack will be lifted into orbit by three space shuttle launches and assembled at the space station. The first launch will carry the laboratory module, the second launch the habitat module, and the third launch solar panels, radiators, and other external structures. GeoShack will be transferred to geostationary orbit using a Space Transfer Vehicle.

Propulsion

Shack will utilize a redundant hydrazine thruster system for repositioning during satellite intercept, for space debris and collision avoidance, and during docking maneuvers.

Attitude Determination and Control

GeoShack will also use the hydrazine thruster system for its attitude control system. Solar pressure and gravity gradient are the primary disturbance torques.

Power

This spacecraft will require approximately 35 kW of power. Primary power is provided by gallium arsenide solar cells on panels. Secondary power is supplied by an energy storage

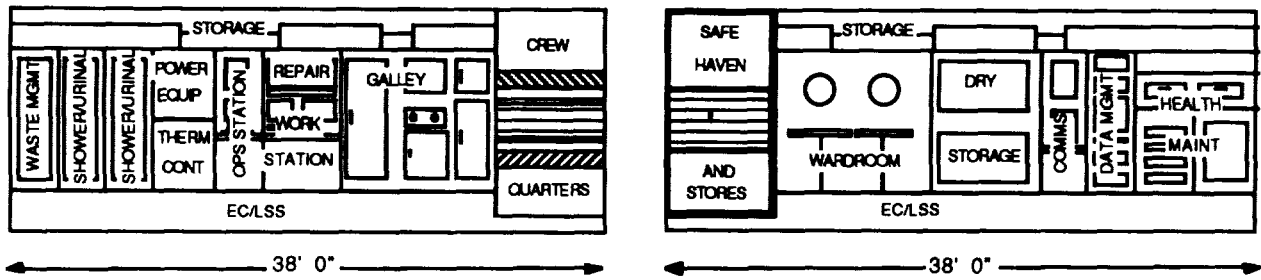


Fig. 5. Habitation Module Interior

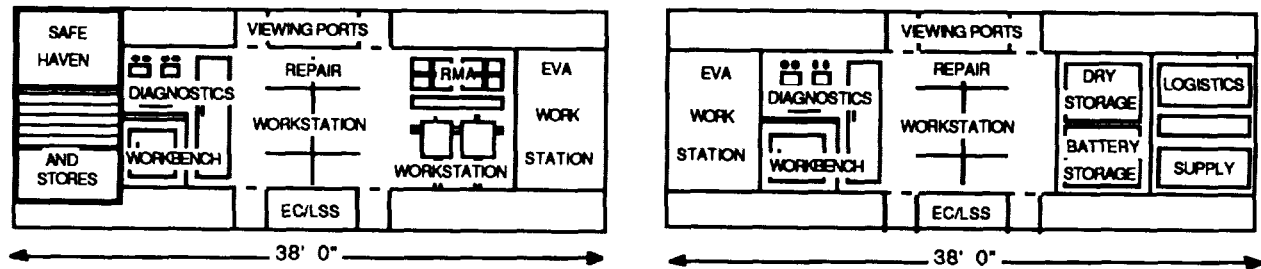


Fig. 6. Laboratory Module Interior

wheel system. An emergency backup system composed of nickel-hydrogen batteries exists to power necessary life support systems.

Thermal Control

The thermal control system consists of two basic loops. Equipment waste heat loads will be acquired via cold plates and transported to heat pipe radiators by a pumped two-phase ammonia loop. Metabolic loads will be acquired via basic air-water heat exchangers. This waste heat will be used in life support systems, and any excess heat will be transferred to the primary thermal control system for rejection.

Environmental Control and Life Support System

This system monitors and controls all systems necessary for maintaining an environment conducive to safe and healthy biological functioning of the astronauts on GeoShack. Components are temperature and humidity controls, pressurization and atmospheric revitalization systems, and water and waste management functions.

Communications, Command and Telemetry, and Data Management

The communications subsystem provides GeoShack with the voice, data, and video links necessary for successful operation. The system utilizes a one-meter parabolic dish at GeoShack and a series of three ground stations for all communications.

Satellite Rendezvous

The primary function of GeoShack is satellite repair. The first step of this process is rendezvous. Rendezvous is accomplished through use of range and range-rate sensors, which determine distance, range rate, and bearing to the target spacecraft.

Telerobotics/Remote Manipulator Arm

GeoShack possesses several automated systems to reduce the required EVA time of its astronauts. These include a four-jointed remote manipulator arm and two telerobots. These systems will be remotely controlled from within GeoShack, will make maximum use of existing technology, and will be upgradable.

EVA System

Extravehicular activity is a driving factor in GeoShack. Satellite repair will dictate that large amounts of time be spent in EVA. The system is composed of an airlock, an Extravehicular Mobility Unit, Advanced Manned Maneuvering Units, and several hard suits.

ACKNOWLEDGMENTS

MIMES team members are David Bouknight, Karl Jensen, John Kracht, Steve Ohmstede, and Jeff Wilson. GEOSHACK team members are Frank Blackburn, Thomas Feddo, Brian Gray, Kelly Hansen, and Kerry Hollenbeck.

20/1/87
P.3
217

MICROSPACECRAFT AND EARTH OBSERVATION: ELECTRICAL FIELD (ELF) MEASUREMENT PROJECT

UTAH STATE UNIVERSITY

N91-18155

INTRODUCTION

Past attempts to map the Earth's electrical field have been severely limited by the lack of simultaneous global measurements. Previous measurements have been made by sounding rocket- and satellite-borne sensors, but these measurements have covered only singular points in the field. These satellite observations are augmented by ground-radar (incoherent scatter) plasma-drift measurements; however, only six ground-based installations are producing such local electrical-field maps. The expansion of this ground-based radar network to meet a global objective is politically and financially impossible. Global electrical-field maps constructed by forcing mathematically formulated models to fit this limited set of data points are not only inaccurate, but the degree of inaccuracy is impossible to evaluate⁽¹⁾. Therefore, we see a need for an inexpensive, extensive, long-lasting global electrical-field measurement system (ELF).

DESIGN CONSIDERATIONS

The primary performance driver for this mission is the need to measure the attitude of each spacecraft very accurately. In addition, it is necessary to know the electrical charge generated by the satellite as it crosses the magnetic field lines ($E = V \times B$). This value must be factored out of the measurements. It will not be necessary to control the attitude of the satellite precisely, but the attitude will have to be known to within $\pm 1^\circ$ to achieve the desired accuracy. Also, the payload sensing booms must rotate in order to balance photoelectric effects and aid in the measurement of the $V \times B$ bias.

In order to achieve the desired global coverage, a constellation of about 50 satellites in at least 18 different orbits will be used as shown by the artist's conception in Fig. 1. To reduce the cost of each satellite, off-the-shelf, proven technology will be used wherever possible. We set a limit of 25 kg and \$500,000 per satellite. We expect the program cost, including the deployment of the entire constellation, to be less than \$100 million. The minimum projected mission life is five years.

Design Evolution

Several designs were considered for the ELF satellite: (1) gravity gradient satellite; (2) dual spinner satellite; and (3) simple spinner satellite.

Gravity gradient satellite. The first design considered was a gravity gradient satellite. This is a satellite in which, because of its mass distribution, one face of the satellite constantly points at the Earth. Because this is a very stable configuration, there is no need for an active attitude control system. This

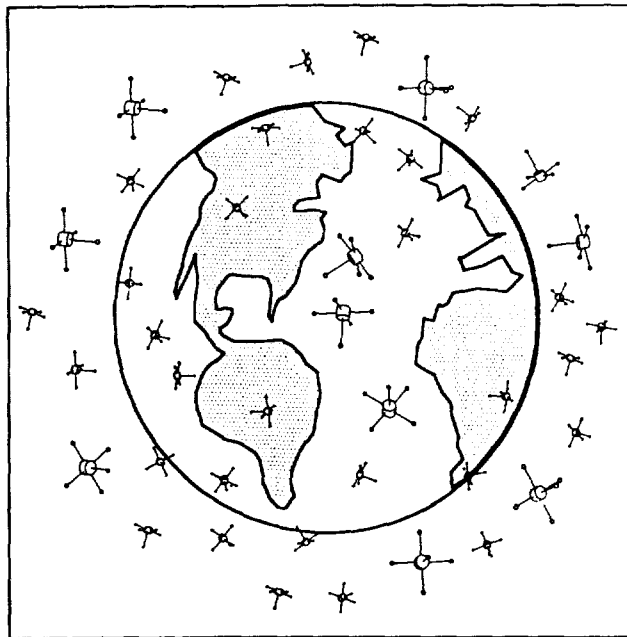


Fig. 1. Artist's conception of the ELF constellation surrounding the Earth.

design was discarded due to the electrical-field sensor requirement that it must spin.

Dual spinner satellite. Second, a dual spinner satellite such as those used for communication purposes was considered. This was in order to satisfy the sensor requirement of spinning as well as to have a face of the satellite constantly Earth-pointing for ease of communication. We abandoned this design due to the unnecessary complications caused by having to interface between the rapidly spinning and slowly spinning platforms of the satellite.

Simple spinner satellite. Last, a simple spinner satellite was considered. With this design, the complexities of interfacing between two platforms spinning at different rates do not exist, yet the sensor requirements are still satisfied. The rest of this document describes this final design configuration.

Electrical-Field Sensing System

The electrical-field sensing system will consist of three orthogonal sets of insulated booms with conductive spheres attached to the ends, as shown by Fig. 2. The electrical potential across each pair of conductive spheres will be

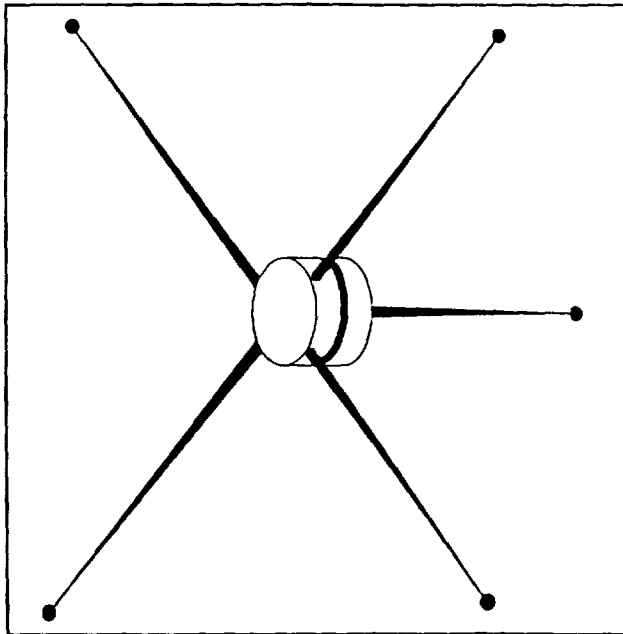


Fig. 2. Close-up exterior view of an ELF satellite.

measured to get the three-dimensional electrical-field measurement at a point. The boom system must be rotating in order to mitigate the photoelectric charge build-up caused by exposure to the sun. To achieve the desired accuracy, the spheres must be separated by at least 1 m and be rotating at no more than 10 rad per sec. Since the rotation causes a sinusoidal variation in the output, potential readings must be taken at least every 0.1 sec to get the desired resolution.

Mission Description

The most dynamic electrical-field activity around the Earth occurs near the poles in the 50° to 70° latitude regions. It is in this region that phenomena such as the aurora are observed most frequently. Little activity of interest occurs in the equatorial regions. Therefore, the ELF satellites will be placed in orbits with inclinations between 45° and 90°. This placement gives good coverage of the poles as well as some coverage of the equatorial regions.

The ELF satellites will be placed at altitudes between 500 and 1000 km. In this range, the Earth's electrical field does not change dramatically with a change in altitude. Also, 500 km is high enough to give the lowest satellite a minimum mission life of 5 years before the orbit decays, and 1000 km is low enough to escape the radiation from the Van Allen belts.

ELF Constellation Deployment

Two deployment scenarios are being considered. The first considers using Orbital Sciences Corporation's Pegasus as a dedicated launch vehicle. The second option looks at piggyback opportunities on McDonnell Douglas's Delta II launch vehicle.

If the Pegasus is used, six satellites will be launched at a time. When the proper orbit is reached, one of the six satellites will be ejected from the Pegasus upper stage. The rest of the cluster will remain attached to the stage. This concept is shown in Fig. 3. The stage will then be maneuvered to a slightly different altitude (about 75 km higher) or a slightly different inclination (about 2.5° difference) where another ELF satellite will be ejected. This sequence will be repeated until all six satellites have been ejected. Launching the satellites in clusters like this reduces the required number of launches. By slightly changing either the altitude or inclination of each satellite in the cluster, the satellites will be dispersed even further by orbital perturbations caused by the Earth's oblateness. This will result in the required global coverage.

The Delta II has the room for four ELF satellites to piggyback on it. The major problem with using this launch vehicle is that the satellites will go to wherever the primary payload dictates. Few polar launches are planned for the 1990s; most launches will be to inclinations below about 35°. Therefore, some sort of onboard propulsion for each ELF satellite will be required to get it into the proper type of orbit and altitude. However, there does not appear to be enough room for such a propulsion system. A possible alternative might be to use a tether deployment system. The details and requirements for this type of launch are still being investigated.

Upon insertion into orbit, a radio signal will be sent to the satellites to activate them. A programmed routine on board the spacecraft will cause the sensor booms to deploy and the attitude control jets to fire, spinning the satellite.

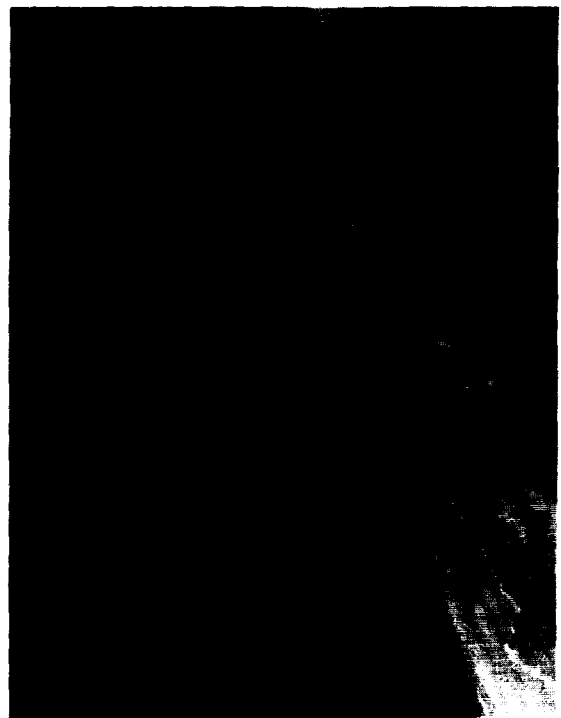


Fig. 3. Artist's conception of an ELF satellite being ejected from the Pegasus's upper stage.

Attitude Control and Determination System

The satellite is modeled as a spinning oblate platform that spins at 10 rpm. The orientation or attitude of each satellite will not be controlled, but the spin rate will be controlled to 10 ± 2 rpm. An onboard cold gas propellant system will be used to spin up the satellite initially, as well as make any necessary spin rate adjustments.

Two 2-axis magnetometers, two sun sensors, and one horizon-crossing sensor are used to determine the attitude of each ELF satellite. By using different combinations of these five sensors, the attitude of the satellite can be determined at all times during the orbit. Some of the data will be redundant, but this redundancy can be used to enhance the accuracy of the readings. These readings will lie within the $\pm 1^\circ$ error margin for attitude knowledge.

Data Processing System

The data processing system is sized to store up to 24-hours' worth of data. These data include the electrical-field potential as well as the attitude readings. This system will also handle housekeeping functions on board the satellite.

Communication System

Because the attitude of each ELF satellite will not be controlled and each satellite can maintain a different orientation, a virtually omnidirectional antenna is needed on board for communication. A stripline wraparound antenna meets this requirement. Frequencies in the S-band will be used for receiving instructions and transmitting the collected data to a ground station. Data will be transmitted twice per day to one ground station. The ground station will use a 4.3-m parabolic dish with tracking capabilities. The actual location of this ground station is yet to be determined. Each satellite will take a maximum of 82 sec to transmit the stored data. It is expected that each satellite will pass within range of the ground station at least twice per day.

Power System

Each satellite's power will come from solar cells wrapped around the exterior of the spacecraft. Since the satellites will not generally be placed in sun-synchronous orbits, they will have to function in the dark as well. Therefore, the solar cells will be backed up with batteries. The minimum power generation will be 12.77 W, which will be sufficient to cover the power requirements of all systems.

ELF Satellite Structure and Configuration

The cylindrical primary structure is 45 cm in diameter and 35 cm high. It will be composed of 0.16- to 0.32-cm-thick aluminum 6061-T6. The primary support plate will be made of 1.25-cm-thick aluminum honeycomb. Most subsystem components will be mounted on this plate as shown by Fig. 4. Individual component covers will provide radiation shielding as required.

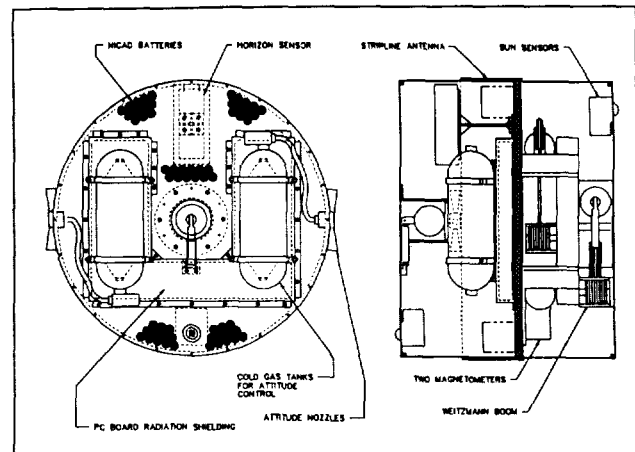


Fig. 4. Internal layout of the subsystem components.

Thermal Control System

The extreme temperatures were determined for the ELF satellites by considering the worst cases of the hottest and coldest orbits. The hottest orbit is one in which one flat face of the satellite constantly faces the sun. If an ELF satellite winds up with this orientation, all onboard components will stay within their temperature ranges. The coldest orbit considered was one in which the flat faces of the satellite never see the sun. The temperature ranges for this case went below the component limits. In order to compensate for this, three 1-W heaters will be used to keep the components within their required operating temperature. These heaters are equipped with their own temperature regulating switches.

Conclusions

Each satellite has a mass of 19.1 kg and will cost less than \$250,000 for the actual hardware. Including deployment costs, the program will cost about \$70 million for 8 Pegasus launches and 48 satellites. Labor costs have not yet been computed.

We expect to be able to deploy about 50 satellites. Because we are deploying a constellation of 50 satellites there is inherent redundancy in this system. The most catastrophic event that could happen is to have the launch vehicle explode. But even this will not affect the system drastically since at the most six satellites will be lost. We expect to lose not more than 10% of the satellites to launch vehicle malfunction, ELF subsystem failure, or space debris impact.

REFERENCES

1. Sojka, J. J., 2-DEF A Two Dimensional Electric Field Mission, Center for Atmospheric and Space Sciences, Utah State University, Logan, Utah, CASS Report #89-5-2, November 1989.

THREE ORBITAL TRANSFER VEHICLES **N 91 - 18156**

VIRGINIA POLYTECHNIC INSTITUTE AND STATE UNIVERSITY

Aerospace Engineering students at the Virginia Polytechnic Institute and State University undertook three design projects under the sponsorship of the NASA/USRA Advanced Space Design Program. All three projects addressed cargo and/or crew transportation between LEO and GEO. Project SPARC presents a preliminary design of a fully reusable, chemically-powered aeroassisted vehicle for a transfer of crew of five and a 6,000-20,000 lb payload. The ASTV project outlines a chemically-powered aeroassisted configuration which uses disposable tanks and a relatively small aerobrake to realize propellant savings. The third project, LOCOST, involves a reusable, hybrid laser/chemical vehicle designed for large cargo (up to 88,200 lb) transportation.

SPACE-BASED AEROASSISTED REUSABLE CRAFT (PROJECT SPARC)

Mission Requirements/Objectives

Project SPARC is designed to transfer crew and cargo between the Space Station at LEO (inclination = 28.5°) and GeoShack at GEO (inclination = 0°). There are three mission scenarios: the "small" mission, a round trip transfer for a crew of five and a 6,000-lbm payload; the standard mission, a round trip transfer for a crew of five and delivery of a 20,000-lbm payload to GEO; and the expendable mission, a one-way transfer of a 28,000-lbm payload to GEO disposing of the vehicle into a higher orbit. Objectives of the project are to design one basic vehicle for all three missions, a reusable aerobrake, and removable components (aerobrake, crew module, and payload bays) to be saved during the expendable mission.

Orbital Mechanics

Hohmann transfers are used for the major impulses required for the mission and a single aeropass is used on the return trip (Fig.1). The minimum altitude of the aeropass is 262,470 ft. Total ΔV required is 22,570 fps, a 26.5% savings over a comparable all-propulsive mission. Total time of flight is 10.6 hr and the synodic period between LEO and GEO is 1.6 hr. A flight summary for the standard mission is shown in Table 1.

Table 1. Flight Plan (Standard Mission)

Impulse	Maneuver	Time (hr)/ Delta V (fps)
1	Decircularize-LEO	0/7929
	LEO-GEO flight	5.3/0
2	Plane change (28.5°)	0/2610
3	Circularize-GEO	0/2610
	Minimum stay at GEO	0.4/0
4	Decircularize-GEO	0/4874
	Plane change (23.82°)	0/2159
5	GEO-atmospheric entry	5.2/0
	Aeropass with 4.68° plane change	0.065/0
	Atmospheric exit-LEO	0.077/0
6	Circularize-LEO	0/193
TOTALS		11.04/22570

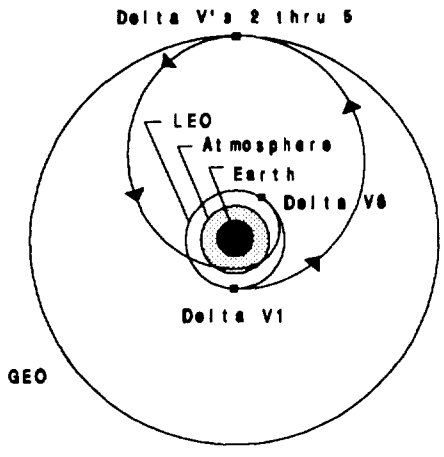
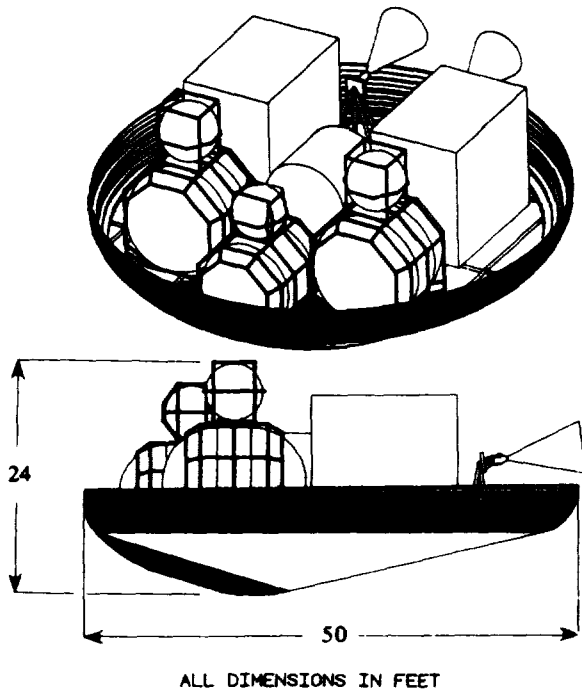


Fig. 1. Flight Path

Configuration

The standard SPARC configuration is shown in Fig. 2. Its major components include the truss structure, aerobrake, propellant tanks, a crew module, payload bays, and engines. The main truss structure consists of twelve graphite polyimide networks oriented in a grid pattern to provide maximum support for the vehicle components. The truss structure is designed with the same shape as the aerobrake to facilitate connection of the two, and it is self-sufficient, allowing vehicle operation without the aerobrake. The truss members have outer radii ranging from 1" to 1.25" with thicknesses from 0.1" to 0.89". All members are connected with titanium silicon carbide joiners.

The aerobrake is constructed with an ellipsoidal nose tangent to an elliptical cone and connected to a toroidal base skirt. The cone is raked at 73° to form a circular base plane 45 ft in diameter. The shell is a rigid graphite polyimide honeycomb sandwich structure supported by graphite polyimide L-beam ribbing mounted flush to the inner surface of the shell at 45° to the longitudinal axis of the base plane. The aerobrake is attached to the main truss structure with graphite polyimide surface mounts. The thermal protection



ALL DIMENSIONS IN FEET

Fig. 2. SPARC Configuration

system consists of a reusable, flexible, quilted multi-layer foiled insulation. The outermost layer is a colloidal silica coating supported by quilted aluminoborosilicate (ABS). Ceramic Q-felt is then followed by ten alternating layers of stainless steel foil and ABS scrim cloth. The innermost layer is ABS fabric again, bonded to the aerobrake shell.

The dimensions of the modular payload bays (14.7 ft long, 10 ft wide, and 13.15 ft high) are such that one is needed for the "small" mission, two are needed for the standard mission, and three are needed for the expendable mission. In the case of the expendable mission, the third payload bay would be mounted in place of the crew module. The crew module (total length = 9.5 ft, radius 4.25 ft) has a maximum capacity of five crew for a two-day mission with a two-day emergency reserve. Life support systems include an open atmospheric control system, contaminant removal, thermal management, and cabin pressurization. The cabin is pressurized to 14.7 psia with 80% nitrogen, 20% oxygen. Five extravehicular mobility units and two manned maneuvering units are carried for each mission and three repressurizations are possible. A safe haven provides protection from solar flare radiation.

Propulsion System

Main propulsion is provided by two modified Pratt & Whitney Advanced Expander Engines, each having a mass of 405 lbm and each providing 16,140 lb thrust. The engines use retractable nozzles which reduce the total engine length from

120" to 40" when stowed during aerobraking. A liquid oxygen/liquid hydrogen propellant is contained at 18 psia, and propellant requirements for each mission are as follows:

"small:"	53,930 lbm
standard:	79,753 lbm
expendable:	71,951 lbm

The main tanks (two fuel, one oxidizer) are designed with the volumetric capacity of the expendable mission, and can therefore accommodate the "small" mission as well. For the standard mission, three smaller spherical auxiliary tanks are added to accommodate the higher propellant requirements, and all tanks are fully reusable. Propellant is carried to the engines through lines which run underneath the main truss structure. Attitude and orientation control is provided by 24 30-lb reaction control system (RCS) thrusters arranged in four packs on the perimeter of the truss structure. The RCS uses a hydrazine monopropellant pressurized by nitrogen.

Docking Scenario

The general docking scenario at the Space Station and at GeoShack consists of the following: (1) maneuvering the vehicle into the docking area with the RCS; (2) attachment to three structural support arms (one fixed and two retractable); (3) removal of payload and crew with an offloading arm capable of reaching all vehicle components; (4) detachment of the aerobrake when necessary with four small aerobrake removal arms; and (5) vehicle storage. It is assumed that there is a hangar and air lock at the Space Station and GeoShack. The docking design is shown in Fig. 3.

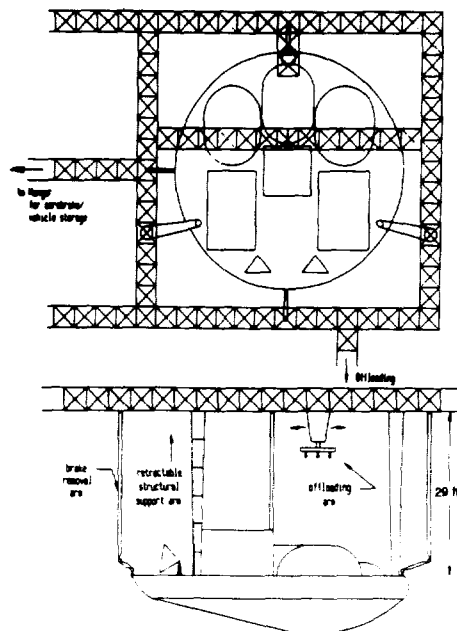


Fig. 3. Docking Scenario

Calculations and Performance Characteristics

Vehicle design and performance calculations included: (1) orbital mechanics; (2) atmospheric heat loading and perigee altitude obtained from an approximate solution by Desautel; (e) nozzle flow calculations obtained from Naval Ordnance Test Station (NOTS); (4) tank insulation and boiloff; (5) aerodynamic and longitudinal stability calculations using modified Newtonian Theory; (6) center of gravity; (7) mass moments of inertia; (8) RCS characteristics derived from the mass moments of inertia values; (9) crew module and payload bay radiation protection; and (10) structural analyses obtained from Structural Analysis Software for Microcomputers (SASM).

The SPARC performance characteristics are listed in Table 2.

Conclusions

Our report has summarized the design specifications of Project SPARC, and results of this design indicate that an aeroassisted vehicle is an attractive mode of orbital transfer. It is expected that the required technical advances in turbomachinery, materials, thermal protection, and other areas will be completed by the time the Space Station is operational, justifying the continuation of research and development of these transfer vehicles.

Table 2. SPARC Performance Characteristics

Characteristic	Small	Standard	Expend.
<i>Propulsion:</i>			
Main engine I_{sp} (sec)	487	487	487
Propellant flow rate (lbm/sec)	35.86	35.86	35.86
Main engine thrust (lbf)	16,140	16,140	16,140
Mixture ratio (W_o/W_f)	6/1	6/1	6/1
RCS I_{sp} (sec)	225	225	225
RCS thrust (lbf)	30 each	30 each	30 each
<i>Masses (lbm):</i>			
Vehicle dry mass, M_s	18,577	20,535	13,469
Payload, LEO-GEO, M_{11}	6000	20,000	28,000
Payload, GEO-LEO, M_{12}	6,000	0	N/A
Propellant used LEO-GEO, M_{p1}	40,627	68,960	71,951
Propellant used GEO-LEO, M_{p2}	13,303	10,793	N/A
<i>Performance:</i>			
Payload-Mass ratio, LEO-GEO { $M_{11}/(M_{p1}+M_s)$ }	0.101	0.233	0.328
Payload-Mass ratio, GEO-LEO { $M_{12}/(M_{p2}+M_s)$ }	0.188	0.0	N/A
Structural coefficient	0.256	0.205	0.158

AEROBRAKING SPACE TRANSFER VEHICLE

The Aerobraking Space Transport Vehicle (ASTV) is a cost effective, reusable orbital transport vehicle to be used in conjunction with the space shuttle, the Space Station, and the GeoShack to transport a payload and/or a crew between the Space Station and the GeoShack.

Three mission scenarios are: (1) deliver 6000 lbm round trip, (2) deliver 20,000 lbm to GeoShack and return empty, and (3) deliver 28,000 lbm to GeoShack and dispose of the vehicle into a higher orbit. The main objectives used as a guide driving the ASTV design process were: (1) reliability and safety, (2) minimize mission costs, and (3) maximize flexibility.

An approximate analysis of projected costs for the thirty mission life ASTV using (a) reusable tank configuration and (b) disposable tank configuration (with \$1000 per lb cost of delivery to LEO projected for 2010) indicated that significant savings can be realized with a disposable tank version.

A typical mission originates at the Space Station with a separation maneuver and a phasing orbit injection followed by an approximate Hohmann elliptical transfer to GEO. Upon reaching GEO, circularization and the 28.5° plane change will be accomplished via single ΔV impulse. At GEO, the vehicle will rendezvous with the GeoShack and the payload will be deployed during which time the ASTV will receive life support from the GeoShack. While in GEO, the vehicle will be able to reach one or more locations for repair or service of satellites and spacecraft. The transfer from GEO back to LEO will begin with a deorbiting impulse to bring the vehicle back into the Earth's atmosphere and to make the plane change from 0.0° to 26.3° inclination. Upon entering the atmosphere, the vehicle will use the lift and drag generated by the aerobrake to achieve the remaining 2.2° of inclination and a decrease in speed of 7690.6 ft/sec. After exiting the atmosphere, the vehicle is placed into a phasing orbit at 350 miles followed by a final Hohmann transfer to LEO.

Figures 4 and 5 show a typical ASTV configuration. Shown are the reduced size aerobrake, the large disposable tanks, and the mission modules. A mass breakdown is provided in Table 3.

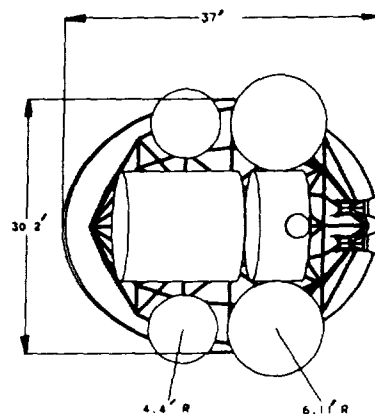


Fig. 4. ASTV Configuration

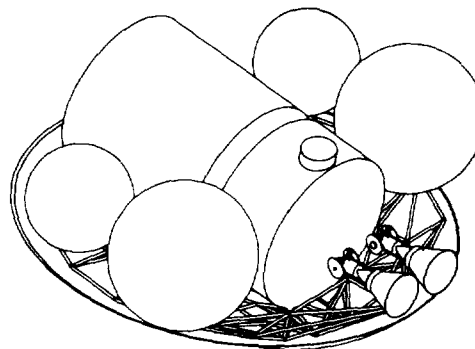


Fig. 5. ASTV Isometric View

Table 3. Vehicle Mass Breakdown

Components	Mass, lbm
Aerobrake System:	
TPS	600
Backing Support (Al)	1,400
Ribbing (Al)	1,250
Frame	1,866
Rails	1,132
Propellant Tanks	1,352
Main Engines	740
RCS	1,320
Propellant Handling	700
Electrical Power	912
Communications	497
GN & C	91
Cargo Modules (2)	1,110
Crew Module	4,890
Cargo	14,000
Total Dry Mass	31,860

The propellant selected for both the main engines and the RCS system is liquid hydrogen/liquid oxygen. The propellant requirements of all three missions are shown in Table 4. These values include a reserve in the event of an emergency return.

Table 4. Propellant Requirements

Mission	Propellant (lbm)
1	50,449
2	62,960
3	59,056

The raked cone aerobrake overall dimensions are shown in Fig. 6. The structure of the brake consists of aluminum-lithium alloy stringers riveted to an aluminum skin. The thermal protection for the aerobrake is provided by a multilayer insulation consisting of aluminoborosilicate cloth, insulation, and stainless steel foil separated by scrim cloth. A one-foot skirt was added around the top of the brake. During the aerobraking maneuver, the aerobrake will provide a .23 L/D at an angle of attack of 13.25° and a maximum deceleration of 3.72 g.

The ASTV main propulsion is provided by two side-by-side engines developing 15 klbf thrust each. These engines have a chamber temperature of 6,660°R, a chamber pressure of 3,000 psi and a nozzle area ratio of 650 resulting in a specific impulse of 498 sec. The turbomachinery consists of a four-stage, centrifugal hydrogen pump driven by a two-stage, axial flow hydrogen turbine and a single-stage, centrifugal oxygen pump driven by a single-stage, axial flow hydrogen turbine.

The engine features a retractable nozzle in which the 33-in extendable portion is retracted prior to the aerobraking maneuver. The engine mounts have electric motors for gimbaling in pitch and propellant driven actuators for gimbaling in yaw. The minimum and maximum pitch angles are -40° and 18° respectively, while the minimum and maximum yaw angles are ±7.5°. Fig. 7 shows the engines rotated to extreme angles in actual operation and Fig. 8 shows them in the stowed position.

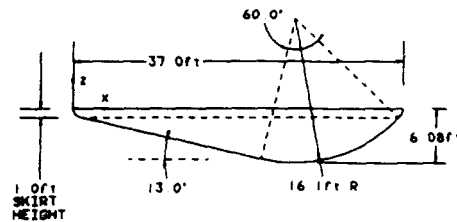
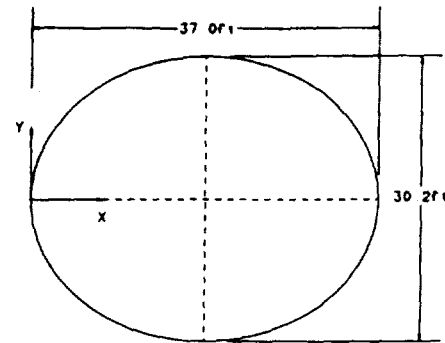


Fig. 6. Aerobrake

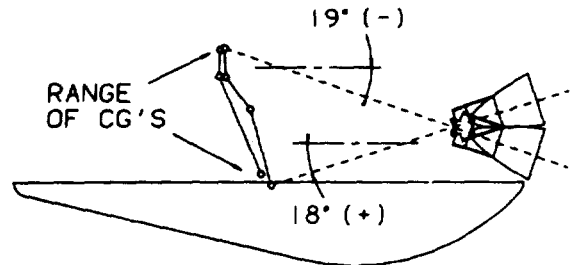


Fig. 7. Thrust Vectoring Through Extreme CG Locations

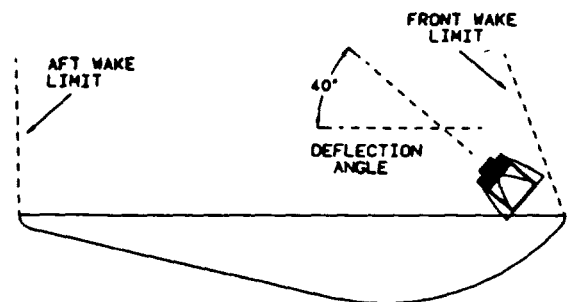


Fig. 8. Engines in Stowed Position

The ASTV comprises four major structural components: a frame, mission modules, propellant tanks and aerobrake supporting structure. The frame is composed of HT graphite/epoxy composite tubes and one square member that are joined at 65 nodes by aluminum endfittings (Fig. 9). Two 27-ft-long aluminum rails are used as a cradle for the mission modules. The frame is connected to the aerobrake via aluminum attachment accessories connected to 11 "Z" type aluminum-lithium stringers.

The propellant tanks fall into two categories: disposable and reusable. There are four large disposable tanks pressurized to 20 psi: two hydrogen and two oxygen tanks. These tanks will be detached by using explosive bolts and a solid rocket motor. A solid shield protects the craft from the rocket blast. The permanent tanks consist of five hydrogen and five oxygen tanks pressurized to 500 psi by a helium-filled bladder. These tanks contain propellant responsible for all maneuvers following the aeropass plus reserve. Insulation and impact protection are provided by stainless steel foils interleaved with Nextel (MLI).

Mission payloads are carried in 8-ft-long by 14-ft-diameter cylindrical cargo modules made of aluminum-lithium. The cargo modules provide mounting platforms, impact and radiation protection and selective positioning for the payload. Up to three modules may be connected to form one 24-ft-long unit, or all three modules could be individually capped, and of course other combinations of modules can be used to fit the needs of the cargo. The cargo modules are mounted to the rails which have connection points spaced at eight-in intervals so that the modules may be connected in a wide range of positions along the length of the rails and thereby adjust the c.g. location.

The crew module is basically a cargo module designed for human transport. The crew module shares the same overall dimensions as the cargo modules so that it too may be connected to other modules and moved around within the ASTV. The crew module can support three adults in an ideal Earth atmosphere for 48 hours with the capability for one full repressurization. A solar flare shelter and a thermal control system are included in the design.

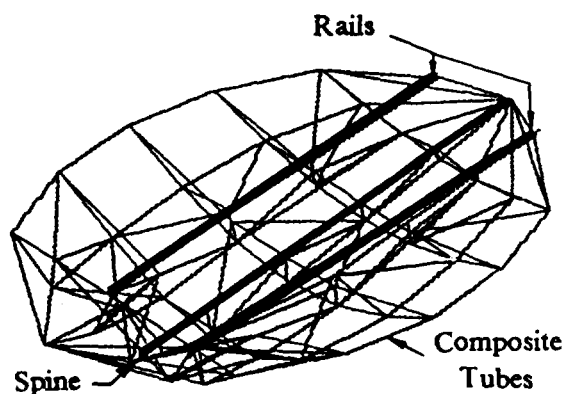


Fig. 9. ASTV Frame

Reaction Control System (RCS) comprises two different sizes of thrusters, 60 lbf and 10 lbf. Overall there are 50 thrusters (34/60 lbf and 16/10 lbf providing double redundancy) located in four clusters around the top of the aerobrake. The clusters are mounted to retractors which draw them inside the aerobrake when not in use.

Navigation is performed by an autonomous inertial system having interfaces with the ground or space stations.

Communication data is transmitted and received to/from the ground, the space shuttle, and the Space Station via K band link.

The electrical power is generated by two 4 kW LOX/LH₂ fuel cells (three during manned missions). The oxygen and hydrogen are drawn from the small permanent tanks. Two nickel/hydrogen batteries are also included.

LASER OR CHEMICAL HYBRID ORBITAL SPACE TRANSFER (PROJECT LOCOST)

Mission Requirements/Objectives

Project LOCOST is an unmanned vehicle that utilizes a hybrid laser/chemical propulsion system to transfer cargo between the Space Station at LEO (inclination = 28.5°) and the GeoShack at GEO (inclination = 0°). The baseline mission scenario is to transfer 20,000 kg of cargo out to GEO and bring 6,000 kg back to LEO. A scenario in which the maximum 40,000 kg of cargo is transferred each way is also analyzed. The laser propulsion system is powered by a Laser Power Station (LPS) orbiting at an altitude of one Earth radius and an inclination of 0°. The basic LOCOST specifications are listed in Table 5.

Table 5. LOCOST Basic Specifications

Orbit Transfer Time	2-3 weeks
Cargo Mass	20,000-40,000 kg
Laser Type	Direct Solar Pumped Iodide
Laser Wavelength	1.313 μm
Laser Power	12 MW
Chemical Rockets	$I_{sp} = 480$ sec
Laser Rocket	$I_{sp} = 1500$ sec
Technology Level	2010

Orbital Mechanics

The laser propulsion system is used to transfer between LEO and GEO on a spiral trajectory. The chemical system is used for circularizations and plane changes. Two Energy Relay Units (ERU), placed 120° ahead of and behind the LPS, allow continuous power for the LOCOST while the LPS is not blocked by the Earth's shadow. A summary of the baseline mission analysis is presented in Table 6.

Table 6. Baseline Mission Analysis

Flight Segment	Delta V (km/s)	Time (days)	Propellant (kg)
Transfer	5.16	9.63	36,393
Circ.	.00575	.0011	1,018
Plane Ch.	1.52	.025	22,879
Plane Ch.	1.52	.0014	12,879
Transfer	3.17	1.74	6,522
Circ.	1.52	.008	7,414
Cargo Transfer	.6 days		
Total Trip Time	12 days		
Laser Propellant	43,202 kg		
Chemical Propellant	44,020 kg		
Thrusting Times:	Laser	83%	
	Chemical	.4%	
	Coasting	17%	

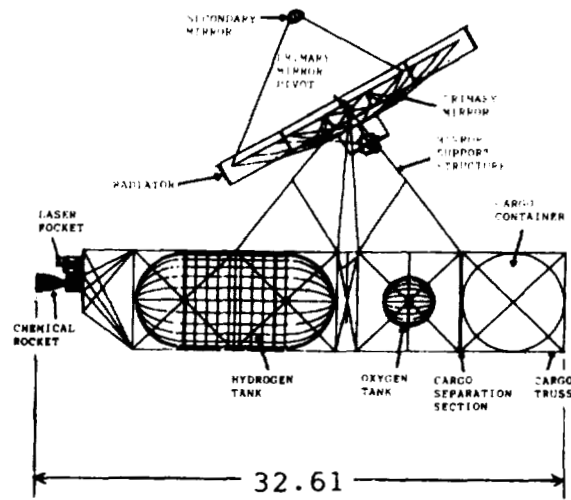


Fig. 11. LOCOST Side View

Configuration

The LOCOST configuration is shown in Figs. 10, 11, and 12.

The major components of the LOCOST are: the main truss, optical system, engines, tanks, and payload module.

The main truss is a rectangular frame 29.11 m x 6.3 m x 18.9 m constructed from 6.3-m truss boxes. The support structure for the mirror assembly extends up 9 m from the top of the main truss. Individual truss members are made from graphite epoxy tubular elements (5.4 cm OD, 5.08 cm ID) joined with titanium fittings.

The payload module is composed of a magnesium alloy cylinder to hold the cargo. The LOCOST has the option of a removable payload canister and a detachable payload module. This allows for greater cargo carrying flexibility and easier transfer.

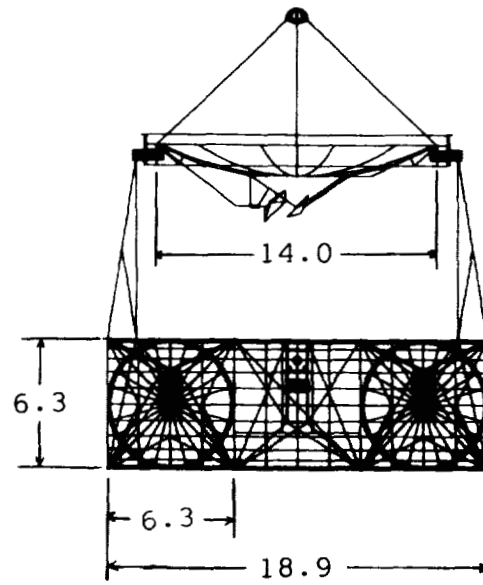


Fig. 12. LOCOST Rear View

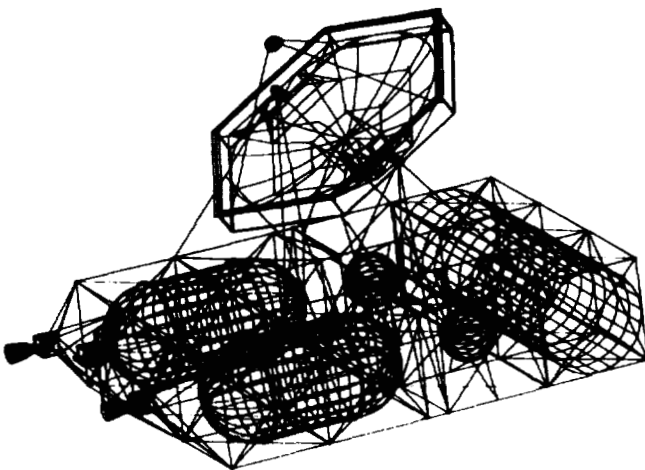


Fig. 10. LOCOST Isometric Schematic

Optical System

The optical system consists of a 14-m-diameter concave parabolic primary mirror and a 1.1-m-diameter convex parabolic secondary mirror arranged in a Cassegrain system. Mirrors 3 and 4, attached to the back of the primary mirror, redirect the laser beam to mirror 5. Mirror 5 redirects and focuses the beam into the laser engine. The entire primary mirror structure pivots through 180° to allow for laser beam collection independent of the vehicle orientation (Fig. 13). All mirror surfaces are dielectrically coated. Mirrors 2, 3, and 4 are cooled by a heat pipe system. Mirror 5 is cooled by hydrogen propellant.

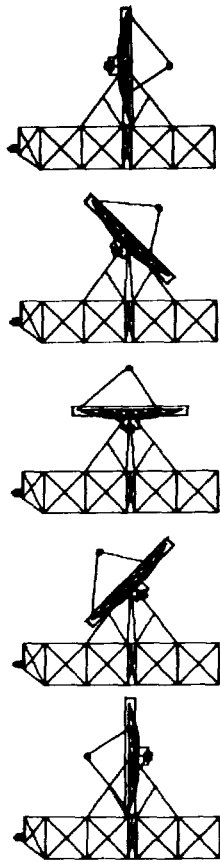


Fig. 13. Primary Mirror Rotation

Propulsion

The laser propulsion system employs the inverse Bremsstrahlung process to couple the laser energy to the thermal energy of the hydrogen propellant. The engine produces a thrust of 768 N. The engine is regeneratively cooled and has a plano-convex sapphire window lens to focus the incident laser beam inside the chamber. The engine is mounted inside a mobile rocket basket which allows for thrust vectoring through the vehicle's center of mass.

The chemical propulsion system consists of two symmetrically placed liquid hydrogen/oxygen rockets. Each engine produces a thrust of 25,000 N. The nozzles of the engines gimbal to track the center of mass.

The hydrogen is stored in two cylindrical tanks with spherical endcaps. The oxygen is stored in two spherical tanks. The tanks are insulated and maintained at an internal pressure of 35 kPa.

Attitude and orientation control is provided by four advanced control moment gyroscopes (CMGs) and eight sets of three hydrazine/oxygen RCS rockets.

Vehicle Characteristics and Performance

Vehicle design and performance calculations included: (1) orbital mechanics; (2) optical system analysis using ray tracing techniques; (3) laser engine performance evaluation; (4) cooling analysis; (5) chemical engine nozzle flow calculations obtained from NOTS; (7) tank insulation and boiloff evaluation; (7) mass and moments of inertia calculations (8) structural analysis obtained with SASM; (9) thermal analysis; (10) estimates of RCS and CMG characteristics derived from the mass and moments of inertia values, and roll rates of the vehicle. A summary of the LOCOST mass breakdown is given in Table 7.

Table 7. LOCOST Mass Breakdown

	Mass (kg)
Structure	
Main Truss	423
Optical System	
Primary Mirror w/support	2110
Secondary Mirror	90
Mirrors 3,4,5	300
Propulsion	
Chemical Rockets	422
Fuel Lines & Mounts	154
Laser Rocket	75
Fuel Lines & Mounts	75
RCSs & CMGs	1100
Docking	50
Communications	110
Payload Module	1100
Total Vehicle Dry Mass	6682

The LOCOST performance characteristics are listed in Table 8.

Table 8. LOCOST Characteristics

Propulsion	
Laser	
Specific Impulse	1500 sec
Propellant Flow Rate	.0522 kg/sec
Thrust	768 N
Chemical	
Specific Impulse	480 sec
Propellant Flow Rate	5.2 kg/sec
Thrust	25,000 N
Masses	
Vehicle Dry Mass	6682 kg
Payload LEO-GEO	20,000 kg
Payload GEO-LEO	6000
Laser Propellant Used	43,202 kg
Chemical Propellant Used	44,020 kg
Performance	
Payload Mass Ratio	.28

Conclusions

This report has outlined an initial configuration study of a hybrid laser/chemical orbital transfer vehicle. The study has indicated that the hybrid propulsion system may be attractive for cargo transportation in the LEO/GEO sphere and that further research is justified.

550 471 229
P. 11

MEGAWATT SOLAR POWER SYSTEMS FOR LUNAR SURFACE OPERATIONS

UNIVERSITY OF WASHINGTON

N91-18157

Lunar surface operations require habitation, transportation, life support, scientific, and manufacturing systems, all of which require some form of power. Nuclear thermal power is often considered to be the only type of power system which can provide a lunar base with power on the megawatt level, but political and technological obstacles may severely limit the application of nuclear power in space. As an alternative to nuclear power, this report focuses on the development of a modular, one-megawatt solar power system, examining both photovoltaic and dynamic cycle conversion methods, along with energy storage, heat rejection, and power backup subsystems. For photovoltaic power conversion, two systems are examined. First, a substantial increase in photovoltaic conversion efficiency is realized with the use of new GaAs/GaSb tandem photovoltaic cells, offering an impressive overall array efficiency of 23.5%. Since these new cells are still in the experimental phase of development, a currently available GaAs cell providing 18% efficiency is examined as an alternate to the experimental cells. Both Brayton and Stirling cycles, powered by linear parabolic solar concentrators, are examined for dynamic cycle power conversion. The Brayton cycle is studied in depth since it is already well developed and can provide high power levels fairly efficiently in a compact, low mass system. The dynamic conversion system requires large scale waste heat rejection capability. To provide this heat rejection, a comparison is made between a heat pipe/radiative fin system using advanced composites, and a potentially less massive liquid droplet radiator system. To supply power through the lunar night, both a low temperature alkaline fuel cell system and an experimental high temperature monolithic solid-oxide fuel cell system are considered. The reactants for the fuel cells are stored cryogenically in order to avoid the high tankage mass required by conventional gaseous storage. In addition, it is proposed that the propellant tanks from a spent, prototype lunar excursion vehicle be used for this purpose, therefore, resulting in a significant overall reduction in effective storage system mass. Emergency backup power is supplied by a nickel-hydrogen battery system derived from the energy storage system to be used on Space Station *Freedom*, in order to save on development costs and to provide one of the most reliable systems available. Structural elements for the entire power system are made of composites and aluminum, keeping system mass to a minimum. All components of the system are designed for transport to low Earth orbit in modular units aboard the Shuttle-C launch vehicle.

INTRODUCTION

Plans for lunar development will ultimately require a large power system to support all of the planned activities. Nuclear energy has usually been the assumed power source due to the high power densities offered, yet nuclear power is far from ideal. There are many problems, including startup of the plant, the large amounts of radiation produced and the need for a large area set aside permanently as a result, the impossibility of maintenance, and very low efficiency. The Space Systems Design Course at the University of Washington has, therefore, performed this design study on the harnessing of solar power for use on the Moon as a cleaner, safer alternative to nuclear power.

This study looks at two basic methods of converting solar energy into electrical power, with the objective of providing one megawatt of electrical power. The first method is the use of direct electrical conversion of solar energy using a new, highly efficient solar cell developed by the Boeing Corporation. The second method is the use of a dynamic cycle operating on energy supplied by a solar concentrator system. The Brayton cycle was chosen for this study for its relatively high efficiency and its availability in the timeframe of the lunar base as a proven and reliable unit. This cycle will also require an extensive heat rejection capability provided by one of two systems examined in this study: an advanced technology heat pipe radiator, or a liquid droplet radiator.

Neither of these power sources will, of course, provide power during the lunar night and, thus, energy is stored using a fuel cell system. Fuel cells similar to those used on the space shuttle, along with cryogenic hydrogen and oxygen stored in the tanks of a spent lunar lander, are employed as the energy storage system. Energy storage is relatively massive, so in order to keep the overall mass of the lunar power system from becoming excessively large, the nighttime energy storage system will provide just 50 kW, rather than a full megawatt. This nighttime power reduction may be offset by adding more photovoltaic arrays or dynamic cycle units, which are far less massive, for increased daytime power production.

The entire power system is designed to be modular, configured in such a way that no single point failures are possible. In the rare event of catastrophic failure, however, emergency power for repair and evacuation procedures is provided. For development, cost, and reliability reasons, the energy storage system from the Space Station *Freedom* was reconfigured to provide the required emergency backup power.

SOLAR PHOTOVOLTAIC POWER SUPPLY SYSTEM

As mentioned above, one of the power generation systems considered makes use of direct conversion via photovoltaic cells. Typical photovoltaic cells used in space and terrestrial

applications are made of gallium arsenide (GaAs) or silicon (Si) and convert only part of the available radiation spectrum into electrical power. These cells usually attain a solar energy conversion efficiency between 14% and 21%. A new tandem cell (Fig. 1) being developed by Boeing Aerospace is used in the present design and consists of two cells of different materials, mechanically stacked on top of one another⁽¹⁾. The upper cell, made of GaAs, absorbs photons with energies above 1.42 eV and has been made transparent to infrared radiation. Infrared radiation passes through the upper cell to a lower cell made of gallium antimonide (GaSb), which absorbs photons with energies as low as 0.72 eV. GaSb was chosen as the infrared sensitive booster cell because it is a direct bandgap material that generates higher currents, its bandgap is significantly lower than that of GaAs, and the voltage produced is nearly one-third that of the GaAs cell⁽²⁾, allowing it to be voltage matched with GaAs in a 3:1 ratio series-parallel arrangement to produce a 1.0 V triplet⁽³⁾, as shown in Fig. 1.

Individual cell efficiencies are enhanced by the addition of prismatic cover slides that fit over the upper gridlines on each cell and direct light toward the cell surface, away from the gridlines. This minimizes reflection losses and increases efficiency by 10% per cell⁽⁴⁾. When tested at a light concentration ratio of 100 times solar intensity (100 suns) in air-mass-zero (AMO) conditions, the individual performance of the GaAs cell was 23.9%, and that of the GaSb cell was 6.9%, for a total of 30.8% solar energy conversion⁽⁴⁾.

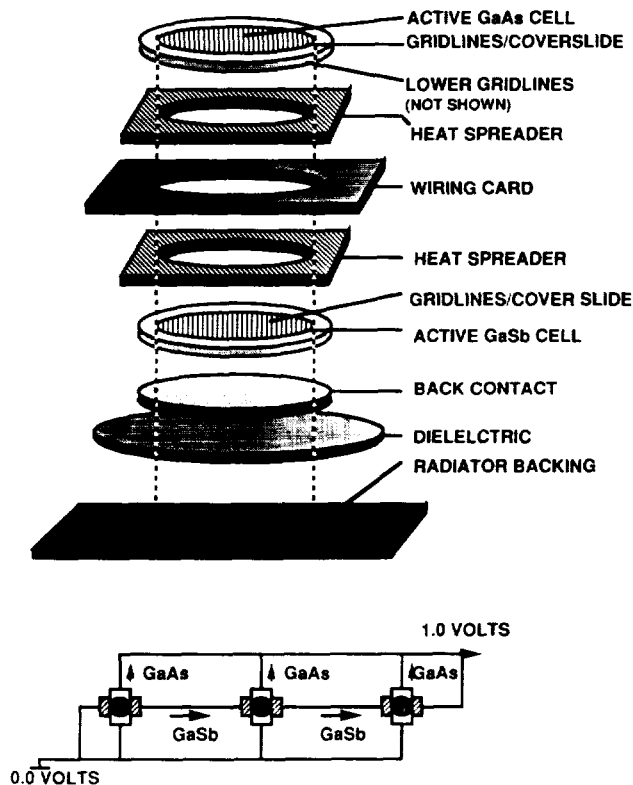


Fig. 1. Cell Assembly and Triplet Formation

To concentrate incoming sunlight to 100 suns, domed Fresnel lenses made by Entech, Inc. are used. These lightweight silicone lenses have a prismatic undersurface, designed to focus light at the center of the cell. A layer of protective microglass is laminated directly to the curved upper surface of the lens to protect it from solar proton flares and micrometeorite damage. Together, the microglass and silicone comprise 27.8% of the total panel mass⁽⁵⁾.

The lenses (which have a 3.75-cm-square cross-section) are fitted into a square aluminum honeycomb housing, so that the lenses lie below the top of the housing. The honeycomb housing is made of 0.15-mm-thick aluminum, 4.05 cm high, with small extensions in the corners to support the lenses⁽⁵⁾. The photovoltaic cells and wiring are attached to a thin aluminum backing, which is placed underneath the honeycomb and lens assembly, as shown in Fig. 2. This backing, coated with alumina for high emissivity, acts as a thermal radiator, rejecting excess heat. When wired into triplets and placed under the concentrating lenses, the entire assembly converts solar radiation to electricity with an overall efficiency of 23.5%, operating at a temperature of 80°C⁽³⁾.

To size the array using the above efficiency, it is necessary to determine what power the lunar base requires and what other subsystem inefficiencies apply. This design was configured for a baseline output of 1.0 MW_e during the day and 50 kW_e at night, provided to the users. During the day, power will be channeled directly through transmission lines which have an efficiency of 94.4%. During the night, energy must be provided from a storage facility which, along with transmission and power conditioning, has an efficiency of 43.2%. Therefore, 1.175 MW_e are needed from the array during the day.

The cells are arranged in panels, 12.5 m × 3.0 m each. Individual panel dimensions are determined by structural and maintenance considerations. In the event of a breakdown, the panels will need to be repaired by an astronaut on site. A width of 3.0 m was chosen, therefore, to allow an astronaut to reach each half of the panel. The panels are supported close to the ground by a central truss, and rotated 0.54° per hour to track the sun, using single-axis tracking. A panel length of 12.5 m

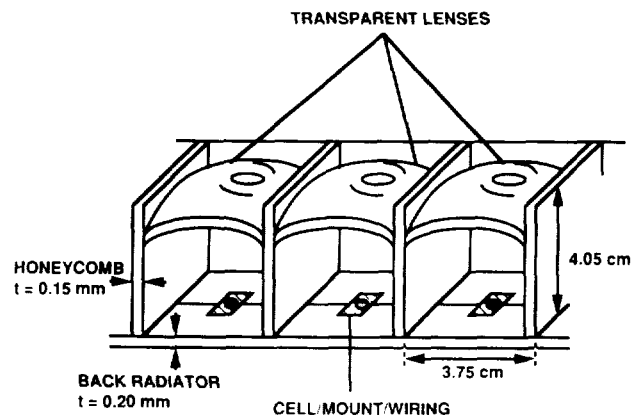


Fig. 2. Honeycomb Section Dimensions

was chosen to minimize structural weight. Two panels are mounted on a support structure with a motor in the center to form a panel set producing 23.85 kW_e at a mass of 183 kg (not including structural members).

Fifty panel sets are required to provide the baseline power output of 1 MW_e. These are arranged in 5 rows of 10 sets each, at a spacing of 15 m to minimize mutual shading effects. When panels are placed in rows facing sunrise or sunset, all panels behind the front row are partially shaded until the sun reaches a certain angle above the horizon. For a total of 50 panels arranged in 5 rows, the minimum is calculated to be 15 m. In this arrangement, the total array has a mass of 9,150 kg (not including structures) and requires a land area of 19,748 m² (4.9 acres).

Since the tandem cell developed by Boeing Aerospace has not been fully tested, an alternative array was also configured using an unconcentrated, single cell produced by TRW. This is intended to provide a comparison using existing technology. The alternative cell is made of GaAs deposited on a germanium substrate and offers an efficiency of 18%⁽⁶⁾. The cells are rectangular (2.0 cm × 4.0 cm × 0.2 mm thick) and require no concentrating lenses or extra housing. They can simply be secured to a radiative backing, placed close together, and wired in series.

The GaAs cells have roughly the same mass as the tandem cells (170 kg/panel set), but due to their lower efficiency, 65 panels are required to provide the same amount of power. Panel sizes are the same as for the tandem cell array: 12.5 m × 3.0 m. This means 15 extra panels are required, which is an addition of 1900 kg to the total system mass (not including structures), or an increase of 21% over the GaAs/GaSb cell array. The panels are arranged in 8 rows of 8 sets each, with one additional panel in the front, at a row spacing of 17 m to minimize shading effects. The total array mass is 11,066 kg (not including structures) and uses a land area of 27,171 m² (6.7 acres).

A comparison of the two alternative arrays is shown in Table 1. Note that the difference in efficiencies of the two cells significantly affects the power density. While the single GaAs cells are appealing in terms of simplicity and availability, the tandem cells, with a higher efficiency, require less mass. Mass is at a premium when all system components must be lifted to orbit, and the lighter weight tandem cell array is recommended.

Table 1. Cell Comparison Summary

	Tandem Cell	GaAs Cell
Array Efficiency	23.5%	18.0%
Concentration Ratio	100	1.0
Power/Area (W _e /m ²)	318	243.3
Total Required Area (m ²)	3750	4825
Number of Panel Sets	50	65
Cell Mass (kg/m ²)	2.44	2.27
Mass/Panel Set (kg)	183	170
Power/Panel Set (kW _e)	23.85	18.26
Total Array Mass (kg)	9150	11066
Power Density (W _e /kg)	130.3	107.3

BRAYTON DYNAMIC POWER SUPPLY SYSTEM

The second power unit considered in this study is the Brayton dynamic cycle conversion system powered by solar radiation concentrated by a parabolic trough collector. The total conversion system is composed of five modules, each with a 250 kW_e output. As shown in Fig. 3, each conversion module is made up of three main elements: the solar collection unit, the dynamic power module, and a heat rejection system. The system configuration was determined by manipulating the Brayton cycle parameters to obtain a system of minimum mass.

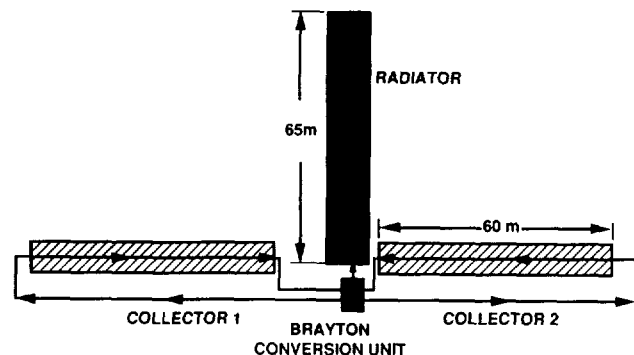


Fig. 3. Dynamic Conversion System Layout

The solar collection unit is designed to concentrate solar radiation onto a receiver through which the system working fluid passes. This fluid is thus heated for delivery to the turbine of the dynamic power module. The solar collection unit consists of two parabolic trough collectors, each 60 m long. Each collector processes half of the required mass flow rate of the system working fluid. The trough collectors are made up of a parabolic reflector surface and a receiver duct mounted at the line focus of the reflector. The reflector consists of a rigid structure that supports a reflective surface of aluminum foil. The reflector has an aperture of 7.0 m and a focal length of 1.0 m. For this design a reflectivity for aluminum foil of 86% was used⁽⁷⁾.

The receiver consists of a 5-cm-diameter duct made of UDE MET 700 alloy with a spectrally selective coating of cobalt oxide that is electroplated onto the duct. It serves to reduce the reradiative loss from the receiver by providing a low surface emissivity at the receiver operating temperature of 780 to 1000 K. The selective nature of the cobalt oxide coating is such that it has a high emissivity for radiation of wavelengths below 3 μm and a low emissivity at longer wavelengths⁽⁸⁾. This provides a solar absorptivity of 95%, with an effective emissivity from 18% to 32% over the entire length of the collector. This allows an efficiency of 63% to be achieved by the collector.

The dynamic power module consists of a regenerative Brayton cycle conversion unit. The cycle parameters used for the optimization of the system were the compressor and turbine inlet temperatures and the compressor pressure ratio. The operating temperature range is determined by considering system mass versus overall cycle efficiency. The compressor

inlet temperature was made as low as possible (330 K) without pushing the radiator mass to extremely high levels. The turbine inlet temperature is driven by two opposing factors. This temperature should be as high as possible to give a high cycle efficiency. However, the efficiency of the collector decreases as its average operating temperature increases. This suggests that there is an optimum turbine inlet temperature. As Fig. 4 shows, this optimum temperature occurs at ~ 1000 K. Based on the selection of the compressor and turbine inlet temperatures, the Brayton cycle efficiency is then maximized with respect to the compressor pressure ratio. The optimum pressure ratio was found to be 1.85 and resulted in a cycle efficiency of 36%.

For the dynamic power module, the compressor and turbine are mounted on the same shaft along with an alternator to produce the electrical power. The turbomachinery chosen for this study consists of a radial compressor and a radial turbine. This choice was made because of the low mass flow rate of the working fluid. Radial compressors require fewer stages than axial flow compressors to obtain the same pressure increase. Also, radial flow components are lighter and more rugged than axial flow components.

Several factors affect the choice of the working fluid: the extreme cold experienced during the two-week lunar night, the need for a noncorrosive gas to limit erosion and breakdown of system components, and the need for a high specific heat to minimize the mass flow rate. Helium was chosen as the working fluid because it does not become liquid at the temperatures reached during lunar night, and it has a high specific heat. Heat engines have higher component efficiencies using working fluids of higher molecular weight, however, any gases heavier than helium will condense out of the mixture at the low temperature of 116 K reached during lunar night.

Two different heat rejection systems were considered for this study. The first is a heat pipe radiator and the second is a liquid droplet radiator. Each requires a different heat

exchanger for the heat rejection from the dynamic power module working fluid. The heat pipe radiator requires a heat exchanger consisting of tubes immersed in the heat pipe fluid through which the helium passes. The liquid droplet radiator requires a heat exchanger that allows the helium to flow around tubes containing the liquid droplet radiator fluid.

The dynamic power conversion system has an overall efficiency of 23% of the incident solar energy. The mass of various components of the cycle, including the waste heat exchanger is given in Table 2, and will be used later to compare the dynamic conversion system to the photovoltaic system.

Table 2. Brayton Engine Mass Breakdown

Component	Mass, kg
<i>Brayton Conversion Unit</i>	
Turbomachinery	234
Regenerator	207
LDR Heat Exchanger	206
HPR Heat Exchanger	148
Gas Supply	8
Total Mass (LDR)	655
Total Mass (HPR)	597
<i>Solar Collector</i>	
Reflector Material	2808
Receiver Duct	15
Piping	105
Support Structure	7977
Total Mass	10,905

THERMAL MANAGEMENT

In any power generating system there will be a requirement for the disposal of a certain amount of waste heat. In the design of a lunar power system, additional complications arise from the lunar environment. The only viable method of heat rejection in the lunar environment is radiation, since the lack of an atmosphere precludes the use of convection and evaporation as methods of rejecting the waste energy. Also, the thermal conductivity of the Moon is very poor, which eliminates the use of conduction of waste heat to the lunar regolith. The waste heat rejection system must take into account any additional background radiation given off by the lunar surface. In addition, the radiator must have a high radiated power-to-mass ratio to minimize its mass, since all the material for the first generation lunar base must be transported from Earth.

The amount of waste heat to be rejected by the radiator varies dramatically between the two power generation systems. The photovoltaic power system is able to reject its own waste heat via the aluminum backing plate on each array, as noted earlier, and does not require a separate heat rejection system. On the other hand, the radiator for the dynamic cycle will be required to radiate away a significant percentage of the incoming solar energy due to the thermal efficiency of the cycle. In order to reject this heat, two possible radiator concepts are considered in this study: the Heat Pipe Radiator (HPR) and the Liquid Droplet Radiator (LDR).

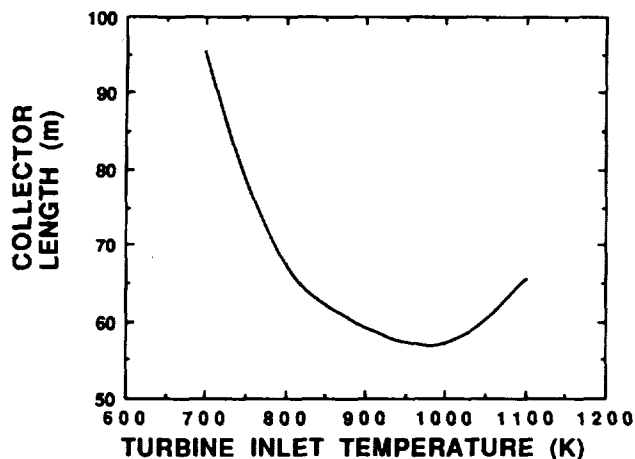


Fig. 4. Variation of Collector Length With Turbine Inlet Temperature

HPRs have been under development since the late 1960s⁽⁹⁾. The device designed for the present purpose uses a horizontal "mother" heat pipe (MHP) to conduct heat to a series of vertical heat pipes (VHP) which are connected to it and aligned with the vertical, as shown in Fig. 5. The VHP units conduct thermal energy to the attached fins, which radiate the waste heat to space. Suitable shading and reflecting surfaces are employed to minimize background input to the radiator. The HPR makes use of low density materials (pyrolitic graphite and graphite epoxy) for weight minimization.

The heat pipe radiator system has many distinct advantages over other heat rejection systems. Heat pipes do not require the use of pumps or moving parts, since they operate via vapor flow and capillary action. The individual VHP sections are independent of one another as well as of the MHP and are, therefore, resistant to single point failure. Another important aspect of the HPR's unique design is its utilization of available technology, reducing the amount of research and development necessary before implementation of the system.

The LDR utilizes a sheet of freely falling liquid droplets to radiate the waste heat^(10, 11). A schematic of the LDR system is shown in Fig. 6. The working fluid receives the waste heat from the power cycle at the heat exchanger. The fluid is pumped up through pipes to an emitter, which sprays the fluid as a vertical sheet of small spherical droplets. The droplets are then captured by a collector at the base of the LDR, and the fluid is recycled through the system. The most attractive aspect of the LDR system is the high surface area to volume ratio of the small spherical coolant droplets, which results in radiating power to mass ratio of 250 W_e/kg for this design.

There are also a number of potential disadvantages with the LDR system. First of all, lunar dust may present a problem by plugging the emitter, which is designed with very small holes in order to form the desired size of droplets in the sheet. Due to the centralized nature of the fluid transfer system, the LDR is not resistant to single point failure in the fluid handling system and the entire radiator would have to be shut down in the event of a system failure. For this design the pumps for the LDR would consume about 10% of the usable power from the Brayton cycle engines, which decreases the total power

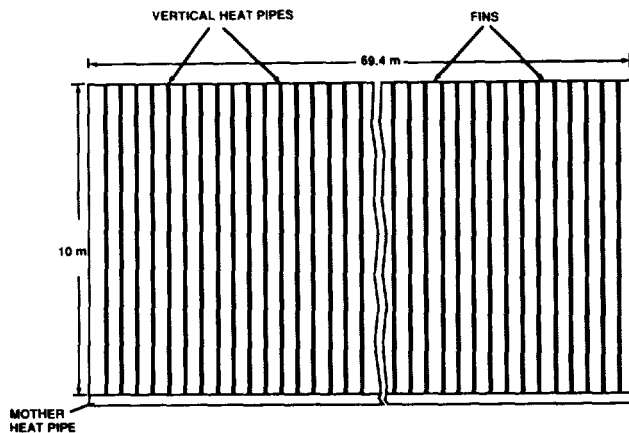


Fig. 5. Lunar HPR Configuration

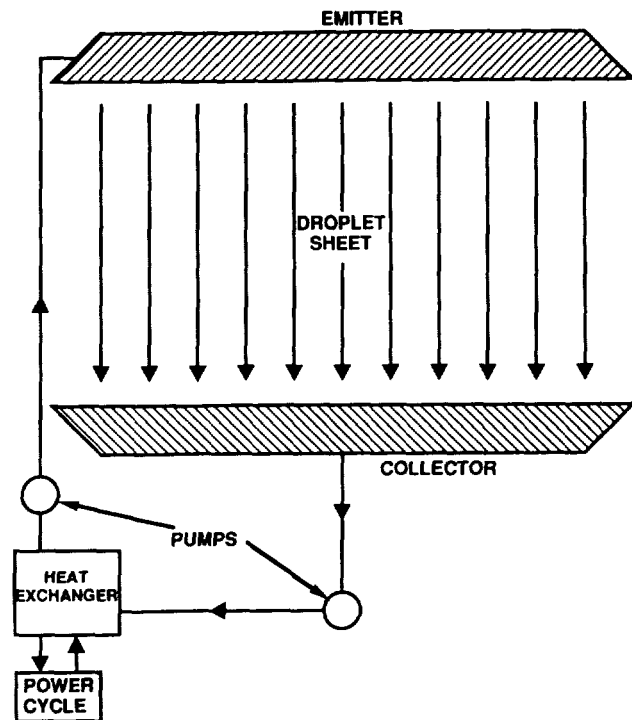


Fig. 6. Liquid Droplet Radiator Schematic

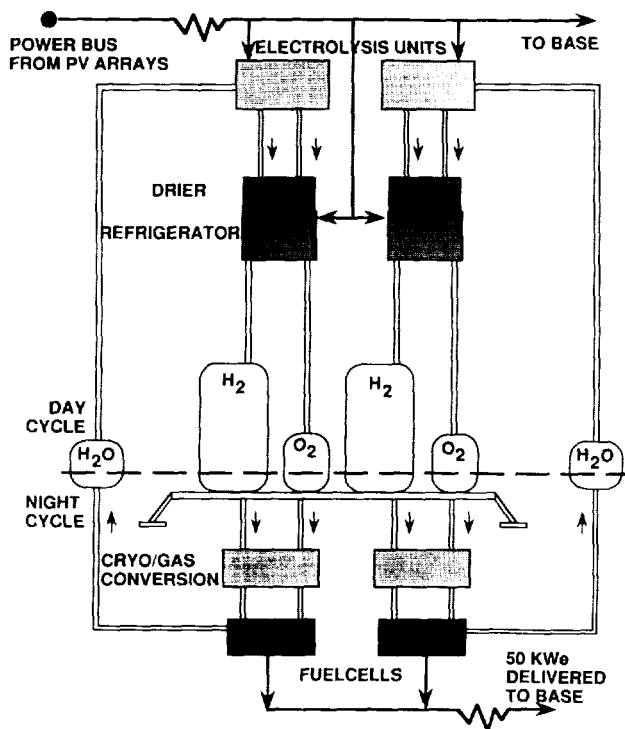
to mass ratio of the lunar power system. A majority of the present research into the LDR is for space-based applications; however, additional research is necessary before this system becomes a viable alternative heat rejection system.

ENERGY STORAGE

Using solar energy to power a manned lunar outpost has one major disadvantage: keeping the outpost fully operational at a 1 MW_e level during the long night would require the storage of more than one trillion joules of energy. Since energy storage tends to be extremely heavy, nighttime operation is limited to 50 kW_e for life-support, astronomy, and reduced research activities.

Recent advances have made the regenerative fuel cell the prime candidate for high power, longterm storage systems⁽¹²⁾. Though fuel cells come in a variety of configurations and operate at various temperatures, each has a basic purpose: the generation of electrical power through the processing of chemical reactants. During the night hours the chemical reactants, H₂ and O₂, enter the fuel cell, where they react to produce electric power and water as a byproduct. During the day, the water produced in the fuel cell is separated back into H₂ and O₂ by electrolysis, which is basically a fuel cell run in reverse. This requires an external energy source (PV array or solar-dynamic cycle) to supply the voltage needed for dissociation of the H₂O.

A schematic drawing of the 50 kW_e system is shown in Fig. 7. It is comprised of two 25 kW_e units, each with separate reactant storage tanks. If one unit were to malfunction, the

Fig. 7. 50 kW_e Energy Storage Schematic

other is capable of providing life-support for the assumed base crew of 8 astronauts (1.5 kW_e/astronaut) plus 13 kW_e which can be used to repair the other unit or for reduced astronomy and research activities.

Two different fuel cells have been considered: the experimental high temperature, monolithic solid-oxide fuel cell (MSOFC)⁽¹³⁾, and today's state-of-the-art low temperature alkaline fuel cell that is used on the space shuttle⁽¹⁴⁾. Table 3 summarizes the system properties associated with each type of fuel cell design. The system masses include the PV array necessary for the recharging of the cell along with the related structures, reactants, and the associated fuel cells. The table shows that the MSOFC does not have an advantage over the alkaline cell. The primary advantage of the low temperature fuel cell is the fact that its reliable operation has been proven and that it is currently in use. Development of MSOFC still faces problems with fabrication and processing of this sophisticated unit. The low temperature fuel cell, due to its availability and reliability, along with an adequate efficiency, was selected for the storage of energy on the Moon.

Table 3. Mass Summary for a 50 kW_e System

	Alkaline Cell	MSOFC
Chem. to Electrical efficiency	70%	60%
Round Trip efficiency	55%	40%
PV Array	1460 kg	2008 kg
Reactant Mass	7125 kg	8315 kg
Fuel cell and electrolysis	748 kg	6 kg
Total Mass	9333 kg	10,329 kg

In conventional energy storage systems, reactants are stored as gases in heavy, pressurized tanks. Satellites in low Earth orbit require storage periods of approximately 40 minutes. In these systems, using Inconel tanks, the tankage mass accounts for only 5.5% of the total system mass. Lunar missions, however, require storage for approximately 360 hours. Here, Inconel tanks account for 83% of the total system mass. Substituting lightweight filament-wound Kevlar 49/epoxy tanks reduces the fraction to 65%. However, by storing the reactants as cryogenic liquids, the tankage mass can be reduced significantly. In a report by L. Kohout of NASA's Lewis Research Center (LeRC), a conceptual design showed that tanks used in storing cryogenic reactants have a mass only 7.4% that of the Kevlar tanks used in the gaseous storage system⁽¹²⁾.

Storing the reactants as cryogenic liquids does require the additional mass of drying and liquefaction plants, as well as additional energy to power them, which means an increase in PV array mass or Brayton unit mass. As the hydrogen and oxygen streams leave the electrolysis unit, they contain a small amount of water vapor that was not completely electrolyzed. This water vapor must be removed before the gases are liquefied so that the water does not freeze and block the flow of reactants. Each dryer (one per 25 kW_e unit) has a daytime energy requirement of 0.3 kW_e and a mass of 28 kg. The liquefaction plants convert the reactants to a cryogenic liquid through a series of compressions and expansions. A reversed Brayton refrigeration cycle was chosen over Stirling, Vuilleumier, and other cycles because it has a lower mass and volume at higher refrigeration capacities. Each H₂ liquefaction unit (one per 25 kW_e unit) has a daytime energy requirement of 3.88 kW_e and a mass of 428 kg. Each O₂ unit has a daytime energy requirement of 1.84 kW_e and a mass of 136 kg⁽¹⁵⁾. However, even with these additional masses the total system mass is reduced by 50% due to the reduced tank mass.

Kohout proposes the construction of special, lightweight tanks for storing the cryogenic fluids, but an overview of the lunar development scenario reveals that there may be no need to design and build tanks especially for energy storage, as a variety of such tanks will be already available. In a conceptual report from Martin Marietta⁽¹⁶⁾, the lunar transit and excursion vehicles (LTV and LEV) will undergo a series of unmanned flight tests from Space Station *Freedom*. On the fourth and final test flight, an LEV will be loaded with cargo and will then land and remain on the Moon while the LTV returns to Space Station *Freedom*. This LEV can provide the reactant tankage for the 50 kW_e energy storage system.

An LEV lands with two LH₂ and two LOX tanks. Each LH₂ tank is capable of storing 1.44 tons of hydrogen and each LOX tank is capable of storing 8.68 tons of oxygen. For the 50 kW_e nighttime power requirement, these tanks will be less than half full (396 kg H₂ and 3166 kg O₂). They remain attached to the LEV, which provides the necessary structural support.

In addition to the LEV tanks, tanks are needed to store the water formed in the fuel cell until it can be electrolyzed in the daytime. The same tanks that were used to transport the reactants (in the form of water) from Earth can be used. These tanks have a volume 110% of that required by the water to accommodate freezing during transportation. Once the energy

storage system is engaged, there will be a constant influx of warm water from the fuel cell during the lunar night, and the water is not expected to freeze. The tanks are made from filament-wound Kevlar/epoxy, and the mass is found to be 148 kg by scaling from Kohout's system using the square-cube rule⁽¹²⁾.

The present design is compared to systems storing the reactants as high pressure gases and Kohout's baseline system utilizing cryogenic storage. Where storing the reactants as cryogenic liquids cuts the total energy storage system in half, the design presented here has an additional 5% reduction in system mass. Using Boeing's tandem photovoltaic cell as the power source for the electrolyzer unit, the PV array mass is reduced. Replacing the pumped loop radiators in the liquefaction plant and storing the cryogenic liquids in the propellant tanks of a spent LEV further reduces the mass.

POWER TRANSMISSION

The storage and transmission of energy require different types of power. For transmission at reasonable voltage over long distances (greater than 200 m), the current must be alternating, at or below a few thousand Hz. For energy storage, the current must be direct. The photovoltaic panels in this study produce direct current at 200 V, which is ideal for the proposed electrolysis units, but not for long-distance transmission. The solar dynamic engines considered in the study produce alternating current at 50 Hz and can be fitted with generators yielding 200 V. This power must be converted to DC for storage, and to higher voltage for long-range transmission. Converting between DC and AC is accomplished with an inverter.

For this study, short (~100 m) transmission distances are used, as a simple power distribution system that operates at the voltage generated by the solar cells requires less mass than a more complicated arrangement that uses high voltage in the lines (see Fig. 8). Also, the only power conditioning required is an inverter between the solar array and the user, plus a smaller inverter downstream of the fuel cells for nighttime power. A 280-kg inverter will be needed between the solar

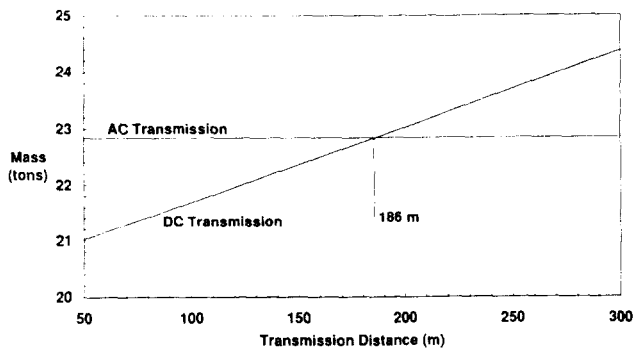


Fig. 8. Effect of Transmission Distance on Total System Mass for AC or DC Transmission

array and the user, and a 14-kg inverter will be required to convert the 50 kW_e nighttime output of the fuel cells into AC for the base⁽¹⁷⁾.

Aluminum cables were chosen for their superior conductivity per unit mass over copper cables (14,240 m²/Ω·kg, compared to 6683 m²/Ω·kg)⁽¹⁸⁾, and it is suggested that the cables be buried in the lunar regolith to avoid any resistivity variations due to temperature changes during the day/night cycle.

For the 1.175 MW_e transmitted (direct power for the base plus charging power for energy storage), the power conditioning mass is roughly 300 kg, and the total mass of the transmission system is 950 kg. This is roughly 5% of the power generation system mass. Note, however, that a distance of only 1000 m between the solar arrays and the base would require a much more complicated system to transmit the power efficiently (see Fig. 9).

STRUCTURAL DESIGNS

The structural designs for the lunar base power system were developed with three primary characteristics in mind. These are that the structural supports for all systems should be easily assembled, they should require no maintenance, and they should be fabricated from materials with the highest specific strength and durability available. All designs take into account the size and mass capacity of the Shuttle-C cargo bay (25 m × 4.6 m diameter, 71-metric-ton payload capacity) on the

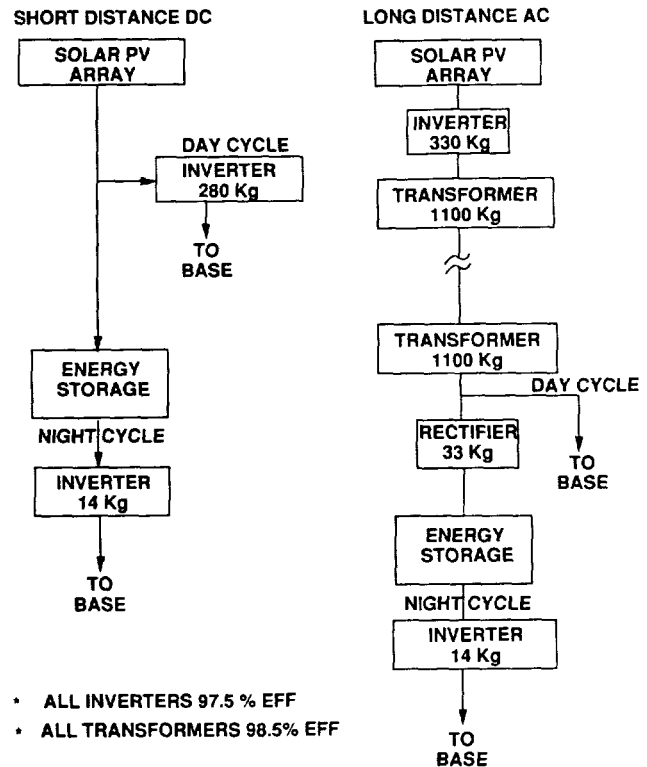


Fig. 9. Solar Photovoltaic Power Transmission

assumption that this is the vehicle that will be available for the delivery of large payloads to low Earth orbit (LEO). Another important criterion in developing the large truss structures was that as few different types of truss members as possible be used, so that a scheme of keeping track of each type (such as color-coding) can be made as simple as possible. Robotic assembly of large truss structures has not been researched in depth for this report, so it was assumed that much of the construction will be performed by astronauts. The four major design sections corresponding to the primary components of the lunar power station are: (1) solar photovoltaic array structural design, (2) solar dynamic parabolic trough collector structural design, (3) thermal management structural designs (including both the HPR and LDR), and (4) lunar concrete structural designs.

The support structure for the solar photovoltaic arrays consists of four different types of members, all fabricated of advanced composite materials. Approximately 3750 m² of Boeing high-efficiency cells are required for the lunar power system, indicating that 50 individual rotating arrays (2 panels \times 12.5 m \times 3 m) will be needed to achieve this surface area. The design concept is termed "backbone and rib" structure and is similar to a human backbone. The "backbone" is a solid, square graphite epoxy composite tube supported on both ends and in the center by rotating bearings (see Fig. 10). A row of graphite epoxy "ribs" filled with a honeycomb core are fitted through the "backbone" at constant intervals, and locked into place. A thin wire mesh is attached to the top of these ribs, and the cell housings themselves are supported by this mesh and the "ribs." This is then supported on each end by a tetrahedral truss structure and in the center by a triangular truss structure. A mass inventory for this design is given in Table 4.

The structural designs for the solar dynamic cycle centered on the design of the parabolic trough collector (see Fig. 11). Approximately 110 m of solar collector is required per engine. This length is divided into 5-m segments, and the basic structural unit is based on this length. Five meters was chosen to minimize unstable bending in the reflecting panels (four around the perimeter of the parabola) while being lifted into

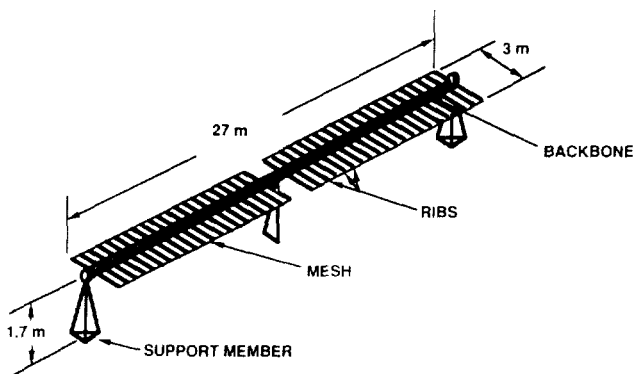


Fig. 10. Solar Array Structure

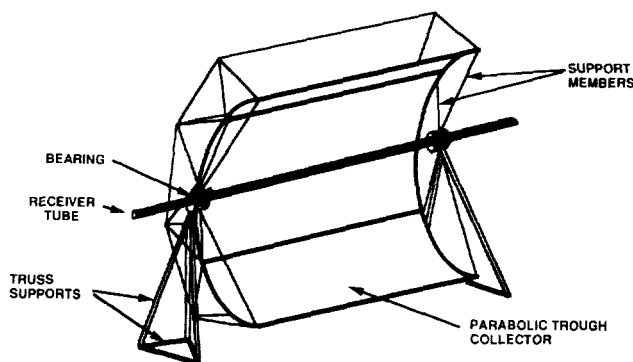


Fig. 11. Isometric View of Solar Trough Collector

position within the support framework. This framework is a system of trusses connected to two stiff graphite epoxy ribs and three support members. The framework holds the shape of the parabola and is strong enough to support the four reflecting panels. In addition, the framework was designed to place the center of mass of the 5-m segment at the point 1 m directly above the apex of the parabola, i.e., the focus. Thus, the concentrator has a mass distribution such that it can be easily rotated about the fluid duct. The reflecting surface will simply be a thin coating over the graphite epoxy honeycomb sandwich panels in order to minimize the mass of the system.

Table 4. Structural Mass Inventory for Solar Array

Member Type	Total Mass Per Array (kg)
Box Beam	70
Ribs	50
Supports	38
Bearings and Nodes	45
Total Mass	203

The four reflecting panels within each 5-m segment have a small space between them and there is a gap between each segment for support structure (a region in which the fluid temperature may drop slightly), both diminishing the system efficiency. To make up for this, two additional 5-m segments are added to the solar collector for each engine, resulting in a total length of 120 m per engine. Thus, twelve 5-m segments will lie on either side of each engine and be supported by tetrahedral trusses at the two ends and triangular trusses in between.

The heat pipe radiator, shown in Fig. 12, consists of four major components: (1) a v-shaped roof, (2) horizontal members that provide lateral stability, (3) vertical members that support the roof, and (4) base support brackets to hold the mother heat pipe and support members. All components are fabricated from advanced composite materials, and designed so that assembly is fast and efficient. The base support brackets are located every 17.5 m along the span of the radiator. The mother heat pipe is laid between these with the vertical heat pipes projecting out of it. The horizontal support members extend out of the bracket along the lunar surface and a guy wire is attached to each, running from the ends to

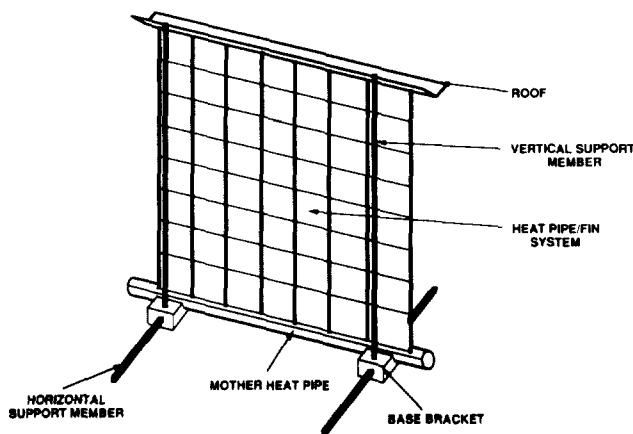


Fig. 12. Isometric View of Heat Pipe Radiator

the roof. Vertical support members project up out of the bracket and support the roof. The guy wires provide support, so that if any kind of lateral load should be applied, the force will be distributed to the horizontal support members on the opposite side and not to the heat pipes.

The liquid droplet radiator, if implemented, would be the largest structural design for the lunar power station (see Fig. 13). It stands 52 m tall and 15 m wide. Many of the major design features were adopted from a previous University of Washington study on nuclear power for a lunar base⁽¹¹⁾. The structure consists of four major elements: (1) erectable masts, (2) a cable-pulley inter-tie system, (3) a longitudinal emitter support truss, and (4) a droplet collector.

On top of each mast a lifting extension truss is fixed. Due to the difficulties involved in the construction of large towers on the Moon, these masts will be built from the top down. This means that the extension truss must be assembled as the first unit to be raised, with each box truss erected beneath

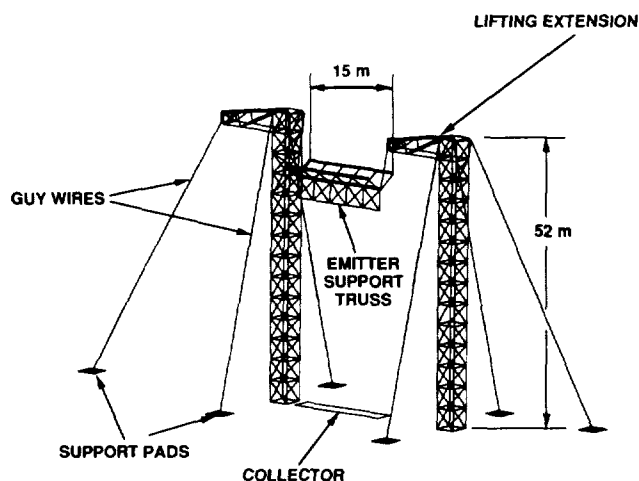


Fig. 13. Liquid Droplet Radiator Structure

it. Attached to each side of the lifting extension are an emitter support bracket and a cable-pulley inter-tie system used to hoist the emitter support truss. The emitter support truss consists of 2-m horizontal and vertical support members with diagonal members placed in between. The emitter will be mounted mechanically to the bottom of the truss before raising it, and the flexible feed line will be attached and allowed to hang freely as it is raised. The liquid droplet collector is placed directly below the emitter and the LDR fluid is pumped out of one end, through the heat exchanger loop and back up to the emitter.

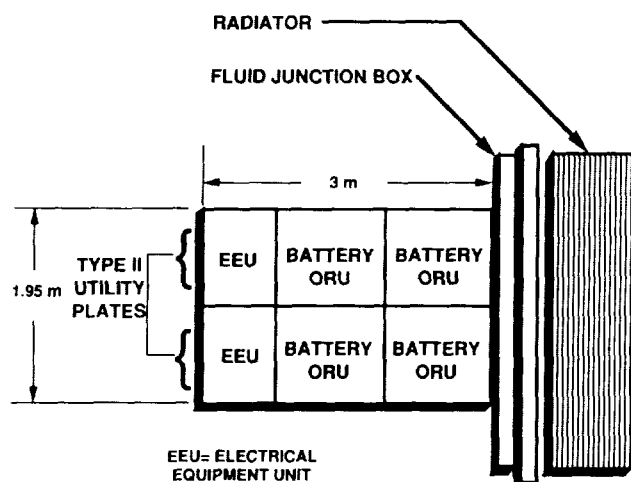
The remainder of each mast consists of twelve 4-m \times 4-m box trusses with guy wires to provide lateral stability. Each box truss is erected one at a time within a framework surrounded by four hydraulic jacks. When each box is assembled, it is raised 4 m by the jacks, allowing the next one to be assembled beneath it. In this way, the entire mast can be constructed on the ground quickly and with little effort.

The possibility of using lunar concrete produced by a method proposed by Shimizu Corporation of Japan was also examined⁽¹⁹⁾. Shimizu studies indicate that a vacuum environment maintained during the hardening of concrete significantly reduces its strength. Because of this and the large mass involved, it was decided that lunar concrete would not be used extensively in the lunar power system design. However, in some applications, such as pads placed beneath truss supports for stability and solid blocks to be used to anchor guy wires, this concept may be worthwhile.

EMERGENCY POWER BACKUP SYSTEM

The lunar power system presented in this report is a modular system with many levels of redundancy. Even so, there is still the chance of some kind of system failure; thus, the decision was made to provide an emergency backup power source. Several candidate power storage methods were examined, including fuel cells and several types of both primary and secondary batteries. After considering the pros and cons of each, nickel-hydrogen secondary batteries were chosen on the basis of their proven record of use in space and their moderately high power density. In order to decrease development costs, and to make use of existing technology, it was decided that a derivative of the power storage system to be used on the Space Station *Freedom* (SSF) be employed as the backup system for lunar operations⁽²⁰⁾.

The basic unit system for backup power is comprised of two 81 Ah, 95 V nickel hydrogen batteries wired in parallel, and the supporting electronics and thermal control equipment (see Fig. 14). After inefficiencies are considered, this is enough energy to supply two persons with 1.5 kW each for approximately 3.5 hours. The components used in the backup power system are designed in modular sections called Orbital Replacement Units for ease of repair. These components are mounted on two standard utility plates that provide structural backing, and coolant fluid pipes. The utility plates will simply be placed where necessary, as opposed to being rigidly connected as on SSF, in order to reduce unnecessary system mass. A modified fluid junction box connects the utility plates

Fig. 14. Space Station *Freedom* Energy Storage System

with the pumped loop ammonia radiator, completing the thermal control loop, as well as the basic unit. These two-person-rated systems may be combined in sufficient quantities, once given the number of occupants at the lunar base.

This battery system turns out to be relatively massive (see Table 5) due to the relatively low energy density of batteries as opposed to fuel cell storage. As stated earlier, the nickel-hydrogen system was chosen because it will be extremely reliable. However, fuel cell systems, when configured in a highly redundant manner, may provide the same power as batteries at a great mass savings, but with increased complexity. When the lunar base is constructed, mission planners will have to decide whether the high mass of the batteries is justified or if some type of fuel cell system should be supplied for emergency backup.

Table 5. Lunar Emergency Backup Power System Components

Component	Mass (kg)	Parasitic Power (kW)	Energy (kWh)	Quantity
Battery ORU	146	-	3	4
EEU	76	0.140	-	2
Utility Plate	136	-	-	2
TCS Pump ORU	36	0.125	-	1
Fluid Junction Box	21	-	-	1
Radiator	125	-	-	1

CONCLUSION

The work presented here shows that a solar power system can provide power on the order of one megawatt to a lunar base with a fairly high specific power. The main drawback to using solar power is still the high mass, and, therefore, cost of supplying energy storage through the lunar night. The use of cryogenic reactant storage in a fuel cell system, however, greatly reduces the total system mass over conventional energy storage schemes.

As shown in Table 6, the advanced new tandem GaAs/GaSb photovoltaic cells provide a specific power nearly four times that of the dynamic cycle conversion scheme. This comparison takes into account all necessary structural, thermal control, and solar collector masses, and suggests that the photovoltaic system is the best system to use. Additionally, the solar cells are passive, with the only moving part being the solar-tracking motor, thereby increasing the system reliability. For these reasons, the photovoltaic array is recommended for use over the dynamic power system.

Table 6. Comparison of Solar Power Systems

	Photovoltaic Arrays	Brayton Cycle
Photovoltaic Array Mass	9,150 kg	-
Structural Mass (PV)	10,150 kg	-
HPR Brayton Engines (5)	-	2985 kg
Solar Collector (5)	-	54,525 kg
Radiator (HPR) (5)	-	17,450 kg
Total Power Supplied	1,175 kW	1,250 kW
Total Specific Power	61.7 W/kg	16.7 W/kg

Obviously, the solar cells produce no power during the night, and since energy storage for the lunar night is so massive when compared to daytime power, cutting back on power during the lunar night is highly recommended. In this system, 50 kW was chosen as the minimum nighttime power in order to greatly reduce overall system mass while still allowing enough power for scientific experimentation. Making use of the spent cryogenic tanks from a lunar excursion vehicle reduces the net mass of the storage system, but not enough to make high power at night economically feasible.

If the dynamic conversion system is used, thermal management should be provided by the heat pipe radiator system because of its fairly high specific thermal power dissipation, and because heat pipe radiator technology is well developed. The liquid droplet radiator is a very promising concept, and may one day surpass conventional systems in performance, but more research needs to be performed first.

If, for some reason, the power system is shut down, a modified version of the Space Station *Freedom* energy storage system is employed to provide the base inhabitants with enough emergency power to escape from the base. This system turned out to be quite massive, and so systems with slightly less reliability may be preferable to help reduce overall system mass.

In conclusion, technology has advanced to the point where a solar power system may now be seriously considered for high power applications on the Moon, as this report has shown. Given all of the problems, both political and technological, with nuclear power, it may be time to reexamine the old idea of using the sun to power the lunar base.

ACKNOWLEDGMENTS

Student authors are B. Adams, S. Alhadeff, S. Beard, D. Carlile, D. Cook, C. Douglas, D. Garcia, D. Gillespie, R. Golingo, D. Gonzalez, P. Gurevich, C. Hansen, W. Hopkins, J. Iacometti, M. Jardin, T. Lipscomb, S. Love, T. Montague, J. Nelson, and D.

Ritter. Editors are David Carlile, John Iacometti, and Matt Jardin. They were assisted by Professors Adam P. Bruckner, and Abraham Hertzberg, and Teaching Assistant Terri Schmitt.

REFERENCES

1. Fraas, L., "Tandem Solar Cells with 31% (AM0) and 37% (AM1.5) Energy Conversion Efficiencies", *IEEE Aerospace & Electronic Systems Magazine*, Volume 4, Number 11, November, 1989, p. 3-9.
2. Henderson, B.W., "Boeing Achieves Major Advance in Space Solar Cell Efficiency", *Aviation Week and Space Technology*, October 23, 1989, pp. 61-63.
3. Fraas, L., "Boeing High Efficiency Solar Cells", Lecture, University of Washington, January 31, 1990.
4. O'Neill, M., Entech, Inc., Personal communication, April 25, 1990.
5. O'Neill, M.J. and Piszczar, M.F. "Development of a Dome Fresnel Lens/Gallium Arsenide Photovoltaic Concentrator for Space Applications", Entech, Inc., 1987.
6. Krueger, M., TRW, Personal communication, May 7, 1990.
7. Duffie, J.A., and Beckman, W.A. *Solar Engineering of Thermal Processes*, John Wiley & Sons, 1980, p. 168.
8. Van der Leij, M., *Spectral-Selective Surfaces for the Thermal Conversion of Solar Energy*, Delft University Press, 1979, pp.64-96.
9. Werner, R. W. and Carlson, G. A., "Heat Pipe Radiation for Space Power Plants," *IECEC 1968 Record*, IEEE, Piscataway, NJ, pp. 487-501, 1968.
10. Mattick, A. T. and Hertzberg, A., "Advanced Radiator Systems for SpacePower", IAF 87-230 38th Congress of the International Astronautical Federation, Brighton, United Kingdom, October 10-17, 1987.
11. AA 420/499 Design Group, "Multimegawatt Nuclear Power System for Lunar Base Application", University of Washington, Department of Aeronautics and Astronautics, NASA/USRA - University Pilot Program, Final Report, June 1986.
12. Kohout, L.L., "Cryogenic Reactant Storage for Lunar Base Regenerative Fuel Cells," Lewis Research Center, NASA TM 011980, June 1989.
13. McPheeters, C.C., et al., "Recent Advances in Monolithic Solid Oxide Fuel Cell Development," *IECEC 889207*, 1988.
14. O'Donnell, P., Deputy Branch Chief, Electrochemical Technology Branch, NASA Lewis Research Center, Private Communication, May, 1990.
15. Bock, E.H., and Fisher, J.G., "In-Space Propellant Processing Using Water Delivered as Shuttle Contingency Payload," *AIAA Paper 78-941*, July 1978.
16. Mitchel, P., *Lunar/Mars Outpost: Interim Review #1*, MCR 89-7505, Martin Marietta Company, 1989.
17. Dickerson, A., *California Polytechnic Institute*, Pomona, Private Communication, February, 1990.
18. Griffiths, D.J., *Introduction to Electrodynamics*, Prentice-Hall, Inc., Englewood Cliffs, N.J., 1981.
19. Namba, H., et. al., "Concrete Production Method for Construction of Lunar Bases," *Academic Papers Regarding Concrete on the Moon*, Shimizu Corporation, Tokyo Japan, 1990.
20. Brandhorst, H. "Challenges for Future Space Power Systems," *NASA-TM-102063*, Cleveland, OH, Oct. 1989.

2005/1/2
P. 14
241

GENESIS LUNAR OUTPOST: AN EVOLUTIONARY LUNAR HABITAT

UNIVERSITY OF WISCONSIN-MILWAUKEE

N 9 1 - 1 8 1 5 8

Students at the University of Wisconsin-Milwaukee Department of Architecture undertook a series of studies of lunar habitats during the 1989-90 academic year. Undergraduate students from architecture and mechanical and structural engineering with previous backgrounds also in interior design, biology, and construction technology were involved in a seminar in the fall semester followed by a design studio in the spring. The studies resulted in three design alternatives for lunar habitation, and an integrated design for a early stage Lunar Outpost.

EARLY STAGE LUNAR OUTPOST

On the 20th anniversary of "One giant leap for mankind," President Bush announced the goal of landing people on the Moon by 2005, and this time to stay. Project *Genesis* is proposed as the first early stage, permanently occupied habitat on the Moon.

Research, design, and development of Project *Genesis* was initiated in 1989 by the University of Wisconsin-Milwaukee (UWM) Center for Architecture and Urban Planning Research and Department of Architecture in cooperation with the College of Engineering and Applied Science. UWM/Architecture is one of only 3 architecture schools in the 44-university NASA/USRA University Advanced Design Program. The program stresses the systems approach to design in which the class works together on a major "real world" project. The objective this year was to design a lunar outpost for the year 2005 based on environment-behavior, architectural, and engineering design concepts.

Genesis is proposed as an evolutionary, long-term testbed for all materials, processes, and development strategies to be employed in a mature lunar colony for the next 20 years, and as a testbed for all processes to be employed in the exploration and settlement of Mars.

Following guidelines provided by aerospace engineers and scientists at NASA's Johnson Space Center (NASA/JSC) and its prime contractors, the UWM Space Architecture Design Group designed *Genesis* for a full-time crew of 8 to 12 persons on rotations of 6 to 9 months with a maximum duration of 20 months. Gender, nationality, and ethnicity are expected to vary as the consortium of world aerospace partners all become involved in free-flowing scientific communication.

Five mission objectives were identified for Project *Genesis*: (1) lunar surface mining and production analysis; (2) lunar construction technology and materials testbed; (3) closed ecological life-support system (CELSS) test facility; (4) lunar farside observatory; and (5) human factors and environment-behavior research facility.

The first crewed mission to establish the outpost, which is expected to land on the Moon in 2005, could last as little as 14 days. The astronauts, architects, and engineers will live inside their lunar landing vehicle (LLV) and spend much of each day performing extra vehicular activities (EVA) involved in base construction. A pressurized construction module will

be the first order of business, followed by the evolutionary development of the rest of *Genesis*. Once all systems, subsystems, and backups have been verified, and the initial operation configuration (IOC) has been put in place, crew change-outs will occur every 9 months to a year as the astronauts and their partners perform research and manufacturing operations.

PROJECT GOALS

This year's project had three goals:

1. **Design solutions.** To develop creative yet realistic architectural and engineering solutions to space design issues in response to human factors and environment-behavior issues, safety, energy, construction technology, and the utilization of natural resources.

2. **Curriculum development and pedagogy.** To enhance, further develop, and maintain courses and studios in the area of space architecture and related subjects in the School of Architecture and Urban Planning in conjunction with the College of Engineering and Applied Science at the University of Wisconsin-Milwaukee, and also to offer the design student the opportunity to become well versed in space and high technology.

3. **Useful information.** To produce information and design solutions useful to the aerospace community, NASA, its prime contractors and subcontractors, and NASA/USRA schools on long-duration habitation design, and to publish this information and disseminate it in a manner that makes is accessible and timely to these communities.

LUNAR BASE MISSION OVERVIEW

A lunar outpost has eight major objectives to satisfy^(1,2):

1. Located at an Earth-facing equatorial location.
2. Constructed of lightweight, durable materials that require little EVA time.
3. Contained within the next generation of Earth-lunar transport systems: (a) U.S. space transport shuttle system, (b) heavy-lift launch vehicle such as the autonomous Shuttle C with cargo capacity of 69,000 kg (150,000 lb) and cargo bay 25 m x 4.5 m diameter (82 x 15 ft), (c) low-Earth-orbit Space

Station *Freedom* (SSF) and associated platforms, and (d) the planned cislunar transport system consisting of an orbital transfer vehicle (OTV) and a separate reusable lunar lander.

4. Capable of housing 8-12 astronauts of different nationalities, genders, and specialties for periods up to 20 months with a normal change-out of 6-9 months.

5. Provision for all life-support systems including (a) human factors, (b) health and safety, (c) environment-behavior issues, (d) habitability of crew areas, crew support, operations of base, and design for productivity, and (e) Controlled Ecological Life-Support Systems (CELSS) and Environmentally Controlled Life-Support Systems (ECLSS).

6. Integration of advanced technologies: (a) space construction technology, (b) advanced systems of energy use and energy conservation, and (c) advanced mechanical systems including power, thermal, air movement, and hydraulic systems.

7. Understanding and response to the physics, geology, and natural environment of the Moon, lunar resource utilization, and appropriate "urban" design to retain the natural qualities of the Moon.

8. Support for five main mission research operations: (a) lunar surface mining and production analysis for lunar oxygen (LUNOX), helium 3 (H₃), and other minerals; (b) lunar construction technology and materials testbed for testing high-technology construction with inflatables, the use of lunar regolith for radiation shielding, lunar glass, lunar concrete, and sintering techniques using advanced telerobotic systems; (c) CELSS test facility; (d) lunar farside observatory; and (e) human factors and environment-behavior research facility including ongoing post-occupancy evaluations (POEs) of *Genesis* itself.

DESIGN METHODOLOGY

To achieve these goals, the project team proceeded in three phases:

1. **Fall semester seminar.** The project began with a fall semester seminar (Architecture 392/792). Twelve students from architecture, interior design, mechanical and structural engineering, and liberal arts/pre-architecture had a series of lectures, extensive readings, and simple sketch designs to learn the material needed to design a lunar habitat. The seminar was under the leadership of Edwin Cordes, a recent graduate of the UWM M.Arch. program and of the International Space University in Strasbourg, France, and Dr. Gary Moore, a research architect and environmental psychologist, the overall project director. The teaching assistant was Mr. Timothy Hansmann, who had been a NASA/USRA intern at JSC. The product was a programming/requirements document⁽¹⁾.

2. **Spring design studio: Preliminary design on three design alternatives.** A space architecture design studio (Architecture 690) was conducted in the spring semester of 1990. Eleven students, most of whom had been in the fall seminar, were drawn from architecture, interior design, and mechanical and structural engineering. Issues included anthropometrics, human factors, health and safety, psychological and social issues, habitability, energy systems, construction

technology, internal and external base operations, and base master planning and phasing. After preliminary exploration of different subsystems of the base (research module, manufacturing areas, habitat module, base planning and layout), three alternative designs were explored in detail and presented at a preliminary design review (PDR) in February 1990 attended by representatives of NASA/JSC, USRA, industry, and academia. Each team was made up of architects and engineers with specialties in environment-behavior studies, interior design, structural or mechanical engineering, and construction technology. This division—vertically by subsystem and horizontally by specialty—insured that each subsystem responded to all design factors and that all subsystems would contribute to an integrated solution.

The product was a set of design drawings and presentation boards, together with a slide presentation. It was presented at several regional and national meetings and received a special student design award from the Environmental Design Research Association at its 21st annual conference.

3. **Spring design studio: Design development of final integrated design solution.** The design concepts and ideas selected at the PDR were further developed. A number of technical issues needed further research, analysis, and design exploration: materials, joining systems, hatches and gaskets, structural system, deployment systems, and regolith containment systems. Each was explored in depth by one or two members of the team with critical input from our NASA/JSC consultants and industry representatives. The project team was subdivided into teams for the further exploration and design development of parts of the overall *Genesis* Lunar Outpost. The three teams were site and master planning, interior configuration, and construction technology.

Three extra-credit students served as team leaders for the design teams; all are now working for NASA or NASA contractors. The product was a set of design development drawings and slide presentation that was presented at the NASA/USRA 6th Annual Advanced Design Program Summer Conference, NASA/Lewis Research Center, and elsewhere in this country and overseas.

THREE DESIGN ALTERNATIVES

As a first design phase, three design alternatives were explored in detail based on differing sets of engineering and architectural assumptions: (1) Space Station *Freedom* (SSF) rigid space structures using clusters of space station-sized pressure vessels, aluminum alloy domes, and interconnect nodes; (2) underground architecture using the natural lunar craters and lava tubes; and (3) inflatables using a laminated Kevlar bladder with a space frame structure.

In each design alternative, separate modules were designed for laboratory and habitation functions. The entire facility was designed to be buried under a sufficient amount of lunar regolith (0.5 to 1.5 m) for proper radiation protection and thermal control.

Concerns of the design teams included provision of public and private spaces for all functions, design for 1/6 gravity of the Moon, systems for multiple uses to conserve space and

weight, accessibility to all areas and components, graphic coding to allow ease of identification by crewmembers, and interior configuration, which includes provisions for life support and power supply systems. The laboratory area includes workstations for eight crewmembers, an exercise facility, a limited hygiene facility, a system for holding a variety of experiments, command and control center, and a storage system for consumables, excess equipment, and personal items. The habitation area includes sleeping and personal areas for the eight crewmembers, hygiene facilities for full body and hand cleansing, meal preparation area, dining area with facilities for teleconferences and meetings, crew health care and emergency medical facility, and storage system for food, medical supplies, and personal items.

Prefabricated Rigid Construction

The first design alternative focused on the use of SSF-type hard modules with connectors and EVA chambers (see Fig. 1). The floor plan has a central command center flanked by science and medical facilities, domestic management, central large domed research and teleconferencing workstations, and crew quarters. Each of the larger modules was designed to fit in a standard space shuttle cargo bay, and would be fully outfitted prior to liftoff.

This alternative would develop through a series of phases (see Fig. 2) with each specified in terms of the number of flights with crew and logistics payloads to construct each phase up to IOC. Phases A, B, and C are the three subphases of

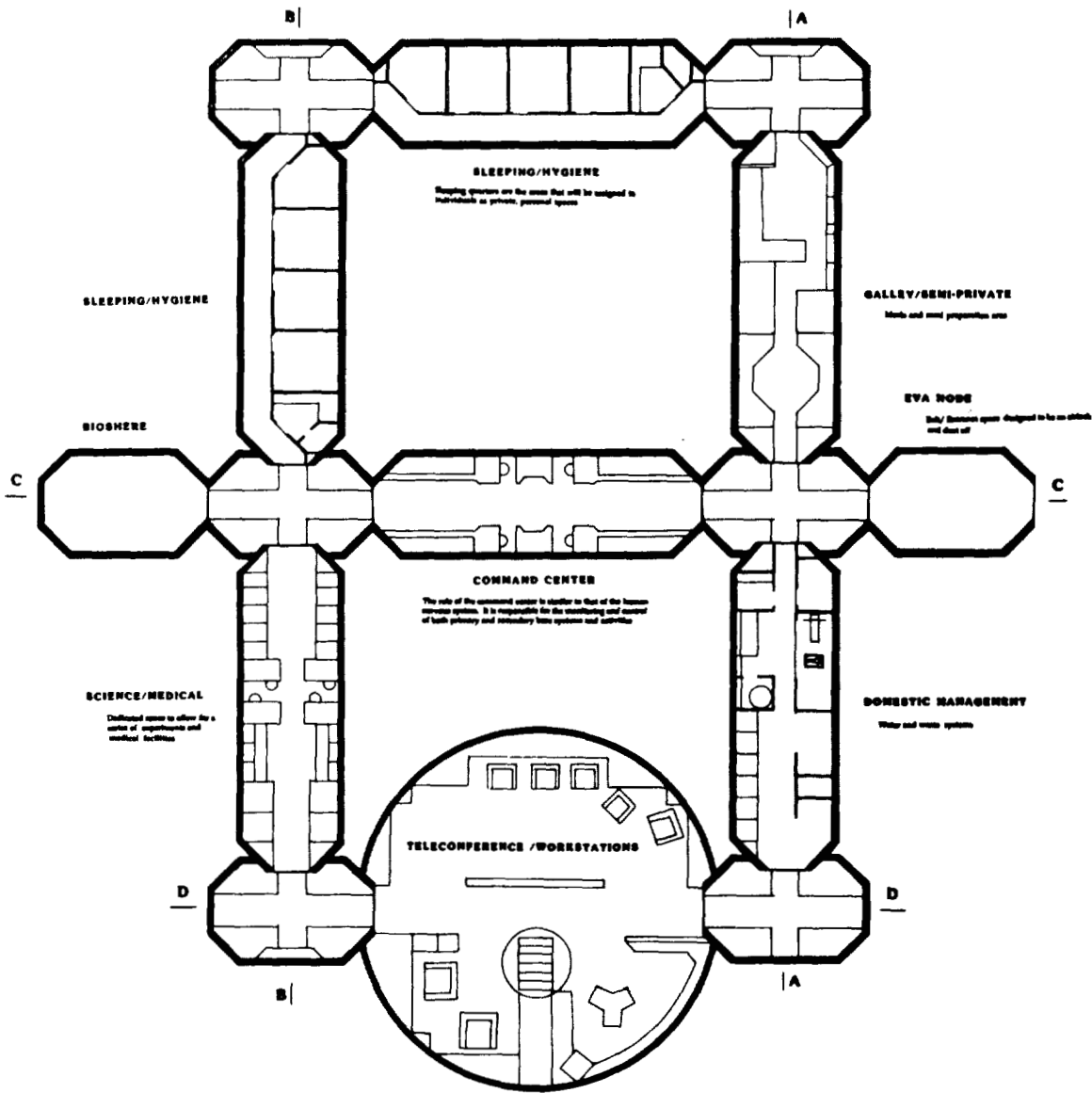


Fig. 1. Design alternative 1: Rigid construction—base floor plan

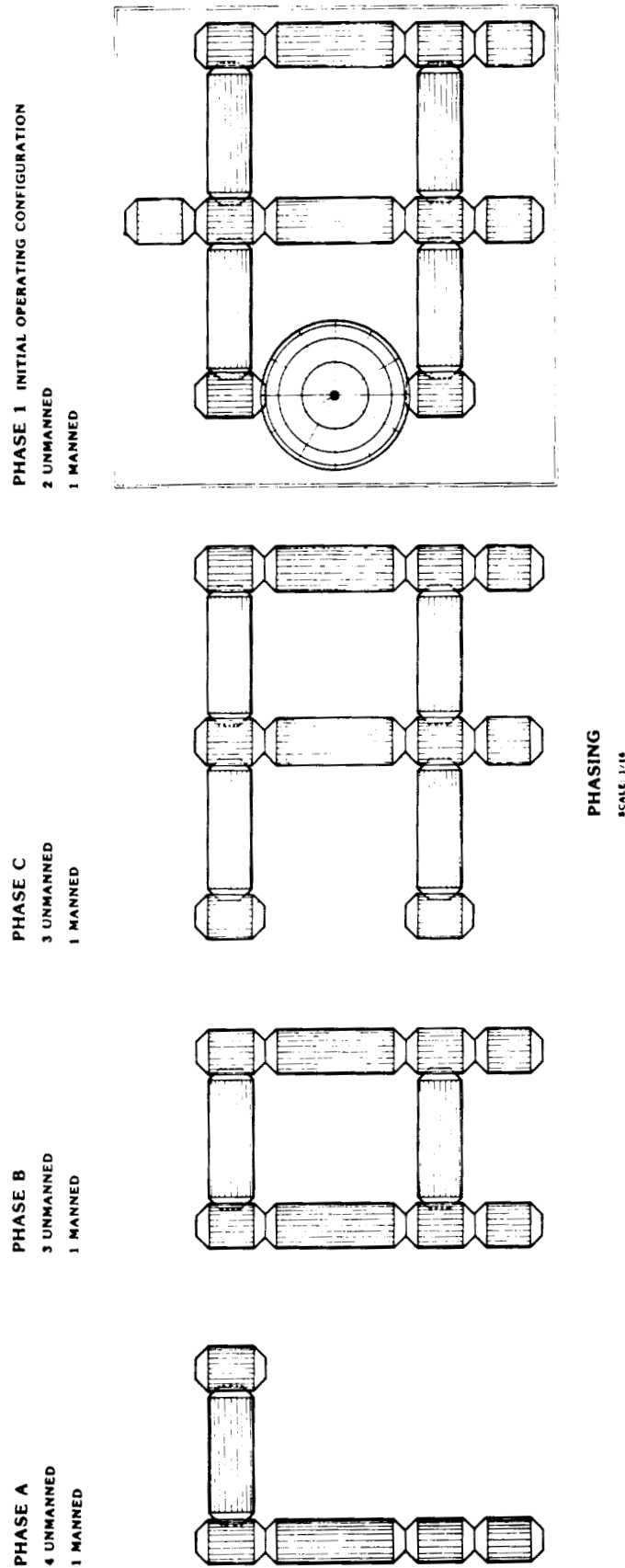


Fig. 2. Initial three subphases leading to IOC

ORIGINAL PAGE IS
OF POOR QUALITY

Phase 1 IOC. The IOC involves a dome habitat center constructed from prefabricated Earth-based construction technology (aluminum sheets, self-rigidizing foam, etc.).

Lunar Craters and Lava Tubes

The second design alternative explored the possibilities of using lunar craters and associated lava tube systems. The design uses a descending lava tube opening (see Fig. 3) with a

command center inside the upper entrance of the lava tube. The walls are formed from a rigidizing foam wall system. As the lava tube continues its steep descent, an electromagnetic elevator system would be installed.

The large, natural, open volume of the lava tube can be converted into a two-story habitat with crew quarters, laundry, meal preparation area, biosphere, conference and library area, laboratory, exercise area, and ball court (see Fig. 4).

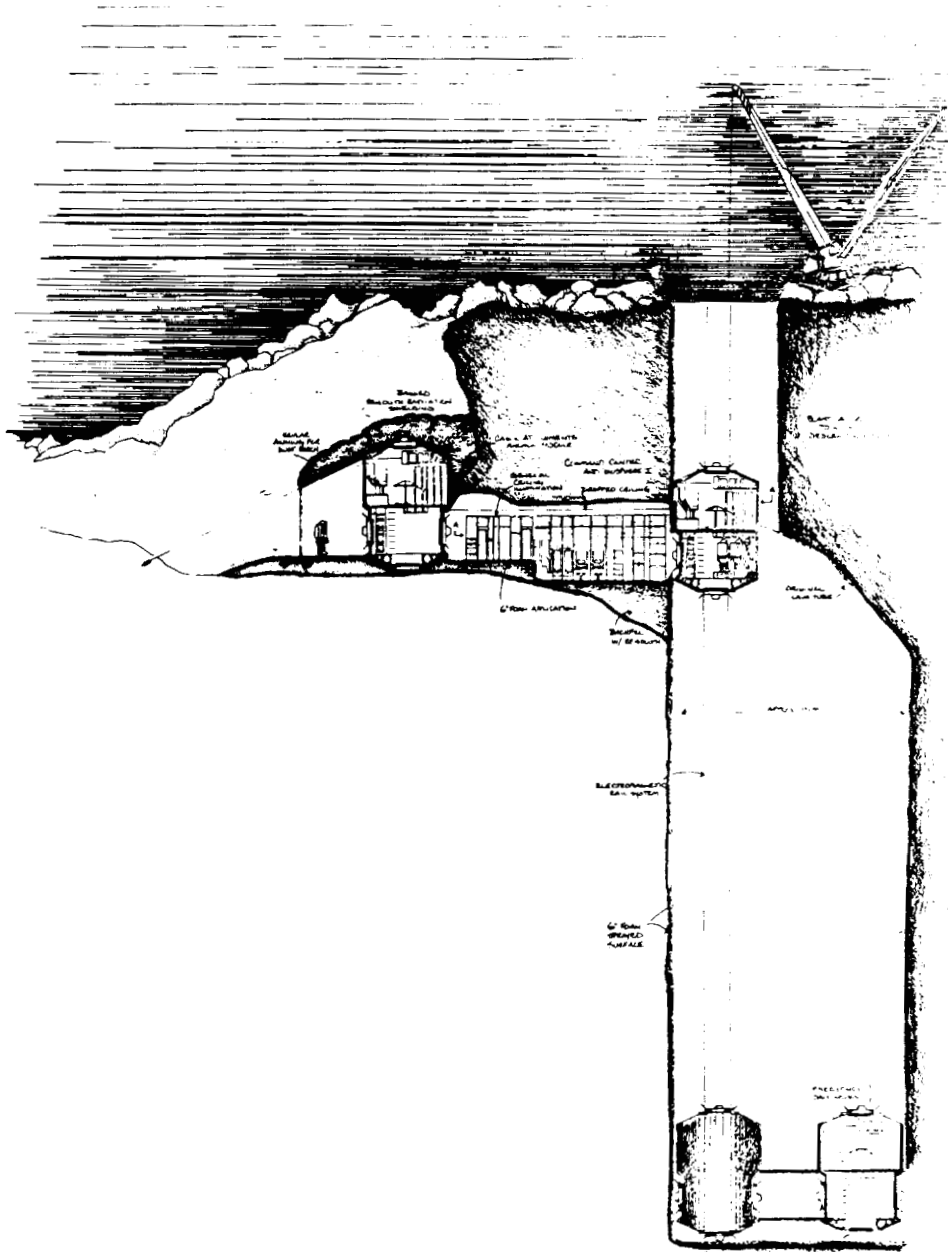


Fig. 3. Design alternative 2: Lava tube construction—entrance to the lava tube from a lunar crater, command center on the surface level, wall section, and electromagnetic elevator

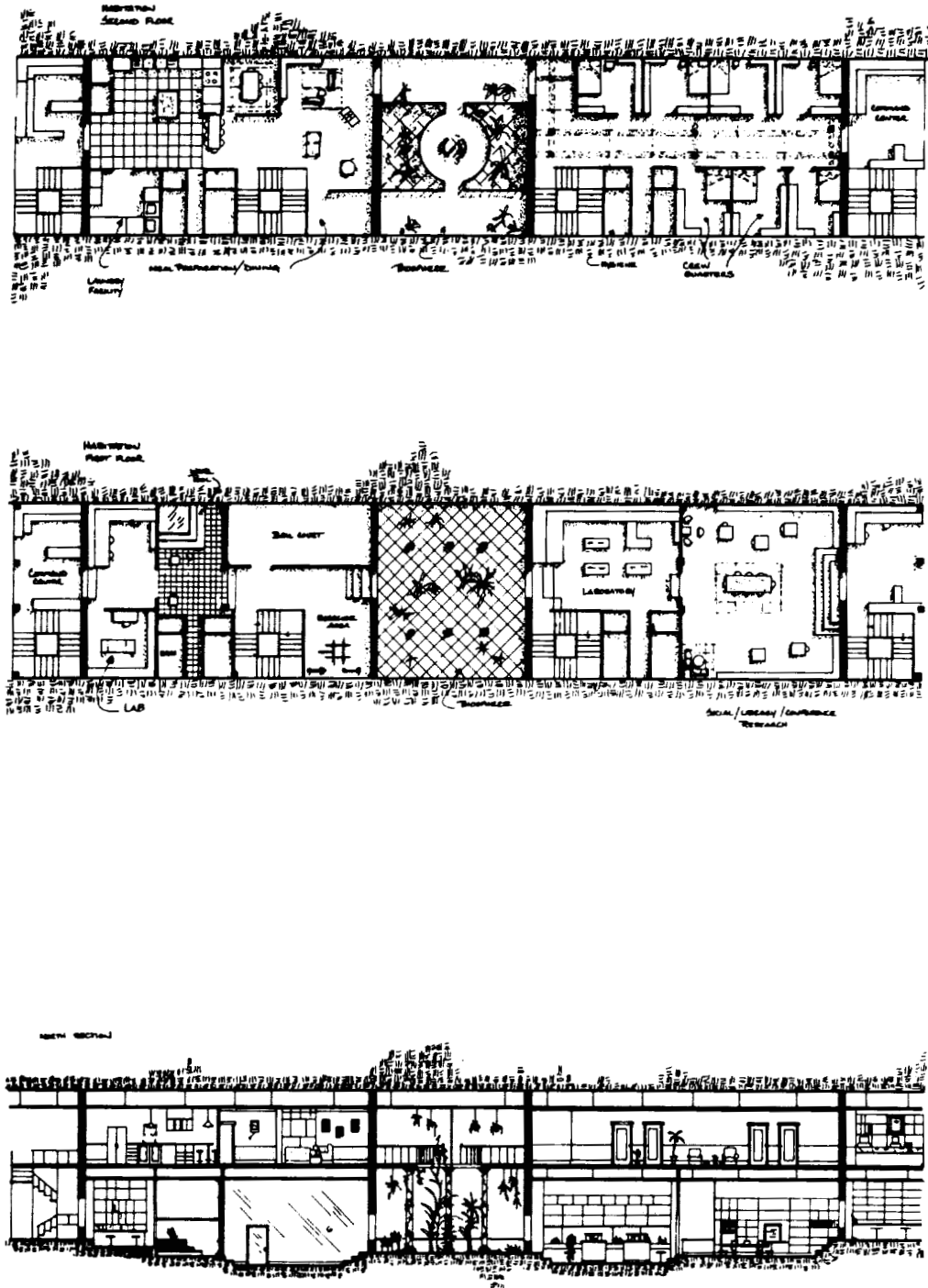


Fig. 4. Lower level floor plan and section of the lava tube design alternative. The two ends of this plan and section connect with the two lower ends of the elevator tubes

ORIGINAL PAGE IS
OF POOR QUALITY

Inflatable Structures

The third design alternative explored the use of inflatables as the primary means of developing a lunar habitat. This scheme also explored site layout and the qualities of "urban design" as well as phasing and deployment of inflatables (see Fig. 5 and 6).

FINAL INTEGRATIVE DESIGN SOLUTION

From the three design alternatives evolved an elaborate but efficient lunar outpost. The final design recommendation consists of standard space station modules, nodes, and inflatables sited near lunar lava tubes. The layout reflects an organizational idea or geometry that allows the base to be understood functionally as well as used efficiently.

Master Plan

The following is a list of master plan components for the proposed base:

- 1. **HLLV (Heavy Lift Launch Vehicle) Base Operations Module.** This module will encase base operations and support functions.
- 2. **Inflatable Habitation Dome #1.** This structure will house the crew support and related activities.

3. **Inflatable Mission Operations Dome #2.** This structure will house mission operations and support functions.

4. **Inflatable Biosphere Dome #3.** This dome will have multiple functions—a biosphere for natural vegetation, entry and gathering place, and storage area.

5. **Standard Crew Support Module #1.** This module will contain additional crew support and hygiene facilities.

6. **Standard Exercise/Health Maintenance Module #2.** This module will house all exercise and health maintenance equipment for the entire base.

7. **Standard Mission Operations Modules #3 and 4.** These modules will contain additional mission operations, research workstations, and support functions.

8. **Logistics Module.** This module supports supply and resupply functions for the crew and base.

9. **Three EVA (Extra Vehicular Activity) Modules.** These modules will house activities pertaining to safety, EVA, and observations.

10. **Three Cupolas.** These spaces will be used to provide a view to the lunar environment.

11. **Launch and Landing Facilities.** These will include remote landing areas with lander servicing equipment and crew/payload transfer systems.

12. **Base Garage Areas.** These will be large nonpressurized hangars with pressurized areas for repairs accessible to all zones until each has its own limited facility.

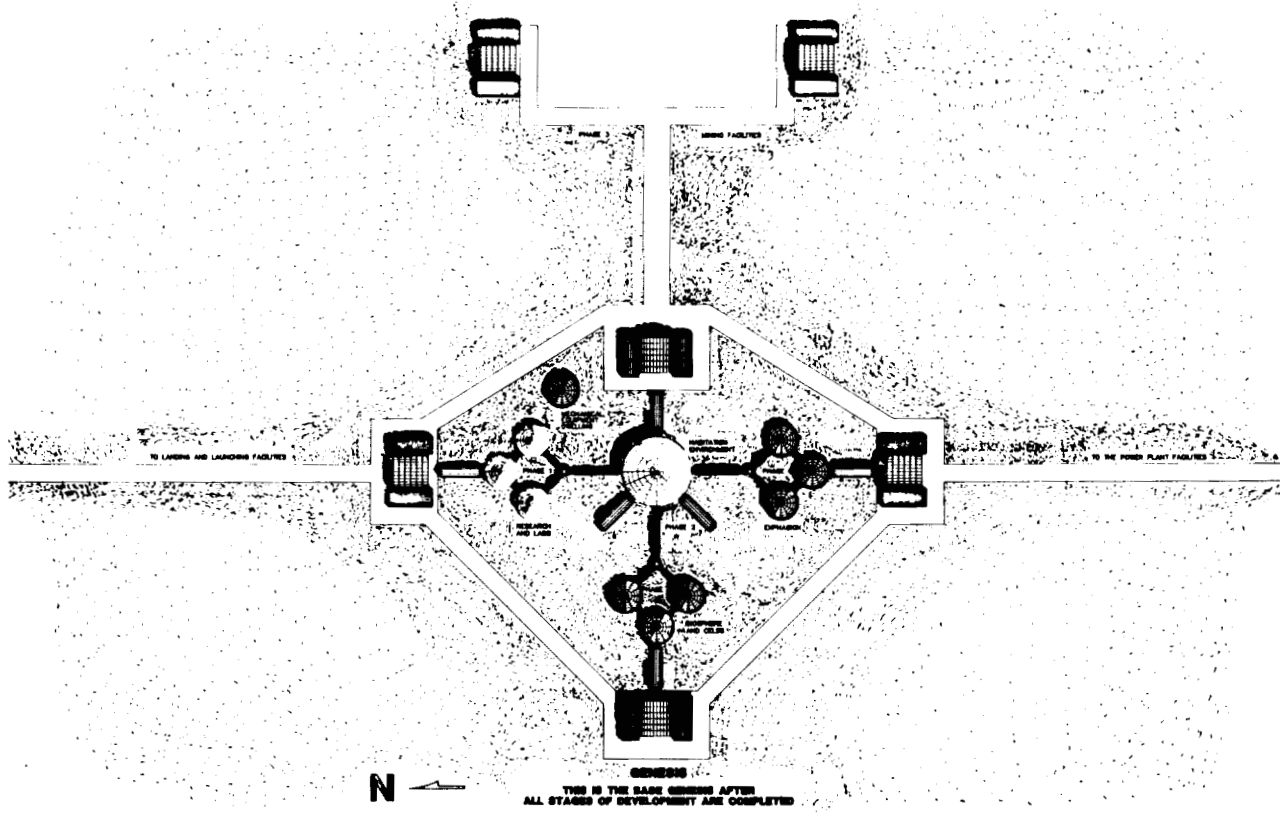


Fig. 5. Design alternative 3: Inflatables—site configuration of an inflatable lunar outpost (north is to the left)

**ORIGINAL PAGE IS
OF POOR QUALITY**

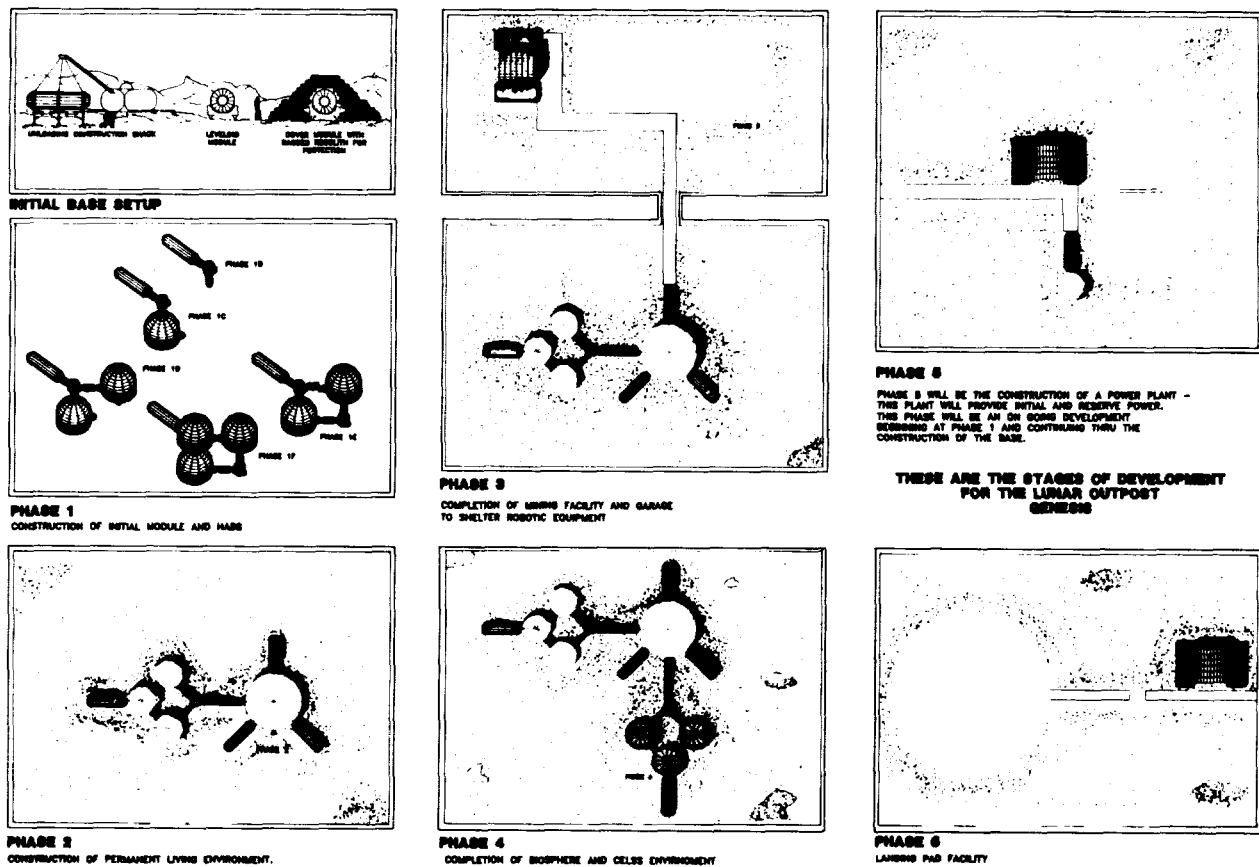


Fig. 6. Phased development of the inflatable site from initial base setup through Phase 1 IOC

13. Transportation Systems. These will provide surface transportation to travel to the more distant base elements as well as transferring payloads or crew.

14. Surface Mining and Production Analysis Operations. Mining and refinement of metals, isotopes (helium-3), lunar oxygen, and other materials.

15. Construction Technology Testbed and Telerobotic Research Laboratories. These will support high-technology construction methods and construction of robotic systems.

16. Power Plant. This will consist of a number of redundant systems including solar array fields, an SP-100 and 550 nuclear power facility, and fuel cells.

Site Plan and Base Layout

The lunar outpost consists of four major areas (see Fig. 7). The first is the centrally located habitat/research area. The second is the permanent power facility located to the north (left, in Fig. 7). The third is the mining and production facility located to the west. The fourth area is dedicated to the launch and landing facility positioned to the south.

The power plant is approximately 1 km to the north of the habitat. It consists of a small nuclear power generator (SP-100) that will be employed in the middle phases of the base development, and a more permanent nuclear facility (550) that

will be set into place at IOC. These facilities are either placed in a crater or surrounded by a lunar berm to provide protection from any leakage of radiation.

The mining and production plant is also located just over 1 km from the habitat to provide safety from dust or objects that may be ejected into the atmosphere. An area of $92\text{ m} \times 92\text{ m} \times 2\text{ m}$ has been projected for an annual mining expedition. In this area, the production of lunar oxygen and other chemicals will be produced to provide *Genesis* with the means of becoming self-sufficient.

There will be two types of launch and landing facilities. The first will be temporary sites to provide ease of construction. These sites will be 250-400 m away from the base location. The second type of facilities will be the permanent launch and landing pads. These sites will be located no less than 3 and preferably about 5 km from the base. These pads will be located in close proximity to those areas of the base most frequently served, i.e., logistics and storage areas. The orientation of the base on the lunar surface was determined by the link it has with Earth. The lunar landers will descend east-west from lunar orbit and must have a clear path to the pads. By having the major axis north-south (perpendicular to the lander orbit) and placing the pads to the south, no base component will be endangered if a lander overshoots its objective.

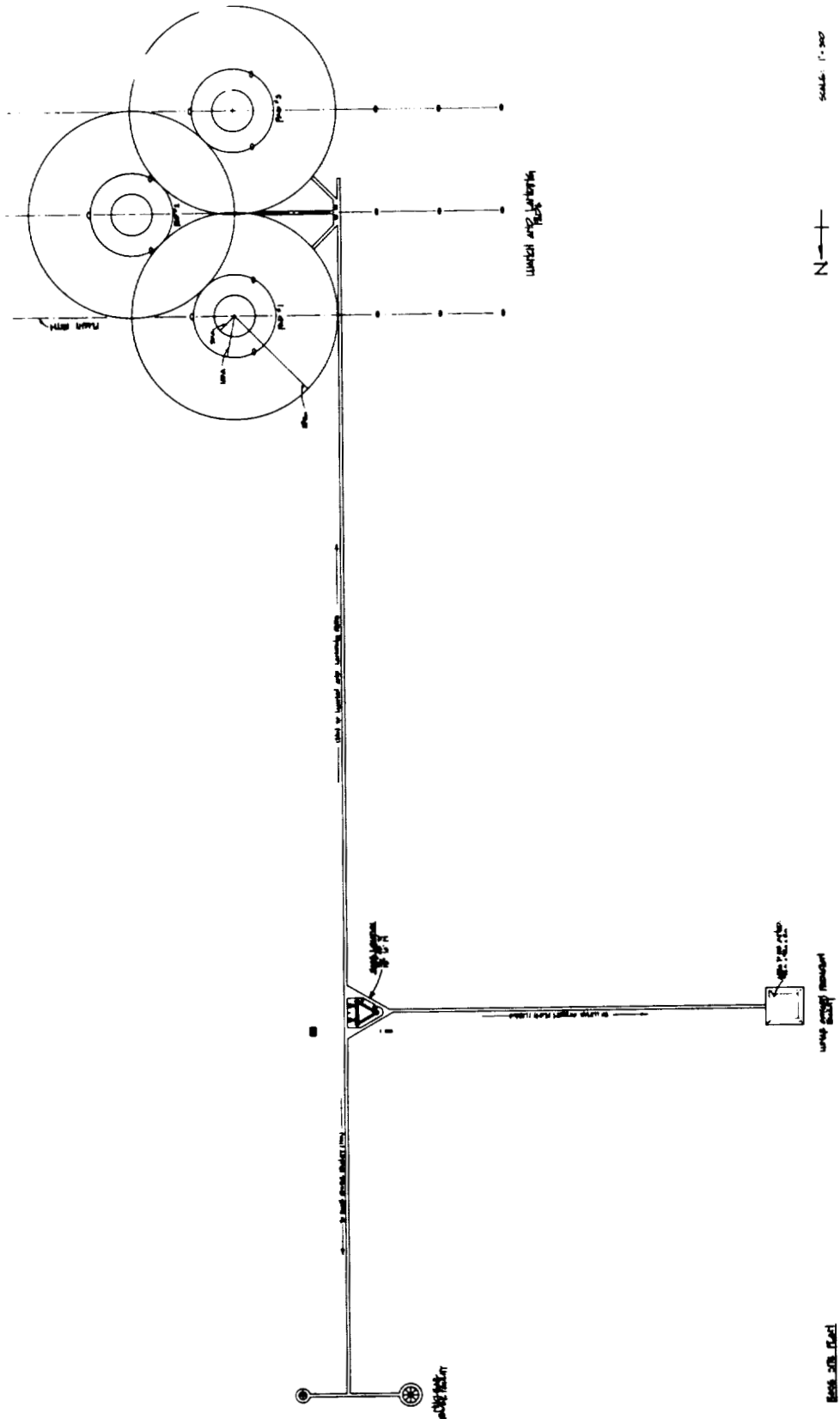


Fig. 7. Genesis Site Plan

ORIGINAL PAGE IS
OF POOR QUALITY

A roadway system will be developed for each phase of the base's development⁽²⁾. Organized roadways between all segments of the base will allow efficient transportation of materials and crew while also giving the base some structure.

Interior Configuration

The interior configuration of the *Genesis* provides space for base operations (command center, communications center), mission operations (workstations for the five research functions), and the crew habitat (crew quarters, recreation, etc.). Key design issues included habitability, anthropometrics, health and safety, psychological and social needs, crew support systems, construction technology, appropriate lighting, and possibilities for expansion. These were organized under four main categories, with four criteria for each (Table 1).

Table 1. Key Design Issues and Evaluation Criteria

Design Issue Categories	Evaluation Criteria
Habitability	Reliability
Safety	Resilience
Constructability	Efficiency
Expandability	Transportability

In Phase 1 (see Fig. 8), the HLLV Base Operations Module is put in place as a command center. The lower level is used for crew support for four people and would consist of a galley,

dining area, group recreation area, medical and exercise facilities, and personal quarters for two crewmembers. The other crew quarters remain in the assembly vehicle.

Phase 2 (Fig. 9) provides for the expansion of base and mission operations. The upper level of the HLLV Base Operations Module remains as originally constructed, but the crew quarters would be shifted into the Inflatable Habitation Dome #1 and associated Crew Support Module #1. The lower level of the HLLV Mission Operations Module would be refitted with operations workstations necessary for base expansion. Inflatable Mission Operations Dome #2 would also be built and fitted during Phase 2 so that about 50% of total research functions could be operational by the end of Phase 2.

Phase 3 (Fig. 10) has added full-scale exercise and health maintenance facilities in Standard Module #2, and expands mission research operations with the addition of Standard Mission Operations Modules #3 and 4. Each is located in proximity to the domes that are the center of research and habitation functions. A temporary flexible connector would connect the entire base into a complete base by the end of Phase 3.

The full IOC (Fig. 11) is realized in Phase 4 by the addition of the multifunctioning Inflatable Biosphere Dome #3 that functions as the major and symbolic entry to *Genesis*, as a place of psychological retreat, and (on the lower level) for storage. The permanent location for the logistics module is now moved near the entry/storage area.

The outpost is covered with 0.5 m of lunar regolith for radiation and thermal control.

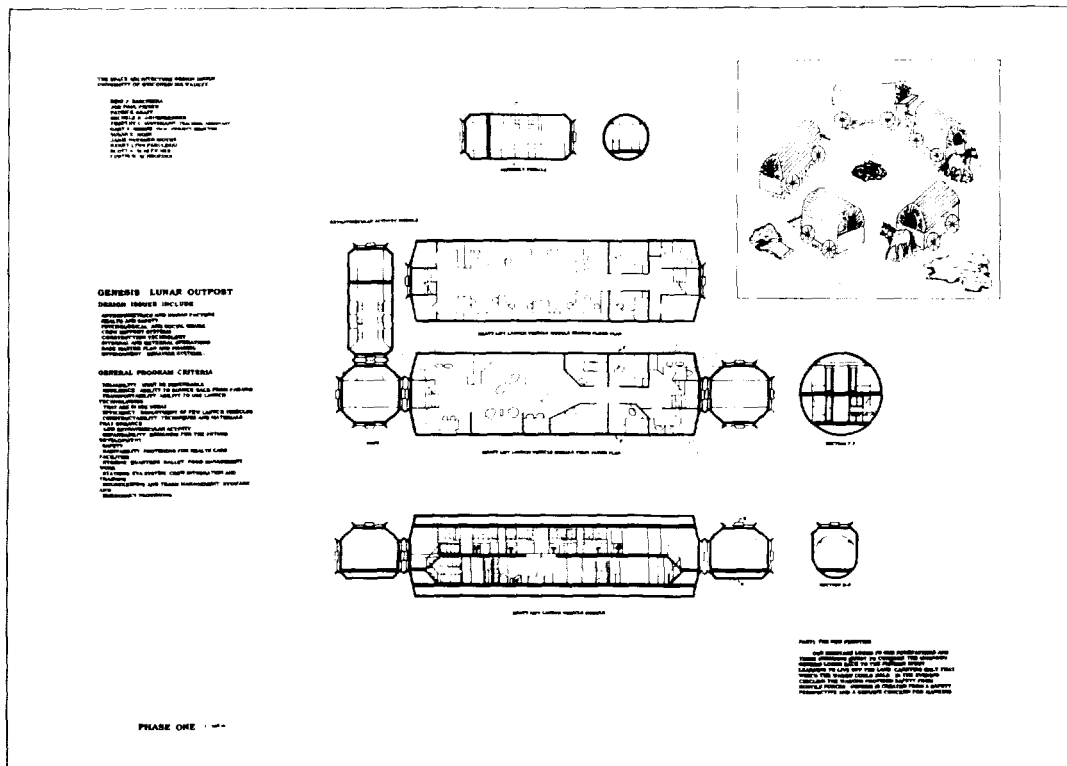


Fig. 8. Phasing of Project Genesis: Phase 1 Emplacement

ORIGINAL PAGE IS OF POOR QUALITY

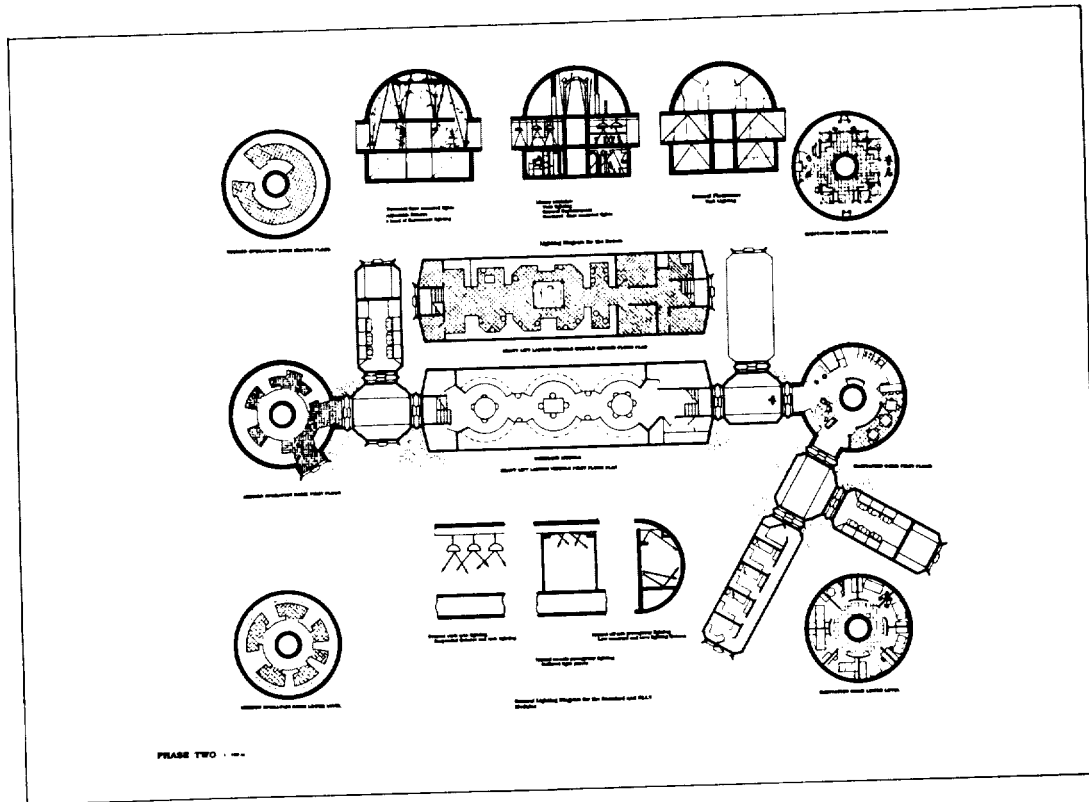


Fig. 9. Phase 2 Integration

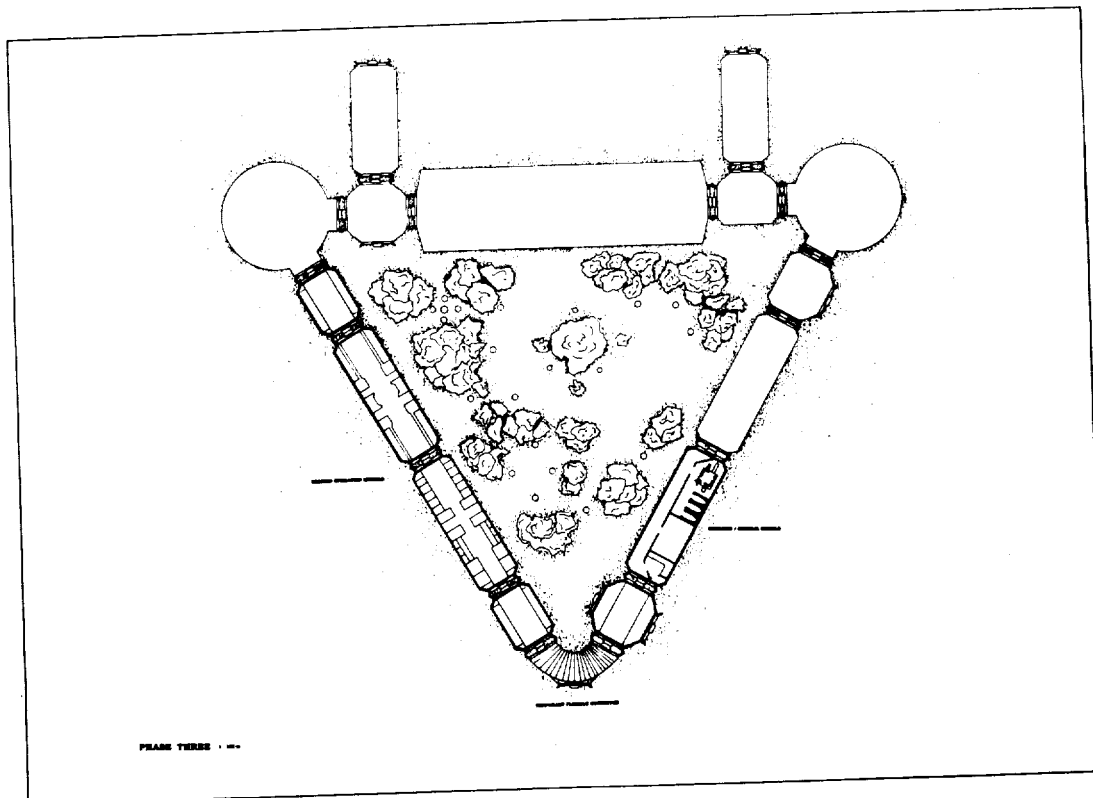


Fig. 10. Phase 3 Completion

ORIGINAL PAGE IS
OF POOR QUALITY

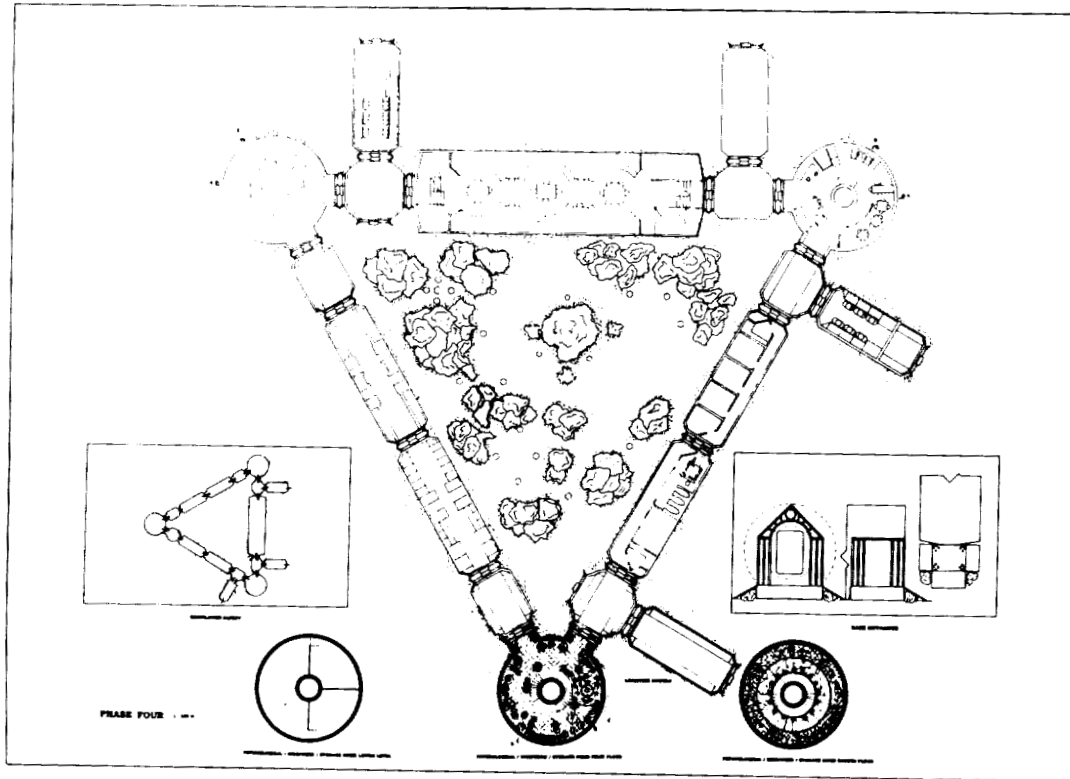


Fig. 11. Complete Initial Operating Configuration (IOC)

Construction Technology

A series of technological issues were addressed by the project team in the design. Chief among these were materials, structural systems, means of deployment and construction, attachment rings, and regolith shielding and containment⁽²⁾.

The two types of modules to be employed are the HLLV module (27.4 m x 7.6 m diameter) and a standard SSF-type module (13.4 m x 2.4 m diameter). The materials of both modules consist of two layers of aluminum enclosing a layer of insulation making a wall thickness of 11 cm. The major difference between the SSF modules and the module designed here is the creation of an airlock opening in the end of the module that accommodates full-sized (1.3 m x 2.1 m) uninhibited walk-through. The modules will be outfitted on Earth, and will employ a rack system to allow components to be easily interchanged or replaced.

The domes will be a half-sphere on top of a cylinder. They will be foam-filled, rib-rigidized, air-supported, single membrane inflatables approximately 10 m in diameter and 10 m at the center (see Fig. 12). The material is proposed to be a laminate membrane composed of Beta cloth (a durability material) for the outermost layer; Kevlar, the main strength material, woven with Spectra to aid in flexibility; Mylar, to provide an air-tight barrier; and Nomex, the innermost material, to protect against fire hazards (Fig. 13).

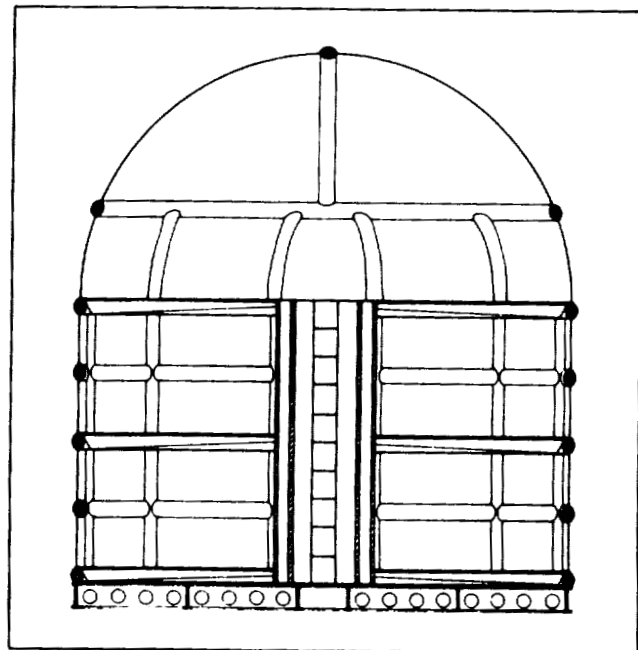


Fig. 12. Section of a foam-filled, rib-rigidized, air-supported, laminate-membrane inflatable

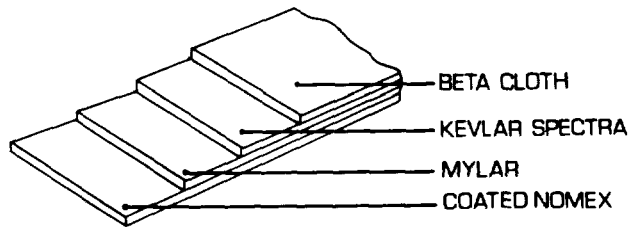


Fig. 13. Inflatable Material Laminate

A rigid platform will spread the weight of the structure over the subregolith and stabilize and level the structures. The foundation will be composed of auger-type bits telerobotically threaded into the regolith. The framework for the base of the inflatable is a lightweight space frame truss (see Fig. 14). The truss radiates outward from a central ring and can fold together for launch and deployment. The truss will be made of aluminum plates and welded channels. The flat surface that covers the truss is made of pie-shaped aluminum panels.

The inflatable membrane will be continuous except for two airlock openings. These openings will be sealed so the entire structure becomes a pressure vessel in which air will be placed at 10855 mbar. The inside of the membrane will be lined with ribs formed by chemically welding the same material to the membrane so a grid is formed. The inside of the ribs will be lined with the two components of the foam, and separated by a form of resin-gel. When the inflatable is ready for deployment, the ribs will be opened to a vacuum, the gel will evacuate, and the components will interact to form a rigid foam. Expanding these ribs will lift the membrane into its approximate form.

The proposed method for attaching a hard module to an inflatable is by using a sandwiched metal ring that will be attached to the inflatable on Earth. The inflatable will be

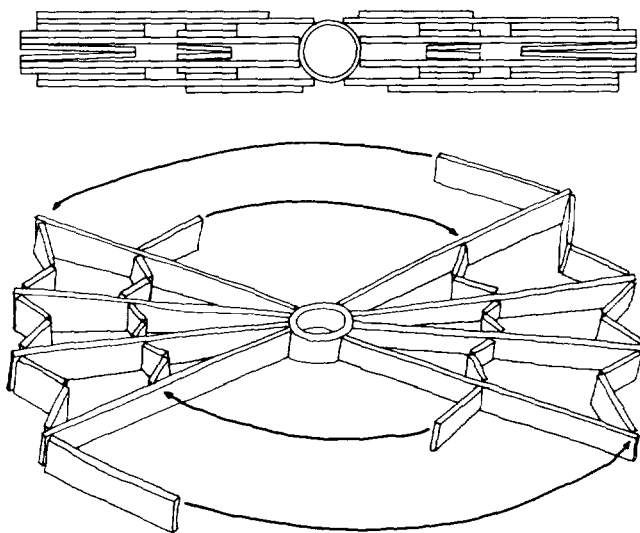


Fig. 14. Lightweight Deployable Space Frame Truss

constructed with the necessary opening left in the membrane. The membrane will have a bead formed at the point where the rib fits into the ring. This bead will be sandwiched between the two metal pieces when they are joined to form an airtight seal.

Regolith shielding will be needed for protection against radiation, micrometeoroid impacts, and thermal regulation. The thickness required has been calculated to be approximately 50 cm. The regolith shielding will be in the form of Beta cloth bags filled with regolith and stacked upon the structures. A specially designed machine will gather regolith, bag it, and transfer these bags to a conveyor that will lift the bags into position (see Fig. 15), thus completing the construction of Project *Genesis* Lunar Outpost.

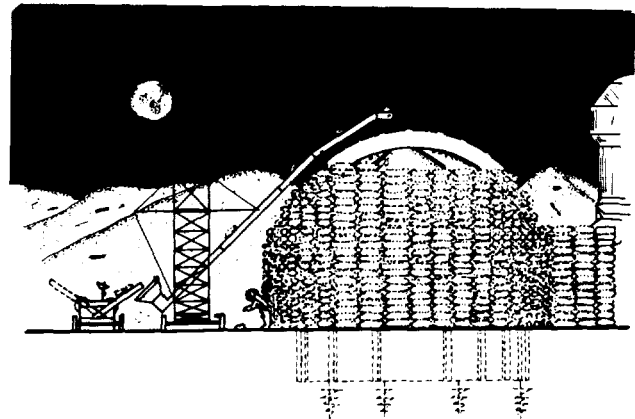


Fig. 15. Concept drawing for lunar regolith bagging and assembly procedure

FUTURE CONSIDERATIONS

There is considerable work still to be done to better understand and design the first lunar habitat. Among the most central issues that need consideration are the following:

1. Comparative, in-depth study of the lunar (versus martian) environment with special attention to atmosphere, radiation levels, solar flares, *in-situ* materials, topography, power sources, temperature extremes, etc.
2. Basic research on long-term effects of reduced gravity and design studies on different approaches to 1/6 gravity.
3. Mass calculations, studies of ways to reduce mass, and rough order-of-magnitude cost estimates.
4. Analysis of total number of flights based on minimum mass calculations.
5. Space allocation study including human factors analysis of the minimum space required for different habitation and research functions.
6. Detailed trade studies of different areas of the lunar habitat, e.g., the health maintenance facility, exercise facility, crew quarters, air locks, and workstation rack designs. Design development studies of these different areas including through study perspectives and/or models.

7. Replacement studies of how to replace/renovate/expand parts of the habitat.
8. Comparative analysis and extraction of design-relevant findings and implications from previous space experience, analogous situations, and simulations, e.g., *Mir* and *Skeylab*, Antarctica and Navy submarines, and *Tektite*, respectively.
9. In-depth mechanical study including more careful radiator study to remove body and machinery heat from under the regolith.
10. Studies of different ways of getting natural light into a regolith-covered lunar habitat without admitting gamma ray particles, including but not limited to partially covered cupolas, flexible light pipes, periscopes, etc.
11. Precise regolith depth studies to protect lunar habitats from radiation and micrometeoroids.
12. Habitability study of the short- and long-term effects of underground environments and windowless environments.
13. Design studies of regolith containment systems, second-generation regolith bagging machines, and processes (including sequences) of habitat construction.
14. Structural calculations for all structural members including but not limited to the structure of lunar inflatable domes.
15. Study of various construction techniques for lunar application including, but not limited to, prefabricated modules, rigid structures, inflatables, and *in-situ* resource utilization.
16. Study of materials for lunar habitat application, especially elastomers and thin films, e.g., Kevlars, Mylars, Spectra, Nomex, aluminums, titaniums, rigidizing foams, and *in-situ* resource utilization of lunar regolith.

These studies will be conducted in subsequent years under USRA and (hopefully) other funding. They will be of two basic types: research and analysis studies, and design and development studies. The results will be reported in future reports and papers.

ACKNOWLEDGMENTS

Designs and illustrations by the Space Architecture Design Group: Dino J. Baschiera, Joe Paul Fieber, Patrick Groff, Michele Gruenberger, Susan E. Moss, Janis Huebner Moths, Kerry Lynn Paruleski, Scott A. Schleicher, and Curtis W. Schroeder; Teaching Assistant Timothy Hansmann. Paper compiled and written by Gary T. Moore, Faculty Advisor, with Dino Baschiera, Joe Fieber, and Janis Moths. This project was supported by an Advanced Design Program grant from NASA/Universities Space Research Association. This paper is a summary of a larger document, *Genesis Lunar Outpost: Criteria and Design* (Hansmann and Moore, 1990) available from the authors. Our thanks to James Burke, NASA/Jet Propulsion Laboratory, and Stephen Paddack, NASA/Goddard Space Flight Center for critical comments.

REFERENCES

1. Baschiera, D. J. et al. (1989). *Genesis Lunar Outpost: Program/Requirements Document for an Early Stage Lunar Outpost*. Milwaukee: University of Wisconsin-Milwaukee, Center for Architecture and Urban Planning Research.
2. Hansmann, T. and Moore, G. T. (Eds.) (1990). *Genesis Lunar Outpost: Criteria and Design*. Milwaukee: University of Wisconsin-Milwaukee, Center for Architecture and Urban Planning Research.

P.10

INTEGRATED SUPPORT STRUCTURE FOR GASCAN II

WORCESTER POLYTECHNIC INSTITUTE N91 - 18159

The focus of the WPI Advanced Space Design Program was the preliminary design of the Integrated Support Structure for GASCAN II, a Get Away Special canister donated to WPI by the MITRE Corporation. Two teams of three students each worked on the support structure: the structural design team and the thermal design team. The structure will carry three experiments also undergoing preliminary design this year: the μ -g Ignition Experiment, the Rotational Flow in Low Gravity Experiment, and the Ionospheric Properties and Propagation Experiment. The structural design team was responsible for the layout of the GASCAN and the preliminary design of the structure itself. They produced the physical interface specifications defining the baseline weights and volumes for the equipment and produced layout drawings of the system. The team performed static and modal finite-element analysis of the structure using ANSYS. The thermal design team was responsible for the power and timing requirements of the payload and for identification and preliminary analysis of potential thermal problems. The team produced the power, timing and energy interface specifications and assisted in the development of the specification of the battery pack. The thermal parameters for each experiment were cataloged and the experiments were subjected to "worst case" heat transfer scenarios. These analyses will be integrated by next year's thermal design team to model the overall performance of the system.

INTRODUCTION

WPI's Get Away Special Canister (GASCAN) Program is now in its eighth year. This program is the result of a cooperative effort by WPI and the MITRE Corporation of Bedford, Mass. MITRE purchased and donated two GASCANs to WPI. The first of these canisters is now scheduled for launch in August of 1990. The second canister, GASCAN II is now undergoing preliminary design. Since 1986, the design of GASCAN II has also been part of the NASA/USRA Advanced Space Design Program.

The task of designing this payload has been divided into the two groups: experiment design and support structure design. The experiments are described in the Payload Description Section. The focus of the AY1989-90 program is the thermal and structural design of the integrated support structure of the GASCAN.

1. Ionospheric Properties and Propagation Experiment
2. Microgravity Ignition Experiment
3. Rotational Fluid Flow in Microgravity Experiment
4. Environmental Data Acquisition System

Ionospheric Properties and Propagation Experiment (IPPE)

The purpose of the IPPE is to correlate the occurrence of radio wave ducting with electron density. This will be accomplished by measuring the electron density in the ionosphere and the signal strength of a 15 MHz signal (radio station WWV in Colorado and Hawaii). Electron density will be determined using an Electrostatic Analyzer (ESA). A radio receiver tuned to 15 MHz will provide the signal strength data.

Radio wave ducting occurs when a high frequency signal is trapped between two ionospheric layers. Theory predicts that ionospheric layers with high electron density will reflect radio waves. If a radio wave is trapped in a layer with a low electron density between two layers with a higher electron density, then that wave will be "ducted." A ducted radio signal will experience less attenuation than a non-ducted signal. The data from the IPPE radio receiver will be analyzed in order to find changes in signal strength attenuation. These changes will indicate ducting of the radio signal.

The basic IPPE system is shown in Fig. 1. The system has four main components: radio receiver, radio antenna, Electrostatic Analyzer (ESA), and a control assembly. Both the ESA probe and the radio antenna will be mounted external to the canister lid (Fig. 2).

PAYLOAD DESCRIPTION

Size and Weight

The maximum volume of our payload will be 5.0 ft³. The maximum weight will be 200 lb.

Experiment Descriptions

We are developing four experiment packages. Each experiment will operate in a stand-alone mode as completely as possible. A brief description of each experiment is presented below. The experiments are as follows:

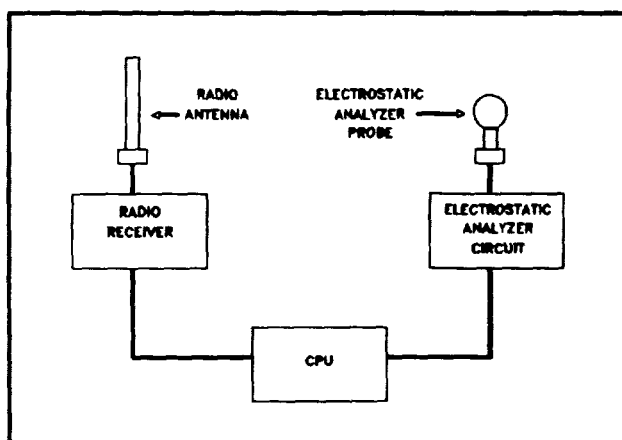


Fig. 1. Schematic of the IPPE

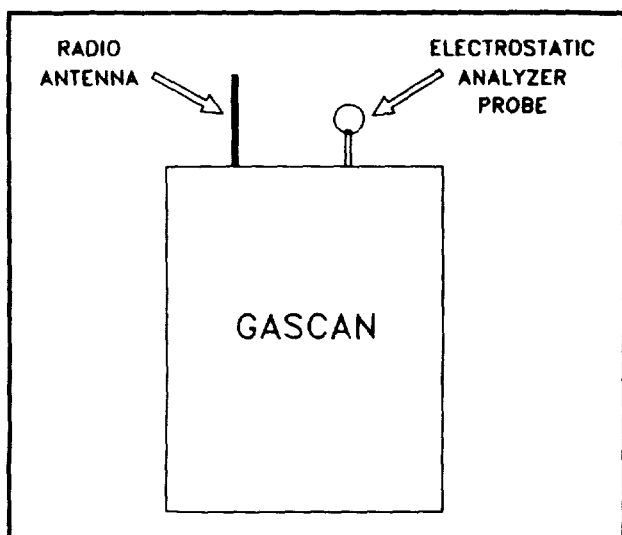


Fig. 2. External View of the Canister

The ESA probe consists of two concentric spheres; the outer sphere is constructed of gold-plated steel mesh, and the inner sphere is a gold-plated hollow aluminum ball. For the experiment to function properly, a voltage potential is maintained between the two spheres. When electrons are drawn onto the inner sphere, a negative current in the range of 10^{-10} to 10^{-5} amperes will be produced. The radio antenna is composed of spring steel. Both the ESA probe and the radio antenna will be mounted to the GASCAN endcap using surface mounts and high impedance vacuum feedthroughs.

The Electrostatic Analyzer circuit inputs the signal from the ESA probe and uses a log electrometer to convert the currents into a 0-5 V range. The control assembly then takes this information, processes the signal as required by the experiment, and stores the necessary information onto an Erasable Programmable Read Only Memory (EPROM).

The unit will be turned on by a shuttle crewmember following the completion of the Rotational Fluid Flow Experiment. At this point the experiment will begin sampling WWV signal strength and ion density at regular intervals.

In order for this experiment to be able to take proper readings within the ionosphere, it must be flown on a high-inclination shuttle flight.

Microgravity Ignition Experiment

The initiation of combustion on Earth is largely controlled by the presence of gravity since natural convection and buoyancy are functions of gravity. By neutralizing the effects of gravity, other mechanisms should become dominant factors in the ignition process. The purpose of this experiment is to compare the ignition characteristics of a material in a microgravity experiment with ignition characteristics established from laboratory experimentation in a 1-g environment.

The experiment has two major subsystems: the combustion chambers and the control system, as shown in Fig. 3. There will be four airtight combustion canisters capable of withstanding five atmospheres of internal pressure. Each of the four containers will have an identical paper target (alpha cellulose) that will be ignited using a high-intensity lamp. Data will be collected from the chambers using temperature, pressure, and heat flux sensors. In addition, an ion sensor will be located above the target to serve as a flame detector.

The control system will contain a microprocessor and an EPROM card for data storage. This system will be responsible for monitoring the experiments and taking appropriate action to shut down a canister if a hazardous condition arises.

This experiment should be turned on by a shuttle crewmember during a period of relative inactivity. Upon activation, this experiment will enter a "sleep mode" for a predetermined time period. At the end of this "sleep phase," the microprocessor will begin the ignition experiments.

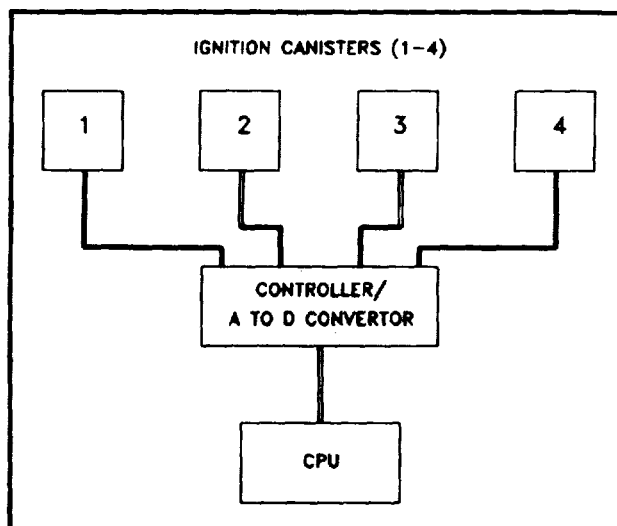


Fig. 3. Schematic of the Microgravity Ignition Experiment

Rotational Fluid Flow in Microgravity Experiment

When a fluid rotates with the axis of rotation normal to a gravitational field, the rotation is accompanied by a decrease in the surface elevation of the fluid at the center of rotation. This phenomenon is referred to as a vortex. Vortex formation is governed by the fluid's angular velocity, viscosity and surface tension. The objective of this experiment is to examine the behavior of a free surface vortex in a microgravity environment.

This experiment has four main components: the rotating platform, the fluid system, the data acquisition assembly, and the control assembly (Figs. 4 and 5). A rotating platform will allow the experiment to utilize its microgravity environment to simulate other gravities, within the range of 10^{-6} to $2.0 g$'s.

The fluid system will be composed of a tank, connecting tubes, and a pump. The working fluid will either be a silicon-based oil or a water/glycerol mixture that will not freeze in the cold of the GASCAN. The fluid will be injected tangentially

into the upper end of the cylinder and drained from the bottom of the tank. This process will induce an angular velocity into the fluid and create the vortex.

The data acquisition assembly will collect data using a camera, an ultrasonic device, and temperature sensors. The ultrasonic sensors will be used for measuring the velocity, and hence circulation, of the fluid within the tank. The camera will be used to measure the actual size of the vortex and will function as a second measure of vortex strength. Not shown in the figures is the gas entrainment detector, which will be located along the piping between the tank outlet and the pump. This device examines the fluid for gas bubbles. If gas is detected within the tubing, the control system stops data collection for that trial.

The control system will use a set of accelerometers to monitor and control the platform's angular velocity. The accelerometers will be aligned to measure the platform's centripetal acceleration.

This experiment will be turned on by a shuttle crewmember by the same switch as the microgravity ignition experiment. Upon activation, this experiment will enter a "sleep mode" until the ignition experiment is finished.

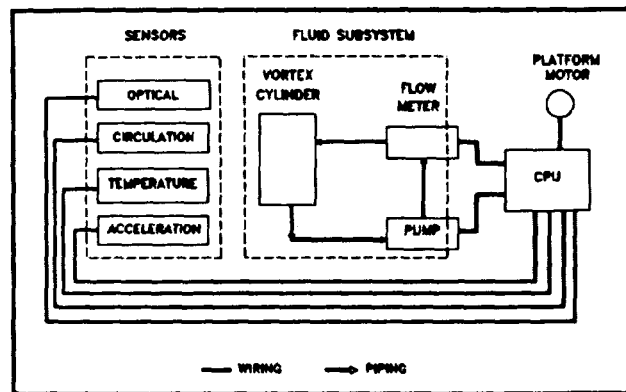


Fig. 4. Schematic of the Rotational Fluid Flow Experiment

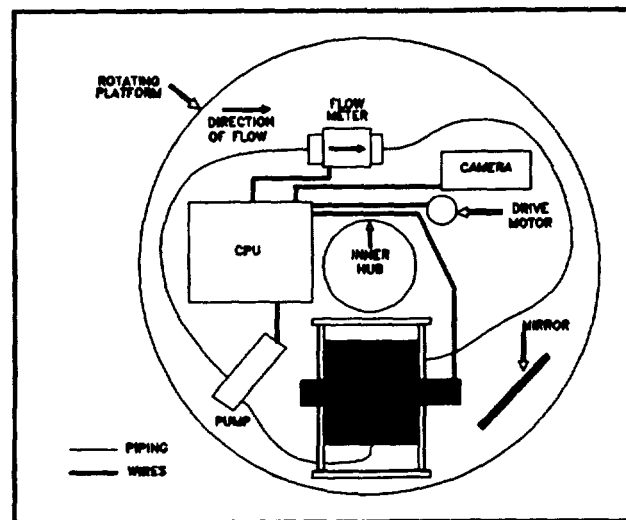


Fig. 5. Rotational Fluid Flow Experiment Layout

Environmental Data Acquisition System

The Environmental Data Acquisition System (EDAS) collects data describing the environment internal to the canister from just after launch until all of the experiments are turned off. The system will be activated by the baroswitch as the shuttle passes through an altitude of 70,000 ft. The system will then begin to sample data for the entire time that experiments are running in the canister. These data will be available for postflight analysis of the experimental data.

STRUCTURAL DESIGN

The objective of the payload structural design group is to integrate all the experiments into a complete package inside the GASCAN II canister while conforming to all NASA structural design requirements. The project is in the preliminary design phase. Emphasis is on adequate structural support of the payload to ensure reliability and safety during flight operation.

General Requirements

Container construction. The standard GAS canister is made of aluminum. There is thermal insulation on the exterior. The top may or may not be insulated depending on the particular shuttle mission and needs of the experimenter. The standard circular endplates are 5/8-in-thick aluminum. The bottom 3 in of the container are reserved for NASA interface equipment such as command decoders and pressure regulating systems. This volume is not included in the space available to the experimenter.

Container size. The container has a volume of 5 ft^3 . The user size is 28.25 in in height and 19.75 in in diameter. The maximum user weight is 200 lb.

Experiment mounting plate. The experiment mounting plate serves three purposes: it seals the upper end of the standard GAS container, provides a mounting surface for the experimental equipment, and acts as a thermal absorption and radiation surface. The inner mounting plate is fitted with 45 holes to accept 10-32 UNF stainless steel screws to a depth of 0.31 in. There are two purge ports for venting gases from the battery pack.

Venting. Batteries, which can produce a combustible mixture of gases, must be housed in a sealed, corrosion proof, vented battery box. Plumbing for the venting of the battery box is to be supplied by the experimenter. The battery box must be vented through the mounting plate and through two 15-psi differential pressure relief valves provided by NASA. All plumbing should be stainless steel.

Lateral load support. Because the experiment structure will be cantilevered from the experiment mounting plate, radial support of the free end of the experiment structure must be provided by at least three equally spaced bumpers between the experiment structure and the standard GAS container.

Load Specifications

Launch:	normal:	3 g RMS, 20-2000 Hz
	adverse:	12 g RMS, 20-1000 Hz
Orbit:	normal:	negligible vibration, 0.1 g with thrusters
Landing:	normal:	negligible vibration, 5 g static along can axis

Payload Integration

Each experiment has characteristics that affect the design. This section will address these design issues and describe the payload layout that will give a structural integrity that meets NASA specifications.

IPPE Experiment. This experiment has some unique requirements that must be adapted into the support structure. Two components, an ion collector and an antenna, are to be protruding out of the experiment mounting plate. These components will be located at a yet to be determined position on the mounting plate and could be anywhere on the diameter. Thus, these components must have access to the entire diameter and must be closely coupled to the IPPE controller box. With these considerations, it is necessary to place the IPPE controller box at the top of the GASCAN II support structure.

Rotational flow vortex experiment. The experiment is completely enclosed within a rotating section of the GASCAN assembly. The experimenters have requested the maximum diameter available in the GASCAN (19.75 in). This will necessitate the placement of support bumpers both above and below the experiment.

Battery and battery box. The battery weight is currently estimated at 79 lb. The battery box must be removable from the structure for installation, checkout, and repair. Vent lines and electrical leads must be accommodated.

Microgravity ignition. The four ignition chambers must be removable and their installation must allow connection of electrical and data lines to the experiment controller.

Initial Design and Design Changes

This design team inherited a design by the previous payload integration structural team which was a year out of date. There were many details that needed to be changed as quickly as possible to allow the other Advanced Space Design project teams to progress with their parts of the design.

The first team had incorrectly allocated the space for the experiment mounting plate within the user interface space. The plate is 5/8-in thick and, therefore, detracted from the amount of space available for the experiments. Also, the previous team had not fully specified how the flange/centerpost assembly would be attached to the mounting plate.

In order to redesign the top of the support structure, the major concern was to do so without altering the space already designated for the IPPE and microgravity combustion experiments. Since it was established that the experiment mounting plate should not have been included in the design, this gave the height of the usable space an additional 5/8 in. Clearance for both the IPPE and microgravity combustion was already sufficient and could only benefit from the additional height. With the exterior components of the IPPE, it was decided that the flanges could be altered such that the IPPE team could have access to the entire diameter to allow them to run their electrical leads to the ion collector and antenna. As this idea developed, it was also discovered that the previous group had not finished the design of the venting mechanism for the battery. From the outset, it was assumed that the venting would be done through the centerpost; however, the routing and connection to the mounting plate had not been established.

Further review of the NASA specifications showed that the battery vent had to be lead to a location within a plumbing circle section of the mounting plate. The mounting plate did not have to be oriented at any particular angle around the diameter; therefore, the team specified that it be oriented above one of the three compartments of the top section of the payload. The next concern was route of the venting line from the centerpost to the plumbing circle.

Taking both the venting and mounting to the mounting plate into account, the top of the support structure was then redesigned. The flanges and centerpost were reduced by 3 in. This 3-in clearance would allow vent lines to exit the centerpost and be directed to the venting apparatus inside the plumbing circle. It would also allow IPPE wiring access anywhere on the plate with the exception of the plumbing circle. The next design change was the mounting of the support structure. Since GASCAN II utilized the same three-flange design as GASCAN I, it was decided to use the same type of mounting brackets.

The next design consideration was the supports around the rotational flow experiment. The earlier design used braces to support the shelves above and below the experiment. The experiment group requested access to the entire diameter of the canister. Therefore, it was decided that the supports of the old design could be removed and replaced by bumpers above or below the rotational area which would give the same support that the previous design would give.

As energy and power requirements for the experiment were developed, it was estimated that 99 lb of batteries and battery box would be required. This weight was much greater than the earlier estimate of 42.6 lb. This discovery caused an immediate review of many of the design aspects. The original design located the battery box as far as possible from the mounting plate. This resulted in a substantial amount of weight supported solely by the centerpost. With this weight so far from the fixed end, the natural frequency of the entire structure would be low, possibly below the minimum requirement of 51 Hz. To help alleviate this problem, the battery box was switched with the rotational flow experiment. This would move the bulk of the weight up the cantilevered structure, increasing the frequency and giving a firmer mounting orientation. This orientation also simplified the installation of the rotational flow device, since the platform will be supported by bearings above and below the system.

The battery box can be slotted to slip over the centerpost and be bolted around the entire diameter of the centerplate. To give the battery box some support at the centerpost, a support ring with a set screw will be welded into place. This ring will also serve as a rigid support for the rotational flow bearing mounts.

Bumpers to stabilize the support structure were the next concern. It was decided that the bumpers could be positioned above the battery box at the ends of the flanges and an additional set could be installed beneath the rotational flow platform and above the bottom plate.

The final layout is shown in Fig. 6.

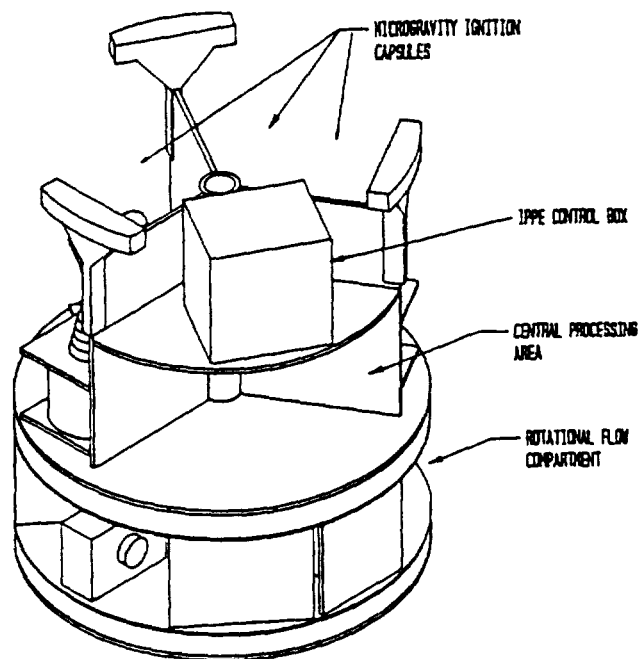


Fig. 6. GASCAN II Layout

ANSYS Introduction

To insure structural integrity of GASCAN II, finite-element analysis was performed using ANSYS. The analysis begins with the orientation of the can with respect to the space shuttle coordinate system. It is along these axes that the loadings are defined.

The most important factor for design purposes is the loadings. These loadings are split into three categories, limit, yield, and ultimate loads. The limit loads are the worst possible loadings that actually may occur. The yield loads are used to insure that the design, within a specified margin of safety, will not undergo plastic deformations. The ultimate loadings are used to insure that the design will be safe when comparing actual loads with the ultimate allowable loads for the materials of the can.

For GASCAN II to become space-qualified, certain safety requirements must be met. The factor of safety is the allowable stress divided by the applied stress. NASA requires that the GASCAN II to meet a Yield F.S. = 1.5 and an Ultimate F.S. = 2.0.

Results and Conclusions

Several structural questions, which would have been difficult or impossible with hand calculations, were addressed using ANSYS. The final models were made using the beam element, the plate element, and the mass element. These elements modeled the experiments and other parts of the can with a minimum amount of input. This was necessary since the ANSYS programs on the WPI campus had a limitation on the size of the model that could be analyzed, and also there was a limit on the time and space available to us on the larger ANSYS program at the MITRE Corporation.

The beam element was used in three places on the can. The first was the center shaft. This element was ideal for the analysis since it gave moments and deflections at the two plates and between the two plates. It also reduced the number of elements necessary to model the center shaft, allowing us to use WPI's computer facilities. The second use of beam elements was in the modeling of the experiments. The element was given a density of near zero and stiffness large enough to eliminate internal deflections in the beam which allowed us to translate the acceleration of a mass into moments and forces at the fastening locations. This provided stresses and deflections in the plates at the experiment locations. The last place the beam element was used was for the mounting brackets, which allowed any forces and moments induced within the beams to be transferred to the plate elements of the flanges.

The plate element was used to model the plates and flanges of GASCAN II. Mass elements were used to represent the masses of the experiments and were attached to the beams as mentioned above. All the elements were then compatible with each other and the model was analyzed.

The first model developed of the can, Model I, consisted of the plates, flanges and center post. To develop forces on GASCAN II, we calculated the force that would be required to accelerate the mass of each experiment at 6 g's. These forces were then applied to GASCAN II at appropriate

locations. The largest deflection that occurred was at node 45, on the outer edge of the bottom plate, and occurred in the z direction. The largest stress in a component direction was at node 140, on the upper corner of a flange, and occurred in the y direction. This was also the location of the highest principal stress. All other high stresses occurred at the bumpers and upper flange locations, the points where the degrees of freedom were fixed. We were not able to determine stresses in the center shaft, but deflections were low, which indicated low stresses. All the stresses that occurred were low in comparison to yield stress and ultimate stress limits, but a more accurate model of the system was required.

The second and third models were identical in structure with the exception of the location of the battery box. The second had the battery box underneath the bottom plate and the third had the battery box above the rotational fluid flow experiment. Additional elements were added to represent the experiments and the mounting brackets, since the first model neglected moments induced by the acceleration of the experiments. These moments added to the stresses in the structure. Another improvement was to accelerate the whole model to take into account the body forces that occur in the parts of the structure.

A further reason for the two models was to compare structural rigidity and vibrational stability. For design reasons, mainly the fastening arrangement of the battery box, the battery box was positioned above the rotational fluid flow experiment. Both designs were analyzed to see if moving the battery box affected the structural integrity of GASCAN II.

As expected, the stresses that occurred in these improved models were much higher than in the simple one. The highest stresses that resulted in both cases were in the direction of the principal stresses for all acceleration directions.

The highest stresses occurred where the nodes were fixed, due to the fact that stress is generally inversely proportional to area. At these points the area is reduced to almost zero and the stresses increase.

The stresses also depended on direction of acceleration and the type of model. The first type was with the battery box on the bottom and the bumpers fixed in all directions. The second type was with the battery box on the bottom and the bumpers free in the z direction. The third was with the battery box above the rotational fluid flow experiment and the bumpers fixed in all directions and the fourth was with the battery box above the rotational fluid flow experiment and the bumpers free in the z direction. The models were each accelerated in the x, y, and z directions.

The lowest stresses occurred when GASCAN II was accelerated in the y direction. Away from the areas around the fixed points, the stresses are in the range of 2000 psi to 5000 psi which is well within the acceptable range for aluminum. The maximum allowable stress for aluminum is 37,000 psi in tension and compression. At the bumpers and mounting brackets, where GASCAN II is fixed, the stresses are in the range of 15,000 psi to 20,000 psi, which is still in the acceptable range. For accelerations in the y direction, the stresses are all within the acceptable range for all four conditions mentioned.

The accelerations in the x direction yielded high stresses at the bumper locations and the mounting brackets. Away from the areas that were fixed, the stresses ranged from 10,000 psi to 13,000 psi. At the bumper locations, the stresses were in the 60,000 psi to 90,000 psi range. In one model the stresses were considerably lower. This was the condition with the battery box above the rotational fluid flow experiment and the bumpers fixed in all directions. The stresses in this model ranged from 2000 psi away from the bumpers to 33,000 psi at the bumper locations. This result was good because it justified moving the battery box above the rotational flow platform.

The accelerations in the z direction were the most important because this is the direction of maximum acceleration requirement. This is also the direction that the bumpers were free to slide. Any movement in the x and y directions would only be from torque. The main concern was the location of the battery box above the rotational fluid flow experiment. In our worst case, where the bumpers would fail and slip, stresses were low in the plates. They were below 7000 psi in the bottom plate, and between 7000 psi and 14,000 psi in the middle plate. The high stresses occurred at the mounting brackets. These were the only three points keeping the entire can from moving and stresses reached the 60,000 psi range, again because of small areas. These stresses carried into the flanges and the shelf and ranged between 25,000 psi and 48,000 psi. Some of these numbers were above the allowed maximums, but might be lower with improved modeling of the bumpers. We found that moving the battery box would not disrupt the structural integrity of GASCAN II. Under certain conditions the stresses were slightly higher, on the order of 1000 psi to 2000 psi, but in others it was considerably lower. To sum up the results, the design with the battery box above the rotational flow platform should meet NASA safety specifications, but must be further analyzed with a finer mesh. Further detailed design of the can should proceed from this design taking into account the problem areas specified above.

THERMAL DESIGN

Introduction

The purpose of the thermal portion of the preliminary design is to identify potential thermal problems and to suggest possible solutions to these problems. In order to identify potential thermal problems, we looked at the thermal energy balance of each experiment and the interaction of each experiment with the surrounding hardware. Through this analysis, we determined if the experiments might fail due to temperature extremes. As a secondary task, this project team was responsible for coordinating and documenting electrical interfaces for GASCAN II, including power requirements, timing of that power, and the subsequent energy requirements. The preliminary electrical interface specification is also part of this project.

C-4

Systems Configuration Diagram

Systems Configuration Diagram, shown in Fig. 7, illustrates all three experiments contained within the GASCAN II. The relationships between each experiment, the GASCAN/NASA Interfaces and the battery pack are also included to give a simplified diagram of all of the systems in the GASCAN II.

Heat Transfer Analysis

Using basic heat transfer theory, often simplified, the thermal analysis of GASCAN II was developed. In the following sections, the methods of analysis, possible thermal design problem areas and recommendations to future groups are presented for each experiment. In addition to the analysis of the experiments, bulk temperature considerations of the GASCAN are discussed in the IPPE section.

IPPE/canister top. The Ionospheric Propagation Properties Experiment (IPPE) consists of a radio receiver, an electrostatic analyzer and the necessary electronics required for the control of the experiment and the storage of data. One of the requirements for this experiment is the external mounting of an ion sensor and an antenna for the radio receiver. Because of this requirement, the insulating cap, which is usually placed on top of the canister, cannot be used.

While the IPPE experiment does not adversely affect the thermal environment in itself, the external mounting of the antenna and the ion probe along with the leads to them does

affect the thermal environment when one looks at the temperature extremes the canister must endure without the insulating cap. While the temperature of deep space has been approximated at 3 K (-270°C), because of the complex radiation that occurs in shuttle bay, the "effective" external temperature experienced by a payload is significantly higher and is directly dependant on the shuttle bay orientation. When the shuttle bay is oriented so that it faces space, as when a satellite is deployed, a heat sink of 173 K (-100°C) should be assumed and, generally, heat will be conducted out of the canister which could result in exceedingly cold temperatures. Similarly, should the shuttle bay face the sun for an extended period of time, the possibility of thermal problems exists because the effective external heat sink temperature is 313 K (+40°C)

There are always potential problems with electronics. If heat generating components are not properly mounted to a conducting surface, they can burn up. It is important to note that while these two scenarios present the extremes that will be encountered, the information gathered from these two situations will provide us with an estimate of the thermal characteristics of the canister and the experiments at any time during the mission.

The following is the methodology for the calculation of the temperatures that will be experienced by GASCAN II as a function of time, shuttle bay orientation, and presence of an insulating cap.

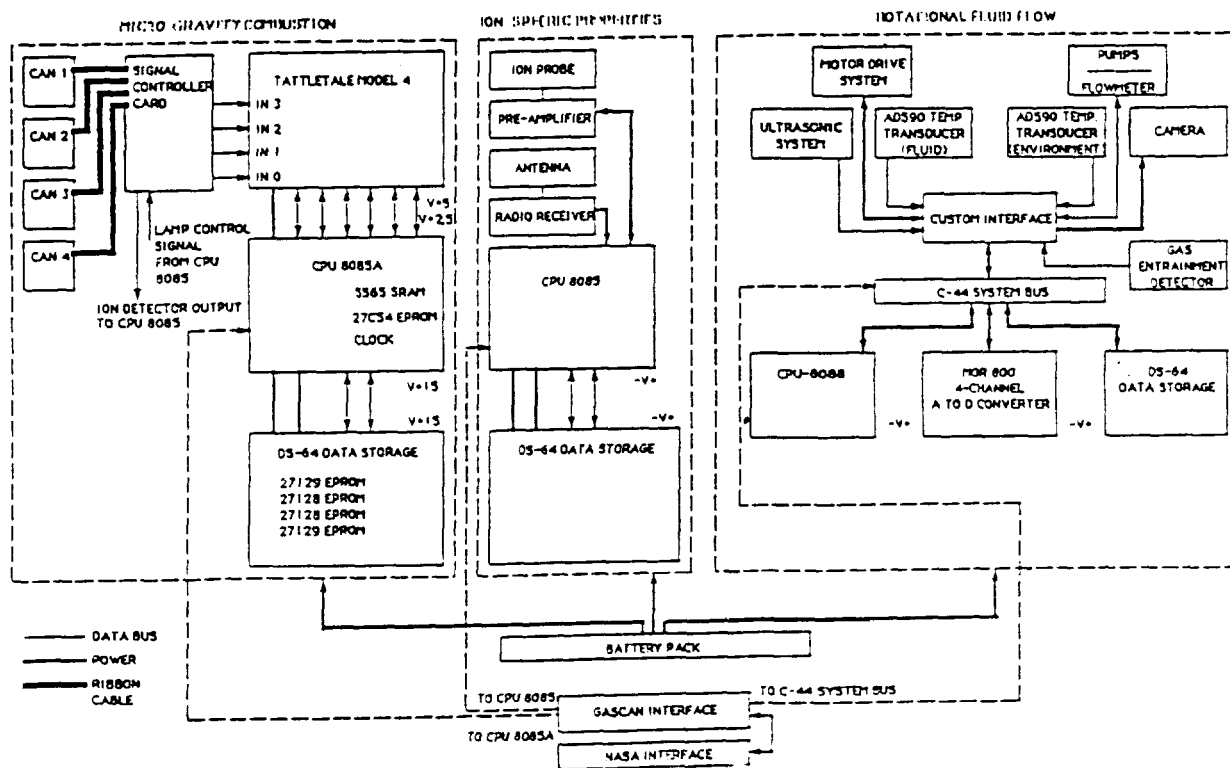


Fig. 7. System Configuration Diagram

ORIGINAL PAGE IS OF POOR QUALITY

Bulk GASCAN II Temperature Calculations

In order to determine the temperature of GASCAN II as a function of time and shuttle bay orientation, the following model was taken from Appendix A of the Get Away Special (GAS) Thermal Design Summary. The following information represents the internal temperature of GASCAN II as a function of time for different shuttle bay orientations for an insulated and uninsulated GASCAN II. It is important to note these temperatures are bulk temperatures for GASCAN II and do not represent the temperature of any individual component. The basic assumption of this analysis is the entire GAS canister is considered to be one thermal mass with the same temperature at any spot in the canister. Obviously temperature variations will exist both from the outside to the inside of the canister as well as the areas around heat generating components.

The resulting differential equations were solved using the ASDEQ, a user friendly, differential equation solver from the Engineering Department of USMA, West Point. The equations are modeled with block diagrams similar to analog computer wiring diagrams. The equation and the resulting ASDEQ block diagram are shown in Fig. 8. After input of the blocks into the program, ASDEQ solves the equations using a fourth order Runge-Kutta scheme and presents data in column or plot formats. Plots of the average GASCAN temperature for three orientations using insulated and uninsulated configurations are shown in Figs. 9, 10, and 11.

For an Earth orientation, the uninsulated GASCAN reaches an equilibrium temperature of 15°C in 70 hr. In comparison, the insulated model does not reach its equilibrium temperature of 5°C even after 150 hr. Similarly, in the sun orientation the uninsulated GASCAN reaches equilibrium with the environment after 60 hr at a temperature of 30°C. The insulated canister approaches its equilibrium temperature of 40°C after 120 hr. Finally in analyzing the space orientation, one sees even after 150 hr neither the uninsulated nor the insulated GASCAN reach their respective equilibrium temperatures of -110°C and -100°C. The uninsulated canister does, however, cool off much more rapidly and a long duration in this orientation will pose problems for GASCAN II.

In all sets of data, there is a "hump" which exists from T+15 until T+30. This increase in temperature is due to the operation of the experiments. One can see a direct correlation between this "hump" and the power requirements for the canister.

It is important to note these calculations assume a shuttle liftoff and subsequent bay orientation immediately after the shuttle is in space. Combinations of these orientations will exist in reality; therefore, the GASCAN may already be at equilibrium in, say, the Earth orientation and then change to a space orientation. This would lead to an initial temperature of 5°C instead of the 27°C modeled here, therefore, reducing the time necessary for the GASCAN to reach critical temperatures. These represent extremes of what could happen to the payload during the shuttle flight.

Thermal Analysis: Microgravity Ignition Experiment

The Microgravity Ignition Experiment consists of four cylindrical canisters each containing a heat lamp, ion detector,

$$\frac{dT_2}{dt} = \frac{1}{C_v M} [\dot{Q}_{int} - \epsilon \sigma A (T_2^4 - T_1^4)]$$

where:

- A Surface Area
- C_v Average Specific Heat
- M Total Mass
- Q̇_{int} Internal Heat Generation
- T₁ Environmental Temperature
- T₂ Mean GASCAN Temperature
- t Time
- ε Effective Emittance
- σ Stephan-Boltzmann Constant

Values of Environmental Temperature, T ₁		
Viewing	Insulated	Uninsulated
Space	173K	163K
Earth	268K	258K
Sun	313K	303K
Values of Effective Emittance, ε		
	0.065	0.16

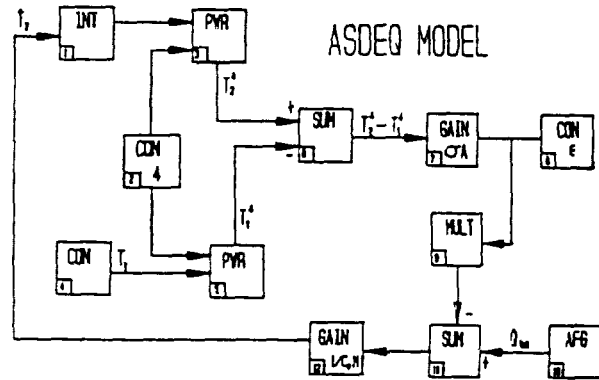


Fig. 8. Thermal Equation and ASDEQ Block Diagram

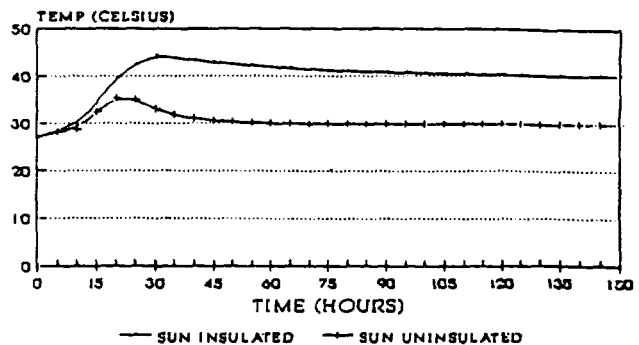


Fig. 9. Thermal Response for Sun Viewing

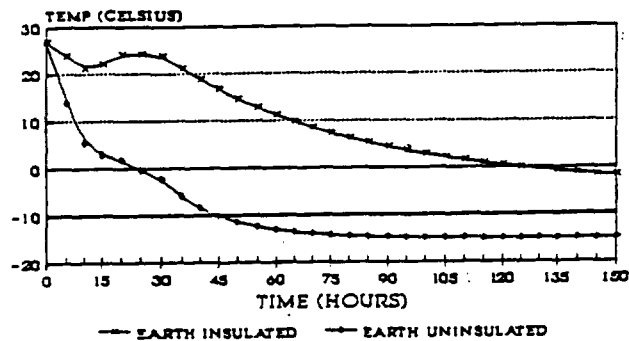


Fig. 10. Thermal Response for Earth Viewing

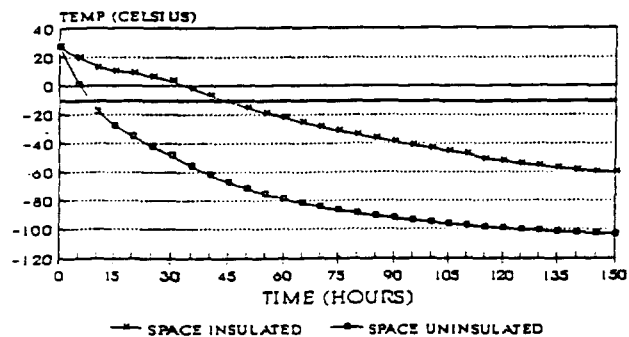


Fig. 11. Thermal Response for Space Viewing

and pressure transducer, as well as material that will be ignited. A custom designed control card, and a Tattletale computer will be used for the control of the experiment as well as data storage. The two major thermal design concerns for this experiment are the presence of four 250-W lamps and the ignition of the combustible material in each of the canisters. Both the lamps and the heat released from the ignited material will cause local hot spots. Analysis of these areas will provide information on the thermal environment of the experiment and its interaction with the other experiments in GASCAN II.

The combination of the lamps and the ignited material will generate heat within each container that could be radiated throughout the compartments the containers are placed in. The electronics for this experiment, primarily the computer components, were determined to generate a minimum amount of heat, which for this analysis is negligible.

The Microgravity Ignition Experiment involves the heating and combustion of a cellulose material inside an aluminum container. The lamp in each of the four canisters will be on for a maximum of 30 sec. It must be determined if for this period of time the temperature rise of the outside of the aluminum chamber will be a safety concern.

The analysis of each individual canister will determine the amount of heat the immediate outside environment must reject from the radiating body (the combustion chamber) assuming

all of the heat generated (from the 250-W lamp and combustion of material) will be radiated through the chamber. Since there is no convection, and conduction is considered to be minimal, this will represent a worst case scenario. The worst case assumptions used are (1) steady state conditions; (2) convection and conduction is minimal; and (3) all of the produced heat is immediately transferred to the environment by means of the aluminum chamber. The heat generated, Q , for 30 seconds inside the chamber is: $Q_{\text{total}} = 10285 \text{ J}$ which results in a temperature rise of the chamber of 16°R .

Experimental results for combustion chamber. Once the approximate temperature rise for the outside of the combustion canister was established, and the components to the microgravity ignition experiment were machined and assembled, a test was performed to determine if the temperature rise calculations were accurate. The experiment was conducted with a thermocouple attached to the outside of the combustion chamber to determine the actual temperature rise due to the heat created by the 250-W lamp for a period of 30 sec.

The results of the experiment yielded only a 4° temperature rise outside of the chamber at the end of the allotted time period. This would support the assumption that there is a minimal temperature rise outside of the combustion chambers. The difference between the analysis and the actual temperature rise is likely because the actual heat release from the paper was very low. Also, the paper mount is an additional mass inside of the combustion chamber and is not considered in the analysis.

Heat Transfer Analysis: Rotational Fluid Flow Experiment

The rotational fluid experiment is the third experiment in the GASCAN II cylinder. The experiment will be isolated from the rest of the GASCAN, in that all of its equipment will be located within the rotating structure. The power supply and interface connections will be the only connections outside the rotational area.

The experiment has possible thermal problems that need to be addressed. The first problem concerns the isolation of the experiment from the rest of the GASCAN. Unlike the other experiments, this experiment is designed so that its interaction with the rest of the canister is minimal. This configuration was chosen to allow smoother rotation of the platform, with less chance of interference from the other experiments. Although this is the desired design, it may create a critical thermal problem. Energy may need to be channelled to or from the experiment to prevent overheating or freezing.

When discussing the channelling of energy, one must realize that in microgravity there is very little natural convection. The amount of free convection is directly related to the gravitational force present. Therefore, in space the amount of free convection will be very close to zero. This prediction is valid for the GASCAN only when the rotational flow experiment is not in operation. During its operation, the initial speed of the platform will create an outer acceleration of approximately 2 g. This will directly affect the convective coefficients and the rate of convection. By doubling the gravitational force, the

Grashof number, Nusselt and Rayleigh numbers will be increased. This increase will raise the rate of free convection at the initial rotation speed in the experiment.

The second potential problem area is the pump and motor-drive systems. With properly instrumented Earth-based testing, the pump system is not expected to be a problem. However, the temperature within the flow experiment compartment must not exceed the acceptable operating temperature spectrum of the pump, which is 210°F.

The motor-drive system is not anticipated to be a problem over the operating time of the experiment. Initially the motor will be brought up to full power. As the experiment continues, the motor speed will be decreased, thereby decreasing heat generation.

Other areas of interest are the bearings in the rotational hub, the camera system, and the viscosity of the fluid. The latter is not anticipated as a problem by the rotational flow MQP team. The viscosity of the fluid remains fairly constant over a wide range of temperatures. The bearings on the other hand may present a problem. If they experience a high degree of friction while in microgravity, heat will result. This heat would then be conducted outward increasing the platform temperature.

Finally the camera system presents a potential problem. The problem does not lie in heat generation, but rather energy absorption. The critical area is the film. Most films can operate

in a temperature spectrum of -10 to 40°C. If the rotational compartment will not be in that temperature range, either an improved thermal design or alternate photography methods may be necessary.

Computer Thermal Analysis

Ultimately, the thermal design of the GASCAN will require a complete thermal analysis, which will show if any of the experiments inside the canister will fail due to temperature extremes.

In order to calculate temperature distribution versus time, a simulation program is needed that keeps track of time varying situations such as ambient conditions and power dissipation.

The program SSPTA (Simplified Space Payload Analyzer), which was provided to previous groups, not only solves transient problems but also provides view factors. Given the material properties, geometry, power dissipation and orbital orientation, SSPTA will allow calculation of temperatures and view factors for each thermal node at specified time intervals. SSPTA can take up to 999 surfaces and 600 thermal nodes.

It is our recommendation that follow-on design teams proceed with the full thermal analysis using SSPTA or similar analysis programs. Particular attention should be paid to those potential thermal problems identified by this design team.

Aeronautics Projects

p.5 267

SUMMARY OF 1989-90 AERONAUTICS DESIGN PROJECTS N91-18160

AUBURN UNIVERSITY

INTRODUCTION

Four design projects were completed at Auburn University this year under sponsorship of the NASA/USRA Advanced Design Program. These projects are summarized below. Three of the topics were suggested by Mr. Shelby J. Morris, NASA mentor at Langley Research Center, and one was chosen from the AIAA design competition topics. The topics were (1) design of a high-speed civil transport; (2) design of a 79-passenger, high-efficiency, commercial transport; (3) design of a low-cost short-takeoff vertical-landing export fighter; and (4) design of an ozone monitoring vehicle.

HIGH-SPEED CIVIL TRANSPORT

The High Speed Civil Transport (HSCT) shown in Fig. 1 is designed to carry 300 passengers at Mach 3 at an altitude of 70,000 ft and have a range in excess of 6000 n.m. Three major areas of concern were configuration, materials, and propulsion.

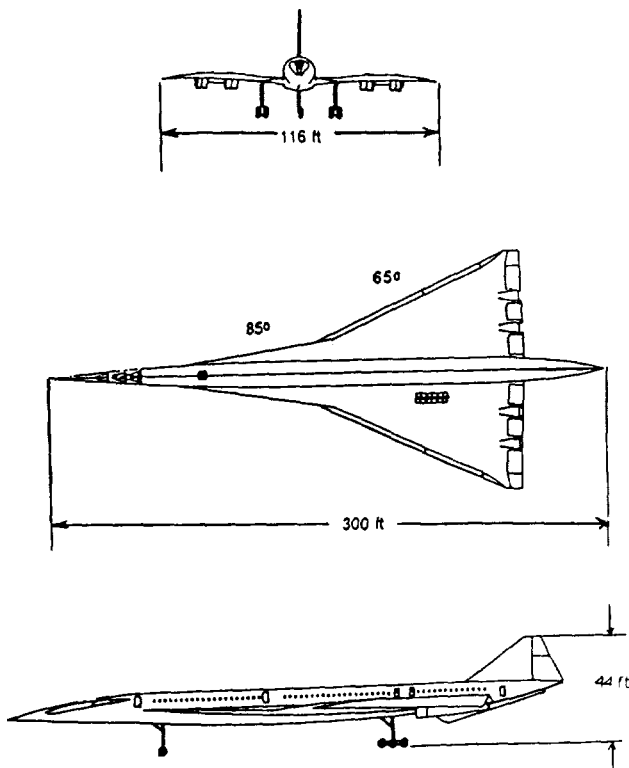


Fig. 1. Basic Configuration of the HSCT

Configuration

The primary goal in configuration design is to minimize drag while maximizing lift. Two wing configurations were considered: a variable-sweep wing and a double-delta planform. The double delta was chosen because of the weight and complexity penalties of the variable-sweep wing. The wing has an area of 9556 sq ft and an aspect ratio of 1.41. Inboard sweep is 85° while the outboard panel is swept 65° . The airfoil is a double wedge airfoil with 5% thickness.

The fuselage is 300 ft long with a diameter of 15 ft. For stability purposes a flight trim fuel tank is located forward of the aircraft center of gravity beneath the passenger compartment.

The HSCT incorporates a vertical tail but no horizontal tail.

Materials

The HSCT will be constructed almost entirely of advanced fiber-reinforced composite materials. Driving forces are the abilities of composites to handle the severe thermal effects induced at Mach 3, and the high strength- and stiffness-to-weight ratios required to keep the weight down. High-temperature areas will use carbon/carbon composites while graphite/epoxy composites will be used wherever possible to reduce cost. Regions susceptible to erosion due to collisions with microscopic materials will be coated with silicon carbide.

Propulsion

Three highly promising engine configurations have been considered: the variable stream control engine (VSCE), the double bypass engine (DBE), and the supersonic through-flow fan engine (STFF). The STFF was chosen because of its lighter weight and better performance over the various flight regimes. The STFF engine concept differs from conventional turbofan designs because the airflow at the fan is supersonic. A schematic of the STFF is shown in Fig. 2. Directly aft of the fan is the engine core inlet. At this point some of the airflow is bypassed while the rest enters the core inlet and is diffused to subsonic speed before reaching the compressor.

Weight savings are seen in the STFF engine in three main areas: the shorter inlet, the simpler single-stage fan, and a lighter, simpler nozzle. The total engine weight savings over the conventional turbofan is estimated at about 31%. A supersonic transport with a gross weight of 760,000 lb is

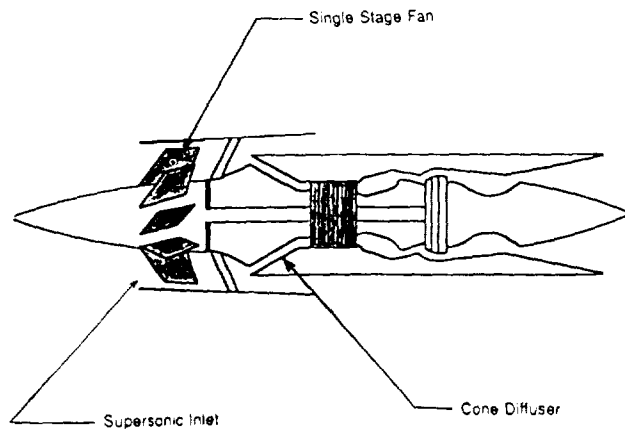


Fig. 2. Schematic of the Supersonic Through-flow Fan

estimated to have 14% greater range. The propulsion weight reduction provides approximately 5% of the range increase while improved specific fuel consumption provides about 9%.

Conclusion

Development of a HSCT at this time will ensure a stronghold in the aerospace industry for the U.S. well into the next century. At a time when foreign competitors have weakened the U.S. economic position in almost every other area, the aerospace industry continues to be one of the U.S.'s best-performing industries. Market studies have shown that the Pacific Rim nations' economies are the fastest growing in the world. This means inevitable increase in the amount of worldwide travel to this area. If the U.S. aerospace community can develop a baseline HSCT in the near future, it may well boost all areas of our economy.

PRELIMINARY DESIGN OF A 79-PASSENGER, HIGH-EFFICIENCY, COMMERCIAL TRANSPORT AIRCRAFT

INTRODUCTION

The Avion is the next step in commercial passenger transport aviation (see Fig. 3). It aspires to capture for the U.S. the growing world market for a 60-90-passenger, short/medium range transport aircraft. Premier engineering achievements of flight technology are integrated into an aircraft that will challenge the current standards of flight efficiency, reliability, and performance. To achieve higher efficiency the features incorporated in the Avion design are a triwing configuration, propfan powerplants, forward swept wings, winglets, aerodynamic coupling, strakes, T-tail empennage, and an aerodynamic tail cone.

Aircraft Configuration

As an evolutionary hybrid from the conventional and canard configurations, a compromise was reached for the Avion with the three-lifting-surface (or triwing) configuration. This

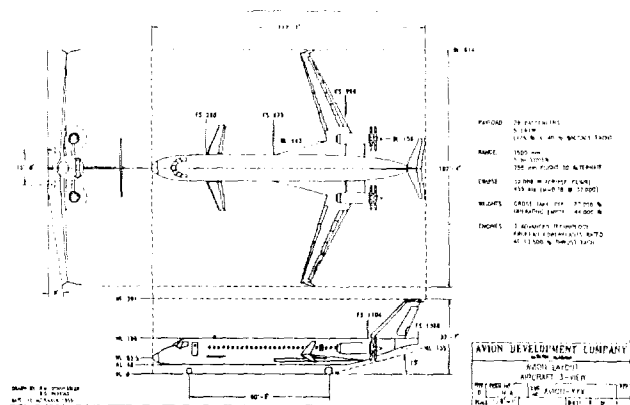


Fig. 3. Avion Configuration 3-View

configuration retains the tail of the conventional arrangement, but uses it as an additional lifting surface rather than a stabilizing (down-loading) surface. Among the favorable attributes of the triwing configuration are (1) higher trimmed cruise lift-to-drag ratios; (2) longitudinal primary and trim controls are incorporated in the horizontal tail; and (3) canard is used to trim flap-induced pitching moments.

The Avion uses forward-swept wings that have a significant stall advantage and a favorable effect on compressibility drag. However, they do possess several disadvantages. First there is a substantial weight penalty, which can be overcome by using composite materials. Then there is a stability problem due to the forward location of the aerodynamic center, which must be overcome by careful center-of-gravity location.

The Avion employs a horizontal and vertical tail in a T-tail arrangement. The increased structural weight of this arrangement is offset by sweeping the vertical tail aft to increase the moment arm and thus reduce the size and weight.

Preliminary Weight Estimate

The difficulty of weight estimation was compounded by the unconventional design of the Avion; however, weight estimation was achieved by the iterative fuel fraction method. The results of this method yielded a takeoff weight of 77,000 lb.

A preliminary component weight estimation was made from averaged data from the McDonnell Douglas DC-9-30 and MD-80, and Boeing 727-100 and 737-200 aircraft. The values were then adjusted as deemed necessary by the preliminary weight estimations and structural concerns.

Performance Design Parameter Estimations

The parameters that have a major impact on performance are wing area, takeoff thrust, and maximum lift coefficient. Sizing to meet FAR requirements yielded a wing loading of 100 lb per sq ft at takeoff and a maximum lift coefficient of 2.4.

ORIGINAL PAGE IS
OF POOR QUALITY

Propulsion System Integration

Propfans are one of the most promising developments for raising propulsive efficiencies at high subsonic Mach numbers. Demonstrations of this new technology on test aircraft have shown that propfans are clearly superior to current turbofan engines in the area of efficiency while still meeting rigid FAR requirements. Two 12,500-lb thrust engines will be used.

After careful consideration, the decision was made to mount the engines at the rear of the fuselage on pylons. This position alleviates the difficulties of exhaust and slipstream interference while maintaining excellent accessibility of the engines for maintenance and repair.

Propfan propulsion is still an evolving technology. Currently, there are no propfans that meet the thrust and configuration requirements of the Avion; therefore, it is assumed that a power plant will be developed for the Avion.

Conclusions

The Avion has evolved from its initial conception into a promising aircraft design. However, there are several areas that need further attention and were not addressed due to time constraints. Some of these areas are (1) control surface sizing, (2) landing gear sizing, (3) dynamic stability and control analysis, (4) internal structural design, and (5) aircraft systems (e.g., fuel, hydraulic, electrical).

**DESIGN OF A LOW-COST
SHORT-TAKEOFF VERTICAL-LANDING
EXPORT FIGHTER/ATTACK AIRCRAFT**

Introduction

In response to the need for a supersonic short takeoff and vertical landing (STOVL) aircraft, AIAA has sponsored a request for proposals (RFP) for a low-cost aircraft meeting these requirements that would be suitable for export and would fill the dual role of a fighter/attack aircraft. These requirements pose several unique design challenges.

Unique Problems of STOVL Design

Since the cost of an aircraft is a function of the amount of new technology that is involved in its development and construction, it is obvious that it will be a major challenge to keep the cost within the range of "low cost." Because of weight minimization needed for vertical flight, lightweight and oftentimes expensive exotic materials will be needed. Also, a new generation of vectored thrust engines will have to be developed since there are no engines on the market that will produce the performance required. One method to contain cost, however, is to use existing avionics packages.

Final Design

After consideration of the many complex design problems concerning STOVL aircraft, and after a considerable amount of

research and analysis, a final design for the supersonic STOVL aircraft (the Gremlin) was achieved (see Fig. 4).

The major design features of this aircraft are as follows:

1. Two seats for reduced workload and reduced vulnerability, as well as the ability to be used as a trainer.
2. Improved Pegasus-type, four-poster, low-bypass turbofan engine.
3. Elliptical under-fuselage air intake for efficient airflow at high angles of attack.
4. Highly swept thin wings for low wave drag at supersonic speeds.
5. Folding wings, with folded semispan of 10 ft to reduce storage space.
6. One-piece acrylic bubble canopy for excellent crew visibility.
7. Avoidance of complex curvature to reduce fabrication costs.
8. Incorporation of easy-access panels to simplify maintenance.

Methods of Analysis

Many analyses of the systems comprising the Gremlin were performed during the design period. An initial analysis of most systems was performed using either historical data or rule-of-thumb guesses. The purpose of these initial analyses was to provide a basis for more detailed analyses that followed.

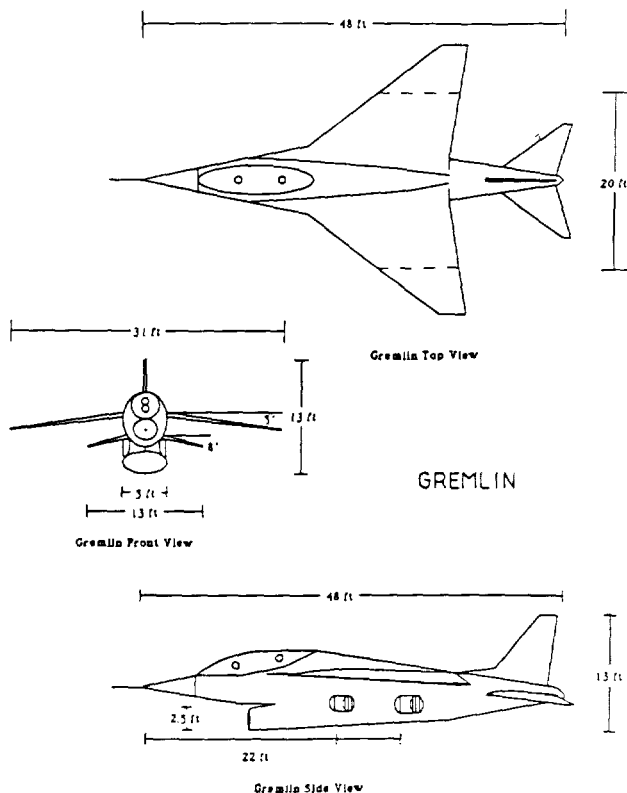


Fig. 4. Gremlin 3-View

Main Systems

The main systems of the Gremlin supersonic STOVL aircraft are as follows:

Avionics. In order to reduce costs, current production systems will be employed. Since the F-18's dual-role mission is very similar to that desired for the Gremlin, its avionics systems will be used.

Fuel system. The fuel system is located as near as possible to the aircraft's center of gravity. A disadvantage of this situation is the proximity of the fuel tanks to the engine. This vulnerability can be reduced by the use of self-sealing fuel tanks and an inert gas to fill voids to reduce the chance of combustion.

Landing gear. The landing gear system consists of two sets of main fuselage gear designed to absorb most of the stress of impact, and two outboard gears designed to maintain the balance and stability of the aircraft during vertical flight landings.

Weapons. The weapons carried by the Gremlin will be controlled by either the front or rear pilot. Wingtip launching rails can carry the AIM-9L Sidewinder missile, and the hardpoint closest to the fuselage on either wing will carry three Mk-82 500-lb bombs on a multiple ejector rack. Another hardpoint will be located farther out on either wing for additional stores.

Performance Requirements

In order to meet the RFP requirement for cruise at a Mach number of 1.5 for 250 nautical miles, a slightly more powerful Pegasus-type engine is required. This engine will allow vertical takeoff in the air-superiority configuration and requires a takeoff roll of only 200 ft in the ground support configuration, thus beating the RFP requirement of a 300 ft takeoff roll.

Material Selection

The combination of vertical flight and other high-performance requirements suggested the use of exotic materials. However, the RFP also required that the STOVL design be "low cost" to be suitable for export. The Harrier AV-8B uses approximately 30% composites throughout the aircraft structure. Many of the experiences learned in the design process of the Harrier could be applied to the Gremlin. However, the supersonic nature of the Gremlin requires that temperature limitations of composites be taken into account.

Aluminum is still the material of choice when constructing airframes and wing boxes. Its relative low cost and ease of fabrication make it an ideal material for restricting the cost of this aircraft. Titanium, although expensive and complicated to machine, will be used in the high-temperature areas of the aircraft, such as around the engine nozzles.

Overall, the weight of the Gremlin is expected to be around 35% composite materials, 60% traditional aluminum alloys, and the remaining amount various specialized materials such as high-strength steel, titanium, and high-strength plastics.

Cost and Management

The AIAA RFP expected a production run of 500 aircraft. By having a large production run the average cost per aircraft is reduced. These aircraft will be produced over a period of five years. Before production begins, one year will be spent in research analyzing test data. Production then begins at the start of the second year by manufacturing two Gremlins each of the first four months. The first four aircraft will be for flight tests. Evaluation of the test flights will begin the third month of production. After testing is completed, full-scale manufacturing of 10 Gremlins per month will occur for production months 9 through 54. As the production schedule nears completion, the rate of production will decrease to allow for personnel to transfer to new programs.

The average cost per Gremlin aircraft for a production run of 500 aircraft was calculated to be \$18.2 million (1990 dollars).

Conclusions and Recommendations

This design group has concluded that the low-cost Gremlin supersonic STOVL fighter/attack aircraft is a viable design. It is expected that the engine technology required for this design will be available by the projected delivery date of 2005. Although the aerodynamic evaluation is not complete, the preliminary analysis predicts very promising performance.

The potential market for such an aircraft is growing. The large number of Harriers and Hornets sold to other countries is an indication of this trend.

HIGH-ALTITUDE OZONE RESEARCH BALLOON

Introduction

The ozone layer shields the Earth from harmful solar radiation that can cause skin cancer, destroy acids in DNA molecules, and have harmful effects on world climate and vegetation. Research has indicated that a seasonal depletion of ozone concentration exists over Antarctica. Can we conclude that this depletion is a natural occurrence, or are we witnessing a decline in ozone concentration that will appear later in other regions of the world?

Because 97% of the ozone molecules are located in the stratosphere, analysis methods are extremely expensive, time consuming, and inadequate. Moreover, atmospheric scientists are concerned with the possible further destruction of the ozone concentration due to the chemical contaminants released from ozone monitoring vehicles. These concerns have caused a renewed emphasis in the development of high-altitude ozone research balloons. However, limited flight duration and lack of vertical and lateral control have severely limited the widespread acceptance of high-altitude research balloons as the primary method for ozone observation and analysis.

Current Limitations

Ozone research requires a vehicle capable of delivering and supporting a scientific payload at an altitude above 25 km. Also, ozone research analysts emphasize the need for variable altitude profile sampling in order to obtain a representative model of ozone concentration. In addition, a long flight duration is desired in order to reduce production costs and increase the amount of data collected per flight.

Presently used high-altitude ozone research balloons are very limited in flight duration. They maintain their altitude by venting helium and dropping ballast. Thus, the length of the mission is limited by the amount of reserve helium and ballast that is initially carried on the support structure of the balloon.

During the day, the balloon is heated by solar radiation impinging on the surface of the balloon film. As the temperature of the film increases, the temperature of the helium within the balloon increases due to natural convection. As a consequence, the helium expands and the balloon rises. When the balloon ascends to an altitude above the desired sampling range, the balloon is remotely vented and helium is released. As the mass of helium is reduced the balloon descends. When the balloon descends below the minimum range of interest, the researchers can either release ballast or perform a controlled addition of reserve helium.

This cycle of venting and ballasting continues throughout the mission. After depletion of ballast and reserve helium, the mission must be terminated. Currently, average flight times for these types of zero-pressure balloons are three to seven days.

HAORB Design Improvements

In order to lengthen flight duration, the conventional method of vertical control must be improved. The High Altitude Ozone Research Balloon (HAORB) is designed to provide this improvement. It will ascend at a slower rate than its conventional counterpart. Consequently, the venting and ballasting process will occur less frequently and the mission duration will be dramatically increased.

The focus of the HAORB design is the control of heat transfer to the balloon film. The polyethylene balloon film is continually heated during the day by direct and indirect solar radiation along with the reflected radiation from the Earth. As the temperature of the balloon film increases, the helium temperature and its volume subsequently increase. This results in a net upward acceleration of the HAORB that is equivalent to its conventional counterpart. The vertical speed of the HAORB will be controlled by removing the heat that is transferred to the balloon film. By limiting the increase in balloon film temperature, less heat is transferred to the helium. Thus, vertical control is achieved by the use of a cooling system on the HAORB.

Cooling System Operation

The cooling system uses cooling ducts and rotary circulation fans to maintain a balance between the temperature of the atmosphere and the temperature of the helium (see Fig. 5).

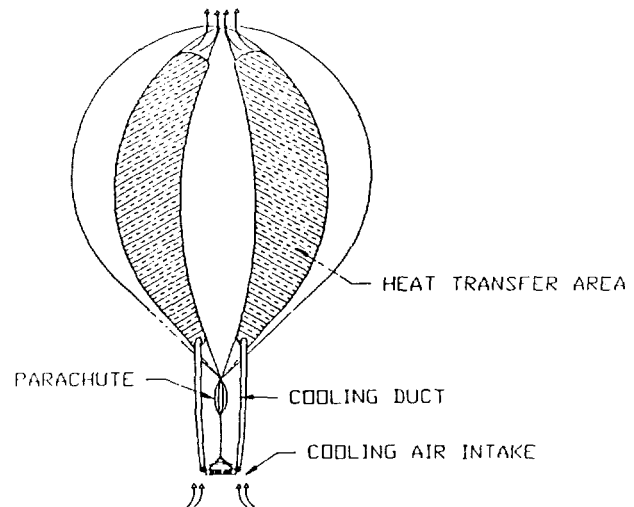


Fig. 5. Configuration of the HAORB at High Altitude

The cooling system cools both the film and the helium. Four cooling ducts are formed by sealing additional panels on the outer surface of the balloon. The four cooling ducts cover approximately one-fourth of the surface area of the balloon, therefore reducing the amount of film surface in contact with the helium that is exposed to solar radiation. The forced circulation of cooler atmospheric air provided by the rotary circulation fans removes heat that would be transferred to the helium from the outer film.

The cooling system receives input from an accelerometer. This information is then used to determine the vertical velocity of the HAORB. As the temperature of the helium increases, the HAORB begins to accelerate upward. When the upward velocity exceeds 0.27 m/sec, the fans are energized. The fans cause forced convection heat transfer from the film to the air. This cools the helium and reduces the acceleration. When the velocity falls below 0.2 m/sec, the fans are secured.

Results

A FORTRAN program was written to facilitate the stepwise integration of the equations describing the vertical motion of both the HAORB and a conventional balloon. The initial conditions assume that the initial velocity and acceleration are zero, the initial film temperature is 5° above atmospheric, and altitude is 26 km. For the test profile conducted from 26 km to 34 km, the HAORB with additional weight of fans, batteries, and solar cells had a substantially longer (about 9 times) mission duration than the conventional balloon with the same reserve helium and ballast.



273
p.1

AUTONOMOUS MARTIAN FLYING ROVER
N91-18161
CALIFORNIA STATE UNIVERSITY, NORTHRIDGE

Future solar system exploration is expected to include manned missions to Mars. The success of these missions can be enhanced through detailed close encounter, precursor surveys of the near-surface environment. A remotely reprogrammable, autonomous flying rover is proposed to extensively survey and map the martian surface environment.

A Mach .3, solar-powered, modified flying wing could cover roughly a 2000-mi range during martian daylight hours. Multiple craft, launched from an orbiting mother ship could provide near-global coverage. Each craft is envisioned to fly at about 1 km above the surface and measure atmospheric composition, pressure and temperature, map surface topography, and remotely penetrate the near subsurface looking for water (ice) and perhaps evidence of life. Data collected are relayed to Earth via the orbiting mother ship. Near-surface guidance and control capability is an adaptation of current cruise missile technology.

The 35-km scientific payload, plus communications and control electronics, is distributed spanwise inside the flying wing, eliminating the need for a traditional fuselage and reducing structural requirements. Mission reliability and, hence, the probability of success are improved by adding a telescoping tail boom that passively enhances flight stability. Thrust is provided with a two-bladed propeller driven by an electric motor powered from high efficiency solar cells supplemented with batteries. Roughly 90% of the required energy comes from the Sun. The final configuration has a payload plus communications-to-gross-weight ratio of 80%.

In summary, a solar powered aircraft, designed to fly in the low-temperature, low-density, carbon dioxide atmosphere near the martian surface appears feasible. Future efforts will optimize the configuration and develop a flying prototype scaled to the Earth's gravity environment.



P. 8

HIGH ALTITUDE RECONNAISSANCE AIRCRAFT

CALIFORNIA STATE POLYTECHNIC UNIVERSITY, POMONA

At the equator, the ozone layer ranges from 65,000 to 130,000+ ft which is beyond the capabilities of the ER-2, NASA's current high altitude reconnaissance aircraft. The Universities Space Research Association, in cooperation with NASA, is sponsoring an undergraduate program which is geared to designing an aircraft that can study the ozone layer at the equator. This aircraft must be able to cruise at 130,000 ft for 6 hr at Mach 0.7 while carrying 3,000 lb. of payload. In addition, the aircraft must have a minimum of a 6,000-mile range. The low Mach number, payload, and long cruising time are all constraints imposed by the air sampling equipment. In consideration of the novel nature of this project, a pilot must be able to take control in the event of unforeseen difficulties. Three aircraft configurations have been determined to be the most suitable for meeting the above requirements, a joined-wing, a biplane, and a twin-boom conventional airplane. Although an innovative approach that pushes the limits of existing technology is inherent in the nature of this project, the techniques used have been deemed reasonable within the limits of 1990 technology. The performance of each configuration is analyzed to investigate the feasibility of the project. In the event that a requirement cannot be obtained within the given constraints, recommendations for proposal modifications are given.

INTRODUCTION

The recent discovery of the ozone hole above the North Pole has prompted the scientific community to accelerate its efforts in investigating man's impact on his environment. The existence of the ozone hole has brought about concern that the predictions of stratospheric scientists may come true. In 1974, two chemists from the University of California, F. Sherwood and Mario Molina, theorized that the ozone layer was being destroyed by chlorofluorocarbons. Unless the ozone depletion in the Earth's atmosphere is controlled, radiation levels at the surface may increase to harmful levels. At the tropics, the ozone layer ranges from 65,000 ft to 130,000+ ft which is beyond the capabilities of the ER-2, NASA's current high altitude reconnaissance aircraft. Therefore, to effectively investigate the ozone layer, NASA needs to develop a high-altitude aircraft that will reach altitudes of 130,000+ ft. To hasten the development of the technology and methodology required to develop an aircraft that can reach these altitudes, the NASA/USRA program has been working closely with industry and universities. Perhaps, with the data retrieved from this aircraft, scientists and politicians will be able to formulate an emissions control plan that will diminish the rate of degeneration of the ozone layer.

DESIGN PROCESS

The 1989-1990 school year was the second in a three-year, ongoing design project geared to the design of a high-altitude reconnaissance aircraft. California State Polytechnic University, Pomona, has its yearly design sequence separated into three consecutive quarters. Basically, the assignment at the beginning of each year is to do a preliminary design analysis to determine the aircraft that best fits the Request for Proposal requirements. If such an aircraft is not deemed feasible, the aircraft must still be designed, with those aspects which are not approachable indicated in the concluding comments. Suggestions for making the Request for Proposal feasible are also requested. During the fall quarter, three groups were formed, aerodynamics,

propulsion, and structures. After a short break, the groups reconvened during the winter quarter to decide on the best possible configurations and commence their design. The final design iteration was completed, and the final report was compiled in the spring quarter.

The three fall quarter groups were given the Request for Proposal and instructed to identify the potential problems in their area of expertise. Once the problem areas were identified, possible solutions were considered and analyzed in detail. From this analysis, the design process was established, and possible configurations were determined. The pros and cons of each configuration as it pertained to the specialty groups of aerodynamics, propulsion, and structures were collected.

At the beginning of winter quarter, the three most plausible designs were chosen based upon the analysis of the previous quarter. For reasons discussed later, the three configurations selected were a conventional twin-boom monoplane design, a joined-wing design, and a biplane design. The three groups were then reassembled into three new teams based upon the configuration of each individual's preference. At the same time, the team leaders from the original groups were assigned to consult the groups on any problem areas that were investigated the previous quarter. If all the groups suffered from the same difficulty during the quarter, the consultant was authorized to temporarily reassemble his original team in an attempt to solve the most common and pressing problems quickly and efficiently. In this manner, the students were given the experience of working with a matrix management system on a small scale.

As the spring quarter commenced, the final configurations were set. Each group wrote a 100-page report on their preliminary design findings. These were assembled into three volumes and made available through the USRA program.

DESIGN SPECIFICATIONS

Ideally, the scientific community would like an aircraft that meets the following specifications:

RFP Specifications

1. The cruise altitude is 130,000 ft.
2. The payload capacity is 3,000 lb.
3. The design cruise Mach number is 0.7.
4. The cruise is a minimum of 6 hr.
5. The range is a minimum of 6,000 miles.
6. There is a minimum of one pilot.
7. The aircraft is to be designed with present technology.

These specifications meet the most optimistic demands of the stratospheric scientists. The results of previous studies have shown that flight at 100,000 ft with a range of 3250 n.m. is possible. Unfortunately, a mission at the lower altitudes would not give an accurate estimate of the chemical activity within the ozone layer at the equator. The ozone layer at the tropics is in the range of 65,000 to 130,000+ ft, as opposed to 50,000 to 100,000 ft at the mid-latitudes and 35,000 to 95,000 ft at the poles. The largest perturbations of the ozone are expected to be at 130,000 ft at the mid-latitudes. This fact coupled with an airplane's ability to follow an experimenter chosen path makes an airplane meeting the above specifications an ideal ozone testing platform⁽¹⁾.

Some of the constraints on the Request for Proposal are imposed by the sampling equipment, which is a modification of that in current use on the ER-2⁽²⁾. The increase in air temperature and the dissociation in the flow cause air samples to lose accuracy as compressibility effects become significant; therefore, the Mach number must be below the transonic regime. At the same time, the low air density (0.0003211 slugs/ft³) at altitude implies low wing loadings and high wing planform areas. Figure 1 illustrates the variation of air density with altitude. All of these adverse effects become more

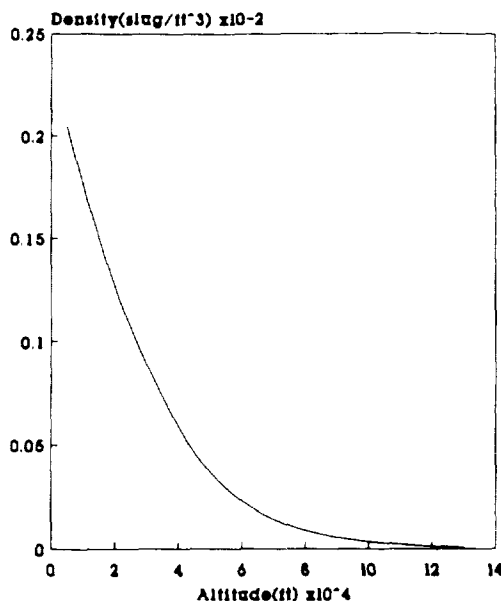


Fig. 1. Air Density vs. Altitude

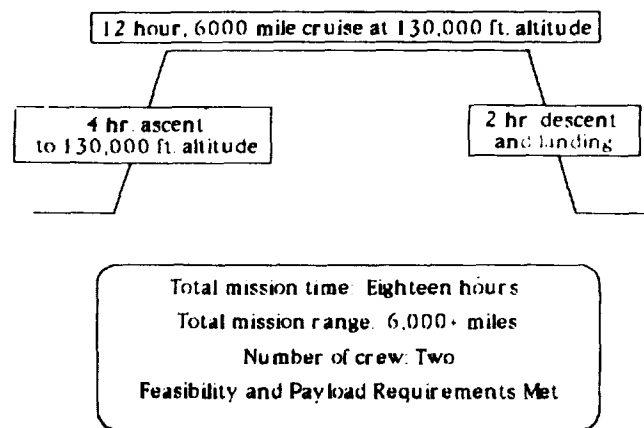


Fig. 2. Mission Profile

significant with decreasing Mach number. A Mach number of 0.7 was chosen to balance the contradicting effects of compressibility and air density. The air sampling equipment also dictates the cruise time and range. Stratospheric scientists are unable to obtain an accurate mapping of the ozone layer without extensive measurements that span a large area. The 6,000-mile range is easily accomplished within the specified minimum time constraints. As shown in Fig. 2, the total mission time is in fact on the order of 18 hours with a 12-hour cruise. The long mission time prompted the groups to design for two pilots in order to diminish fatigue.

The present technology requirement is desirable in order to acquire the maximum utility from this vehicle. In mid-1993, the Cryogenic Limb Array Etalon Spectrometer (CLAES), an instrument designed to monitor the ozone layer on the Upper Atmosphere Research Satellite scheduled for launch in 1991, will become inoperational. The first Earth Observing System (EOS) sensors are scheduled to become operational in 1996, at the earliest. It is during this testing gap that the results from a high altitude aircraft will be most crucial. After the EOS comes on-line, the aircraft will be used to cross-calibrate the measurements from the EOS and ground-based sensing instruments⁽¹⁾.

CONFIGURATIONS

The configurations considered for this aircraft are (1) Flying wing, (2) Monoplane-conventional, (3) Monoplane-twin-boom, (4) Canard, (5) Joined wing, and (6) Biplane-twin-boom.

The flying wing has a high aerodynamic efficiency due to the lack of a horizontal tail. However, it has the disadvantage of stability problems coupled with poor takeoff rotation. These factors rendered this design undesirable.

The monoplane with the conventional fuselage tends to be stable and predictable. The large wingspan required would produce excessive bending moments that a single fuselage could not counteract. On the other hand, a twin boom fuselage structure would relieve the structural loads while maintaining

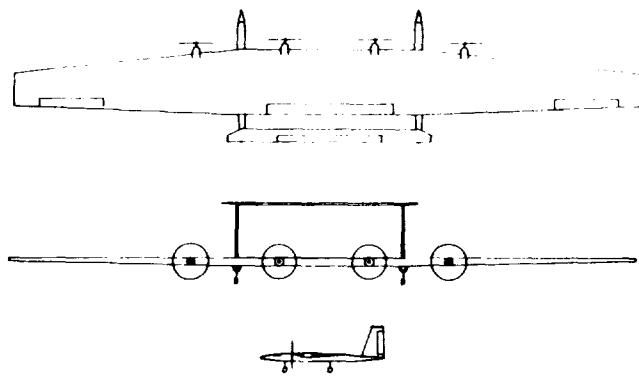


Fig. 3. Global Sentry

the advantages of stability and ease of analysis. The final design for the twin-boom monoplane is shown in Fig. 3⁽³⁾.

A canard configuration is similar to a flying wing in that it has many of the same advantages and disadvantages. No justification for using a canard configuration could be found.

The joined wing aircraft at first seems ideal with its high aerodynamic efficiency and high structural strength. Unfortunately, a joined wing aircraft is not a proven design. Therefore, the extra testing may render it not cost effective. Despite this possible failure, the aircraft appears to be worth analyzing. The three-view for this aircraft is shown in Fig. 4⁽⁴⁾.

A twin-boom biplane is structurally sound, minimizes the span, has good propeller clearance, and has a large frontal area. Its only apparent disadvantage is the interference from the wing struts. Considering the possibility that the strut interference may not be sufficient to undermine the advantages of the design, this aircraft is being considered further. Figure 5 shows a three-view.

In summary, the three designs chosen for further investigation were the twin-boom monoplane, the joined wing, and the twin-boom biplane. The three projects are called *Global Sentry*, *Icarus*, and *Hi-Bi*, respectively.

AERODYNAMICS

The two design drivers in the area of aerodynamics are airfoil selection and propeller design.

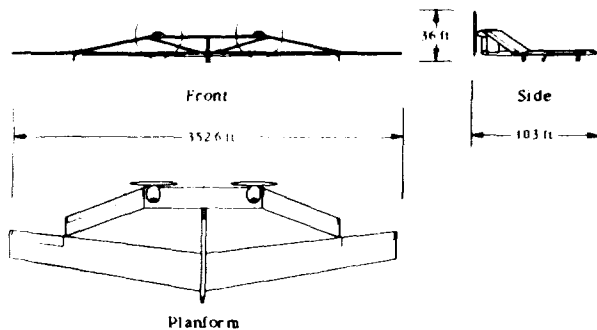


Fig. 4. Icarus High Altitude Aircraft

Airfoil Design

The airfoil design criteria are high lift and low drag at cruise conditions. In addition, the rarefied flow at the cruise altitude introduces low Reynolds number aerodynamic phenomena. For this reason, the airfoil has a tendency toward laminar separation bubbles and compressibility effects, which must be avoided. For the conventional configuration, a low pitching moment is required, but for the joined wing configuration it is not so crucial, since the moment can be balanced with the other wing. To accommodate fuel storage requirements, a maximum thickness ratio at 10% of the chord is preferred.

In general, supercritical airfoils conform to these criteria. A modification of Richard Eppler and Dan M. Somers' ES-989 was found to best suit the needs of all three configurations. A computer code authored by Mark Drela called XFOIL was used to modify and analyze the airfoil. The code was able to tailor the pressure distribution to reduce shocks and flow separation. The resulting pressure distribution is shown in Fig. 6. XFOIL is prone to errors in integration. This manifests itself in excessive peaks in the pressure distribution at the leading edge and a slightly higher Mach number distribution as compared to test data for similar airfoils. However, despite these potential problems the performance characteristics of the final modification compare well with published data for similar airfoils designed for low Reynolds number flight⁽⁶⁾.

Propeller Design

Initially, XFOIL's counterpart, XROTOR, was considered for the propeller design. Unfortunately, it was found that XROTOR's tendency to optimize the propeller blade loading produced excessive propeller root chords on the order of 50 ft. As a result, the propellers were hand designed. They were optimized to produce the lowest section drag coefficients. There were two main criteria for designing the propellers. The first and foremost was that the tip velocities can not exceed

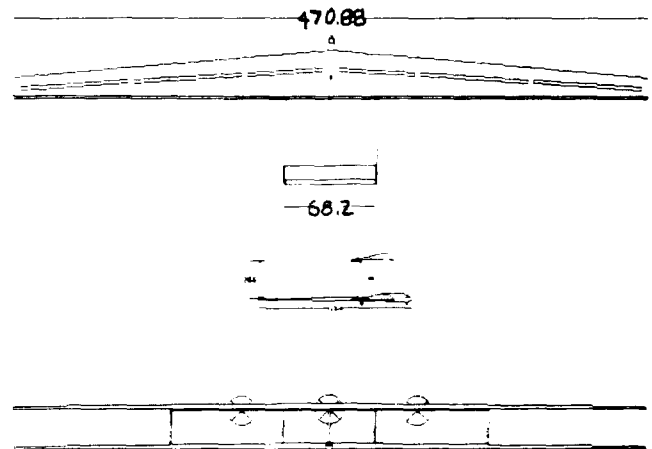


Fig. 5. Hi-Bi

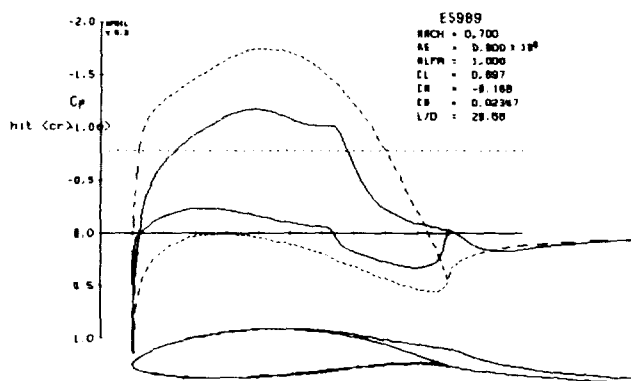


Fig. 6. XFoil

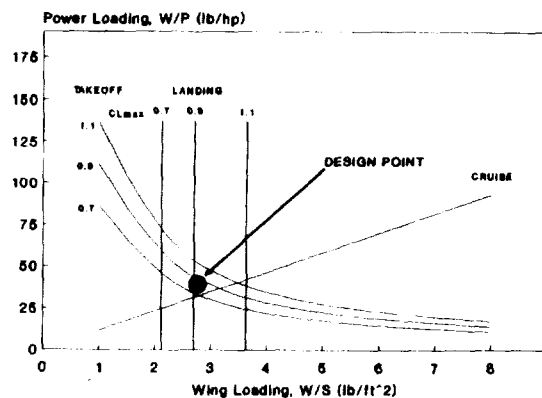


Fig. 8. Preliminary Sizing

the drag divergence Mach number. Since the air density is so low, the rpm and diameter need to be high.

Because of differences in ground-tip clearance, each configuration has a slightly different propeller design. The data for the six-blade, single-rotating propeller system that the *Icarus* chose, shown in Fig. 7, is a typical example.

Performance

From the sizing chart shown in Fig. 8, it is evident that in order to meet the constraints imposed by the Request for Proposal, the wing loading is limited to a range of approximately 2.8 to 3.2 psf⁽⁷⁾. With these wing loadings, takeoff is not a problem. The takeoff distances are rather short, and high lift devices in the form of flaps and slats are generally considered unnecessary. Figure 9 shows a typical take-off analysis chart.

The best rate of climb is chosen from the rate of climb versus velocity graph shown in Fig. 10. For the *Icarus* project, the time to climb was chosen to be 3.87 hr. This is shown

in Fig. 11. With this knowledge the fuel weight for climb is estimated to be 1330.75 lb. The time to climb for each configuration varied from 1.5 hr to 3.87 hr depending upon what parameter was optimized.

The flight envelope for all three aircraft is similar. The aircraft are constrained by the laminar stall velocity at lower speeds and by maximum power at higher speeds. Typically, high altitude aircraft have a very narrow flight envelope. These three designs are no exception as shown in Fig. 12.

Figure 13 shows the power required curve as a function of altitude. Figure 14 emphasizes the cruise condition. It is clear that the aircraft is flying within its power requirements at all times.

The landing characteristics are summarized in Fig. 15. The total landing distance is approximately 640 ft.

PROPULSION SYSTEM

The mission profile for this aircraft sets very stringent requirements for the propulsion system. The powerplant for

- Number of Blades 6
- Diameter 30 feet
- Revolutions 572.96 rpm
- Advance Ratio (J) 2.59
- Phi .7R (helix angle) 61 degrees
- Activity factor 1000 (166.67 per blade)
- Mach tip .85
- Propeller section Naca 16-series
- Cruise Overall Efficiency 75.7 %

Fig. 7. *Icarus* Propeller Data

- STALL VELOCITY = 44 ft./sec.
- C-L max = 1.3
- WING LOADING = 3.1
- THRUST LOADING = .25
- ROLLING COEFFICIENT = .03

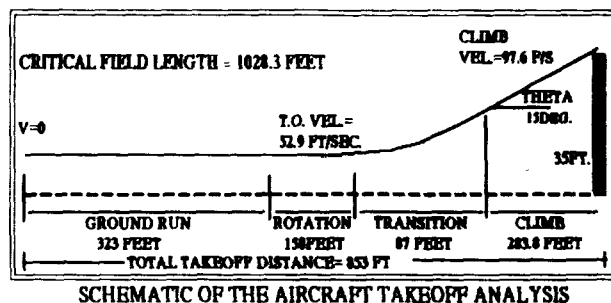


Fig. 9. Takeoff Analysis

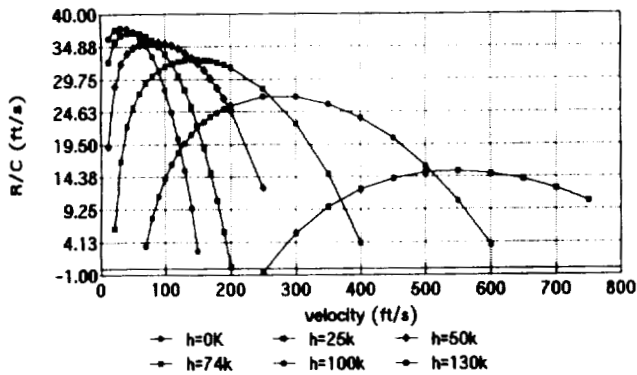


Fig. 10. Rate of Climb as A Function of Airspeed and Altitude

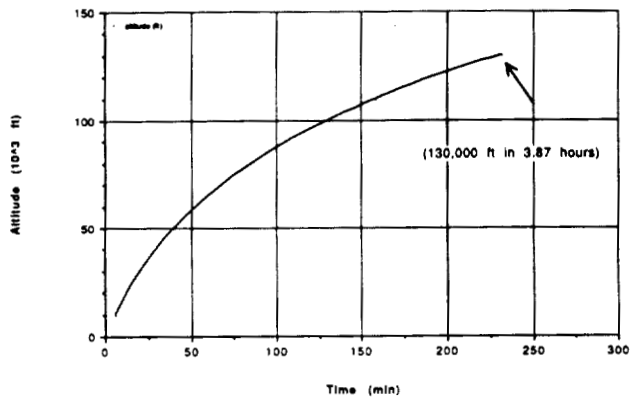


Fig. 11. Time to Climb

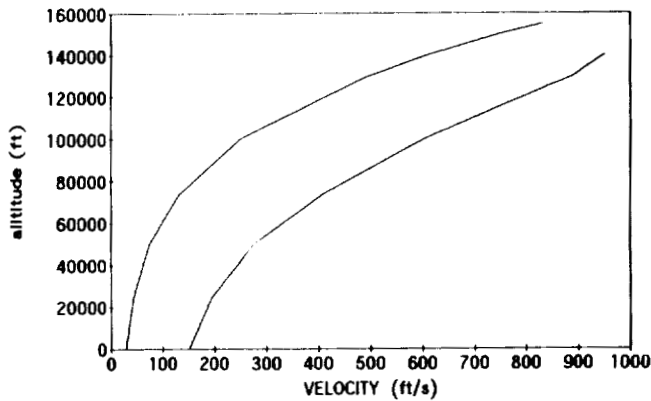


Fig. 12. Hi-Bi Flight Envelope

this aircraft must be able to operate with a low specific air consumption. The 6,000-mile range requirement necessitates that the powerplants have a low specific fuel consumption to reduce the amount and weight of fuel needed to complete the mission. Since the aircraft operates at subsonic velocities and very high altitudes, the aircraft's wings are large and heavy. This requires an engine that is capable of producing large amounts

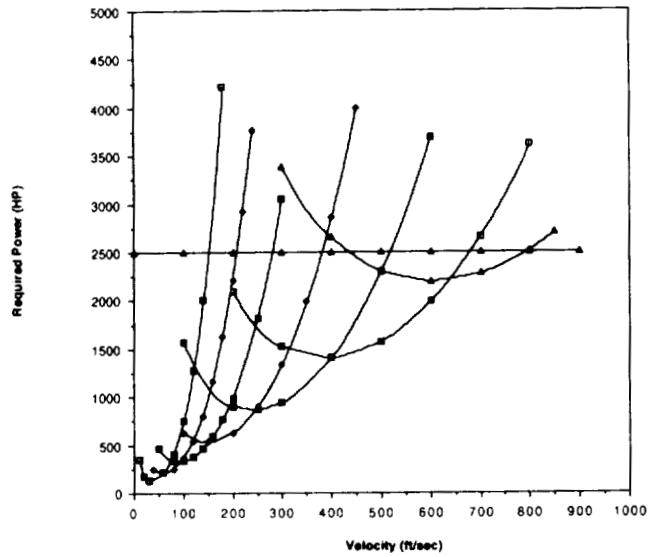


Fig. 13. Power Required Curve

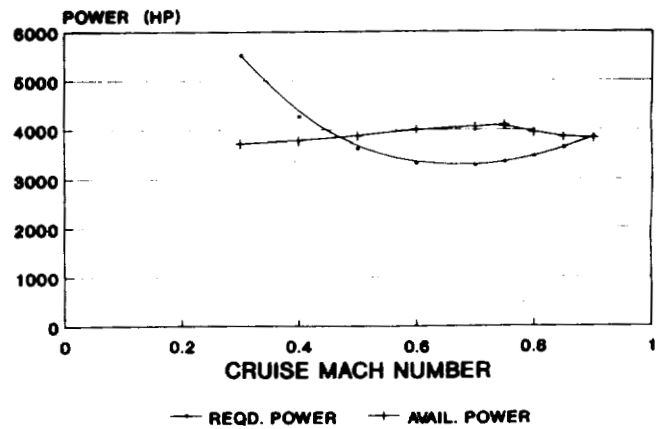


Fig. 14. Power Optimization

STALL VELOCITY = 33.85 ft./sec.
 C-L max. = 1.3
 WING LOADING = 1.92
 THRUST LOADING = .2
 BRAKING COEFFICIENT = .1

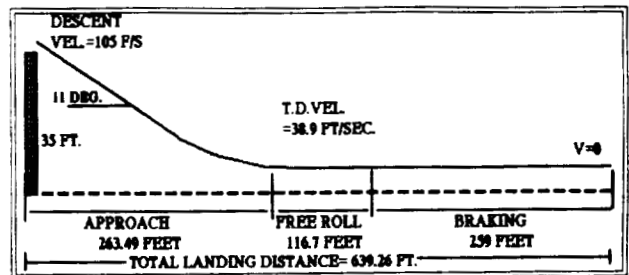


Fig. 15. Landing Analysis

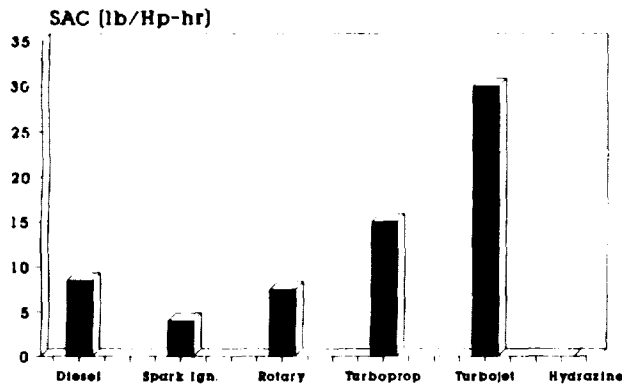


Fig. 16. Specific Air Consumption for Various Engine Types

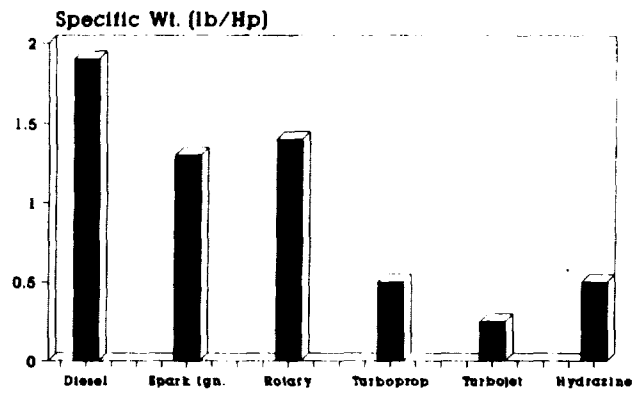


Fig. 18. Specific Weight for Various Engine Types



Fig. 17. Specific Fuel Consumption for Various Engine Types

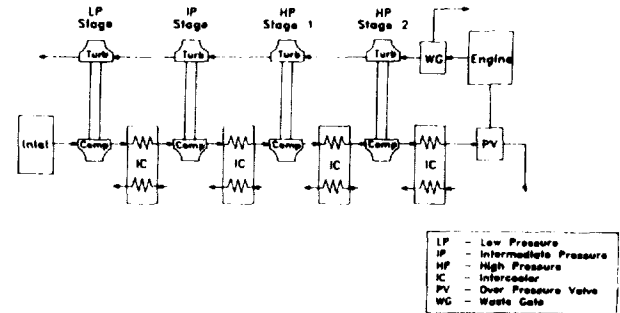


Fig. 19. Schematic of the Four Stage Turbocharging System

of power at altitude. The final requirements are to keep the engine and its systems as light as possible and to develop this system with current technology.

Powerplant Selection

The driving constraint in the engine selection process is the air consumption of the engine at altitude. The air consumption has to be low for the engine to produce power at altitude. Figure 16 shows typical specific air consumption values for the engines examined. The second constraint is the propulsion system weight, which has to be kept as low as possible. Figures 17 and 18 show typical specific fuel consumption and specific weight values for the engines examined.

The low density of air at altitude and subsonic cruise velocity combined with the engine's high specific air consumption make it impossible for any turbojet or turbofan engine to produce any meaningful thrust. Turboprops follow the same trend as the turbojet producing little power at altitude. The hydrazine engine is also an unlikely candidate since it has an extremely high specific fuel consumption and is extremely toxic.

Internal combustion engines have a relatively low specific air and fuel consumption. Nonetheless, they are unable to produce enough power at altitude without some type of turbocharging. The Lockheed HAARP Project designed a turbocharging system to operate with an internal combustion engine at an altitude of 100,000 ft. Of the three internal combustion engines examined, diesel, rotary, and spark ignition, the spark ignition engine had the best mix of s.a.c., s.f.c., and specific weight.

Other engine technologies such as microwave propulsion, laser propulsion, nuclear propulsion, and electrical propulsion were examined. Practical versions of these engines are not feasible with present day technology; therefore, there is no merit in further investigation. Thus, the spark ignition engine was selected as the best choice for the high altitude propulsion system.

Engine Configuration

The concept is based on an engine designed by Continental Teledyne Motors. It is a 500 hp engine designed to cruise at 100,000 ft with three stages of turbocharging.

Turbocharger Type	Radial
Over All Pressure Ratio	432:1
1st Stage Pressure Ratio	3:1
2nd Stage Pressure Ratio	4:1
3rd Stage Pressure Ratio	6:1
4th Stage Pressure Ratio	6:1
Maximum Mass Flow Rate	120.5 (lb/min)
Maximum Pressure	
Obtained at 130,000 ft.	1788 (psia)
Inlet Size	8.7 (ft²)
System Weight	900 (lb)

Fig. 20. Specifications of the Four Stage Turbocharger System

Engine Type	IC Spark Ignition
Number of Cylinders	8
Cylinder Arrangement	Horizontal Opposed
Bore and Stroke	5.25 in and 6.5 in
Displacement	1125 cu in
Compression Ratio	10:1
Width and Height, Engine	38 in and 29.25 in
Width and Height, Installed	41 in and 59.8 in
Length and Frontal Area, Engine	33.6 in and 7.7 sq ft
Length and Frontal Area, Inst.	69.6 in and 16.4 sq ft
Engine Weight	11177 lb
Total Weight, Installed	2077 lb
Weight/Horsepower	1.89 lb/Hp
Fuel Grade	100 LL
SFC, Cruise and Max Power	0.357 and 0.383 lb/Hp-hr
SAC, Cruise and Max Power	5.684 and 5.45 lb/Hp-hr
Cruise Power	962 Hp/3900 RPM @ 130k ft.
Max Power	1194.9 Hp/4250RPM @ S.L.
	1100 Hp/4250 RPM @ 130k ft.

Fig. 21. Performance Specifications, 960 hp Engine

The engine designed for this project uses four stages of turbocharging to allow it to operate at a higher altitude. Turbocharging was selected over supercharging so that the minimum engine power is required to run the engine. Figure 19 shows a schematic of the turbocharging system. Figure 20 tabulates the specifications of the system. The turbochargers are each composed of a radial compressor and a radial turbine. Each of the four turbocharger stages are intercooled with a crossflow air to air heat exchanger.

The high altitude engine is arranged in a horizontal opposed configuration to reduce frontal area and allow an aerodynamic cowling to be fitted around the engine. The block is composed of two forged aluminum alloy pieces bolted together vertically. The crank shaft is a forged steel, eight-throw, one-piece design and is supported by five journal bearings. The engine has eight, 10:1 compression ratio, aluminum alloy pistons displacing 1125 cu in.

The powerplant is modeled on a modified engine program⁽⁸⁾. Figure 21 shows the specifications and performance for the engine. Figure 22 gives the cycle information.

WEIGHTS AND STRUCTURES

Of the three configurations, the joined wing was found to be the most structurally sound. It was modeled on NASTRAN

with the joint at 70% of the semi-span and graphite/epoxy honeycomb sandwich spars. The composite fiber orientation is 0, 45, 90, -45, 0, -45, 90, 45, 0. The wing configuration, wing box, shear force and bending moment diagrams are shown in Fig. 23-25. The maximum deflection is 10.4 feet at the tip of the front wing. The total gross takeoff weight is 41,200 lb.

RELIABILITY

Figure 26 shows the results of a reliability analysis for the Global Sentry. All three aircraft yield comparable results. The graph indicates the probability of a component failing as a function of mission time. Generally, the mission would have to be aborted 43% of the time⁽¹⁰⁾.

CONCLUSIONS

The mission would be more likely to succeed if the Request for Proposal is modified. There is some doubt as to whether the aircraft necessary to meet the constraints can be built using present technology. This conclusion concurs with parallel analyses being conducted by NASA and Lockheed⁽¹⁹⁾.

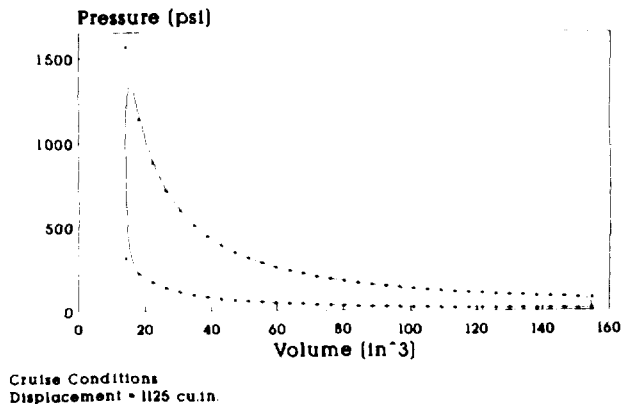


Fig. 22. Pressure vs. Volume Diagram, 960 hp Engine

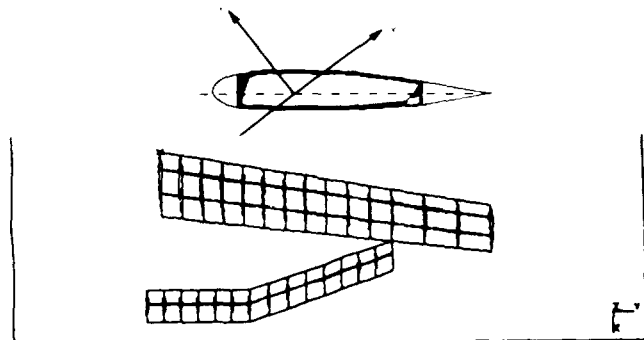


Fig. 23. Wing Box for Joined Wing

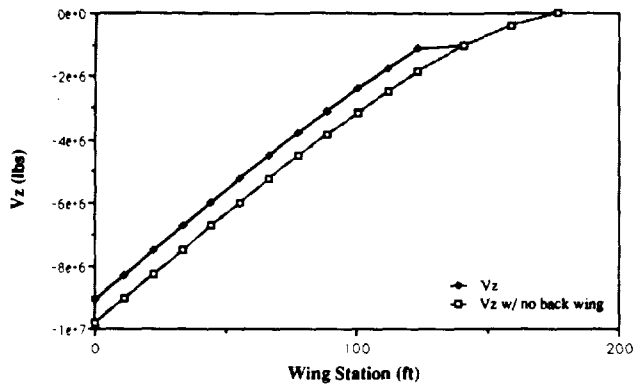


Fig. 24. Shear Force Diagram

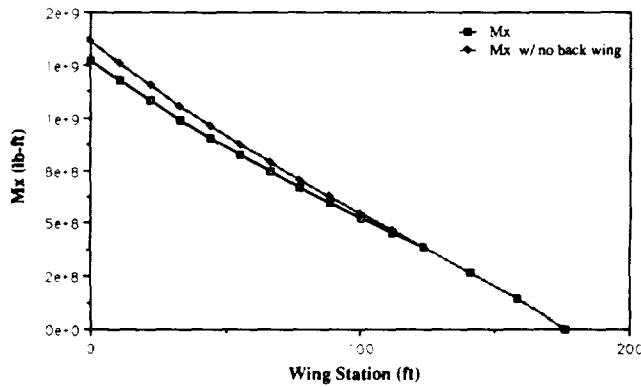


Fig. 25. Bending Moment Diagram

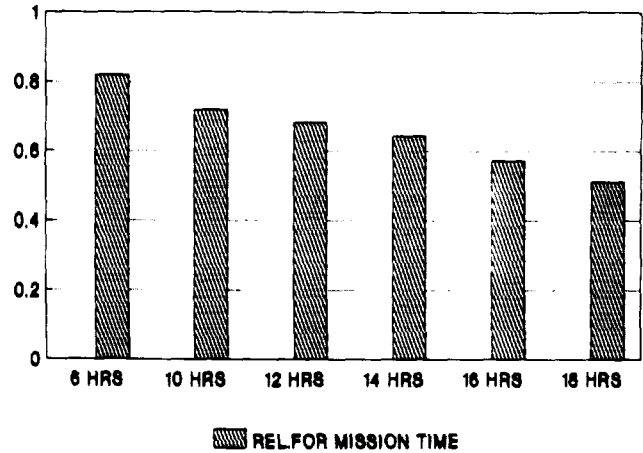


Fig. 26. Reliability Analysis of the *Global Sentry*

Lisa Alexandru, the group leaders. We would also like to acknowledge the hard work of the individual team members. Our NASA sponsor George Kidwell did much to keep us on track. Bob Antoniewicz and many others at NASA gave their time and energy to assist us. The USRA staff gave us the opportunity to participate in the program and then taught us how to make the most of the opportunity. The Lockheed Corporation as well as Hughes Aircraft provided us with insight into the problem from industry's standpoint. We were also privileged this year to have two wonderful instructors, Professor P.A. Lord and Professor C.F. Newberry.

REFERENCES

- 1 "Global Stratospheric Change," NASA Conference Publication 10041, July 15-16, 1989.
- 2 Memorandum dated July 13, 1988- To: Distribution, From: SSG/Chief, Atmospheric Experiments Branch, Subject: Very-High-Altitude Platform Aircraft Exploratory Studies, Reply to Attn of: SSG:245-5/136.
- 3 Cronin, Donald L. and Selberg, Bruce P., "Aerodynamic-Structural Study of Canard, Dual Wing and Conventional Wing Systems for General Aviation Applications," NASA CR- 172529, February, 1985.
- 4 Wolkovitch, J., "The Joined Wing: An Overview," *Journal of Aircraft*, Volume 23, Number 3, March 1986, p.161-178.
- 5 Drela, Mark, XFOIL and XROTOR software, MIT.
- 6 Miley, S.J., "A Catalog of Low Reynolds Number Airfoil Data for Wind Turbine Applications," Rockwell International Corporation, Subcontractor No. PFY12781-W, February 1982.
- 7 Roskam, Jan, *Airplane Design Part I: Preliminary Sizing of Airplanes*, Roskam Aviation and Engineering Corporation, Ottawa, Kansas, 1985.
- 8 Benson, R.S., and Whitehouse, N.D., *Internal Combustion Engines*, Pergamon Press Inc., New York, 1979.
- 9 "High Altitude Atmospheric Research Platform, Information Package," The Lockheed Corporation, Burbank, California, February 1990.
- 10 Myer, Peter, Hughes Aircraft Corporation.

Suggested modifications to the Request for Proposal are as follows:

1. Decrease the cruise altitude to 100,000 ft with possible zooms to 130,000 ft.
2. Split the mission into a 6,000-mile unmanned mission and a 6-hour manned mission.
3. Decrease the cruise Mach number to 0.6.

These modifications should act to decrease the span which in turn makes the aircraft manufacturable and increases structural integrity. The present spans, which range from 400 to 450 feet, render it impossible to land at most airports. It would be more reasonable to design for a 150-ft-wide runway with four foot-high obstacles located 20 ft off the runway. Furthermore, the reliability will increase with the decrease in mission time. The four-stage, turbocharged propulsion system could be brought down to three stages, which are generally considered possible. Some work has been done on a three-stage engine in recent years but none on the four-stage.

ACKNOWLEDGMENTS

The authors, Renee Anna Yazdo and David Moller, thank Chris Higa, Tai Kim, Hector Lopez, Michael Medici, and Mona-

P.4

THE CALIFORNIA CORRIDOR TRANSPORTATION SYSTEM: A DESIGN SUMMARY

N 9 1 - 1 8 1 6 3

CALIFORNIA POLYTECHNIC STATE UNIVERSITY, SAN LUIS OBISPO

INTRODUCTION

The systems approach to engineering design demands that any factor that may have some bearing on the project be identified, evaluated, and allowed to influence the design. The extent of this influence needs to be determined through a logical analysis of all competing factors. To this end a design group was assembled to find and research criteria relevant to the design of a California Corridor Transportation System. The efforts of this group included defining the problem, conducting a market analysis, formulation of a demand model, identification and evaluation of design drivers, and the systematic development of a solution. The results are summarized in the following pages.

The California Corridor contains a complex, expanding system of transportation, with requirements set by a wide variety of system users. The corridor is defined as a region where significant demand for transportation exists, along a line between major cities. This definition incorporates transportation demands both within and surrounding these cities. For the purposes of this study, California was selected, because of its intrinsic, generic qualities, and four of its major cities, Sacramento, San Francisco, Los Angeles, and San Diego, for the axis. The users are loosely categorized under the headings of commuters, transients, miscellaneous travelers, and freight, while the types of trips they take are categorized as capillary trips, intra-corridor, and inter-corridor.

The problems of the current system were analyzed and used to determine "design drivers," which were divided into the broad categories of cost, convenience, feasibility, environment, safety, and social impact. The relative importance of individual problems was addressed, resulting in a "hierarchy" of design drivers. Where possible, methods of evaluating the relative merit of proposed systems with respect to each driver were developed.

THE SYSTEM

The system envisioned by the design team is brought about through a controlled evolution of the present day system.

Beginning in the near future, a measured series of changes are proposed that will offer consistent improvements in the areas of each design driver, eventually bringing to the corridor in the year 2020 a transportation system that better serves the interests of the citizen.

This gradual evolution begins in the year 1995, with a ground transportation network of highly efficient jitneys and buses, offering near door-to-door service on a scheduled basis for metropolitan commuters. Both these vehicles are refined versions of existing technology, using clean-burning, com-

pressed natural gas for fuel, and following closed routes through neighborhoods and along reserved highway lanes. They interact with each other and with other forms of transportation through specially designed modeports, strategically located near the intersections of major freeways, in order to reduce the time and inconvenience of transferring from one vehicle to another.

Longer distance travelers are accommodated by a new aircraft, the QSTOL, which stands for Quiet, Short-Takeoff-and-Landing. The QSTOL carries 100 passengers, and is configured with 3 lifting surfaces and counterrotating propfans. It is specifically designed to minimize environmental impact, offering improvements in its noise signature and pollution levels, as well as enhanced abilities to serve smaller, more numerous airports. By utilizing these, air traffic congestion will be diffused over wider regions, providing larger margins of safety without raising community noise levels or building new airports.

Ten years later, in 2005, significant advances are made with the introduction of two innovative new public transportation modes. The first is a group of giant, hybrid aircraft, called CCATs for Corridor Combined Aircraft Transit System. These semi-buoyant helipsoids are turboprop-driven lifting bodies, reminiscent of airships and capable of carrying 600 passengers in luxury, comfort, and safety. These aircraft will fly closed routes, like great, airborne buses, over major cities and along the length of the corridor. Immense savings in time and cost are gained through the procedure of maintaining the aircraft in constant flight, boarding passengers and freight with tiltrotor shuttles that ferry between a boarding port on the upper surface of the aircraft and conveniently located ground stations. The ability of this fleet to transport vast numbers of people will be essential to meet the large increases in demand anticipated in the foreseeable future.

The Personal Rapid Transit (PRT), will introduce a quick, convenient, and cost effective method for everyday travelers to get around in congested downtown areas, where the jitney's effectiveness is reduced by the same congestion that makes automobiles so inefficient. PRTs are four-passenger, automated, electric rail coaches that travel along elevated monorails at speeds up to 40 mph. They offer the privacy and convenience of automobiles, high average speeds in congested areas, minimal noise and pollution, freedom from parking headaches, and the luxury of travel time spent as leisure.

Five years after this, in 2010, the completion of two Corridor Access Ports (CAPs) are anticipated. Situated near the extremities of the corridor, the CAPs are gigantic, high-capacity

airports, designed to eliminate congestion from the skies over larger cities by rerouting all transient and out-of-corridor traffic away from major metropolitan airports. They will be capable of expanding to meet the needs of the future without conflicting with the surrounding communities and will act as ports-of-entry for the entire southwest coast. The CAPs will be served by the QSTOL, the CCATS tiltrotor, long-distance conventional aircraft (CTOLs) going out of the corridor, and another new mode of mass transportation, the magnetically levitated train.

Expected to become fully operational at the same time as the CAPs, the mag-lev trains will carry 250 passengers at an average speed of 230 mph. They will follow a route along the inland valleys of the corridor that leads from the Los Angeles basin to the Bay Area. Fast, quiet, and clean, the mag-lev train is designed to offer a groundbased alternative to the CCAT and the QSTOL.

The final step in the implementation of the system is in 2020, when the Chicken Air Taxi service is expected to become fully operational. Beginning with a design philosophy of "a chicken in every pot, and a tiltrotor in every garage," (hence the name) the original concept was intended to eclipse the automobile in its level of personal service and independence. The design eventually evolved, through a series of compromises with the design drivers, into a single seat, fully automated, electric helicopter taxi that will take the discriminating traveler where he wants to go, when he wants to go there. Operating under the constant surveillance of an omnipotent air traffic control system based on the interaction between satellites and computers, the Chickens will operate between literally thousands of destinations throughout metropolitan areas.

Thus, over a period of 25 years, the corridor transportation system is seen to evolve from its present state of inefficiency and congestion to one of vastly improved service, satisfying the needs of travelers of all income levels, and covering a wide spectrum of destinations. The expense of implementing the system is rendered inconsequential when one compares the benefits of the invigorated economy this system will help to promote, to the losses, waste, and damage California will endure, should we choose to remain idle. Among the anticipated benefits are significant improvements in the quality of life and the environment, as well as increased personal liberty.

CONCLUSION

The approach taken in designing the California Transportation System is concerned with the needs of California. The solution addresses the demand for all levels of transportation, within, between, and out of major metropolitan areas. The solution deals with both the present demands and those anticipated in the future. It is an approach concerned with the "total picture" of transportation, and as such, it is a model for other transportation studies both in other regions and in the future.

Transportation is a dynamic enterprise, and must be assessed on a continuous, systemwide basis. It is emphasized that studies of transportation system integration, impact, and

evolution must be continued, and that the resulting solutions be designed and implemented in a macroscopic fashion. Only by applying a systems approach to transportation engineering can problems be solved without creating others.

ADDITIONAL PROJECTS

Phoenix

As a senior design project, the Hybrid Tandem Fan team was required to design a low-cost, export, short-takeoff, vertical-landing (STOVL) supersonic fighter. The specifications used were acquired from the 1989/1990 AIAA/General Dynamics Corporation Team Aircraft Design Competition's request for proposal. The Phoenix (Fig. 1) is our team's design answer to this proposal.

The propulsion system we have selected is the Hybrid Tandem Fan (HTF). The HTF is similar to conventional turbofan jet engines, but includes two separate compression fans. There are two modes in which the engine can operate; parallel and series. Parallel mode is used for takeoff, landing, and subsonic cruise. Series mode, which provides about 20% more thrust, is used for acceleration, supersonic flight and high-g maneuvers. The side and rear nozzles are all vectorable for vertical flight and combat maneuvers. The side and rear nozzles are all vectorable for vertical flight and combat maneuvers. The Phoenix can cruise at a maximum speed of Mach 1.5. It has a statically stable flight control system for lower cost and ease of maintainability.

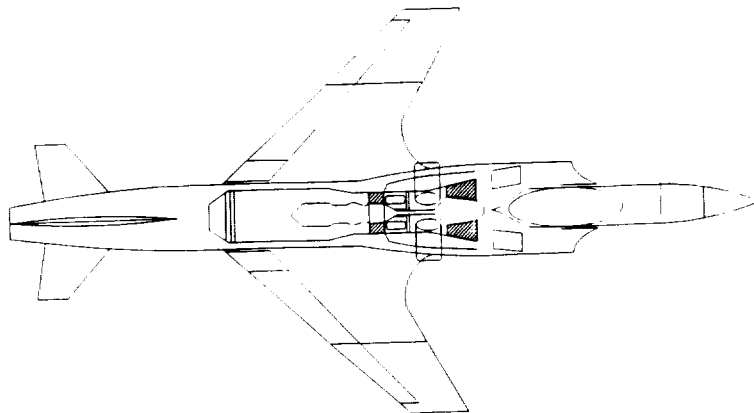
In our preliminary design, we are using conventional vertical and horizontal tails and a forward swept wing. We chose a forward swept wing (FSW) configuration because of its better performance in the transonic flight regime, higher lift coefficient, more effective ailerons, since a FSW stalls at the roots first, and reduced suckdown during vertical landing. However, there is a weight penalty with a forward swept wing due to structural divergence. The use of composites will help to lower the weight.

The Phoenix answers the need for a low cost, highly maneuverable, and extremely versatile airplane for export to less economically and technically advanced countries.

ASTOVL - Vectored Thrust Concept

The Ariel, a low cost, Advanced Short-Takeoff-Vertical landing (ASTOVL) supersonic fighter, is a proposal for the 1989/1990 AIAA/General Dynamics Corporation Team Aircraft Design Competition. The Ariel incorporates an advanced turbofan engine with three full-vectoring nozzles, two fore, with plenum-chamber burning, and one aft, to achieve the vertical thrust used in take-off/landing and increased maneuverability in combat. The intent of this design is to provide a low-cost, high-performance aircraft for export to countries without the means to build their own, and yet retain sufficient range, maneuverability, and weapons payload to be competitive in today's combat arena.

Figure 2 shows a three-view representation of the Ariel and provides some of its important geometric parameters. The maximum range, which compensates for ascent to and descent



	WING	VERTICAL TAIL	HORIZONTAL TAIL
Area (sq ft)	277.8	81	58.5
Span (ft)	31.2	9	12
MDC (ft)	9.8	8.9	4.69
Aspect Ratio	3.53	1.0	2.55
LE Sweep (deg)	-30	48.2	42
Taper Ratio	.35	.293	.369
Root Chord (ft)	13.2	13.82	6.4
Tip Chord (ft)	4.82	4.06	2.4
Thickness Ratio	.05	.04	.04
Dihedral (deg)	-2.35	80	8
Incidence (deg)	1.5	0	variable
Airfoil	(see sec 5.2)	0004	0004
Aileron Chord Ratio	0.3c	Rudder Chord Ratio	0.3c
Aileron Span Ratio	0.63 - 0.95c	Rudder Span Ratio	0.11 - 0.7c
Flap Chord Ratio	0.3c	Flap Span Ratio	0.17 - 0.62c
	EXTERIOR	COCKPIT	OVERALL
Length (ft)	80	9	80
Maximum Height (ft)	10.8	11.5	20.2
Maximum Width (ft)	8.4	3	31.2

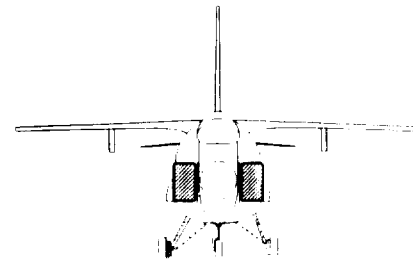
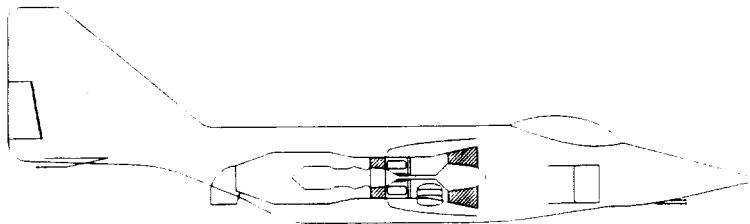


Fig. 1. The Phoenix

length	44.33 ft
span (wings deployed)	35.06 ft
span (wings stored)	20.50 ft
height (wings deployed)	13.77 ft
height (wings stored)	13.77 ft
takeoff weight (mission 1)	21,900 lbs
empty weight	14,592 lbs
inlet area (total)	10 ft ²

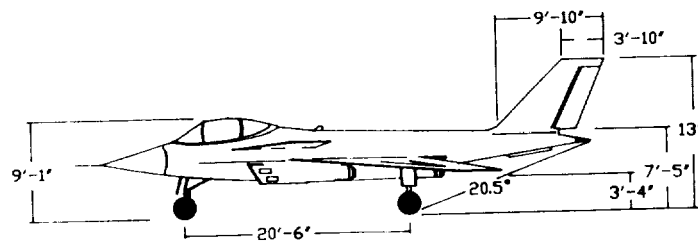
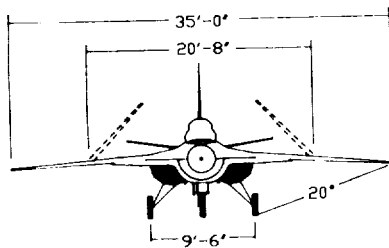
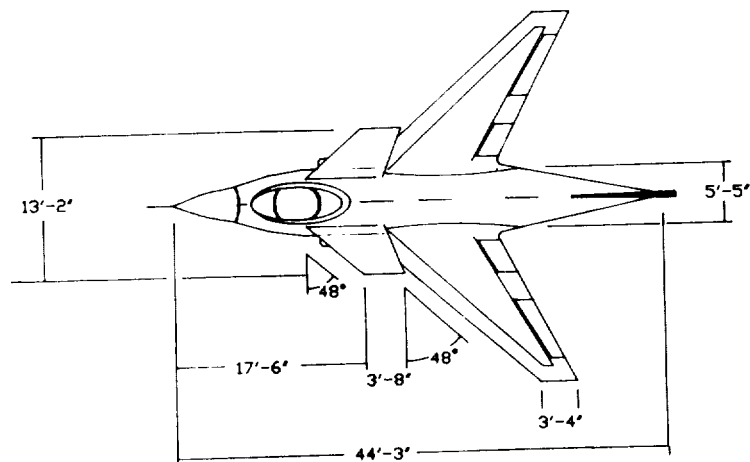


Fig. 2. Ariel

ORIGINAL PAGE IS
OF POOR QUALITY

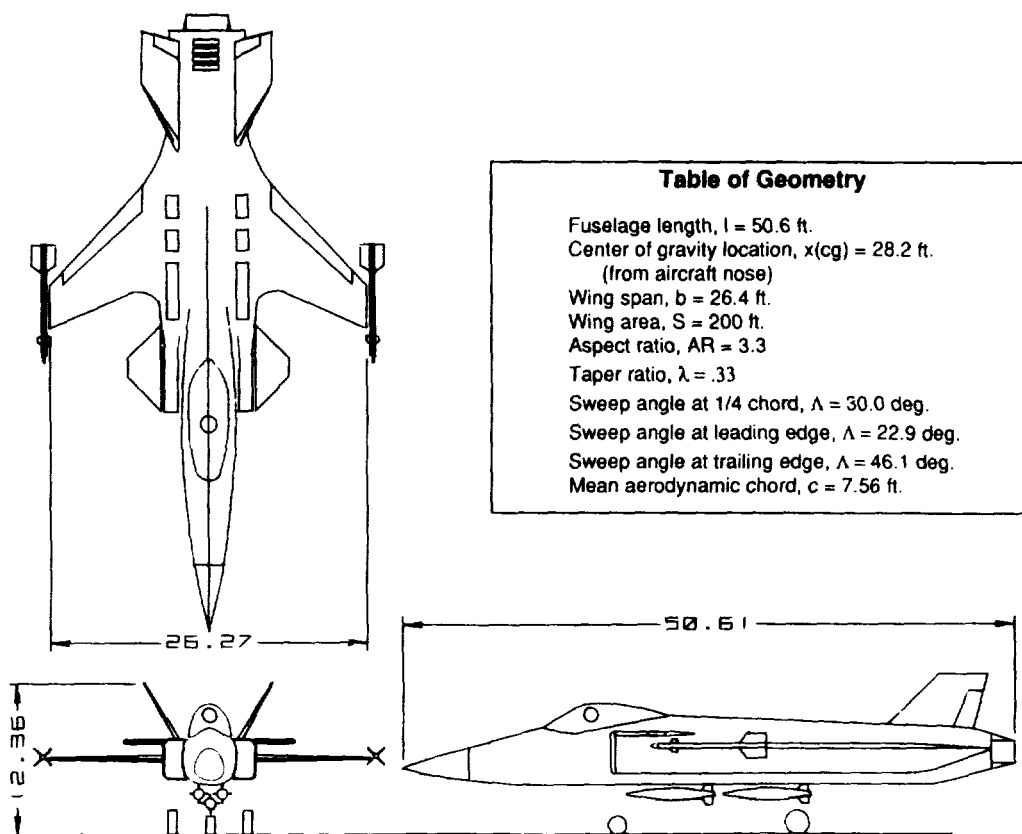


Fig. 3. Sea Hawk

from the best cruise altitude of 40,000 ft and best cruise Mach is 0.89. The Ariel was designed to take off in less than 300 feet and to land vertically; however, with a thrust to weight ratio of 1.26, a vertical takeoff is possible if necessary. The maximum shift in c.g. location during the Air-Ground mission is 1.2" which is only a 1.1% change in static stability, and during the Air Superiority mission the shift is 1.9", a static change 1.7%. These small changes in the static margin will not noticeably affect handling qualities throughout the range of flight.

The Ariel is designed to be a low-cost, high-performance military fighter. At under 15 million 1990 dollars, the Ariel is in the optimum price range for third world countries' military needs. At the same time, the Ariel has the capability to perform high-speed Air Superiority and Air-Ground missions. It can also sustain speeds of Mach 1.5 in both cruise and constant altitude turn. Another major advantage of Ariel is its STOVL capability. The Ariel has the ability to hover and land vertically, thereby reducing the amount of landing area required by the airplane.

Ejector Concept Design: "Sea Hawk"

The Sea Hawk is a low cost, export, supersonic short-takeoff and vertical-landing (STOVL) jet fighter (Fig. 3). The design was based on the AIAA Team Aircraft Design competition request for proposal.

The Sea Hawk is powered by an advanced concept turbofan engine similar to the Pratt and Whitney F100-220 turbofan. This provides a static sealevel thrust of 24,000 lbs giving the Sea Hawk a thrust loading at takeoff of 1.2. Vertical thrust is attained through the use of an ejector vertical thrust system similar to that on the E-7 experimental aircraft. The ejector system consists of a primary jet shrouded by a diffuser duct. The primary flow entrains a secondary flow which increases the mass flow rate through the diffuser and hence, increases the thrust of the ejector. Forward swept wings were utilized to decrease transonic and supersonic drag, provide sufficient stability, and give the agility needed for a fighter aircraft. The wings are strengthened by the use of composites and titanium. Agility is also improved through the use of a 2-D vectorable nozzle and through the use of forward canards, which are also used for trim. Twin, canted vertical tails are used for lateral-directional control. A reverse thruster and a reaction control system are used to aid maneuverability in the hover mode. These components combine to create a new advanced STOVL fighter at a low cost of approximately 16 million 1989 US dollars.

300 478
P. 4

O-THREE: A HIGH ALTITUDE, REMOTELY PILOTED VEHICLE

CASE WESTERN RESERVE UNIVERSITY N91-18164

INTRODUCTION

A conceptual design for a remotely piloted vehicle to be used for ozone research above 80,000 ft was developed as part of the one-semester NASA/USRA Aerospace Design course at Case Western Reserve University in Fall 1989.

The O-THREE design team chose as its mission requirements: a cruise altitude of 100,000 ft, a range of 1000 n.m., an endurance of 6 hr, a 1,000-lb payload, and a power to payload of 2 kW. These are based on the Boeing requirements for an ozone research vehicle. In addition, the vehicle should not be restricted to operation over any particular global location. Efforts were made to minimize atmospheric contamination that might increase the rate of ozone depletion and could cause discrepancies in data accuracy. Design was not limited to today's level of technology.

The design team was divided into four groups: Propulsion, Aerodynamics, Structures, and Stability and Control. Each group faced a unique design problem resulting from the unusual mission requirements. The Propulsion Group was concerned with the ability to operate at 100,000 ft where the density of air is 1/70th that of sea level. Because of the low dynamic pressure, the main Aerodynamic Group design goal was to find a high lift coefficient, low Reynolds number airfoil. The primary issue facing the Structures Group was to find strong, lightweight materials.

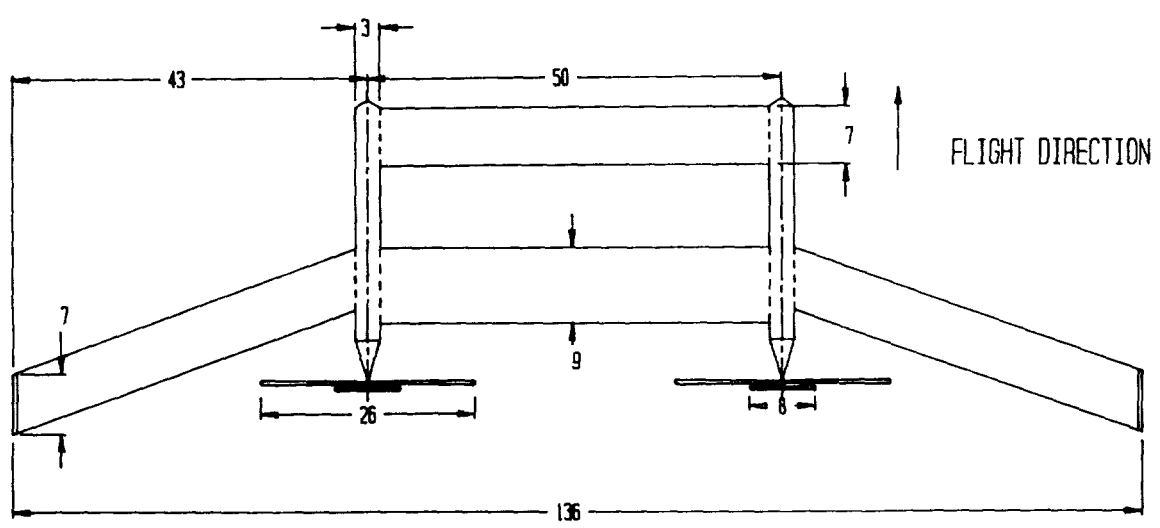
FINAL DESIGN

The final configuration can be found in Fig. 1. Specifications and weights are given in Tables 1 and 2, respectively. Performance estimates for cruise at altitude are listed in Table 3.

DISCUSSION

The Propulsion Group investigated possible propulsion devices and power sources to select a feasible propulsion system. Feasible was defined as a system capable of producing the required thrust at the working altitude. This was accomplished by a joint iterative process with the Aerodynamics Group.

From among the list of potential propulsion devices (turbofan, turboprop, turbojet, internal combustion engine, rocket, balloon, Stirling engine, electric motor) the electric motor was chosen for its high efficiency, low specific weight, and minimum environmental impact. The final airplane configuration necessitated the use of two motors, one per fuselage. Samarium-cobalt electric motors were selected. These motors use rare-earth permanent magnets to achieve efficiencies of 90-95% and lightweight composite materials for an expected specific weight of 0.57 lb/hp. Their brushless design eliminates the arcing problems associated with conventional motors operating in such a low-density atmosphere.



TOP VIEW

Fig. 1. Vehicle Configuration

ORIGINAL PAGE IS
OF POOR QUALITY

Table 1. O-THREE Specifications

Airfoil	LNV109A
Power plant	Solid oxide fuel cells
Engines	Samarium cobalt electric motors
Weight at takeoff	8198 lb
Weight at cruise	7853 lb
Weight empty	5558 lb
Wing span	136 ft
Wing area	1402 ft ²
Aspect ratio	17.6 ft
Distance between fuselages	50 ft
Fuselage diameter	3 ft
Fuselage length	30 ft
Small propeller diameter	8 ft
Large propeller diameter	26 ft
Canard	
Span	50 ft
Chord	7 ft
Area	350 ft ²
Max thickness	0.9 ft
Midsection wing	
Span	50 ft
Chord	9 ft
Area	450 ft ²
Max thickness	1.2 ft
Swept wing	
Span	43 ft
Chord	7 ft
Area	283 ft ²
Sweep angle	20°
Taper ratio	1.0

Table 2. O-THREE Weight Distribution, Cruise Conditions

	(lb)
Propulsion	
Fuel	
Oxygen (gaseous)	2040
Hydrogen (gaseous)	256
Electric motors (2)	400*
Fuel cells (12)	1000*
Electric converters (2)	100*
Large propellers (2)	200*
Small propellers (2)	100*
Structures	
Midsection wing	523
Swept wing (2)	909
Canard	438
Vertical stab/winglet (2)	100
Fuselage (2)	607
Other	
Landing gear (4)	120*
Payload	1000
Controls	60*
Total	7853

* Allocated weight

Table 3. Performance Characteristics

Takeoff velocity	44 mph
Endurance at cruise (100,000 ft)	6 hrs
Cruise velocity	0.55 Mach
Power required (cruise)	250 kW
Lift-to-drag ratio (cruise)	25
Range	1930 n.m.
Glide angle	2.3°

The possible power sources were constrained by the choice of propulsion device to those that produced electric power. From the list of potential power sources (solar, hydrocarbon fuels, laser-plasma, microwave, nuclear, battery, fuel cells) fuel cells were chosen, since cutting edge fuel cell technology provided the highest specific power, the best competitive overall efficiency, and the most compact package of any power source investigated.

The AIRResearch Division of the Garrett Corporation (Torrance, CA) has developed a monolithic solid-oxide fuel cell design that utilizes a ceramic honeycomb structure to provide a compact package. Garrett's goal for the 1990s is a 9-in × 9-in cross-section producing an output of 67 hp. The fuel cell's specific power is about 0.37 hp/lb. This is 4.5 times greater than the specific power for a diesel generator and 7.5 times greater than that of a conventional fuel cell. Fuel cells tested have demonstrated a 60-70% efficiency. The only product generated by the reaction is water. This solves the concern over polluting the atmosphere. Argonne National Laboratories has operated cells for up to 700 hr without any noticeable degradation. Finally, the fuel cells are modular so that units can be stacked to increase power output, while the monolithic design provides a strong structure and the ability to automatically seal at the edges.

The final propulsion system configuration would consist of the following:

1. Monolithic solid-oxide fuel cells utilizing hydrogen and oxygen as fuel and oxidizer, respectively;
2. Power conversion units to transform the fuel cell electrical output to an acceptable motor electrical input;
3. Two samarium-cobalt permanent magnet electric motors;
4. Reduction gear box to match each motor with the necessary propeller speeds;
5. Two pairs of pusher propellers, one size for takeoff and the other for cruise.

Aerodynamics

Subsonic flight at 100,000 ft posed several unique aerodynamic problems.

Airfoil selection. Low dynamic pressure is the consequence of cruising at 100,000 ft near the minimum power required condition. Based on preliminary estimates, chord Reynolds numbers were expected to range between 200,000 and 600,000. Therefore, a broad search of the technical literature on low Reynolds number airfoils was conducted. The criteria used for selecting an airfoil were: (1) high lift coefficient, $C_L > 1$; (2) predictable performance at Reynolds numbers between 200,000 and 600,000; and (3) minimum thickness-to-chord ratio. A high lift coefficient was sought to reduce the wing area and flight speed. The second criterion was established to eliminate any airfoil displaying lift hysteresis at the cruise Reynolds numbers. In general, lift hysteresis was a concern only at Reynolds numbers below 375,000. Minimum thickness-to-chord ratio was desired to reduce weight. The Liebeck airfoil, LNV109A, was one that met all three conditions. Maximum performance for this airfoil occurred for Reynolds numbers greater than 400,000. The characteristics of the LNV109A can be found in Fig. 2. The operating lift coefficient was chosen to be 1.2 at an angle of attack of 8°.

AIRFOIL CHARACTERISTICS

Airfoil: LNV109A
 Designers: R.H. Liebeck and P. P. Comacho
 Douglas Aircraft Company

(t/c) max = 13%
 Location of (t/c) max = 0.25c
 Design Re = 400,000
 $0.5 < C_L < 1.5$
 $C_{L \text{ stall}} = 1.8$
 $\alpha_{\text{stall}} = 14^\circ$
 $C_m = -0.05$

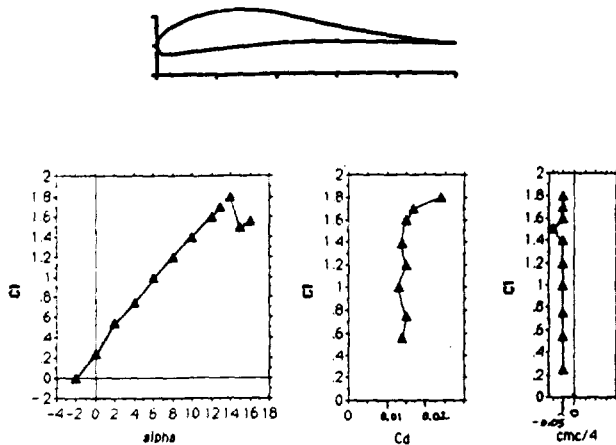


Fig. 2. Airfoil Characteristics

Configuration. The twin fuselage configuration was chosen primarily for structural reasons. In order to lift approximately 8000 lb with an operating lift coefficient of 1.2, 1402 ft² of wing area was needed. This wing area is divided into four sections: a canard, a main wing midsection, and two swept wings. Because performance degradation occurs for Reynolds numbers below 375,000, chordlengths were chosen to maintain chord Reynolds numbers of 400,000 or greater. The Mach number at cruise is 0.55.

The outboard wings were swept 20° in order to keep the wingtips as far aft of the center of gravity as possible since the vertical stabilizers would be mounted there. Pusher-props were used to eliminate the detrimental effects of propwash over the main lifting surfaces.

Drag power required estimation. The BASIC Aircraft Performance Analysis program developed by Kern International was used to predict the drag of the entire airplane. Modifications were made to the program's atmosphere subroutines using the equations given by the 1976 U.S. Standard Atmosphere. Also, because the Kern program could accept only conventional designs, O-THREE was modeled as a sailplane with a wingspan of 136 ft and a total wing area of 1402 ft². From this, a new aspect ratio and chord length were calculated. Secondly, a single fuselage equivalent of the twin fuselage arrangement was obtained by keeping the wetted area and the front area constant.

The parasite drag coefficient at cruise is 0.0156. This is probably a conservative estimate of the drag coefficients because the skin friction coefficient was evaluated for turbulent flow. The effects of sweeping the two outboard wings were also not taken into consideration and would act to reduce drag.

The power required for level, unaccelerated flight at 100,000 ft at $M = 0.55$ is about 250 kW. This is close to the minimum power required condition.

Structures

The structural analysis of O-THREE was conducted for cruise conditions at 100,000 ft. The structural design process began when the geometry of the plane (Fig. 1) and an estimation of the weight (8000 lb) were determined.

Using the initial weight estimate of 8000 lb and a wing area of 1402 ft², a wing loading of 5.71 lb/ft² was calculated. The wing weight was estimated at 1.3 lb/ft² from a Lockheed technical report that used lightweight composites. The structural forces and moments were obtained by integrating over strips in a spanwise direction. The net force was the difference between the lifting force and the weight. The initial assumption was that every part of the wing produced ideal lift.

The main spar of the swept wings was modeled as a cantilever beam. The midsection wing and canard were beams fixed at both ends by the fuselage. A wing loading of three times that of cruise or 17.12 lb/ft² was used in the calculations.

Two types of spar geometries were examined, a shear web and a circular tube. The circular tube was chosen for its potential to store fuel in the center. The midsection spar contains enough empty volume to carry 45.6 ft³ of gaseous hydrogen at 1 atm, and the canard spar can hold 22.8 ft³ of gaseous oxygen. This is the fuel needed for a 6-hr endurance.

The material chosen for the spar was a graphite (50%) epoxy composite. The estimated yield strength was 110,000 lb which was used for σ_{allow} . This material was chosen for its strength-to-weight ratio, its superior fatigue properties, and corrosion resistance as compared with typical aircraft materials. The spars can be manufactured using an autoclave.

The maximum deflection of these spars under a wing loading of 17.12 lb/ft² was calculated using the same beam models. The maximum deflection for the tips of the swept wing was 70.6 in. This includes a point force of 50 lb hanging on the tip due to the vertical stabilizer/winglet. The maximum deflection of the midsection wing and the canard is 8.2 in and 8.9 in, respectively. This maximum occurs at the center of the wing. Time has not permitted the iteration of these calculations for cases when the spars are fueled up.

The ribs are formed of rigid polyurethane (Pur) foam, 3/4-in thick, and wrapped in 1/32-in Kevlar 49 (K49). The ribs form the shape of the LNV109A airfoil. The compressive strength of the foam combined with the tensile strength of the K49 make a strong sandwiched composite.

The ribs were held to the spars in two different ways. On the midsection wing, spar caps were placed on each side of the rib and adhere to the rib and spar. On the swept wings and canard the spar spacers were adhered between the spar and the ribs.

Table 4. Structural Specifications

Item	Material	Weight	Dimensions
1. Midsection Wing			
a. Spar	GR/EP	167 lb	Ro = 6.625, Ri = 6.5 in L = 50 ft
b. Ribs (25)	Pur/K49	84 lb	T = .75 in W = .5 in
c. Skin	GR/EP	219 lb	T = 1/32 in
d. Trailing edge	Pur/EP	51 lb	L = 50 ft, W = 6.4 in T = airfoil shape
e. Spar caps (50)	GR/EP	3 lb	L = 4 in, W = .5 in
2. Canard			
a. Spar	GR/EP	119 lb	Ro = 4.725, Ri = 4.6 in L = 50ft
b. Ribs (25)	Pur/K49	65 lb	(Same as 1.b)
c. Skin	GR/EP	170 lb	(Same as 1.c)
d. Trailing edge	Pur/K49	82 lb	L = 50 ft, W = 2.25 in T = airfoil shape
e. Spacers (25)	GR/EP	2 lb	(Same as 1.e)
3. Swept wings (2)			
a. Spars	GR/EP	408 lb	Ro = 4.5, Ri = 4.25 in L = 45.7 ft
b. Ribs (50)	Pur/K49	130 lb	(Same as 1.b)
c. Skin	GR/EP	293 lb	(Same as 1.c)
d. Trailing edges	Pur/K49	75 lb	L = 45.7 ft, W = 2.25 in T = airfoil shape
e. Spacers (50)	GR/EP	3 lb	(Same as 1.e)
4. Fuselage (2)			
a. Bulkheads (20)	GR/EP	231 lb	W = 1, T = 1.5 in
b. Stringers (16)	Pur/K49	239 lb	W = 2, T = .75 in L = 30 ft
c. Skin	GR/EP	137 lb	(Same as 1.c)
Total		2478 lb	

The trailing edges of all the wings were also constructed using a Pur core wrapped in K49. This piece was fastened onto the end of the ribs with adhesive. The skin for all the wings and the fuselage are graphite epoxy face sheets of 1/32 in. The fuselage consisted of graphite epoxy bulkheads with polyurethane Kevlar sandwiched stringers.

All the structural data can be found in Table 4. No consideration was made for twist about the spar due to the pressure distribution over the wing. The next iteration in this ongoing design process will be to replace the estimated wing weight per area (1.3 lb/ft²) with the results of this first analysis. The exact configuration of the control surfaces and landing gear also needs to be completed.

Stability and Control

Static longitudinal stability. O-THREE utilizes a long-coupled canard in that the forward plane is placed at an appreciable distance in front of the main wing. Since O-THREE is an unconventional design, several simplifying approximations were made. The main wing was modeled as a rectangular wing even though the two outboard wings were swept 20°. Dimensions of the rectangular main wing model are: chordlength of 7.7 ft and a wingspan of 136 ft. The maximum lift coefficients, assumed at both takeoff and cruise, of all lifting surfaces was 1.2. The aerodynamic center was calculated to be 6.34 ft behind the leading edge of the main wing midsection. The center of gravity was computed to travel from 4.55 ft in front of the main wing leading edge at the beginning of cruise, to 0.51 ft in front of the main wing leading edge when the fuel is depleted. The neutral point moves correspondingly from 2.33 ft behind the main wing leading edge to 0.9 ft behind the main wing leading edge. O-THREE did meet the criteria for static longitudinal stability with static margins for takeoff and cruise calculated to be 86% and 16%, respectively. Static directional and dynamic stability analyses were not completed because of time constraints.

It is suggested that pitch control be achieved by flaps attached to the main wing midsection. Roll would be controlled by spoilers located on the outboard swept wings, and yaw control by two rudders attached to the vertical stabilizers on the wingtips. Additional yaw control could be achieved by varying the propeller speeds.

44-05
 25-7-11
 P.10

PRELIMINARY DESIGN OF A SUPERSONIC SHORT-TAKEOFF AND VERTICAL-LANDING (STOVL) FIGHTER AIRCRAFT

UNIVERSITY OF KANSAS, LAWRENCE **N91-18165**

A preliminary design study of a supersonic short-takeoff and vertical-landing (STOVL) fighter is presented. Three configurations (a lift + lift/cruise concept, a hybrid fan-vectored thrust concept, and a mixed-flow-vectored thrust concept) were initially investigated with one configuration selected for further design analysis. The selected configuration (the lift + lift/cruise concept) was successfully integrated to accommodate the powered-lift short takeoff and vertical landing requirements as well as the demanding supersonic cruise and point performance requirements. A supersonic fighter aircraft with a short takeoff and vertical landing capability using the lift + lift/cruise engine concept seems a viable option for the next generation fighter.

NOMENCLATURE

BAI	Battlefield Air Interdiction
CA	Counter Air
c.g.	Center of Gravity
FS	Fuselage Station
HFVT	Hybrid Fan-Vectored Thrust
LIFT	Lift + Lift/Cruise
MFVT	Mixed-Flow-Vectored Thrust
n.m.	Nautical Mile
STOVL	Short Takeoff, Vertical Landing

PHASE I AIRCRAFT STUDY

Mission Profiles and Specification

The mission profiles for the Phase I study (Figs. 1 and 2) show the design defensive counter air superiority mission and the fallout battlefield air interdiction mission. The mission specification (Table 1) shows the armament carried for each mission and the point performance requirements.

INTRODUCTION

The survivability of long, hard-surface runways at Air Force Main Operating Bases is fundamental to the current operations of the Air Force Tactical Air Command. Without the use of these runways, the effectiveness of the Tactical Air Command is severely degraded⁽¹⁾. One possible solution to this runway denial situation is to include a short takeoff and vertical landing capability in a supersonic fighter/attack vehicle. An aircraft with this capability is envisioned as the next multirole fighter to replace the F-16 in the 2000-2010 time period⁽²⁾.

Design teams at the University of Kansas, through the sponsorship of the NASA/USRA Advanced Design Program, have completed a conceptual design study of a supersonic STOVL aircraft. Phase I of the study began with a brief historical survey of powered-lift vehicles followed by a technology assessment of the latest supersonic STOVL engine cycles under consideration by industry and government in the U.S. and U.K. A survey of operational fighter/attack aircraft and the modern battlefield scenario was completed to develop, respectively, the performance requirements and mission profiles for the study^(3,4). Three aircraft were considered for initial investigations⁽⁵⁻⁷⁾. They employed the following engine cycles: a lift + lift/cruise cycle, a hybrid fan-vectored thrust cycle, and a mixed-flow-vectored thrust cycle. Phase II of the study consisted of comparing the three configurations of Phase I and selecting one configuration for further design analysis. This paper (1) briefly presents the results of the Phase I aircraft study; (2) discusses the considerations for the selection of and modifications made for the Phase II aircraft; and (3) presents the design analysis performed on the Phase II aircraft.

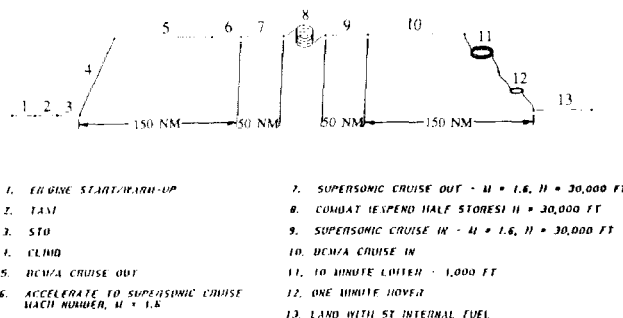


Fig. 1. Counter Air Mission Profile

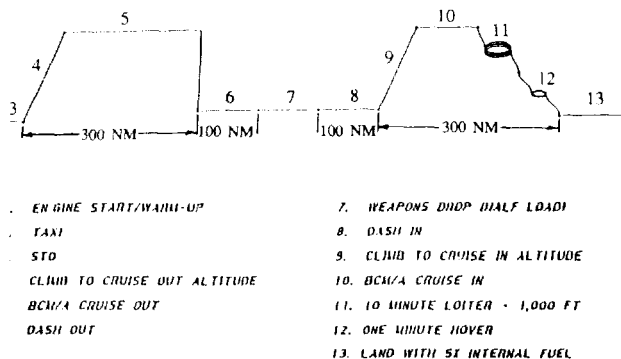


Fig. 2. Battlefield Air Interdiction Mission Profile

ORIGINAL PAGE IS
 OF POOR QUALITY

Table 1. Mission Specifications

Crew:	One Pilot (225 lb)
Armament:	One internal M61A1 Vulcan cannon and 400 rounds of 20 mm ammo
Payload:	Counter Air Two ASRAAMs (stored internally) and two AMRAAMs (stored internally) Battlefield Air Interdiction Six Mk 82 Bombs (externally stored), or Six AGM-65 Mavericks (externally stored) Four AGM-88A HARMs (externally stored)
Performance:	
Performance Characteristic	Value
Time to Climb	40K in 2 min
1 g Specific Excess Energy	
(2A) 30K Mach 0.9	500 ft/sec
(2B) 10K Mach 0.9	1000 ft/sec
Sustained Turn Rate	
(3A) Mach 0.8/15K ft	15°/sec
(3B) Mach 0.9/30K ft	9°/sec
(3C) Mach 1.2/30K ft	8°/sec
(3D) Mach 0.9/15K ft	6.5 g
(3E) Mach 1.6/30K ft	4.5 g
Acceleration	
(4A) 30K ft Mach 0.9 to Mach 1.6	70 sec
(4B) Mach 0.5 to Mach 1.4	80 sec
(4C) 10K ft Mach 0.3 to Mach 0.9	22 sec
Landing Distance	
Without Chute	2200 ft
Groundrun: Takeoff - 300 ft, Vertical Landing	
Certification: Military	

Lift + Lift/Cruise Configuration Description

The LIFT configuration consists of a conventional wing and fuselage with a canard and strake. Figure 3 shows a three-view drawing of the LIFT configuration. The mid-fuselage-mounted wing, using full-span leading and trailing edge surfaces to provide for high lift and lateral control, incorporates a strake allowing for delayed wing stall at high angles of attack. The empennage consists of an all-moving canard and a single vertical fin using a two-surface rudder to enhance redundancy against battle damage. Considerations for the fuselage layout included internal packing of the counter air mission weapons and lift engine, as well as shaping for reduced wave drag.

The engine cycle of the LIFT configuration consists of a 28:1 thrust-to-weight lift engine just aft of the cockpit and a conventionally located lift/cruise engine. The lift/cruise engine employs a single ventral nozzle that opens aft of the last turbine stage. The afterburner flame holders double as turning vanes for the flow. Flow turning is also enhanced by a main nozzle capable of choking down its exit area. A three-axis reaction control system is required for hover and transition control. An auxiliary inlet on the upper surface of the fuselage is opened to reduce hot gas reingestion and foreign-object damage.

Hybrid Fan-Vectored Thrust Configuration Description

The HFVT configuration consists of a twin boom, high forward swept wing, and an aft swept inverted vertical tail.

Figure 4 shows a three-view drawing of the HFVT configuration. The combined vertical thrust of the two forward posts and single aft post of the HFVT engine cycle (described

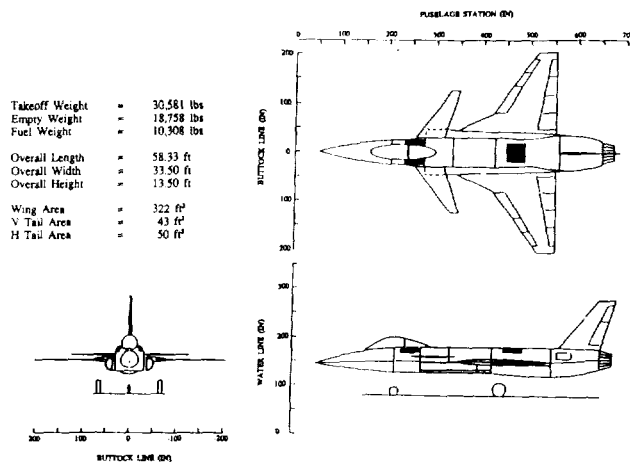


Fig. 3. Lift + Lift Cruise Configuration Three View

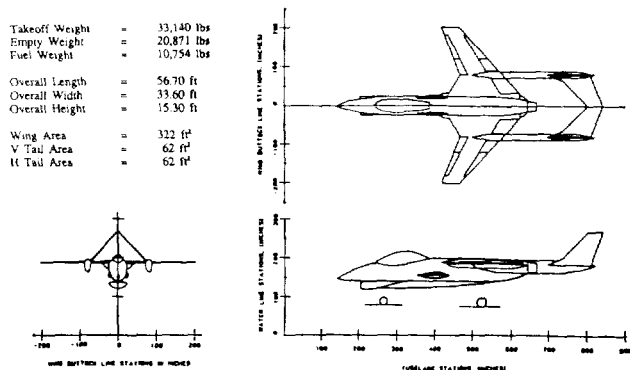


Fig. 4. Hybrid Fan-Vectored Thrust Configuration Three View

below) acts at approximately one-third of the engine length. The resulting hover balance lends itself to the engine being driven forward to the middle of the aircraft, thus the twin boom configuration. The forward swept wing and inverted vertical tail are aimed to achieve structural synergism. The wing rear main spar is synergistic with the main engine mount and the inverted vertical tail acts as an efficient structural tie between the booms.

The HFVT engine cycle consists of a mixed augmented turbofan driving a remote front fan through a shaft. The front fan is connected to the rest of the engine by an interduct. At the forward end of the interduct is a diverter valve to allow two modes of operation for the engine: (1) Parallel—the front fan flow is diverted to a plenum and fed to two unaugmented, fully vectoring front nozzles. The core air is fed by a ventral auxiliary inlet behind the cockpit. (2) Series—the auxiliary inlet and front nozzles are shut off and the front fan air passes through the valve to the rest of the engine for maximum power. The parallel mode is used for the powered lift requirements and subsonic cruise where the higher bypass

ratio may improve the specific fuel consumption. The series mode is for point performance and supersonic flight where the front nozzles are faired in by a retractable ramp to minimize drag. A two-axis reaction control system is required as the front nozzles differentially vector to provide lateral control.

Mixed-Flow-Vectored Thrust Configuration Description

The MFVT configuration consists of a high aft swept wing, twin vertical tails, and all moving horizontal stabilizers. Figure 5 shows a three-view of the MFVT configuration. The large flow transfer ducts required for the MFVT engine cycle (described below) dictated the middle and aft fuselage width, while the cockpit and radar volume sized the forward fuselage. Fuel volume and internal bays for the medium-range missiles sized the fuselage length. Volume beneath the engine inlet and ducts was dedicated to the main landing gear and internal short-range missiles. A conventional aft swept wing was selected for simple construction with adequate performance. The strake provides improved aircraft lift and maintains adequate airflow to the bifurcated inlet at high angles of attack.

The MFVT engine cycle consists of a single cruise engine with a block-and-turn main nozzle and two flow transfer ducts. In powered-lift operation, the mixed turbine and bypass flow, completely blocked by the main nozzle, is transferred forward to the c.g. of the aircraft and exhausted. The two-variable area, vectoring exhaust nozzles, along with the 5%-thrust, longitudinal trim valve, provide complete control in hover, eliminating the need for a reaction control system. In up-and-away flight, the forward exhaust nozzles are stowed and the transfer ducts are closed off to allow for conventional operation.

PHASE II AIRCRAFT STUDY

Selection of Phase II Aircraft

The LIFT configuration was selected for the Phase II aircraft study based on a comparison of the Phase I aircraft using the following considerations: (1) aircraft weight and cost, (2) aircraft area rule distribution, and (3) aircraft components required for STOVL capability.

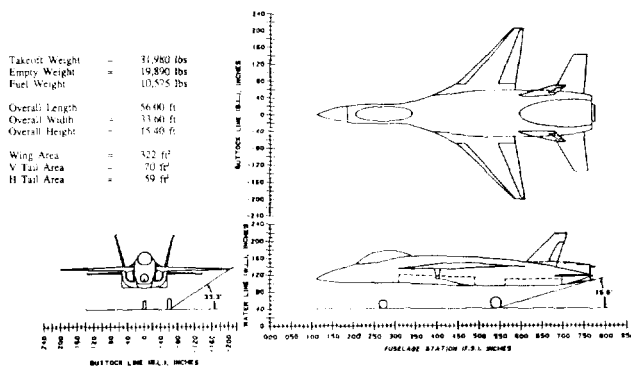


Fig. 5. Mixed-Flow-Vectored Thrust Configuration Three View

The LIFT configuration was 1400 lb lighter than the MFVT and 2400 lb lighter than the HFVT. The added cost of the lift engine negated its lighter weight as the cost of the three configurations was similar.

The more conventional internal packaging of the LIFT configuration compared to the other concepts allowed it a favorable area rule distribution. The HFVT configuration area distribution suffered due to the large loss of cross-sectional area in the boom region. The large transfer ducts required by the MFVT cycle increased the mid and aft fuselage width resulting in a large gap in cross-sectional area between the canopy and mid fuselage.

The component weights and volumes required for the short takeoff and vertical landing capability of each configuration were estimated. The results are shown in Table 2. The HFVT configuration suffers the most from the STOVL equipment for two reasons. First, the engine components required for flow shifting are heavy and require a large volume (the annular inverter valve and interduct). Second, the engine thrust split requires a mid-aircraft-mounted engine and thus some sort of boom configuration. The LIFT and MFVT configurations have similar weight penalties but the MFVT has a larger volume penalty due to the transfer ducts.

Modifications for the Phase II Study

The lessons learned in Phase I were adapted to the study plan of Phase II. Modifications were made regarding (1) the mission profiles and specifications and (2) the overall configuration of the lift + lift/cruise aircraft.

The fuel fractions (fuel weight/takeoff weight) for the Phase I aircraft were unrealistically high⁽⁸⁾. The design CA mission was scaled down to a 100-n.m. subsonic cruise with a 50-n.m. supersonic cruise. The fallout BAI mission was scaled to a 200-n.m. subsonic high-level cruise with a 80-n.m. low-level dash.

Table 2. Weights and Volumes for Components Required for STOVL Capability

	Volume (ft ³)	Weight (lb)
Lift		
Lift Engine	21	647
Ventral Nozzle and Turning Vanes	•	300
RCS System	8	390
Total	29	1337
HFVT		
Flow Switching Mechanism and Extended Power Shaft	83	1351
Front Vectoring Nozzles	2	•
Rear Vectoring Nozle	•	•
Penalty for Booms	117	1112
RCS System	6	423
Total	208	2886
MFVT		
Block and Turn Nozzle	•	450
Transfer Ducts	92	465
Front Clamshell Nozzles	2	450
Total	94	1365

The BAI mission payloads were changed to reflect more realistic missions⁽⁹⁾. The mission payloads were changed to allow carrying radar-guided weapons along with unguided weapons, thus having the aircraft able to deliver munitions if the target shuts off its radar. The BAI missions (two of them) were changed to (1) BAI Mission #1: Four Mk-82s and two HARMs, and (2) BAI Mission #2: Four AGM-65s and two Mk-82s.

A horizontal stabilator replaced the canard on the LIFT configuration to reduce the complexity in the main and lift engine inlet region, to provide more favorable stability margins (less trim drag), and to move the hover c.g. further aft. Moving the hover c.g. aft (or moving the rear thrust post forward) decreases the thrust required of the lift engine. Toward this end, the avionics were moved aft behind the internal weapons bay. The internal short-range missile requirement was dropped and the missile was wingtip mounted since (1) prelaunch target acquisition is required and (2) the wingtip launchers provide the missile with a larger field of view. The final modification of the LIFT configuration was replacing the single ventral nozzle with two variable-area ventral nozzles allowing for a three-post configuration, reducing the suckdown, and providing lateral control in hover. The effect on suckdown of a two- vs. three-post configuration was estimated and is shown in Fig. 6.

CONFIGURATION DESCRIPTION

The Phase II lift + lift/cruise aircraft consists of a mid-wing with split leading and trailing edge flaps, an all moving horizontal stabilator, and a single vertical fin. Figure 7 shows a three view of the configuration. The internal layout is shown in Fig. 8 with the resulting cross-sectional area distribution as shown in Fig. 9. The configuration highlights are discussed below.

The lift engine and lift/cruise engine combine to decouple the short takeoff and vertical landing requirements from the supersonic-cruise and point-performance requirements. The

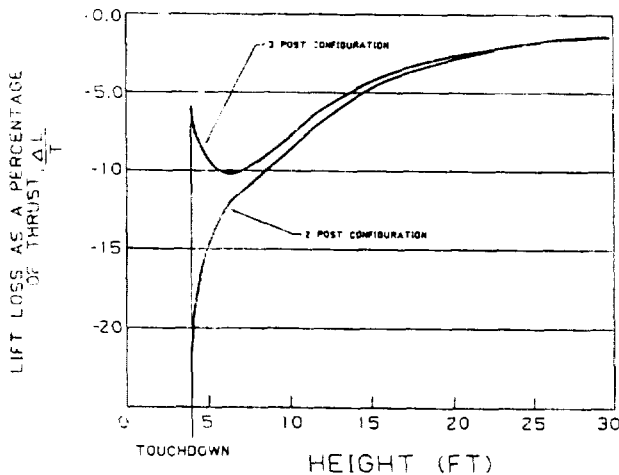


Fig. 6. Effect of Number of Thrust Posts on Suckdown

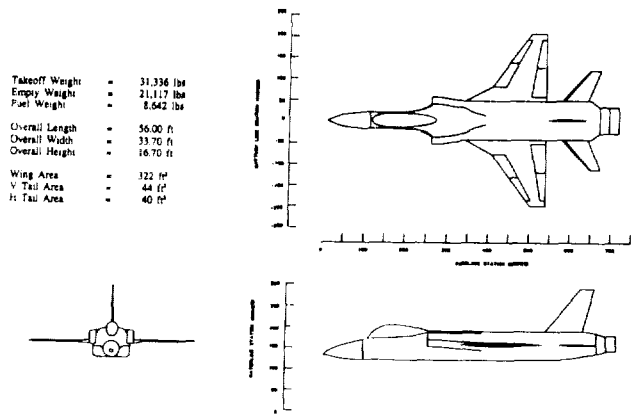


Fig. 7. Lift + Lift/Cruise Configuration Three View

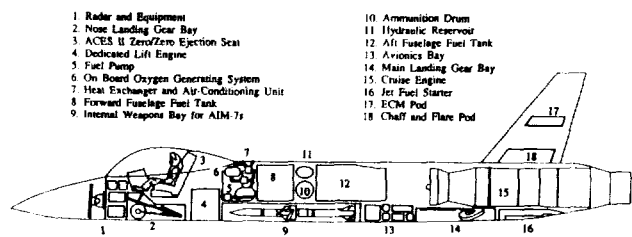


Fig. 8. Lift + Lift/Cruise Configuration Internal Layout

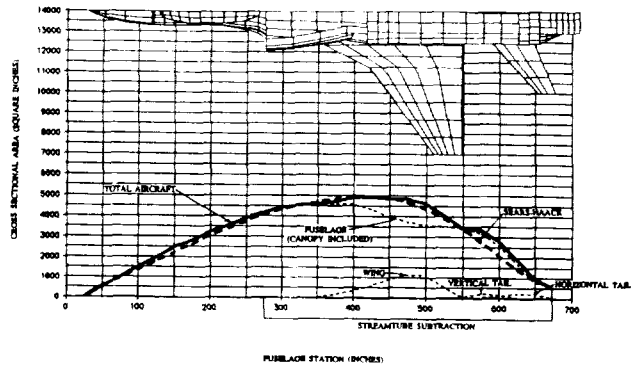


Fig. 9. Lift + Lift/Cruise Configuration Cross-Sectional Area Distribution

configuration is area ruled to closely match the ideal Sears-Haack shape considering the two internal medium-range missiles, the lift engine volume, and the large soft-field capable and high-sink-rate (17 ft/sec) landing gear. The high main inlet placement provides for less severe hot gas reingestion and reduces foreign-object damage. The pitch and yaw vectoring main engine nozzle allows for the removal of the rudder, a reduction in the vertical tail size, and for enhanced maneuverability at post-stall angles of attack.

WEIGHT DATA

The weight data are shown in Table 3. STOVL equipment weight includes that of the lift engine and nozzles, the lift/cruise engine nozzles, the reaction control system ducting and nozzles, and the lift/cruise engine tailpipe extension.

Table 3. Weight Statement (lb)

	CA	BAI #1	BAI #2
Structure	(9,498)		
Fuselage	4,385		
Wing	2,490		
Tails - Vertical	256		
- Canard	295		
Landing Gear - Main	1,249		
- Nose	220		
Launch Mechanisms (Int. Weap)			
ASRAAM	40		
AMRAAM	262		
Ventral Clamshell Nozzles	300		
Propulsion	(6,139)		
Cruise Engine	3,557		
Lift Engine	480		
Cruise Engine Tailpipe Ext	300		
Cruise Engine Nozzle	420		
Air Induction	773		
Fuel Bladder	415		
Fuel Dumping	24		
Engine Controls	45		
Starting System	125		
Fixed Equipment	(5,480)		
Flight Control	1,021		
Avionics	1,517		
Electrical System	596		
Air Conditioning	301		
Oxygen System	17		
APU	298		
Furnishings	277		
Gun and Provisions	630		
Auxiliary Gear, Paint	418		
RCS Ducting and Nozzles	405		
Total Empty Weight	21,117	21,117	21,117
Crew	225	225	225
Total Fuel	8,642	8,642	8,642
Armament	(1,196)	(4,074)	(3,316)
ASRAAMS	332		
AMRAAMS	654		
HARM		1,614	
Mk-82s		2,240	1,120
Mavericks			1,976
Ammo - (200 rounds)	220	220	200
Takeoff Weight	31,336	34,400	33,642

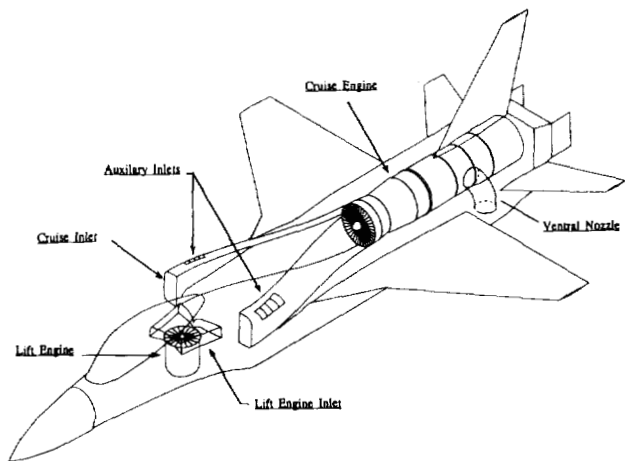


Fig. 10. Propulsion System Integration

The lift/cruise engine,⁽¹⁰⁾ sized by the point-performance requirements, has a maximum sea-level static thrust of 35,573 lb. For hover, the dry thrust required included the following: (1) 1.00 g to counter the aircraft weight, (2) 0.10 g to arrest a sink rate, (3) 0.13 g to counter suckdown (assumed), and (4) 0.07 g to support reaction control (assumed). The calculated required thrust loss due to suckdown and bleed required for reaction control were less than that assumed and so resizing was not required.

The ventral nozzles are of the clamshell type. Figure 11 shows the integration of the ventral nozzles and the tailpipe extension. In powered-lift operation, while the main nozzle blocks the flow, the turning vanes direct the flow through the transfer ducts to the clamshells. In conventional flight, the turning vanes block off the transfer ducts and the clamshell nozzles are retracted into the fuselage. This nozzle arrangement allows for a three-post configuration as well as lateral control in hover, thus reducing the required reaction control bleed.

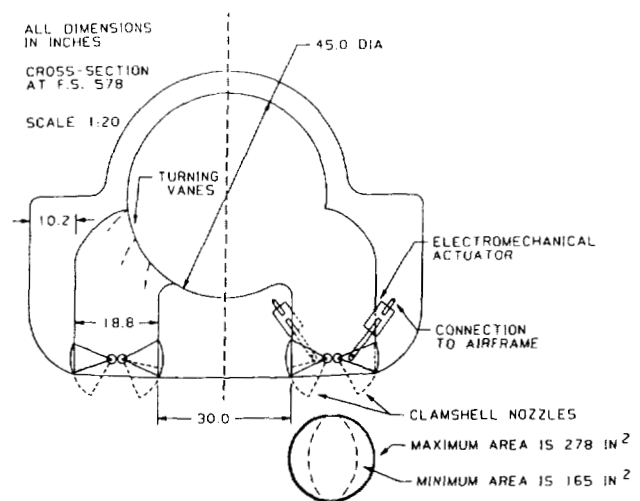


Fig. 11. Lift/Cruise Engine Ventral Nozzles

PROPULSION SYSTEM INTEGRATION

The overall propulsion system integration is shown in Fig. 10. The integration consists of a lift/cruise engine with two ventral nozzles and a main pitch and yaw vectoring nozzle, and a lift engine with a pitch vectoring nozzle. Auxiliary inlets are used for the lift/cruise engine to accommodate the increased mass flow required for powered-lift operation.

The lift/cruise engine main nozzle has 20° pitch vectoring and 25° yaw vectoring, with a block and turn capability. Figure 12 shows the lift/cruise engine main nozzle. The yaw capability of the nozzle was calculated to have enough control power to eliminate the rudder and to provide adequate stability to reduce the size of the vertical tail by 30%. Removing the rudder reduces the complexity and cost of the flight control system and reducing the vertical tail size allows a more favorable aft end area distribution. The pitch vanes of the nozzle close together to block the flow and turn its direction for hover and transition.

The lift engine⁽¹¹⁾, sized by the hover balance, has a maximum installed thrust of 12,105 lb. The lift engine along with its nozzle arrangement is shown in Fig. 13. The unmixed turbofan employs a large amount of advanced composites, which enables the uninstalled thrust-to-weight to reach 28. To achieve the lightest possible engine while maintaining acceptable jet exhaust conditions, a high bypass ratio (1.5) is implemented. A smaller diameter engine with a higher specific thrust could have been used to decrease the engine volume, but this would have led to an increase in engine weight and/or more severe exhaust conditions.

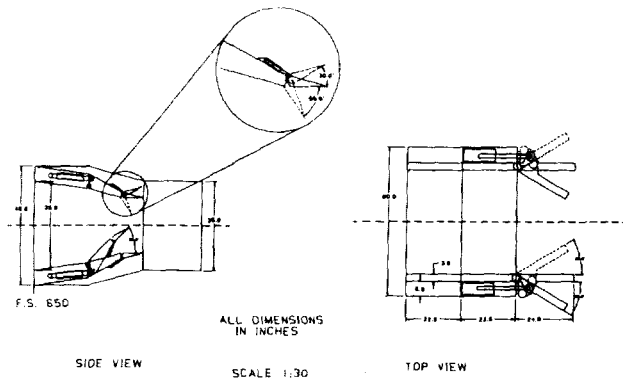


Fig. 12. Lift/Cruise Engine Main Nozzle

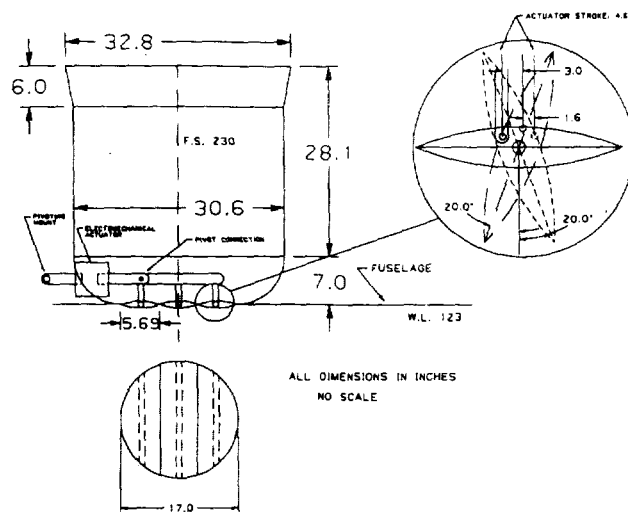


Fig. 13. Lift Engine Nozzle Arrangement

In conventional flight, the lift engine nozzle vanes were designed to fold into the fuselage underside to avoid fuselage doors. The 20° fore and aft capability of the nozzle was included to assist in pitch control in takeoff and transition.

TAKEOFF, TRANSITION, AND HOVER ANALYSIS

Takeoff

At brake release the main engine, operating at maximum dry thrust, has its nozzle vectored slightly downward to balance the thrust of the idling lift engine. During groundroll the lift engine reaches maximum thrust while the main engine thrust is shifted from the main nozzles to the ventral nozzles. When the combined lifting force of the engines and wing reaches the weight of the aircraft, the lift engine retards its thrust while the main engine thrust is shifted back to the main nozzle. During the groundroll, the composite thrust forces are balanced independently of the aerodynamic forces on the aircraft. Rotation was not investigated since the ventral nozzles, not capable of vectoring, would produce a component of thrust to counter the forward motion of the aircraft.

The resulting takeoff groundroll distances for CA, BAI, and an overload mission are shown in Fig. 14.

Transition

The transition of the aircraft between powered-lift and wingborne flight was investigated using a time-stepping technique. Figure 15 shows an example of the transition between powered-lift to wingborne flight, starting with takeoff. An effort was made to achieve gross thrust vectoring with the combination of the lift/cruise engine main and ventral nozzles and the lift engine nozzle. Idling back the lift engine thrust and transferring the main engine thrust from the ventral to main nozzle occurs at a rate at which the aircraft remains at a constant altitude since the decrease in vertical thrust equals the increase in lift from the wing.

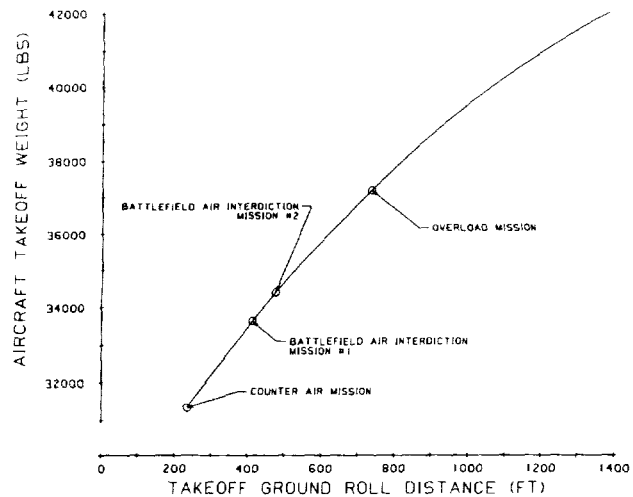


Fig. 14. Takoff Ground Run Distances

SCALE: 1/500
ALL DIMENSIONS INCHES
VECTOR MAGNITUDE:
1 INCH = 50,000 LBS
NOTE: SMALL VECTORS ARE THE THRUST FROM EACH NOZZLE
AND THE LARGE VECTOR IS THE EQUIVALENT THRUST

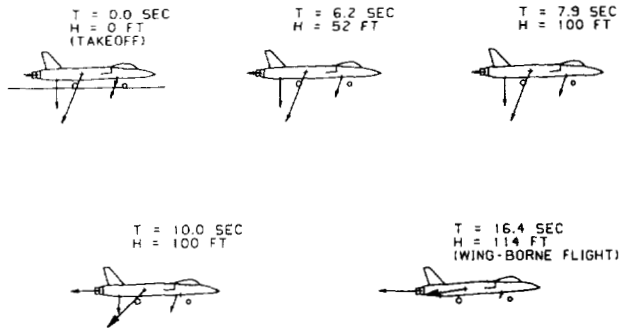


Fig. 15. Takeoff to Wingborne Transition

Control requirements and the pilot workload for STOVL aircraft are higher than that of conventional aircraft, thus a digital fly-by-wire flight-control system with advanced software and integrated propulsion control is required.

Hover

A reaction control system maintains control about the pitch and yaw axes in hover. The Level 1 flying qualities for hover control from AGARD 577 and MIL-F-83300 were used to calculate the required engine mass flow bleed rate. A total of 2% of the lift/cruise engine mass flow rate is required for adequate control in hover, 1.2% for pitch control and 0.8% for yaw control. The reaction control system layout is shown in Fig. 16.

The hot gas reingestion (HGR) problem is very configuration-dependent and thus difficult to identify without extensive theoretical research and experimentation. However, major determinants of the severity of HGR are the number and location of the vertical jet exhaust nozzles. Figure 17 shows a top view of the aircraft with the location of its nozzles and the fountain created by the jet exhaust. The flow walls do not concentrate themselves in an inlet region and thus it is predicted that the aircraft will not have severe HGR problems.

STABILITY AND CONTROL

The stability and control derivatives were calculated for seven flight conditions that were selected to represent critical points in the flight envelope. Pitch trim diagrams were plotted to assure that the aircraft was longitudinally trimmable at each flight condition. The aircraft was verified to not have severe spin-departure characteristics and the inertia coupling of the aircraft was alleviated with feedback to compensate the short period and dutch roll frequencies and damping ratios. A low-level ride qualities analysis indicated that the aircraft may need a ride quality augmentation system throughout most of the flight envelope.

Digitally controlled stability augmentation systems were designed for each of the three aircraft axes: pitch, roll, and yaw. A sampling frequency of 100 Hz was implemented for the digital controllers. The directional stability augmentation system block diagram is shown in Fig. 18. As shown, yaw rate is derived by (1) the deflected thrust of the yaw vanes and (2) the aerodynamic force produced by the yaw vanes as they are deflected. The unaugmented z-plane root locus, shown in

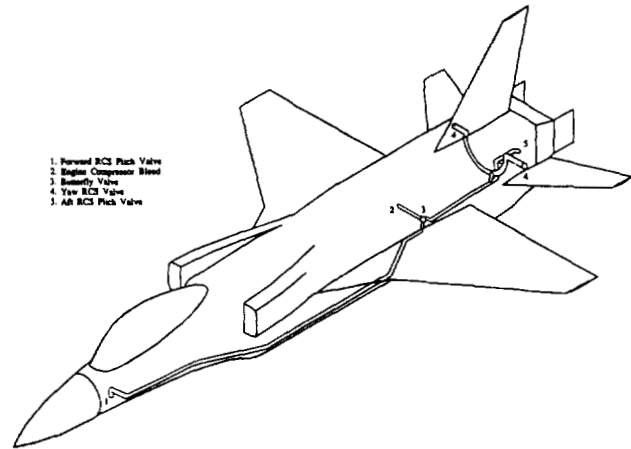


Fig. 16. Reaction Control System Layout

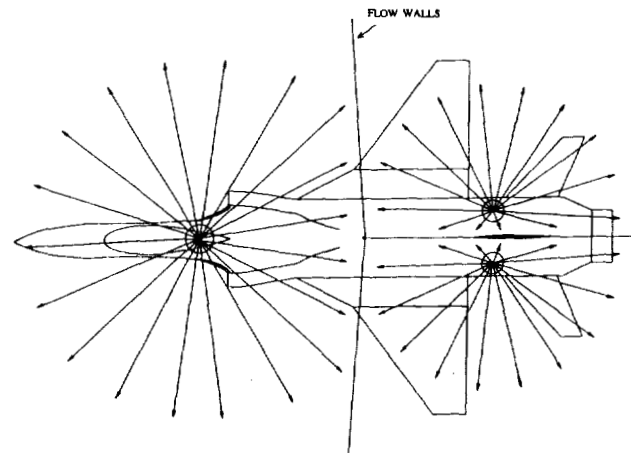


Fig. 17. Flow Walls of the Jet Exhaust

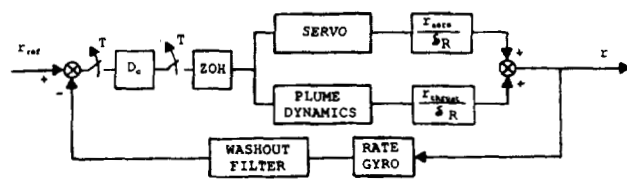


Fig. 18. Directional Stability Augmentation System Block Diagram

Fig. 19, indicates that the dutch roll is neutrally stable. The digital compensator selected is shown below.

$$D_c(Z) = \frac{Z^2 - 1.9978Z + 0.9978}{Z^2 - 1.9766Z + 0.9773}$$

The augmented dutch roll z-plane root locus, shown in Fig. 20, shows that for a gain of -0.1, the dutch roll meets the Level 1 requirements with a damping ratio of 0.6 and a frequency of 2.25 rad/sec.

MATERIALS SELECTION

Weight savings, damage tolerance, and cost were the primary considerations for the materials selection, with the material mechanical properties and fabrication characteristics being secondary considerations. An exploded view showing the material selection is given in Fig. 21. Weight savings are achieved through the use of composite materials and materials with high strength-to-weight ratios. Damage tolerance is achieved by using materials having high toughness and

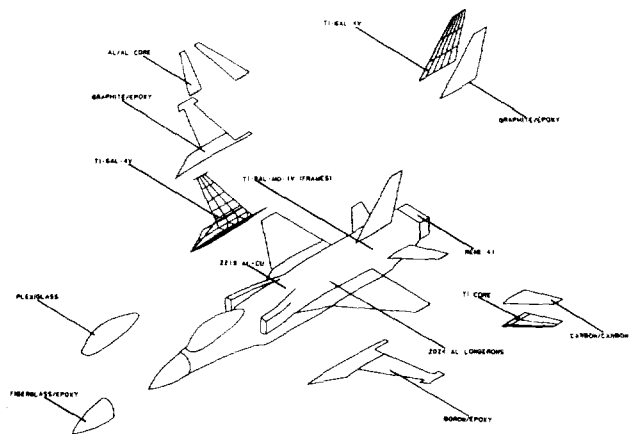


Fig. 21. Materials Selection Exploded View

redundant structure. Although many of the materials selected have high initial cost, the good fatigue properties of the materials (reduced maintenance) may allow the costs to be regained throughout the aircraft's life cycle.

PERFORMANCE AND MISSION CAPABILITY

The point-performance requirements of the mission specification were met, as shown in Table 4, with the exception of the very demanding 1000-ft/sec specific excess energy requirement. The point performances were specified at half fuel, two short-range missiles, and half ammo resulting in a performance wing loading of 76 lb/ft². The turn performance of the aircraft is shown in Fig. 22. The aircraft sustains high rates of turn over the operating Mach number range due to its high thrust engine. The maximum sustained turn rate at 15,000 ft for the aircraft is 16.9°/sec (thrust limited) and the maximum instantaneous turn rate is 17.3°/sec (lift/load factor limited).

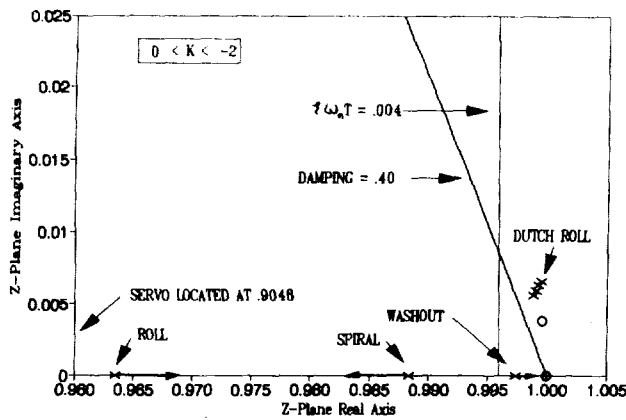


Fig. 19. Unaugmented Z-Plane Root Locus

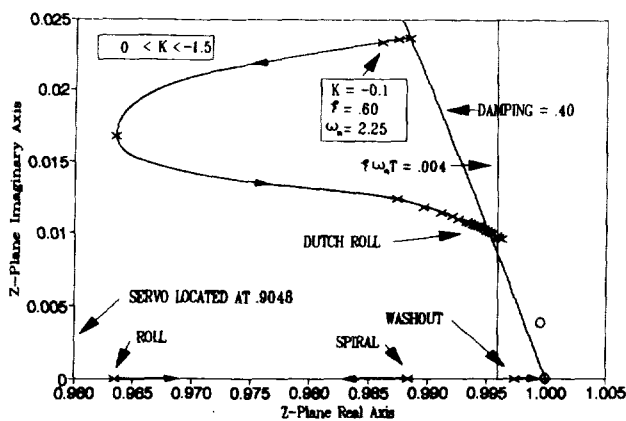


Fig. 20. Augmented Z-Plane Root Locus

Table 4. Point Performance Verification

Performance Requirement	Required Value	Monarch Value
<i>Time to Climb</i>	40K in 2 min	1.75 min
<i>1 g Specific Excess Energy</i>		
(2A) 30K Mach 0.9	500 ft/sec	505 ft/sec
(2B) 10K Mach 0.9	1000 ft/sec	920 ft/sec
<i>Sustained Turn Rate</i>		
(3A) Mach 0.8/15K ft	15°/sec	15°/sec
(3B) Mach 0.9/30K ft	9°/sec	10°/sec
(3C) Mach 1.2/30K ft	8°/sec	9.9°/sec
(3D) Mach 0.9/15K ft	6.5 g	7.75 g
(3E) Mach 1.6/30K ft	4.5 g	8.70 g
<i>Acceleration</i>		
(4A) 30K ft Mach 0.9 to Mach 1.6	70 sec	47.3 sec
(4B) Mach 0.5 to Mach 1.4	80 sec	62.1 sec
(4C) 10K ft Mach 0.3 to Mach 0.9	22 sec	18.4 sec
<i>Landing Distance (ground roll)</i>		
Without Chute	2200 ft	2100 ft

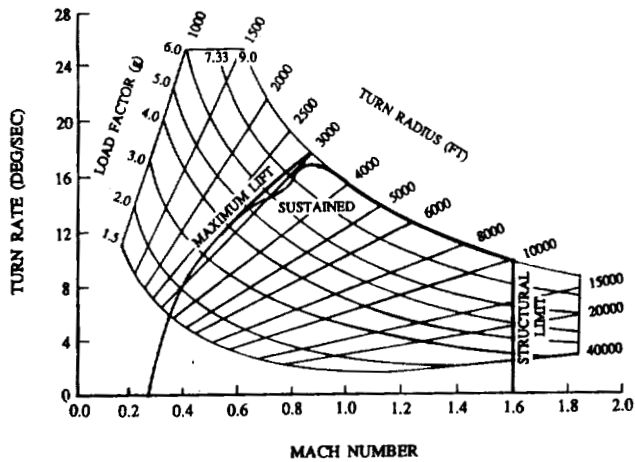


Fig. 22. Turn Performance at 15,000 ft

The 1-g specific excess energy for the flight envelope is shown in Fig. 23. The aircraft has a 1000 ft/sec specific excess energy capability at high subsonic Mach numbers and altitudes below 10,000 ft. As shown, a specific excess energy of 600 ft/sec is achievable over a wide portion of the flight envelope.

The mission capability of the aircraft was measured by (1) verifying the CA and BAI mission profiles and (2) taking the aircraft through typical fighter/attack missions to determine the aircraft's capability as a multirole fighter. Tables 5 and 6, respectively, show the CA and BAI (heaviest ordnance) mission fuel usage. As shown, the supersonics (acceleration to and sustaining supersonic flight) of the CA mission and the low-level dash of the BAI mission dominate the aircraft fuel usage. Figures 24 and 25, respectively, show the aircraft's capability in a mass intercept mission and a STOVL two-stage mission. The two-stage mission shows the advantage of a STOVL aircraft in that it can operate from dispersed bases and thus save fuel and cut down on response time.

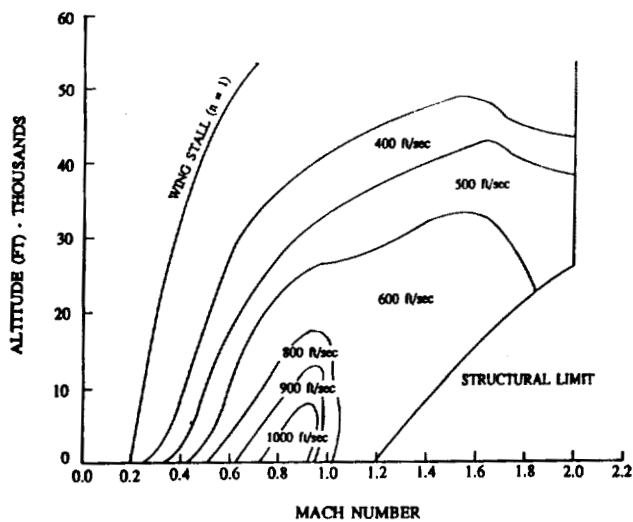


Fig. 23. Specific Excess Energy

Table 5. CA Mission Fuel Usage

Phase	Fuel Burn (lb)
Engine Start/Warm Up	327
Taxi	307
Short Takeoff	376
Acceleration to Climb Speed	308
Climb	538
Subsonic Cruise - 200 n.m.	1331
Sea Level Dash In - 80 n.m.	1204
Strafe Run	864
Sea Level Dash Out - 80 n.m.	1110
Climb	326
Subsonic Cruise - 200 n.m.	1124
Hover	246
Landing	121
Reserves	432
Total	8614

Table 6. BAI Mission Fuel Usage

Phase	Fuel Burn (lb)
Engine Start/Warm Up	314
Taxi	279
Short Takeoff	360
Acceleration to Climb Speed	313
Climb	485
Subsonic Cruise - 100 n.m.	531
Acceleration to Supersonic Cruise	620
Supersonic Cruise - 50 n.m.	1334
Combat	1728
Supersonic Cruise - 50 n.m.	1325
Subsonic Cruise - 100 n.m.	571
Hover	227
Landing	114
Reserves	432
Total	8634

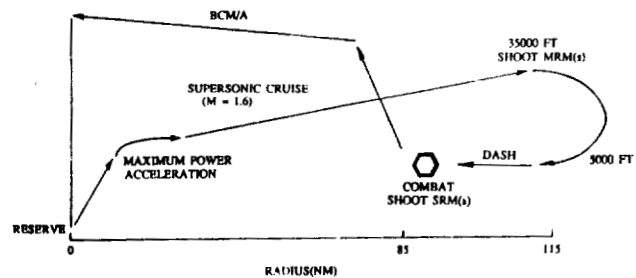


Fig. 24. Mass Intercept Mission

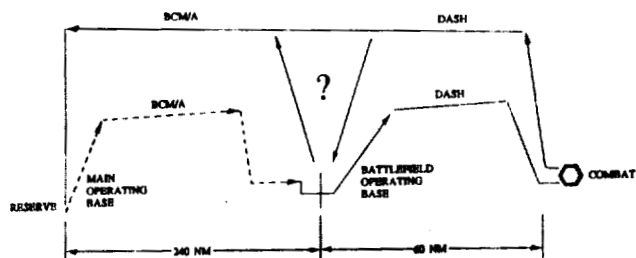


Fig. 25. STOVL Two-Stage Mission

LIFE CYCLE COST ANALYSIS

The life cycle cost of the aircraft was estimated. The results are summarized in Table 7 with a life cycle cost breakdown shown in Fig. 26. The results shown are for a production run of 500 aircraft and in 2005 dollars. The average estimated price per fighter is \$32.6 million.

Table 7. Summary of Life Cycle Cost

Research, Development, Test, and Evaluation
 Number of Airplanes Built for RDTE = 10
 Engineering Manhour Rate = \$105.00
 Manufacturing Manhour Rate = \$68.00
 Tooling Manhour Rate = \$83.00
 RDTE Cost = \$3.716 Billion

Acquisition
 Number of Aircraft Produced Per Month = 10
 Test Flight Hours Before Delivery = 20
 ACQ Cost = \$12.206 Billion

Operating
 Number of Flight Hours Per Year = 325
 Number of Years in Active Duty = 25
 OPS = \$28.88 Billion

Disposal
 1% Program Life Cycle Cost
 DISP = \$0.456 Billion

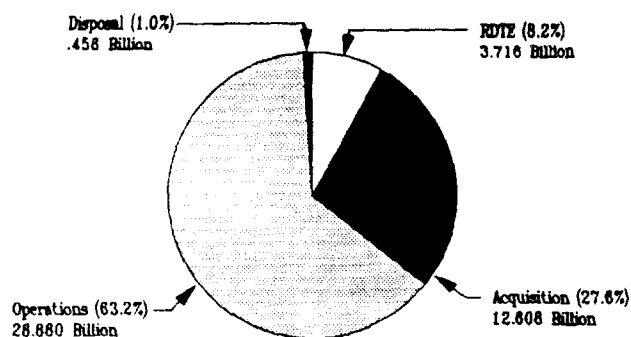


Fig. 26. Life Cycle Cost Breakdown

CONCLUSIONS AND RECOMMENDATIONS

The results of an investigation of three STOVL configurations indicated that a lift + lift/cruise concept was the most promising configuration for continued design analysis. The lift + lift/cruise aircraft suffered the least penalty due to equipment required for STOVL capability. The aircraft's engine cycle, consisting of a lift engine and a lift/cruise engine, decouples the short takeoff and vertical landing requirements and the supersonic requirements. Flexible nozzle integration allows for a three-post design that is critical to acceptable suckdown and to control power requirements in powered-lift operation. The aircraft has the ability to take off in short distances, transition to wingborne flight, complete its mission, transition to powered lift, and land vertically. Inertial coupling

and spin departure tendencies were reduced via the digital fly-by-wire flight control system. Materials for the aircraft were selected by balancing their high initial cost with their increased performance throughout the aircraft's life cycle. The aircraft does not suffer from the STOVL requirement as shown by its high level of performance. Also, the aircraft's mission capability is adequate to the point that it may be considered a multirole fighter.

Further design analyses are necessary to determine if the hot exhaust gases interfere with the engine operation in close proximity to the ground and to develop highly redundant integrated flight and propulsion controls to assure successful takeoff and transition of the aircraft.

ACKNOWLEDGMENTS

The following are recognized as contributors to the success of this design study: the students of the AE 621 and AE 622 design courses for their design analyses, the members of the Technology Assessment Division of the Wright Research and Development Center (particularly Lieutenant Gerald Swift) for their (his) technical support and data packages, the members of the Powered Lift Branch of NASA Ames Research Center (particularly Andrew Hahn) for their (his) technical support and data packages, Dr. Roskam for his guidance and support to the design team, Shelby J. Morris as the NASA monitor, and the Universities Space Research Association for sponsoring the Advanced Design Program.

REFERENCES

- Byrnes, J. M. and Lowry, R. B., Views on V/STOL Tactical Fighter Aircraft: Technology Needs and Relationships to the Runway Denial Problem, AGARD Conference, Proceedings, Number 313 June 1984.
- Tamplin, G. C., Hammond, D. L., and Fredette, R. E., Assessment of A Post 2000 STOVL Fighter, SAE Aerospace Atlantic Paper 901031, April, 1990.
- Cox, Brian, et al., Preliminary Performance Assessment for a Supersonic STOVL Fighter, University of Kansas, AE 621, September, 1989.
- Cox, Brian, et al., Battlefield Arena in 1995-2000, University of Kansas, AE 621, September 1989.
- Cox, Brian, et al., Preliminary Design of a Supersonic STOVL Aircraft Using a Hybrid Fan Vectored Thrust Engine Cycle, University of Kansas, AE 621, December 1989.
- Cox, Brian, et al., Preliminary Design of a Supersonic STOVL Aircraft Using a Lift + Lift/Cruise Engine, University of Kansas, AE 621, December 1989.
- Cox, Brian, et al., Preliminary Design of a Supersonic STOVL Aircraft Using a Mixed Flow Vectored Thrust Engine Cycle, University of Kansas, AE 621, December 1989.
- USAF Wright Research and Development Center Presentation at the University of Kansas, Presenter: Ray Fredette, University of Kansas, January, 1990.
- NASA Ames Research Center Presentation at the University of Kansas, Presenter: Andrew Hahn, University of Kansas, February 1990.
- Pratt and Whitney Advanced Engines Performance, Weights and Dimensions Model, Fighter/Attack/Interceptor Applications, Provided by Public Release from Wright Research and Development Center, January 1990.
- Rolls-Royce, ASTOVL Direct Lift Engine, Performance and Installation Data Package, July 1989.

301, 6, 00
p. 8 301

DESIGN OF A REMOTELY PILOTED VEHICLE FOR A LOW REYNOLDS NUMBER STATION KEEPING MISSION

UNIVERSITY OF NOTRE DAME

N91-18166

Six teams of senior level Aerospace Engineering undergraduates were given a request for proposal, asking for a design concept for a remotely piloted vehicle (RPV). This RPV was to be designed to fly at a target Reynolds number of 1×10^5 . The craft was to maximize loiter time and perform an indoor, closed-course flight. As part of the proposal, each team was required to construct a prototype and validate their design with a flight demonstration.

INTRODUCTION

There has been a growing interest in flight applications in the low Reynolds number range, specifically near 10^5 . At these low Reynolds numbers, many different phenomena occur. One particular example is lift hysteresis. As an airfoil increases angle of attack in this flow regime, separation bubbles form that alter boundary layer development and influence both lift and drag performance. Through a small angle-of-attack range, these bubbles augment the overall lift of the airfoil. At higher angles of attack, the bubbles break down and may cause a sudden decrease in lift. If the angle of attack is then slowly decreased the bubble may reform and the increase in lift would again be present. There are also significant form-drag penalties associated with this Reynolds number regime.

Another problem faced in this particular application is that of weight constraints. Since the aircraft is flying a constrained, closed course and loiter time is to be maximized, optimally the cruise velocity should be kept to a minimum. This will keep the chord length, and hence the aircraft size, in a limited range. Therefore, for a given velocity range and limited planform size, there is a finite amount of lift that can be generated by the craft. Therefore, to take off and maneuver, it is critical that the RPV is weight efficient. This requires selecting a proper propulsion system and aerodynamic configuration for this specialized mission.

There are several applications for which low Re RPVs may be used, both at high and low altitudes. At high altitudes they could be used for meteorological, communications, or reconnaissance purposes. At lower altitudes they could be used for surveillance, or in a rescue mission to locate survivors. Since this study involved nonconventional (nonairbreathing) propulsion systems, they could be used in any hostile environment, ranging from martian topography mapping to volcanic monitoring on Earth. Another use for these RPVs is in radiation-contaminated areas where human-operated craft would be unsafe.

REQUEST FOR PROPOSALS

The mission and semester project details were defined in the following request for proposals. This request placed some additional requirements and constraints on the basic mission

specifications. The design teams were notified that certain aspects of the mission were open for modification, given sufficient justification for these changes.

FLIGHT AT VERY LOW REYNOLDS NUMBERS: A STATION KEEPING MISSION

Opportunity

Most conventional flight vehicles are designed to operate in a flight regime such that the Reynolds number based on mean wing chord is in excess of 10^6 and some currently operate approaching 10^5 . Recently there has been interest expressed in vehicles that would operate at much lower Reynolds numbers, less than 10^5 . Particular applications are low-speed flight at very high altitudes, low-altitude flight of very small aircraft, and flight in the atmospheres of other planets atmospheres such as Mars. There are many unique problems associated with low-speed flight that pose challenges to the aircraft designer and that must be addressed in order to understand how to exploit this low Reynolds number flight regime. Since many of the anticipated missions for this type of aircraft are unmanned, it is necessary to couple developments in unmanned aircraft development with our knowledge of low Reynolds number aerodynamics in order to develop an aircraft that can fly as slowly as possible at sea-level conditions. This study will help to better understand the problems associated with flight at these very low Reynolds numbers. Considering the potential applications, the aircraft must also be very robust in its control and be highly durable.

Objectives

1. Develop a proposal for an aircraft and associated flight control system that must be able to (a) Maintain level controlled flight and fly a closed-course at flight speeds corresponding to Reynolds numbers less than 2×10^5 and as close to 1×10^5 as possible. The greatest measure of merit is associated with achieving the lowest mean chord Reynolds number possible and maximizing the loiter time on a closed course. (b) Be maneuverable and controllable so that it can

fly a closed pattern and remain within a limited airspace. (c) Use a propulsion system that is nonairbreathing and does not emit any mass. (d) Be able to be remotely controlled by a pilot with minimal flying experience or an autonomous onboard control system. (e) Carry an instrument package payload that weighs 2.0 oz and is 2" × 2" × 2" in size.

2. Take full advantage of the latest technologies associated with lightweight, low-cost radio-controlled aircraft and unconventional propulsion systems.

3. All possible considerations must be taken to avoid damage to surroundings or personal injury in case of system malfunction.

4. Develop a flying prototype for the system defined above. The prototype must be capable of demonstrating the flightworthiness of the basic vehicle and flight control system. The prototype will be required to fly a closed figure-eight course within a highly constrained envelope. A basic test program for the prototype must be developed and demonstrated with flight tests.

5. Evaluate the feasibility of the extension of the aircraft developed under this project to high-altitude station keeping application for atmospheric sampling.

System Requirements and Constraints

The system design shall satisfy the following: (1) all basic operation will be line-of-sight with a fixed ground-based pilot, although automatic control or other systems can be considered; (2) the aircraft must be able to take off from the ground and land on the ground; (3) the aircraft must be able to maximize loiter time within a restricted altitude range on a figure-eight course with a spacing of 150 ft between the two pylons that define the course; and (4) the complete aircraft must be able to be disassembled for transportation and storage and fit within a storage container no larger than 2' × 2' × 4'.

In order to successfully satisfy the mission objectives, Design Requirements and Objectives (DR&O) were established by each design team. Principally, the constraints imposed by the confined flight course (see Fig. 1), by maximizing loiter time, and by the necessity for ease of installation and assembly had to be addressed and target parameters identified.

Evaluation of the mission requirements enabled each group to categorize the primary constraints. The ability to take off and land in a 150-ft strip, to establish effective stability and control for all flight speeds, and to execute low-speed turns while maintaining altitude were of extreme importance to satisfy the confined environment constraints. The ability to climb to cruising altitude in a reasonable time and to complete three figure eight patterns around two pylons were main considerations to satisfy the endurance requirements. Ease of installation of the instrument package and compactness for transportation were necessary to satisfy assembly constraints.

General guidelines allowed for minimum performance limits for the RPVs capabilities to be determined. The mission was to simulate low-speed flight at high altitudes, low-altitude flight of very small aircraft, or flight in another planet's atmosphere. In order to approximate these conditions, most groups chose a target Reynolds number of 10^5 .

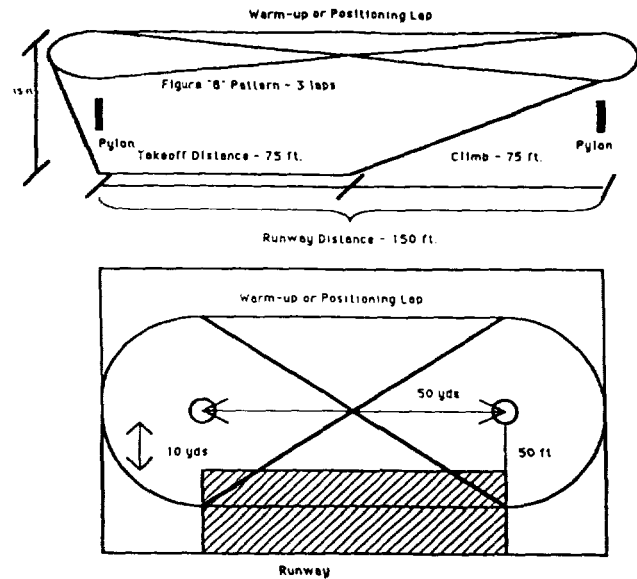


Fig. 1. Schematic of Closed Figure "8" Course

CONCEPT DESCRIPTIONS

The following summaries provide an overview of each of the six concepts. These summaries describe the final concept and address specific technical merits and limitations. Included are selected three-view representations of the aircraft. These summaries are meant to give a brief description of each design, and further technical detail on each proposal is available upon request.

The Drag-n-Fly

The Drag-n-Fly (see Fig. 2) is a remotely piloted, low Reynolds number vehicle. It was designed to maintain level controlled flight and fly a closed course at flight speeds corresponding to Reynolds number of 1×10^5 . The success of the mission will be associated with achieving the lowest mean chord Reynolds number possible and maximizing loiter time on the course. The flight plan for the Drag-n-Fly calls for the vehicle to climb to a cruise altitude of 25 ft. Once achieved, the Drag-n-Fly will fly within a restricted altitude range on a figure eight course, complete three laps, and then a final oval to bring the RPV back around in preparation for landing.

The Drag-n-Fly is a high-wing, high-aspect ratio monoplane. The airfoil selected for the Drag-n-Fly was a Spica chosen for its high lift coefficient at low Reynolds number. The wing span is 8.5 ft with total surface area of 6 sq ft and aspect ratio of 12. There is no sweep or twist associated with the wing and the taper ratio is 1.0. The wing loading is approximately 7.1 oz/ft².

The propulsion system for the Drag-n-Fly consists of a 10"-diameter propeller mounted on the front of the vehicle. The 10-6 propeller is driven by the ASTRO 05 electric motor using eight 500 MAH nickel-cadmium batteries. This motor/battery combination was selected not only because it is capable of

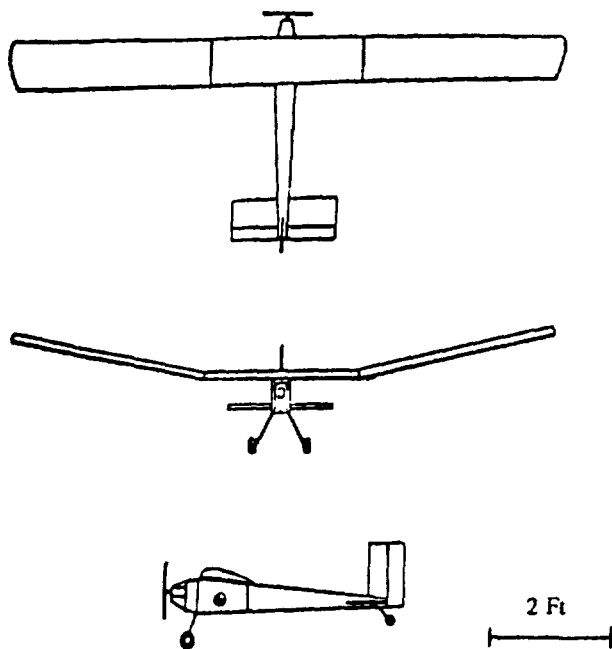


Fig. 2. Drag-n-Fly

providing the thrust needed to accomplish the mission, but also because of its light weight. An electronic speed control was also used to maintain altitude through the turns.

The primary fuselage structure was provided by four longerons running the length of the fuselage. The strongest part of the aircraft is the forward fuselage, since the motor and avionics are located in this region. This area will be reinforced by panels to increase the strength of the front fuselage. The spar/multirib wing design was selected for light weight and durability.

The vertical tail area is 0.5 sq ft and the horizontal tail area is 1.05 sq ft. Two movable control surfaces are used for maneuver control. A rudder will be implemented to control yaw and an elevator to control the pitch during the flight course, and both control surfaces will be actuated by microservos. Pitch-yaw coupling through wind dihedral is used.

The design for the Drag-n-Fly will meet the criteria for the present mission. Some areas of concern are accurate wing construction, control of the aircraft in flight (will the control surfaces deflect enough to maneuver the aircraft?), and very limited fabrication experience by the entire team.

The Stealth Biplane

The Stealth Biplane (see Fig. 3) was developed to serve as a remotely piloted vehicle designed to navigate a low-level figure-eight course at a target Reynolds number of 10^5 . The basic biplane configuration was selected in order to increase the wing area while maintaining the required mean chord and still satisfying the "storage" requirements. This flight vehicle will combine the latest in lightweight radio-controlled hardware in conjunction with current low Reynolds number aerodynamic research to demonstrate feasible operation in a

variety of applications. These potential low Reynolds number applications include high-altitude atmospheric sampling and search-and-rescue operations.

The completed prototype is designed to operate within a confined, closed course. Briefly, this course requires an unassisted ground takeoff followed by a climb to cruise altitude of 20 ft, in position to make the first left hand turn. Upon completion of the turn, a slight loss of altitude is predicted; however, during the straight cruise portion of the flight, this lost altitude can be regained. A similar right-hand turn and subsequent straight cruise completes one full lap around the course. Upon the completion of three full laps around the course, the Stealth Biplane will need to loiter back to the opposite end of the field for the landing run, where a full-stop ground landing will then be executed. This flight plan fulfills all imposed design requirements for normal operation.

Safe operation around such a course can be accomplished by an experienced ground-based pilot, but the pilot workload should be sufficiently light such that even an amateur can control the Stealth Biplane. In order to successfully rotate the Stealth Biplane and ascend to the mission altitude of 20 ft, a powerful propulsion system is required.

The electric motor that was selected to fulfill all the mission requirements was the Peck Silver Streak 035M electric motor, capable of producing a maximum static thrust of 11 N and a maximum power of 95 W. At this power setting, the engine operates at 13,000 rpm and uses an 8-in diameter, 4-in pitch propeller. This propulsion system derives its power from a power pack of 10 AA nickel-cadmium 1.2-V, 600-MAH rechargeable batteries. This entire powerplant will allow the aircraft to achieve its required cruising velocity of 28 ft/sec, with a maximum velocity of 40 ft/sec. This propulsion system was selected for its relatively low weight of only 10.6 oz,

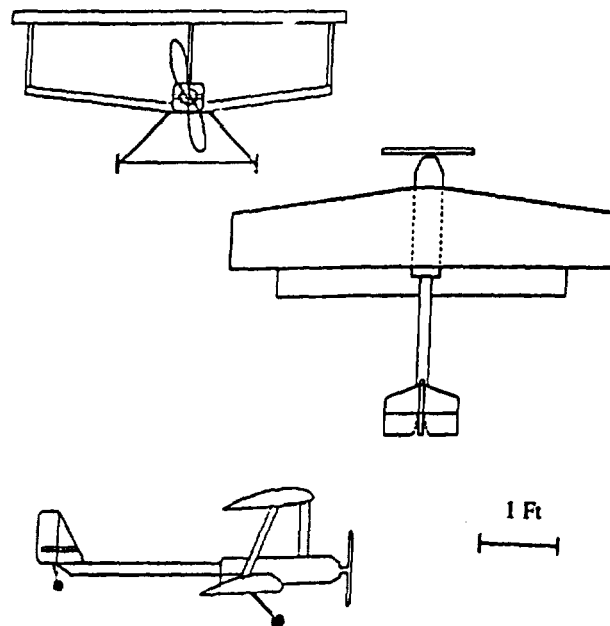


Fig. 3. Stealth Biplane

lowering the total aircraft weight significantly. The most important factor in selecting the aircraft propulsion system was obtaining the necessary power required for take off.

The Stealth Biplane will be receiving its lift from twin lifting surfaces in the form of a staggered biplane wing configuration. The top or main wing measures 4 ft in span, with a root chord length of 8 in, a taper ratio of 0.65, and a mean chord length of 6.6 in. The lower, staggered wing measures 3 ft in span, with the same root chord, taper ratio, and mean chord length as the top wing. The lower wing is staggered 3.2 in aft and 9 in below the leading edge of the main wing. Neither surface is swept; thus, the surface areas of the wings measure 2.2 ft² and 1.65 ft² for the top and bottom wings respectively. The airfoil selected for both surfaces is the Wortmann FX 63-137 airfoil. However, the lower wing has been augmented with a 5° droop of 13% of the chord at the leading edge, for an overall increase in L/D for that surface.

The construction of the Stealth Biplane requires a variety of fabrication techniques; the wing ribs, spars, and stringers will be fabricated from balsa, and the wing skin will be a mylar-based derivative. The fuselage is constructed from four balsa sheets in a boxlike configuration, with the propeller in the front of the aircraft and the components strategically placed to ensure static and dynamic stability of the Stealth Biplane. The empennage is a simple 1.5-in diameter cylinder that will connect the horizontal and vertical tails with the main fuselage. This length of the tail boom has been designed to provide optimum tail control while still minimizing the overall weight of the aircraft. The empennage (movable rudder and elevator) is constructed from simple flat plates of solid balsa, and the components are controlled by two microsensors.

The Penguin

The Penguin is a low Reynolds number remotely piloted vehicle. It has been designed to fly three laps indoors around two pylons in a figure-eight course while maximizing loiter time. Although the Penguin's mission seemed quite simple at first, the challenges of such low Reynolds number flight are quite unique. In addition to the constraint of low Reynolds number flight, the aircraft had to be responsive in its control, highly durable, and very lightweight.

The Penguin's flight plan begins with takeoff on a runway of 150 ft. It will actually lift off in approximately 50 ft, and the remaining runway distance will be used to climb to the cruise altitude of 15 ft. The aircraft will then begin its three laps around the pylons. After completing the last lap, the Penguin will land and come to a stop in approximately 30 ft.

Aerodynamically, the Penguin is similar to standard taildragger sailplane designs. The 7-ft-span rectangular wing is mounted on the top of the fuselage and is canted at a 3° dihedral. It uses the Wortmann FX63-137 airfoil. The long fuselage is rectangular and is highly tapered aft of the wing. The empennage has standard horizontal and vertical tail surfaces.

Supporting the structure of the Penguin are two box beams for the fuselage and wing, and two simple beams in each of the horizontal and vertical tails. The box beam in the wing

is located at the maximum thickness of the wing, while the simple beams in the empennage are located at the leading edge and the trailing edge (just prior to the control surfaces). The fuselage box beam runs the entire length of the aircraft. The forward section of the fuselage is much stronger than the aft since it supports the engine and the avionics as well as the load from the wings.

The Penguin is driven by an ASTRO 15 electric motor that provides more power than the RPV will need. The excess power may prove to be useful in a stall situation that may arise since the Penguin will cruise at a velocity close to the stall velocity ($V_{\text{cruise}} = 1.3 V_{\text{stall}}$). A two-blade, 10-in-diameter propeller provides the thrust.

Since the RPV had to be highly maneuverable, it makes use of large rudder, aileron, and elevator surfaces. Its large horizontal and vertical tail surfaces are located far aft of the wing in order to provide static stability and are placed in the wash of the propeller for added effectiveness. The dihedral of the wing provides roll static stability.

Scream-J4D

The Scream-J4D (see Fig. 4) is a remotely piloted airplane with a high-aspect-ratio main wing and a conventional empennage giving it a "sailplane" appearance. It is designed to satisfy the required mission using a flight plan that calls for ascent to cruise altitude at 20 ft and then perform three figure-eight turns around pylons. Once completed, the pilot is to make use of any remaining power by loitering before landing the plane.

The propulsion system of the J4D consists of a propeller-electric motor combination with the engine mounted at the front of the fuselage. The 10-in diameter, 6-in pitch, two-bladed propeller is powered by an ASTRO 05 electric engine with 7 AA nickel-cadmium batteries. The system is capable of maximum power output of 50 W and has throttling capabilities. Of the available propellers, the 10-6 was best suited for the takeoff distance and maximum current draw constraints. The 05 engine was chosen for being most lightweight while still supplying adequate power.

In order to provide sufficient lift for low-speed flight, the J4D has an aspect ratio of 11.7 with an 8.2-in mean chord. The wing consists of a spar and rib construction with thin

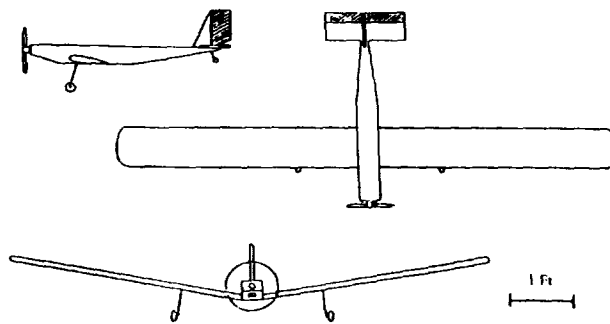


Fig. 4. SCREAM-J4D

plastic film skin. Its low mount and dihedral, in combination with the vertical tail, were designed to augment maneuverability. A major problem, however, is that due to the nature of a low-speed mission, there is little margin for error between the cruise and stall velocities. A square fuselage will contain the servos, engine, and payload, with adequate excess space so that the c.g. of the airplane is kept at about 33% of the chord.

A combination of directional and longitudinal control will enable the J4D to perform the figure-eight maneuvers. However, in order to avoid the construction and servo weight of ailerons, the rudder was designed to be over one-half the size of the vertical tail to insure that the proper roll control could be attained.

The Dawdler

The Dawdler (see Fig. 5) is a remotely piloted airplane designed to fly at low Reynolds numbers (10^5). The airplane will be flying a closed course in a controlled environment. The purpose of the design is to study the difficulties that arise in the design of a low Reynolds number aircraft. The Dawdler is a canard configured aircraft. It can also be considered a tandem wing configuration. The canard is designed to produce 30% of the total lift necessary to keep the aircraft in steady level flight. This configuration was chosen in order to attain an upward lifting force from the horizontal stabilizer.

The aircraft is designed to fly at 25 ft/sec, which requires a relatively small amount of power from the engine. However, a large amount of power is required for the aircraft to climb to the design altitude of 20 ft. Neglecting the takeoff performance of the aircraft, it was decided that the ASTRO 035 motor would supply enough power to keep the aircraft in steady level flight. One of the main reasons for picking the engine is its relatively light weight.

The takeoff will be accomplished via a remotely controlled, motorized cart assisted launch. The aircraft will be placed on top of a motorized cart that will accelerate the aircraft to a velocity of 45 ft/sec. At this speed, the aircraft will have enough kinetic energy to lift itself up to its cruise altitude. Once the aircraft reaches this velocity, the pilot can begin to raise the nose to lift it off the cart.

The Dawdler has a vertical tail mounted behind the wing for lateral stability and a rudder for yaw control. A 13° dihedral angle will be incorporated into the wings to assist roll control.

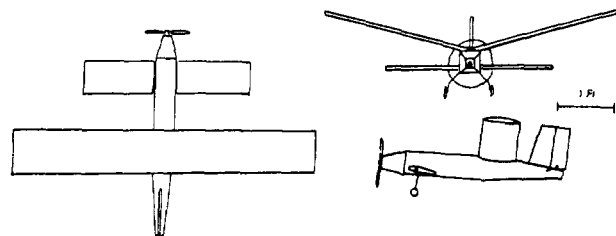


Fig. 5. Dawdler

Ailerons have been omitted from the design to reduce the number of servos and the associated structural complexity and weight. The canard will be fully movable for pitch control.

FX/90

The FX/90 is a remotely piloted vehicle designed to satisfy the mission requirements and to investigate the unique problems involved in low Reynolds number flight. The aircraft will operate in a steady flight environment, free from significant atmospheric turbulence and weather effects. The aircraft will take off within 75 ft, and will climb to an altitude of 20 ft within an additional 90 ft of ground distance. The aircraft will then commence its flight plan, which consists of three figure-eight loops around two pylons spaced 150 ft apart. Upon completion of the three laps, the aircraft will travel around the flight envelope and return to the pit area for landing. It can do so under powered flight, or it can travel an additional 60 ft and then glide the remaining distance.

The F-90 has a 39-in fuselage constructed of balsa and plywood. The fuselage consists of two sections. The forward section is a 3.5 in \times 3.5 in \times 17 in rectangular structure in which the propulsion and flight control systems are located. The rear section is a 22-in boom with a truss structure and a square cross section that tapers to a point. The boom provides a moment arm for the tail surfaces. The length of 22 in is a compromise between the advantages of a longer moment arm and the disadvantages of the associated increase in weight. The truss construction was chosen for its high strength and torsional stiffness with minimal weight.

The landing gear for the aircraft is a detachable carriage on which the aircraft rests prior to takeoff. The aircraft accelerates for takeoff while on the carriage. At takeoff, the aircraft lifts off the carriage, and completes its flight plan without landing gear. Landing is accomplished by setting down on the smooth lower surface of the fuselage. The propulsion system uses a foldable propeller to prevent damage during landing.

The aerodynamic planform is a rectangular wing (no taper or sweep) with a chord of 9 in, a wingspan of 72 in, and is constructed entirely out of styrofoam. Styrofoam was chosen for its low weight and relative ease of construction. "Aircraft quality" styrofoam was chosen for its high strength and hardness and its smooth surface, which eliminates the need for a coating material. Special care must be taken when handling the wings, particularly the thin trailing edges.

The propulsion system consists of an ASTRO 05 engine and a 10-6 two-bladed propeller. The ASTRO 05 engine was chosen for its light weight and adequate available power. The 10-6 propeller was chosen for its efficiency in conjunction with the 05 engine and for its moderate diameter. The maximum velocity and rate of climb, as well as the maximum range and endurance, all exceed the design requirements due to an excess of available power and battery energy storage.

Control of the aircraft is accomplished through the use of two movable control surfaces: elevators for pitch control and a rudder for yaw control. In addition, a large dihedral angle was used to couple the yaw and roll axis. This allows for roll maneuvers to be accomplished through the use of the rudder,

as well as providing adequate spiral stability. Ample rudder was provided in order to allow a high maneuverability, as required by the flight plan.

There are several areas of concern. At takeoff, the landing gear will detach while traveling at approximately 24 ft/sec, which is a safety concern. The aircraft flies at a high angle of attack, giving the aircraft a low tolerance to gusts, and is near stall during maneuvers. The impact of a landing without landing gear, as well as its effects on components of the aircraft, is relatively uncertain. Finally, the performance of the foldable propeller is not well documented, and its influence on the propeller performance was not evaluated.

System Technical Areas

The following brief sections address the problems in the five major technical areas: weights, structures, propulsion, aerodynamics, and stability/control. A final paragraph will then describe the concept prototypes and their flight demonstrations. Some of the basic parameters can be found in Table 1.

Weights

Each team was concerned about keeping the overall weight to a minimum. Table 1 also shows the overall aircraft weights. Each team used various means to cut weight. The FX/90 used detachable landing gear, while the Dawdler, which has no gear, was launched from a radio-controlled cart. Some teams chose smaller engines, while others built their fuselages with a lightweight truss design. The results were six strong aircraft with a maximum weight of 50.7 oz. Table 2 shows the weight fractions for each aircraft.

Structures

The structural problems consisted of constructing a lightweight aircraft that could withstand the loads required during flight, especially takeoff and turns, and the structures needed to be both lightweight and durable. Another problem consisted of providing adequate interior space to keep the center of gravity at the designed location. Material selection was a crucial part of the structural design, and Table 3 shows the materials used in each aircraft. Most of the truss configurations were modeled and examined using a finite element analysis program.

Propulsion

Perhaps one of the most challenging areas was propulsion. Each team needed an adequate propulsion system that would satisfy the nonairbreathing requirement. Electric, stored mechanical energy (rubber band) and stored compressed gas (CO₂) systems were considered. Only the electric systems appeared to provide the duration needed for this mission. Limited technical data were available on the lightweight, DC electric motors. Integration of the battery storage, electric motor performance and propeller selection proved to be critical in determining the success of the concepts. Takeoff power requirements far exceeded the low-speed steady-cruise requirements. Three groups decided on the ASTRO 05 engine, one chose the ASTRO 035, one the ASTRO 15, and one group used a Peck Silver Streak 035M. Some of the propulsion characteristics are found in Table 4.

Table 1. Basic Aircraft Parameters

Parameter	Drag-n-Fly	Stealth Biplane	Penguin	Scream-J4D	Dawdler	FX/90
V _{cruise} (ft/sec)	25.0	25.0	25.0	23.0	25.0	24.0
Endurance (min)	3.2	4.3	1.8	3.9	3.2	8.5
Weight (oz)	43.7	41.6	50.7	48.0	37.2	45.3
Area (ft ²)	6.0	2.2/1.65	4.67	5.46	3.25	4.38
Span (ft)	8.5	4.0/3.0	7.0	8.0	5.0	5.8
Length (in)	41.0	33.0	42.0	37.0	37.0	43.0
AR	12.0	7.3/5.5	10.5	11.7	7.7	7.8
Airfoil	SPICA	FX63-137	FX63-137	NACA 4415	Clark Y	FX63-137

Table 2. Structural Component Weight Percentages

Aircraft	Propulsion	Wing	Fuselage Empen.	Landing Gear	Avionics	Payload
Drag-n-Fly	30.7	19.2	19.2	8.1	18.3	4.5
Stealth Biplane	28.0	26.7	5.3	6.6	29.0	4.4
Penguin	34.1	16.8	21.9	8.0	15.2	4.0
Scream-J4D	33.7	28.5	20.2	5.0	8.6	4.0
Dawdler	29.5	21.4	21.2	7.7	15.2	5.0
FX/90	29.5	22.2	28.5	-	15.6	4.2

Aerodynamics

The primary purpose of the design project was to evaluate the influence that the very low Reynolds number flight regime would have on the aircraft design. Some of the problems in aerodynamics dealt with choosing an airfoil that would produce high lift coefficients without the risk of stall throughout the mission. Airfoil selection then involved investigating lift hysteresis, minimizing drag, and choosing the planform parameters. The airfoils that were selected ranged from the Wortmann FX63-137 (improved aerodynamics), to a traditional Clark-Y (ease of manufacturing). Profile drag prediction was complicated by the lack of data in this Reynolds number range particularly in the area of interference effects. Induced drag was minimized primarily by using the high-aspect-ratio wing planforms. In hindsight, the low Reynolds number aspect of the mission primarily influenced the selection of the mean chord since cruise speed requirements were dictated by initial minimum weight estimates and predicted available $C_{L,max}$.

Stability and Control

Control concerns were primarily those of maintaining adequate static-pitch stability and the roll control necessary to perform the closed-course maneuvers. This was usually accomplished with two channels of control, elevator and rudder, in order to eliminate the weight and complexity of the additional control for ailerons. This was accomplished by using large dihedral and oversized rudders. This allowed the aircraft to turn by coupling the yaw and roll axes. The main concern in the area of stability involved static, longitudinal stability.

Static margins were kept at 5-10%, and the center-of-gravity location was crucial to the success of each aircraft. Subsequent flight tests indicated that acceptable remote pilot control required even greater static margins.

Technology Demonstrators

Each design team constructed their prototypes during the last three weeks of the project. They were issued Futaba Attack 4 radio systems, as well as their respective engines. All construction took place in the Notre Dame Aerospace Design Lab, where simple construction equipment was provided for the students. At the end of the three weeks, a series of taxi tests was performed to test the systems and to check the aircraft for basic flightworthiness and controllability. All six aircraft experienced problems, especially in the areas of center-of-gravity placement, tuning of the control surfaces, landing gear stiffness and alignment, and propulsion system battery performance.

On 4 May, 1990, the flight demonstrations were held. Five of the six craft successfully performed at least a single complete figure eight. The sixth aircraft, the Stealth Biplane, was underpowered and could not takeoff unassisted. A hand launch was attempted that proved unsuccessful. Three of the aircraft, Drag-n-Fly, Scream-J4D, and the FX-90 exceeded the range requirements completing as many as 10 laps of the course. Most appeared to exceed their target cruise speeds but handled very well under the control of an experienced pilot. Considering the lack of experience of the builders and the time constraints placed on the teams, this flight demonstration was considered a great success, and showed the students the difference between a conceptual success and success in the real world.

Table 3. Structural Materials

Aircraft	Wing	Fuselage	Empennage
Drag-n-Fly	Spruce/Balsa	Spruce/Balsa Plywood	Spruce/Balsa
Stealth Biplane	Balsa	Balsa	Balsa
Penguin	Spruce/Balsa	Spruce/Balsa	Spruce/Balsa
Scream-J4D	Spruce/Balsa	Spruce/Balsa Plywood	Spruce/Balsa
Dawdler	Spruce/Balsa	Balsa	Balsa
FX/90	Styrofoam	Plywood/Balsa	Balsa

Table 4. Propulsion Systems

Aircraft	Motor Type	Prop	Batteries	Volts	System Weight (oz)	Weight Fraction (%)
Drag-n-Fly	Astro 05	10-6	8 × 500 mah AA NiCad	9.6	11.3	34.8
Stealth Biplane	Peck 035	8-4	10 × 600 mah AA NiCad	12.0	12.6	28.1
Penguin	Astro 15	10-4	13 × 270 mah AA NiCad	15.6	15.3	30.1
Scream-J4D	Astro 05	10-6	7 × 600 mah AA NiCad	8.4	16.2	33.7
Dawdler	Astro 05	9-6	5 × 500 mah	6.0	11.3	35.4
FX/90	Astro 05	10-6	7 × 500 mah AA NiCad	8.4	16.0	36.3

CONCLUSIONS

The purpose of this course is multifaceted. The students entered the course with the knowledge required to complete the mission. The learning process involved the ability to incorporate that information into a design. They were shown the design process from start (the request for proposals) to finish (the prototype). They were immersed into many real world problems faced by engineers. These included working in a team and integrating seven engineers' ideas and work into one design. They were given the opportunity to experience the construction process, and how one must "bridge the gap" between a concept on paper and a flightworthy aircraft.

The students' results, namely their proposals and prototypes, indicate that the goals were achieved. Although they may soon forget their aircraft's design, hopefully what they have learned will help them wherever their careers take them.

ACKNOWLEDGMENTS

This project was supported by NASA/USRA Advanced Aeronautics Design Program. Technical assistance and guidance was provided by the Boeing Company under the coordination of Mr. Cal Watson and Mr. Robert Wickemeyer. The course was presented by Dr. Stephen M. Batill, and graduate teaching assistants David M. Carey and Todd V. Graves. Sections of this report have been edited from the final proposals submitted by each design group. Finally, thanks must go to Mr. Joseph Mergen, Mr. Joel Preston, and Mr. Mike Swadener for their technical assistance and advice throughout the semester.

476-05
P. 9 / 309

A HYPERSONIC RESEARCH VEHICLE TO DEVELOP SCRAMJET ENGINES

THE OHIO STATE UNIVERSITY **N91-18167**

Four student design teams produced conceptual designs for a research vehicle to develop the supersonic combustion ramjet (scramjet) engines necessary for efficient hypersonic flight. This research aircraft would provide flight test data for prototype scramjets that is not available in groundbased test facilities. The design specifications call for a research aircraft to be launched from a carrier aircraft at 40,000 ft and a Mach number of 0.8. The aircraft must accelerate to Mach 6 while climbing to a 100,000-ft altitude and then ignite the experimental scramjet engines for acceleration to Mach 10. The research vehicle must then be recovered for another flight. The students responded with four different designs, two piloted, waverider configurations, and two unmanned vehicles, one with a blended wing-body configuration, the other a delta wing shape. All aircraft made use of an engine database provided by the General Electric Aircraft Engine Group; both turbofanramjet and scramjet engine performance using liquid hydrogen fuel was presented. This paper describes the students' conceptual designs, and the aerodynamic and propulsion concepts that made their designs practical, as well as touching upon interesting problems that surfaced during the design process.

INTRODUCTION

The Ohio State University (OSU) Advanced Aeronautical Design Program (ADP) has focussed upon hypersonic vehicle design concepts for the last three years. With the assistance of staff from the NASA Lewis Research Center, OSU has developed conceptual hypersonic designs of both commercial, 250-passenger aircraft and 10-passenger executive jets. These craft, weighing near one million pounds and 200,000 pounds, respectively, could cross the Pacific in less than three hours. This year, the design project continues the hypersonic tradition with the task of designing a Hypersonic Research Vehicle (HRV) that would be used to develop and flight test the specialized air-breathing, supersonic combustion ramjet engine called a scramjet.

The earlier OSU design concepts operated at Mach numbers below Mach 6, a flight regime that allows variable-cycle air-breathing engines that can use subsonic combustion processes. However, as flight Mach numbers increase above Mach 6, scramjet engines become the only viable air-breathing concept as shown in Fig. 1, a graph of specific impulse versus flight

Mach number for several candidate engines. Conceptual designs at these high Mach numbers must, therefore, employ scramjets. The National Aerospace Plane (NASP), for example, now scheduled for first flight in the later part of this decade uses scramjets to accelerate to near orbital speeds.

Although the concept of scramjet engines has been studied for many years, the practical application of the supersonic combustion process has not been tested extensively. One reason is the lack of adequate ground simulation facilities that can duplicate the high temperatures and pressures the engine will encounter during hypersonic flight. Figure 2 illustrates the ascent and descent trajectories of a single stage to orbit (SSTO) air breather and superimposes the groundbased facilities presently available to these scramjet propulsion concepts. The newest facility, the Rocketdyne Hypersonic Flow Laboratory (RHYFL) appears to cover a reasonable range of flight conditions, but its duration of operation is in the millisecond range, making engine testing difficult. Before risking new aircraft designs on a relatively undeveloped engine concept, it

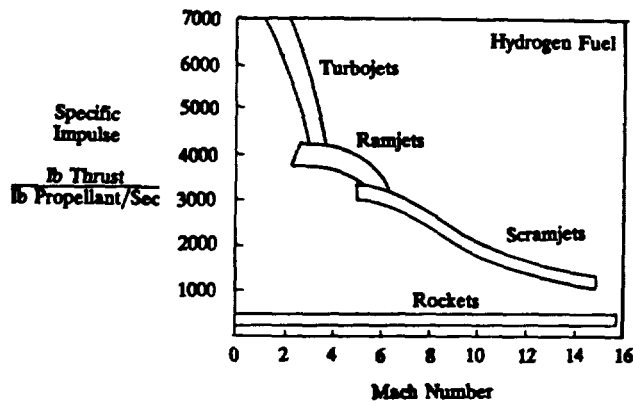


Fig. 1. Propulsion System Operating Regimes

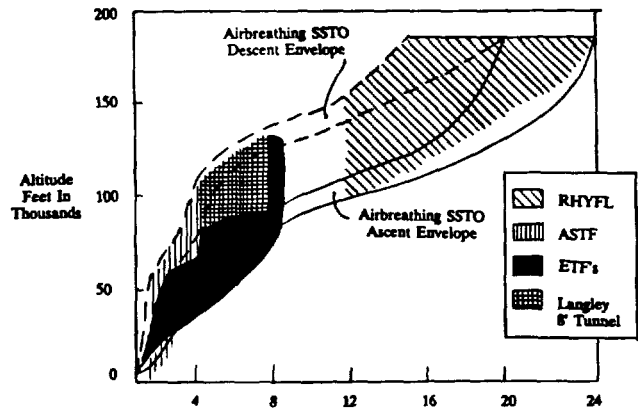


Fig. 2. Ground Test Facility Capability

ORIGINAL PAGE IS
OF POOR QUALITY

appears prudent to develop a test vehicle that can expose the scramjet to the actual flight environment.

The OSU design specification (Table 1) evolved from this desire to provide just such a flying platform to test the scramjet engines. In an effort to reduce costs and fuel weight, the HRV is to be carried to altitude by another aircraft, dropped at Mach 0.8, and then accelerate and climb to Mach 10 at 100,000 ft. The HRV must maintain steady, level flight for two minutes to allow engine performance data to be recorded and then return to base. The vehicle may be either piloted or unmanned, but the intent was for an aircraft that would be well instrumented and used for many engine development flights. The means to accelerate from Mach 0.8 to Mach 6 was not specified.

Table 1. HRV Specifications

<ul style="list-style-type: none"> • Air lifted and dropped from carrier aircraft at Mach 0.8 and 40,000 ft • Accelerate and climb to Mach 6 and 100,000 ft • Ignite scramjet engine(s) and accelerate to Mach 10 • Maintain Mach 10 at 100,000 ft for two minutes • Return and land at base

Four design teams were formed to develop the HRV to these specifications. Two teams chose to design manned vehicles, two selected unmanned concepts. All design groups had engine data packages from the General Electric Aircraft Engine Group. The packages provided engine net thrust, air flow, and fuel flow rates for two types of engines, a turbofanramjet and a scramjet. Full-scale turbofanramjets, shown in Fig. 3, can produce 20,000 lb of thrust at Mach 0.8 and 40,000 ft, and can operate to Mach 6 at 100,000 ft. The scramjet module, also shown in Fig. 3, produces 5,000 lb of thrust at Mach 10 and 100,000 ft. GE also provided the scaling laws to allow the design groups to tailor the engines for their particular configuration.

The four design concepts are presented in the following section. The teams were designated Red, White, Blue, and Gold with the Red and White groups working on the manned aircraft and the Blue and Gold teams developing unmanned vehicles.

The aircraft that would drop the HRV was not considered by the OSU student teams. In a unique international cooperative effort, students from Ecole Polytechnique Feminine designed the carrier aircraft.

AIRCRAFT DESIGNS

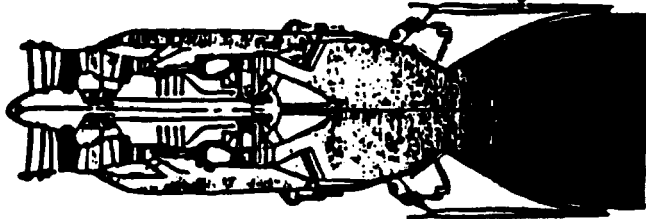
The Red group aircraft, Figure 4a, is a waverider configuration to take advantage of the high lift-to-drag ratios that can be obtained using this shape. It is a manned aircraft; therefore, it must carry life support systems. The Red team's configuration is the largest aircraft having a planform area of 2,300 sq ft and a drop weight of 59,000 lb. It uses two turbofanramjets, scaled at 65%, outboard of four scramjet modules. Since the turbofanramjets are outboard, they are not completely contained in the waverider shape. This separation of engines allows the inlets for each propulsion system to be optimized for its own operating range.

The White group's aircraft is also a waverider and is shown in Fig. 4b. It has a drop weight of 53,000 lb and a planform area of 2,100 sq ft. Five scramjet modules are located on the bottom surface of the body under the two, 80%-scaled turbofanramjets, providing an over-under engine configuration. A single inlet for both engine systems is possible with this arrangement and the turbofanramjets can be completely contained in the waverider body. This aircraft is the second manned configuration.

The major design thrust of the Blue group was to design a small aircraft to make the carrier's job easier. This was accomplished using the blended wing-body configuration shown in Fig. 4c and a rocket assist. Drop weight is 44,000 lb and planform area is 1,711 sq ft. A feature of this aircraft is its separate inlets for the three scramjet modules and the 92% turbofanramjet. The turbofanramjet engine is located on the bottom surface of the body; conversely, scramjets are on the top surface of the body. For each system the inlet and the respective forebody are integrated to give the best system performance. This configuration is the first of the unmanned aircraft.

The Gold team designed a delta configuration (Fig. 4d). It uses one, 100% turbofanramjet and four scramjet modules to power the vehicle. As with the Blue team they use a rocket assist for the initial acceleration from the drop. This was done to minimize fuel usage and to increase acceleration in going to the test conditions. Higher accelerations can be used because it is the second unmanned configuration. The drop weight of 62,000 lb includes the weight of the solid rocket boosters; the planform area is 720 sq ft.

General Electric Turbofanramjet



General Electric Scramjet Module

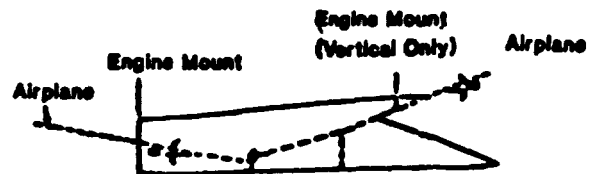
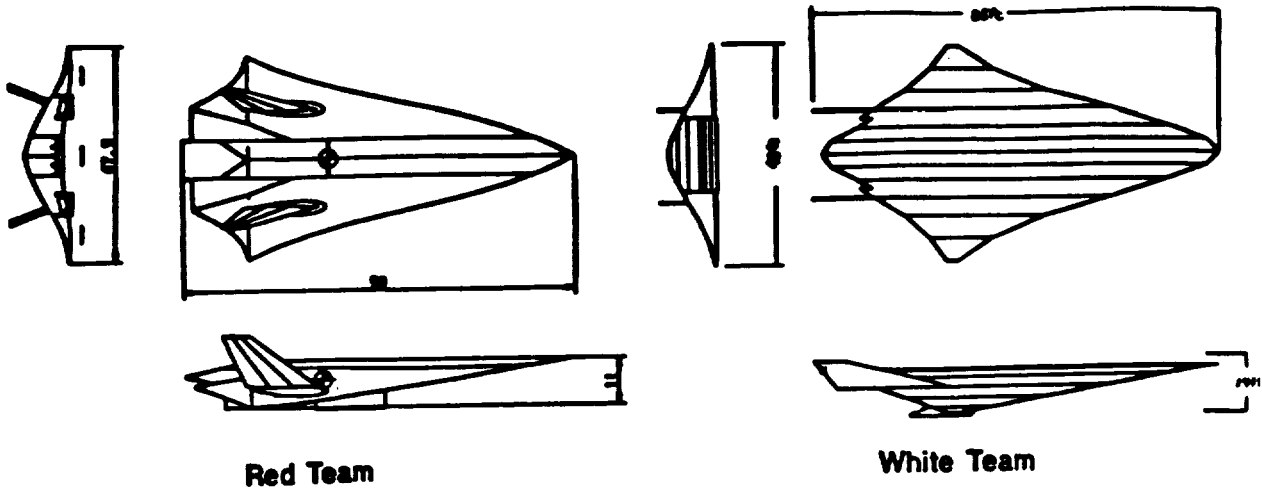


Fig. 3. Propulsion Systems

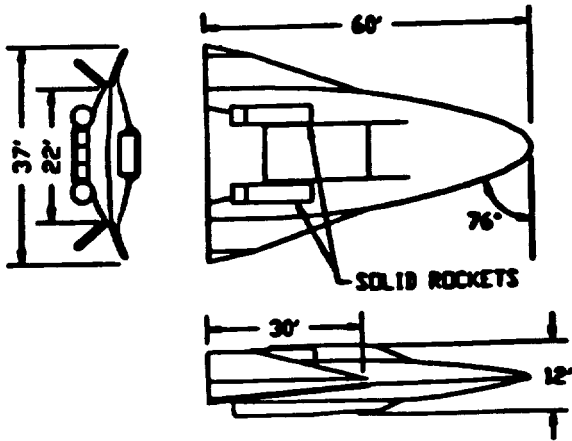


Specifications
Manned
 Planform Area: 2300 sq. ft.
 Wing Loading: 20.85 psf. (Landing)
 Drop Weight: 88,000 lbs.
 Dry Weight: 47,500 lbs.
Propulsion
 Turbofan/jets: 2 @ 85%
 Scramjets: 4

Figure 4a

Specifications
Manned
 Planform Area: 2100 sq. ft.
 Wing Loading: 18.8 psf. (Landing)
 Drop Weight: 83,000 lbs.
 Dry Weight: 39,172 lbs.
Propulsion
 Turbofan/jets: 2 @ 80%
 Scramjets: 5

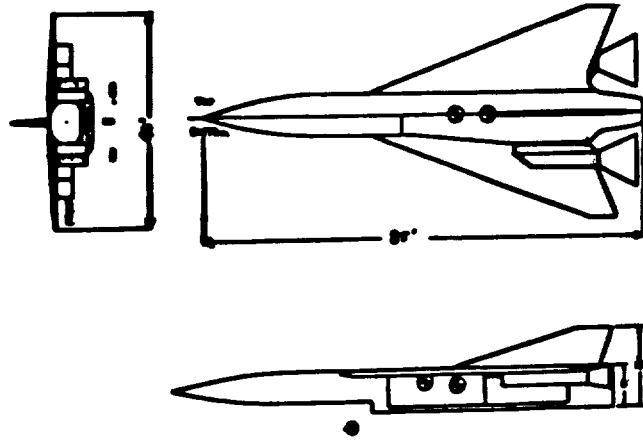
Figure 4b



Blue Team

Specifications
Unmanned
 Planform Area: 1711 sq. ft.
 Wing Loading: 87.44 psf. (Landing)
 Drop Weight: 44,000 lbs.
 Dry Weight: 30,400 lbs.
Propulsion
 Turbofan/jets: 1 @ 82%
 Scramjets: 3

Figure 4c



Gold Team

Specifications
Unmanned
 Planform Area: 720 sq. ft.
 Wing Loading: 81.08 psf. (Landing)
 Drop Weight: 62,000 lbs.
 Dry Weight: 36,774 lbs.
Propulsion
 Turbofan/jets: 1 @ 100%
 Scramjets: 4

Figure 4d

Fig. 4. Aircraft Configurations

ORIGINAL PAGE IS
 OF POOR QUALITY

DESIGN RESULTS

Each design group did a comprehensive study of their configuration weight, aerodynamics, propulsion system (including inlet configuration), and heating. There is not space to review all the details of each design here; instead representative results from the teams' designs will be discussed to provide a flavor of the HRV design process.

Weight Estimate

Several weight estimating methods were used by the design groups. Methods in Nicolai⁽¹⁾ and Roskam⁽²⁾ texts and a NASA Lewis Research Center WAATS program⁽³⁾ provided empty and gross weight estimates. The HRV's drop weights ranged from 44,000 lb to 62,000 lb. The unmanned vehicles had the lowest empty weights, 30,400 lb and 36,800 lb for the Blue and Gold teams respectively, while the manned vehicle empty weights were 47,500 lb and 39,200 lb for the Red and White designs.

Figure 5a illustrates the component weight distribution for the White and Blue team designs. The heavier White manned aircraft had a structure and engine weight of 28% and 32% of the total drop weight of 53,000 lb. The unmanned Blue HRV had a structural and engine weight of 13% and 22% for its drop weight of 44,000 lb. The distribution of the fuel used for the three phases of powered flight: acceleration under turbofanramjet to Mach 6, acceleration of Mach 10 during scramjet operation, and the fuel used during the two-minute, steady flight, is also shown in Fig. 5b. While the waverider uses

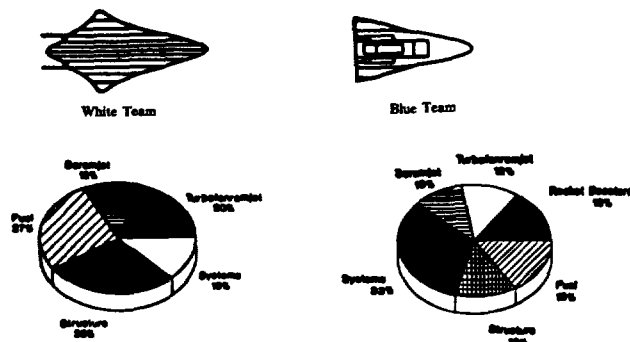


Fig. 5a. Weight Percentage Distribution

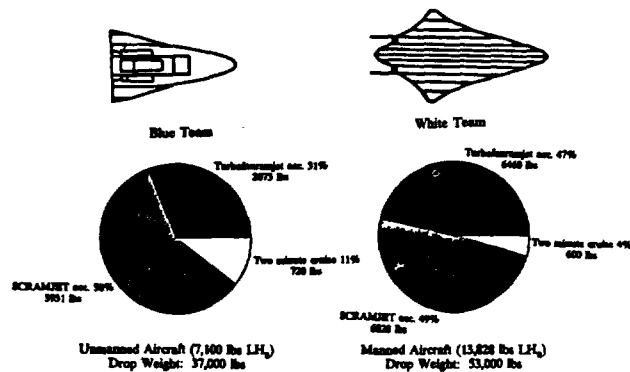


Fig. 5b. Fuel Weight Percentage Distribution

47% of its fuel during turbofanramjet acceleration, the unmanned Blue HRV uses but 31% since the Blue vehicle uses a short rocket boost. On the other hand, the Blue HRV burns 720 lb in two minutes at Mach 10, whereas the White, low-drag waverider, uses but 600 lb.

Engines

One of the first considerations when deciding on the propulsion system was the type of fuel to be used. Figure 6a shows a comparison of mass energy density and volumetric energy density for three fuels liquid hydrogen (LH₂), liquid methane (LCH₄), and Jet A. Although LH₂ has a high mass density, a penalty is paid because of its low volumetric density. The Candidate Engine Performance presented earlier indicates good performance for all the engine systems using hydrogen fuel; therefore, all groups decided to use the LH₂ and take the volumetric penalty. The Candidate Engine Performance Chart also shows the performance of solid rockets in the range of the proposed mission. Early in their design studies, the teams found that if their aircraft were to use solid rockets exclusively for the acceleration, the fuel weight would be prohibitively high because of the low specific impulse of rockets. None of the four configurations used solid rockets as the only acceleration system.

Because of the volume penalty when using liquid hydrogen, the design groups used several methods for reducing the fuel weight. A large portion of the fuel is used during the scramjet burn during the acceleration from M=6 to M=10. The White team did a trade study to determine the optimum number of scramjet engines to minimize the fuel while limiting the weight penalty of additional scramjet modules. Figure 6b shows the number of engines versus the fuel weight to accelerate the HRV. As modules are added the required fuel weight is reduced. The students determined that the optimum number of scramjets is five because the weight penalty paid for having the sixth scramjet module is greater than the fuel savings.

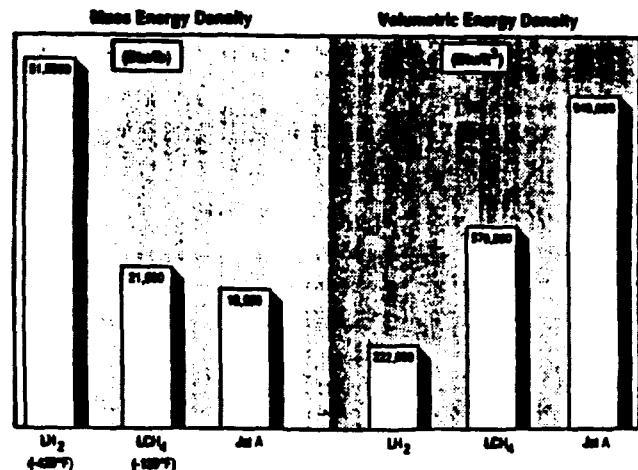


Fig. 6a. Fuel Comparison

ORIGINAL PAGE IS OF POOR QUALITY

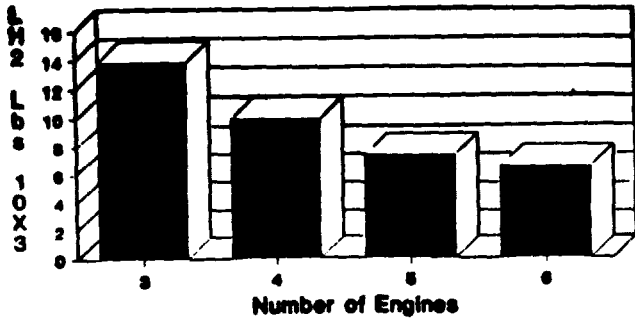


Fig. 6b. Number of Engines vs. Fuel Weight for Scramjet Operation

Typical performance data obtained from the engine data for the two types of engines are presented in Fig. 7. The thrust as a function of Mach number for the turbofanramjets is shown as a function of altitude. The engine thrust increases with Mach number, but decreases significantly with altitude. The scramjet engine Mach number performance is shown as a function of Q, the dynamic pressure, a convenience, since many climb trajectories are performed at constant Q. Again, the decrease in net thrust with altitude (lower Q at fixed Mach number) is observed.

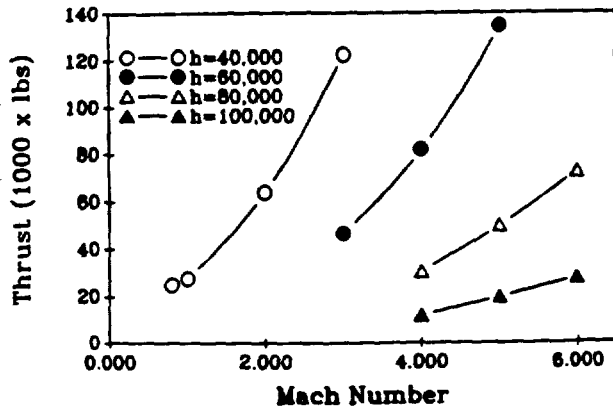


Fig. 7a. Turbofanramjet Performance

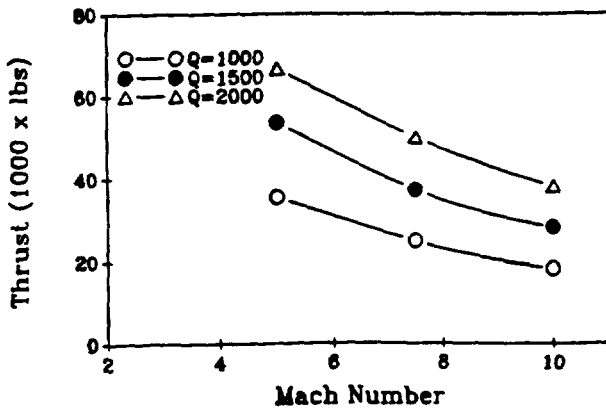


Fig. 7b. Scramjet Performance

An integral part of the propulsion installation is the inlet design. Each group had different inlet designs; inlet configurations varied from completely separate engine systems, as in the Blue design, to common inlets for both engine types, as in the White design. The inlet designs shown in Fig. 8 are representative of the inlet configurations examined by the student teams. All are variable geometry inlets, necessary to accommodate the changing capture areas required for the large range of Mach numbers and altitudes. An example of the pressure recovery for two inlets is shown, one for the turbofanramjet and another for the scramjet inlet. The figure is for the Red aircraft which had separate inlets for both engines; the turbofanramjet inlet is axisymmetric, while the scramjet inlets are two-dimensional.

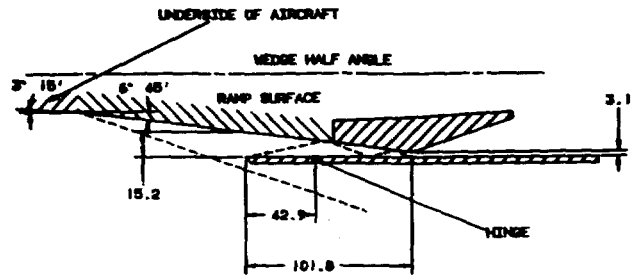


Fig. 8a. Scramjet Inlet M = 6.0

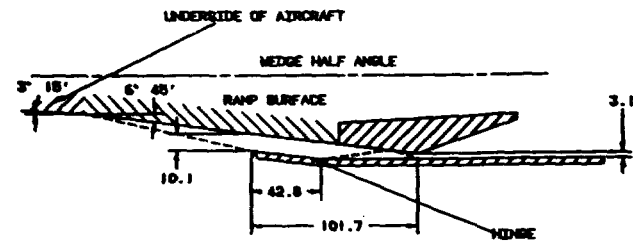


Fig. 8b. Scramjet Inlet M = 10.0

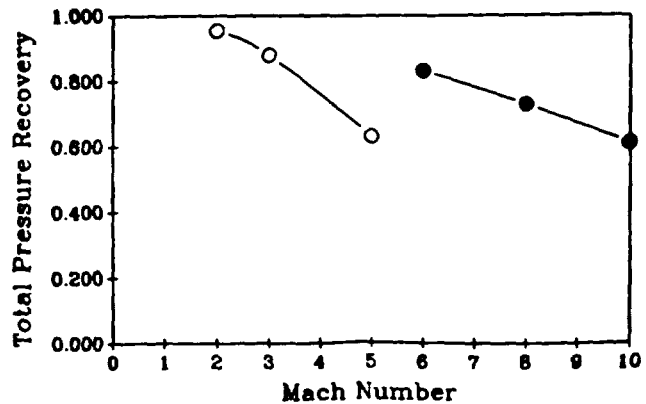


Fig. 8c. Inlet Pressure Recovery

Aerodynamics

A vital part of the design is the vehicle aerodynamics. Because each aircraft flies through subsonic, supersonic, and hypersonic regimes, several methods were used to determine the aerodynamic characteristics. Primarily, the methods outlined in Nicolai's book, *Fundamentals of Aircraft Design*⁽¹⁾ were used to determine the subsonic and supersonic characteristics. Other methods incorporated included shock expansion theory and Newtonian methods for hypersonic flows.

The two manned aircraft that used a waverider configuration developed the shape using a program called MAXWARP developed by Dr. S. Corda and Dr. J. Anderson at the University of Maryland⁽⁴⁾. Since a waverider is optimized for a certain Mach number and altitude, initially there was a question of the validity of using a waverider shape for these aircraft since they will not be at any particular Mach number for an extended period of time. Figure 9 shows a comparison of waverider shapes at Mach numbers of 6, 8, and 10. After comparing these shapes and consulting with the University of Maryland, it was determined that the off-design characteristics of the waveriders will be good enough to justify their use in the designs. Using the methods discussed above, plots of the Red group's waverider drag polar and lift-to-drag ratios versus Mach number were generated and are shown in Fig. 10. Note the

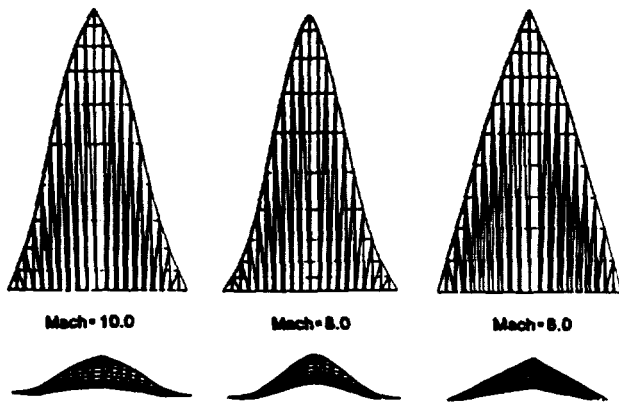
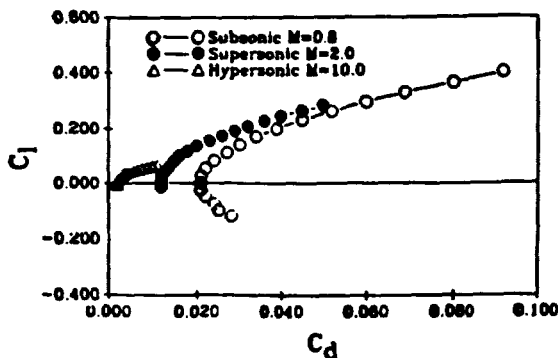


Fig. 9. Waverider Comparison



thrust "pinch" as the vehicle accelerates through Mach 1 and the increasing lift-to-drag ratio as the waverider reaches its design flight condition.

A model test of the Red group's waverider was conducted in the OSU 3' x 5' subsonic wind tunnel using a 1/72 scale model. Lift and drag coefficients were found as a function of angle of attack using a three-component balance. These data, shown in Fig. 11, agree well with the subsonic aerodynamic estimates.

Heating and Cooling

In any hypersonic design, aerodynamic heating is an important concern. Since the HRV is to fly at hypersonic speeds for less than 15 minutes, questions were raised about the time required to reach equilibrium skin temperature. After discussing this problem with engineers at NASA Lewis Research Center, the OSU mentor center, it was determined that the vehicles could heat to steady state in less than a second and there would be no need to account for unsteady heat transfer. The worst case of steady-state heating was considered by each group; that is, the highest skin temperature was reached when the convective heat input was balanced by radiative output. This equilibrium temperature distribution for the Red team's aircraft is shown in Fig. 12.

Because of these high temperatures, over 3500°F at the nose and inlets, special materials and several methods for cooling are required. Wherever possible radiative cooling of the structure is used because it requires no coolant to be carried. Hastelloy-x is used in these areas. Other systems incorporated are liquid convective cooling and a carbon/carbon integrated heat pipe structure for the leading edges, shown in Fig. 12. At the nose, a JTA graphite composite must be used. While this material can sustain high temperatures, it must be replaced after a few flights.

Flight Profile

One of the interesting operational aspects of this project was examining the flight profile of a typical research flight. By optimizing the climb trajectory, a substantial saving in fuel can be obtained. Figure 13 shows one of these optimized

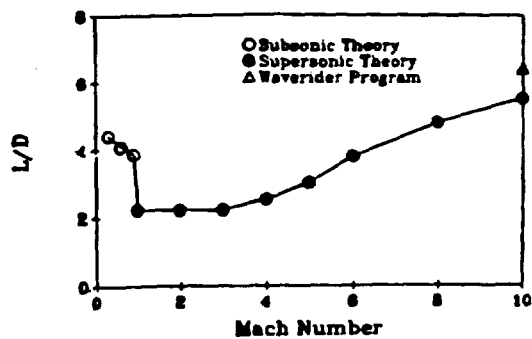


Fig. 10. Theoretical Aerodynamics

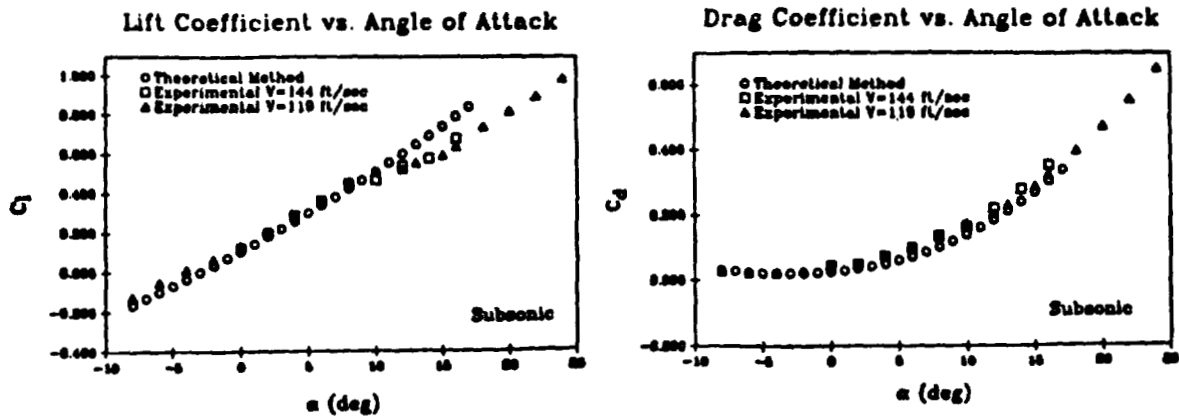


Fig. 11. Wind Tunnel Data

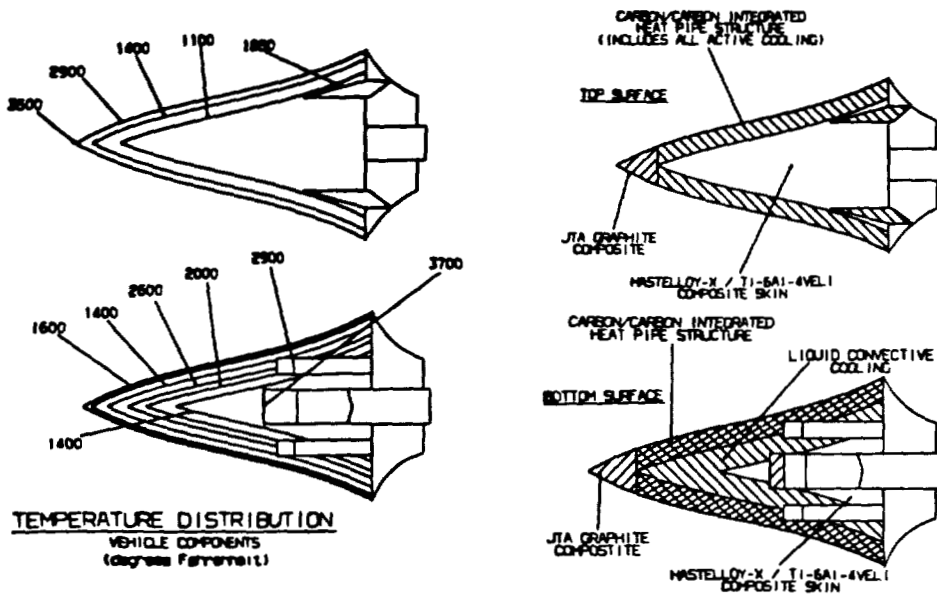


Fig. 12. Equilibrium Temperature Distribution and Materials

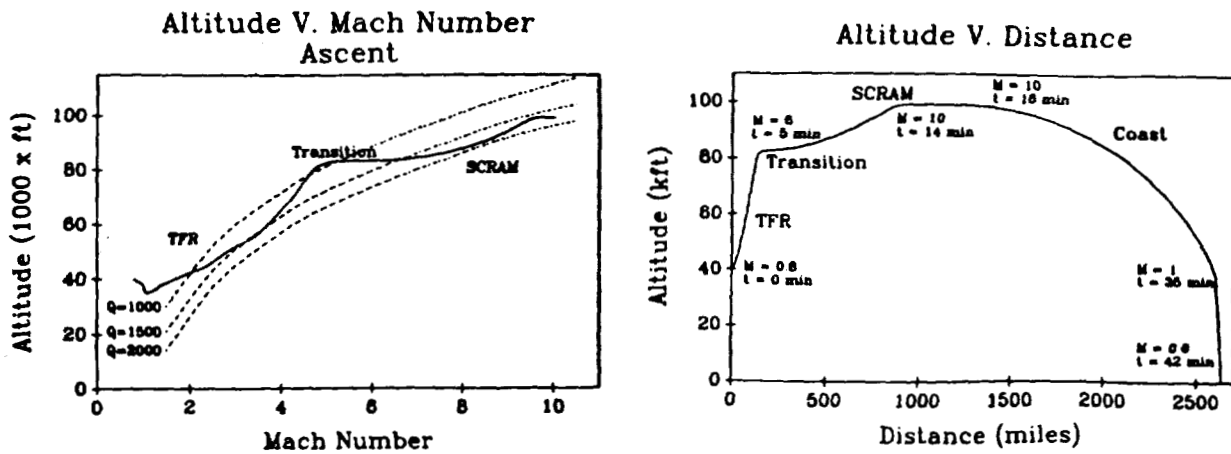


Fig. 13. Flight Profile

trajectories. Also shown is the transition from turbofanramjet to scramjet operation. A somewhat unexpected result is the distance required for a research flight. Accelerating to Mach 10 and maintaining Mach 10 for two minutes requires a straight line distance in excess of 1500 miles.

The large distance to accelerate and slow down creates a problem of where to fly the research vehicle. Two prospective flight paths are depicted in Fig. 14. One path is a drop just off the coast of Alaska with a landing at NASA Dryden Flight Testing Center; the other is a drop in Maine and a landing at NASA Kennedy Space Center in Florida. At this time the west coast site would probably be used, because all four of the research vehicle designs have skids for landing gear and the Dryden site is the dry lake bed rather than concrete. The drop location also impacts the carrier aircraft design, requiring the carrier aircraft to fly out a considerable distance with the HRV.

A final observation is that the flight paths are all over water. This is done so that any sonic booms created by the aircraft do not disturb populated areas. An estimate of the largest overpressure caused by a sonic boom is shown in Fig. 14. Of interest is the overpressure of one lb/ft² which may be a tolerable sonic boom pressure over land.

SUMMARY

Four conceptual designs for a hypersonic research vehicle have been developed by four design teams. Two concepts are manned vehicles, two are pilotless. The motivation behind these designs was to allow supersonic combustion ramjets to be tested and refined in the actual flight environment, since ground based facilities cannot duplicate the extreme pressures and temperatures of hypersonic flight. Characteristics of the four configurations are presented in Fig. 15.

The summary table (Fig. 15) presents a comparison of pertinent performance data for the four HRVs. For example, the low wing loading of the waveriders in contrast to the unmanned vehicles can be noted on the order of 20 lb/ft



Type	Manned	Manned	Unmanned	Unmanned
Gross Weight	59,000 lbs	53,000 lbs	44,000 lbs*	62,000 lbs*
Empty Weight	47,600 lbs	39,172 lbs	37,000 lbs**	47,000 lbs**
Length	90 ft	85 ft	60 ft	85 ft
Span	.48 ft	48 ft	37 ft	40 ft
W/S (Landing)	20.6 paf	18.6 paf	37.4 paf	51.0 paf
T/W (Drop)	0.42	0.57	1.59 *	1.2 *
L/D (M=10)	6.5	6.2	0.35 **	0.44 **
Cost (Billions)	\$4.79	\$4.45	\$3.7	\$3.3

*with booster rockets
**without booster rockets

Fig. 15. Aircraft Summary

compared with double that value for the unmanned aircraft. The low wing loading, of course, will allow low landing speeds for the waveriders. Similarly, the thrust-to-weight ratios for the waveriders are significantly lower than the rocket-boosted, unmanned HRVs, requiring longer acceleration times and increased hydrogen fuel usage. On the other hand, the efficient lift-to-drag ratios near L/D = 6 of the waveriders can be compared with the lower L/D values of the more conventionally configured aircraft.

Cost of producing a single research aircraft is also shown in Fig. 15, with the manned aircraft approximately a billion dollars more expensive than the unmanned HRVs. Whether this cost can be borne by the United States over the next five or six years to develop an operational scramjet engine with the potential for efficient air breathing flight to near orbital speed was not a consideration for the students. The students did consider the merits of a manned machine versus an unpowered vehicle with each group supporting its design view. Manned

**ΔP vs Altitude
Boom Pressure**

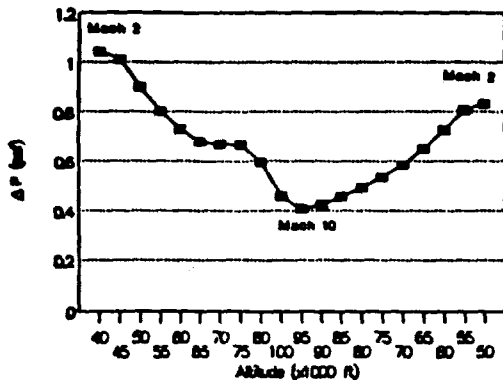


Fig. 14. Sonic Boom Overpressure and Flight Path

vehicles would be flexible with pilots handling unexpected engine problems and research opportunities at the expense of weight and life support systems, while unmanned vehicles would not endanger a pilot's life, be cheaper and lighter in weight. Yet, a successful manned HRV would provide much operational hypersonic flight experience, once the engines were proven. While these questions remain, the design task was certainly well worth the student effort, with the results a contribution to this controversial problem.

REFERENCES

1. Nicolai, L.M., *Fundamentals of Aircraft Design*. San Jose, CA: METS, Inc., 1974.
2. Roskam, J., *Airplane Design*. University of Kansas, 1986.
3. Glatt, C.F., *Weights Analysis of Advanced Transportation Systems*. NASA CR-2420.
4. Corda, S., "Viscous Optimized Hypersonic Waveriders Designed from Flows over Cones and Minimum Drag Bodies". University of Maryland, 1988.



CARRIER AIRCRAFT
ECOLE POLYTECHNIQUE FEMININE

N 91 - 18168

This year the Ohio State University planned to conduct a conceptual design of a single research aircraft that could be used to explore the flight regime from Mach 6 to Mach 12.

Since this aircraft will be a special purpose vehicle, it need not take off and land in a conventional manner. Indeed, if this aircraft were launched from a larger aircraft that carried it to altitude, then conventional landing gear would not be needed, and the extra weight of the fuel to take off and climb into the stratosphere would be eliminated.

The focus of EPF students' project was on the design of a carrier aircraft answering to the specifications. Its mission is

to take off with the research aircraft from runways of less than 15,000 ft, climb to 40,000 ft, and release the hypersonic aircraft at the speed of Mach 0.8, and return to base. The range of this mission is 2000 n.m.

This study includes the conception of an optimized aircraft (geometry, weights, propulsion, aerodynamics, interactions between the two aircraft, etc.), the longitudinal stability of the composite, and the separation critical phase.



DESIGN OF A HIGH SPEED BUSINESS TRANSPORT

P.4

PURDUE UNIVERSITY

N91-18169

The design of a High Speed Business Transport, the HSBT, was considered by the Aeronautical Design Class during the academic year 1989-90. The project was chosen to offer an opportunity to develop user friendliness for some computer codes such as WAVE DRAG, supplied by NASA/Langley, and to experiment with several design lessons developed by Dr. John McMasters and his colleagues at Boeing. Central to these design lessons, used at the beginning of each semester, was an appeal to marketing and feasibility considerations from the very beginning and the emphasis upon simplified analytical techniques to study trades and to stimulate creative thinking before committing to extensive analytical activity.

All design teams considered the same general category of aircraft, one that was to fly supersonically to foreign business regions. Neither the Mach number nor the range were specified by the instructor. The choice of number of passengers was also undefined initially. As a result, no design group developed exactly the same RFP. Although a number of excellent designs were developed, two designs stood out above all the rest because of the depth of thought and consideration of alternatives. These two designs used quite different methods to meet approximately the same RFP.

One design, the Aurora, used a fixed wing design to satisfy the design mission, while the other design, the Viero, used a swing wing configuration to overcome problems related to overland supersonic flight. The Aurora design was composed of seven students led by Mr. Lyle Dailey, while the Viero group consisted of five students led by Mr. Dan Cler. What follows is a summary of each of those designs.

AURORA DESIGN SUMMARY

A Request For Proposal (RFP) was developed for a Mach 2.2, 8-passenger business transport with a range of 4980 n.m. capable of serving transpacific business routes. The Aurora will have an approach speed of 160 kts. The target date for delivery of the Aurora is the year 2005. The Aurora can deliver passengers from Los Angeles to Tokyo in 4.43 hours, approximately one-third the travel time of current subsonic aircraft. Figure 1 provides a three-view of the Aurora together with several cabin arrangements.

The Aurora has an overall length of 110 ft and wing span of 47.2 ft. The external hull diameter is 6.5 ft at its maximum dimension. The cabin section has a length of 24 ft 8 in (including flight deck) and an internal diameter of 5 ft 8 in, allowing an aisle height of 5 ft 6 in. The cabin has first class seating with an 18-in aisle width and 44-in seat pitch.

A three engine configuration is used to satisfy FAR 25 one-engine-inoperative safety requirements for transoceanic flight.

One podded engine is located under each wing, with the third engine placed on top of the aft fuselage extending through the vertical tail.

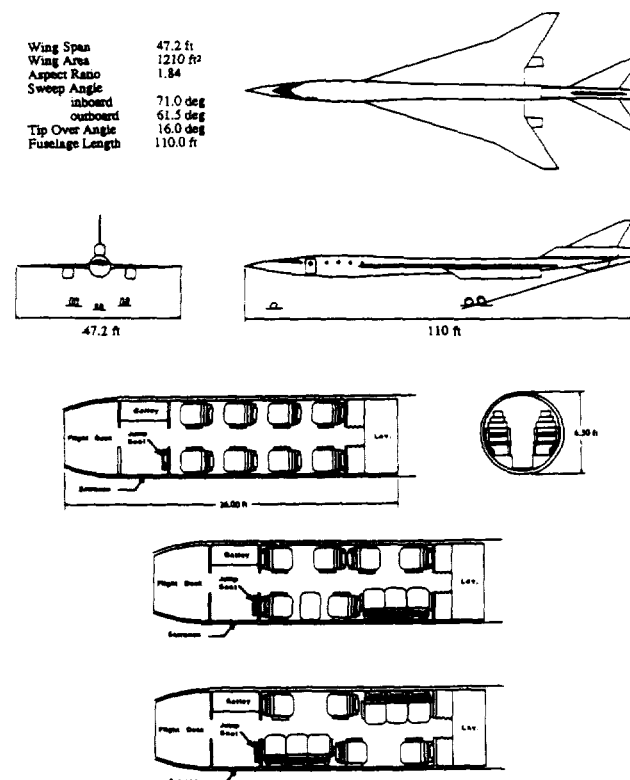


Fig. 1. Aurora Three View and Cabin Layout

Aurora Design Features

A long-range supersonic transport such as the Aurora requires high aerodynamic efficiency, measured by the lift-to-drag ratio (L/D) during supersonic cruise, to minimize fuel requirements and to maximize range. However, supersonic transports must also operate effectively at subsonic speeds, especially for takeoff and landing.

Because of these requirements, a highly swept, low aspect ratio, modified arrow wing was selected because of its low supersonic cruise drag. Wing geometry information is contained in Table 1. The Aurora has a trimmed supersonic L/D of 7.07 at cruise.

Table 1. Aurora Planform Geometry Parameters

Wing Area:	1210 ft ²	Aspect Ratio:	1.84
Wing Loading:	90 lb/ft ²	Wing Span:	47.2 ft
Root Chord:	48.3 ft	Tip Chord:	4.21 ft
Mean Aerodynamic Chord:	34.5 ft	Tip-Root Chord Ratio:	0.076
Wing Length:	65.2 ft	Box Ratio:	0.362
Thickness-Chord Ratio:	0.06		

The inadequate subsonic performance of an arrow wing requires that leading edge vortex flaps and trailing edge flaps be incorporated into the Aurora design to provide high lift during takeoff and landing. For trimmed takeoff, with leading edge flaps deployed, the Aurora needs a lift coefficient of 0.7, requiring a wing angle of attack of 10°, and a trailing edge flap deflection of 5°. During subsonic cruise at Mach 0.85, the Aurora has an L/D of 9.5.

The total net thrust required at takeoff is 40,900 lb. This thrust is produced by three non-afterburning turbojet engines that satisfy one-engine-inoperative criteria. With one engine out, the Aurora can still take off at a throttle setting of 97%. For supersonic cruise at Mach 2.2 ft, the thrust specific fuel consumption is 1.192 lb/lb/hr. At this condition, each engine produces 10,700 lb of thrust. During subsonic operation at Mach 0.85 and 30,000 ft, each engine produces 8308 lb of thrust.

The aircraft has a TOGW of 104,500 lb, determined using the Flight Optimization System (FLOPS). The Aurora has eight fuel tanks; three are located in each wing and two are located in the aft fuselage. This configuration allows a fuel burning sequence that keeps the static margin between 5 and 24%.

The Aurora employs a tricycle landing gear configuration. The nose gear has a length of 10.0 ft and uses a dual wheel arrangement, while the main gear has a length of 11.5 ft and uses a twin tandem wheel configuration. A tipback angle of 16° allows safe rotation for takeoff and landing and a turnover angle of 57° provides sufficient ground maneuverability.

Aluminum was selected as the primary material for the Aurora because of its low cost. At the cruise Mach number and altitude, stagnation temperatures will reach 310°F. Aluminum will lose 15% of its yield strength at this temperature; as a result, titanium is used in the higher temperature regions such as leading edges, engine nacelles, and the nose cone. Titanium was not used as the primary material, even though it has better temperature strength, temperature, and fatigue characteristics, because the cost per aircraft would increase by 60%.

Providing the stability and control necessary for the mission involves meeting three requirements. These requirements are that the aircraft is stable, can be controlled, and can be trimmed. Achieving these requirements involves empennage design, static stability analysis, and trim analysis.

Empennage design efforts resulted in a conventional tail arrangement employing "all-moving" horizontal and vertical tail surfaces. The horizontal tail was sized to meet the requirements of rotation on takeoff. The result was a 140-ft² horizontal tail which must be deflected 18° leading edge down for

takeoff. The vertical tail was sized to meet the one-engine-inoperative condition. This requirement produced a 69.2-ft² vertical tail which needs to be deflected 10° to maintain a zero sideslip angle with one engine inoperative.

An attempt was made to keep the static margin between 5 and 10%. The subsonic static margin was between 5% and 16%, while the supersonic static margin is between 18 and 24%.

The aircraft trim was determined for several different flight conditions. As expected, the low-speed trim angles α and δ_c are rather large (5 to 10°), while the high-speed angles are very small (less than 3°). These small trim angles at supersonic speeds cause very little trim drag, and thus improve performance.

Cruise range, operation altitude, and trip time are measures of the overall aircraft performance. Other areas of interest include the ability of the aircraft to take off and land under off-design conditions. The Aurora was designed to meet the goals set by the RFP and an analysis of the final design showed that, with the exception of the takeoff field length, all those goals were met. A field length of 8800 ft, 300 ft greater than the target stated in the RFP, is needed for takeoff. All of the major and international airports that were targeted for the normal flight operation of the Aurora have runways that exceed 10,000 ft. As a result, the takeoff field length of 8800 ft will not restrict the normal operation of the Aurora.

The total cost of an aircraft from its design to its retirement is defined as the Life Cycle Cost (LCC). Included in the LCC are research, development, test, and evaluation (DT&E), acquisition, and operations. The research phase includes the research, exploratory and advanced development efforts needed to initiate the design process. Research cost is not included in the cost analysis due to the difficulty in its determination. The DT&E phase determines the cost to design and develop a working aircraft to satisfy the needs of the customer and the industry.

The development cost for the Aurora HSBT is \$1.93 billion. The production cost is the cost to produce the aircraft and results in a price per copy. The total production cost for the Aurora HSBT is \$6.4 billion, and the total price per aircraft, based on 150 aircraft, is \$47.3 million.

Direct operating costs involve fuel and oil consumption, maintenance, and the number of crew needed to operate the aircraft. Other factors included are depreciation and insurance. The direct operating cost per flight for the Aurora, based on 110 flights per year, is approximately \$47,000 for a 4980 n.m. trip.

The Aurora HSBT bears a striking resemblance to the Gulfstream/Sukhoi HSBT design. The development cost for the Gulfstream HSBT is over \$1 billion compared to \$1.93 billion for the Aurora. The price per aircraft for the Gulfstream is \$50 million compared to \$47.3 million for the Aurora.

THE VIERO VARIABLE - SWEEP TRANSPORT

The Viero design team chose a cruise Mach number of 2.5, a cruise range of 4750 n.m., and a payload of nine first-class, business passengers with a crew of two. The Viero, with its

variable-sweep wing shown in Fig. 2, was designed to meet the needs of fast and long-range business travel. It also must have a substantially better subsonic cruise efficiency than a typical supersonic transport to be competitive with current business aircraft. Table 2 presents performance parameters of the Viero.

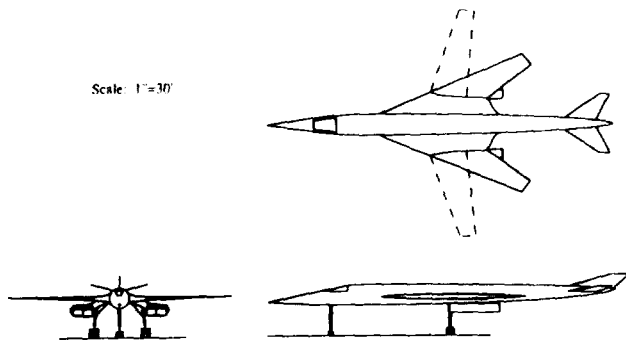


Fig. 2. Three-View of the Viero Executive Jet

Table 2. Viero Performance Parameters

Cruise Mach Number	2.5
Cruise Altitude	73,000 ft (supersonic) 35,000 ft (subsonic)
Takeoff Gross Weight	128,348 lbs
Payload	1,881 lbs
Operating Empty Weight	54,264 lbs
Fuel Burned	73,724 lbs (JP8)
Range	5,262 n.m. (including reserves)
Block Time	4 hrs 34 min (including reserves)
Block Fuel	72,206 lbs
Takeoff Distance	3,357 ft
Takeoff g's	0.12 g's
Landing Distance	4,610 ft
Rate of Climb	3,000 ft/s (cruise) 9,300 ft/s (sea level)
Thrust	17,000 lbs per engine
Cruise Specific Fuel Consumption	1.192 lbs/lbs/hr (supersonic) 0.8 lbs/lbs/hr (subsonic)
Wing Reference Area	1,032 ft ²
Wing Spans	89 ft (unswept), 55 ft (swept)
Aspect Ratio	7.624 (unswept), 2.931 (swept)
Wing loading	120.9 lbs/ft ² (max)
Cruise Lift-To-Drag Ratio	6.3 (supersonic), 14.7 (subsonic)

The Viero payload-range curve (Fig. 3) indicates that the Viero payload has little effect on range because the maximum payload is less than 1.5% of the takeoff gross weight. For most commercial transports the payload can comprise almost 50% of the takeoff gross weight.

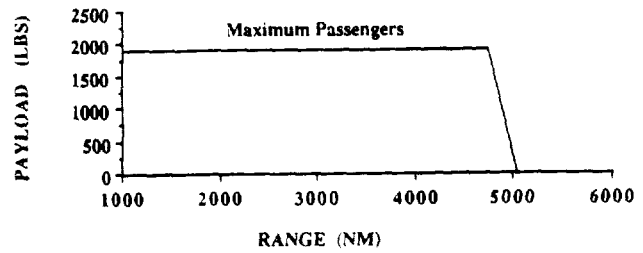


Fig. 3. Viero Payload-Range Curve

The Viero's takeoff and landing field lengths allow the use of smaller airports. The FAR 25 balanced takeoff distance is 3300 ft. The balanced landing distance is 4700 ft.

Figure 4 shows the fuel burned during a Viero mission per trip cost is more than \$17,700, since 73,700 lb of JP8 fuel are used based on \$1.50 per gallon (typical private aircraft fuel costs).

The Viero is compared to the Concorde in Fig. 5. The structure of the Viero is designed to keep the empty weight to a minimum. By using integrally stiffened skin panels and lightweight composite materials for the structural cover, the weight is reduced by about 10% when compared to a similar aircraft constructed of aluminum.

The cabin layout shown in Fig. 6 will seat nine first-class, business passengers. Several aspects of the Viero make it stand out from other HSBTs. The high cruise wing loading creates a smooth and comfortable ride by not being so sensitive to atmospheric disturbances. The swing wing utilized on the Viero not only allows for supersonic flight but enables efficient subsonic cruise over land where supersonic flight is not allowed. The variable-sweep wing allows takeoffs and landings from smaller, less congested airports.

Based on an operating empty weight of 52,000 lb, a design speed of Mach 2.5, and an estimated production quantity of 200 between the years 2002 and 2016, the Viero cost is

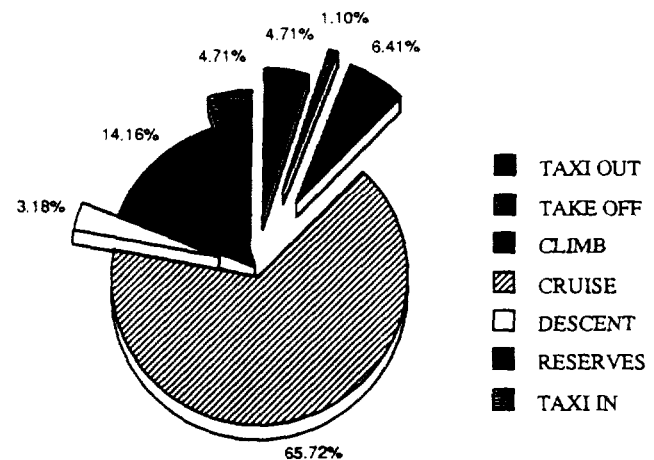


Fig. 4. Viero Fuel Burned as Percentage of Total Used

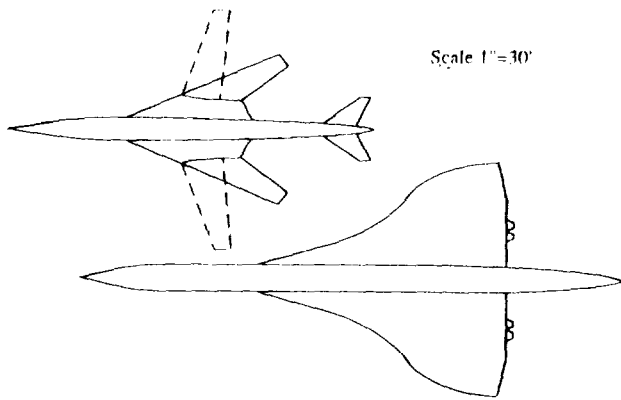


Fig. 5. Planform Comparison: Viero and Aerospatiale/BAC Concorde

estimated to be \$47.5 million. With engine costs of around \$1 million each, this brings the Viero's selling price up to \$51.5 million. Initial estimates of quantity to produce and orders to be taken indicate a project net present value (year 2002) of over \$60 million. Direct operating costs based on \$1.50 per gallon of fuel are shown in Table 3.

Table 3. Direct Operating Costs (1989 dollars)

Fuel	\$16,870
Crew	\$1,045
Maintenance	\$1,329
Depreciation	\$8,141
Insurance	\$577
Total	\$27,963
Cost Per Passenger	\$3,107
Seat-Miles Flown	\$2,750
DOC/Mile (\$/Mile)	\$5.89
DOC/Seat-Mile (\$/ASLM)	\$0.65

These costs combined with comparable indirect operating costs (overhead, ground facilities depreciation, customer service, etc.) lead to a round trip ticket price per passenger of around \$6,000, competitive with that of the Concorde.

SUMMARY

Two designs for a High Speed Business Transport were developed in response to a similar RFP. These design efforts showed the enormity of the cost of such a project. The integrated use of empirical estimation techniques, together with sophisticated analytical prediction enhanced the design effort. Inclusion of cost estimation at the earliest possible time emphasized the design trade-offs.

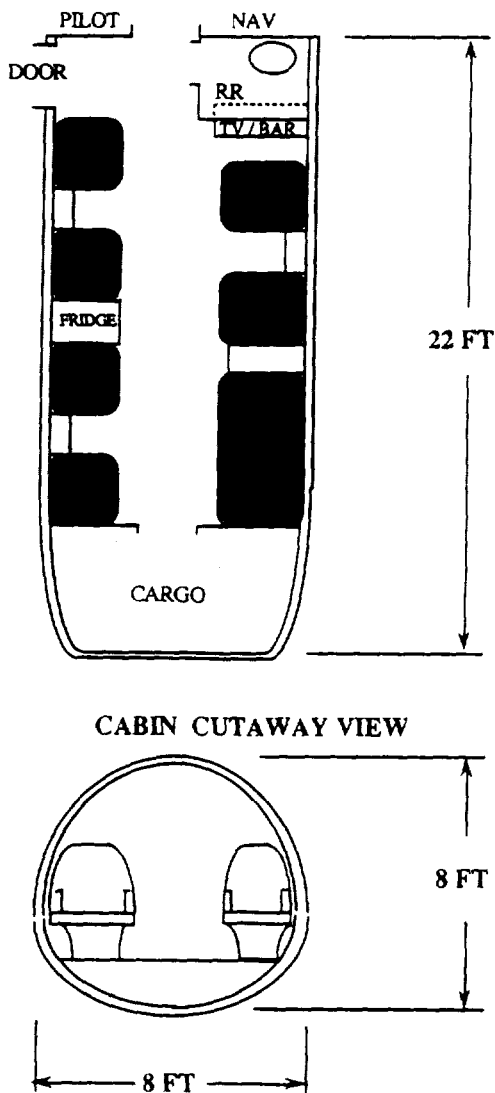


Fig. 6. Cabin Layout of the Viero

325
p.1

HIGH ALTITUDE, MICROWAVE-POWERED ATMOSPHERIC SAMPLING AIRCRAFT

N91-18170

WORCESTER POLYTECHNIC INSTITUTE

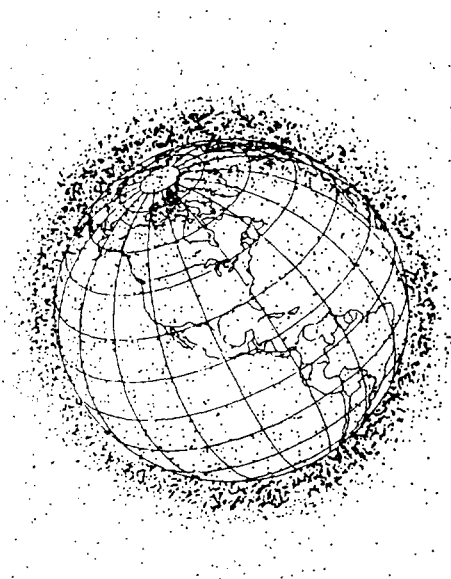
The preliminary design of a high-altitude, remotely piloted, atmospheric sampling aircraft powered by microwave energy beamed from a ground-based antenna has been completed. The vehicle has a gross weight of 6720 lb, and is sized to carry a 1000-lb payload at an altitude of 100,000 ft. The underside of the wing serves as the surface of a rectenna designed to receive microwave energy at a power density of 700 W per m²; the wing has a planform area of 3634 sq ft to absorb the required power at an optimum Mach number, $M = 0.44$, and an airplane lift coefficient, $C_L = 0.65$. The aircraft utilizes a horizontal tail and a canard for longitudinal control and to enhance the structural rigidity of the twin fuselage configuration. The wing structure is designed to withstand a gust-induced load factor, $n = 3$, at cruise altitude, but the low wing

loading of the aircraft makes it very sensitive to gusts at lower altitudes, where induced load factors may be in excess of 20. A structural load alleviation system is, therefore, proposed to limit actual loads to the designed structural limit. Losses will require transmitted power on the order of megawatts to be radiated to the aircraft from the ground station, presenting environmental problems. Since the transmitting antenna would have a diameter of several hundred ft, it would not be readily transportable, so we propose that a single antenna be constructed at a site from which the aircraft is flown. The aircraft would be towed aloft to an initial altitude at which the microwave power would be utilized. The aircraft would climb to cruise altitude in a spiral flight path and then orbit the transmitter in a gentle turn.

Alumni Projects

p. 3

ORBITAL DEBRIS REMOVAL AND SALVAGE SYSTEM

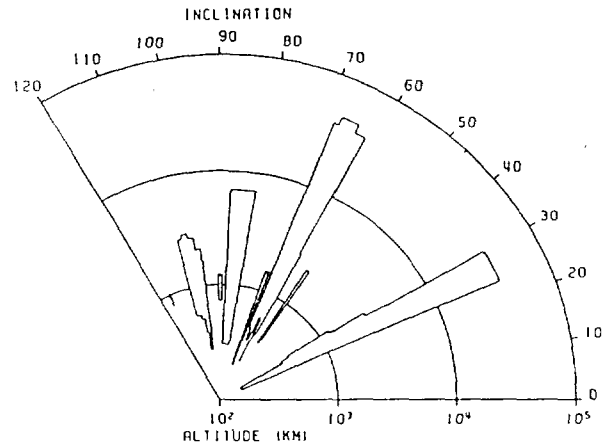


"Birds-Eye" View of Near-Earth Satellites

The near-Earth environment is becoming increasingly hazardous. There are at least 10,000 known debris objects in orbit that are larger than 4 cm in diameter and the number of objects smaller than 4 cm is expected to be even greater. The situation has become so desperate that a critical part of satellite design is protection from debris. One instance of damage from debris collision was a 1-cm pit in the window of the space shuttle caused by a 0.2-mm fragment of paint. It is estimated that the Hubble Space Telescope has a 1% chance of being destroyed by a collision during its lifetime. The probability of satellite destruction will continue to increase as more and more launches are performed annually. At this point in time, the danger is not large enough to necessitate countermeasures. However, by the early- to mid-twenty-first century, countermeasures will be imperative.

The purpose of this design is to eliminate a majority of the orbital debris. The Orbital Debris Removal and Salvage System (ODRASS) will push the smaller particles into lower orbits where their orbits will decay at a higher rate. This will be done with momentum transfer via a laser. The salvageable satellites will be delivered to the Space Station by an Orbital Transfer Vehicle. The rest of the debris will be collected by Salvage I. This will provide an active means of orbital debris management.

Acknowledgments. Project Team Members were Todd Shelton, Doug Cramer, and Matt Dougherty



Orbital Debris Distribution as a Function of Altitude and Orbital Inclination

DESIGN OF A SPACE-BASED SATELLITE SYSTEM TO PREVENT THE DEPLETION OF ATMOSPHERIC OZONE/OPTIC

The first purpose of this design is to attack one of the many problems facing the environment and explore a possible solution. Our design group has chosen to focus on the problem of ozone depletion in the Antarctic. We propose using a space-based system to interact with the stratospheric region over the Antarctic. This task will be accomplished by using an orbiting solar array system designed to transmit microwaves at a frequency of 22 GHz over the region in order to dissipate polar stratospheric clouds (PSC) that form during the months beginning in August and ending in October. The solar array system will be driven by a satellite system in a polar orbit at an altitude of 1000 km (621.4 mi). This altitude corresponds to an orbital period of 105.0 minutes. At an altitude of 1000 km, the solar satellite system will be able to beam microwaves into the PSC for 32.7 minutes every orbit. We have determined that the amount of microwave energy necessary to dissipate the PSC is approximately 3.44×10^{16} J. We have calculated that a PSC can be dissipated in approximately 38.8 days by a system incorporating two microwave emitting satellites inputting 5×10^{15} J every 32.7 minutes every orbit. Each satellite will collect energy using a system incorporating solar cells in conjunction with storage batteries for nine months of the year. The energy will be transferred to flywheels that will be sized to discharge energy at a rate of 25.5 GW/orbit for the required three-month period.

The second purpose of this environmental intervention design study is to provide a fundamental understanding of the chemistry of ozone depletion over the Antarctic. We hope that

Results of Hurricane Seeding Experiment

Hurricane	Dates	Number of seedings	AgI used (kg)	Maximum wind change (%)
Unnamed	13 Oct 1947	1	Unknown	Unknown
Esther	16 Sep 1961	1	35	-10
Esther	17 Sep 1961	1	35	0*
Beulah	23 Aug 1963	1	220	0*
Beulah	24 Aug 1963	1	335	-14
Debbie	18 Aug 1969	5	185	-30
Debbie	20 Aug 1969	186	-15*	
Ginger	26 Sep 1971	2	7	0†
Ginger	28 Sep 1971	3	96	decrease†

* Suitable clouds not seeded
 † Large old decaying storm with few seedable clouds

the ideas presented within our paper will spark creative new ideas. It is also our hope that our work will encourage others to look more closely into the problems facing our world. We hope to promote an awareness of the problems mankind has bequeathed to future inhabitants of the planet Earth.

PROJECT POSEIDON: A CONCEPTUAL DESIGN OF A SPACE-BASED HURRICANE CONTROL SYSTEM

Project Poseidon is a conceptual design for a space-based hurricane control system. The project was undertaken in response to an initiative from Lyle M. Jenkins of the Johnson Space Center on the topic of environmental intervention from space. Project Poseidon consists of a network of 21 low-orbiting laser platforms arranged in three rings designed to heat the upper atmosphere of a developing tropical depression. Fusion power plants are proposed to provide power to the lasers. The necessary tracking information will be provided by existing weather satellites and ground stations. Cooling for the optics and electronic components will be provided by sorption refrigeration. The target launch date for the proposed network is 2025 to 2050. Necessary assumptions were made in the conceptual design phase on the achievable technology level by this time period.

Acknowledgments Project Members were Kyle Cooper, Jorge Frank, and Michael Kalinowski.

Reduction in Destructive Force with Respect to Wind Speed

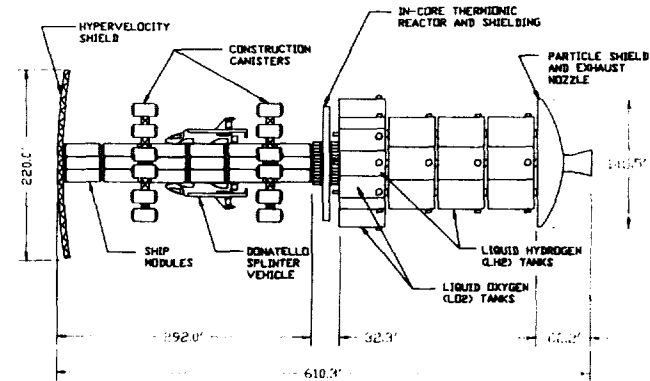
Reduction in wind speed (%)	Reduction in destructive force (%)
10	27
20	49
30	66
40	78

PROJECT DONATELLO: A PROPOSED MARS EXPLORATION INITIATIVE FOR THE YEAR 2050

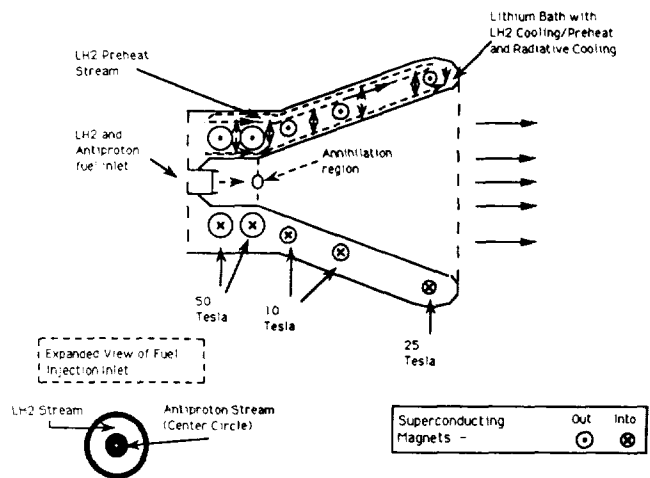
This project is a conceptual design for a futuristic superfreighter that will transport large numbers of people and supplies to Mars for the construction of a full-scale scientific and manufacturing complex. Code named "Project Donatello,"

the freighter will be assembled at the first libration point (L1) of the Earth-Moon system. The ship will be constructed with materials supplied by Heavy Lift Launch Vehicles (HLLVs) from Earth and from Orbital Transfer Vehicles (OTVs) from the large lunar base.

Donatello will utilize an antimatter propulsion system that will drastically reduce Mars trip time and the fuel mass



Donatello: Superfreighter to Mars



Anti-proton/Liquid Hydrogen Annihilation Propulsion Engine (A/LH-APE)

requirements of the ship. Upon arrival at Mars, two smaller transfer ships will carry railroad boxcar sized payload canisters into the martian atmosphere and to the vicinity of the existing Mars outpost. The canisters will be parachuted to the surface allowing the transfer ships to make numerous runs with low fuel consumption. The vehicles will also have vertical takeoff and landing (VTOL) capabilities when transporting fuselage canisters containing the Mars base personnel.

The canisters will contain construction materials for an advanced Mars base, including material processing components, airshells, life support systems, power supplies, scientific and industrial equipment, and food production systems.

Acknowledgments. Project Members were John G. Vandegrift, Kenneth, E. Brunsen, Timothy F. Dawn, and Brian H. Kendall.

N91-18172

UNIVERSITY OF WISCONSIN-MADISON

P.1

MARS PENETRATOR SAMPLE RETRIEVAL SYSTEM

Because of the high probability of manned Mars expeditions in the future, a greater understanding of the planet's subsurface conditions has become necessary. NASA is considering using a penetrator to acquire and analyze soil samples from a region approximately 15-30 ft below the martian surface. The purpose of this study is to propose and describe a drilling mechanism that will be used in a penetrator to collect and deliver an uncontaminated, thermally unaltered soil sample to the penetrator instrumentation for analysis. A preliminary design, utilizing a percussive drilling motion, was the basis for a prototype model in which design principles were analyzed and tested. This unique design uses a drill bit with three cutting tips arranged in a radially terraced formation. The bit is indexed after each percussion, excavating a terraced hole. Curved scoops on the drill head encourage soil particles to enter the drill tube where the sample retrieval system, using the percussive action of the drill, migrates sample backwards through the drill and out exit holes. Special conditions unique to a martian penetrator sampling system have been recognized in this design. They include size and weight limitations, temperature restrictions, extremely high *g* loads and the ability to dispose of contaminated soil. Our paper describes the drill design, prototype test set-up, and methods of analysis.

Acknowledgments. Project members were James R. Bilodeau, Christopher W. Byrne, Stephan J. Caravella, Cynthia G. Kurek, Andy J. Provenza, and Kristin C. Schad

MARS EGG

One of NASA's primary areas of interest in the near future is the determination of martian surface properties in preparation for a sample return mission or manned mission to Mars. The Mars Egg is a small surface analyzer that would be dropped on the surface of Mars from an orbiter and would analyze the gases present in the surface soil over a period of

one martian year to determine the diffusivity of the soil. Our study includes analysis of reentry dynamics, impact with the Mars surface, repositioning after impact to access undisturbed soil, and actuation of the test apparatus. The egg contains a gas chromatograph, radio transmitter, and the necessary power supplies.

Upon deployment of the egg from an orbiting satellite, the egg free falls until it reaches the martian atmosphere. The probe is protected by an ablative heat shield that dissipates most of the heat caused by friction with the atmosphere during reentry. A ballute and parachute system is used for speed reduction during reentry. The ablative shield is released when the parachute is deployed, and the egg is slowed to an impact velocity of < 10 m/s. To obtain the gas samples, a porous hollow tube is inserted into uncontaminated soil and gases are evolved by heating the soil with resistive coils. The gases are drawn into the probe and analyzed by a gas chromatograph. The output signal of the chromatograph is then transmitted to the orbiting satellite.

DESIGN OF A GEOSHACK

The purpose of the study is to present the initial design of a Geosynchronous Operations Support Center, or GeoShack. A GeoShack is a manned or unmanned "mini-space station" in geosynchronous orbit, designed for the repair, attitude correction, and general upkeep of satellites stationed in geosynchronous orbit. Our paper presents the conceptual design and initial engineering design of several components of the vehicle, including the pressure vessel, satellite berthing structure, and payload berthing pins for accommodation in the shuttle orbiter bay. In addition, engineering studies of material selection, attitude control, orbital stability, and a remote manipulator are presented. Our paper represents engineering design strategies taught by the University of Wisconsin-Madison Engineering Mechanics Department.

1. Report No. NASA CR-187041		2. Government Accession No.		3. Recipient's Catalog No.	
4. Title and Subtitle Proceedings of the 6th Annual Summer Conference: NASA/USRA University Advanced Design Program				5. Report Date November 1990	
				6. Performing Organization Code	
7. Author(s)				8. Performing Organization Report No. None	
				10. Work Unit No. 505-90-53	
9. Performing Organization Name and Address Universities Space Research Association (USRA) 17225 El Camino Real, Suite 450 Houston, Texas 77058				11. Contract or Grant No. NASW-4435	
				13. Type of Report and Period Covered Contractor Report Final	
12. Sponsoring Agency Name and Address National Aeronautics and Space Administration Washington, D.C. 20546-0001				14. Sponsoring Agency Code	
15. Supplementary Notes Project Manager, Sheree McGee, University Programs, NASA Headquarters.					
16. Abstract <p>This document contains the reports presented at the Sixth Annual Summer Conference of the NASA/USRA University Advanced Design Program, cosponsored by NASA and USRA, and hosted by NASA Lewis Research Center, on June 11-15, 1990. The University Advanced Design Program brings together NASA engineers, students, and faculty from United States engineering schools by integrating current and future NASA space/aeronautics engineering design projects into the university curriculum. Topics studied cover a broad range of potential space and aeronautics projects which could be undertaken during a 20- to 30-year period beginning with the deployment of Space Station Freedom scheduled for the mid-1990s. Both manned and unmanned endeavors are embraced, and the systems approach to the design problem is emphasized.</p>					
17. Key Words (Suggested by Author(s)) Aerospace engineering; Aircraft design; Manned orbital laboratories; Orbit transfer vehicles; Space habitats; Space stations; Spacecraft design; Space probes			18. Distribution Statement Unclassified - Unlimited Subject Category 12		
19. Security Classif. (of this report) Unclassified		20. Security Classif. (of this page) Unclassified		21. No. of pages 319	22. Price* A14